AGARD-CP-373

AGARD

ADVISORY GROUP FOR AEROSPACE RESEARCH & DEVELOPMENT

7 RUE ANCELLE · 92200 NEUILLY SUR SEINE · FRANCE

AGARD CONFERENCE PROCEEDINGS No.373

Flight Test Techniques

NORTH ATLANTIC TREATY ORGANIZATION

DISTRIBUTION AND AVAILABILITY
ON BACK COVER

COMPONENT PART NOTICE

THIS PAPER IS A COMPONENT PART OF THE FOLLOWING COMPILATION REPORT: A

(TITLE): Flight Test Techniques. Proceedings of the Flight Mechanics Panel Symposium Held in Lisbon, Portugal on 2-5 April 1984.

(SOURCE): Advisory Group for Aerospace Research and Development, Neuilly-sur-Seine (France).

TO ORDER THE COMPLETE COMPILATION REPORT USE AD-A147 625.

THE COMPONENT PART IS PROVIDED HERE TO ALLOW USERS ACCESS TO INDIVIDUALLY AUTHORED SECTIONS OF PROCEEDINGS, ANNALS, SYMPOSIA, ETC. HOWEVER, THE COMPONENT SHOULD BE CONSIDERED WITHIN THE CONTEXT OF THE OVERALL COMPILATION REPORT AND NOT AS A STAND-ALONE TECHNICAL REPORT.

THE FOLLOWING COMPONENT PART NUMBERS COMPRISE THE COMPILATION REPORT:

AD#:	TITLE:
AD-P004 098	Determination of External Store Drag.
AD-P004 099	The Flight Test of an Automatic Spin Prevention System.
AD-P004 100	High Angle of Attack Test and Evaluation Techniques for the 1980s.
AD-P004 101	Determination of Performance and Stability Characteristics from Dynamic Manoeuvres with a Transport Aircraft Using Parameter Identification Techniques.
AD-P004 102	Application of Advanced Parameter Identification Methods for Flight Flutter Data Analysis with Comparisons to Current Techniques.
AD-P004 103	A Technique to Determine Lift and Drag Polars in Flight.
AD-P004 104	Flight Testing a Digital Flight Control System: Issues and Results.
AD-P004 105	Aircraft Tests in the Clearance Program for the Use of a Combat Aircraft from a Runway After Damage Repair.
AD-P004 106	The Handling and Performance Trials Needed to Clear an Aircraft to Act as a Receiver During Air-To-Air Refuelling.
AD-P004 107	Reference Systems for the Evaluation of Dead-Reckoning Navigation Equipment.
AD-P004 108	Autopilot Performance Evaluation: Tornado Experience and Future Applications.
AD-P004 109	Assessing Pilot Workloads in Flight.
AD-P004 110	Simulation Applied to the Avionics System Testing in the F/A-18.
AD-P004 111	Flight Test Techniques Employed in the Nimrod MR MK 2 Weapon System Performance Trials.
AD-P004 112	F-16 and A-10 Diffraction Optics Head-Up Display (HUD) Flight Test Evaluation.
AD-P004 113	In-Flight Accuracy and Coverage Tests of ESM and ECM Systems.
AD-P004 114	Flight Test Techniques Used for Proof of Structural Integrity of Tornado When Carrying External Stores.

COMPONENT PART NOTICE (CON'T)

AD#:	TITLE:
AD-P004 115	Real Time Testing - The Next Generation.
AD-P004 116	Using an Airborne CO_2 CW Laser for Free Stream Airspeed and Windshear Measurements.
AD-P004 117	NAVSTAR GPS Applications to Test and Training.
AD-P004 118	An Extended Real-Time Microwave Airplane Postion System.
AD-P004 119	General Integrated Multipurpose Inflight Calibration System.
AD-P004 120	The Development of an Airborne Instrumentation Computer System for Flight Test.

NORTH ATLANTIC TREATY ORGANIZATION

ADVISORY GROUP FOR AEROSPACE RESEARCH AND DEVELOPMENT

(ORGANISATION DU TRAITE DE L'ATLANTIQUE NORD)

AGARD Conference Proceedings No.373

FLIGHT TEST TECHNIQUES

Papers presented at the Flight Mechanics Panel Symposium held in Lisbon, Portugal, 2 - 5 April 1984.

THE MISSION OF AGARD

The mission of AGARD is to bring together the leading personalities of the NATO nations in the fields of science and technology relating to aerospace for the following purposes:

- Exchanging of scientific and technical information:
- Continuously stimulating advances in the aerospace sciences relevant to strengthening the common defence posture;
- Improving the co-operation among member nations in aerospace research and development;
- Providing scientific and technical advice and assistance to the North Atlantic Military Committee in the field of aerospace research and development;
- Rendering scientific and technical assistance, as requested, to other NATO bodies and to member nations in connection with research and development problems in the aerospace field;
- Providing assistance to member nations for the purpose of increasing their scientific and technical potential;
- Recommending effective ways for the member nations to use their research and development capabilities for the common benefit of the NATO community.

The highest authority within AGARD is the National Delegates Board consisting of officially appointed senior representatives from each member nation. The mission of AGARD is carried out through the Panels which are composed of experts appointed by the National Delegates, the Consultant and Exchange Programme and the Aerospace Applications Studies Programme. The results of AGARD work are reported to the member nations and the NATO Authorities through the AGARD series of publications of which this is one.

Participation in AGARD activities is by invitation only and is normally limited to citizens of the NATO nations.

Published July 1984

ISBN 92-835-0359-7

Printed by Specialised Printing Services Limited
40 Chigwell Lane, Loughton, Essex IG10 3TZ

PREFACE

The techniques used in flight testing undergo continual development to accommodate the new concepts that have to be tested and to improve the accuracy and efficiency of flight testing.

In recent years novel flight control systems have greatly increased the scope of handling qualities clearance work to include violent manoeuvring at high angle of attack, decoupled manoeuvres, etc.

Determination of aircraft position has been developed for greater convenience and better accuracy and satellite based systems are now being introduced for navigation assessment. These reflect the constant struggle for the flight test techniques and instrumentation to stay ahead of the systems they are assessing in terms of accuracy.

The major advances made in pilot's displays have led to the development of new test techniques for their assessment. Meanwhile the real time display of information to the flight test engineer in the ground station and the rapid processing and interpretation of results on the ground have continued to advance.

At the same time there are always novel and interesting applications of quite simple techniques which are of real interest and value to the flight test community.

The Flight Mechanics Panel has held a symposium on flight testing every four years or so since its early days and it was decided to follow up the symposia in 1976 and 1980 by a further one on "Flight Test Techniques". This led to the symposium, held in Lisbon, Portugal, in April 1984, which is reported in these proceedings.

The Symposium included many interesting papers and provided a valuable opportunity for the AGARD flight test community to meet and discuss broader issues such as the cost effectiveness of the complex techniques and sophisticated equipment now emerging.

It is important that such meetings should continue to be organised by the Flight Mechanics Panel on a regular basis so that new techniques for flight testing, instrumentation and data analysis can be disseminated to ensure that safe, efficient and timely testing is accomplished.

A.D.PHILLIPS
Member, FMP

T.B.SAUNDERS
Member, FMP

CONTENTS

DETERMINATION OF EXTERNAL STORE DRAG

by

K. Lutz, R. Matecki
DORNIER GMBH
Postfach 1420
D-7990 Friedrichshafen

1. INTRODUCTION

"External store drag" is a title of a wide field of aerodynamical and flight mechanical problems. Our considerations are based on ALPHA-Jet work and thus are only valid for stores in the subsonic flight region. Until now no exact methods for preestimation of single or multiple store arrangements are commonly known. The only successfully used methods are of semi-empirical nature for which the most critical problem, i.e. the estimation of the interference drag, is to be taken from statistical material based on a greatest possible number of flight test results.

Before presenting typical results from the evaluation of ALPHA-Jet flight tests with external stores, the philosophy of the flight test evaluation itself is described shortly. The external store drag values from flight tests, evaluated since 1975, are not only registrated for performance purposes and documentation in the pilots operating handbook, but they are also analysed in regard to the causes of the differences in values, to the individual contribution of the interference drag and to the possibilities to define poor drag configurations. The latter ones are limited due to several constraints which cannot be changed (e.g. shape and aerodynamic cleanliness of the store itself). Here only the importance of better aerodynamic design of future stores can be emphasized.

The evaluation of external stores which is presented here concerns single store configurations and double store configurations. In the final chapter the necessary considered further work for completing external store statistical basic data is listed up.

2. TECHNIQUE OF EXTERNAL STORE DRAG EVALUATION FROM FLIGHT TESTS

The external store drag is to be evaluated in a classical manner for all configurations and configuration components beginning with the clean aircraft as first reference configuration and than evaluating step by step additional components (e.g. gun-pod, pylons, tanks e.a.). Our main efforts were directed on under-wing stores, as the ALPHA-Jet has only one under-fuselage station for a gun-pod.

To come to reliable results for the drag values, the main condition is the availability of individually calibrated engines for a certain test sequence. This calibration is done for all engines in a ground test facility and for some cases in an altitude simulation facility. The results are adopted together and the brochure data set of the engine manufacturer (for a minimum engine) is fitted to the calibration results by correction factors. Every time the engines are replaced by others these correction factors were also to be checked or changed. And as a result of this, new reference flights were necessary, which were the starting point for the evaluation of further added store components. The primary engine signals which could be used to calculate the actual thrust (beside mass and atmospheric data) were RPM, nozzle pressure and fuel flow. In the first time we used nozzle pressure and fuel flow parallelly, but in later time we only used the "fuel-flow-method" because of the best reliable results. By using the equilibrium of forces equations we come to polar curve points C_L, C_D (M, α) which were filtered in a last computation step. The interesting drag contribution of a certain store including the interference drag is found as the difference between the drag with this store and the configuration without that (in the same test sequence). An angle of attack dependency in the practically used angle of attack range was never found. The additional store drag always resulted only in a corresponding parallel shift of the drag polar curves of the clean aircraft.

3. TEST RESULTS FROM SINGLE MOUNTED STORES UNDER PYLONS

Fig. 1 shows the evaluated additional drag curves from flight test for some single mounted stores under pylons in terms of drag aereа $\Delta C_D \cdot S$ where the pylon contribution itself is excluded but the interference between store and wing is included. The curve for the training system CBLS-200 (Carrier Bomb Light Store) was evaluated for an asymmetric mounted case i.e. only one store at the aircraft. This result with the very high drag contribution of one store only was somewhat unexpected in this amount, because first preestimations and the following wind tunnel test phase let hope for a considerably lower additional drag. The trim drag contribution for this asymmetrical case was checked to be negligible. Not only the evaluation of several flight test sequences but also additional evaluation of later German Airforce flights confirmed this result.

The lower curves of drag aereas are valid for two stores in symmetric mounted configurations. Whereas the 230 L-tanks are mounted always under the outer wing pylons, the other store drags are always evaluated for the position under the inner pylons. For some of the smaller stores also the position under the outer pylons where checked, but no considerable difference was found. It was always in the (fairly small) scatter range of the evaluation points.

A comparison of these drag curves does not lead to further unexpected conclusions. Due to the Re-number influence, the curves are going first down at low Mach-numbers until the compressibility influences let them go more or less steep up. The drag level corresponds in all cases with the aerodynamic cleanliness and with the wetted store surface. The importance of aerodynamic cleanliness can best be seen at the example of the 2xMK 82, a typical low-drag bomb. For the case with a crude nose initiator the store drag is double as high as for the case with the smooth regular conical nose.

In fig. 2 the results of the drag evaluation for three types of single mounted launchers are shown. They were mounted symmetrically under the inner pylons and in some cases also under the outer pylons. Comparing the results for the two positions, again the differences were within the evaluation points scatter.

The launchers were tested for the cases "full" and "empty". The geometric dimensions as well as the surface aerea were within the same order of magnitude, so that the differences in the results are caused only by the individual aerodynamic cleanliness. A table in the lower part of this figure gives a first impression of the surface quality "full" and "empty" with results in the logical differences of the drag level. But because of one unexpected result, some additional remarks must be made to this figure:

For the case "full", due to the smooth plastic covered nose the LAU 5003/A has the lowest drag values, and due to the uncovered rocket holes the LAU-51A shows the highest values. The values for the LR-155 ND are placed between those others.

For the case "empty" the sequence is otherwise ordered. The additional drag curve of the LAU-51/A empty is not only placed lower than those of the other two launchers, it is even a little bit lower than for the LAU-51/A "full". For the preestimation it was commonly assumed that an empty launcher always must have a higher drag than a full one because of the larger wetted aerea (rocket holes) and intake perturbations. But as can be seen here the combined detail contributions are more complicated. For the LAU-51/A the open uncovered rocket holes in the loaded configuration obviously generate disturbances which yield to a relatively high drag. In the unloaded case these disturbances vanish, the intake flow is relatively regular and the base drag is decreased by ventilation. The additional friction drag is lower than the sum of the above mentioned contributions, so that the result for the empty LAU-51A is lower than for the full case.

For the other two launchers the drag behaviour is of somewhat other nature. In the full case the flow around the covered nose is relatively clean (better for the LAU 5003/A). But in the empty case, this cover is perforated by the fired rockets, the inlets are irregular and generating disturbances outside the stores. The flow velocity through the holes is lower than in the case of LAU-51A, thus yielding to lower additional friction drag, but also avoiding the full decreasing of the base drag by ventilation. As a sum of all detail contributions, the overall launcher drag for these two types is higher in the empty case than in the full case.

4. ANALYSIS OF DRAG TEST RESULTS FOR SINGLE STORE CONFIGURATIONS

It is not a satisfying work to evaluate the external store drag, thinking about why the drag of one store is more or less different than that of an other and than to document it. For future preestimations it is desirable to go into more details, to get also information of the very important interference drag between store and wing as statistical values which allow also to come to conclusions for special low drag arrangements. Concerning the interference drag contribution it is desirable to know the influencing parameters quantitatively. In combination with the external store drag evaluation from Alpha-Jet flight tests the following approach to analize the store drag was chosen:

- *assuming the measured drag of a store under an a/c, interference drag included, is valid and*
- *assuming the semiempirically estimated free flight store drag without interference is also valid*
- *in this case the difference between these two values must be the interference drag contribution.*

The second of the above assumptions will accept a certain scatter in the results but seldom massive deviation will occur (in our cases estimation of the CBLS e.g.).

If now as much as possible values of external stores are evaluated in this way and documented with all possibly contributing characteristical informations, it can be attempted to answer to the question *"what parameters are influencing the interference drag in which way?"*.

And if this is known all informations for future low store drag arrangement are available.

The technique of evaluating the store drag from flight tests was already shortly described in chapter 2. Fig. 3 shows the steps for estimating the external store drag beginning with step 1 by determining the friction and pressure drag, continuing by adding the different contributions of step 2 thru 4 and summing all these steps up to the so-called "free flight store drag" without interference, which is to be compared in one actual case with the flight test results to analyze the interference contribution. For unknown store-arrangements the "free flight store drag" must be multiplied with the interference factor for the interaction between wing and body and perhaps also for double body arrangements. But the aim of our efforts was to come to these interrerence factors by the above described comparing method.

About 10 years ago, Mr. Berry [1] from the ARA in GB published a very useful extensive paper in the AGARD Lecture Series Nr. 67, where he combined empirical methods with wind-tunnel measurements. We now attempted a similar approach by combining flight test results on the ALPHA-Jet with semiempirical methods to come to a diagram of interference factors equivalent to that of Mr. Berry. Our results are presented in fig. 4 for axis-symmetrical stores. A similar one was evaluated for flat stores like pylons. The used symbols are the same as defined by Mr. Berry: E = factor of aerodynamic cleanliness (ratio of free flight drag and friction drag); ΔM = difference between actual Machnumber and drag rise Mach-number of wing; K_s = interference factor (ratio of store drag under wing pylon and free flight drag). Here the often found results are demonstrated, that the "cleanier" the store is (low E), the higher will be the interference factor.

Compared with the corresponding diagram of Mr. Berry it is to be stated that the whole carpet is shifted to higher values. Values extremely below $K_s = 1.0$, due imaginable, were not found during the ALPHA-Jet flight test evaluation.

Further it is to be stated that the diagram is of limited validity. Two examples may illustrate this: The external 320-l-tank of the ALPHA-Jet is of extreme aerodynamic cleanliness (E ∿ 1.6) but the resulting interference factor is about K_S = 1.0. The aerodynamically very dirty CBLS-200 (E ∿ 7) shows an interference factor about K_S ∿ 2. Especially the first case, where the quite long tank (3,5 m) is mounted under the outer wing pylon with a local wing chord of only 1,8 m an influence of these geometrical relations is to be suspected. Some attempts were made with the ALPHA-Jet external store flight test data to construct diagrams including such geometrical influences, but until now these efforts were without success, as not enough values were available.

Thus the interference drag diagram of fig. 4 is only be considered as a first approach for average external store dimensions.

5. TEST RESULTS FROM DOUBLE MOUNTED STORES UNDER TWIN CARRIERS

During the ALPHA-Jet flight tests some double mounted stores configurations for different stores and different twin carriers were evaluated. Fig. 5 gives a first selection of drag values of double mounted stores, including all interferences (to the wing and between one another), but without the drag contribution of pylons and twin carriers.

This figure gives a first impression of the importance of the choice of the twin carrier type on the double stores drag. It should however be noted that this is only one contribution to the sum of the drag including the carrier's own drag, too.

First the case of 2x2 BL755 in the upper part of the figure should be considered. The flat twin carrier MLr in its origin configuration led to the highest double stores arrangement of the 4 BL755. A small modification at the carrier MLr (shortened = rogné) decreased the drag only a little bit. The body shaped carrier Y-DC, which was better was only evaluated for comparison, but the special development of the A-formed carrier Y-ES 1954 with an extreme spacing of the stores decreased the drag of 4xBL755 by about 30 %. Comparing this curve with that in fig. 1 for 2xBL755 under single pylons shows that the interference factor for double stores is reduced by the spacing of the twin carrier to 1.0, i.e. the drag of one store under the Y-ES 1954 corresponds to a single mounting.

Further interesting results are the lowest two curves, each for only one BL755 under the twin carrier MLr. The second store, which is mounted at the side of a first already tested store has only half the amount of drag. This would result into the conclusion that for this configuration - the stores are in a very tight, nearly touching position - a favourable double - stores effect exists. Summing up the values of the two lowest curves and multiplying with 2 leads to the result of 4xBL755 at MLr in the upper part of the figure. It is to be noted that the latter curve is taken from the early time of flight test evaluation whereas the lower ones are from a far later test period; but the results are fitting well together. (A further evidence of existing favourable double store interference in this special case was found during a wind tunnel test serie concerning a study for low drag arrangements [2]. A fairing around the front and side parts of the MLr with two BL755 led to an overall increased drag.) The other stores under MLr (SAMP 250 kg and MK82) show lower drag values, corresponding to their smaller dimensions.

But as already stated above, the drag of the stores with all interferences is only a part of the total additional drag which includes also the contribution of pylons and twin carriers, and which is finally of interest for the performance. An impression of such a comparison gives the diagram in fig. 6, which shows the total drag of 4 x Matra SAMP 250 kg stores with two pylons and two twin carriers of different types.

The best (lowest drag) with nearly no compressibility effect shows the configuration with tandem store mounting, as a result of the well known favourable low drag interference and the own low drag of the carrier itself. The case with the fairly small flat ALKAN 4020 with tight parallel positioning of the SAMP-stores has also good results in the low Mach-number region, but with a steep drag creep at higher Mach-number values. The difference between configurations with the body-shaped AU-Fl-standard and AU-Fl-modified is caused by an other solution for the store rack system with identical stores and stores spacing. The Refaut twin carrier is also body shaped. The overall additional drag with this carrier is similar with the modified AU-Fl-configuration in the lower Mach-number range but with a steeper drag creep. The highest overall additional drag is found for the case with MLr.

6. ANALYSIS OF DRAG TEST RESULTS FOR DOUBLE STORE CONFIGURATIONS

With this analysis some knowledgement about the mutual interference between two double arranged stores should be found. Again Mr. Berry from the ARA in GB presented in the above referenced report [1] a first diagram for double store mutual interference, where this factor K_D is the quotient of the drag of two stores in double configuration and that of two corresponding single store arrangements, which it a function of the store spacing and the flight Mach number.

The analysis of our flight test results is a little bit more complicated because the several results for different spacing are found for

- different twin carrier types with different store rack systems (crutch arms e.g.) which can have not negligible influence and which cannot be separated from the interference drag factor K_D in the case of consideration of the same store types;
- different combinations of stores with the same twin carrier type. It is imagineable that an individual different contribution caused by different store body shapes occurs.

It must be taken in mind that these two influences during our analysis of double mounted stores must necessarily be neglected. It is supposed but not demonstrable that these influences in most cases can be neglected. But a certain scatter in the results of the analyses must be expected to be existant.

In fig. 7 the evaluated double store interference factor as defined above is shown for always the same store type (2 x SAMP 250 kg) under different twin carriers (the relative spacing of each is noted) as a function of Mach number for the above assumptions. The lowest K_D-factor is found below 1.0 for the stores under the tandem carrier, where no spacing can be defined. A K_D-factor of 1.0 independent from Mach number is characteristic for the stores under the specially constructed A-pylon with a very larger spacing ($y/D \approx 1,9$). At low Mach-numbers for the mounting under the flat ALKAN 4020 with very tight spacing ($y/D \approx 1,17$) similar results for K_D are found (remember the favourably appearing interference effect for the second BL755 under MLr in fig. 5). The highest values for K_D are shown for the mounting under MLr for medium spacing with the actual store at about $y/D \approx 1.37$. Higher spacing with $1.57 \approx y/D \approx 1.68$ for the carriers AU-F1 and Rafaut lead to K_D-factors between maximum, and minimum values. But it is note worthy that the evaluation for the AU-F1 standard total configuration and for the AU-F1 modified total configuration leads to the result, that the higher total drag of the first one as shown in fig. 6 is part of the drag of the twin carrier only and not part of the interference drag, so that the same K_D-value for the double mounting of the store is found in both cases. This result lets hope that the above assumed neglection of such influences is not totally unacceptable. The same result that for very tight spacing and very wide spacing of stores the lowest K_D-factors are found also in the curves of fig. 8 where three cases of positioning different stores under the same twin carrier (MLr) are drawn. The actual spacing values are given numerically. The case of the two stores BL755 is evaluated from the already presented results with the favourably appearing interference effect in fig. 5.

For summarizing the foregoing results fig. 9 is drawn with K_D as a function of the relative spacing and with curves of constant Mach-number. The case for stores under the tandem carrier is excluded here. The evaluated value range of the interference factor K_D is marked for each carrier configuration at the actual spacing position as solid bars for the case of SAMP 250 kg and as dashed bars for other external store types.

The characteristics of the curves are to be considered with the following reservations:

- At the high spacing of about $y/D \approx 2.0$ the curves must come together asymptotically, because the mutual interferences vanish independently of the Mach number; but the results can only be a first approximation.

- At very tight spacing with $y/D \approx 1.0$ the evaluation led also to relatively low K_D-values but with a relatively higher scatter. But all discussed detail results seem to support the conclusion that tighten the spacing below a certain value will lower the K_D-factor. For this case remember again the test results for the contribution of each of the two double mounted BL755 under MLr. Nevertheless for assuring this result further test values for this region in the diagram are desirable.

- Regarding only the results in combination with flat plate similar twin store carriers (MLr, ALKAN 4020 and Y-ES) the total scatter of the values in this diagram is somewhat lower. But also in these cases influences of different body shapes and rack systems are to be accepted. Therefore a much higher number of evaluated double mounted stores is desirable; and as long as these are not available, this diagram must be regarded as being preliminary.

7. SUMMARY

Experience of several years in evaluating the additional drag of external stores shows that enough confidence exists in the standardized methods in flight tests with the most important condition of availability of individually calibrated engines.

But more analizing work on additional other external stores, carriers and airplanes is necessary, especially for more statistical values concerning the interference drag. Additionally further efforts are necessary for incorporating the surely existing geometrical dependencies between stores, pylons and wing in new interference diagrams.

Concerning the twin store carrier configurations, also further additional evaluations for other store types in combination with the already known carriers as well as for new carrier types are necessary with the aim to get more informations about the double store interference factor. This is especially desirable for configurations with fairly tight spacing.

Not included in this report are evaluations of multiple carrier interferences with more than two stores because they were not tested on the ALPHA-Jet. Systematical work with analysis concerning these configurations is unknown.

Summarizing the above statements: Further efforts are necessary for completing the statistical values of external store drag with all influencing parameters with the aim to be sure in preestimation of not tested new stores especially in low drag arrangement.

8. REFERENCES

[1] J.B. Berry:
"External Store Aerodynamics for Aircraft Performance Prediction", AGARD-Lecture Series No. 67 on "Prediction Methods for Aircraft Aerodynamic Characteristics"

[2] R. Matecki, e.a.:
"Widerstandsarme Anbringung von Außenlasten bei Kampfflugzeugen", Dornier-Berichte 79/47 B und

Fig. 1

Single Mounted External Stores Under Pylons
Flight Test Results from Alpha Jet

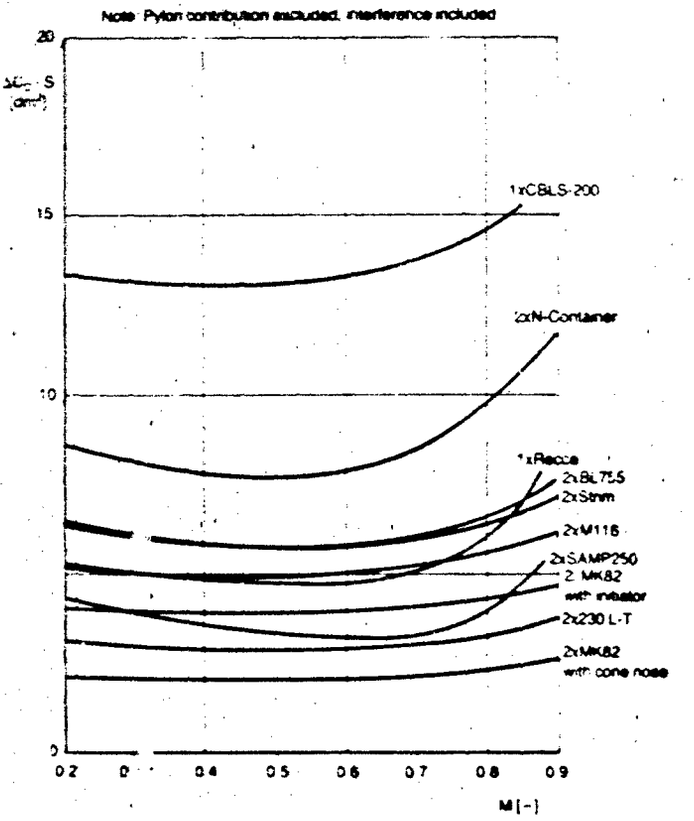

Single Mounted Launchers Under Pylons
Flight Test Results from Alpha Jet

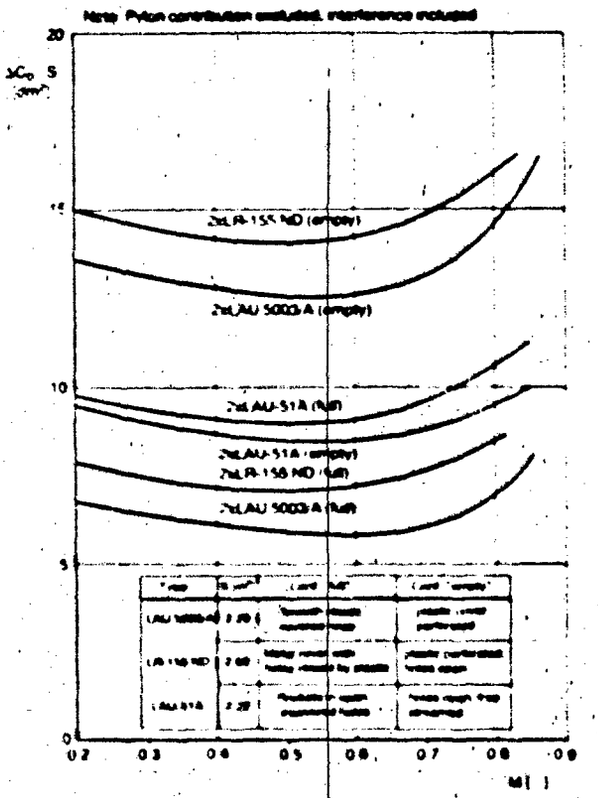

① Friction drag and pressure drag for equivalent streamline shaped bodies (or wings)

② Influence of cylindrical middle part, non-circular cross section, excrescences, initiator, stabilizer e.g.

③ Base drag contribution

④ Interference between store parts (corners between stabilizer and body e.g.)

⑤ FREE FLIGHT STORE DRAG Σ ① ÷ ④

⑥ Factor of interference between wing and body

⑦ Factor of interference for double body arrangement

⑧ TOTAL EXTERNAL STORE DRAG UNDER WING ⑤·⑥·⑦

Fig. 3 **Semiempirical External Store Drag Estimation**

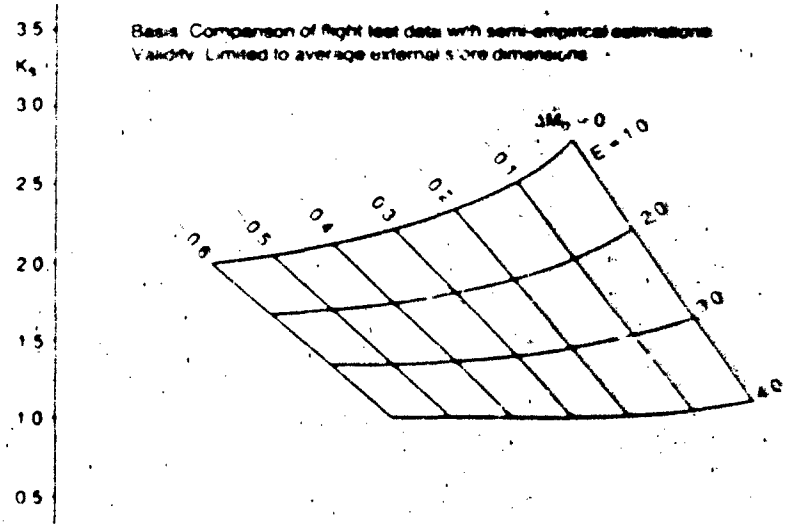

Interference Factors for Axis-Symmetrical External Stores at Alpha Jet

Fig. 4

Fig. 5

Double Mounted Stores under Twin-Carriers
Flight Test Results from Alpha Jet

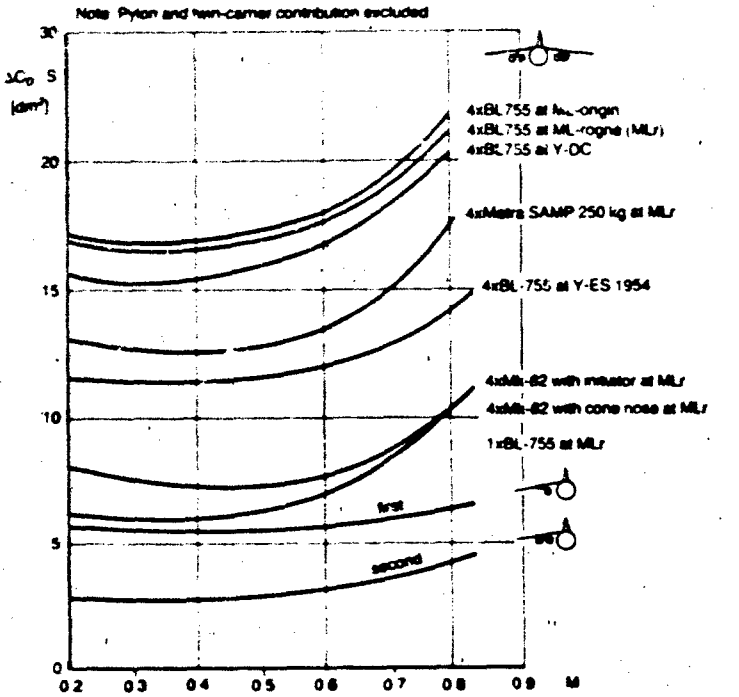

Fig. 6

Comparison of Twin Carrier Configurations
with Identical Stores
Flight Test Results from Alpha Jet

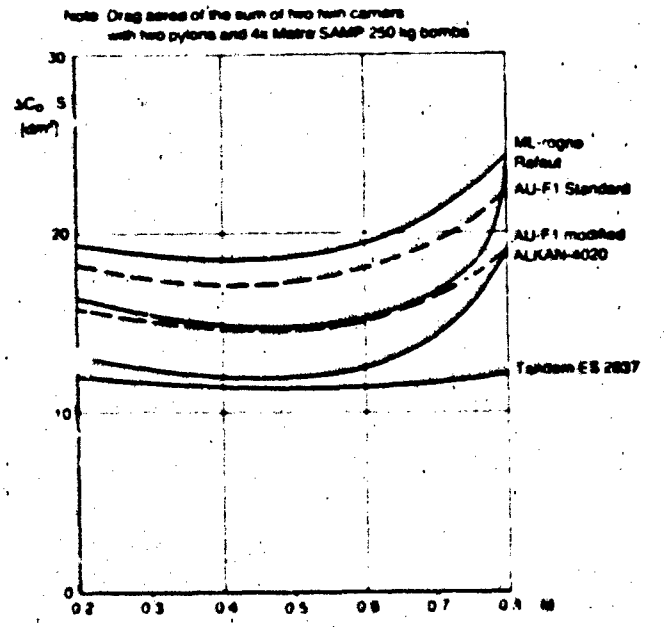

Fig. 7

Interference Factor

for Double Mounting SAMP 250 kg

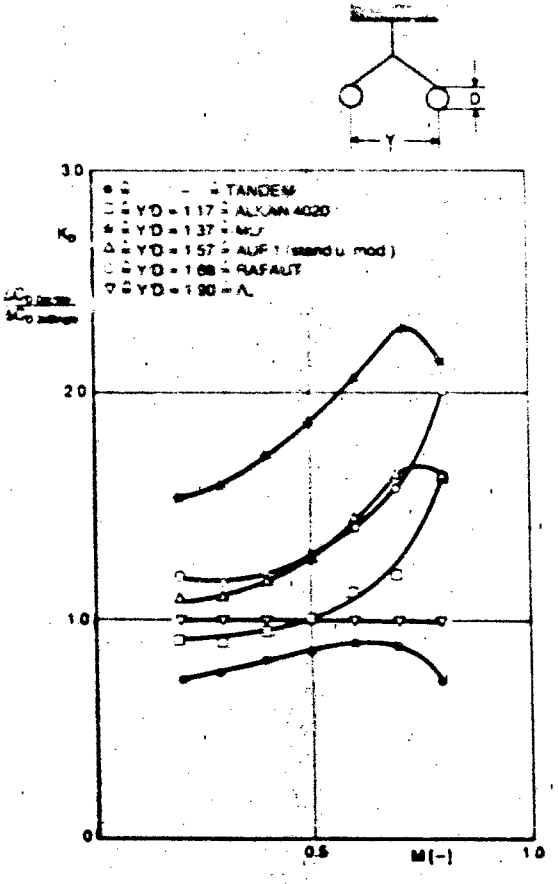

Fig. 8

Interference Factor for Double Mounted Stores under Twin Carrier MLr

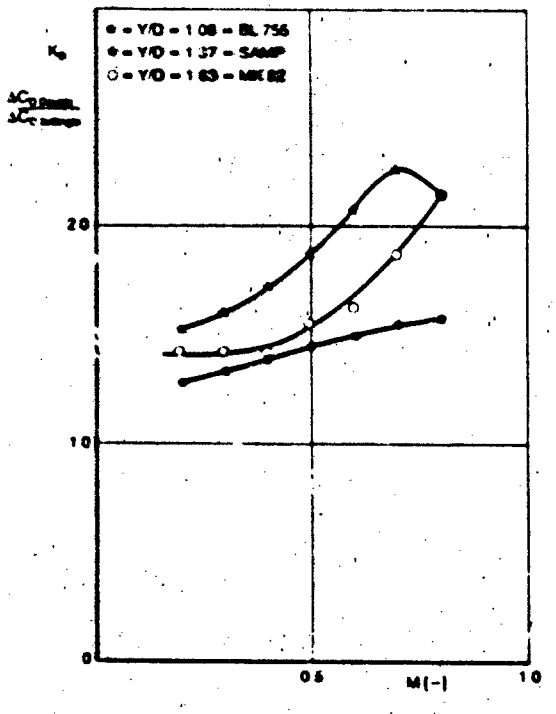

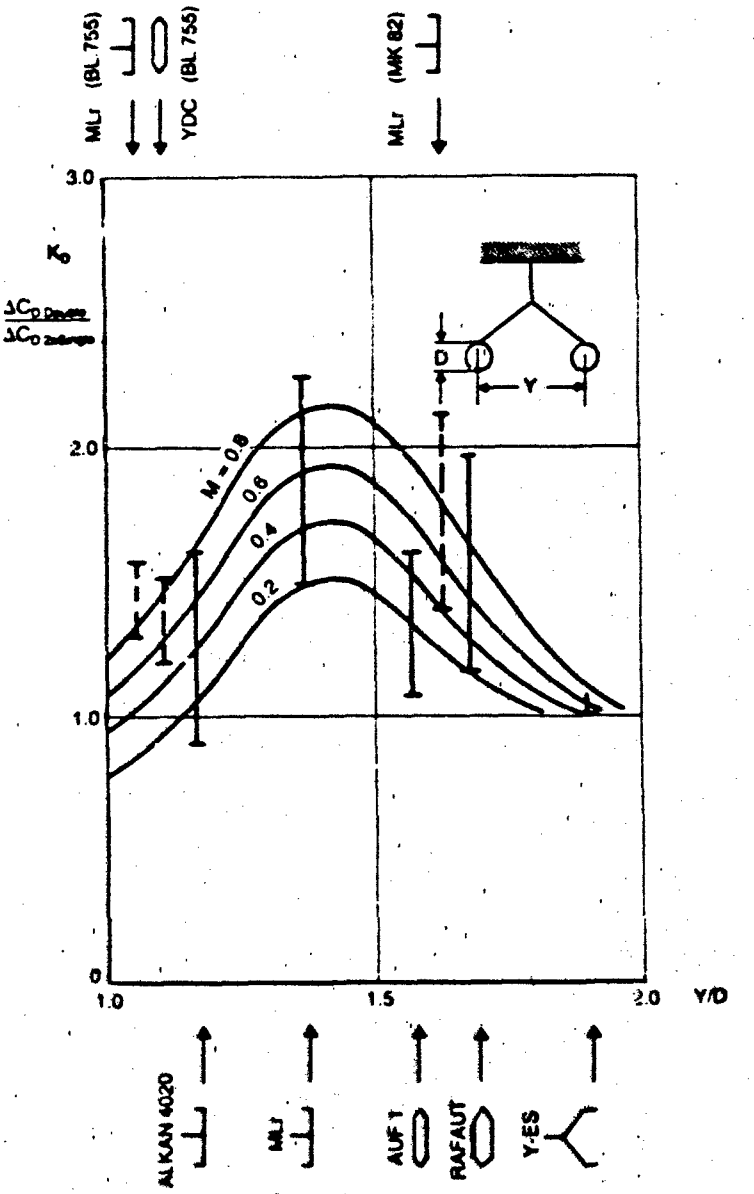

Comparison of Twin Carriers:
Interferences for ⟶ = SAMP 250 kg
⟵ = OTHERS

Fig. 9

THE FLIGHT TEST OF AN AUTOMATIC SPIN PREVENTION SYSTEM

by

P. S. Butcher - Flight Test Engineer

and

K. McKay - Senior Aerodynamicist
British Aerospace, Aircraft Group
Warton Division
Warton Aerodrome
Preston
PR4 1AX
England

SUMMARY

The paper describes the flight testing of the Spin Prevention and Incidence Limiting System (SPILS) now fitted to the Tornado aircraft. The trial was carried out in parallel with the conventional stalling and spinning trial and the special aircraft equipment and test procedures were common to both trials for much of the time. The use of telemetry was of particular importance to the conduct of the trial and is considered in some detail. The paper then describes the SPILS flight testing, with and without stores, and describes the reasons for the control law modifications required to "fine tune" the performance of the system. In conclusion, consideration is given to the lessons learned from the flight trial.

1. INTRODUCTION

The potential of "fly-by-wire" flight control systems to modify aircraft handling characteristics is by now well known. This potential extends to the possibility of reducing pilot workload by providing automatic protection from departures and spins. However, the number of aircraft which have been introduced into service equipped with such systems is as yet small. This paper describes the flight development of an automatic spin prevention system for the Tornado which will be the first aircraft in operational service in the U.K., Germany and Italy to be so equipped.

When considering the design of the Tornado Spin Prevention and Incidence Limiting System (SPILS), the following factors had to be taken into account:

a) The aircraft has variable geometry wings and is designed to carry large varieties of external stores, resulting in a very large number of different configurations to be protected.

b) The basic flight control system (called the Command and Stability Augmentation System or CSAS) had been designed to specific stability criteria without reference to the possibility of an extra control loop.

c) The CSAS is a triplex analogue system and thus less flexible to control law changes than digital systems.

d) The addition of automatic spin prevention allows the pilot to demand more from his aircraft and thus designers have to protect the aircraft against unusual combinations of control inputs applied at very high rates.

The SPILS was therefore designed to be an addition to the already proved CSAS. It was a design constraint that the only CSAS modifications allowed would be in the interface and that only existing sensors could be used to provide inputs to the SPILS. The design was primarily carried out in the U.K. However, since MBB in Germany held System Design Responsibility (SDR) for the CSAS they were closely involved in ensuring that the SPILS did not destablise the CSAS.

The SPILS is a duplex analogue computer and functions in two ways (figure 1):

a) Angle of Attack (AoA) is limited by augmenting pitch stiffness. This is achieved by feedback of AoA and pitch rate signals into the pitch axis of the CSAS.

b) Lateral control authority is reduced at high AoA to levels which will not provoke departure.

Note that no restriction of load factor is provided, and no account is taken of the aircraft's configuration, either in terms of wing sweep or store load.

As far as the pilot is concerned, he notices that pitch stick force is increased at high angle of attack, compared with a non-SPILS Tornado, and in most cases full back stick can be reached without departure. Also, numerical AoA limitations on the use of lateral control are removed and full lateral stick and full pedal can be applied at full back stick without endangering the aircraft. Should a system failure be detected, an alarm is sounded and the SPILS is disconnected from the CSAS. A reset can be attempted and, if successful, full SPILS functions are restored.

2. FLIGHT TRIAL OBJECTIVES

The objectives of the flight trial were:

a) To demonstrate that SPILS protected the aircraft against loss of control and define the wider clearance envelope therefore available.

b) To demonstrate the increased manoeuvrability available to a SPILS equipped aircraft, relative to a non-SPILS aircraft obeying its limitations.

c) To demonstrate that the SPILS would not impair control of the aircraft within the SPILS cleared envelope.

d) To demonstrate satisfactory engine, intake, CSAS, airdata and systems performance at the angles of attack achievable with SPILS.

3. TEST VEHICLE

The flight testing of the SPILS was carried out in parallel with the conventional stalling and spinning trial using the second Tornado prototype, PO2. Both of these trials were designated as "high risk" programmes and thus the aircraft was specially equipped for recovery from out-of-control situations. The reason for this classification is obvious when considering the spinning trial but perhaps not so when referring to SPILS. In the latter case, although the SPILS was designed to protect against loss of control, it was considered important, as a matter of philosophy, to anticipate departures from controlled flight - even when not predicted or expected - until the system had been proved by vigorous testing. Only when departure protection had been confirmed would the safety devices be removed so that their aerodynamic effect could be shown to be negligible.

Considering now the particular safety devices fitted, the most noteworthy items were (figure 2):

a) An anti-spin parachute fitted to an external gantry.

b) A hydrazine powered emergency power unit (EPU) and a battery powered electro-hydraulic pump (EHP), providing two levels of back-up hydraulic power in the event of a double flame out.

c) A D.C. fuel pump powered in the event of a double flame out.

d) Special cockpit displays to help the pilot recognise the aircraft's motions and thus determine the correct control inputs for recovery (figure 3).

e) The aircraft was converted to single crew operation for the duration of the trials. The rear cockpit was occupied by parts of the emergency hydraulic equipment.

f) A comprehensive flight test instrumentation fit was installed which could be broadcast via a telemetry link to Warton Airfield for real time monitoring. The most essential parameters were arranged to be powered in the event of a double flame out.

g) The telemetry system also allowed continuous two-way voice contact between the pilot and the ground monitoring station. A "hot-mike" system allowed the pilot to talk without having to operate switches. This facility was additional to the normal radios, used for air traffic control purposes in the normal way.

4. TELEMETRY

The use of the telemetry facility was extremely important to both the SPILS trial and the spinning trial and will therefore be considered in some detail. Although the risk of a developed spin during the SPILS trial was considered low, it could not be ruled out. Hence all of the special facilities developed for the spinning trial were also used when testing the SPILS.

For all stages of SPILS development flying (and, of course, the spinning trial) full, real time telemetry cover was mandatory. Any telemetry system failure required high angle of attack testing to be abandoned until it was repaired.

The telemetry monitoring team was specially trained and comprised engineering specialists in aircraft handling, aircraft systems and engines, plus a safety pilot. The safety pilot was the only member of the telemetry team in radio contact with the aircraft pilot and was usually a qualified Tornado spinning pilot for familiarity with the pilot's workload during testing.

Each monitoring team member was trained according to his individual role using a simulation system connected to the normal telemetry displays. Of particular note is the fact that the safety pilot and senior handling engineer assisting him were trained to recognise spin modes additional to those predicted by the theoretical analysis of the aircraft. This gave maximum confidence that they would not be "taken by surprise" by any unusual aircraft behaviour which might occur.

Parts of the telemetry room were specially configured for the trials, with only the most essential information for aircraft recovery being presented to the safety pilot and handling engineer. Secondary information was monitored by the other team members and instructions were passed to the safety pilot by intercom using pre-defined phrases to avoid confusion.

The philosophy of the telemetry team was to assist the aircraft pilot in recognising the motion of the aircraft, advise him of the correc. recovery controls and also advise him when vital actions were required, for example, when passing critical heights or when an engine shutdown was necessary. The pilot, of course, remained in command of the aircraft at all times.

The use of telemetry in this way was vital to the safety of the trial and also allowed the most efficient use of flight time within the safety constraints.

5. HIGH ANGLE OF ATTACK TEST PROCEDURE

In addition to the retention of the telemetry monitoring techniques developed for the spinning trial, the special aircraft operating procedures used in the spinning trial were retained until the departure protection offered by SPILS had been successfully demonstrated.

In all but the final phase of the SPILS trial, the testing was carried out at 35000 feet (10667m) in a designated spinning area near Warton. The spinning area was selected to be free of air traffic control restrictions and over an unpopulated area. The aircraft was flown in a racetrack pattern allowing an economical climb to reach operating altitude at the spinning point after the descent during the previous manoeuvre (see figure 4).

Critical heights were defined such that the anti-spin parachute would be streamed if the aircraft was out of control at 25000 feet (7620m) and that the aircraft would be abandoned if there were no signs of recovery at 15000 feet (4572m). Thankfully the latter criterion was never approached, but rescue helicopter cover was provided during all test periods.

Strict weather minimum conditions were defined for high angle of attack testing.

Once departure protection had been demonstrated, the anti-spin gantry was removed and the requirement to use the spinning area dropped. As a result, this phase of testing was mostly carried out over the sea. Also testing at lower altitudes was now permitted in order to expand the IAS/load-factor envelope tested.

6. ENGINEERING ASSESSMENT

Before the initial flight clearance could be given, extensive simulation and rig testing were carried out to ensure satisfactory system operation. Also ground resonance tests were made to ensure that the closure of the extra control loop did not have unfortunate consequences for the stability of the aircraft's structural modes.

The first flights with the SPILS fitted were then devoted to an engineering assessment of the system. For this the SPILS was powered and operating, but not connected to the CSAS, during clean aircraft spin testing. The instrumentation was used to calculate the effect that the SPILS would have had, had it been connected, and hence evaluate whether actual departures would have been prevented (see figure 5). Thus confidence was gained that the SPILS was able to protect against departure of the aircraft and was operating as designed.

Additionally, the engineering assessment confirmed that the in-line monitor thresholds had been set correctly to avoid nuisance disconnects. Particularly, it was shown that, should the SPILS not prevent departure during development testing it would disconnect itself automatically due to the disparity between the two angle of attack sensors. It will be appreciated that the spin is a very high angle of attack motion and thus, if the SPILS remained engaged, all lateral control authority would be lost, preventing application of recovery controls. In order to positively prevent this, the pilot was provided with an Instinctive Cut Out (ICO) facility to disconnect the CSAS and SPILS if required, reverting the tailerons to mechanical control but leaving spoilers and rudder under electrical control. However, the results of the engineering assessment showed that in a departure case the SPILS would disconnect automatically and no impedance of the recovery controls would occur.

After satisfactory results had been obtained from the in-flight engineering assessment and ground rig testing, clearance to conduct flight tests with SPILS engaged was given. However, it is worth noting that even after the SPILS engaged testing had begun, the SPILS was monitored during intervening spinning flights, as a continuation of the engineering assessment.

7. TESTING WITH SPILS ENGAGED, MARKS 1 TO 3

The first flights with SPILS engaged were carried out in the clean (no stores) configuration. Simple wind-up-turns and slowdowns to full back stick were made at low speed in each wing sweep to confirm that angle of attack was limited to predicted values. Then, full lateral and directional control inputs were made at full back stick to prove the lateral authority scheduling functions.

Having successfully demonstrated that the SPILS held the aircraft within the departure boundary previously identified, testing proceeded to more vigorous control inputs. These specifically included inputs which had been shown to provoke departure without SPILS and included rapid roll reversals at full back stick, rapid breaks with simultaneous application of pitch and roll stick, deliberate mishandling at full back stick with crossed controls, and rapid pitch inputs (roller coasters). These inputs were significantly more brutal than could be considered for a combat aircraft without departure protection.

The testing demonstrated that the basic philosophy of the SPILS design was sound, efficient AoA limiting and lateral authority scheduling being provided (see figure 5). However, some weaknesses were exposed in the course of testing which required the control laws to be modified in order to "fine tune" the performance of the system. These were insufficient pitch axis stability in response to very rapid snatches, and insufficient departure protection in a few cases in response to gross mishandling of the controls.

As each successive standard of SPILS was introduced, the same basic set of control inputs was repeated, together with particular tests designed to exercise the modifications made and thus demonstrate their efficacy.

Testing of the marks 1 and 2 was confined to the clean (no stores) configuration and was preceded in each case by an engineering assessment as described above. In the case of the mark 3 however, sufficient confidence had been gained to proceed directly to testing with SPILS engaged and gross mishandling of the controls. Also the mark 3 testing saw the first assessment with external stores fitted.

The non-SPILS high angle of attack evaluation of Tornado with stores was based on two "key" configurations from which other configurations could be cleared by analogy. The same philosophy was followed for SPILS but the non-SPILS testing was required to be underway before the SPILS trial commenced.

The configurations evaluated were (see figure 6):

a) A heavy wing configuration with no stores underfuselage (minimum longitudinal stability, aft CG, high roll inertia).

b) A heavy fuselage configuration with no stores underwing (minimum directional stability).

The test manoeuvres followed the pattern established in clean aircraft testing.

The results with the mark 3 standard were extremely encouraging, departure protection being demonstrated in all cases except when rapid inertially coupled inputs were made in the heavy fuselage configuration. However, on the 18th flight with this standard, a large amplitude, undamped pitch oscillation was encountered during the recovery from a test manoeuvre. This resulted in the suspension of testing of the mark 3. Sufficiently good results had been demonstrated, however, for an investigation and redesign to be initiated aimed at overcoming the problem.

8. INVESTIGATION AND REDESIGN

Prior to the flight oscillation which caused the suspension of the trial, the vast majority of the rig and simulation results had been satisfactory from the stability point of view. However, some damped oscillatory behaviour had occurred on the rig in the rate limited regime which had not been fully explained using the available computer models. In the light of this a critical review of the system models was undertaken aimed at identifying the nature of the model behaviour as well as the root of the flight problems and hence identifying the necessary cure. This was undertaken both at MBB and BAe since the combination of CSAS and SPILS had to be understood as well as the SPILS itself.

It was quickly shown that the aerodynamic model was satisfactory by calculating the response to the flight measured control angles. An almost exact match was obtained so attention turned to the modelling of the system itself. Fortunately the comprehensive instrumentation of the test aircraft allowed comparison of computed responses and flight data at various points in the flight control system. This comparison showed that the problem lay in the modelling of the taileron actuator characteristics. Rig tests were then put in hand to measure accurately the actuator's response over a range of frequencies and amplitudes, including those of the flight oscillation. This showed that the gain and phase of the actuator were worse than predicted theoretically, even allowing for rate limiting. Hence with SPILS engaged the system exhibited an unstable mode resulting in a limit cycle.

Increasingly sophisticated computer models, and much original thought, were required by the flight control system designers before satisfactory modelling of the inner and outer loop characteristics of the actuator was finally accomplished. The essential features added to the model were the current limits which give rise not only to rate limiting of the actuator, but also to acceleration limits which reduce the actuator's capability to reverse direction.

Once the cause of the instabilities had been established, a cure was designed. This required the introduction of tailplane position feedback into the pitch rate channel of the SPILS. This effectively provides extra phase advance to the angle of attack signal, warning the system of large aircraft response before it occurs, hence reducing the system input. The new SPILS standard was designated the mark 5 (see figure 7).

Following hardware modification, further intensive rig tests were undertaken including attempts to provoke instability by large amplitude stick pumping, abrupt checks and reversals. These tests having been completed satisfactorily, aircraft resonance checks were carried out, resulting in the introduction of notch filters in the pitch rate loop. After a retest, the clearance to flight test the system was restored.

9. HIGH ALTITUDE TESTING, MARK 5 SPILS

Clearly, the first object of the mark 5 SPILS flight trial was to verify that the pitch axis modifications had been successful. After progressive pitch stick snatching to part and full back stick, an attempt was made to reproduce exactly the manoeuvring which had led to the mark 3 oscillation. Once these tests had been carried out without exciting any instability, further testing included vigorous stick pumping, as well as single direction "snatch" inputs where stick rates over 80 degrees per second were achieved in each direction without inducing any kind of oscillation (see figure 8). Close tracking tasks were also examined, both air-to-air (against a target aircraft) and air-to-ground. It was demonstrated that air-to-air tracking was particularly smooth and easy due to the more precise control of AoA available and the lack of requirement to monitor AoA.

The pitch axis having been proved, testing progessed to demonstration of departure resistance in the same "key" stores configurations as described above. In addition to the manoeuvres already described, a further inertially coupled manoeuvre was introduced. This involved a full stick rapid roll at 1g, followed by a maximum rate pitch stick snatch to full back stick as the bank angle passed through 90 degrees, the roll control being held on (see figure 9). By inducing a rapid AoA increase at maximum sideslip, this provided the most severe test of the SPILS yet devised, but in all cases the aircraft remained fully under control.

Additional testing comprised combat manoeuvring sequences to demonstrate that the more clinical test manoeuvres were adequate to allow clearance of operational manoevring of the aircraft.

The success of the SPILS in protecting the aircraft against departure, while allowing improved manoeuvrability over the non-SPILS aircraft is seen by comparing the achieved SPILS envelope in all test manoeuvres with the departure points established in the non-SPILS testing, and the numerical AoA limits required without SPILS (see figure 10). It is also worth noting that some manoeuvres which are quite safe to fly with the SPILS could not even be considered in an unprotected aircraft - allowing the Tornado pilot extra combat flexibility.

10. LOW ALTITUDE TESTING - MARK 5 SPILS

The final stage of the flight trial required removal of the anti-spin devices and thus could not be attempted until departure protection had been proved. This testing progressed to lower altitudes and higher airspeeds than had been possible hitherto.

This phase posed special clearance problems since it required rapid rolling at angles of attack above those normally cleared, and at airspeeds higher than had been achieved previously at high AoA. Effectively, the flight envelope was to be extended in several directions at once (see figure 11).

The solution to the problem of clearance to test was the production of acceptable loads boundaries in terms of handling parameters which could be measured - for example, AoA, sideslip, control surface angles, IAS (figure 12). Provided the parameters remained within the defined boundaries, the loads must have been satisfactory.

Prediction of aircraft responses to representative control inputs was then carried out using at 6 degree-of-freedom computer model. The responses were monitored against the loads boundaries, giving confidence that the manoeuvres could be attempted in flight without endangering the aircraft.

It was then arranged to monitor the most critical boundaries in real time in telemetry using specially installed displays. Hence if it was surpected that the aircraft had been overstressed, testing could be aborted immediately and the aircraft returned to base for inspection. In the event, no inspections were ever required.

In flight, some check manoeuvres were first carried out at high altitude to verify that the anti-spin gantry had not materially affected previous results. Then a progressive work down to low altitude was carried out. This followed the pattern established during previous phases although the pilot's workload was now increased by the requirement to monitor load factor.

Since departure protection had now been established, additional stores configurations were introduced in this phase. These were more representative of those seen operationally and ranged from a light air-to-air combat configuration to a heavy ground attack configuration, including eight 1000lb (454 kg) bombs. Departure free handling was demonstrated in all cases.

11. CONCLUSIONS

The major lesson of the SPILS development trial is that, while flight testing is essential, its risks and expense can be minimised by demanding complete understanding of the design and rig test results beforehand. This requires a clear understanding of the total flight control system design and the implications of hardware characteristics.

Designers must also be aware that pilots will, quite rightly, take full advantage of any capability increase offered. Thus, systems such as SPILS must be designed with extreme inputs in mind and must be tested to the limits of their capability before being released to Service.

The final lesson is that when a high risk trial is undertaken, the targets of testing aircraft and systems to their limits, while minimising the risks to aircrew and aircraft, can only be achieved by taking special care with test procedures and monitoring. Proper consideration must be given to the best use of the telemetry facilities available and extensive training must be given to aircrew and groundcrew. It is worth noting that the Tornado SPILS and spinning trials were carried out over a period of 3 years, requiring 75 SPILS and 100 non-SPILS flights. During that time the required data was gathered without any damage to the aircraft.

The successful conclusion of this difficult flight trial means that the Royal Air Force is now receiving its first aircraft type with automatic spin protection, and aircraft for the German and Italian Air Forces will soon follow.

FIGURE 1 SPILS FUNCTIONS

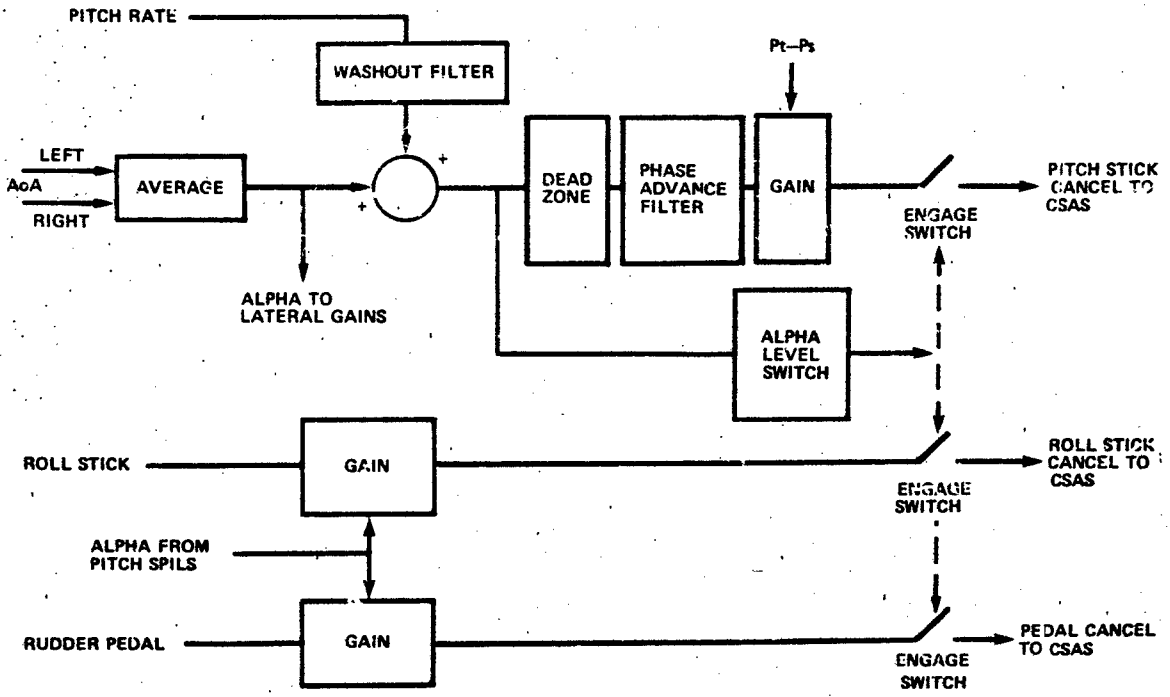

FIGURE 2 SAFETY DEVICES

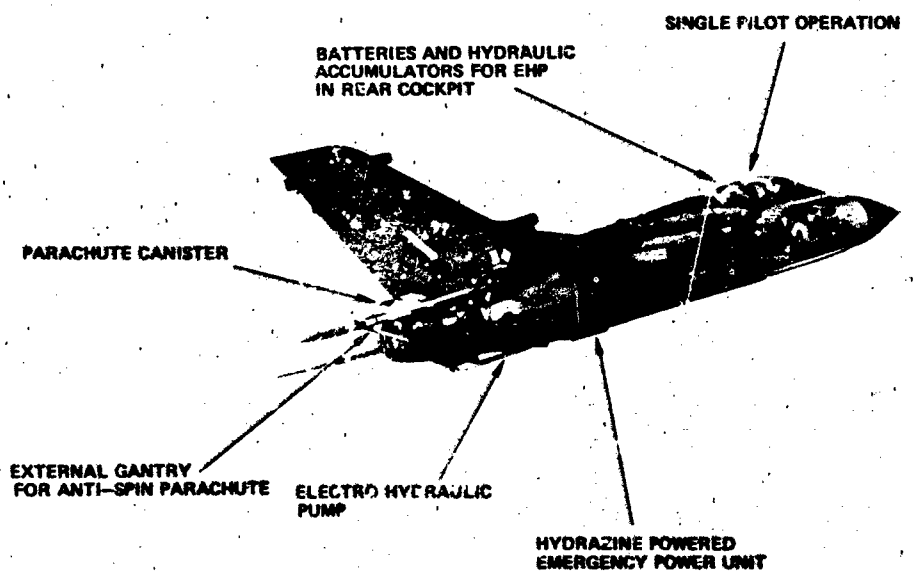

FIGURE 3 SPECIAL COCKPIT DISPLAYS FOR HIGH AoA TESTING

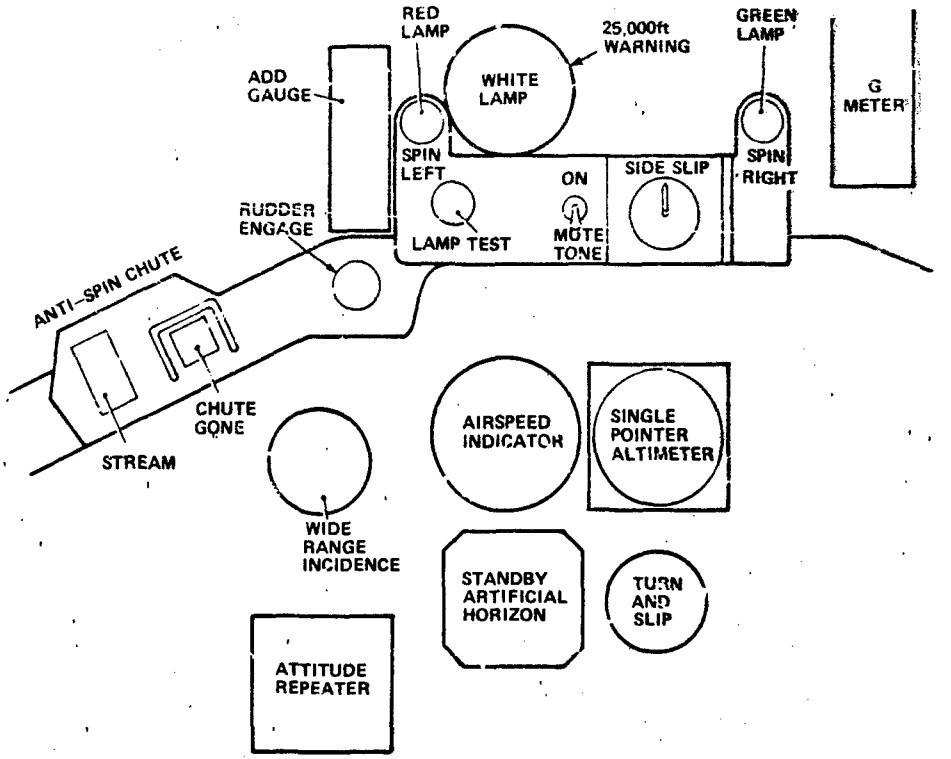

FIGURE 4 SPINNING PATTERN

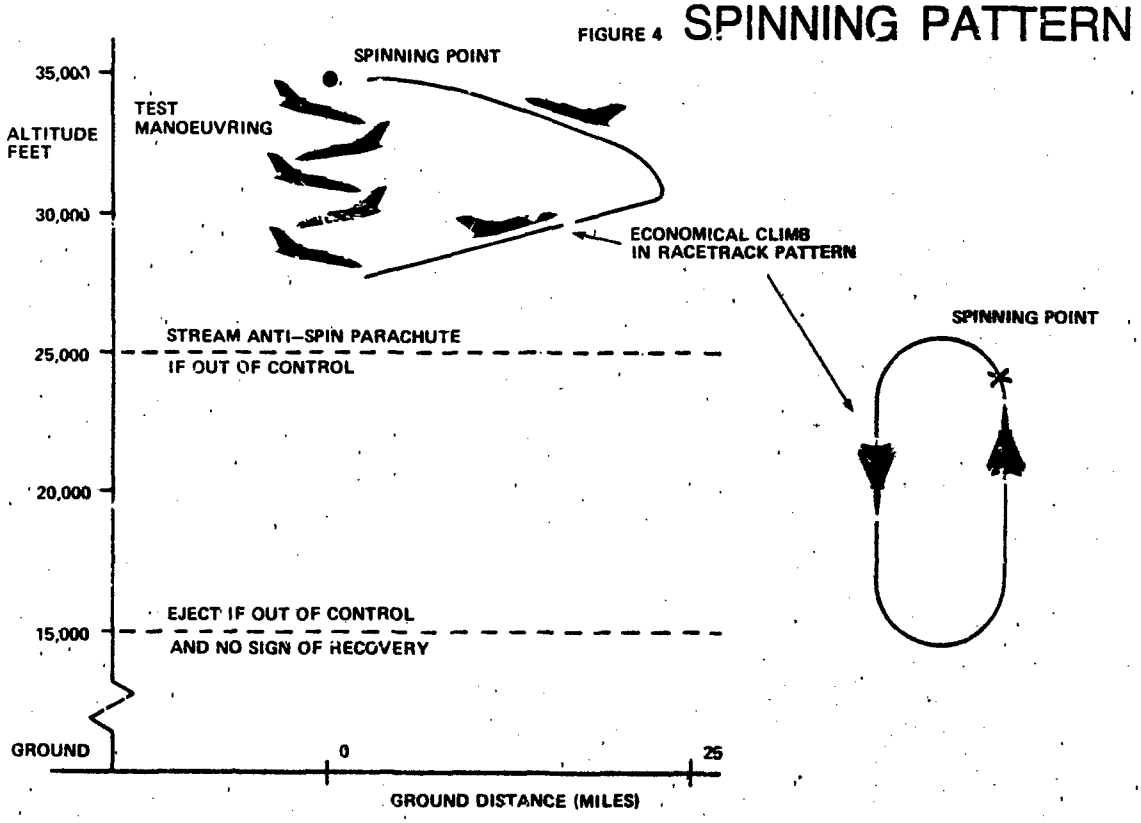

FIGURE 5 ENGINEERING ASSESSMENT

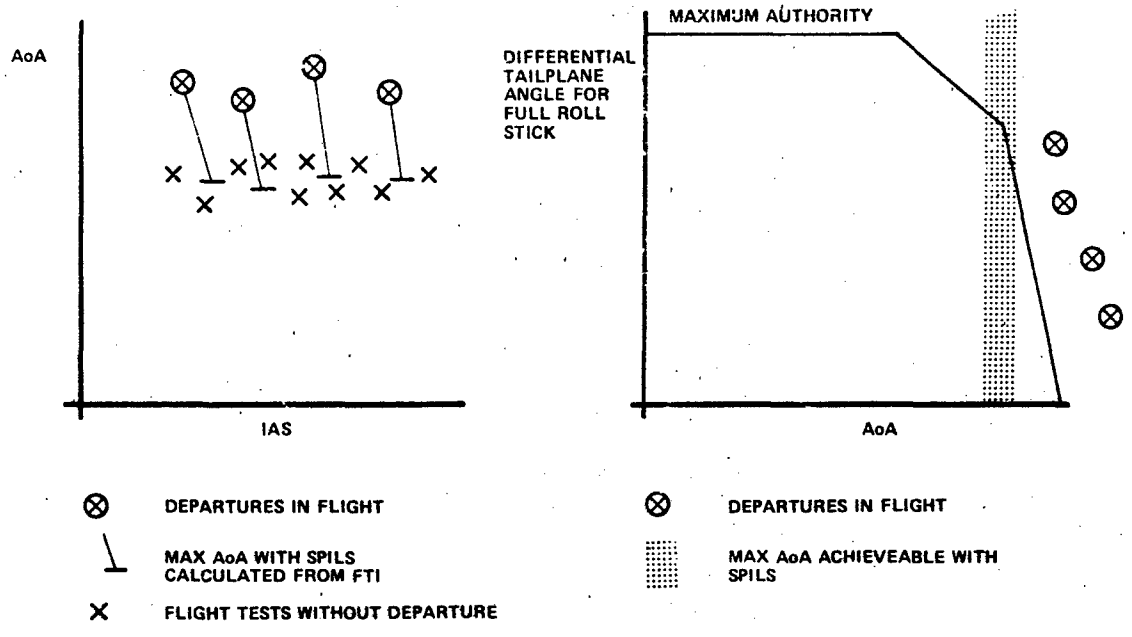

FIGURE 6 KEY STORES CONFIGURATIONS

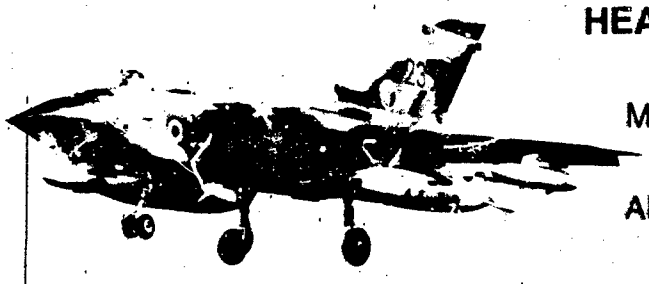

HEAVY WING CONFIGURATION

MINIMUM LONGITUDINAL STABILITY

AFT CG

HIGH ROLL INERTIA

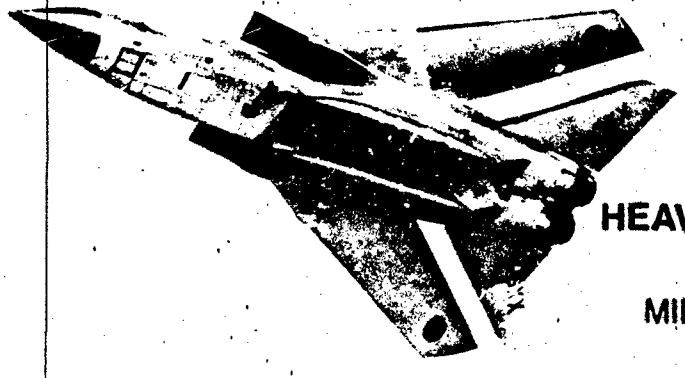

HEAVY FUSELAGE CONFIGURATION

MINIMUM DIRECTIONAL STABILITY

FIGURE 7 MARK 5 SPILS

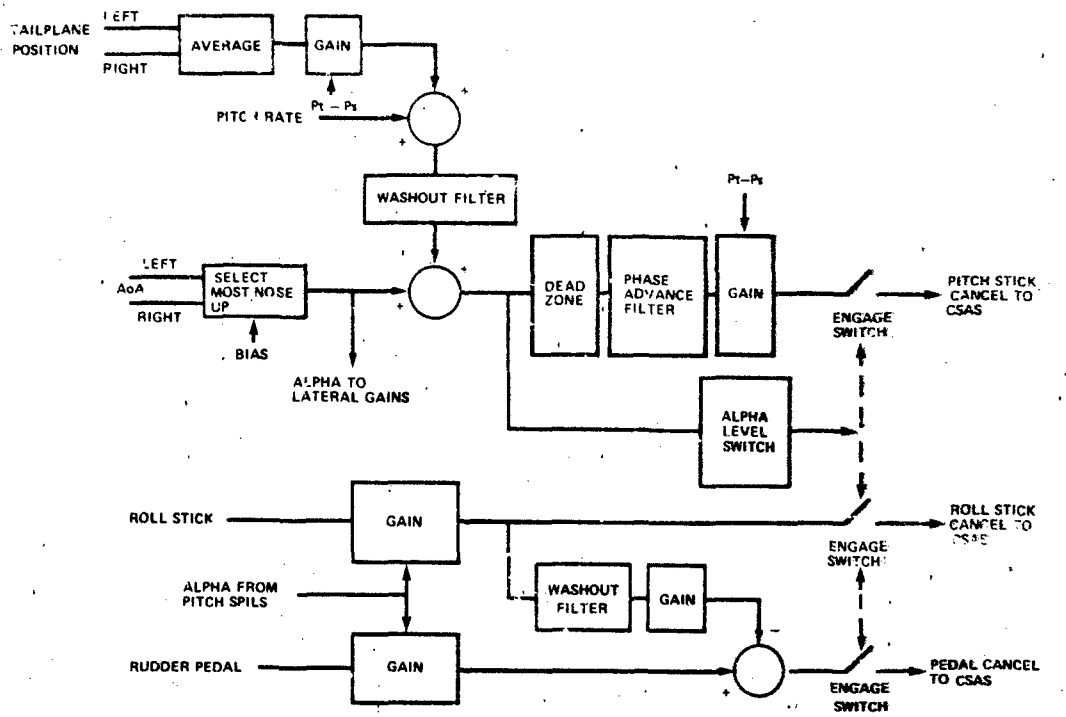

FIGURE 8 LEVEL BREAK MANOEUVRE WITH STICK PUMPING IN A DIVE

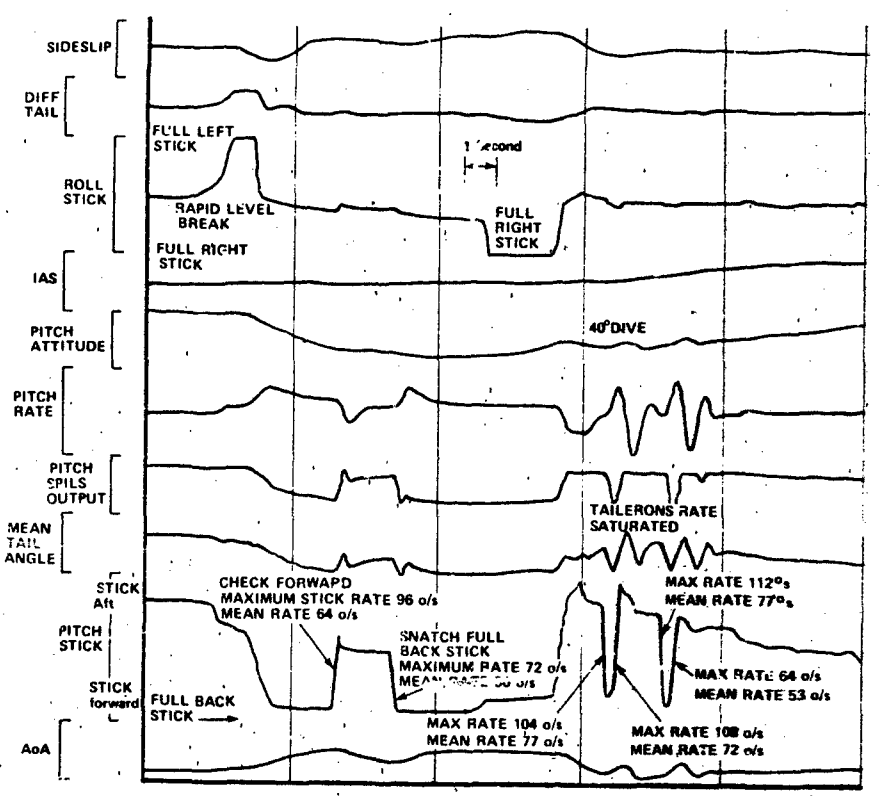

FIGURE 9 INERTIALLY COUPLED MANOEUVRE

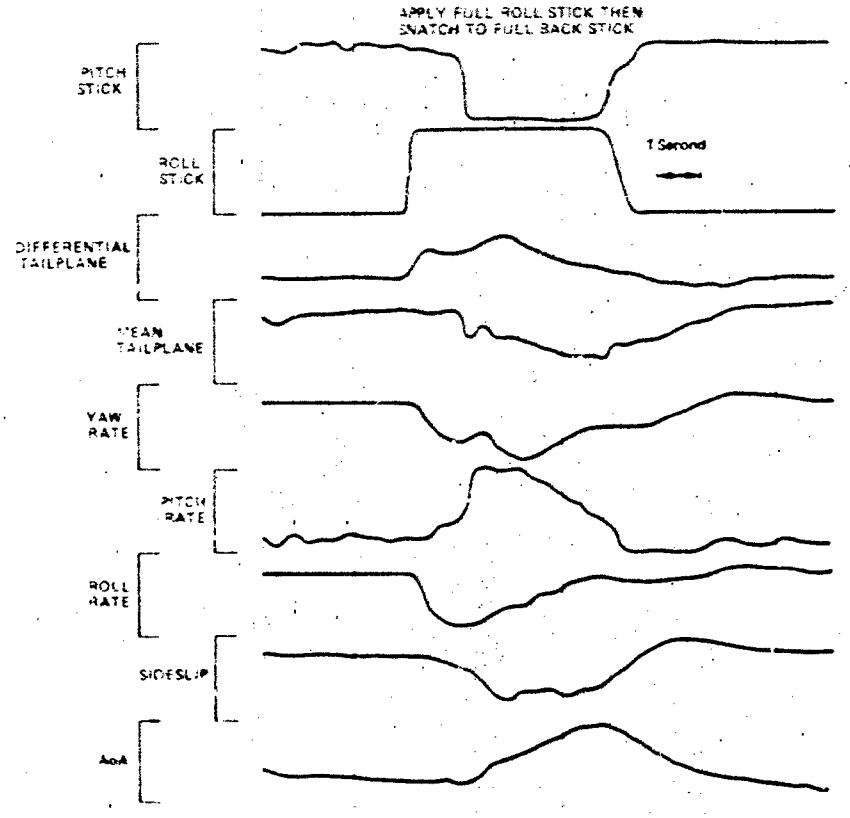

FIGURE 10 SPILS PROTECTION

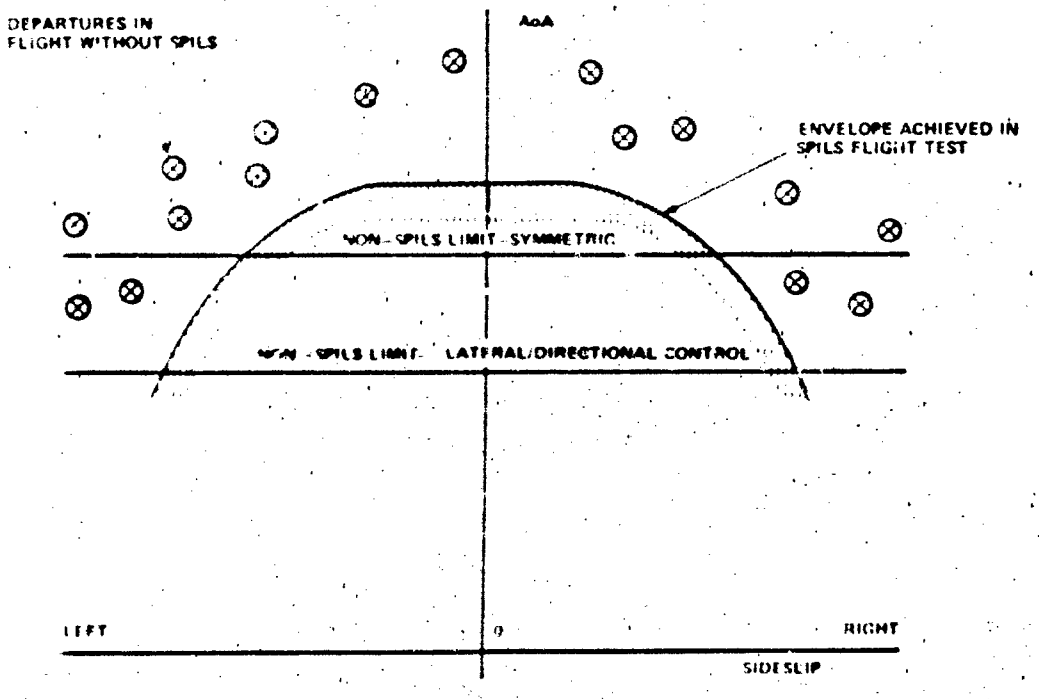

FIGURE 11 ENVELOPE EXPANSION

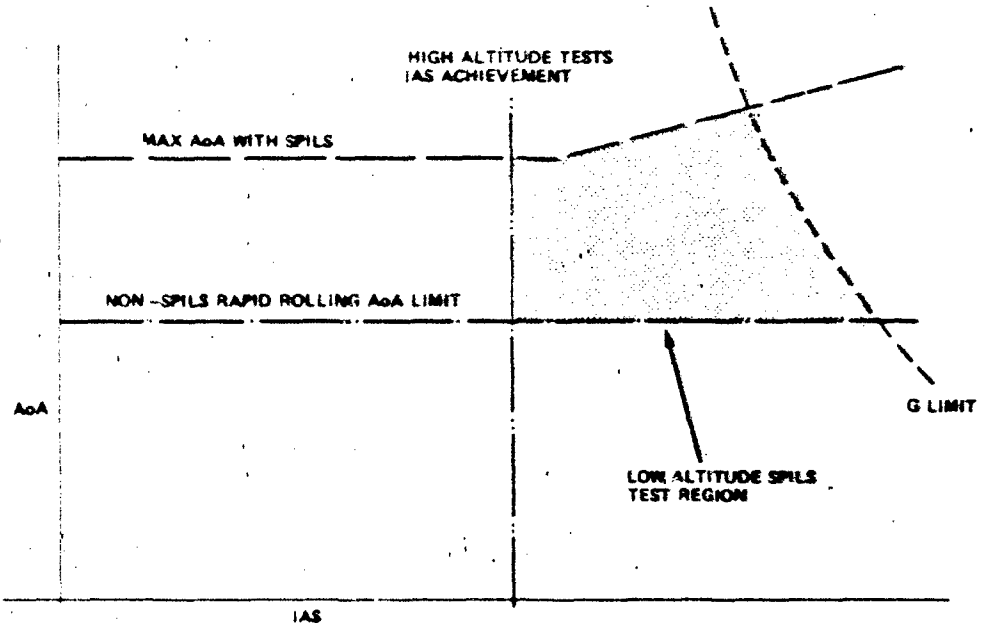

FIGURE 12 EXAMPLE LOADS BOUNDARIES

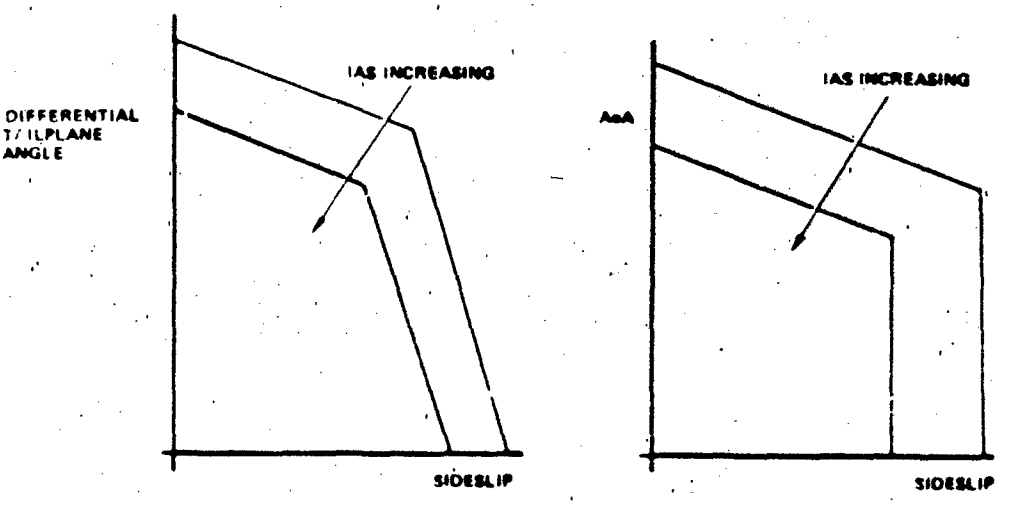

HIGH ANGLE OF ATTACK TEST AND EVALUATION TECHNIQUES FOR THE 1980s

Gerald L. Jones
Flight Test Engineering Supervisor
6520th Test Group
AFFTC, Edwards AFB, CA 93523

ABSTRACT

The implementation of USAF Stall/Post-stall/Spin Flight Test Demonstration Specification, MIL-S-83691, in the early 1970 s, introduced major changes to the techniques used at the AFFTC in test and evaluation of maneuvering-type military aircraft near stall/departure angles of attack. The basic objectives of each high AOA flight test program since that time have been the determination of departure characteristics and the development of methods for departure prevention and spin avoidance. Along with the emphasis on departure prevention came an increased attention to flight dynamic prediction methods and an increased utilization of open-loop and pilot-in-the-loop simulations which are continually updated to stay abreast of the flight test program and to assist in flight planning. The highly nonlinear and complex nature of aircraft dynamic behavior at high angles of attack coupled with poorly understood aerodynamics has made this task difficult at best. One additional factor that aggravates the problem of correlating flight test results with wind tunnel and simulator predictions is that airspeed, angle of attack and angle of sideslip, measured onboard the flight test aircraft by means of noseboom pitot-static and vane sensors, yield erroneous and misleading information at high angle-of-attack. State-of-the-art inertial navigation systems, however, have recently provided a tool to accurately determine these parameter values and to do a considerably better job of correlating flight test results with predictions and thus allow improved estimates of aircraft dynamic characteristics at more adverse flight conditions. Even though more sophisticated prediction and analysis methods are being continually sought, the development flight test program and especially the test pilot continue to be the key elements in synthesizing the final aircraft/flight control system configuration with optimized operating procedures to get the best performance from the man-machine system under combat conditions. Today's properly structured development flight test program follows a safe and efficient buildup approach with concurrent simulation efforts to assist in flight planning. It has built-in flexibility to allow pursuit of an alternate course of action from that which was originally planned if flight test and simulation results indicate the need. It also includes operational-type maneuvers to provide the test pilot with an insight as to how the aircraft will perform the operational task. This paper will take a brief look at the principles that guided the development of MIL-S-83691 and at how recent flight test experiences at the AFFTC have modified and expanded upon those ideas over the past decade.

INTRODUCTION

In the thirteen-year period since the publication of MIL-S-83691 on 31 March 1971, the United States Air Force has conducted approximately sixteen high angle-of-attack (AOA) flight test programs on four different series of fighter-attack aircraft at the Air Force Flight Test Center (AFFTC), Edwards Air Force Base, California. The basic objectives of each one of those programs have emphasized the determination of departure characteristics and the development of methods for departure prevention and spin avoidance. The physical nature of these methods took many forms:

A. Limiters designed into the aircraft flight control system to automatically prevent the pilot from maneuvering the aircraft into a departure/spin susceptible region of the flight envelope.

B. Modifications to the flight control system to automatically apply to the proper controls to recover the aircraft from an out-of-control condition.

C. Aerodynamic modifications to the aircraft to prevent departure in an otherwise useable portion of the flight envelope.

D. Aerodynamic modifications to the aircraft to improve its out-of-control characteristics and to facilitate a more rapid return to controlled flight.

E. Development of flight manual limitations and out-of-control recovery procedures that reduce the probability that an unrecoverable departure and spin will be encountered.

At about the same period of time that MIL-S-83691 was being written and published, the United States Air Force was entering into a new era of weapon system development and test policy. This policy, directed by Air Force Regulation 80-14, specified that all military development test programs would be jointly conducted. The joint test approach was not unique to high AOA testing, but, it did provide the necessary impetus for the implementation and application of the principles of MIL-S-83691. With the AFFTC as the responsible test organization and with the using command and the airframe and engine contractors as participants, Air Force personnel became deeply involved in the initial test planning efforts of, (1) defining the engineering parameters to be measured

and the instrumentation hardware to be used, (2) writing the detailed test plan that defined the test maneuvers, and (3) developing the data processing and analysis methods that were to be used to report the test results and convey the proper message to the operational pilots. The joint test team concept served to minimize duplication of effort while assuring that the contractor collected sufficient data to demonstrate specification compliance and the Air Force retained an operational perspective on the test results. Air Force involvement also assured that corporate knowledge was being passed on from one test program to the next to avoid rediscovering old mistakes.

TEST PLANNING

The USAF demonstration specification MIL-S-83691 is demanding in its objectives; there is a desire to determine all warning, recognition, and recovery characteristics of real and apparent out-of-control situations and make recommendations most beneficial to the user. The specification is designed to be a guide for planning a stall/post-stall spin test program and there is sufficient flexibility in the four test phases to achieve these goals through logical test progression. In test phase A, recovery is initiated as soon as the pilot has a positive indication of a stall (per the MIL-F-8785C definition of stall). In test phase B, an attempt is made to aggravate the stall by misapplying control inputs immediately upon recognition of the stall. In test phase C, the effects of delays in applying proper recovery controls as well as improper control inputs are tested. If no out-of-control motions have occurred by this time, test phase D is included to provide for attempts to force the aircraft into an out-of-control condition.

It is neither feasible nor desireable to plan a flight test program to demonstrate every possible airplane/flight control system configuration (including failure cases) at every set of entry conditions with all possible combinations and permutations of control inputs, etc. It is rather the task of the flight test engineer to define and test those conditions that are most likely to exhibit the entire spectrum of modes and motions that the aircraft may encounter during its operational use. The intelligence with which to make these initial decisions must, by necessity, come from predictive studies performed using the results of static wind tunnel tests, rotary balance tests, free-flight model tests, spin tunnel tests, and finally simulations. It cannot be overemphasized, however, that extreme caution must be exercised in interpreting the results of these studies. Predictive studies of one particular kind cannot be analyzed independently from the results of the others and must be cross-checked repeatedly. Conversely, the results of one study should never be completely discounted because it did not agree with the results of the other studies. Each predictive study is of value only in proportion to its contribution to meeting a development or test objective and must be weighted according to the assumptions and limitations of the study in order to size and direct the flight test plan. There have been instances where flight test results were precisely opposite to the prediction, not because the predictive method was invalid, but, because it did not follow ground rules used in performing the flight tests or in analysing their results.

When writing the high AOA test plan, deliberations as to the order of test points, the types of recovery techniques to be evaluated, and the hazard factors believed to be characteristic to the particular airplane probably receives the most attention. Flight test personnel do not necessarily have an easy time projecting dynamic behavior and recovery capability of the full-scale airplane from the predictive studies, however. This can be an uncomfortable situation since a degree of precision is needed when allocating time, manpower, physical resources, and funds to a flight test program. Consequently, the test plan should be as flexible as possible, incorporating decision points where the program could change in scope and direction pending initial results.

The first three test phases of MIL-S-83691 do not require any given mode of aircraft motion after the entry conditions are achieved; rather these are phases of discovering what the airplane does under increasingly adverse flight conditions. A number of flight test experiences have verified that post-stall motions do not always conform to preflight desires or expectations, resulting in delayed or improperly applied recovery controls being applied by the pilot. The hazards of these possibilities can be minimized by adequate pre-test planning with the aid of pilot-in-the-loop simulation. Here again, it is essential that the limitations and assumptions of the simulation are clearly understood before a level of confidence can be established for the results. It is at this point where the test pilots who are acutally going to fly the test aircraft come into the picture. Their operational experience is invaluable in determining which test maneuvers and which subsequent recovery procedures should be carried into the flight test program. Out of these tests will also come the initial trend charts summarizing the simulator results of the recommended flight test maneuvers and which will eventually be used in following the progress of and directing the flight tests.

The high AOA flight test vehicle is an expensive, one-of-a-kind item for a once-only (hopefully) test program. With special cockpit displays and full flying qualities and propulsion system data recording and telemetry, and onboard film or video cameras, it is evident that these test modifications must be done carefully so that their effect on aircraft flight characteristics are minimal. With some aircraft test installations, these effects may be difficult to predict (e.g., test noseboom and spin recovery chute installations), so, provisions for doing wind tunnel tests and/or flight tests with and without these items installed may be necessary. Photographic documentation of the high AOA flight tests is extremely important. The onboard and ground-based cameras that serve to document aircraft motion are operated at a true-time frame rate allowing

production of briefing and training films from the test documentary collection with minimal effort and loss of quality. A cockpit camera with an over-the-shoulder field of view provides a pilots-eye view of the aircraft motions.

The flight test plan is a key document which describes in detail the testing that is to be done and directly impacts mission accomplishment, program objectives, safety and expenditure of resources. Any agency conducting tests at the AFFTC utilizing AFFTC resources must have a test plan approved by the AFFTC Commander before testing can begin.

A thorough technical review of each test plan or major revision to an existing test plan is required by AFFTC Regulation 80-1 to insure adequate planning and preparation. If appropriate, a technical review board, set up by the office of primary responsibility for the test, will conduct the technical review. The project manager, engineering, and test operations personnel responsible for conducting and supporting the test program participate in the review. The test force director or project manager is responsible for ensuring that the test plan is prepared and submitted for review in time to meet program requirements. The technical review board, through discussions with the individuals who prepared the plan, evaluates the requirement for the test, addresses the test objectives, ensures that the overall approach relates to the objectives, evaluates the technical adequacy of the plan and verifies that the objectives can be met effectively with acceptable risks and minimum expenditure of resources. Individuals assigned to the technical review board are chosen on the basis of their expertise. This expertise should be broad enough to critically review all aspects of the planned tests.

A safety review of all tests requiring the use of AFFTC resources is also required, and is covered by AFFTC Regulation 127-3. The purpose of the safety review is to: (1) identify hazards generated by each test and ensure adequate action is taken to eliminate or control these hazards to an acceptable level of risk; (2) ensure a thorough and impartial review of the safety aspects of test activities which involve AFFTC personnel, aircraft, ranges, or airspace; and (3) advise the AFFTC Commander and other responsible supervisors and agencies of the degree of risk that the planned testing will present. Safety review board members are normally selected from supervisory positions within test operations and engineering agencies having project responsibilities. They should have project familiarity, but, without sufficient project involvement to present a personal conflict of interest. During the safety review meeting, the designated project personnel present the test plan objectives, proposed tests, and test methods to the safety review board. The safety review board establishes any open items that must be resolved before testing can begin, identifies additional procedures to enhance test safety, and assigns risk levels to the tests. Following the safety review, the test plan, minutes of the technical review meeting, minutes of the safety review meeting, and a final operational hazard analysis are prepared and briefed to the AFFTC Commander for his approval.

TEST CONDUCT

Stall/spin training for the test pilots involved is the test agencies first active flying step in the conduct of the actual high AOA flight test program itself. While it is desirable to select a training aircraft for its similarity in control applications and sequence to those predicted for the test aircraft, the primary purpose of the training is to subject the pilots to the out-of-control or spinning environment in as many types of aircraft as possible. This variety of experience enhances the pilots ability to cope with any situation which could arise while testing an aircraft with undefined out-of-control characteristics. When possible, however, the training is concluded with the aircraft which has recovery techniques most similar to those predicted for the test aircraft. Obviously, each pilot uses this valuable training time to increase his proficiency in observing departure and spin motions as well as in manipulating the aircraft controls in the correct sequence. Also, he reevaluates his procedures and preferences for tightness of pilot restraints, for seat and rudder pedal adjustment, and relates each one of these to what will be required in the test aircraft. While performing this training, the test pilot also considers his requirement for a command-and-response checklist to be used in the test aircraft. The items to be listed are considered very carefully and limited to those which are essential steps to be accomplished before and after each maneuver. Items that go on this checklist include such things as emergency systems checks and test data management actions.

Several test aircraft flights are initially required to qualify systems unique to the high AOA flight testing. Antispin chute system qualification is always done on the test aircraft after installation. Static deployments are done on the ramp initially to check the functional operation of the sytem followed usually by a low speed deployment during a taxi test at approximately 100 knots on the runway. Finally, at least one in-flight deployment is accomplished near the maximum dynamic pressure condition for the chute to check the system deployment and release characteristics under actual flight conditions. Recovery of the test aircraft using emergency backup systems are also done when practical to determine any in-flight operating restrictions and allow development of emergency recovery patterns and procedures. Training for engine-flameout landings is also accomplished in the test aircraft at this time. This flameout landing practice is initiated from locations, altitudes, and airspeeds which are representative of the worst conditions which could be encountered during the actual high AOA tests.

These flights also present an opportunity to link together all of the support required to conduct the high AOA test flights and to provide familiarization for the test pilots, ground support personnel, and chase crews if applicable, on what will be expected of them. The test pilot is able to work out procedures to be followed in setting up and performing the test maneuvers. Actual data cards are checked for completeness, simplicity and accuracy. Flying actual mission profiles determine pilot workload. The controllers in the ground tracking stations are able to practice positioning the test aircraft in the proper airspace. Different headings into the spin area are tried to determin the best telemetry reception and sun angle for ground and airborne chase photographers as applicable. The duties and responisbilities of mission control room personnel in monitoring the test proceedings are also worked out during these flights. Key personnel develop procedures and select their operating locations so that they will have the proper real time data available to assist the test pilot in the conduct of the tests and provide aid in making stop-or-continue decisions.

During the conduct of each of the sixteen high AOA test programs at the AFFTC, the test maneuvers performed on those aircraft that employed the conventional stick and rudder pedal controls, were very similar. They were performed in order of severity beginning with very benign maneuvers designed to gather quantitative stability and control data and progressed to more aggressive maneuvers which employed large and sustained control inputs, both coordinated and aggravated. Finally, operational-type maneuvers were performed that incorporated one or more of the previous manuevers into a tactical scenario to evaluate the operational significance of the demonstrated characteristics. These maneuvers aided in the establishment of any flight manual restrictions that might be necessary and in developing unusual attitude recovery procedures. A list of representative test maneuvers are, in order:

A. One-g deceleration to maximum AOA. Maximum AOA is defined as the maximum for controlled flight or the maximum permitted by the flight control system.

B. Pitch, yaw, and roll doublets performed at one-g in even increments of AOA up to maximum.

C. Wings level sideslips performed slowly to full rudder deflection or loss of control at one-g in even increments of AOA up to maximum.

D. Windup turn performed by slowly increasing g to maximum AOA at constant Mach.

E. Pitch, yaw, and roll doublets performed at even increments of AOA up to maximum at constant Mach and elevated-g.

F. Constant-bank sideslip performed slowly to full rudder deflection out of the turn or to loss of control at even increments of AOA up to maximum at constant Mach and elevated-g.

G. Constant-g decelerating turn to maximum AOA in a level turn at 2 or 3 g-levels to maximum g.

H. Roll briskly to 90 degrees bank followed by abrupt full aft stick application to achieve maximum AOA.

I. 360-degree rolls at one-g in even increments of AOA up to maximum.

J. 360-degree or 180-degree rolls at elevated-g in even increments of AOA up to maximum at constant Mach.

K. Elevated pitch-attitude decelerations to maximum attainable AOA at 2 or 3 pitch attitudes up to 90 degrees.

L. Negative-g (180 degrees bank) deceleration to maximum negative AOA.

M. Aggravated single- and multiple-control inputs at maximum AOA for up to 15 seconds duration (Phase D, MIL-S-83691).

N. Tactical maneuvers/unusual attitude recoveries.

TYPICAL TEST RESULTS

As previously stated, trend charts, summarizing the results of simulator predictions and supplemented with the results of flight tests as each manuever is flown, play a critically important role in guiding the progress of today's high AOA flight test program. MIL-S-83691 defines departure as "the event in the post-stall flight regime which precipitates entry into a post-stall gyration, spin, or deep-stall condition. The departure may be characterized by divergent, large-amplitude, uncommanded aircraft motions such as a nose-slice or pitch-up. Departure is synonomous with complete loss of control." The degree of susceptibility of a modern, highly-maneuverable, fighter aircraft to departure and spins depends on its roll-coupling characteristics more than any other single factor. The following equations are useful for explanation of high AOA roll coupling characteristics:

$$\dot{q} = pr(I_z - I_x)/I_y + (r^2 - p^2)I_{xz}/I_y + (\dot{p} + qr)I_{xy}/I_y + (\dot{r} - pq)I_{yz}/I_y - r\Omega_e I_e/I_y + M_{aero}/I_y \qquad (1)$$

$$\dot{r} = pq(I_x - I_y)/I_z + (\dot{p} - qr)I_{xz}/I_z + (p^2 - q^2)I_{xy}/I_z + (\dot{q} - pr)I_{yz}/I_z + q\Omega_e I/I_z + N_{aero}/I_z \quad (2)$$

$$\dot{\alpha} = q - (\dot{V}/V)\tan\alpha - (p - \dot{\beta}\sin\alpha)\tan\beta/\cos\alpha + (\cos\theta\cos\phi - N_{aero}/W)g/V\cos\alpha\cos\beta \quad (3)$$

$$\dot{\beta} = p\sin\alpha - r\cos\alpha - (\dot{V}/V)\tan\beta + (\cos\theta\sin\phi + Y_{aero}/W)g/V\cos\beta \quad (4)$$

Of primary importance during high AOA rolling maneuvers, from a departure susceptibility standpoint, is inertial coupling and kinematic coupling into the pitch or yaw axis. The primary inertial coupling term in the pitch axis is $pr(I_z - I_x)/I_y$ of equation (1) referred to here as the inertial pitch acceleration. All other inertial terms of equation (1) are insignificant for a symmetrically loaded aircraft because of extremely small products of inertia and engine rotating inertia. A coordinated roll in either direction causes a nose-up contribution to pitch acceleration with a body-loaded mass distribution, and must be counteracted with an aerodynamic moment. Similarly, the primary inertial coupling term in the yaw axis is $pq(I_x - I_y)/I_z$ of equation (2) referred to here as the inertial yaw acceleration. Again, all other inertial terms of equation (2) are insignificant for a symmetrically loaded aircraft. The inertial yaw acceleration term causes a moment opposite to the direction of roll and results in an adverse sideslip contribution. In kinematic coupling, the $-(p - \dot{\beta}\sin\alpha)\tan\beta/\cos\alpha$ term of equation (3) results in a positive $\dot{\alpha}$ contribution when rolling with proverse sideslip and a negative contribution when rolling with adverse sideslip. Therefore, sideslip angle directly affects longitudinal characteristics during rolling maneuvers. Equation (4) shows that the primary kinematic coupling term is $p\sin\alpha - r\cos\alpha$. The $\dot{\beta}$ kinematic coupling characteristics result primarily from a balance between roll rate and yaw rate.

Figures 1 and 2 show typical trend charts that have been developed to summarize the characteristics of an aircraft that had a tendency to depart longitudinally during rolling maneuvers both at one-g and at elevated-g. Roll-coupled departure trends could be plotted from simulator tests and compared with flight test results as the maneuvers were being flown to predict, with reasonable certainty, when a departure was likely to occur. As the flight tests progressed from rolls at benign conditions to the more adverse conditions in a buildup fashion, trends were usually very evident. The plotted flight test data in figure 1 show that rolls initiated at increasing trim angles of attack produced, in this case, a relatively constant nose-down stabilator increment and angle of attack overshoot from trim conditions up until control surface saturation occurred. Beyond that point, angle of attack overshoots began to increase because of the unbalanced inertial pitching moment. The simulator results, though not plotted, showed the same trends. In figure 1, it should also be pointed out, three maneuvers were flown where full rudder deflection was applied in the direction of the roll. This was not an advisable thing to do, as it turned out, because the increased proverse sideslip and increased yaw rate produced by the rudder inputs aggravated the roll coupling and resulted in stabilator saturation at a lower angle of attack and increased angle of attack overshoots. It is also interesting to point out that no improvement in roll rate was achieved by the application of rudder. Figure 2 shows trends with rolls initiated at full aft stick and increasing trim airspeed conditions. The worst condition in this case was at approximately 250 knots indicated airspeed and was less severe above and below that. The same adverse trends are evident with the application of rudder during a roll at the worst case conditions. The fact that the worst case condition would be at the 250-knot point was predicted by the simulator and was due to the flight control system design.

The inertial effect of wing-mounted stores resulted in a degradation of roll-coupled departure resistance for the aircraft mentioned above. Inertial pitch acceleration was not increased since the inertia ratio $(I_z - I_x)/I_y$ of equation (1) was essentially unchanged with the addition of wing-mounted stores and the maximum roll rates were decreased over those with no wing-mounted stores. Kinematic coupling, however, was significantly affected. Wing-mounted stores increased the roll inertia more than the yaw inertia; therefore, roll acceleration was reduced proportionally more than the yaw acceleration. The resulting change in the balance between roll rate and yaw rate resulted in less adverse (or even proverse) sideslip buildup per the $p\sin\alpha - r\cos\alpha$ term of equation (4). Also contributing to the tendency toward less adverse sideslip was a decrease in the inertial yaw acceleration due to a significant decrease in the inertia ratio $(I_x - I_y)/I_z$ of equation (2). This reduced adverse (or more proverse) sideslip characteristic of loadings with wing-mounted stores resulted in the kinematic coupling term $-(p - \dot{\beta}\sin\alpha)\tan\beta/\cos\alpha$ being less negative (or even positive). Therefore, the effect of wing-mounted stores was an increased tendency for angle of attack to overshoot during rolling maneuvers and thus a requirement for more nose-down aerodynamic moment to maintain angle of attack within satisfactory bounds.

Asymmetric store loadings also reduced the aircraft's resistance to roll-coupled departure, especially for rolls performed in the direction away from the heavy wing. The decrease in roll-coupled departure resistance was due primarily to kinematic coupling effects. Trim requirements to balance asymmetries in roll and yaw resulted in a sideslip angle with the heavy wing into the wind. Rolls performed away from the heavy wing, therefore, were initiated with a preestablished proverse sideslip angle, while rolls into the heavy wing had a preestablished adverse sideslip angle. The $\dot{\beta}$ kinematic

coupling term was less negative (or more positive) for rolls away from the heavy wing and more negative for rolls into the heavy wing when compared with symmetric loadings. Therefore, rolls away from the heavy wing were more critical due to kinematic coupling. Even without the aircraft being trimmed with the preestablished sideslip mentioned above, the tendency toward less adverse (or more proverse) sideslip during rolls away from the heavy wing would still occur. The inertial yawing moment due to the product of inertia terms $(p^2-q^2)I_{xy}/I_z$ and $(q-pr)I_{yz}/I_z$ become significant and produce increased yaw acceleration in the direction away from the heavy wing.

Additional roll coupling effects were evident when abrupt longitudinal inputs were applied during rolling maneuvers. Abrupt aft stick inputs increased positive pitch rate which then coupled with roll rate to produce an increase in inertial yaw acceleration opposite to the direction of roll. Yaw rate, therefore, was increased and sideslip increased adversely per equations (2) and (4). Likewise, abrupt forward stick inputs decreased the amount of positive pitch rate during a roll and thus resulted in a decrease in adverse (or increased proverse) sideslip. A small to moderate inadvertent longitudinal input during maximum command rolling maneuvers did not normally produce any significant adverse effects on rolling characteristics. There was, however, some increase in adverse sideslip and reduced roll response for aft stick inputs and some decrease in adverse sideslip and increased roll response for forward stick inputs. Abrupt full aft stick inputs during rolls, however, often resulted in divergences both in sideslip and in angle of attack. The sideslip divergence was due to inertial yaw coupling from the $pq(I_x-I_y)/I_z$ term of equation (2), while the angle of attack divergence was due to the aircraft nose-up command (full aft stick) in combination with the inertial pitch acceleration generated by the roll. Abrupt full aft stick inputs produced the most adverse characteristics when they were applied after 180 degrees of roll during maximum command, one-g, 360-degree rolls. During roll/pull maneuvers at low to medium angles of attack, sideslip and angle of attack overshoots were often excessive. Roll/pull maneuvers initiated at higher angle of attack generally did not result in departures because very large pitch and roll rates could not be developed.

The autoroll, named for its autorotative rolling characteristics, was an out-of-control mode exhibited by one aircraft at moderate angles of attack. The autoroll could not be terminated by neutral controls. The roll was sustained through dihedral effect by a proverse sideslip angle and angle of attack was sustained by the roll and yaw rates through inertial pitch coupling. The roll continued with neutral controls because the sideslip was sustained by inertial coupling, and by mechanical hysteresis and roll rate feedback in the aircraft flight control system. The negative pitch rate, associated with rotating about the stability axis with proverse sideslip, inertially coupled with roll rate to produce an inertial yaw acceleration through the $pq(I_x-I_y)/I_z$ term of equation (2). These effects sustained the sideslip because the aircraft static directional stability was low. The autoroll was usually encountered during rudder rolls at moderate angles of attack. Lateral stick applied opposite to the roll, in an attempt to recover, accelerated the yaw rate, increased the angle of attack, and eventually resulted in a departure. As little as three seconds of full lateral control opposite the roll was all that was required to depart the aircraft. The best recovery technique was to apply rudder pedal opposite to the roll. This reduced sideslip, inertial yaw acceleration and angle of attack and thus resulted in immediate recovery.

Initial tests on one recent high AOA flight test program indicated severely degraded high angle of attack characteristics for a modified version of an aircraft that had previously demonstrated excellent high AOA characteristics. The test aircraft encountered several departures and one spin during relatively benign maneuvers. This differed significantly from the characterisitics of the unmodified aircraft. Data analysis indicated that a reduction in departure and spin resistance occurred only above 40 degrees angle of attack. Test data indicated that large asymmetric yawing moments above 40 degrees angle of attack were the cause of the degraded characteristics but the source could not be conclusively determined. Subsequent testing of another similarly modified aircraft, a two-seat model without flight test instrumentation, exhibited characteristics inconsistent with those of the test aircraft. Since the external differences between the two aricraft was the larger canopy of the two-seat aircraft and the presence of the flight test noseboom on the single-seat test aircraft, further tests were conducted with the test aircraft with the noseboom removed in an attempt to isolate the cause. Test results indicated that the flight test noseboom had an adverse influence on the High AOA dynamics of the aircraft. It was theorized that the noseboom (a circular cross-section) altered the forebody configuration sufficiently to produce large vortex systems at the apex of the aircraft nose. This vortex system separated asymmetrically at approximately 40 degrees angle of attack generating large side forces that produced severe yawing moments due to the distance from the aircraft center of gravity. Figures 3 and 4 show time histories of two similar maneuvers flown in the test aricraft with and without the flight test noseboom installed. The maneuver shown in figure 3 is the same maneuver that produced the one spin encountered during the test program. Figure 5 shows a comparison of the aerodynamic yawing accelerations produced during the two maneuvers versus angle of attack up to the point of departure. At approximately 40 degrees angle of attack, a large yawing moment occurs with the noseboom-configured aircraft which produced the resultant spin. Evidently, the only reason why the unmodified test aircraft (also configured with a noseboom) did not exhibit these adverse effects was because: (1) angles of attack of 40 degrees or more were only achievable under very dynamic conditions with the unmodified aircraft and (2) slightly reduced longitudinal stability characteristics of the modified aircraft allowed stabilized angles of attack of 40 degrees or more to be achieved with full aft stick commands. These results demonstrated a case where the flight test configuration severely affected

the aircraft flight characteristics at high AOA. Future test of production-configured aircraft should and will be tested in the high AOA regime to insure that test results from instrumented aircraft were not influenced by the test configuration (e.g., noseboom, spin chute, mass characteristics, etc.).

DATA ANALYSIS AND REPORTING

Meaningful, accurate and timely data analysis is an absolute necessity in conducting a safe and efficient high AOA flight test program. As stated earlier, much of this data analysis is performed prior to and during the conduct of the test maneuvers themselves. Virtually all test maneuvers that are planned for the flight test program are first performed on the simulator to establish predictive trends. Trend charts such as the ones previously discussed are used in the control room between maneuvers to compare the test results with predictions. The closeness with which the predicted data matches the flight test results and the amount of control margin remaining then dictates if the next test maneuver can be flown as planned or if additional buildup points are to be flown first. If the comparison of test results with predictions yields poor agreement, the flight is usually terminated so that the contractor and Air Force engineers can have a closer look at the data, come up with explanations for the mismatch and make recommendations on how to proceed with the remaining tests. The emphasis in the early stages of the flight test program, is to prevent a departure and avoid a spin whenever possible. Only after accomplishing everything in phases A through C of MIL-S-83691 that can possibly be done without departing the aircraft, are the departure and post-departure characteristics of an aircraft intentionally evaluated during phase D.

A significant factor in early attempts at correlating simulation predictions with flight test results was an inability to calculate accurate aircraft flightpath angles and velocities at very low speeds with the standard flight test noseboom pitot-static pressures and angle of attack and sideslip vanes. The spin maneuver depicted in figure 3 graphically shows what happens to pitot-static airspeed measurements at high angles of attack. For this particular pitot-static head, it appears that the total pressure source stalls out and becomes virtually useless above approximately 45 degrees angle of attack. Since angle of attack and sideslip measurements are subject to large errors due to angular rates of the vanes about the aircraft center of gravity and since the only way to correct for these errors is with an algorithm that includes true airspeed in its formulation, these parameter values become useless as well. Because the pitot-static and vane measurements become unreliable at high angles of attack and because of the possibility that asymmetric vortex shedding from the noseboom will make the test results suspect, serious questions are now being raised within the flight test community about the liabilities imposed by its use. Fortunately, technology has provided an answer to the dilemma. The quality of modern inertial navigation systems (INS) have reached the level which qualifies them as viable candidates to be used as flight test instrumentation sensors. There have been many symposium papers written to date on the successes of using INS systems for other types of testing such as aircraft performance determination. High AOA testing, as well, has benefitted from the use of INS systems recently. Figure 6 shows airspeed, angle of attack and angle of sideslip as calculated from INS attitudes and velocities. No rigorous proof will be given in this paper to show that the INS values shown represent true values of these parameters; however, computer-generated visual displays of the spin maneuver and others show a considerably more steady velocity vector that transitions very smoothly from level flight to near vertical with very little oscillation. We have also had a great deal more success lately in correlating simulator predictions with the results of flight tests.

The final task of any high AOA test program is getting the information to the user. Methods of reporting this information have taken the form of technical reports, briefings, training films, flight demonstrations, and flight characteristics sections of Flight Manuals rewritten to reflect flight test results. Along with words on paper, which dictate his actions while operating the aircraft, the operational pilot needs face-to-face verbal exchanges, pictures, and hands-on demonstrations to explain the <u>why</u> behind those words.

A major step in the reporting process is to prepare the final technical report. The more complete this report can be, the more meaningful it will be later when those involved have forgotten the more subtle aspects of the test program. While it is important to condense the "meat" of the program into a concise package which is useful to higher management for decision-making without subjecting them to a myriad of detail, it is also important to record those details so that the next program can benefit from the information. The AFFTC has wrestled for years with the dichotomy created by the need to get bottom-line results to the management decision-makers in a timely manner versus the need to document the technical details for the "millions of questions" that are always asked about the tests throughout the operational life of the aircraft. Within the last year, it was decided to split the reporting function into two parts to better satisfy the needs of both groups. The bottom-line results are first assembled into a quick-response briefing to be presented up the Air Force chain of command as far as necessary to satisfy the need of the decision-makers. The final technical report is then prepared to document the technical details. A briefing tour, flight demonstration program, and/or a training film are also prepared as necessary at this time to meet the needs and desires of the user. These items provide the necessary measure of visible competence and assurance to the operational pilot who has just been handed a Flight Manual or safety supplement with descriptions of out-of-control characteristics and recovery procedures that are totally unfamiliar and on which he is expected to rely. The briefing tour has significant two-way benefits. Test projects personnel can receive

valuable insight to the operators special problems, and then in future test efforts, address test techniques more properly to these areas. Also, the briefing forces the tour team to "talk in useable language" to an audience possessing less expertise in the high AOA area. The effectiveness of disseminating complex test results in a simple, useable format is then assessed and reapplied to the training film or flight demonstration program as applicable.

SUMMARY

High AOA flight testing is still very exploratory in nature. Although wind tunnel test techniques and analytical methods are becoming more sophisticated, they still do not serve with the same accuracy as similar studies applied in the low AOA range because of more acute Reynolds number and flow separation problems. With stall/spin predictive studies tempered by such uncertainty, it is increasingly vital that suitable flight test techniques be employed and continually refined to obtain results useful to the operational pilots. As a representative for all present and future service pilots, the test pilot must prepare himself to be an accurate witness to rapidly transpiring events, many of which are likely to be unscheduled. When the results are determined and conclusions made, they must be promptly and properly reported. To the designers, quantative data is needed to back up the qualitative conclusions if aircraft modifications are warranted. To the operators in the field whose lives or mission success depend upon an incisive Flight Manual writeup, a face-to-face briefing, a flight demonstration, and/or a training film is appropriate.

Using the guidance provided by MIL-S-83691, emphasis in high AOA flight testing is now directed toward departure prevention and spin avoidance as well as spin recovery. Today's high AOA test program is systematic, flexible and user-oriented, following a gradual buildup approach supplemented with concurrent simulation efforts. The AFFTC has now completed approximately sixteen high AOA flight test programs in the last decade totaling more than 600 test flights without the loss of a single test aircraft and with only three unplanned spin chute deployments. It is a record we are proud of and we hope will continue for some time to come.

REFERENCES

1. Sharp, Patrick S., and McElroy, Collett E., Captain, USAF, Background Information and User Guide for MIL-S-83691, AFFTC-TD-73-2, Air Force Flight Test Center, Edwards AFB, California, March 1974.

2. Stall/Post-stall/Spin Symposium, ASD/AFFDL Proceedings, Wright-Patterson AFB, Ohio, 15-17 December 1971.

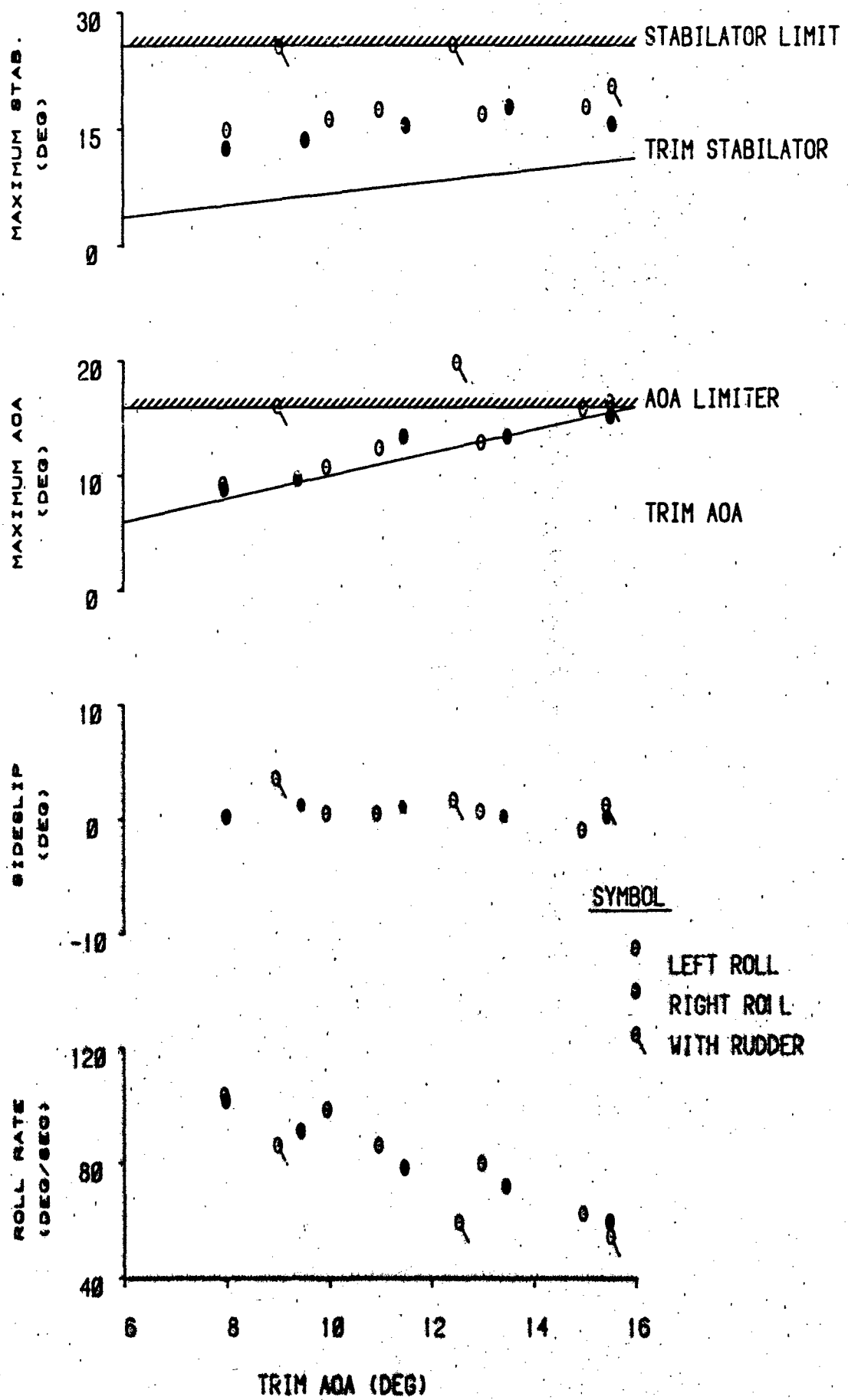

FIGURE 1. ONE-G ROLLS

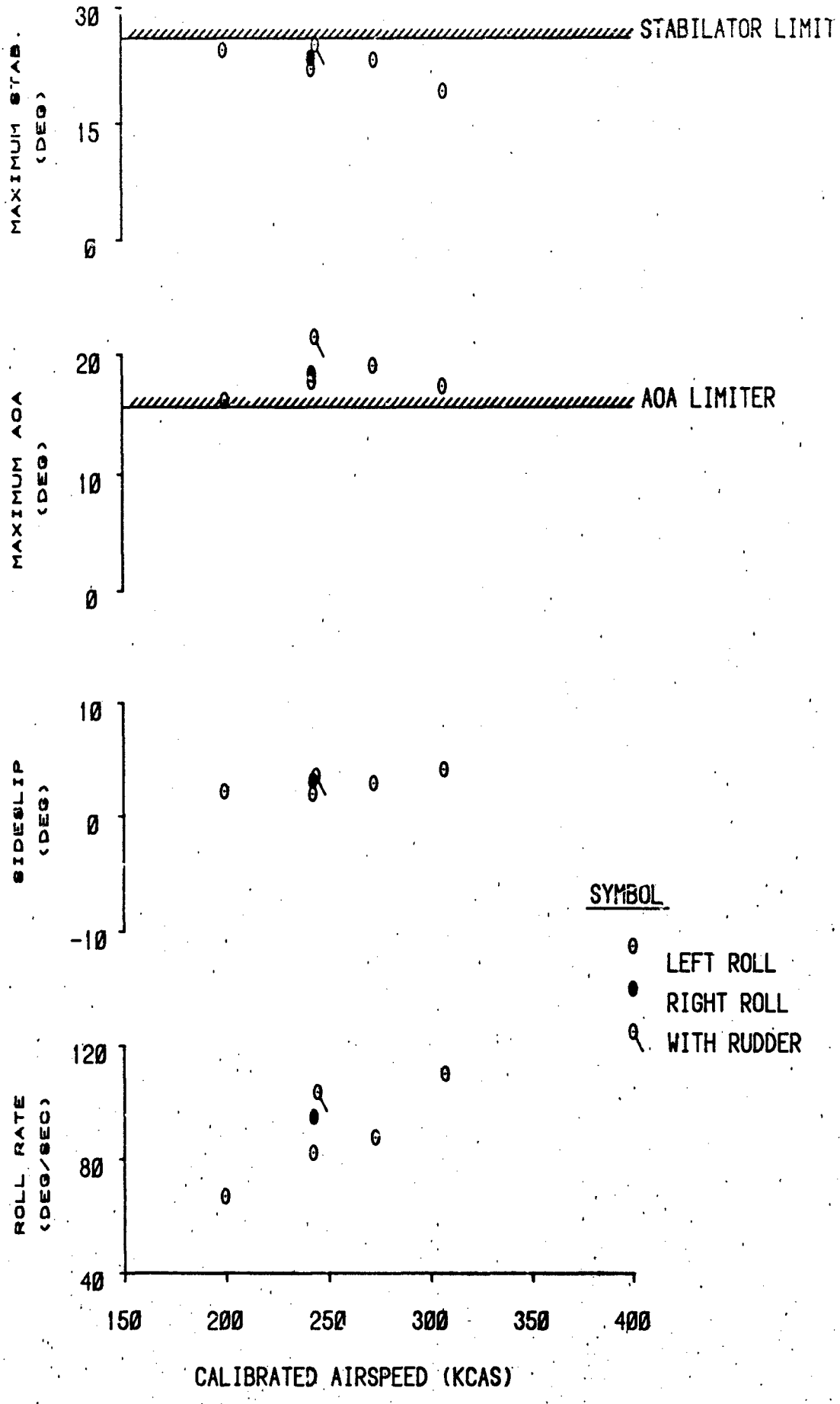

FIGURE 2. MAXIMUM-G ROLLS

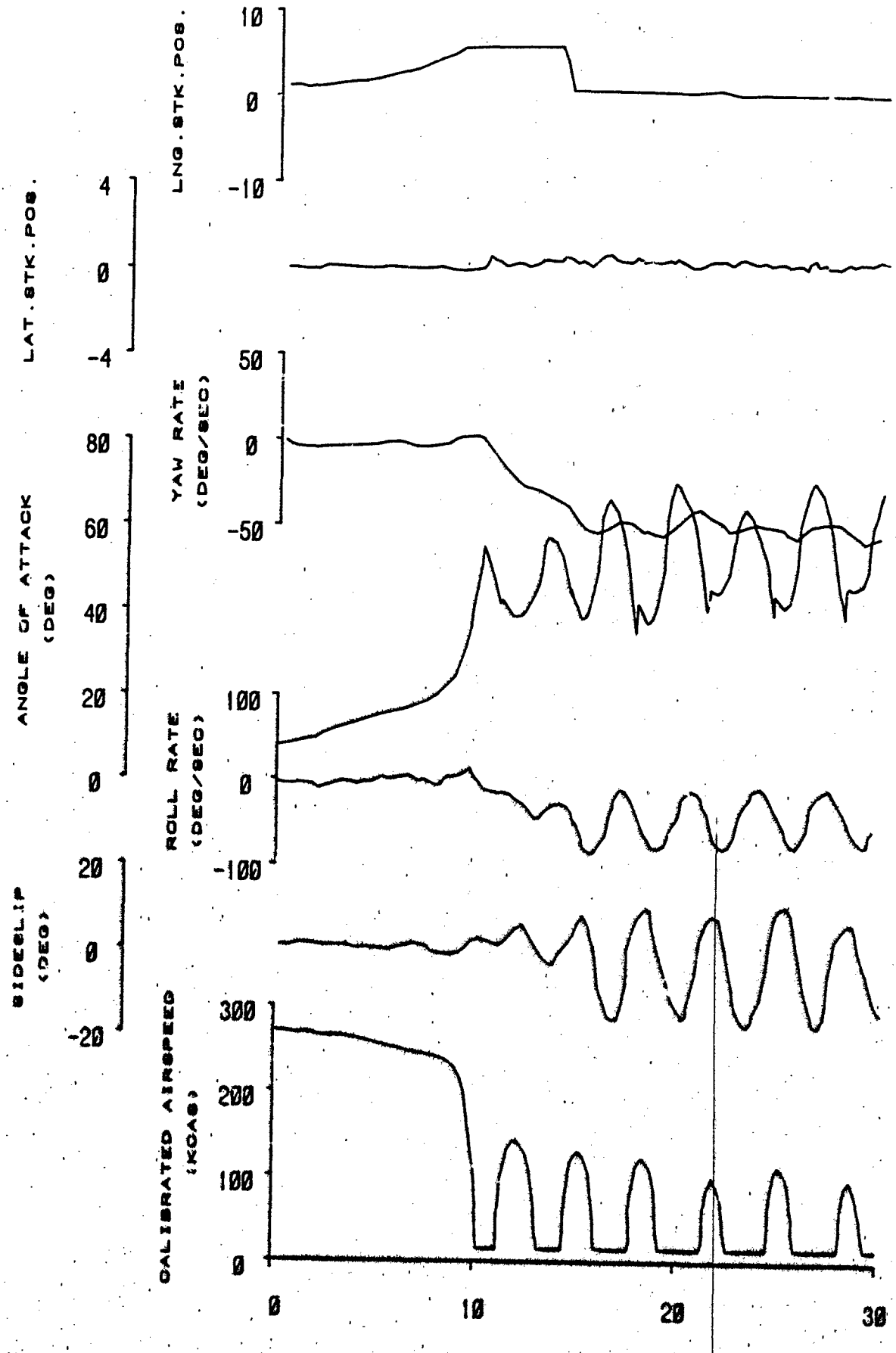

FIGURE 3. WINDUPTURN - NOSEBOOM ON

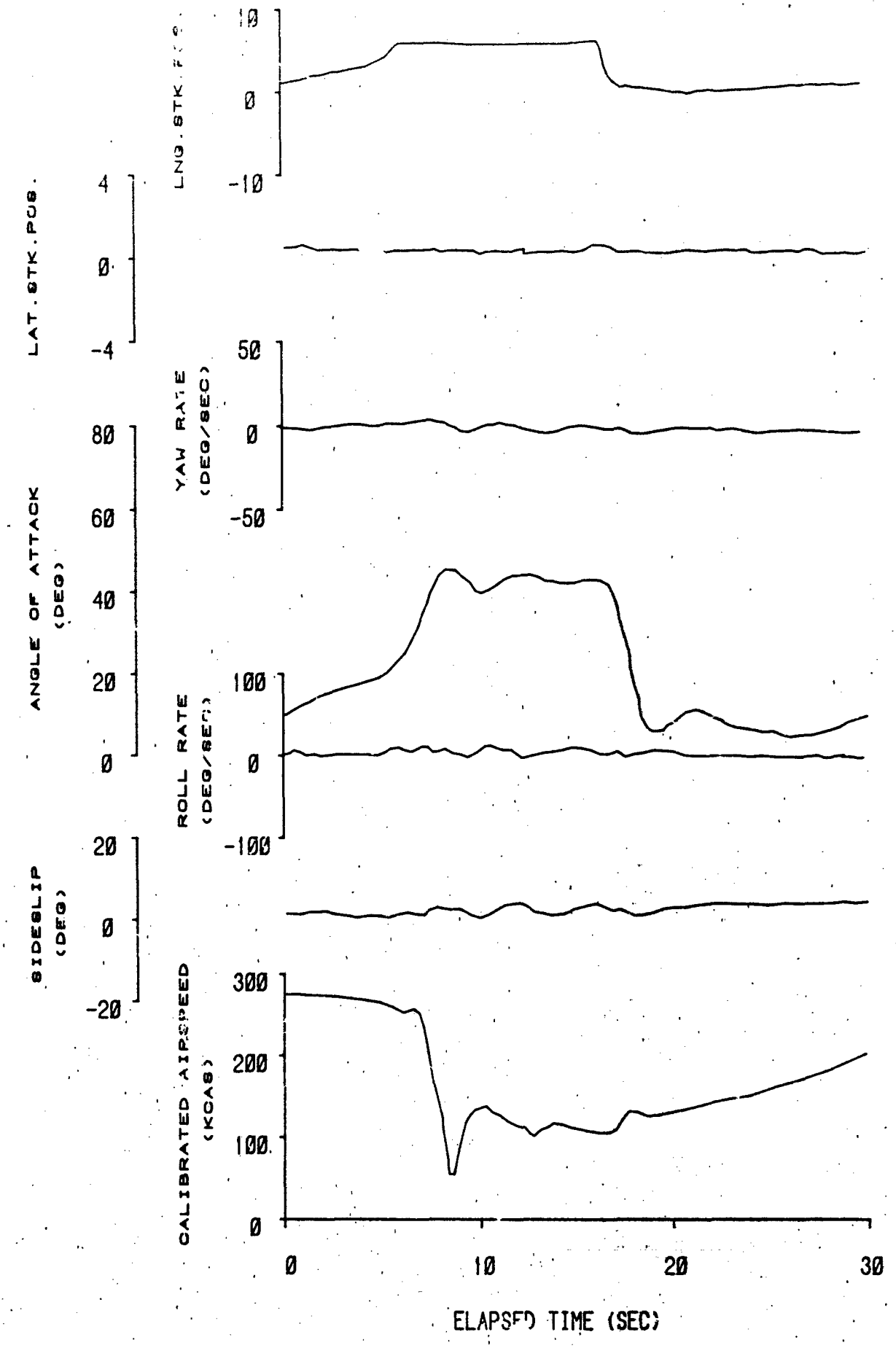

FIGURE 4. WINDUP TURN - NOSEBOOM OFF

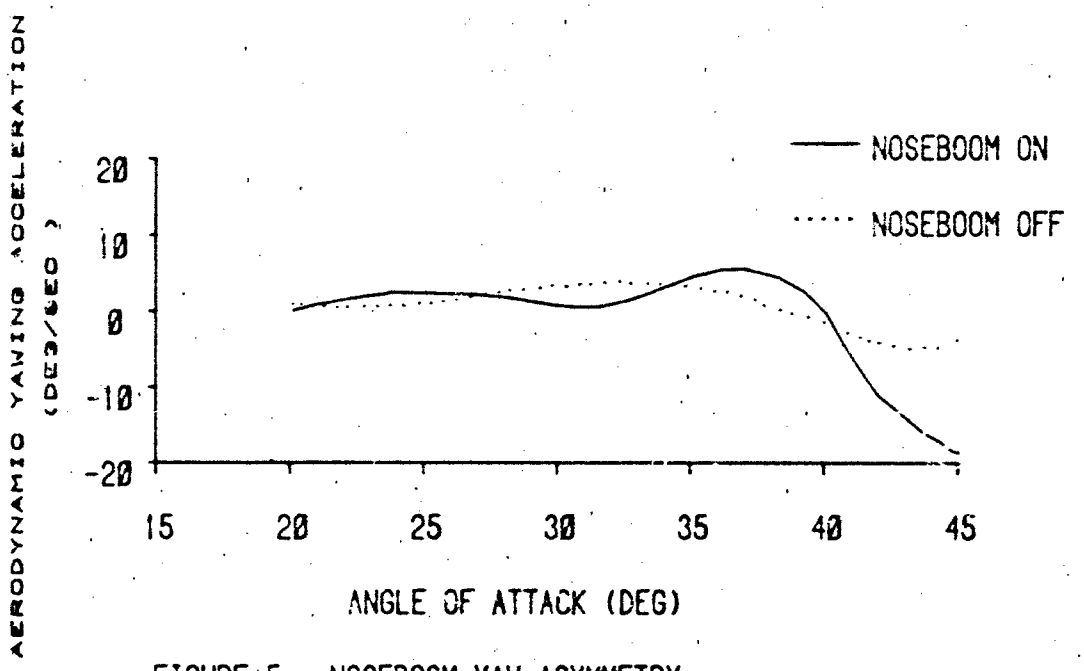

FIGURE 5. NOSEBOOM YAW ASYMMETRY

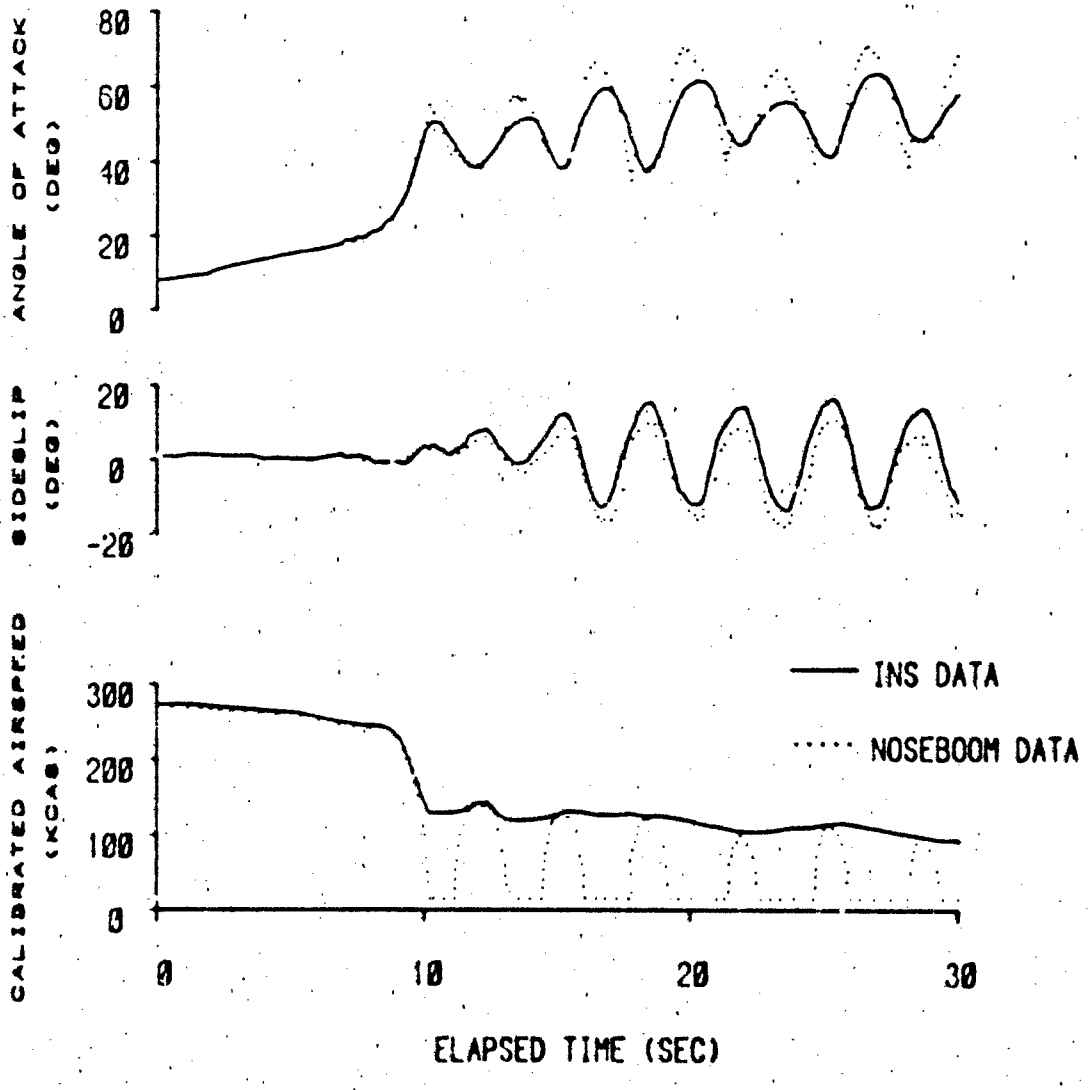

FIGURE 6. NOSEBOOM VS INS DATA COMPARISION

DETERMINATION OF PERFORMANCE AND STABILITY CHARACTERISTICS FROM DYNAMIC MANOEUVRES WITH A TRANSPORT AIRCRAFT USING PARAMETER IDENTIFICATION TECHNIQUES

by

J.H. Breeman, L.J.J. Erkelens and A.M.H. Nieuwpoort
National Aerospace Laboratory (NLR)
Anthony Fokkerweg 2
1059 CM Amsterdam
The Netherlands

SUMMARY

A flight test program was executed with the Fokker F28 transport aircraft to investigate whether it is possible to determine performance and stability characteristics from dynamic manoeuvres using parameter identification techniques, with sufficient accuracy for certification purposes.
A research moving base flight simulator, programmed with the F28 aerodynamic model derived from conventional flight tests and wind-tunnel data, was used to select an optimal set of manoeuvres from which the desired characteristics could be determined with a satisfactory degree of accuracy.
Flight test data was analysed, using the so-called 'Two-Step method' developed in The Netherlands by Delft University of Technology and NLR. This method starts by reconstructing the aircraft flight path as the first step. The second step is the calculation of all aerodynamic coefficients using straightforward regression analysis techniques. The advantage of this method over the more often used maximum likelihood estimation methods is that a large number of alternative non-linear aerodynamic models can be investigated in a short time using an interactive program.
The flight test results are compared with results derived from conventional test programmes. From this comparison it is clear that the above-mentioned goal has been reached.

LIST OF SYMBOLS

A_x, A_y, A_z	specific forces along the body axes (X, Y, Z)	(ms^{-2})
a_n	normal acceleration	(ms^{-2})
b	wing span	(m)
C_X, C_Z	dimensionless coefficients of total forces (see Eq. 2.10)	
C_D, C_L, C_Y	dimensionless coefficients of aerodynamic forces (see Eq. 2.14)	
C_l, C_m, C_n	dimensionless coefficients of aerodynamic moments (see Eq. 2.14)	
C_{D_0}, C_{D_α}, etc.	coefficients in taylor expansion of aerodynamic coefficients (see eq. 2.15 and 2.16)	
$\bar{c}$	mean aerodynamic chord	(m)
D	drag	(N)
g	acceleration due to gravity	(ms^{-2})
h	altitude	(m)
Δh	altitude variation with respect to initial altitude	(m)
L	lift	(N)
l	rolling moment	(Nm)
M	pitching moment	(Nm)
M	Mach number	(-)
m	aircraft mass	(kg)
N	yawing moment	(Nm)
n	normal load factor	
n_{HP}	engine rpm (high pressure shaft	(rpm)
p, q, r	components of angular rate along body axes (X, Y, Z)	$(deg\ s^{-1})$
S	wing area	(m^2)
x	vector of independent variables in aircraft model (see eq. 2.11)	
T_e	nett engine thrust (both engines)	(N)
t	time	(s)
U	system input vector	
u, v, w	components of V_a along body axes (X, Y, Z)	(ms^{-1})
V_a, V	velocity of the aircraft w.r.t. the air mass	(ms^{-1})
V_i	velocity of the aircraft w.r.t. the surface of the earth	(ms^{-1})
V_s	stalling speed	(ms^{-1})
V_w	wind velocity	(ms^{-1})
x_{cg}, z_{cg}	location of centre of gravity with respect to the X- and Z-axes	(m)
X	system state vector	
Y	measurement vector	
Y	side force along Y_s axis	(N)
α	angle of attack	(deg)
β	angle of sideslip	(deg)
δ	coefficient of C_L^2 in the lift-drag polar	(-)
γ	flight path angle	(deg)
δ_a	aileron deflection	(deg)
δ_e	elevator deflection	(deg)
δ_r	rudder deflection	(deg)
δ_s	horizontal stabilizer deflection	(deg)
θ	angle of pitch	(deg)
μ_c	non-dimensional aircraft mass $(m/\rho SF)$	
ρ	density of air	$(kg\,m^{-3})$
ρ	simple correlation coefficient	(-)
σ	standard deviation	
ϕ	angle of roll	(deg)
ψ	angle of yaw	(deg)

Superscript

$\dot{x}$ time derivative of x

Subscripts
1 values pertaining to actual flight conditions
2 values pertaining to standard conditions
a with respect to the surrounding air mass
i inertial
w wind
m air data measurements

Reference systems (see figure 1)
(O, X, Y, Z) Aircraft body-fixed reference frame (body axes)
(O_a, X_a, Y_a, Z_a) Air-trajectory reference frame (wind axes)

1. INTRODUCTION

Dynamic flight test techniques allow the determination of performance as well as stability and control characteristics. These techniques already have a long history, but until recently they were mainly applied to military aircraft (Refs. 1, 2, 3). In 1976 the NLR initiated a research program to investigate the applicability of the so-called Two-Step Method to commercial jet transport aircraft. The research concentrated initially on the determination of performance characteristics, because of the potential reduction in flight test time and the improvement in accuracy. In autumn 1977 a series of four test flights were executed with the prototype of the Fokker F28 (see Fig. 1), using a specially designed instrumentation system (Refs. 4,5). The main results of this flight test program are presented in Section 3.

Later the emphasis shifted to the determination of stability and control characteristics. The main reasons for this change are the increased importance of realistic flight simulators and the potential improvement in the design of autopilots. The first flight tests already included a few stability and control measurements, but they were confined to longitudinal motion. The results of these measurements were encouraging, but it was decided to do some further research using the NLR moving base simulator. The objectives of this research were the design of a set of manoeuvres which will allow the determination of all the major aerodynamic coefficients under the condition that these manoeuvres are simple enough to be flown manually by a test pilot. An additional aim was to prove that even "standard" flight test manoeuvres (e.g. rudder doublets, turns) can be used, provided that they are suitably combined with each other. The main conclusions of this research are presented in section 4.2.

In the spring of 1983, Fokker decided to execute a short flight test program in order to validate its simulator model for the F28 Mk4000 for Phase 3 use. It was decided to perform some of the planned manoeuvres in the same way as in the simulator program described in section 4.2. This provided an in-flight verification of these theoretical results. Since the standard NLR flight test instrumentation system, that has been installed in the aircraft for a long time, was not designed to the specifications for dynamic flight testing, a Honeywell laser strapdown Inertial System was added in order to obtain the needed accurate inertial measurements. Some results of these flight tests are presented in section 4.3.

2. THEORY

2.1 Introduction

The Two-Step method as used by NLR was developed by the Department of Aerospace Engineering of the Delft University of Technology (Ref. 1). As the name implies the method uses two distinct steps.

Figure 2a gives an overview of the first step of the data processing. The first phase is called "pre-processing" and involves e.g. the application of the sensor calibrations and position error corrections, the correction of vane angles for dynamic errors, the correction of pressure measurements for time lags and the reduction of the acceleration measurements to the center of gravity. After the pre-processing the state trajectory of the aircraft with respect to the surrounding air mass is reconstructed, this crucial procedure is described in more detail in section 2.2. The last phase is the calculation of the engine thrust components. Correcting the inertial measurements for the thrust components yield the aerodynamic forces and moments. The end result of the first step is the smoothed time histories of the dimensionless aerodynamic forces and moments and of the aircraft state variables.

In the second step (Fig. 2b) there are two options:
1. A program which reduces the measurements in dynamic flight to equivalent steady-state conditions. This allows the determination of performance characteristics and trim curves (see section 2.3).
2. An interactive parameter identification program based on linear regression techniques. This allows the determination of the coefficients of an aerodynamic model (see section 2.4).

2.2 Flight path reconstruction

The flight path reconstruction procedure is an essential part of the Two-Step method. This procedure makes use of the redundancy present in the recorded inertial and air data variables in order to obtain the best estimate of the state variables of the aircraft during the dynamic manoeuvre. The most important result is the estimate of the angle of attack, which is very difficult to measure accurately with vanes, especially during a dynamic manoeuvre.

For a flat and non-rotating earth and for constant wind, the equations of motion expressed in body axes are (see figure 1):

$$
\begin{aligned}
\dot{u} &= A_x - g \sin\theta \qquad\quad - qw + rv \\
\dot{v} &= A_y + g \cos\theta \sin\phi - ru + pw \\
\dot{w} &= A_z + g \cos\theta \cos\phi - pv + qu \\
\dot{\phi} &= p + q \sin\phi \tan\theta + r \cos\phi \tan\theta \\
\dot{\theta} &= \qquad q \cos\phi \qquad - r \sin\phi \\
\dot{\psi} &= \qquad q \sin\phi \sec\theta + r \sec\theta \cos\phi \\
\dot{h} &= u \sin\theta - v \sin\phi \cos\theta - w \cos\phi \cos\theta
\end{aligned}
\qquad (2.1)
$$

The important variables V_a, α and β can be calculated by

$$V_a = \sqrt{u^2 + v^2 + w^2} \tag{2.2}$$

$$\alpha = \arctan\left(\frac{w}{u}\right) \tag{2.3}$$

$$\beta = \arcsin\left(\frac{v}{V_a}\right) \tag{2.4}$$

We define the state vector as

$$X = (u, v, w, \phi, \theta, \psi, \Delta h) \tag{2.5}$$

and the inertial measurements as the input vector

$$U = (A_x, A_y, A_z, p, q, r) \tag{2.6}$$

This allows us to write (2.1) as

$$\dot{X} = f(X,U) \tag{2.7}$$

This differential equation cannot be integrated to yield the state vector trajectory of the aircraft during a manoeuvre, because the initial state is not known accurately and because the input vector is corrupted with measurement errors. This problem is solved by using the air data measurement vector

$$Y = (V_m, \Delta h_m, \beta_m) \tag{2.8}$$

and applying the well-known Kalman filter methodology. The exact algorithm is described in more detail in reference 4 and 6, while references 7 and 8 give additional theoretical background.

In the original implementation the errors on the inertial quantities were modelled as a constant bias plus a noise process. In practice the bias estimates were very close to zero, although the estimation of the bias errors in the first tests did uncover an error in the calibration coefficients of one of the gyroscopes. Therefore, it was decided to remove the bias terms from the model.

The quality of the flight path reconstruction can be judged by examining the so-called residuals, i.e. the difference between the Kalman filter estimate of Y and the measured Y. The difference between the estimated and the measured angle of attack α also yields important independent information because it is not used in the Kalman filter procedure. While there is a significant bias on the measured α_m, this bias should be expected to reproduce under similar conditions. The residuals are invaluable for tracing any uncorrected errors in the air data system, such as time delays or dynamic effects.
Nevertheless, the final criterion for the quality of the reconstruction is the lift-drag polar curve, because any deviation in the estimated angle of attack has a very large effect on this curve.

Closer examination of systematic deviations between lift-drag polars from one flight revealed the importance of changes in wind velocity for the performance results. Although it is in theory possible to estimate the change in wind velocity by incorporating it in the error model, in practice this can only be succesful if the inertial measurements are of so-called navigation accuracy. Therefore, it was decided in 1981 to replace the NLR developed inertial sensor package by a strapdown navigation system. As mentioned above, this system was used in the 1983 flight tests. The advantages of such a system for flight tests are:
- the ground speed error is small and, more important, changes very slowly,
- it provides the attitude angles with high accuracy (0.02 degree),
- it provides the accelerations and angular rates in body axes,
- it does the integrations of the inertial sensors internally at very high speed, which simplifies the data processing on the ground,
- it is commercially available.

With this equipment the wind velocity vector can be determined by subtracting the airspeed vector from the inertial speed vector:

$$\vec{V}_w = \vec{V}_i - \vec{V}_a \tag{2.9}$$

This measurement is very noisy, so smoothed estimates of the two horizontal wind components V_{w_x} and V_{w_y} are obtained by adding them to the state vector and by adding (2.9) to the measurement vector Y. Based on the flight test results the wind velocity is modelled as varying with time, distance and altitude. Especially the variation with altitude was very significant at times, which could be noticed by systematic deviations in the lift-drag polar curves derived from measurements in opposite flight directions. The variation with distance may be even more important, however, because it has the same effect on the lift-drag polar curves in both flight directions, which means that the deviations will not average out.

2.3 Reduction to steady-state conditions

The performance characteristics as well as the trim curves can be derived from the forces and moments acting on the aircraft in steady, trimmed flight conditions. However, during an accelerated run the measured forces and moments apply to the actual flight condition, which is nonsteady and untrimmed. In addition the altitude, the center of gravity location and the mass of the aircraft vary continuously during the flight. The reduction procedure uses a model of the aircraft to calculate the forces and moments corresponding to a prescribed steady-state condition with standard values of altitude, c.g. location and mass. This is possible, because the complete state of the aircraft is available after the flight path reconstruction.

The dimensionless forces and moments acting on the aircraft in symmetric flight are defined as:

$$C_X = \frac{mA_x}{\frac{1}{2}\rho V^2 S}$$

$$C_Z = \frac{mA_z}{\frac{1}{2}\rho V^2 S} \tag{2.10}$$

$$C_m = \frac{I_y \dot{q}}{\frac{1}{2}\rho V^2 S \bar{c}}$$

If the aerodynamic model of the aircraft and the engine thrust T_e are known, it is possible to write C_X, C_Z, C_m as:

$$\begin{aligned} C_X &= C_X(\alpha, V, q, \dot{\alpha}, \delta_e, \delta_s, h, T_e) \\ C_Z &= C_Z(\alpha, V, q, \dot{\alpha}, \delta_e, \delta_s, h, T_e) \\ C_m &= C_m(\alpha, V, q, \dot{\alpha}, \delta_e, \delta_s, h, T_e, C_X, C_Z, x_{cg}, z_{cg}) \end{aligned} \tag{2.11}$$

We will now denote the actually measured variables with the subscript 1 and the reduced variables with the subscript 2. The standard condition is completely prescribed by the altitude in the standard atmosphere h_2 (which fixes ρ_2 and T_2), the mass m_2 and the center of gravity location x_{cg2} and z_{cg2}. In addition we assume $T_{e_2} = T_{e_1}$ which is reasonable for a jet engine, and we choose $\alpha_2 = \alpha_1$ in order to stay close to the measured condition. Steady trimmed flight is described by:

$$\begin{aligned} C_{m_2} = q_2 = \dot{\alpha}_2 = \delta_{e_2} = 0 \\ \sqrt{C_{X_2}^2 + C_{Z_2}^2} = \frac{m_2 g}{\frac{1}{2}\rho_2 V_2^2 S} \end{aligned} \tag{2.12}$$

In principle the set of equations (2.11) and (2.12) can be solved for the unknowns C_{X_2}, C_{Z_2}, V_2 and δ_{s_2}. This would yield the required results without any use of the measurements! However, the model (2.11) is not accurate enough for the calculation of performance characteristics, although it can describe the changes in the forces and moments over small changes in the variables very well. Therefore, the model (2.11) is replaced by a model based on the actual flight measurements:

$$\begin{aligned} C_{X_2} &= C_{X_1} + [C_X(s_2) - C_X(s_1)] \\ C_{Z_2} &= C_{Z_1} + [C_Z(s_2) - C_Z(s_1)] \\ C_{m_2} &= C_{m_1} + [C_m(s_2) - C_m(s_1)] \end{aligned} \tag{2.13}$$

where the vector s consists of the 12 independent variables in equation (2.11). The set of equations (2.12) and (2.13) is solved with Newton-Raphson iteration.

An important aspect of the reduction procedure is that it is an extrapolation based on the aerodynamic model. This means that the more the standard condition differs from the actual flight condition, the more the reduction relies on the accuracy of the aerodynamic model. In the case of the accelerated runs the flight condition is in fact very near steady, trimmed flight. This means that in this case the accuracy of the aerodynamic model is not critical. An important advantage of reduction to standard conditions is that all results from different recordings can be compared directly, such as C_L-α curves, etc. The effect of the reduction can be seen in the trim curve (Fig. 5) discussed in section 3.2.

Finally, it should be noted that there are many possible choices for the standard condition. An example is steady manoeuvring flight which would be useful for the determination of stickforce per g. The reduction procedure is described in more detail in references 4, 7 and 10.

2.4 Aerodynamic model identification

The aerodynamic model identification was performed with the aid of a computer program called "Parameter estimation using an Interactive Adaptive System" (PIAS). This program is based on the linear regression technique, which is implemented using Householder transformations and Givens rotations (Ref. 4). This results in a system which yields accurate parameter estimates within a negligible time delay and, therefore, can be used interactively. The program contains extensive graphical facilities, which allows the analyst to evaluate the results for a particular aerodynamic model very quickly.

A significant feature of the program is that the form of the aerodynamic model can be changed interactively by the analyst. Since the calculation of the coefficients of a new model is virtually instantaneous, the analyst is capable of evaluating a large number of alternative models until he is satisfied with the result. The program always starts with a model with a chosen maximum set of parameters and then allows the removal of parameters from the model or the specification of linear dependencies between the parameters.

After choosing one particular form of the aerodynamic model the program can be run in batch mode on all available flight data and the results presented in the form of graphs (see section 4). This last step is very important, because the analysis is only completed if the results from the batch run show that the parameter estimates are consistent for all available data. If this is not the case further analysis in the interactive mode is necessary.

An advantage of the linear regression method in comparison with e.g. Maximum Likelihood methods for parameter identification is the fact that the method does not rely on the temporal relation between the processed data points. This allows the analyst to concatenate several separate recordings and thus obtain a data set which allows the identification of all model parameters, whereas the individual recordings will not allow this identification. Another option which was used extensively in the analysis presented in section 4, is the deletion of those parts of a recording which the analyst does not want to take into account, because either these parts are corrupted by errors or the incorporation of these parts would force him to use a more complex aerodynamic model, e.g. in order to describe nonlinear behaviour or Mach number coefficients. Reference 8 contains some simple examples of the use of the PIAS program features.

The analysis was based on dimensionless coefficients corrected for the known (geometric) effects of the engine thrust defined as:

$$C_D = \frac{D}{\frac{1}{2}\rho V^2 S} \qquad C_Y = \frac{Y}{\frac{1}{2}\rho V^2 S}$$

$$C_L = \frac{L}{\frac{1}{2}\rho V^2 S} \qquad C_\ell = \frac{\ell}{\frac{1}{2}\rho V^2 S b} \tag{2.14}$$

$$C_m = \frac{M}{\frac{1}{2}\rho V^2 S \bar{c}} \qquad C_n = \frac{N}{\frac{1}{2}\rho V^2 S b}$$

The force coefficients (C_D, C_L, C_Y) were chosen in the air-trajectory reference frame, because in this frame the large lift force is separated from the smaller drag and side forces. The moment coefficients (C_ℓ, C_m, C_n) were chosen in the body axes frame, because the contributions of the horizontal and vertical tail surfaces act in this frame. This eliminates one source of a dependency in the moment coefficients. The general form of the aerodynamic model was based on the existing Fokker simulator model, since it appeared to describe the aircraft dynamics well. The model equations, divided into separate sets for the longitudinal (2.15) and lateral-directional (2.16) motion are:

$$C_D = C_{D_0} + C_{D_\alpha}\alpha + C_{D_{\alpha^2}}\alpha^2 + C_{D_q}\frac{q\bar{c}}{V} + C_{D_{\dot{\alpha}}}\frac{\dot{\alpha}\bar{c}}{V} + C_{D_{\delta_e}}\delta_e + C_{D_{\delta_s}}\delta_s + C_{D_M}M$$

$$C_L = C_{L_0} + C_{L_\alpha}\alpha + C_{L_{\alpha^2}}\alpha^2 + C_{L_q}\frac{q\bar{c}}{V} + C_{L_{\dot{\alpha}}}\frac{\dot{\alpha}\bar{c}}{V} + C_{L_{\delta_e}}\delta_e + C_{L_{\delta_s}}\delta_s + C_{L_M}M \tag{2.15}$$

$$C_m = C_{m_0} + C_{m_\alpha}\alpha + C_{m_{\alpha^2}}\alpha^2 + C_{m_q}\frac{q\bar{c}}{V} + C_{m_{\dot{\alpha}}}\frac{\dot{\alpha}\bar{c}}{V} + C_{m_{\delta_e}}\delta_e + C_{m_{\delta_s}}\delta_s + C_{m_M}M$$

$$C_Y = C_{Y_0} + C_{Y_\beta}\beta + C_{Y_p}\frac{pb}{2V} + C_{Y_r}\frac{rb}{2V} + C_{Y_{\delta_a}}\delta_a + C_{Y_{\delta_r}}\delta_r + C_{Y_{\dot{\beta}}}\frac{\dot{\beta}b}{2V}$$

$$C_\ell = C_{\ell_0} + C_{\ell_\beta}\beta + C_{\ell_p}\frac{pb}{2V} + C_{\ell_r}\frac{rb}{2V} + C_{\ell_{\delta_a}}\delta_a + C_{\ell_{\delta_r}}\delta_r + C_{\ell_{\dot{\beta}}}\frac{\dot{\beta}b}{2V} \tag{2.16}$$

$$C_n = C_{n_0} + C_{n_\beta}\beta + C_{n_p}\frac{pb}{2V} + C_{n_r}\frac{rb}{2V} + C_{n_{\delta_a}}\delta_a + C_{n_{\delta_r}}\delta_r + C_{n_{\dot{\beta}}}\frac{\dot{\beta}b}{2V}$$

Depending on the type of analysis several of these coefficients were deleted from the model. In particular in most analysis work the model was limited to one single Mach number and the M-terms were deleted.

2.5 Comparison with other methods

Today the Maximum Likelihood or Modified Newton-Raphson methods are widely used for parameter identification (Ref. 2). It seems appropriate to make an attempt to compare the Two-Step method with its main rival.

In the ML method the combined state-estimation/parameter identification problem is solved in one step. This means that the estimates of the aerodynamic model coefficients directly influence the estimated trajectory. In the case that the aerodynamics are relatively well-known and the measurements of the state are relatively inaccurate this seems plausible and even convenient. But in the case of high accuracy state measurements the assumption that these measurements alone should be sufficient to obtain an accurate trajectory estimate seems to be more appropriate.

More important are the practical differences. The combined problem is highly nonlinear and requires an iterative solution and some care to assure convergence. Therefore it is an expensive program to run, which would not be so bad if you used it only once. But in a realistic aerodynamic model development a number of alternative model structures have to be investigated, each requiring the solution of the full problem (although starting from previous estimates should help).

In the case of the Two-Step method the trajectory reconstruction is also a nonlinear problem, although the accurate measurements will prevent large deviations from the true trajectory, which assures convergence. It is also an expensive program to run, comparable to the ML-method, with one important difference: you only have to run it once! The aerodynamic model investigation is based on linear regression techniques which are very inexpensive and can handle very complicated models quite easily. This allows the investigation of a large number of models in a short time on an interactive basis.

3 PERFORMANCE

3.1 Flight test technique

For the determination of the aircraft performance characteristics a flight test manoeuvre has been developed whereby the aircraft is slowly accelerated from nearly steady flight at low speed, approximately 10 % above the stalling speed, to the maximum allowable or practicable airspeed. During an accelerated run the complete speed range of the aircraft for a single configuration is covered. Measurements in decelerating flight were not contemplated, because of the inaccurate determination of the (low) engine thrust in these conditions.

In figure 3 time histories of six motion and control variables for a typical accelerated run are shown. The manoeuvre is carried out by applying stepwise changes in the stabilizer setting, while the elevator is used for fine control of the manoeuvre. The following phases can be distinguished:

1. Steady level flight at the required altitude and at an airspeed of approximately 1.3 V_s. Stabilization at a lower speed proved to be impracticable due to the proximity of the stall.
2. Engine stabilization at the required power setting for at least 30 seconds. The airspeed is decreased slightly to around 1.1 V_s, while the increased engine power is taken up by going into a climb.
3. Measurement interval during which the aircraft is accelerated at a rate of between 0.5 and 1 m/s^2.
4. Return to initial altitude in preparation for the next run.

5. Steady level flight to allow the calibration of the air data system.

The flight test manoeuvre was practised by Fokker pilots on the NLR moving base simulator, which had been programmed with the Fokker F28 simulation model. The evaluation of the test manoeuvres on the simulator resulted in the ultimate shape of the manoeuvre. At the same time the sinusoidal elevator input signals for the determination of longitudinal stability and control characteristics were practised. These manoeuvres will be discussed in section 4.1. More details on the preparation for the 1977 flight test program can be found in reference 9.

3.2 Results

In the 1977 flight test program a total of 45 accelerated runs were executed for 11 different aircraft configurations (flap setting, undercarriage selection, altitude, power setting, etc.). In addition 27 partial climbs were executed for 4 different configurations in order to investigate whether the results of the dynamic flight tests accurately represent the static performance characteristics (Ref. 10).

The primary aim of the research was to establish the repeatability of the performance results. Therefore, each configuration was measured at least three times while the more important configurations were measured up to six times, divided over two different flights. In the analysis each individual measurement was fitted to the second degree polynomial:

$$C_D = C_{D_0} + \beta C_L^2 \qquad (3.1)$$

From the individual estimates of C_{D_0} and β overall estimates for C_{D_0} and β were calculated, together with the corresponding sample standard deviations $\sigma_{C_{D_0}}$ and σ_β and the sample correlation coefficient $\rho_{C_{D_0},\beta}$.

Figures 4a, 4c and 4e present the results for the 3 most important configurations. These configurations are respectively:
- clean aircraft, two engines (6 runs from two flights),
- slats extended, one operating engine (5 runs from two flights),
- slats extended, 25 degrees flap, one operating engine (4 runs from two flights).

In each figure all datapoints from all accelerated runs for a particular configuration are plotted. In addition the overall estimates for C_{D_0} and β were used to draw the lift-drag polar curve (heavy line). The estimates for $\sigma_{C_{D_0}}$, σ_β and $\rho_{C_{D_0},\beta}$ were used to calculate 3 sigma confidence boundaries for the lift-drag polar as indicated by the broken lines. Approximately 99 % of all polar curves derived from one single accelerated run would be expected to fall between these boundaries. The figures show that even the large majority of the datapoints stay within these boundaries, although there is some evidence that the strictly quadratic model does not apply.

In figures 4b, 4d and 4f the corresponding results for the partial climbs are compared to the lift-drag polar curve as derived from the accelerated runs. It is evident that the results are mutually consistent although 6 or 7 partial climbs are hardly enough to verify the dynamic results to their full accuracy. It does show, however, that the two-step method does not introduce a bias in the estimated lift-drag polar curves.

Table 1 presents an overview of the sample standard deviation of these estimates for C_{D_0} and β for all configurations, expressed as a percentage of the full value of those coefficients. From this table it can be concluded that over all configurations the average standard deviation of the C_{D_0} estimates was 1.4 % and the average standard deviation for the β estimates was 2.0 %. The results for configurations 2 and 4 show the largest deviations. Closer investigation of those measurements revealed that the wind velocity changed appreciably during those manoeuvres, an effect which can also be seen in the results for the partial climbs.

Figure 5 presents a typical result for a trim curve derived from an accelerated run. The stabilizer angle δ_s is shown as a function of angle of attack α over the speed range of the aircraft. The dots correspond to the actual measurements, while the solid curve represents the results of the reduction to steady-state flight with $\delta_e = 0$ and standard c.g. location, mass and altitude.

4. STABILITY AND CONTROL

4.1 Initial results

As mentioned before, a small part of the 1977 flight test program was devoted to the determination of longitudinal stability and control characteristics (Ref. 10).

The elevator control input signal was computed with an optimization program developed by Delft University of Technology (see reference 11). The optimization procedure was constrained to produce an input signal which would be as simple as possible to allow the pilot to fly it manually and which would be very smooth in order to prevent the excitation of bending modes in the airframe. In addition some time was spent in practising the input signal on the flight simulator. The final input signal consisted of a two-period control movement with a sinusoidal shape (see figure 6). The signal was adapted for the various flight conditions by adapting its frequency to the short period frequency.

In order to investigate the repeatability of the results a number of similar elevator inputs were executed during each measurements. The time interval between the inputs was kept as small as possible in order to maximize the number of usable responses.

From this flight test program longitudinal stability and control derivatives were determined over a large area of the flight envelope. In figure 7 the estimated coefficients of the pitching moment control for a measurement at M = 0.52 and h = 8830 m consisting of a series of four individual elevator inputs are presented. In addition the results of combining the four elevator inputs is shown. As can be noted from this figure the repeatability of the estimated coefficients is quite good, with the exception of the α and $\dot{\alpha}$ coefficients of the second manoeuvre. In addition the calculated standard deviations appear to be consistent with the actual spread in the results.

Since there is a strong coupling between the α, $\dot{\alpha}$ and q motion during the oscillations the corresponding coefficients cannot be estimated independently of each other. Therefore, it was necessary to use a priori information in the estimation procedure. Based on theoretical assumptions a ratio of 3 between the q and $\dot{\alpha}$ derivatives was used in the analysis.

4.2 Manoeuvre design

4.2.1 Introduction

In continuation to this program a further investigation on the flight simulator of NLR was carried out with the objective of establishing flight test manoeuvres from which the complete set of either the longitudinal or the lateral-directional stability and control derivatives can be determined without the use of any prior knowledge of coefficient values or of ratios of coefficients.

The objectives in the design of the flight test manoeuvres have been:
- the manoeuvres should be simple to perform manually, without requiring exceptional piloting skill,
- the data measured during the different manoeuvres should contain sufficient information to allow an accurate estimation of the stability and control derivatives.

In reference 12 five different types of input signals have been tested with respect to their usefulness for the determination of longitudinal and lateral-directional stability and control derivatives from dynamic manoeuvres. It turned out that two of these input signals provide accurate results and moreover are very easy to perform manually. These input signals are the classical doublet and the 3211 multistep, which is described in section 4.2.2.

The aircraft response to a single control input does not contain all the information required for an accurate determination of the complete set of derivatives. However, by considering a combination of different manoeuvres a series of measurements can be arranged, which provide sufficient information for an accurate identification of the derivatives. An important advantage of the applied regression technique is that the time sequence of the datapoints is not important, which allows the use of an arbitrary combination of manoeuvres in the analysis.

In order to select an optimal combination of flight test manoeuvres from which the desired derivatives, both longitudinal and lateral-directional, can be determined with a satisfactory degree of accuracy, an investigation was carried out on the NLR moving base simulator. The simulator had been programmed with the Fokker F28 simulation model. The data was analyzed with the PIAS program.

Various types of manoeuvres and combinations of manoeuvres have been evaluated. As a result of this study two sets of manoeuvres were established which appeared to be very promising with a view to provide data from which accurate estimation of the aerodynamic coefficients could be obtained. These sets contained both doublet and multistep input signals, but also other types of manoeuvres were included to attain the proposed objective.

A distinction has been made between manoeuvres for the identification of the longitudinal and of the lateral-directional stability and control derivatives.

4.2.2 Longitudinal derivatives

The manoeuvres investigated for the determination of the longitudinal derivatives were:
- 3211 manoeuvre (multistep elevator input)
- Level turn manoeuvre
- Pull-up/Push-over manoeuvre
- Untrimmed flight

In the following a brief description is given of each manoeuvre individually:

3211 manoeuvre (multistep elevator input)

The 3211-signal consists of a series of alternating step inputs of which the duration satisfies the ratio 3:2:1:1 (i.e. 3 time units positive, 2 negative, 1 positive and 1 negative). Because of its simplicity the manoeuvre is very easy to perform manually. The multistep signal has a rather wide bandwidth compared to the other input signals. This allows an effective excitation of the aircraft over a large frequency range. By proper selection of the time unit the maximum of the energy spectrum can be concentrated around the short period frequency of the aircraft.

Figure 8a presents time histories of this input signal and of the resulting aircraft response. Since there is a strong resemblance between the $\dot{\alpha}$ and q motion variables, it is unlikely that a good estimate of the $\dot{\alpha}$ and q derivatives can be obtained from this type of manoeuvre.

Level turn manoeuvre

During this manoeuvre the aircraft is banked into a 45 degree roll attitude, which is kept steady for several seconds, after which the aircraft is rolled to a 45 degree bank into the opposite direction. After some seconds this steady turn is completed with a roll to the initial wings level condition. A constant altitude is maintained during the manoeuvre by the application of additional power. The result is an S-type flight path in the horizontal plane whereby the headings at beginning and end of the manoeuvre are approximately equal.

The objective of this manoeuvre is to obtain a decoupling of the $\dot{\alpha}$ and q motion. During the steady part of the turns the angle of attack is constant, while the pitch rate follows from:

$$q = \frac{g}{V} \tan \phi \sin \phi \qquad (4.1)$$

Note that this manoeuvre always yields positive pitch rates q for both positive and negative bank angles ϕ. Time histories of this manoeuvre are presented in figure 8b.

It should be emphasized that the measurements do not only include the quasi-steady parts of the manoeuvre, but also the non-steady initiation and roll-out of the turn.

Pull-up/push-over manoeuvre (pupo)

During this manoeuvre, also called a "roller-coaster" manoeuvre, the aircraft is pulled up with a certain normal acceleration e.g. 1.5 g and after that pushed over with about 0.5 g. For configurations in the low speed regime the speed will vary considerably, whereas for high speed the speed remains almost constant. For low speeds it is recommended to carry out this manoeuvre in the reversed sequence in order to prevent the aircraft from stalling. Time histories of a pupo are shown in figure 8c. This figure shows that $\dot{\alpha}$ and q are very different in a pupo, but that there is a strong correlation between α and q.

In Appendix A it is shown that the same relation exists between α, $\dot{\alpha}$ and q in a 3211 as in a pupo. In a level turn this relation is different (see figure 9a), so it can be expected to yield the additional information. In addition the ratio between the pitch rate and the normal acceleration is also more favourable in the level turn (see figure 9b). Therefore, the pupo can only be recommended in the case that a strong interference between the lateral and the longitudinal motion is expected in the level turn.

Untrimmed flight

In all the previous manoeuvres the stabilizer setting was kept constant, consequently these manoeuvres do not provide the necessary information for the determination of the stabilizer derivatives. In order to obtain this information, an untrimmed flight manoeuvre was introduced. During this manoeuvre the stabilizer angle is changed by means of the trim switch, while at the same time the pitching moment balance is maintained by an equivalent amount of elevator deflection. This exchange between elevator and stabilizer control is performed over a large range of stabilizer angles to both sides of the initial trim condition. The aircraft state variables such as airspeed, attitude and altitude are kept as close as possible to the initial reference condition. Hence this is more or less a steady flight condition and only information about the (ratio of) the control derivatives can be derived.
Summarizing it can be stated that the complete set of longitudinal stability and control derivatives can be obtained from a 3211, a level turn and an untrimmed-flight manoeuvre.

4.2.3 Lateral-directional derivatives

The manoeuvres investigated for the determination of the lateral-directional stability and control derivatives were:
- roll manoeuvres
- rudder doublets

A brief description of these manoeuvres is given below.

Roll manoeuvres

Roll manoeuvres have been included for the determination of the aileron and roll rate derivatives. The manoeuvre starts with an aileron step input to the left, whereby the rolling motion is continued until a bank angle of about 45 degrees is reached. Then the ailerons are neutralized for a short time, after which an aileron step input to the right is applied, until a wings-level attitude is reached. Finally the same procedure is repeated rolling to the right. Thus each roll manoeuvre includes four step aileron inputs and covers a bank angle range from 45 to -45 degrees.

Time histories of the motion variables for a typical roll manoeuvre are presented in figure 10a.

Rudder doublets

For the determination of the rudder and yaw rate derivatives a rudder doublet has been included in the set of lateral-directional flight test manoeuvres. The duration of the doublet signal is adapted to the frequency of the dutch roll mode of the aircraft. Figure 10b shows a typical aircraft response to a rudder doublet.

During a rudder doublet the $\dot{\beta}$ are r signals are very similar (although in opposite phase). Hence it is not possible to identify the individual stability derivatives for both the $\dot{\beta}$ and r derivatives from only a rudder doublet. This correlation between $\dot{\beta}$ and r is much less during a roll manoeuvre, consequently the corresponding derivatives can be identified better in this manoeuvre. This is true notwithstanding the fact that magnitude of $\dot{\beta}$ and r is much less during a roll manoeuvre.

The results of the simulator investigation confirm that the use of a combination of a roll manoeuvre and a rudder doublet yields good estimates not only for the rudder and aileron derivatives, but also for the rate and sideslip derivatives. Another interesting result was that the addition of measurements from steady sideslips did not improve the results at all, consequently the recommended set of lateral-directional stability and control manoeuvres consists of roll manoeuvres and rudder doublets.

4.3 Test results

4.3.1 Introduction

The various manoeuvres have been evaluated for different flight conditions and aircraft configurations during the flight simulator investigation. The 23 recorded motion and control variables were analyzed with the PIAS program. A limited flight test program was carried out subsequently, with the Fokker F28-A1 prototype aircraft, in order to check the simulation results with results obtained in the real flight environment.

Flight test experience regarding the determination of the longitudinal stability and control derivatives was already obtained during the previous flight test program whereby results obtained from the sinusoidal elevator input signals were evaluated. Therefore, during the recently executed flight tests emphasis was given to the manoeuvres concerning the determination of the lateral-directional stability and control derivatives.

In the present section the results of both simulator tests and flight tests will be discussed.

4.3.2 Longitudinal

The simulator tests, concerning the determination of the longitudinal stability and control results included the three considered manoeuvres.
- 3211 elevator manoeuvre
- level turn manoeuvre
- pull-up/push-over manoeuvre

Furthermore the ratios between the stabilizer and elevator derivatives were determined from a simulated untrimmed flight manoeuvre.

The measurement data were analyzed for the three aerodynamic models viz. the drag, lift and pitching moment model. In order to improve the realism of the simulator measurements, noise was added to the synthetic data. Both individual manoeuvres and combinations of manoeuvres were processed. In total 7 different cases (3 individual and 4 combinations of manoeuvres) were considered hereby.

By way of illustration in figure 11 the pitching moment results are shown for a high speed cruise condition and forward center of gravity. The plots in this figure show clearly that, in order to obtain the most accurate coefficients, combinations of manoeuvres have to be processed, instead of making separate analyses for individual manoeuvres. Moreover it appears that a combination has to include a level turn manoeuvre (see nr. 5, 6 and 7), since the combination of 3211 and pupo manoeuvre (nr. 4) does not yield satisfactory results. An explanation for this has been given in appendix A. Similar results were obtained for the coefficients of the lift and drag models.

4.3.3 Lateral-directional

Simulator tests were also carried out for the roll manoeuvres and the rudder doublets, which are intended to provide the lateral-directional stability and control derivatives. Measurements were executed for flight conditions and aircraft configurations that covered the greater part of the flight envelope. Noise was added to the recorded (noise-free) simulation data, before the coefficients in the side force, rolling moment and yawing moment models were determined by the regression program.

As an example the estimated coefficients of the yawing moment model are presented in figure 12, which belong to a high speed cruise condition with forward center of gravity.
The plots show the various coefficients as derived from processing the data of an individual manoeuvre (nr. 1 and 2), and of an analysis of a combination of both manoeuvres (nr. 3). These results show that processing of the data of two different manoeuvres together yield a better result than the processing of each manoeuvre individually. Although it is not shown by these plots, it turned out that the addition of data from steady sideslips has no effect on the final result.

In a following flight test program with the Fokker F28 A1 prototype aircraft the results of this simulator investigation have been validated. As an example of these flight test results the estimated coefficients of the lateral-directional model have been presented in figure 13 for a flight condition which is almost the same as that of the simulator results discussed previously. The main difference between the simulated and the flight test condition is a difference in centre of gravity position (simulated: forward c.g. flight test: aft c.g). The reference values depicted in the plots have been derived from the Fokker F28 flight simulator data.

Results have been presented for two rudder doublets and two roll manoeuvres. Both results of individual manoeuvres (nrs. 1 and 2 in the plots) and results of combinations of different manoeuvres (nr. 3) have been depicted. The result of the combination of two rudder doublets and two roll manoeuvres is indicated by nr. 4.

Also for this case applied that the best results are obtained by processing combinations of different types of manoeuvres. Taking into account the magnitudes of the standard deviations, a comparison with the reference values learns that all identified coefficients except the yaw rate derivatives, are in good agreement with the reference values. Moreover the consistency of the results is also satisfactory.

So far as the discrepancies in the yaw rate derivatives are concerned, it has to be remarked that the considered model did not include $\dot{\beta}$-terms. The differences between the reference values and the quantities derived from the flight test measurements may partially be attributed to $\dot{\beta}$ effects. Since the flight simulator model does not incorporate $\dot{\beta}$ effects, these differences did not appear in the simulator results of figure 12. It has to be remarked, however, that the reference values for the yaw rate derivatives, such as C_{Y_r} and C_{ℓ_r}, have been derived from theoretical methods of which the accuracy is uncertain.

Finally the flight test results confirm the results of the flight simulator investigation, concerning the importance of processing combinations of different types of manoeuvres.

5. CONCLUSIONS

The research described in this paper applied the Two-Step method to extract performance and stability and control characteristics from dynamic manoeuvres for a jet transport aircraft. The following conclusions can be drawn based on the results reported in this paper:

- Successful application of dynamic flight test techniques requires an accurate instrumentation system, proven flight test manoeuvres and sophisticated data processing and analysis software.
- Performance characteristics can be determined accurately from dynamic flight tests. The accuracy is only limited by the uncertainty in the calculation of the engine thrust and by changes in the wind velocity. The application of inertial navigation equipment allows a further improvement in the latter factor.
- The determination of stability and control characteristics from a suitable selection of simple, manually flown manoeuvres is possible by combining the manoeuvres in the analysis.
- The Two-Step method makes the rapid evaluation of a large number of alternative aerodynamic models possible. Due to the interactive nature of the analysis program full use can be made of the engineering judgement of the analyst.
- The use of a moving-base simulator is of great value in the preparation of dynamic flight tests. It allows the evaluation of the manoeuvres as well as the familiarization of the pilot in a controlled environment.

6. POSTSCRIPT

Currently work is going on at NLR in two major areas. The first is the evaluation of the method for turboprop powered aircraft. A first flight test in a Fokker F27 is now being analyzed. The second is the improvement of the processing and analysis software which will allow the operational use of this method.

The main emphasis in the improved software will be on the traceability of the results. The results do not only depend on the flight test data, but also on a large body of additional information, such as calibration data, position error corrections, sensor positions, data selections, processing options, a priori aerodynamic models used in the reduction program, e.g. location, etc. This problem will be solved by archiving the final results together with the original flight test data and all additional information necessary to reproduce these results. In the process an attempt will be made to reduce the manual labor in the operation of the programs and improve the user interface.

7. REFERENCES

1. Gerlach, O.H., Analysis of a possible method for the measurement of performance and stability and control characteristics of an aircraft in non-steady symmetric flight (in Dutch). Delft University of Technology, Department of Aerospace Engineering, Report VTH-117, 1964.
2. Maine, R.E. and Iliff, K.W., Identification of dynamic systems. AGARD Flight Test Techniques Series AGARDograph, AG-300 (to be published).
3. Breeman, J.H., Parameter identification results of tests in non-steady symmetric flight with the Hawker Hunter Mk VII, 1983, NLR TR 83042 L.
4. Breeman, J.H. and Simons, J.L., Evaluation of a method to extract performance data from dynamic manoeuvers for a jet transport aircraft, 11th Congres of the ICAS, Lisbon, 1978 (NLR MP 78021 U).
5. Pouwels, H., Instrumentation for the determination of aircraft performance from dynamic maneuvers. ISA 25th International Instrumentation Symposium, Anaheim, 1979 (NLR MP 79001 U).
6. Wilt, M. v.d., Flight path reconstruction of symmetric unsteady flights, 1976, NLR TR 76133 U.
7. Jonkers, H.L., Application of the Kalman filter to flight path reconstruction from flight test data including estimation of instrumental bias error corrections. Delft University of Technology, Department of Aerospace Engineering, Report VTH-162, 1976.
8. Mulder, J.A., Jonkers, H.L., Horsten, J.J., Breeman, J.H., Simons, J.L., Analysis of aircraft performance, stability and control measurements. AGARD Lecture Series LS-104 on Parameter Identification, 1979.
9. Boer, I. de, Determination of performance and stability characteristics from dynamic longitudinal manoeuvres with a Fokker F28 transport aircraft; Execution of the flight trials, 1978, NLR TR 78005 L.
10. Nieuwpoort, A.M.H., Breeman, J.H., Determination of performance and stability characteristics from dynamic longitudinal manoeuvres with the Fokker F28 transport aircraft; Summary of flight test results. 1983, NLR TR 83126 C.
11. Plaetschke, E., Schulz, G., Practical input signal design. AGARD Lecture Series LS-104 on Parameter Identification, 1979.
12. Plaetschke, E., Mulder, J.A., Breeman, J.H., Flight test results of five input signals for aircraft parameter identification. IFAC Symposium on Identification and System Parameter Estimation, Washington, 1982.

TABLE 1

Repeatability of the measured polars

polar: $C_D = C_{D_0} + \beta C_L^2$

configuration	standard deviations	
	$\sigma_{C_{D_0}}$ (%)	σ_β (%)
1	0.5	0.9
2	4.1	2.4
3	0.4	2.5
4	2.1	3.8
6	1.2	2.3
7	1.4	0.6
8	1.7	1.8
9	0.3	2.1
11	1.2	1.8
total	(1.4 ± 1.2)	(2.0 ± 0.9)

APPENDIX A

Relation between α, $\dot{\alpha}$ and q in the longitudinal manoeuvres

In symmetric manoeuvres, such as the 3211 and the pupo, the elevator input causes an increase in lift

$$\Delta L = m\, a_n$$

in which

$$\Delta L = \tfrac{1}{2}\rho V^2 S\, C_{L_\alpha}\, \Delta\alpha$$

and

$$a_n = V\dot{\gamma} = V\,(q-\dot{\alpha}) \quad .$$

Hence

$$\frac{\frac{q\bar{c}}{V} - \frac{\dot{\alpha}\bar{c}}{V}}{\Delta\alpha} = \frac{\rho S \bar{c}}{2m}\, C_{L_\alpha} = \frac{C_{L_\alpha}}{2\mu_c} \quad . \tag{A.1}$$

Since this relation holds for both the 3211 and the pupo manoeuvre, it is clear that for C_{L_α} = constant and for μ_c = constant the identifiability of the stability derivatives like C_{m_α}, $C_{m_{\dot{\alpha}}}$ and C_{m_q} from a 3211 or a pupo or from a combination of both manoeuvres will be poor.

The lift increase during the steady part of a level turn with bank angle ϕ satisfies the equation:

$$\Delta L = m\, g \left(\frac{1}{\cos\phi} - 1\right)$$

and also

$$\Delta L = \tfrac{1}{2}\rho V^2 S\, C_{L_\alpha}\, \Delta_\alpha \quad .$$

Hence

$$\Delta\alpha = \frac{2\, m\, g}{\rho V^2 S\, C_{L_\alpha}} \left(\frac{1}{\cos\phi} - 1\right). \tag{A.2}$$

For the pitch rate during the turn applies

$$q = \frac{g}{V} \tan\phi \sin\phi = \frac{g}{V}\,(1-\cos^2\phi)/\cos\phi \tag{A.3}$$

Dividing (A.3) by (A.2) yields

$$q/\Delta\alpha = \frac{\rho\, V\, S}{2m}\, C_{L_\alpha}\,(1+\cos\phi)$$

or

$$\frac{q\bar{c}/V}{\Delta\alpha} = \frac{C_{L_\alpha}}{2\,\mu_c}\,(1+\cos\phi) \tag{A.4}$$

A comparison of expression (A.4) with the corresponding expression for that part of the pupo (A.1) where the $\dot{\alpha} = 0$, shows that the $q\bar{c}/V/\Delta\alpha$ ratios for the two manoeuvres differ by a factor $1+\cos\phi$. This relation is shown in figure 9a. The ratio is about 2 for small bank angles and reduces to 1 for large bank angles, which means that in the latter case the identification of C_{m_α}, $C_{m_{\dot{\alpha}}}$ and C_{m_q} will again be poor. Although the $1+\cos\phi$ relation suggests that bank angles close to zero would yield the largest separation between the derivatives, it is clear that this also means very small pitch rates. The simulator tests showed that a bank angle of 45 degrees yields a reasonable compromise.

The pitch rate during the section of the pupo were $\dot{\alpha} = 0$ equals

$$q = \frac{g}{V}\,(n-1) \tag{A.5}$$

whereas for the level turn the pitch rate amounts to

$$q = \frac{g}{V}\,(n-1/n) \tag{A.6}$$

Figure 9b presents qV/g as a function of n for both types of manoeuvres, which shows that the level turn is also more efficient in producing pitch rates than the pupo.

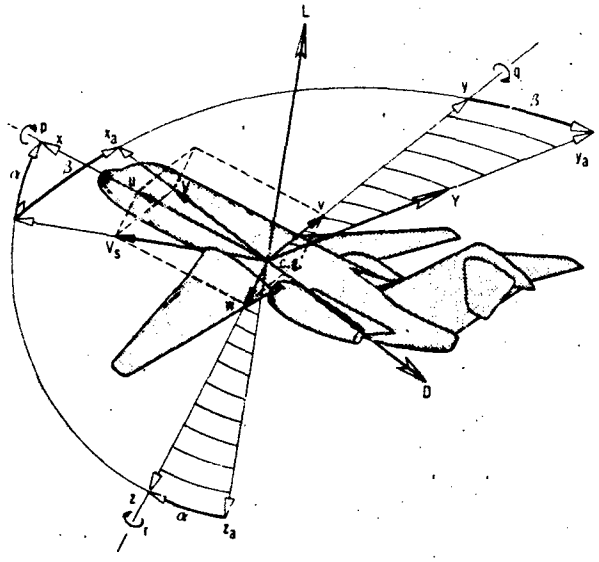

Fig. 1 Body fixed and air-trajectory reference frames

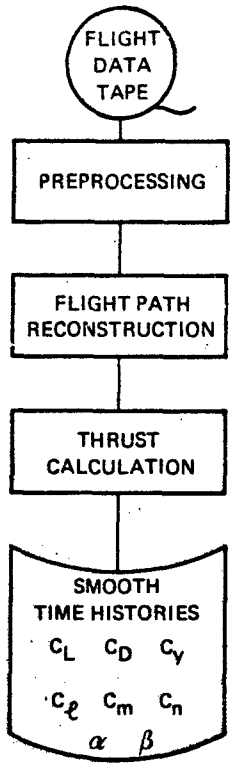

Fig. 2a Processing of dynamic manoeuvres

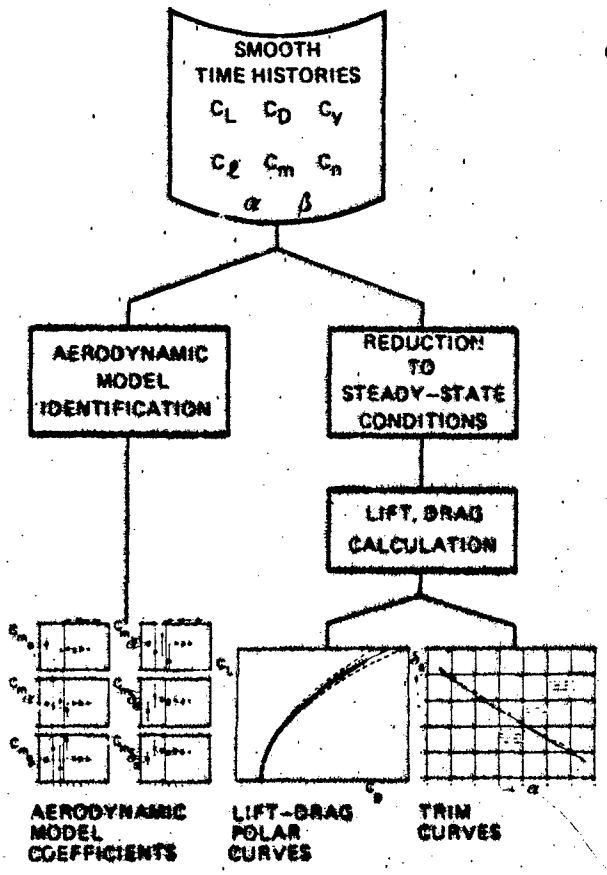

Fig. 2b Analysis of dynamic manoeuvres

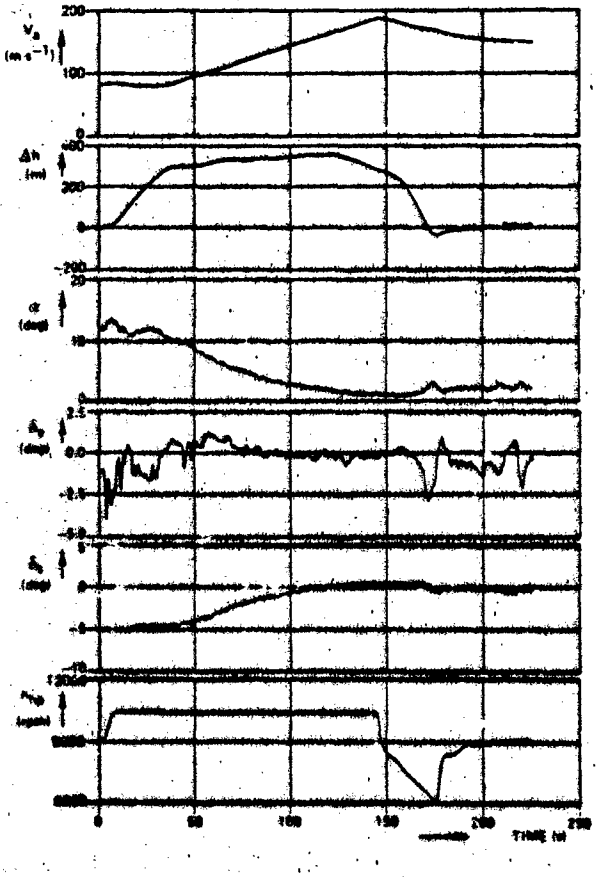

Fig. 3 Time histories of the motion and control variables during an accelerated run

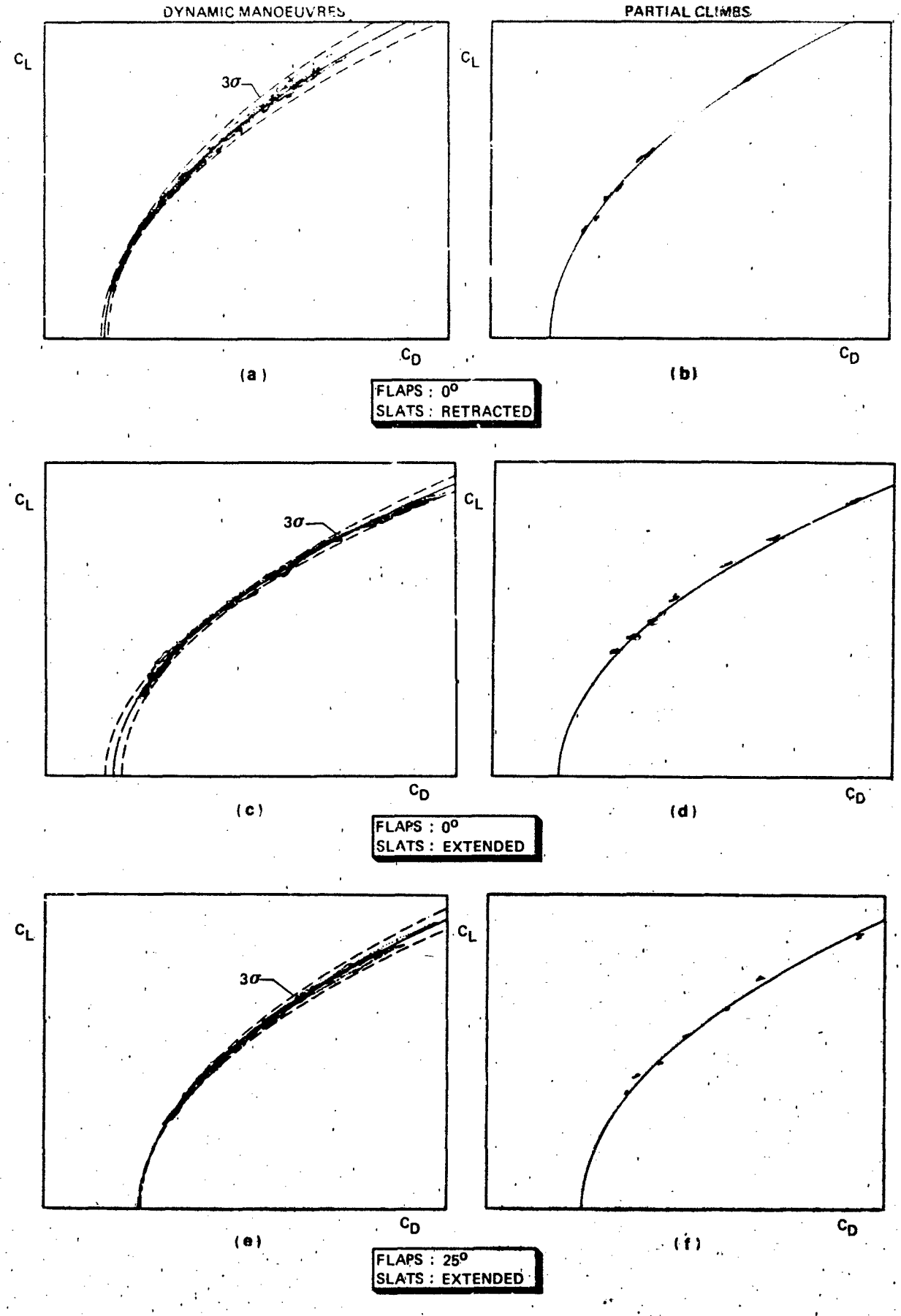

Fig. 4 Survey of the lift-drag polar measurement results

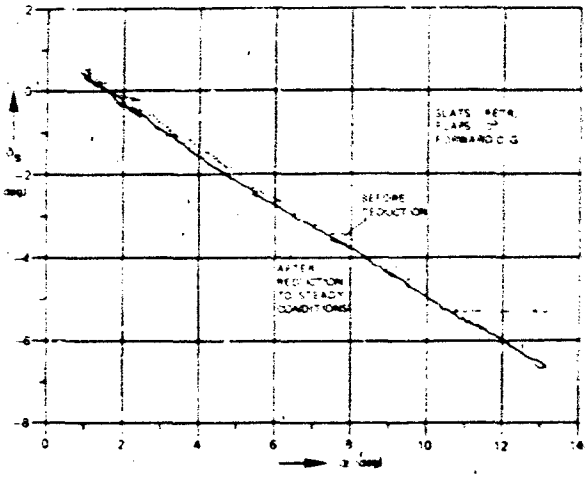

Fig. 5 Stabilizer trim curve

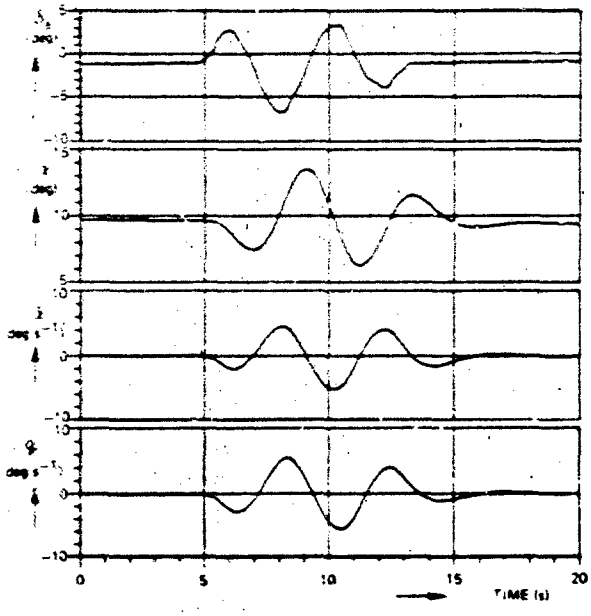

Fig. 6 Time histories of the sinusoidal elevator input signals and the resulting aircraft response

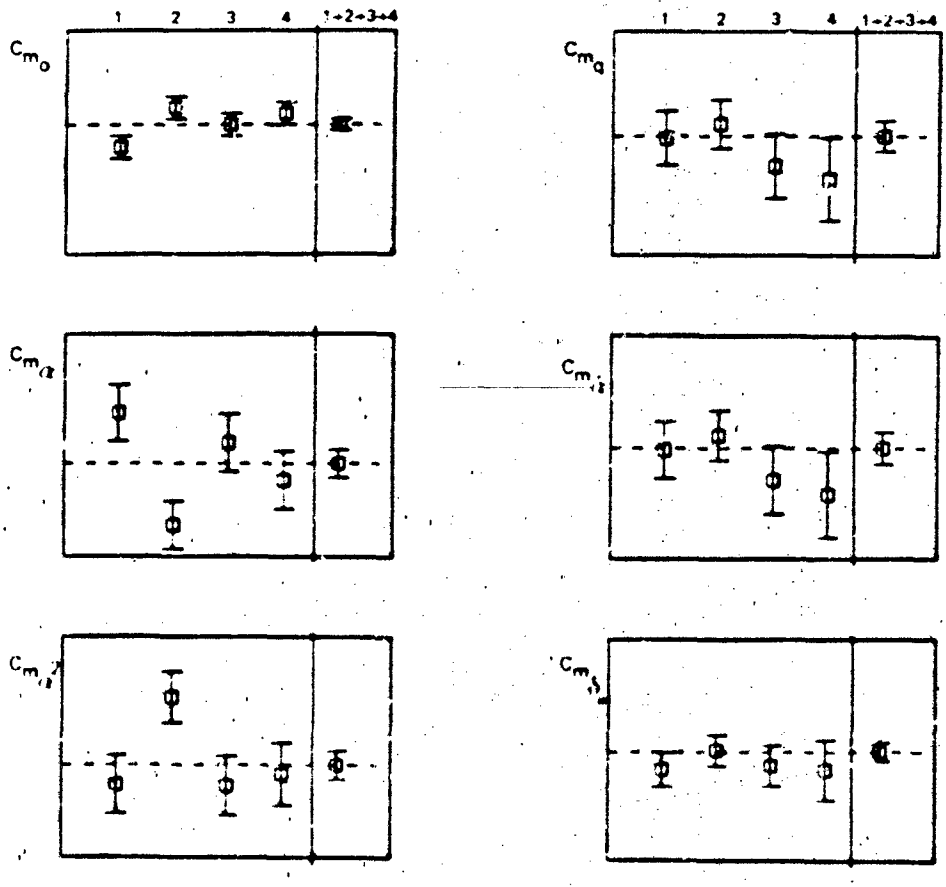

Fig. 7 The coefficients of the pitching moment model as obtained by the sinusoidal elevator input signal from flight test measurements

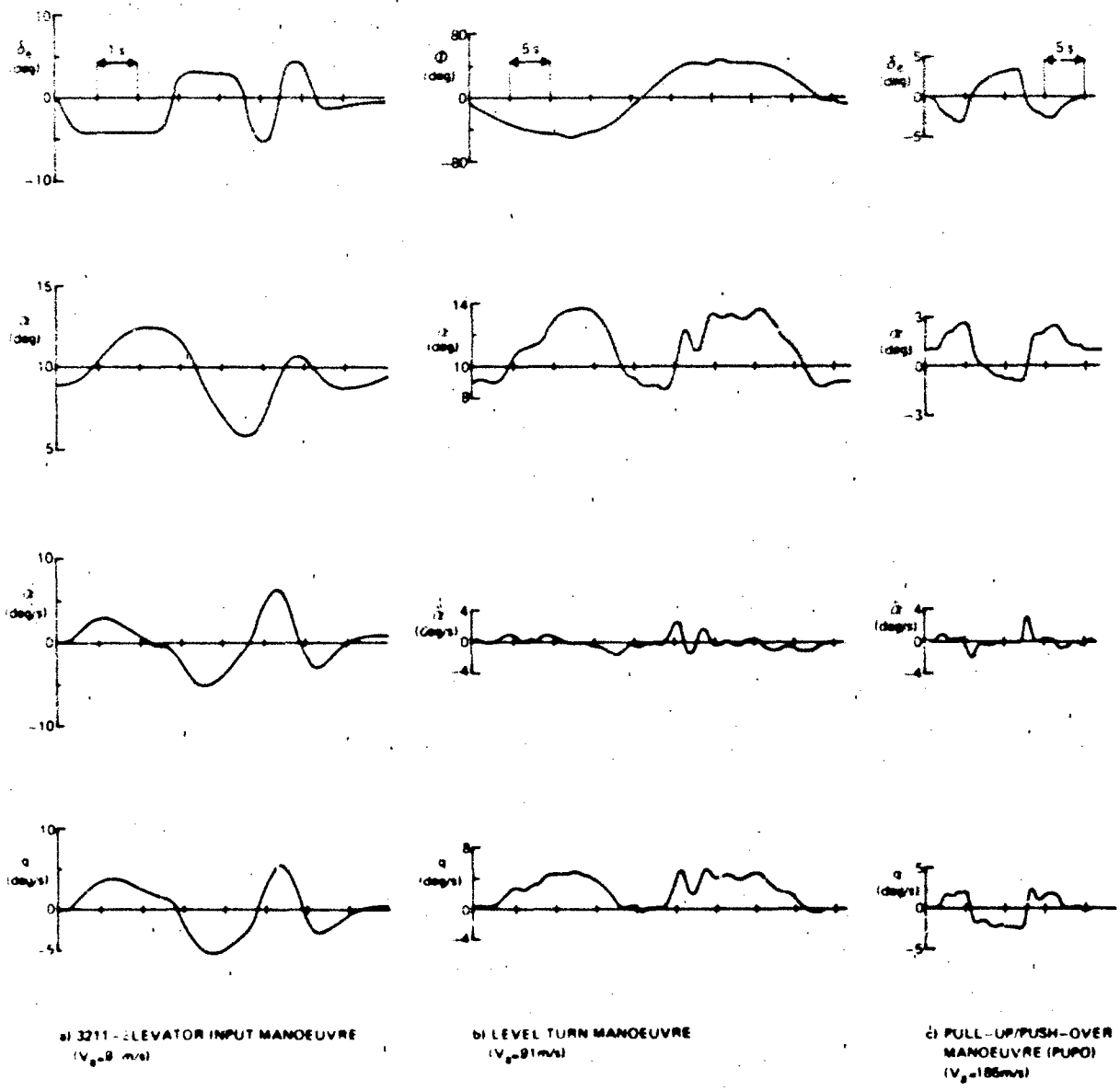

Fig. 9 Time histories of aircraft response during the manoeuvres considered for the determination of the longitudinal stability and control derivatives

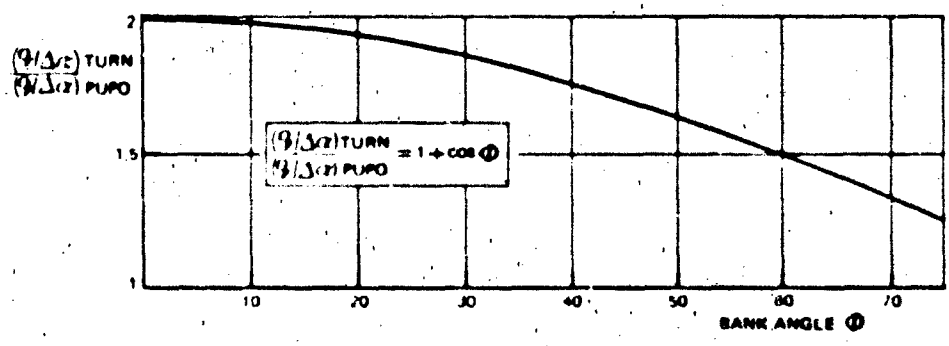

Fig. 9a Comparison between the $\frac{\partial n}{\partial \alpha}$ ratios for the level turn and the pull-up/push-over (pupo) manoeuvres

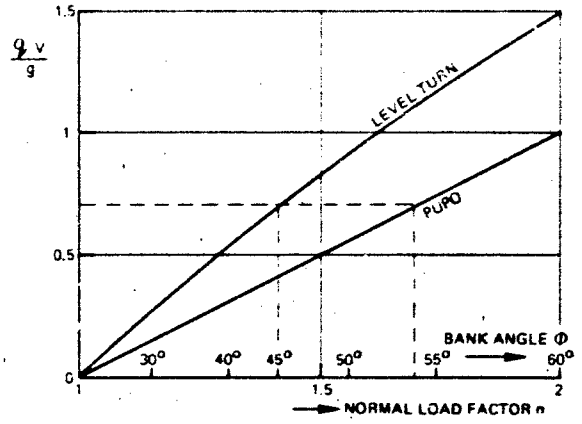

Fig. 9b Amount of pitch rate produced by the level turn and the pull-up/push-over manoeuvres as a function of the normal load factor

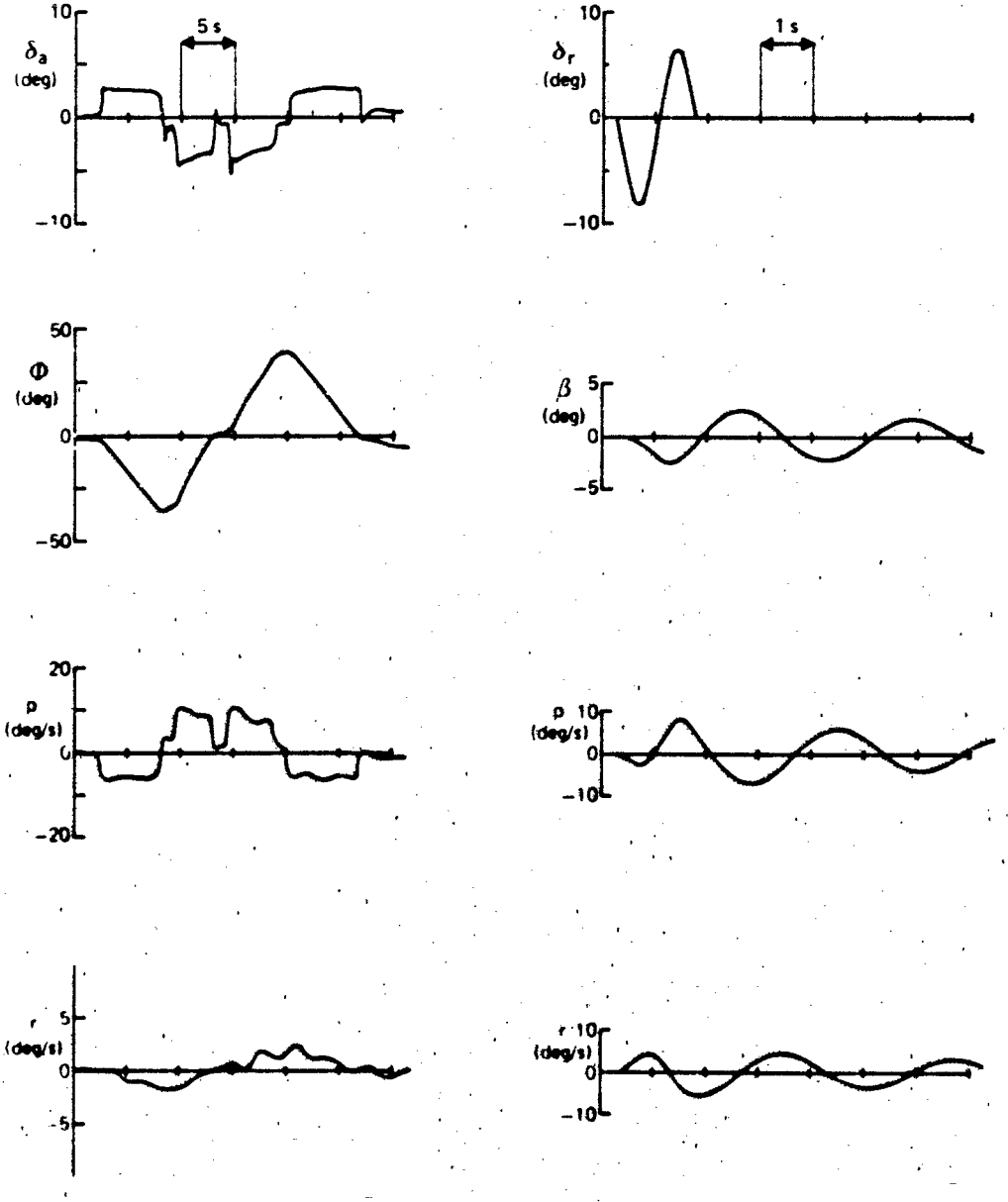

a) ROLL MANOEUVRE (V_a=185m/s)

b) RUDDER DOUBLET (V_a=185m/s)

Fig. 10 Time histories of the aircraft responses to the manoeuvres considered for the determination of the lateral-directional stability and control derivatives

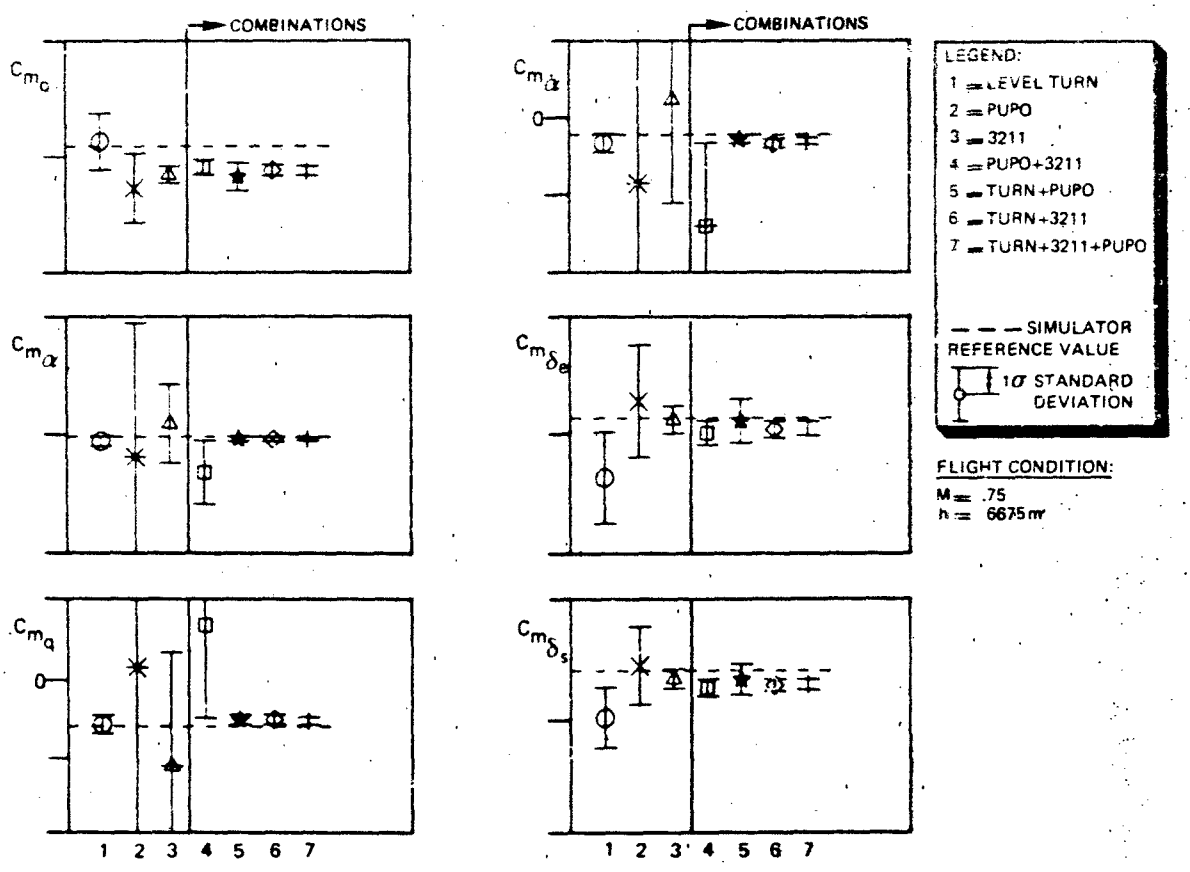

Fig. 11 Coefficients of the pitching moment model as derived from the simulated data

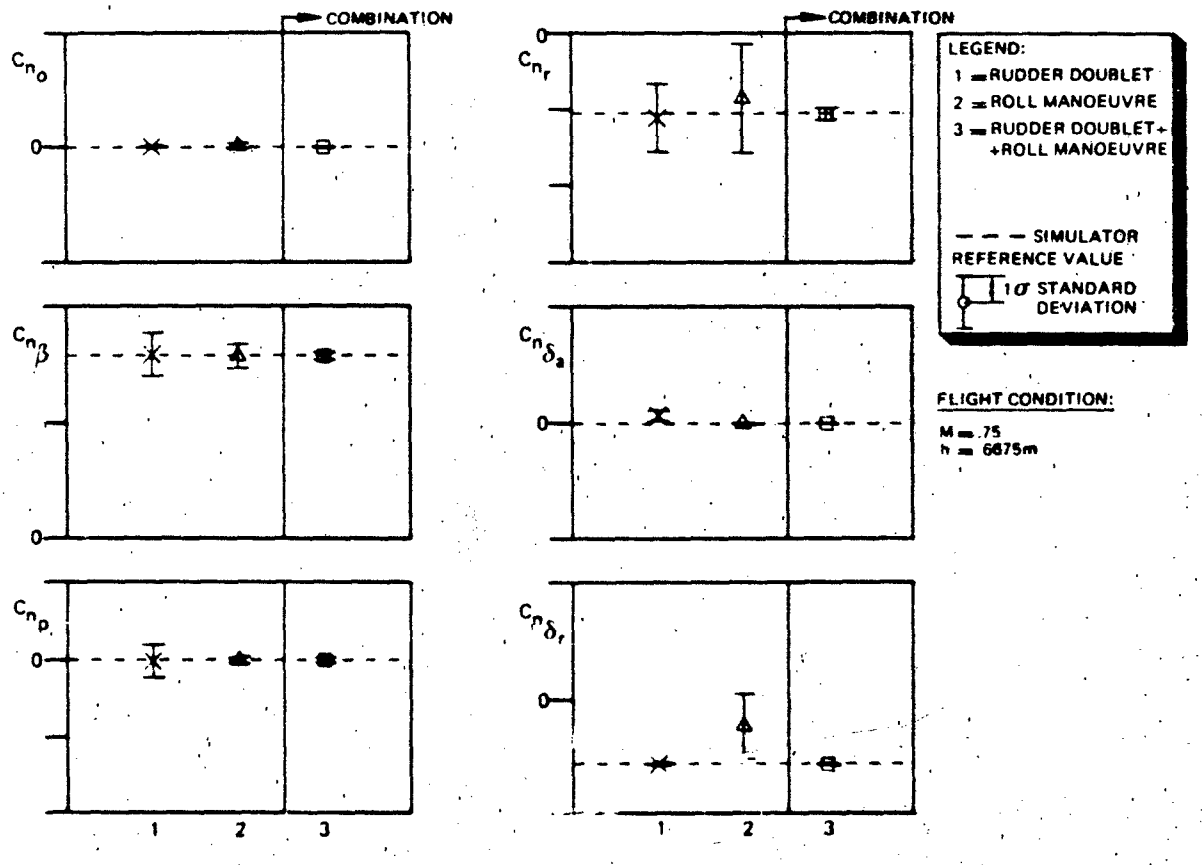

Fig. 12 Coefficients of the yawing moment model as derived from the simulated data

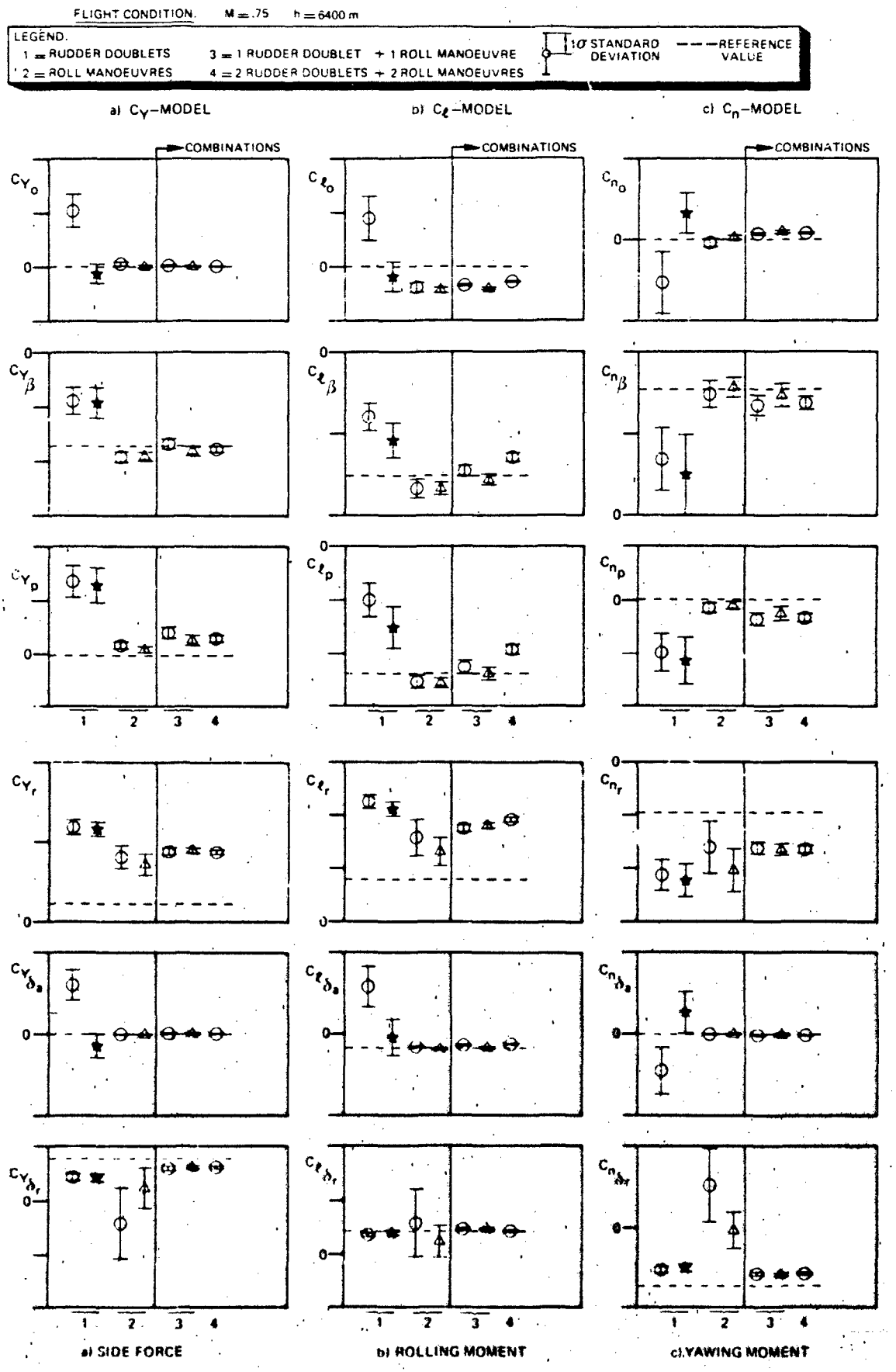

Fig. 13 Coefficients of the lateral-directional model as derived from flight test measurements

APPLICATION OF ADVANCED PARAMETER IDENTIFICATION METHODS FOR FLIGHT FLUTTER DATA ANALYSIS WITH COMPARISONS TO CURRENT TECHNIQUES

Henry J. Perangelo
Assistant Director, Test Systems
Grumman Data Systems Corporation
Calverton, New York

Paul R. Waisanen
Manager, Flight Dynamics & Loads, Flight Test Department
Grumman Aerospace Corporation
Calverton, New York

SUMMARY

Grumman has been pursuing the implementation and evaluation of advanced parameter identification software for use in flutter test data processing operations at its Automated Telemetry Station. They have been motivated by aircraft design tending toward thin, lightweight aircraft structures, which make it difficult to use authoritative shaker systems, and the continuing development of high-speed digital computer technology. Started in 1981, this development activity is aimed at establishing an on-line processing capability, in the 1985 time frame, that will initially use the maximum likelihood parameter identification algorithm in conjunction with a detailed physical aeroelastic aircraft model to perform optimal flutter test data analysis. Extended Kalman filtering is being considered for eventual use as a second advanced parameter identification method. A mathematical description of the advanced parameter identification approach and Grumman's current least-squares flutter analysis procedures are presented. In addition, a comparison between this current analysis capability and prototype code for the maximum likelihood parameter identification algorithm on response data excited randomly (via atmospheric turbulence) and by swept frequency shaker inputs indicates a significant improvement in analysis results with the advanced method.

1. INTRODUCTION

Grumman Aerospace Corporation has been using parameter identification methods to analyze flight test flutter response data from the early 1970s when its Automated Telemetry Station in Calverton, New York, first became operational. This facility was built to reduce the time required to complete the F-14A and subsequent aircraft flight test programs. In addition to telemetry data acquisition, mass data storage, and visual display equipment, the station contains a high speed digital mainframe computer to allow ground personnel to analyze aircraft flight test data as it is being generated. This on-line processing system was designed to enable test engineers to use relatively complex analytical algorithms on telemetered test data to maximize the answers obtained during a flight and provide a means for achieving rapid envelope expansion.

Before the availability of on-line digital-computer-aided data analysis, flutter testing methods relied primarily on manual and analog techniques such as log decrement signatures from multiple abrupt control surface inputs or numerous shake and stops, reciprocal amplitude trends and extrapolations using mass shakers, vector plotting techniques, etc. These methods for determining aeroelastic stability were adequate for handling the classical analysis of clean signals which contained modes that were not strongly coupled. But, they degraded significantly in the presence of turbulence, or on multimodal or highly damped response signals. It was obvious to Grumman that computer compatible versions of these older methods could not satisfy the F-14A test program requirements for a fast and accurate flutter data analysis capability.

In 1969, a parameter identification method was proposed for the eventual analysis of F-14A flutter response data in the Automated Telemetry Station. The proposed technique used a linear system difference-equation model of flutter dynamics and a least-squares equation-error identification algorithm

to extract modal resonant frequency and damping coefficient information from digitally filtered excitation and response data. This approach was readily accepted because of its clear superiority over the older methods. The technique was computationally efficient and could handle fast shaker sweeps (2 to 70 Hz in 15 sec) enabling it to rapidly analyze data in a near-real-time environment. Variable sized difference equation models could be used to process multimodal (highly coupled) response data. Highly damped response signals could also be analytically handled. Starting in 1971 this technique was successfully used on the F-14A flutter program where the bulk of the data consisted of swept frequency shaker excited signals having a relatively high signal to noise ratio. As initially installed on a Control Data Corporation 6400 computer, analysis time per 15 sec sweep typically averaged less than 1 min with less than one-half of the computer's resources devoted to the on-line processing task.

Development and refinement of the least-squares difference-equation identification software continued at Grumman through 1976. Most of the development activity was centered on reducing algorithm susceptibility to noise effects and providing options to analyze data excited via random sources such as atmospheric turbulence. This processing capability was necessary in order to handle test situations where authoritative shaker systems were not available or economically feasible. The ability of the technique to handle noisy data was significantly improved by optionally replacing filtered response and excitation data with specially computed cross and autocorrelation functions of these signals. However, the proper use of correlation methods generally required longer data records and a significant increase in computational time. Reference 1 gives a detailed description of how cross-correlation, autocorrelation, random decrement signature, and frequency domain windowing techniques were used in conjunction with the least-squares difference-equation identification approach to determine the frequency and damping of flutter modes from data excited either by deterministic or random means. With the exception of some software repackaging and minor operational modifications aimed at simplifying software use (completed by 1976) the analytical capabilities defined in Reference 1 essentially reflect Grumman's current techniques for on-line flutter test data processing. A mathematical description of this processing capability is contained in subsection 3.3.

The long-standing goals for on-line flight test data analysis are to improve safety of flight and reduce overall program cost. In aircraft flutter testing, improved safety of flight can be realized by implementing more comprehensive analysis methods for accurately determining aeroelastic stability at a given test point and for predicting the stability margin at the next flight condition. Cost reduction can usually be tied to shortening the flight test program and minimizing the requirement for high quality shaker systems. In 1981, Grumman initiated an advanced development project aimed at providing a state-of-the-art flutter test data analysis capability for both on-line and off-line support of aircraft test programs for the mid-1980s and beyond. A major improvement in flight flutter data analysis capability was needed with new aircraft designs tending toward thin, lightweight aerodynamic structures that inhibited installation of traditional forced excitation devices. Grumman's specific requirement is for analysis procedures that will handle randomly excited (shakerless) or poor quality shaker excited data in an optimal fashion, in a near-real-time operating environment. An overview of the approach Grumman is pursuing is contained in Section 2. This is followed in Section 3 by a mathematical description of the new and existing techniques. Preliminary analysis results obtained in evaluating the relative accuracy of the new and existing methods are demonstrated in Section 4.

2. ADVANCED FLUTTER DATA ANALYSIS CAPABILITY

Continued advances in high-speed computer technology have made it feasible to consider using advanced parameter identification methods in the on-line analysis of aircraft flutter response data. These advanced methods can be interfaced with detailed physical (engineering) models for aircraft flutter dynamics to produce software capable of performing analysis on shakerless or shaker excited data in an optimal fashion. As long as processed software test results coincide with dynamic model extrapolations, large incremental steps can be taken during aircraft envelope expansion testing. This mode of operation reflects a significant departure from extrapolating measured modal frequency and damping results to obtain estimates for flutter stability margin. Scatter in results extracted from measured data with existing analysis methods (particularly damping values) often makes such predictions risky (see Reference 2). The goal this new approach is to use measured test data to confirm the validity of rigorously derived engineering flutter models. These models would be used as the basic means of making accurate flutter margin projections. Significant discrepancies between projected and measured results would signal an evaluation and possible adjustments to the models to reflect unexpected effects existing in the measured test data.

Figure 1 represents a conceptual overview of the advanced flutter test data analysis capability as it would eventually be used in on-line test support. Most significantly, when engineering flutter dynamic models were available (which would generally be true for Grumman flutter test programs), they would

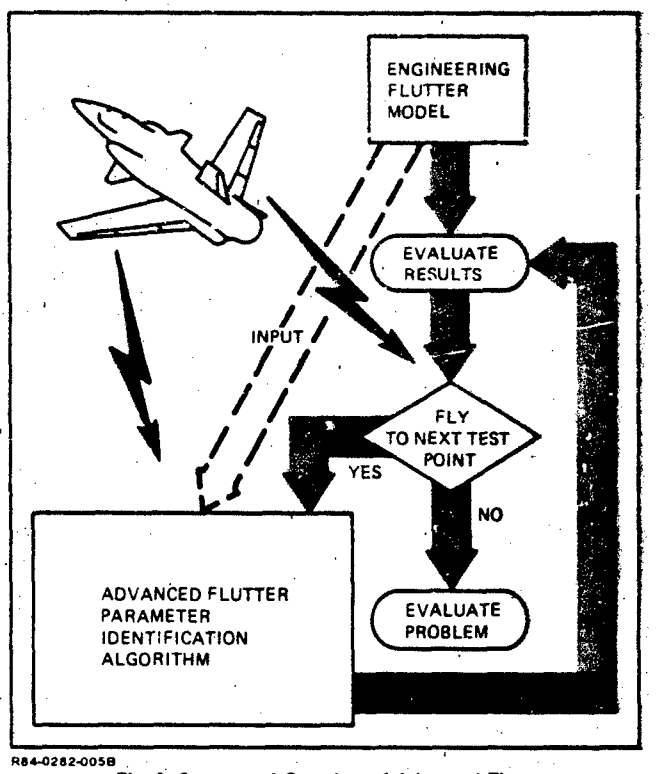

Fig. 1 Conceptual Overview of Advanced Flutter Test Data Analysis Capability

be used to initialize parameter identification software models for analyzing data at specific test points, and to extrapolate anticipated test results at upcoming test points. Agreement between calculated and extrapolated results would allow larger speed increments to be taken during envelope expansion. Thus, the successful tie-in of advanced parameter identification test data analysis with detailed engineering flutter models can result in a large pay-off in reduced test duration, increased safety of flight, and confirmation of flutter dynamic modeling techniques. When engineering flutter models were not available or when minor discrepancies between modeled and parameter identification results existed, smaller steps would be taken during expansion testing. In either event, the improved accuracy of the advanced parameter identification methods would minimize the risk associated with making flutter margin extrapolations from measured modal frequency and damping results.

For flutter test data analysis, the parameter identification process consists of determining estimates for the lumped parameter coefficients in the linear equations of motion for aircraft flutter dynamics at a given test condition. In turn, these coefficients are used to define the margin of stability at the test condition (normally quoted in terms of associated modal damping coefficients). The advanced parameter identification methods being considered by Grumman are the maximum likelihood and extended Kalman filter procedures. To minimize the time required for a prototype capability, Grumman decided, in late 1982, to implement and evaluate the maximum likelihood method (considered to be more computationally efficient and rigorously derived) before proceeding with the extended Kalman filter method. Both of these methods require an initial estimate for the flutter equations of motion which are being implemented to permit the analyst to select variable sized dynamic models. When available, these models would coincide with engineering flutter models for the test conditions to be flown, otherwise, they would be determined from frequency domain analysis of the actual test data or from models supplied by cognizant test personnel.

Maximum likelihood and extended Kalman filter methods have replaced least-squares equation-error parameter identification techniques as state-of-the-art procedures (reference 3), and are likely to remain at the forefront of parameter identification activity for the foreseeable future. Both approaches use a Kalman filter as an inherent part of their identification algorithm. This makes them particularly well suited to identifying system parameters in the presence of both measurement and process noise (in flutter test data analysis gust or atmospheric turbulence is a process noise effect that is often dominant in the response data). Both techniques are capable of analyzing randomly excited (shakerless) flutter response data as well as shaker-excited data in a near-optimal fashion. Optimal implies parameter estimates that are statistically consistent, asymptotically unbiased, and asymptotically efficient in the absence of significant modeling errors.

When compared to least-squares equation-error techniques these advanced parameter identification methods require a significant increase in computational capability. However, Grumman estimates that they can be effectively implemented in support of on-line test data analysis activities on modern high-speed peripheral array processors. When one considers the near-term availability of supercomputers and the relatively long development time required to perfect effective operational software, it is wise to initiate new development activities several years in advance of actual hardware availability. Grumman is presently modernizing its on-line processing capability at the Automated Telemetry Station. The station will be reconfigured to reflect a distributed data processing architecture (see Reference 4) with both minicomputers and mainframes communicating via a high speed data network to mutually participate in on-line test data analysis operations. One of the minicomputers will have a dedicated attached Floating Point Systems 164 array processor to support computationally intensive processing tasks such as the subject advanced flutter data analysis capability. An operational interactive version of this capability on the 164 array processor is presently targeted for late 1984 with on-line capability ready in mid-1985. Network communications with the existing mainframe at the Automated Telemetry Station (presently a Cyber 740) or a remote Cray 1 supercomputer (to be network connected via a microwave link) will be available to supplement data processing capacity.

3. MATHEMATICAL DESCRIPTION

3.1 Physical System Modeling

The aircraft aeroelastic equations of motion and corresponding measurement relationship, comprising the engineering flutter dynamic model, can be defined in the following physical first order form

$$\begin{aligned} A\,\underline{\dot{y}}' + B\,\underline{y}' &= G'\underline{u} + W'\underline{w}_G \,, \\ \underline{z} &= H'\underline{y}' + \underline{\mu} \,. \end{aligned} \tag{1}$$

Actual system measurements are elements of the vector $\underline{z}$. H' is the constant element measurement matrix and $\underline{\mu}$ represents measurement noise. The physical state vector $\underline{y}'$ has elements corresponding to the generalized modal and unsteady aerodynamic coordinates the aeroelastic system. A, B, G', and W' are all treated as constant element matrices. Actually, many elements vary with aircraft altitude and velocity, but these latter quantities are generally held constant over the interval of interest (test condition). The term $\underline{u}$ represents an intentionally introduced excitation vector (elements corresponding to shaker inputs, etc.) while $\underline{w}_G$ represents the process noise excitation vector corresponding to gust effects (atmospheric turbulence) as defined by the equation

$$\underline{w}_G = \frac{\partial}{\partial t}\int_0^t \left[1 - a' e^{\alpha'(t-\tau)}\right] \underline{w}_T(\tau)\, d\tau \,. \tag{2}$$

In the derivation of Eqs. (1) and (2), (see Reference 5) it is assumed that the pressure distribution on the aircraft can be approximated by constant pressures on a set of aerodynamic boxes into which the surface of the aircraft has been subdivided. As defined in Eq. (2), the elements of the vector $\underline{w}_T$ represent the time varying gust intensity on each box. The constants a' and α' are chosen to reflect the indicial response characteristics of the aircraft. The pressure distribution on the boxes is directly proportional to $\underline{w}_G$ with the elements of W', see Eq. (1), providing generalized force scaling.

An alternate form for definition of the engineering flutter dynamic model is

$$\begin{aligned} \dot{\underline{X}} &= F_e\underline{X} + G_e\underline{u} + W_e\underline{w}_b \,, \\ \underline{z} &= H_e\underline{X} + \underline{\mu} \,. \end{aligned} \tag{3}$$

This classical first order form is convenient for numerically calculating system response to known excitation and noise signals. However, in the analysis of flutter flight test data, process and measurement noise effects are unknown. The advanced parameter identification algorithms require integration of the assumed system equations of motion which they accomplish via a Kalman filter state estimator (see Reference 6). This estimator statistically accounts for process and measurement noise effects by considering them to originate from uncorrelated zero-mean Gaussian white sources. In particular, the identification procedures require that the dynamic model of the system be put in the form

$$\begin{aligned} \dot{\underline{x}} &= F\underline{x} + G\underline{u} + W\underline{\eta} \,, \\ \underline{z} &= H\underline{x} + \underline{\mu} \,. \end{aligned} \tag{4}$$

Here $\underline{\eta}$ is a two-element noise vector representing vertical and lateral gust inputs (the effect of longitudinal gusts are generally assumed to be negligible). The important aspect is that both $\underline{\mu}$ and $\underline{\eta}$ be zero-mean uncorrelated Gaussian white noise processes, with

$$\begin{aligned} &E[\underline{\eta}(t_i)] = 0 , \\ &E[\underline{\eta}(t_i)\underline{\eta}^T(t_j)] = Q\delta_{ij} , \\ &E[\underline{\mu}(t_i)] = 0 , \\ &E[\underline{\mu}(t_i)\underline{\mu}^T(t_j)] = R\delta_{ij} , \\ &E[\underline{\mu}(t_i)\underline{\eta}^T(t_j)] = 0 . \end{aligned} \tag{5}$$

for all i, j. Q and R are the process and measurement noise covariance matrices, respectively. $\delta_{ij} = 0$ for $i \neq j$, $= 1$ otherwise. Here, $E[\cdot]$ denotes the expectation of the quantity in brackets.

With today's modern instrumentation systems it is reasonable to assume measurement noise with nearly zero-mean Gaussian white characteristics. Certainly the measurement noise is uncorrelated with the process noise and it is possible to make a reasonable estimate for the R matrix. The process noise represents low frequency gust effects which are correlated. However, this noise effect can be modeled as the output of shaping filters (one for vertical and one for lateral effects) which, when driven by zero-mean Gaussian white noise, approximates the gust spectrum. Conceptually this filtered output represents the gust intensity at a reference spatial location at some instant of time. The gust intensity acting on each aerodynamic box (i.e., the intensity represented by each element of the vector $\underline{w}_T$ in Eq. (2)) is a time delayed version of the filter's output. This delay is a function of aircraft speed and box location on the airframe. The method currently being implemented, is to model the gust shaping filter with a third order transfer function defined by

$$\frac{w_F(s)}{\eta(s)} = K_F \sum_{i=1}^{3} \frac{b_i}{s - a_i} . \tag{6}$$

Here s is the Laplace operator and w_F the shaping filter output at the reference spatial location due to input η.

A number of different gust modeling approaches, of varying complexity, could be used to reflect the lag effects between w_F and the elements of $\underline{w}_T$ and augment Eq. (3) into the form of Eq. (4). At present, only the simplest approach has been utilized, since it is anticipated that detailed modeling of this effect will not significantly improve the performance of the advanced parameter identification algorithms. In this simplified approach, the lag effects between the gust intensity on each aerodynamic box are neglected. Thus all elements of the vector $\underline{w}_T$ are equal to their respective vertical or lateral gust shaping filter output. From Eqs. (2) and (6), it follows that the transfer function between a given element of $\underline{w}_G$ (denoted by the scalar quantity w_G) and either the vertical or lateral white gust source (denoted by the scalar quantity η) is of the form

$$\frac{w_G(s)}{\eta(s)} = \frac{(1 - a')s - \alpha'}{s - \alpha'} K_F \sum_{i=1}^{3} \frac{b_i}{s - a_i} . \tag{7}$$

The simplified gust modeling approach replaces Eq. (7) with a first order filter that matches the roll-off and white noise energy transfer characteristics of the fourth order transfer function defined by Eq. (7). Using this approach allows Eq. (3) to be augmented into the form of Eq. (4) by adding a single state for vertical and a single state for lateral gust effects. If only one of these gust effects is modeled then only a single state need be added.

The advanced parameter identification procedures can be implemented using the model defined by Eq. (4) or some linearly transformed version of this model. One can define a non-singular transformation matrix T such that

$$\underline{x} = T\underline{y} . \tag{8}$$

By applying this transformation on Eq. (4) it follows that

$$\begin{aligned} \dot{\underline{y}} &= T^{-1}FT\underline{y} + T^{-1}G\underline{u} + T^{-1}W\underline{\eta} \\ &= F_0\underline{y} + G_0\underline{u} + W_0\underline{\eta} , \\ \underline{z} &= HT\underline{y} + \underline{\mu} \\ &= H_0\underline{y} + \underline{\mu} . \end{aligned} \tag{9}$$

The dynamic behavior of the systems defined by Eqs. (4) and (9) are identical. The matrix T is selected so that the non-zero elements of the F_0 matrix correspond to the real and imaginary parts of the system eigenvalues in a tridiagonal pattern. The same transformation can also be set to normalize a given column of the G_0 or W_0 matrix to contain 0, 1 pairs corresponding to complex eigenvalues and to contain ones for real eigenvalues (at least for those elements that were not correspondingly zero to begin with). The resulting sparse nature of these transformed matrices and the explicit representation of system eigenvalues allows the identification algorithm to be implemented in a computationally efficient manner.

To obtain the system model defined by Eq. (9) from a supplied engineering dynamic model a number of steps must be taken depending on the starting point. First, if the model is initially defined by Eq. (1), it must be transformed to the classical form denoted by Eq. (3). Since the A matrix in Eq. (1) is not generally invertible, the transformed system could be reduced in dimension. Of course, the engineering model could have been defined in the form of Eq. (3) to begin with. The next step involves augmenting this model for zero-mean Gaussian white gust effects as previously outlined. The final step entails transforming the model to the form implied by Eq. (9), as required for initiation of the parameter identification process in the current implementation. The analyst always has the ability to directly define the system model in this final form, if desired, or when necessary to handle those situations where an engineering flutter dynamic model is not available to begin with.

3.2 Advanced Parameter Identification Methods

3.2.1 *MAXIMUM LIKELIHOOD APPROACH*

A high level mathematical description of the maximum likelihood identification algorithm is covered below. A somewhat more complete explanation, paralleling that given here, is contained in Reference 7. The maximum likelihood parameter identification procedure is based on the premise that the outcome of an experiment depends on unknown parameters (denoted as elements of the vector $\underline{\theta}$). The method effectively estimates the set of parameter elements (denoted as $\hat{\underline{\theta}}$) that maximize the likelihood function, which is taken to be the conditional probability density function of the observations $Z_N = [\underline{z}(t_1), \underline{z}(t_2), \ldots \underline{z}(t_N)]$, given the assumed value of the system parameters. Mathematically, the likelihood function is defined by

$$L(\underline{\theta}) = p[Z_N/\underline{\theta}]$$
$$= \prod_{n=1}^{N} p[\underline{z}(t_n)/Z_{n-1}, \underline{\theta}] , \tag{10}$$

where $p[\cdot]$ denotes the probability density function of the quantity in brackets.

In order to define the actual probability distribution associated with $p[\underline{z}(t_n)/Z_{n-1}, \underline{\theta}]$, it is necessary to first define the expected value of $\underline{z}(t_n)$ given all measurements up to and including the previous data point by

$$E[\underline{z}(t_n)/Z_{n-1}, \underline{\theta}] \equiv \hat{\underline{z}}(n/n-1) , \tag{11}$$

and its covariance by

$$E[\underline{\nu}(n)\underline{\nu}^T(n)] \equiv B(n) , \tag{12}$$

where

$$\underline{\nu}(n) = \underline{z}(t_n) - \hat{\underline{z}}(n/n-1) . \tag{13}$$

The assumption that the innovations $\underline{\nu}(n)$ are Gaussian distributed leads to the following relationship

$$p[\underline{z}(t_n)/Z_{n-1}, \underline{\theta}] = \exp\{-\tfrac{1}{2}[\underline{\nu}^T(n)B^{-1}(n)\underline{\nu}(n)]\}/(2\pi)^{m/2}|B(n)|^{1/2} , \tag{14}$$

where m is equal to the number of measurements. For parameter identification manipulations, it is generally more convenient to deal with the natural log of the likelihood function which is valid since both $L(\underline{\theta})$ and the $\ln L(\underline{\theta})$ have the same extrema. From Eqs. (10) and (14) it follows that the natural log of the likelihood function is defined by

$$J(\underline{\theta}) \equiv \ln L(\underline{\theta}) = -\frac{1}{2}\sum_{n=1}^{N}[\underline{\nu}^T(n)B^{-1}(n)\underline{\nu}(n) + \ln|B(n)|] + \text{constant} . \tag{15}$$

Thus, the problem becomes one of maximizing Eq. (15) with respect to the unknown parameter set $\underline{\theta}$.

Maximizing the likelihood function is an optimization problem. We are using the modified Newton-Raphson technique which is an iterative procedure requiring multiple data passes to establish the parameter set $\hat{\underline{\theta}}$ that maximizes $J(\underline{\theta})$. This is a second order gradient method requiring the computation of the

first and second order partials of $J(\underline{\theta})$. The technique is established by taking the first order Taylor series expansion for the gradient of $J(\underline{\theta})$ about the operating point $\underline{\theta}_k$ (the value of $\underline{\theta}$ determined on the k th data pass) as defined by

$$\underline{g} = \underline{g}_k - M_k(\underline{\theta} - \underline{\theta}_k) , \tag{16}$$

where

$$\underline{g} = \frac{\partial J(\underline{\theta})}{\partial \underline{\theta}} , \quad \underline{g}_k = \left.\frac{\partial J(\underline{\theta})}{\partial \underline{\theta}}\right|_{\underline{\theta}=\underline{\theta}_k} \quad \text{and} \quad M_k = -\left.\frac{\partial^2 J(\underline{\theta})}{\partial \underline{\theta}\,\partial \underline{\theta}^T}\right|_{\underline{\theta}=\underline{\theta}_k} .$$

By setting the left hand side of Eq. (16) to zero, the following recursive relationship for parameter updates is obtained

$$\underline{\theta}_{k+1} = \underline{\theta}_k + M_k^{-1}\,\underline{g}_k . \tag{17}$$

It follows from Eq. (15) that the first order partial of $J(\underline{\theta})$ with respect to the i th element of vector $\underline{\theta}$ is

$$\frac{\partial J}{\partial \theta_i} = -\sum_{n=1}^{N}\left[\underline{\nu}^T\left(B^{-1}\frac{\partial \underline{\nu}}{\partial \theta_i} - \tfrac{1}{2}B^{-1}\frac{\partial B}{\partial \theta_i}B^{-1}\underline{\nu}\right) + \tfrac{1}{2}\,\mathrm{trace}\left(B^{-1}\frac{\partial B}{\partial \theta_i}\right)\right] , \tag{18}$$

where the argument n on variables $\underline{\nu}$ and B have been dropped to simplify notation. For the modified Newton-Raphson technique the second order partials of the innovations $\underline{\nu}$ and its covariance B are dropped. Therefore, the i j th element of the second order partials of $J(\underline{\theta})$ is defined by

$$\frac{\partial^2 J}{\partial \theta_i \partial \theta_j} = -\sum_{n=1}^{N}\left[\frac{\partial \underline{\nu}^T}{\partial \theta_j}B^{-1}\frac{\partial \underline{\nu}}{\partial \theta_i} - \underline{\nu}^T\left(B^{-1}\frac{\partial B}{\partial \theta_j}B^{-1}\frac{\partial \underline{\nu}}{\partial \theta_i} - B^{-1}\frac{\partial B}{\partial \theta_j}B^{-1}\frac{\partial B}{\partial \theta_i}B^{-1}\underline{\nu}\right)\right.$$
$$\left. - \frac{\partial \underline{\nu}^T}{\partial \theta_j}B^{-1}\frac{\partial B}{\partial \theta_i}B^{-1}\underline{\nu} - \tfrac{1}{2}\,\mathrm{trace}\left(B^{-1}\frac{\partial B}{\partial \theta_j}B^{-1}\frac{\partial B}{\partial \theta_i}\right)\right] , \tag{19}$$

where θ_i and θ_j correspond to the i th and j th elements of the parameter vector $\underline{\theta}$. Note that all summations in Eqs. (18) and (19) are with respect to time.

The innovations and innovations covariance are obtained as outputs of a Kalman filter state estimator (see References 6 and 8) corresponding to the linear aeroelastic system defined in Eq. (9). These Kalman filter equations are defined in terms of propagation (or prediction) and measurement update equations as represented by:

- The state propagation equation

$$\underline{y}(n/n-1) = \Phi\,\underline{y}(n-1/n-1) + \Gamma\,G_0\,\underline{u}(n-1) , \tag{20}$$

  where $\underline{y}(n/n-1)$ is the expected value of $\underline{y}(t_n)$ using all measurements up to time t_{n-1} given that $\underline{y}(t_{n-1}) = \underline{y}(n-1/n-1)$. Φ and Γ represent the modeled system transition and superposition matrices, respectively.

- The state covariance propagation equation

$$P(n/n-1) = \Phi\,P(n-1/n-1)\Phi^T + \Gamma\,W_0\,Q\,W_0^T\,\Gamma^T , \tag{21}$$

  where $P(n/n-1)$ is the state covariance matrix at time t_n using all measurement information up to time t_{n-1}. Q represents the process noise covariance matrix identified in Eq. (5).

- The Kalman gain equation

$$K(n) = P(n/n-1)H_0^T\,B^{-1}(n) , \tag{22}$$

  where the innovations covariance is defined by

$$B(n) = H_0\,P(n/n-1)H_0^T + R , \tag{23}$$

  with R being the measurement covariance matrix identified in Eq. (5).

- The state measurement update equation

$$\underline{y}(n/n) = \underline{y}(n/n-1) + K(n)\,\underline{\nu}(n) , \tag{24}$$

  where the innovations at time t_n are given by

$$\underline{\nu}(n) = \underline{z}(n) - H_0\,\underline{y}(n/n-1) . \tag{25}$$

- The state covariance measurement update equation

$$P(n/n) = [I - K(n)H_0]\,P(n/n-1)[I - K(n)H_0]^T + K(n)R\,K^T(n) . \tag{26}$$

Equations (20) through (26) represent the Kalman filter equations needed to define $\underline{\nu}(n)$ and B(n) for use in establishing unknown system parameter estimates via equations (17) through (19). These equations also need the partial derivatives of the innovations and its covariance with respect to each unknown parameter. The required derivatives are derived from sensitivity filters obtained by taking the partials of Eqs. (20) through (26). To simplify notation, all variable arguments will be dropped and plus (+) and minus (-) superscripts will be used to reflect propagated and updated variables, respectively. With this in mind, the typical sensitivity filter with respect to the j th unknown parameter is expressed by:

- The state propagation sensitivity equation

$$\frac{\partial \underline{y}^+}{\partial \theta_j} = \Phi \frac{\partial \underline{y}^-}{\partial \theta_j} + \frac{\partial \Phi}{\partial \theta_j}\underline{y}^- + \left(\frac{\partial \Gamma}{\partial \theta_j}G_0 + \Gamma \frac{\partial G_0}{\partial \theta_j}\right)\underline{u} \,. \tag{27}$$

- The state covariance propagation sensitivity equation

$$\frac{\partial P^+}{\partial \theta_j} = \Phi \frac{\partial P^-}{\partial \theta_j}\Phi^T + \Phi P^- \frac{\partial \Phi^T}{\partial \theta_j} + \left(\Phi P^- \frac{\partial \Phi^T}{\partial \theta_j}\right)^T + \Gamma\left[W_0 \frac{\partial Q}{\partial \theta_j}W_0^T + W_0 Q \frac{\partial W_0^T}{\partial \theta_j} + \left(W_0 Q \frac{\partial W_0^T}{\partial \theta_j}\right)^T\right]\Gamma^T + \Gamma W_0 Q W_0^T \frac{\partial \Gamma^T}{\partial \theta_j} + \left(\Gamma W_0 Q W_0^T \frac{\partial \Gamma^T}{\partial \theta_j}\right)^T \,. \tag{28}$$

- The Kalman gain sensitivity equation

$$\frac{\partial K}{\partial \theta_j} = \frac{\partial P^+}{\partial \theta_j}H_0^T B^{-1} + P^+ \frac{\partial H_0^T}{\partial \theta_j}B^{-1} + P^+ H_0^T \frac{\partial B^{-1}}{\partial \theta_j} \,, \tag{29}$$

where

$$\frac{\partial B^{-1}}{\partial \theta_j} = -B^{-1}\frac{\partial B}{\partial \theta_j}B^{-1} \,,$$

$$\frac{\partial B}{\partial \theta_j} = H_0 \frac{\partial P^+}{\partial \theta_j}H_0^T + H_0 P^+ \frac{\partial H_0^T}{\partial \theta_j} + \left(H_0 P^+ \frac{\partial H_0^T}{\partial \theta_j}\right)^T + \frac{\partial R}{\partial \theta_j} \,. \tag{30}$$

- The state measurement update sensitivity equation

$$\frac{\partial \underline{y}^-}{\partial \theta_j} = \frac{\partial \underline{y}^+}{\partial \theta_j} + K\frac{\partial \underline{\nu}}{\partial \theta_j} + \frac{\partial K}{\partial \theta_j}\underline{\nu} \,, \tag{31}$$

where

$$\frac{\partial \underline{\nu}}{\partial \theta_j} = -H_0 \frac{\partial \underline{y}^+}{\partial \theta_j} - \frac{\partial H_0}{\partial \theta_j}\underline{y}^+ \,. \tag{32}$$

- The state covariance measurement update sensitivity equation

$$\frac{\partial P^-}{\partial \theta_j} = [I - K H_0]\frac{\partial P^+}{\partial \theta_j}[I - K H_0]^T + [K H_0 - I]P^+ \frac{\partial H_0^T}{\partial \theta_j}K^T + \left([K H_0 - I]P^+ \frac{\partial H_0^T}{\partial \theta_j}K^T\right)^T + K\frac{\partial R}{\partial \theta_j}K^T \,. \tag{33}$$

Equations (17) through (33) define all the information necessary to implement the modified Newton-Raphson parameter optimization procedure. The Kalman and sensitivity filter equations are executed for each measurement vector in the data record establishing the information required by Eq. (17) to recursively compute refined parameter estimates. A block diagram showing the computational flow of the maximum likelihood parameter identification algorithm is contained in Fig. 2. The algorithm is capable of identifying elements of the statistical covariance matrices Q and R, as well as, elements of F_0, G_0, W_0, and H_0. The complex conjugate eigenvalues of F_0, estimated as elements of this tridiagonal matrix, are used to establish modal frequency and damping values.

3.2.2 *STATISTICAL CHARACTERISTICS*

The maximum likelihood estimation process has a number of highly desirable statistical properties. As noted in Reference 3, the most significant are:

Parameter estimates are asymptotically unbiased, as expressed by

$$\lim_{N\to\infty} E[\underline{\theta}] = \underline{\theta}_t \,,$$

which indicates that the expected value of an estimate $\underline{\hat{\theta}}$ approaches the true value $\underline{\theta}_t$ as more data is used (i.e., as N increases).

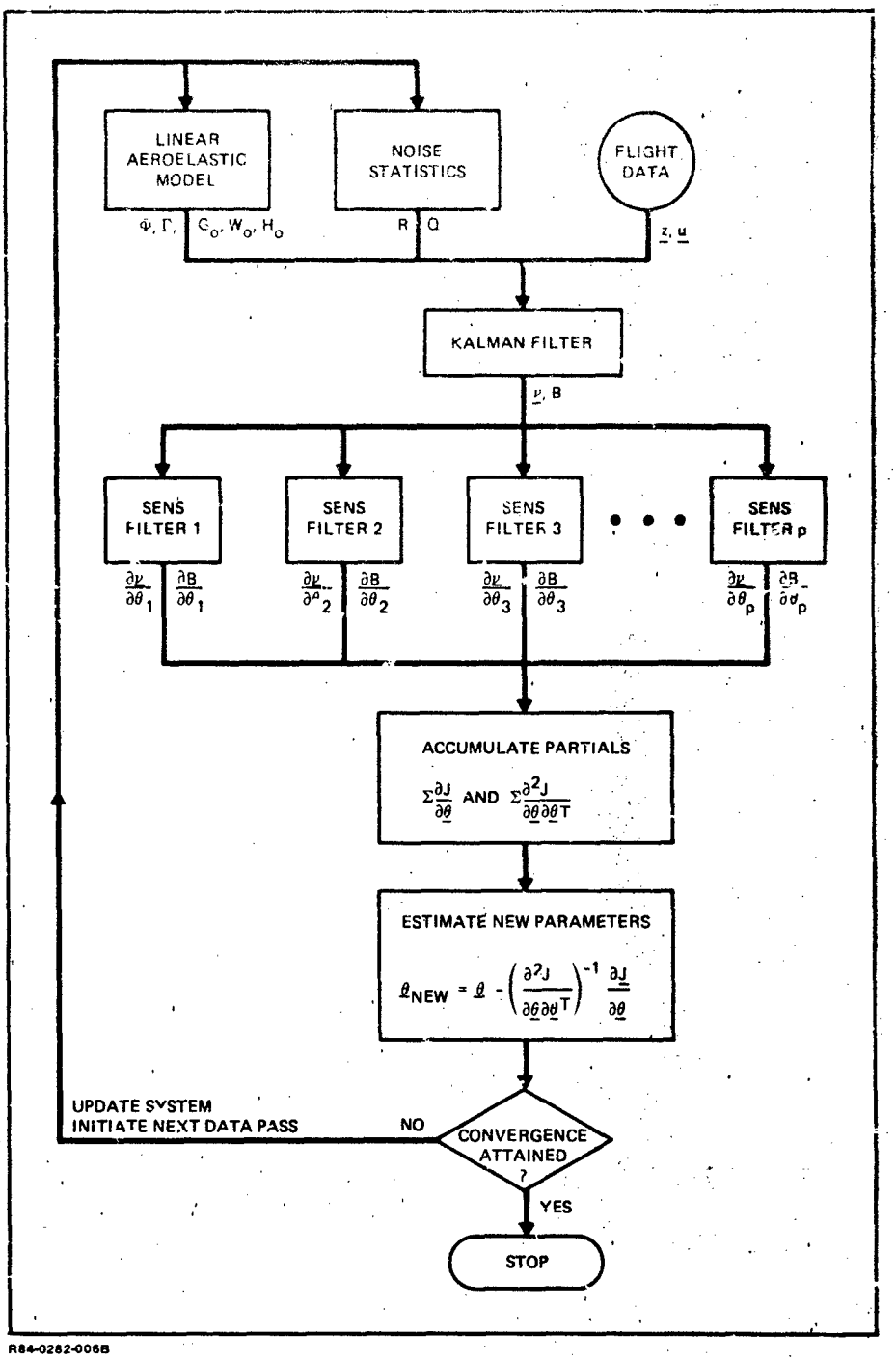

R84-0282-006B

Fig. 2 Computational Sequence for Maximum Likelihood Parameter Identification Algorithm

Parameter estimates are consistent which implies that

$$\lim_{N\to\infty} \text{Prob}[\,|\hat{\underline{\theta}} - \underline{\theta}_t| \le \epsilon\,] = 1 \ ,$$

where Prob $[\cdot]$ indicates the probability of the quantity in brackets, with ϵ being an arbitrarily small positive number.

Parameter estimates are asymptotically efficient with

$$E[(\hat{\underline{\theta}} - \underline{\theta}_t)(\hat{\underline{\theta}} - \underline{\theta}_t)^T] \le -E\left[\frac{\partial^2 J(\theta)}{\partial \underline{\theta}\, \partial \underline{\theta}^T}\right] \equiv M \ ,$$

where M is the Fisher information matrix. The inverse of this matrix provides a lower bound on parameter estimate covariances known as the Cramer-Rao bound which is considered the maximum achievable estimation accuracy.

Parameter estimates are asymptotically normal in that they approach the Gaussian distribution with

3.2.3 *SIMPLIFIED COMPUTATIONAL CIRCUMSTANCES*

In our application we are dealing with a time invariant linear system with uniformly sampled measurements. For our system, the process and measurement noise covariance matrices, defined by Q and R, are assumed to be constant. Under the above stated conditions the Kalman gain and the innovations and state covariances approach constant steady state values defined by

$$P(n-1/n-2) = P(n/n-1) = P^{*} ,$$

$$K(n-1) = K(n) = K ,$$

$$B(n-1) = B(n) = B ,$$

$$P'(n-1/n-1) = P(n/n) = P^{*} .$$

Similar steady state conditions will also prevail in the sensitivity filters. In practice, the Kalman and sensitivity filters are in statistical steady state for almost the entire duration of the analysis interval. Under steady state conditions the computation of Eqs. (20) through (33) can be reduced to only the computation of Eqs. (20), (24), (25), (27), (31), and (32). This is a substantial reduction in computations and a key factor in enabling the maximum likelihood parameter identification technique to be used in on-line processing situations at the present time.

Another simplification in computational requirements can be realized when process noise levels are negligible. In the absence of process noise, the Kalman gain matrix K(n) will go to zero as time increases. This fact is obvious when the initial state of the system is known, since the covariance of the error in predicted state would then be zero and it follows from Eq. (22) that the Kalman gain matrix would be zero. Here the innovations are the output error

$$\underline{\nu}(n) = \underline{z}(n) - H_1 \underline{y}(n) ,$$

where system state $\underline{y}(n)$ is propagated (integrated) via the equation

$$\underline{y}(n) = \Phi \underline{y}(n-1) + \Gamma G_0 \underline{u}(n-1) . \tag{34}$$

The innovations covariance matrix is defined by

$$B(n) = R ,$$

which is the constant measurement covariance matrix. The log of the likelihood function becomes

$$J(\underline{\theta}) = \ln L(\underline{\theta}) = -\frac{1}{2}\sum_{n=1}^{N} \underline{\nu}^{T}(n) R^{-1} \underline{\nu}(n) + \text{constant} ,$$

where R can be estimated by

$$\hat{R} = \frac{1}{N}\sum_{n=1}^{N} \underline{\nu}(n)\, \underline{\nu}^{T}(n) . \tag{35}$$

The equality in Eq. (35) holds only for those elements of R which are not considered known. If R is known to be diagonal the off diagonal terms in the matrix computed via Eq. (35) should be set to zero.

Here, the same modified Newton-Raphson optimization procedure is used to calculate parameter updates via Eq. (17). The corresponding first and second partials of $J(\underline{\theta})$ are defined by

$$\frac{\partial J}{\partial \theta_i} = -\sum_{n=1}^{N} \underline{\nu}^{T}(n) \hat{R}^{-1} \frac{\partial \underline{\nu}(n)}{\partial \theta_i} , \tag{36}$$

and

$$\frac{\partial^2 J}{\partial \theta_i \partial \theta_j} = -\sum_{n=1}^{N} \frac{\partial \underline{\nu}^{T}(n)}{\partial \theta_j} \hat{R}^{-1} \frac{\partial \underline{\nu}(n)}{\partial \theta_i} . \tag{37}$$

The corresponding sensitivity equations are

$$\frac{\partial \underline{\nu}(n)}{\partial \theta_i} = -H_0 \frac{\partial \underline{y}(n)}{\partial \theta_i} - \frac{\partial H_2}{\partial \theta_i} \underline{y}(n) , \tag{38}$$

where $\underline{y}(n)$ is defined by Eq. (34) and

$$\frac{\partial \underline{y}(n)}{\partial \theta_i} = \Phi \frac{\partial \underline{y}(n-1)}{\partial \theta_i} + \frac{\partial \Phi}{\partial \theta_i} \underline{y}(n-1) + \left(\frac{\partial \Gamma}{\partial \theta_i} G_0 + \Gamma \frac{\partial G_2}{\partial \theta_i}\right) \underline{u}(n-1) . \tag{39}$$

The bulk of the computational activity is involved in the propagation of system state and sensitivity relationships, via Eq. (34), (38) and (39), and the accumulation of the first and second partials of J, via Eq. (36) and (37).

3.3.4 *EXTENDED KALMAN FILTER APPROACH*

The extended Kalman filter was developed for handling system state estimates of nonlinear systems (see Reference 8). This filter is not optimal in any proven sense but has worked well on a wide variety of problems. Parameter identification problems for linear systems can be approached by declaring unknown parameters of the system as state variables (see Reference 3). This creates a set of nonlinear system equations with parameter state variables that can be estimated as the output of the corresponding extended Kalman filter. Our linear aeroelastic system has been defined by Eq. (9). Here, specific elements of F_0, G_0, W_0, and or H_0 could be selected as elements of the parameter vector $\underline{\vartheta}$ and added to the original linear system state vector $\underline{y}$ to create an augmented state vector $\underline{\delta}$. The resulting system would then be defined in the generalized nonlinear form

$$\dot{\underline{\delta}} = \underline{f}_0(\underline{\delta}, \underline{u}) + W_0(\underline{\delta})\underline{\zeta} ,$$

$$\underline{z} = \underline{h}_0(\underline{\delta}) + \underline{\mu}$$

where functional arguments have been noted within brackets. Specifically,

$$\underline{\delta}^T = [\underline{y}^T, \underline{\vartheta}^T] , \quad \underline{\zeta}^T = [\underline{\eta}^T, 0] ,$$

$$\underline{f}_0(\underline{\delta}, \underline{u}) = \begin{bmatrix} F_0 \underline{y} - G_0 \underline{u} \\ 0 \end{bmatrix} ,$$

$$\underline{h}_0(\underline{\delta}) = H_0 \underline{y} , \quad W_0(\underline{\delta}) = W_0 ,$$

where it should be noted that since selected elements of $\underline{\vartheta}$ can correspond to elements in F_0, G_0, W_0, and H_0 these latter matrices can be functions of $\underline{\delta}$. The noise sources $\underline{\zeta}$ and $\underline{\mu}$ are assumed to be independent with zero-mean Gaussian white characteristics.

The derivation of the extended Kalman filter is patterned on concepts established for the linear Kalman filter, as defined by Eqs. (20) through (26), resulting in corresponding propagation and measurement update relationships which are identified by:

- System state propagation via the integration of the nonlinear differential equation

  $$\dot{\underline{\delta}} = \underline{f}_0(\underline{\delta}, \underline{u}) ,$$

  to obtain propagated state $\underline{\delta}(n/n-1)$ at the required iteration times t_n, using all measurements up to time t_{n-1}, subject to the assumption that $\underline{\delta}(t_{n-1}) = \underline{\delta}(n-1/n-1)$.

- System state covariance propagation via the equation

  $$P(n/n-1) = \Phi(n, n-1)\, P(n-1/n-1)\, \Phi^T(n, n-1) + \Gamma(n, n-1)\, W_0 Q W_0^T \Gamma^T(n, n-1) .$$

  The above relationship is a linearized equation and is, therefore, similar in form to Eq. (21). However, both Φ and Γ vary with time and so will W_0 if any of its elements are considered unknown parameters. Here, the transition matrix is the solution to the differential equation

  $$\dot{\Phi}(t, t_{n-1}) = F(t)\, \Phi(t, t_{n-1}) ,$$

  where $t = t_{n-1}$, $\Phi(t_{n-1}, t_{n-1})$ = the identity matrix I, and

  $$F(t) = \left. \frac{\partial \underline{f}_0}{\partial \underline{\delta}} \right|_{\underline{\delta} = \underline{\delta}(n/n-1)}$$

  It follows that

  $$\Gamma(t, t_{n-1}) = \int_{t_{n-1}}^{t} \Phi(t, \tau) d\tau .$$

  Elements of W_0 that are considered unknown parameters would be set equal to their corresponding values in vector $\underline{\delta}(n/n-1)$.

- Kalman gain computation using the linearized equation

  $$K(n) = P(n/n-1) H_0^T(n) [H_0(n)\, P(n/n-1)\, H_0^T(n) + R]^{-1} ,$$

  where

  $$H_0(n) = \left. \frac{\partial h_0}{\partial \underline{\delta}} \right|_{\underline{\delta} = \underline{\delta}(n/n-1)}$$

- System state measurement update using the nonlinear relationship

$$\underline{\delta}(n/n) = \underline{\delta}(n/n-1) + K(n)\left[\underline{z}(n) - \underline{h}_0(n)\right],$$

where

$$\underline{h}_0(n) = \underline{h}_0(\underline{\delta})\Big|_{\underline{\delta}=\underline{\delta}(n/n-1)}.$$

- System state covariance measurement update via the linearized equation

$$P(n/n) = [I - K(n)H_0(n)]\,P(n/n-1)[I - K(n)H_0(n)]^T + K(n)\,R\,K^T(n),$$

with $H_0(n)$ as defined in the Kalman gain computation.

The relationships identified in the bulleted items define the extended Kalman filter parameter identification procedure required to recursively process each measurement vector in a data record. A block diagram depicting the computational flow of the algorithm is shown in Fig. 3. The extended Kalman filter essentially makes maximum likelihood estimates and therefore, has statistical properties similar to those previously mentioned for the maximum likelihood algorithm. However, the maximum likelihood algorithm has the advantage of being able to determine process and measurement noise covariance statistics as parameter estimates. This is not possible with the extended Kalman filter approach. These noise statistics could be difficult to assess quickly in an on-line test environment.

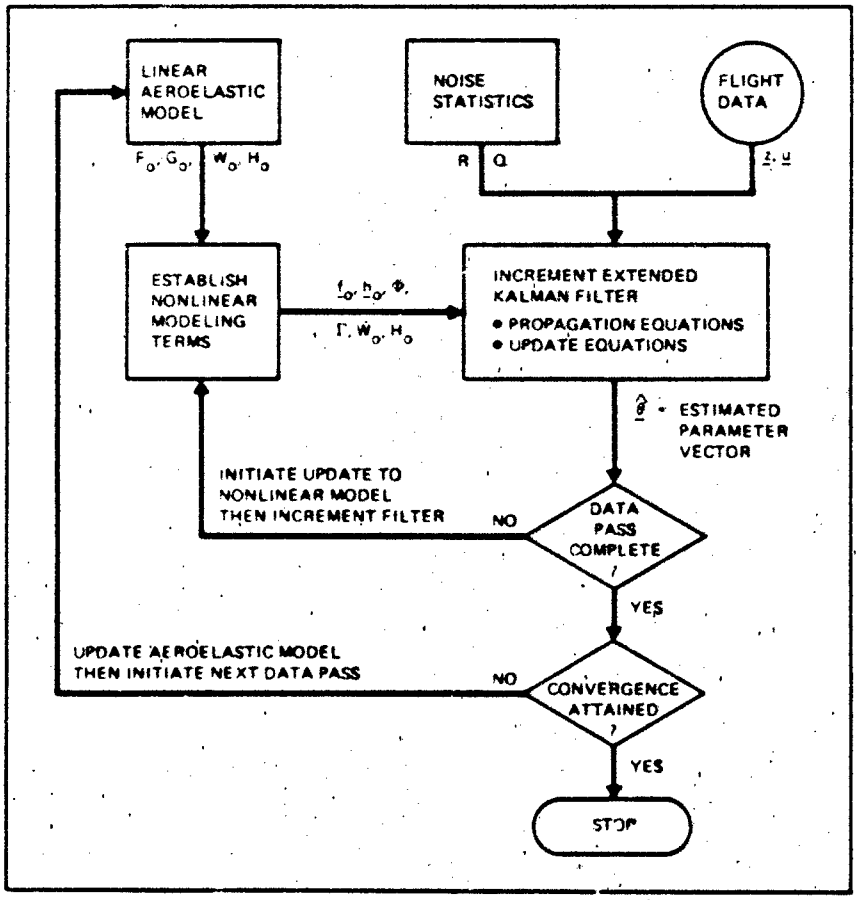

Fig. 3 Computational Sequence for Extended Kalman Filter Parameter Identification Algorithm

3.3 Current Analysis Techniques

The current processing methods used by Grumman in the on-line analysis of flutter response data, all use a least-squares difference-equation identification algorithm to establish modal frequency and damping characteristics. Differences in the processing methods primarily reflect the techniques used to precondition the test data before it is presented to the identification algorithm. This preconditioning is necessary to suppress noise effects, which can significantly degrade the accuracy of the basic equation-error identification algorithm which is well known to be a biased parameter estimator (see Reference 3). Even though the basic approach is susceptible to noise effects the filtering, correlation, and frequency domain

windowing methods employed in the processing software have enabled the identification algorithm to produce consistent results (even when compared to more advanced methods) on shaker excited response data. Up until the early 1980s this had been the dominant means used at Grumman for generating flutter test data.

The fundamental assumption underlying software analytics is that aeroelastic system dynamics are linear. Taking that into effect, system dynamics can be represented by an ordinary differential equation the form

$$\sum_{n=0}^{N} d_n \frac{d^n y}{dt^n} = \sum_{m=0}^{M} c_m \frac{d^m u}{dt^m} , \tag{40}$$

where $y = y(t)$ is the system response and $u = u(t)$ the input excitation signal. Here, c_m and d_n are constant coefficients ($d_N = 1.0$) and it is generally assumed that $N \geq M$. The assumed form of Eq. (40) classifies the system as linear, time-invariant, and causal. The properties of such systems have been extensively covered in literature and imply the following convolution integral relationship between system input and output, when it is assumed that $u(t) = 0$ for $t < 0$

$$y(t) = \int_0^t u(\sigma)\, g(t-\sigma)\, d\sigma = \int_0^t u(t-\sigma)\, g(\sigma)\, d\sigma , \tag{41}$$

where $g(t)$ represent the system's impulse response.

Using lower case nomenclature to denote variables in the time domain and upper case for frequency domain variables it follows by taking the Laplace transform of Eq. (41) that

$$Y(s) = G(s)\, U(s) \tag{42}$$

where s is the Laplace operator and G(s) is the system transfer function. The actual form of G(s) is established by taking the Laplace transform of Eq. (40), assuming the system to be initially at rest, resulting in

$$\frac{Y(s)}{U(s)} = G(s) = \frac{\sum_{m=0}^{M} c_m s^m}{\sum_{n=0}^{N} d_n s^n} = \frac{c_m \prod_{m=1}^{M} (s - q_m)}{\prod_{n=1}^{N} (s - p_n)} , \tag{43}$$

where q_m are the zeros of G(s) and p_n the poles which correspond to the eigenvalues of the system. Modal frequency and damping coefficients are determined from the complex conjugate pole pairs. If a typical pair had a real part equal to $-\alpha$ and an imaginary part equal to β, then the damped natural frequency of the mode would be defined by

$$f_d = \beta / 2\pi ,$$

and the corresponding damping coefficient by

$$g = 2\alpha / \sqrt{\alpha^2 + \beta^2} .$$

The least-squares difference-equation identification algorithm is predicated on single-input single-output system transfer function relationships like Eq. (43). As explained in Appendix A of Reference 1, G(s) can be approximated with a Z-transfer function relationship which leads directly to a time domain difference equation in the form

$$y(kT) = -\sum_{n=1}^{N} a_n\, y(kT - nT) + \sum_{n=1}^{N} b_n\, u(kT - nT) , \tag{44}$$

where T is the data sampling period. The identification algorithm uses Eq. (44) as its dynamic model of the system and determines the a_n and b_n coefficients that best match the test data in a least-squares equation-error sense. Basically the technique determines the difference equation coefficients which minimize the cost function J defined by

$$J = \sum_{k=k_1}^{k_2} e_k^2 = \sum_{k=k_1}^{k_2} \left[\mu + \sum_{n=0}^{N} \hat{b}_n f_{k-n} - \sum_{n=1}^{N} \hat{a}_n r_{k-n} - r_k \right]^2 , \tag{45}$$

where the subscript k implies the value of the variable at time kT. Here, e_k is the difference equation error and r_k and f_k represent preconditioned response and excitation signals, respectively. The parameter μ has been added to the difference equation model to account for bias errors in the measurement data.

The procedure for minimizing J is defined by setting the partial derivatives of J with respect to the difference equation coefficients to zero, resulting in a set of 2(N+1) linear equations in 2(N+1) unknowns which can be solved for the estimated coefficient information (i.e., $\hat{a}_n$ and $\hat{b}_n$) using the matrix equation

$$\underline{\hat{\theta}} = [B^T B]^{-1} B^T \underline{v} , \tag{46}$$

where

$$\underline{\hat{\theta}}^T = [\mu, \hat{b}_N, \cdots \hat{b}_0, -\hat{a}_N, \cdots -\hat{a}_1] ,$$

$$\underline{v}^T = [r_{k_1}, r_{k_1+1}, \cdots r_{k_2}] ,$$

$$B = \begin{bmatrix} 1 & f_{k_1-N} \cdots f_{k_1} & r_{k_1-N} \cdots r_{k_1-1} \\ \vdots & \vdots \quad \vdots & \vdots \quad \vdots \\ 1 & f_{k_2-N} \cdots f_{k_2} & r_{k_2-N} \cdots r_{k_2-1} \end{bmatrix} .$$

The poles of G(s) and the a_n difference equation coefficients are related by the following polynomial equation

$$1 + \sum_{n=1}^{N} a_n z^{-n} = \prod_{n=1}^{N} [1 - \exp(p_n T) z^{-1}] , \tag{47}$$

where z corresponds to the Z-transfer function operator. Using the estimated parameters $\hat{a}_n$ in Eq. (47) it follows that

$$\hat{p}_n = \frac{1}{T} \ln(\hat{\gamma}_n) ,$$

where $\hat{\gamma}_n$ is the n th root of the polynomial defined in Eq. (47). Modal frequency and damping coefficients can then be determined from the estimated complex conjugate pole pairs in a manner similar to that previously defined for the complex conjugate pole pairs of G(s).

In Eq. (45) r_k and f_k were defined as preconditioned response and excitation signals. As noted in Appendix A of Reference 1, these preconditioned signals can be digitally filtered or specially computed correlation functions of these signals. Since correlation signal processing involves the handling of functions that are not zero for negative time delays it proves expedient to express frequency domain relationships using the Fourier rather than the unilateral Laplace transform. In terms of the Fourier transform the system transfer function relationship defined in Eq. (42) becomes

$$Y(i\omega) = G(i\omega)\, U(i\omega) , \tag{48}$$

where $Y(i\omega)$, $U(i\omega)$ and $G(i\omega)$ are the Fourier transforms of y(t), u(t) and g(t), respectively. If one filters the measured system response signal y(t) with a linear filter having a transfer function $F(i\omega)$ it follows that the filtered response signal is defined by

$$Y_f(i\omega) = Y(i\omega)\, F(i\omega) ,$$

and it follows from Eq. (48) that

$$Y_f(i\omega) = G(i\omega)\, U(i\omega)\, F(i\omega) = G(i\omega)\, U_f(i\omega) . \tag{49}$$

Equation (49) states that the filtered response and excitation signals are dynamically related to each other through the same transfer function as the unfiltered signals. This implies that the filtered signals satisfy difference Eq. (44) in the same manner as the unfiltered signals.

In contrast to direct digital filtering of measurement signals, a somewhat higher level of noise rejection can be obtained if correlation methods are used. Since noise effects are generally uncorrelated with the applied system excitation signal, the cross-correlation method provides a particularly good means for suppressing noise effects (provided sufficient test signal is available for data averaging). Consider the cross-correlation of some arbitrary signal w(t) with y(t) and u(t) over the finite interval of time ranging from t_1 to t_2 sec as denoted by

$$\phi_{wy}(\tau) = \frac{1}{t_2 - t_1} \int_{t_1}^{t_2} w(t)\, y(t+\tau) dt ,$$

and

$$\phi_{wu}(\tau) = \frac{1}{t_2 - t_1} \int_{t_1}^{t_2} w(t)\, u(t+\tau) dt .$$

The cross-correlation functions shown above satisfy the following cross-spectral relationship

$$\Phi_{ww}(i\omega) = G(i\omega)\,\Phi_{wu}(i\omega)\ , \tag{50}$$

where $\Phi_{ww}(i\omega)$ and $\Phi_{wu}(i\omega)$ are the Fourier transforms of $\phi_{ww}(\tau)$ and $\phi_{wu}(\tau)$, respectively. In particular

$$\Phi_{ww}(i\omega) = W(-i\omega)\,Y(i\omega)\ ,$$

$$\Phi_{wu}(i\omega) = W(-i\omega)\,U(i\omega)\ .$$

Equation (50) shows that the cross-correlation functions $\phi_{ww}(\tau)$ and $\phi_{wu}(\tau)$ are mathematically related to each other in the same manner as the actual system response and excitation signals. Thus, these cross-correlation functions satisfy difference Eq. (44) and provide a low noise level signal input into the least-squares identification algorithm. For cross-correlation signal processing w(t) is generally set equal to the excitation signal u(t) digitally filtered to emphasize the modal frequency range of interest. In addition, data is only analyzed over that interval of time when the excitation signal is supplying energy in the frequency range of interest, which is also the case when direct digital filtering is used.

Response signal correlation analysis corresponds to the case where w(t) is set equal to a digitally filtered version of the system response signal. For this form of preconditioning Eq. (50) becomes

$$\Phi_{y_f y}(i\omega) = G(i\omega)\,\Phi_{y_f u}(i\omega)$$

$$= G(i\omega)\,G(-i\omega)\,F(-i\omega)\,\Phi_{uu}(i\omega)\ . \tag{51}$$

The cross-correlation of filtered and unfiltered response signals does not effectively reject noise within the filter pass-band. Thus, excitation signal cross-correlation analysis is generally preferred. However, it should be noted that if $\Phi_{uu}(i\omega)$ is broadband-flat then Eq. (51) reduces to

$$\Phi_{y_f y}(i\omega) = G(i\omega)\,G(-i\omega)\,F(-i\omega)\ . \tag{52}$$

The above relationship indicates that the time domain function $\phi_{y_f y}(t)$ is equivalent to the system output response resulting from an excitation signal equal to the filtered system impulse response function folded about the t=0 axis. For values of $t>0$ it follows that $\phi_{y_f y}(t)$ is actually the free decay of the system to the aforementioned input. Equation (52) involves only response signal measurements and has proved of value in analyzing flutter response data obtained from an aircraft excited by a driving function possessing an impulsive autocorrelation function. Random excitation having either a spectrum which is broadband-flat or one which can be considered as the output of a linear system which is driven by a broadband-flat random input satisfy this requirement. This random excitation can be obtained either naturally from a source such as atmospheric turbulence or artificially via random shakers.

The above mentioned preconditioning methods are all time domain processing techniques. Grumman's current flutter analysis software also provides the capability to precondition test data by first computing frequency response functions by three different methods. When an excitation signals is available, the cross-spectral density between system excitation and response, and the power spectral density of the excitation signal are computed. In this case, the frequency response function is computed by dividing the cross-spectral density by the power spectral density over the frequency range of interest. For the analysis of random data, particularly when no excitation signal is available, the frequency response function is computed by taking the discrete Fourier transform of the positive lags of the response signal's autocorrelation function or its random decrement signature. Although the three indicated frequency response functions are somewhat different in form, they all can be considered representative of a transfer function characteristic possessing poles identical to the actual system under test.

For modal identification purposes, rectangular windows are applied to the calculated frequency response function and the windowed frequency response information inverted into the time domain for analysis. The windowed frequency response information reflects the response of a system having the calculated frequency response characteristic to an excitation signal having a rectangular frequency domain amplitude function with zero phase angle. The time domain form of the artificially created excitation signal is analytically computed and used along with the inverted response signal to determine system frequency and damping coefficient information for those modes within the windowed frequency range using the least-squares difference-equation identification algorithm. Digital bandpass filtering of the raw time domain signals is employed to minimize the effects of neighboring modes whose resonant frequencies are close to the windowed frequency range. This frequency domain windowing method has proved to be a most effective means for minimizing noise effects. When this method of analysis is employed, frequency response functions computed from the Z-transforms corresponding to each identified difference equation model are available to the analyst for comparison with the actual function computed from the test data. This information is often helpful in establishing the validity of calculated results. The analysis results contained in subsection 4.2 were all obtained using this frequency domain windowing method of analysis.

4. ANALYSIS RESULTS

4.1 Maximum Likelihood Analysis

At the present time, prototype software has been developed for the maximum likelihood identification method that enables analysis to be carried out in either an interactive or batch data processing environment. Figure 4 contains a block diagram defining the maximum likelihood identification algorithm as implemented in the prototype software. The processing activities shown in Fig. 4 correspond to the mathematical description explained in subsection 3.2. The software was developed on the Cyber 740 at the Automated Telemetry Station and then converted to run on a Cray 1 supercomputer. All the lengthy evaluation runs on simulated randomly excited data were conducted on this computer. The analysis of short duration data records such as the simulated swept frequency data (of 10 sec duration) and the analysis of F-14A randomly excited fin response data (of 24 sec duration) were carried out on the Cyber 740. To minimize execution time on all runs, the Kalman filter gain propagation and update calculations were terminated 1 to 2 sec into each data pass with the remaining data in each record analyzed with the last calculated value for the gain matrices.

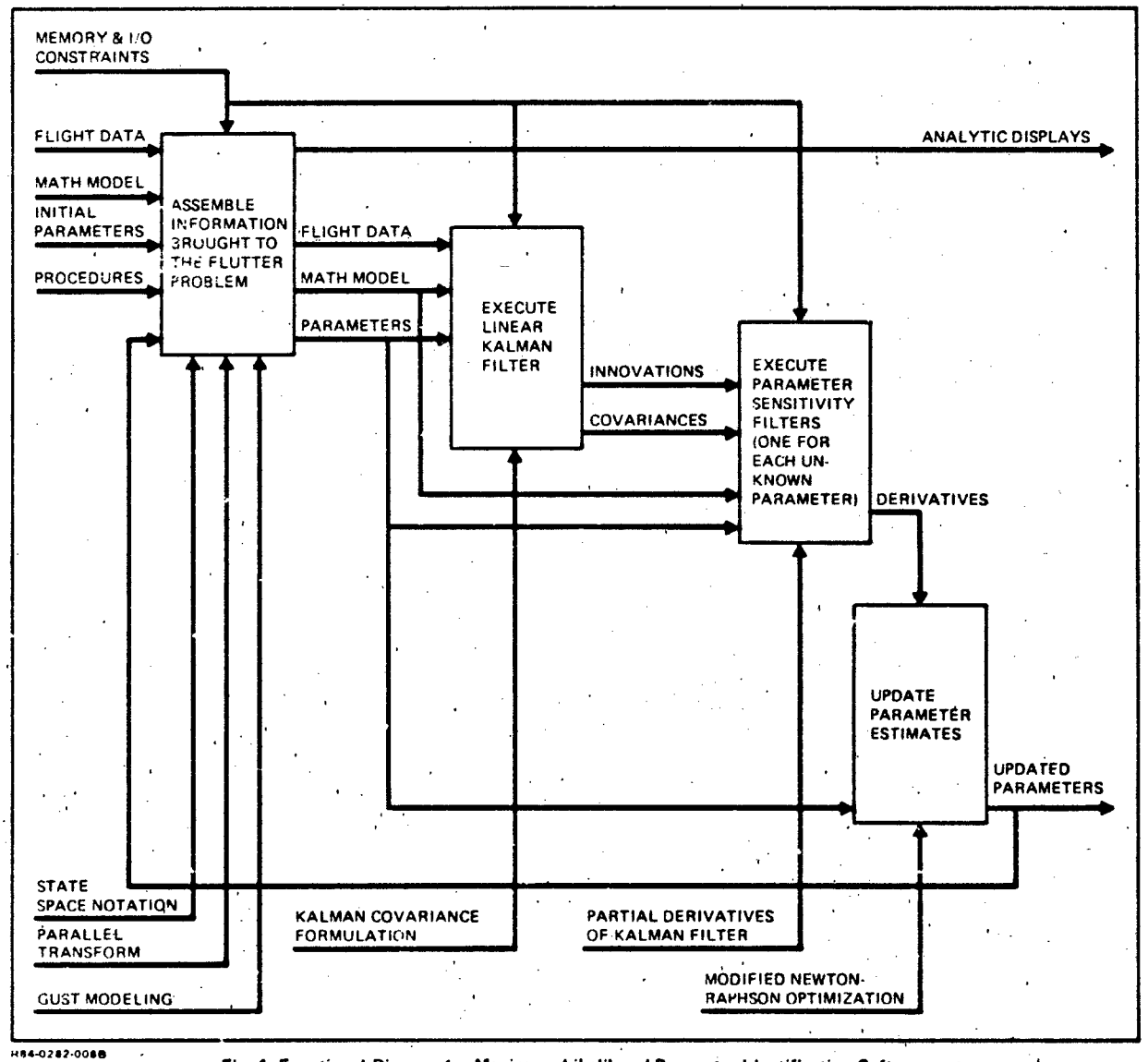

H84-0282-008B

Fig. 4 Functional Diagram for Maximum Likelihood Parameter Identification Software

In all simulated runs, data was generated at a sample rate of 250 Hz by an 11-state aeroelastic model driven by zero-mean Gaussian white noise to approximate atmospheric gust effects plus a shaker excitation signal in the cases pertaining to swept frequency data. Gaussian white zero-mean noise was added to each of two generated response measurements. The characteristic roots (eigenvalues) of the simulation model were defined by

$$\lambda_{1,2} = -147.964 \pm 64.3410i\,, \quad \lambda_{3,4} = -11.8078 \pm 61.7156i\,,$$

$$\lambda_{5,6} = -1.45901 \pm 19.7414i\,, \quad \lambda_{7,8} = -106.626 \pm 17.8611i\,,$$

$$\lambda_{9} = -145.492\,, \quad \lambda_{10} = -55.9049\,, \text{ and } \lambda_{11} = -3.1400\,.$$

This model contained two flexible modes. The first corresponds to roots 3 and 4 with a damped natural frequency (f_d) of 9.83223 Hz and a damping coefficient (g) of 0.3758. The second corresponds to roots 5 and 6 with $f_d = 3.1419$ Hz and $g = 0.1474$. Roots 1, 2, 7, 8, 9, and 10 pertained to the modeling of unsteady aerodynamic effects with root 11 corresponding to the simplified gust shaping-filter defined in subsection 3.1.

Simulated data analysis was accomplished using both an accurately defined eleventh order model and an approximate fifth order model. In the uncoupled form used by the maximum likelihood algorithm, the eleventh order state equations were defined by

$$\begin{bmatrix} \dot{y}_1 \\ \dot{y}_2 \\ \dot{y}_3 \\ \dot{y}_4 \\ \dot{y}_5 \\ \dot{y}_6 \\ \dot{y}_7 \\ \dot{y}_8 \\ \dot{y}_9 \\ \dot{y}_{10} \\ \dot{y}_{11} \end{bmatrix} = \underbrace{\begin{bmatrix} \alpha_1\beta_1 & & & & & & & & & & \\ -\beta_1\alpha_1 & & & & & & & & & & \\ & \alpha_2\beta_2 & & & & & & & & & \\ & -\beta_2\alpha_2 & & & & & & & & & \\ & & \alpha_3\beta_3 & & & & & & & & \\ & & -\beta_3\alpha_3 & & & & & & & & \\ & & & \alpha_4\beta_4 & & & & & & & \\ & & & -\beta_4\alpha_4 & & & & & & & \\ & & & & \lambda_9 & & & & & & \\ & & & & & \lambda_{10} & & & & & \\ & & & & & & \lambda_{11} & & & & \end{bmatrix}}_{F_0} \begin{bmatrix} y_1 \\ y_2 \\ y_3 \\ y_4 \\ y_5 \\ y_6 \\ y_7 \\ y_8 \\ y_9 \\ y_{10} \\ y_{11} \end{bmatrix} + \underbrace{\begin{bmatrix} 0 \\ 1 \\ 0 \\ 1 \\ 0 \\ 1 \\ 0 \\ 1 \\ 1 \\ 1 \\ 1 \end{bmatrix}}_{G_0} u + \underbrace{\begin{bmatrix} w_1 \\ w_2 \\ w_3 \\ w_4 \\ w_5 \\ w_6 \\ w_7 \\ w_8 \\ w_9 \\ w_{10} \\ w_{11} \end{bmatrix}}_{W_0} \eta \,,$$

with corresponding measurements (z_1 and z_2) defined by

$$\begin{bmatrix} z_1 \\ z_2 \end{bmatrix} = \underbrace{\begin{bmatrix} h_{1,1} & h_{1,2} & h_{1,3} & \cdots & h_{1,11} \\ h_{2,1} & h_{2,2} & h_{2,3} & \cdots & h_{2,11} \end{bmatrix}}_{H_0} \begin{bmatrix} y_1 \\ y_2 \\ y_3 \\ \vdots \\ y_{11} \end{bmatrix} + \begin{bmatrix} u_1 \\ u_2 \end{bmatrix} .$$

Accordingly the fifth order analysis model was described by

$$\begin{bmatrix} \dot{y}_1 \\ \dot{y}_2 \\ \dot{y}_3 \\ \dot{y}_4 \\ \dot{y}_5 \end{bmatrix} = \begin{bmatrix} \alpha_1\beta_1 & & & & \\ -\beta_1\alpha_1 & & & & \\ & \alpha_2\beta_2 & & & \\ & -\beta_2\alpha_2 & & & \\ & & & & \lambda_5 \end{bmatrix} \begin{bmatrix} y_1 \\ y_2 \\ y_3 \\ y_4 \\ y_5 \end{bmatrix} + \begin{bmatrix} 0 \\ 1 \\ 0 \\ 1 \\ 1 \end{bmatrix} u + \begin{bmatrix} w_1 \\ w_2 \\ w_3 \\ w_4 \\ w_5 \end{bmatrix} \eta \,,$$

and

$$\begin{bmatrix} z_1 \\ z_2 \end{bmatrix} = \begin{bmatrix} h_{1,1} & h_{1,2} & h_{1,3} & h_{1,4} & h_{1,5} \\ h_{2,1} & h_{2,2} & h_{2,3} & h_{2,4} & h_{2,5} \end{bmatrix} \begin{bmatrix} y_1 \\ y_2 \\ y_3 \\ y_4 \\ y_5 \end{bmatrix} + \begin{bmatrix} u_1 \\ u_2 \end{bmatrix} .$$

In analysis runs with the eleventh order model the eigenvalues corresponding to the flexible modes were initially offset 10 to 20% from their true values with corresponding elements in the measurement matrix (H_0) offset by approximately 10%. All other parameter values were left at their true values with the maximum likelihood algorithm directed to establish estimates for all offset parameters. The purpose of these runs was to determine the best possible results obtainable with an accurate model and perfect knowledge of gust and unsteady aerodynamic effects. On the other hand, the purpose of the analysis runs made with the fifth order model was to determine what results could be expected with little knowledge of a good physical model. Here, the model completely ignored unsteady aerodynamic effects, the

four eigenvalues corresponding to the flexible modes were offset by the same 10 to 20% (reflecting what might be expected in actual practice), the elements of the H_0 and W_0 matrices were offset by orders of magnitude, and the eigenvalue corresponding to the fifth gust modeling state offset and maintained at a value 20% in error. In the fifth order model runs, the maximum likelihood algorithm was directed to establish parameter estimates for the eigenvalues of the flexible modes, all elements of the H_0 matrix, and the first four elements of the column matrix W_0 for the swept frequency data (the W_0 elements were set and fixed at the same 0 and 1 normalized values as the G_0 matrix when analyzing randomly excited response data since these values can be arbitrarily set with no loss in generality when u = 0).

Results obtained in analyzing 16 independent randomly excited simulated data records of 10, 20, 30, 60, and 90 sec duration are shown in Table 1 for the eleventh order analysis model and Table 2 for the fifth order analysis model. Typical power spectral density plots for the simulated measurement signa-

Table 2 — Statistical Results for 16 Simulated Randomly Excited Data Runs (at Each of Five Different Durations) Using the Maximum Likelihood Method & a 5th Order Analysis Model

	Mode 1 true f_d = 3.1419 Hz true g = 0.1474		Mode 2 true f_d = 9.8223 Hz true g = 0.3758		Run Duration
	Freq (f_d)	Damp. (g)	Freq (f_d)	Damp. (g)	
Mean	3.1706	0.1433	9.7007	0.3770	10 sec
Std dev	0.0859	0.0454	0.2208	0.0572	2500 points
Mean	3.1496	0.1421	9.7436	0.3641	20 sec
Std dev	0.0610	0.0295	0.1126	0.0327	5000 points
Mean	3.1375	0.1435	9.7236	0.3541	30 sec
Std dev	0.0496	0.0277	0.0898	0.0261	7500 points
Mean	3.1378	0.1376	9.7216	0.3760	60 sec
Std dev	0.0271	0.0146	0.0693	0.0224	15,000 points
Mean	3.135	0.1368	9.7138	0.3777	90 sec
Std dev	0.0188	0.0085	0.0494	0.0161	22,500 points

R84-0282-002B

Table 1 — Statistical Results for 16 Simulated Randomly Excited Data Runs (at Each of Five Different Durations) Using the Maximum Likelihood Method & a 11th Order Analysis Model

	Mode 1 true f_d = 3.1419 Hz = 0.1474		Mode 2 true f_d = 9.8223 Hz true g = 0.3758		Run Duration
	Freq (f_d)	Damp. (g)	Freq (f_d)	Damp. (g)	
Mean	3.1689	0.1587	9.8544	0.3664	10 sec
Std dev	0.0907	0.0411	0.1902	0.0492	2500 points
Mean	3.1534	0.1517	9.8837	0.3535	20 sec
Std dev	0.0584	0.0293	0.1422	0.0341	5000 points
Mean	3.1410	0.1518	9.8472	0.3552	30 sec
Std dev	0.0449	0.0274	0.0977	0.0245	7500 points
Mean	3.1407	0.1492	9.8397	0.3680	60 sec
Std dev	0.0279	0.0134	0.0762	0.0231	15,000 points
Mean	3.1386	0.1473	9.8294	0.3701	90 sec
Std dev	0.0198	0.0090	0.0567	0.0149	22,500 points

R84-0282-001B

are shown in Figs. 5 and 6 revealing that the response level of the 9.8223 Hz mode relative to the 3.1419 Hz mode was almost negligible on the first measurement and very low on the second. Despite this fact, the results shown in Tables 1 and 2 indicate that the maximum likelihood technique was able to obtain good results for the frequency and damping of both modes using either an eleventh or fifth order analysis model. Scatter plots for data record lengths of 10, 30, and 90 sec are shown in Figs. 7 and 8. The results of these figures emphasize that the maximum likelihood results were statistically consistent with either analysis model, asymptotically unbiased when the proper eleventh order analysis model was used, and contained an insignificant bias error when the inexact fifth order analysis model was used.

Typical time histories for simulated swept frequency measurements are shown in Figs. 9 and 10. The exponential shaker sweep covered the 1 to 20 Hz frequency range in 10 sec. Figures 11 and 12 contain scatter plots obtained in analyzing 16 noisy 10 sec simulated swept frequency data records with eleventh and fifth order models, respectively. Here again the difference between results obtained with the

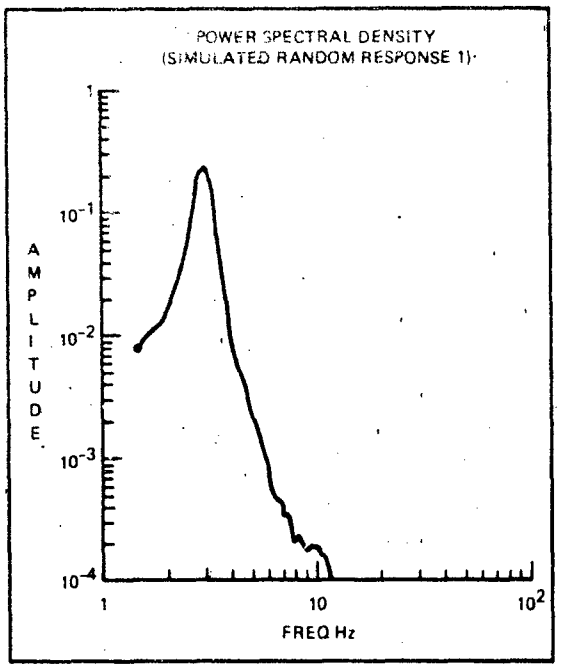

Fig. 5 Typical Power Spectral Density for 1st Simulated Randomly Excited Measurement

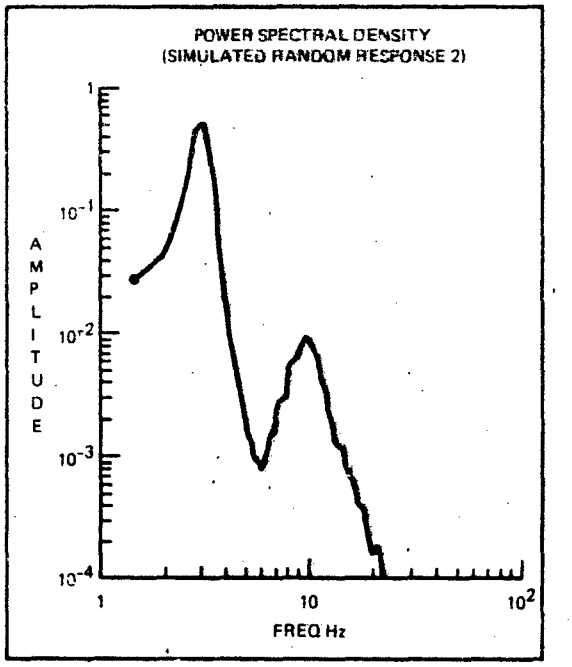

Fig. 6 Typical Power Spectral Density for 2nd Randomly Excited Measurement

eleventh and fifth order analysis models did not appear to be significant. The accuracy of the results for the 10 sec sweep were better than the results obtained in analyzing the 10 sec randomly excited data records. This is undoubtedly due to the more pronounced response level of the 9.8223 Hz mode in the measurement data. It should be noted that in the swept frequency analysis runs, parameter values for modal damped natural frequency and for elements of the H_0 matrix could be quickly brought close to their true values by ignoring process noise and using the simplified maximum likelihood algorithm (discussed in subsection 3.2) on the first few data passes and then completing the analysis with the generalized algorithm.

Our prime interest in the analysis of real flight test data has centered on evaluating the ability of the maximum likelihood algorithm to analyze response data excited by atmospheric turbulence. Since the analysis of this type of data was not extensively pursued by Grumman on past flight test programs, the availability of actual data is somewhat limited. However, some preliminary impressions have been obtained from F-14A fin and wing response data excited by atmospheric effects. Here, dynamic models in the 10 to 20-state range have been used to evaluate flexible modes in the 5 to 65 Hz frequency band. In these preliminary runs, model structure has been determined from power spectral density analysis of the actual test data. In effect, the number of states in the model reflect the number of modes (flexible and rigid) observed in the data, plus an added state to roughly account for low-frequency turbulence inputs. Thus far, the maximum likelihood algorithm has demonstrated the ability to take crudely defined initialization models and converge on final system models that yield good modal frequency and damping estimates.

When analyzing real data, there are no absolute references for establishing accuracy. One must rely on trusted results obtained under similar test conditions via other methods or on engineering judgement. In this latter category, we have been encouraged to see that the spectral characteristics of identified system models agree with those of the actual test data. As indicated in Reference 2, this does not necessarily ensure the accuracy of modal frequency and damping estimates. However, our experience has indicated that the accuracy of identified results is normally poor when a good spectral match is not achieved. Further confidence can be gained by inspecting the identified system Kalman filter residuals, $\underline{\nu}$, which tend to be low level and noise-like when parameters are correctly identified. Obtaining convergence of the algorithm is by no means trivial, but our experience has indicated that strategies can be devised for varying parameters on a pass-by-pass basis that will work most of the time for a given set of measurements.

Figure 13 shows a 24 sec segment of randomly excited F-14A fin velocity response data and a corresponding power spectral density estimate computed from the signal. In addition to fin first bending, rudder rotation, and rudder torsion (which were the modes of interest for this measurement, accounting

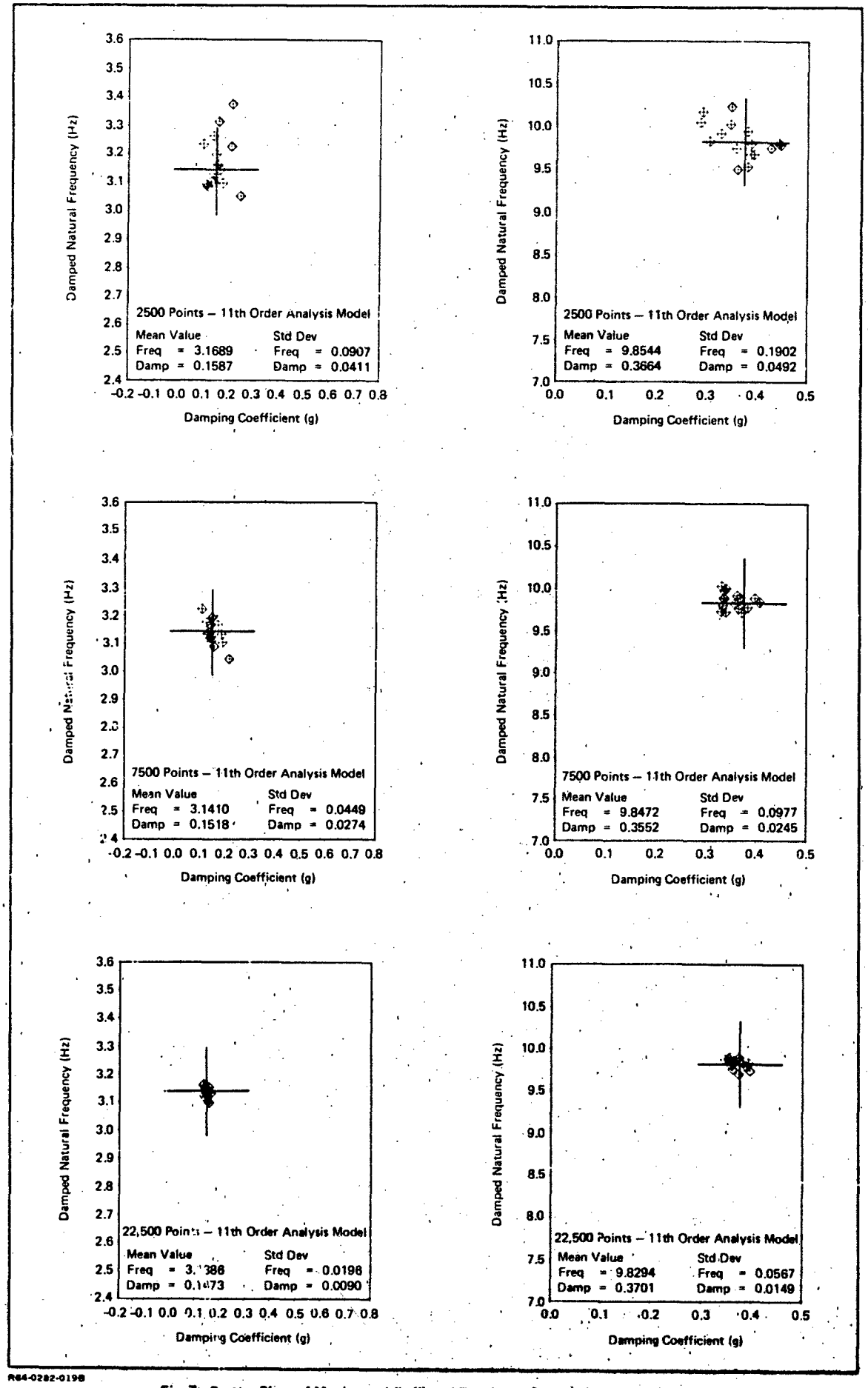

R84-0282-019B

Fig. 7 Scatter Plots of Maximum Likelihood Results on Randomly Excited Data Using a

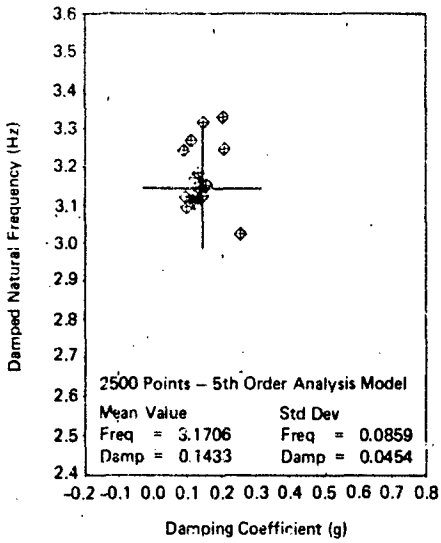
Damped Natural Frequency (Hz)
3.6
3.5
3.4
3.3
3.2
3.1
3.0
2.9
2.8
2.7
2.6
2.5
2.4
2500 Points – 5th Order Analysis Model
Mean Value
Freq = 3.1706
Damp = 0.1433
Std Dev
Freq = 0.0859
Damp = 0.0454
-0.2 -0.1 0.0 0.1 0.2 0.3 0.4 0.5 0.6 0.7 0.8
Damping Coefficient (g)

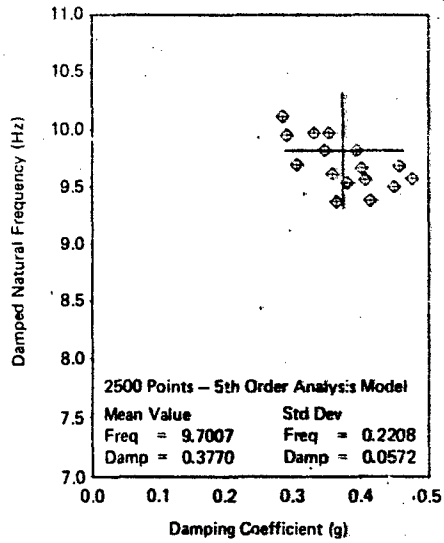
Damped Natural Frequency (Hz)
11.0
10.5
10.0
9.5
9.0
8.5
8.0
7.5
7.0
2500 Points – 5th Order Analysis Model
Mean Value
Freq = 9.7007
Damp = 0.3770
Std Dev
Freq = 0.2208
Damp = 0.0572
0.0 0.1 0.2 0.3 0.4 0.5
Damping Coefficient (g)

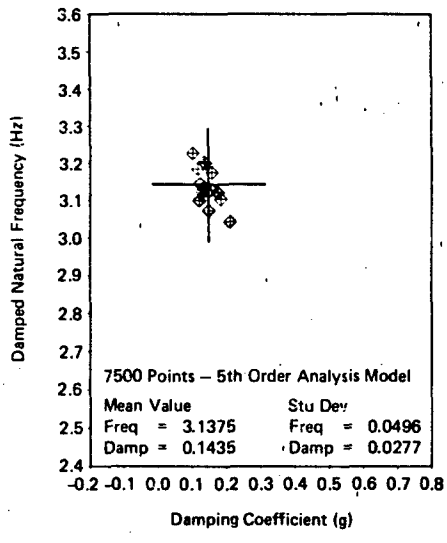
Damped Natural Frequency (Hz)
3.6
3.5
3.4
3.3
3.2
3.1
3.0
2.9
2.8
2.7
2.6
2.5
2.4
7500 Points – 5th Order Analysis Model
Mean Value
Freq = 3.1375
Damp = 0.1435
Std Dev
Freq = 0.0496
Damp = 0.0277
-0.2 -0.1 0.0 0.1 0.2 0.3 0.4 0.5 0.6 0.7 0.8
Damping Coefficient (g)

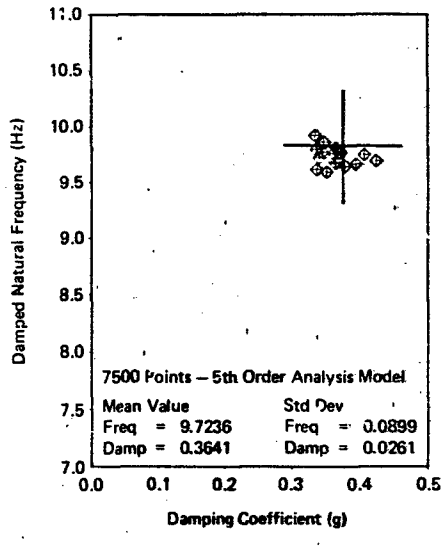
Damped Natural Frequency (Hz)
11.0
10.5
10.0
9.5
9.0
8.5
8.0
7.5
7.0
7500 Points – 5th Order Analysis Model
Mean Value
Freq = 9.7236
Damp = 0.3641
Std Dev
Freq = 0.0899
Damp = 0.0261
0.0 0.1 0.2 0.3 0.4 0.5
Damping Coefficient (g)

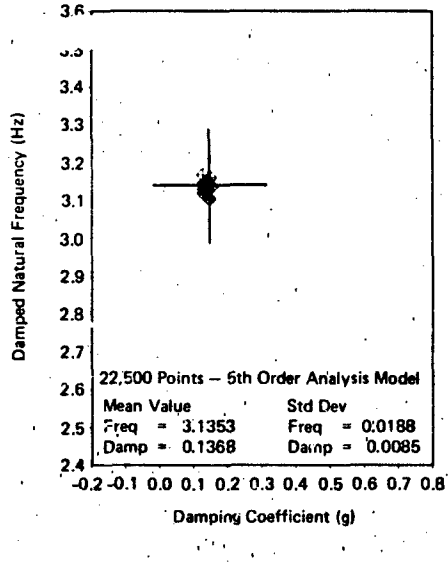
Damped Natural Frequency (Hz)
3.6
3.4
3.3
3.2
3.1
3.0
2.9
2.8
2.7
2.6
2.5
2.4
22,500 Points – 5th Order Analysis Model
Mean Value
Freq = 3.1353
Damp = 0.1368
Std Dev
Freq = 0.0188
Damp = 0.0085
-0.2 -0.1 0.0 0.1 0.2 0.3 0.4 0.5 0.6 0.7 0.8
Damping Coefficient (g)

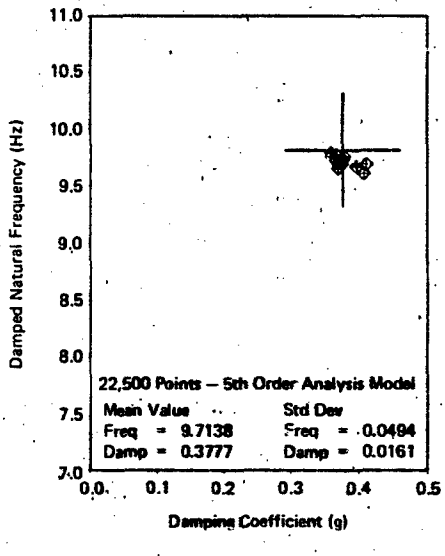
Damped Natural Frequency (Hz)
11.0
10.5
10.0
9.5
9.0
8.5
8.0
7.5
7.0
22,500 Points – 5th Order Analysis Model
Mean Value
Freq = 9.7138
Damp = 0.3777
Std Dev
Freq = 0.0494
Damp = 0.0161
0.0 0.1 0.2 0.3 0.4 0.5
Damping Coefficient (g)

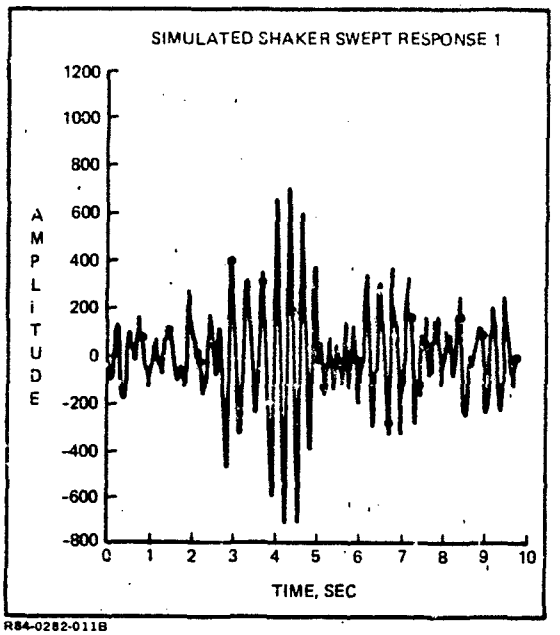

Fig. 9 Typical Time History for 1st Simulated Swept Frequency Measurement

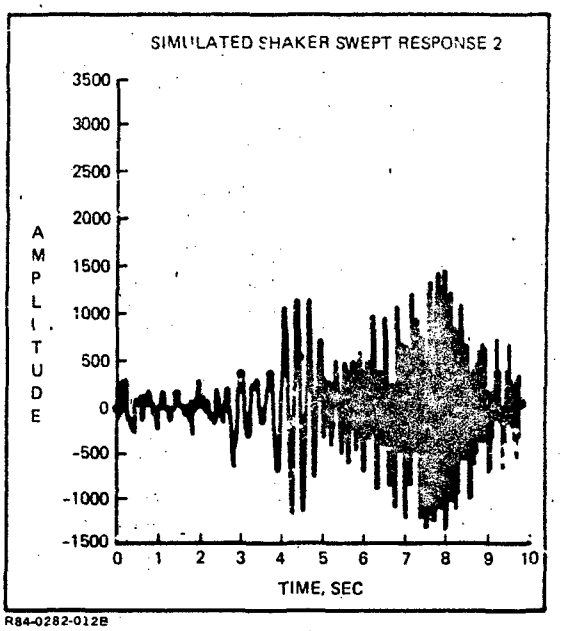

Fig. 10 Typical Time History for 2nd Simulated Swept Frequency Measurement

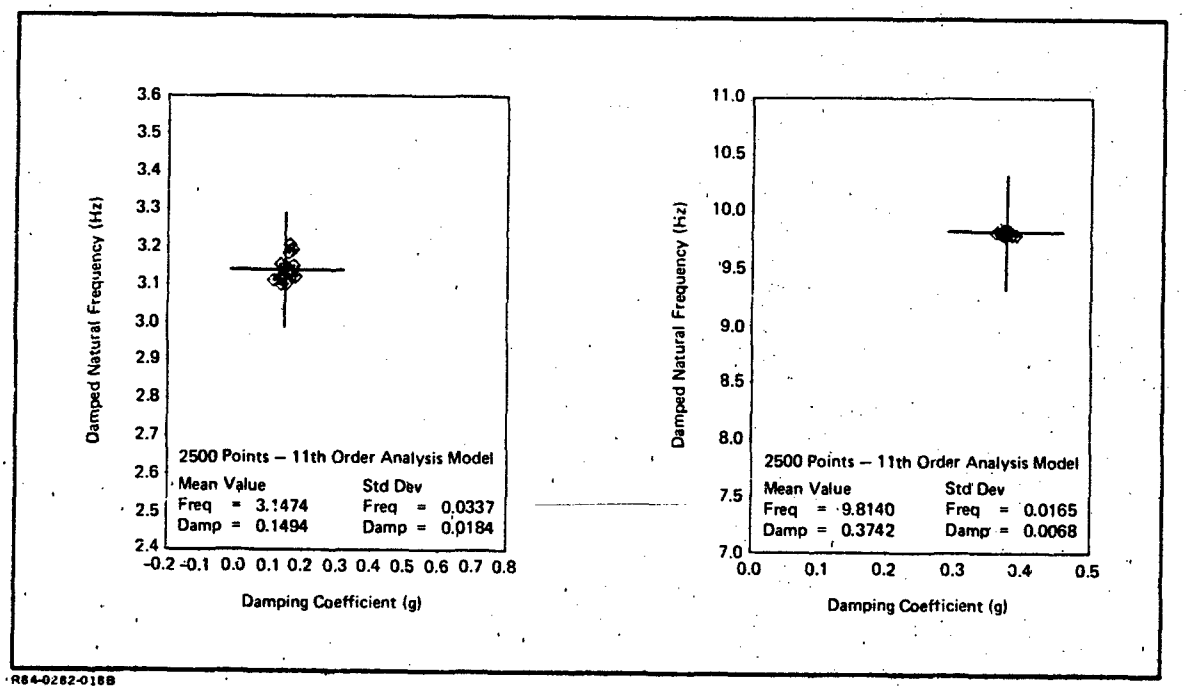

Fig. 11 Scatter Plots of Maximum Likelihood Results on Data Excited Via a 10 sec Shaker Sweep Using a 11th Order Analysis Model

for the resonant peaks at approximately 12.5, 44, and 63 Hz, respectively) the spectral information indicated a low frequency mode (perhaps short period rigid body motion) and resonances which happened to coincide with first and second wing bending modes (at approximately 5.5 and 16 Hz, respectively). Therefore a thirteenth order model was used to analyze the data, 12 states to model the apparent modal content of the response signal and a thirteenth state to account for gust modeling. Figure 14 shows the power spectral density estimate calculated from a 24 sec randomly excited data segment generated with the thirteenth order model obtained via maximum likelihood analysis of the fin data. The modeled spectral information compares favorably with that obtained from the actual test data, as set forth in Fig. 13. In addition, Fig. 15 shows a high resolution (1 sec snapshot) time history of the actual measurement data and the corresponding low-level noise-like Kalman filter innovation signal achieved with the estimated system model. Finally, the damped natural frequencies and damping coefficients determined for fin first bending, rudder rotation, and rudder torsion agreed closely with results obtained with current least-squares identification software from a fin shaker sweep at the same test condition (frequencies agreed within 1.6% and damping values within 7.5%).

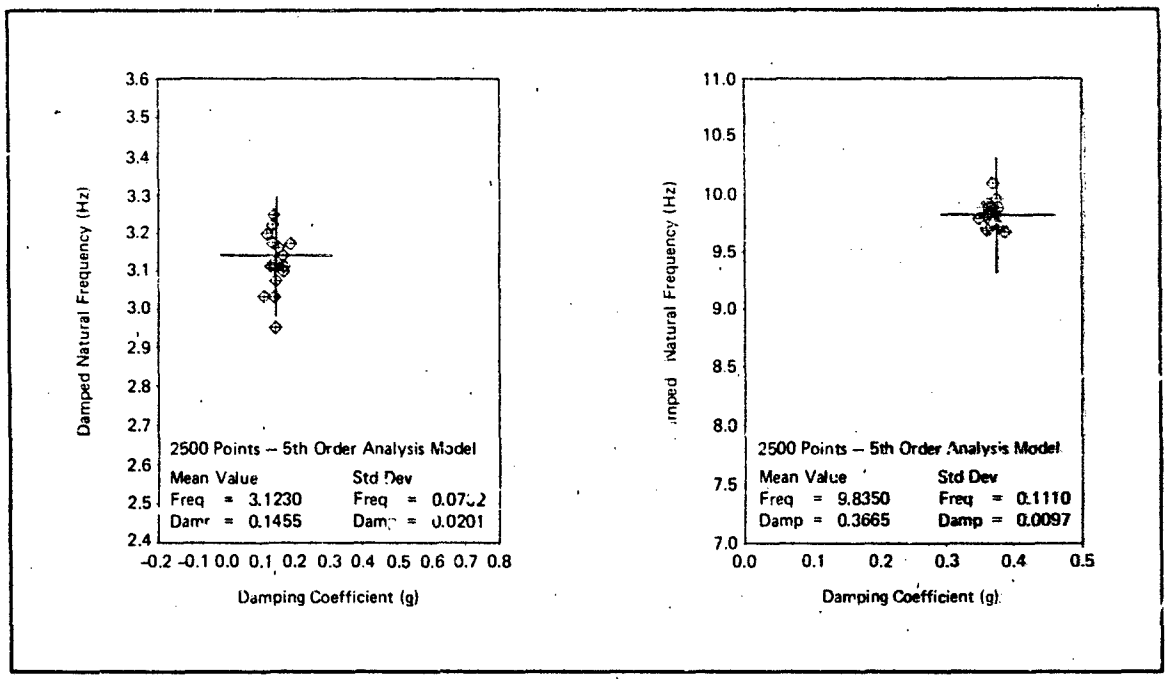

R84-G282-017B

Fig. 12 Scatter Plots of Maximum Likelihood Results on Data Excited Via a 10 sec Shaker Sweep Using a 5th Order Analysis Model

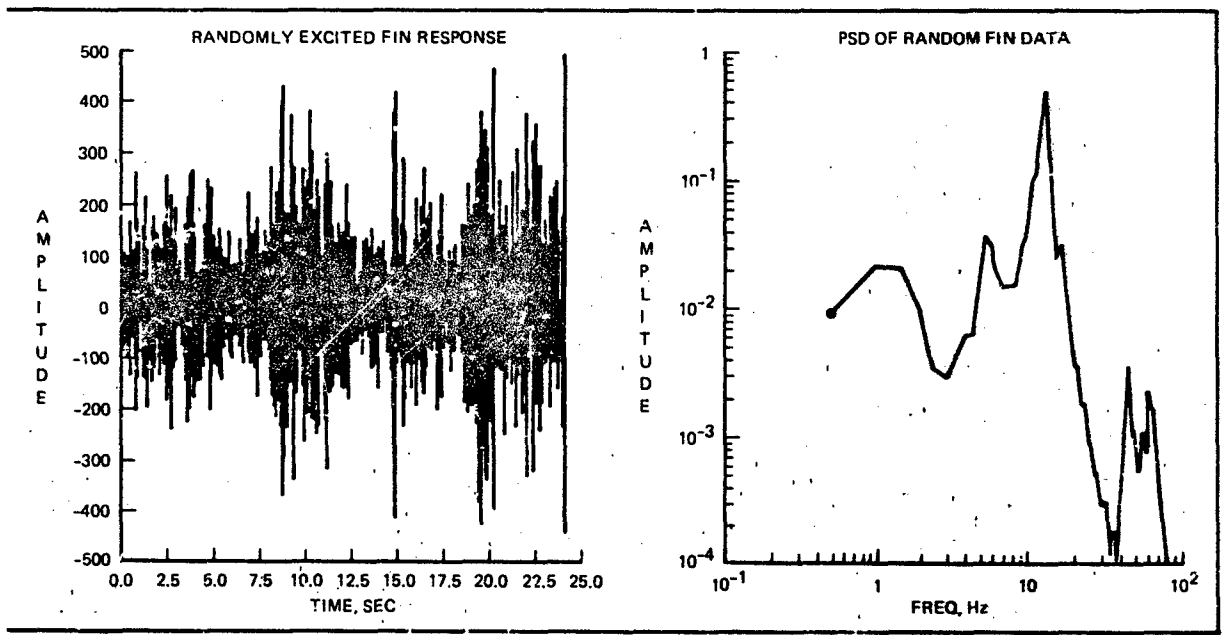

84-G282-013B

Fig. 13 Time History & Corresponding Power Spectral Density for F-14A Randomly Excited Fin Response Data

4.2 Comparison to Least-Squares Analysis

To obtain a comparison between the maximum likelihood method and our current analysis techniques, the simulated randomly excited and swept frequency data were analyzed using the frequency domain windowing method described in subsection 3.3. Both types of data were analyzed using normal processing procedures. This consists of first reviewing the frequency response data and selecting at least two sets of rectangular windows that best bracket the resonances in the data. Second, difference equation model sizes are chosen for use on the windowed signals (inverted from the frequency into the time domain) that are equal to and slightly larger than that necessary to accommodate the number of modes observed in the windowed frequency range. For the simulated data, which contained two flexible modes, fourth and sixth order difference equation models were used in each analysis window. Modeled frequency domain plots calculated by the software for each identified difference equation model in each

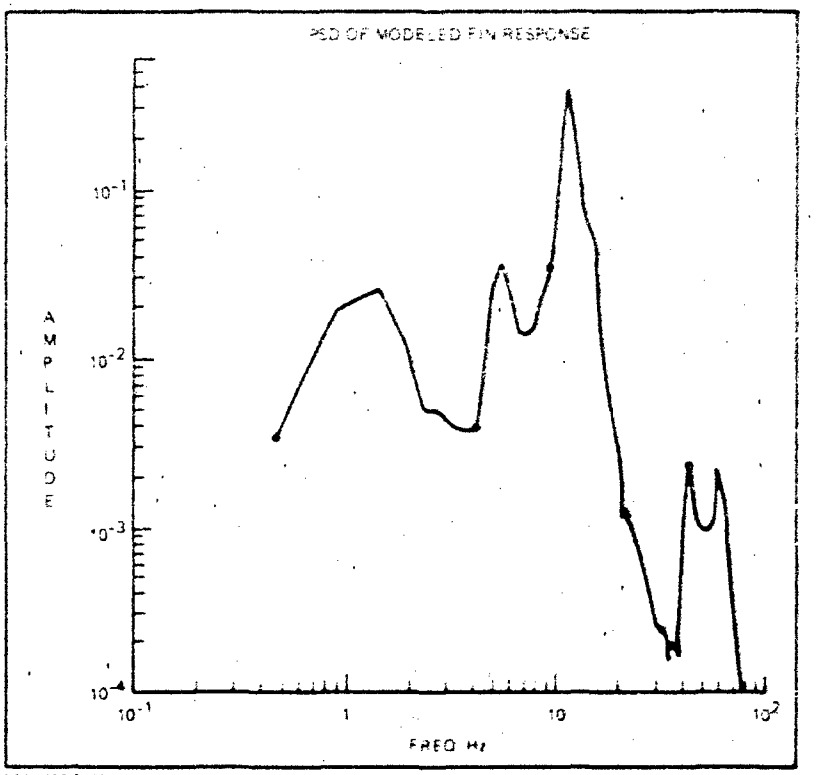

Fig. 14 Power Spectral Density for Modeled F-14A Fin Response Data (Model Determined via Maximum Likelihood Identification Analysis)

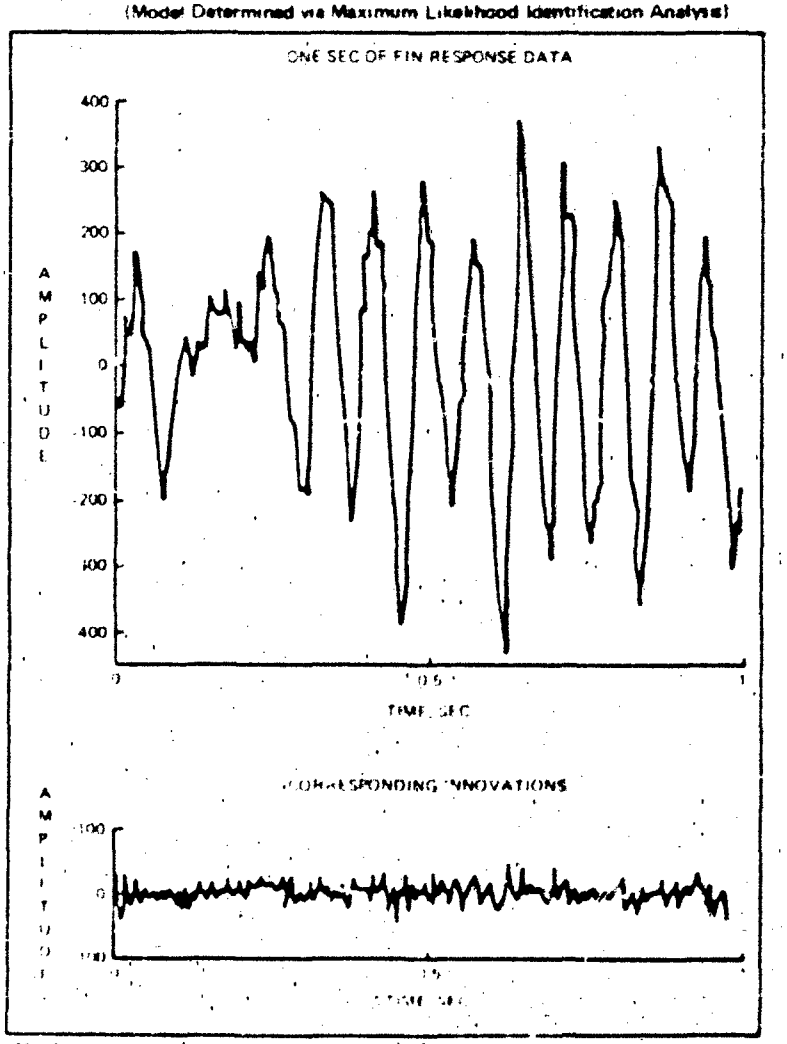

Fig. 15 Typical High Resolution Comparison of Actual F-14A Fin Response Data Segment & Maximum Likelihood Innovation Signal Level

analysis window were used for comparison with the corresponding frequency response information calculated from the actual data. This latter comparison of identified model and calculated raw data frequency response information helps the analyst to eliminate results which are obviously in error as indicated by a poor match. The accuracy of the results can be quite sensitive to both window and model order variations generally requiring an experienced analyst to interpret the results obtained. A significant advantage that the maximum likelihood method has over the current technique is that only one all-encompassing model is used for analysis. An additional advantage is that all the data in the measurement record is used, thus eliminating the need for windowing information.

The statistical results displayed in Tables 3 and 4 reflect the performance of current least-squares analysis software in processing the simulated randomly excited and swept frequency data, respectively.

Table 3 – Statistical Results for 16 Simulated Randomly Excited Data Runs (of Varying Duration) Using the Current Least-Squares Method

	Mode 1 true f_d = 3.1419 Hz true g = 0.1474		Mode 2 true f_d = 9.8223 Hz true g = 0.3758		Analysis Variables D = run duration W = analysis window M = model order
	Freq (f_d)	Damp. (g)	Freq (f_d)	Damp. (g)	
Mean	3.0591	0.1174	9.3068	0.2029	D = 10 sec 2500 points W = 1.0 to 15.0 Hz M = 4th order
Std dev	0.0885	0.0511	0.7409	0.1088	
Mean	3.1002	0.1367	9.3309	0.3144	D = 30 sec 7500 points W = 1.0 to 15.0 Hz M = 4th order
Std dev	0.0756	0.0294	0.5187	0.0381	
Mean	3.1384	0.1415	9.5198	0.3804	D = 90 sec 22,500 points W = 1.0 to 15.0 Hz M = 4th order
Std dev	0.0341	0.0204	0.5166	0.0581	
Mean	3.1515	0.1372	9.8633	0.1988	D = 90 sec 22,500 points W = 2.0 to 13.0 Hz M = 4th order
Std dev	0.0373	0.0190	0.3337	0.0393	
Mean	3.1436	0.1442	10.3687	0.2345	D = 90 sec 22,500 points W = 1.0 to 15.0 Hz M = 6th order
Std dev	0.0348	0.0251	0.9486	0.0987	
Mean	3.1456	0.1335	11.0567	0.0997	D = 90 sec 22,500 points W = 2.0 to 13.0 Hz M = 6th order
Std dev	0.0393	0.0196	0.7042	0.0558	

H84-0282-00 3B

Table 4 – Statistical Results for 16 Noisy Simulated Swept Frequency Data Runs of 10 Sec Duration (2500 Points) Using the Current Least-Squares Method

	Mode 1 true f_d = 3.1419 Hz true g = 0.1474		Mode 2 true f_d = 9.8223 Hz true g = 0.37[illegible]		Analysis Variables W = analysis window M = model order
	Freq (f_d)	Damp. (g)	Freq (f_d)	Damp. (g)	
Mean	3.1768	0.1525	9.6811	0.3698	W = 1.2 to 13.0 Hz M = 4th order
Std dev	0.0765	0.0371	0.1477	0.0224	
Mean	3.1533	0.1615	9.4483	0.3879	W = 2.0 to 12.0 Hz M = 6th order
Std dev	0.0792	0.0424	0.2016	0.0185	
Mean	3.2108	0.4801	10.0765	0.2408	W = 1.2 to 13.0 Hz M = 4th order
Std dev	0.1154	0.1630	0.2015	0.0541	
Mean	3.0981	0.2802	9.7556	0.1224	W = 2.3 to 12.0 Hz M = 4th order
Std dev	0.0740	0.1164	0.1118	0.0425	

A84-0282-00 4B

Scatter plots of the random analysis results for the best analysis window (1 to 15 Hz with a fourth order model) are shown for data record lengths of 10, 30, and 90 sec in Fig. 16. These results are inferior to those obtained for the maximum likelihood technique (see Fig. 7), specifically with respect to the low-level 9.8223 Hz mode. The last three entries in Table 3 show that minor variations in frequency windowing and model order caused the results for the low-level mode to degrade significantly, even with 90 sec of data available for analysis. In practice, the scatter introduced by small window and model order differences proves to be one of the more significant shortcomings of the current least-squares analysis approach and often makes evaluation of the test data difficult. The results shown in Table 4 and Fig. 17 show similar performance on the simulated swept frequency data. For this data analysis, the best results were obtained with a window of 1.2 to 13 Hz and a sixth order difference equation model. Here the low-frequency mode was more difficult to analyze due to the short duration shaker sweep. The high-frequency mode was driven out relatively well on the second measurement signal (see Fig. 10) which was the only signal used in the least-squares analysis. From the standpoint of accuracy, the results indicate that the maximum likelihood algorithm is clearly superior to the least-squares approach.

5. CLOSING COMMENTS

The preliminary results discussed in Section 4 indicate that the maximum likelihood technique is analytically capable of accurate determining modal frequency and damping estimates from noisy flutter response signals. Its ability model both process and measurement noise enable it to consistently outperform older methods. Most notably, the method can accurately determine modal characteristics in those flight test situations where the measured data is dominated by or solely due to the aircraft's aeroelastic response to atmospheric turbulence. In light of these results, the ability to use the maximum likelihood method to confirm the validity of a detailed physical aeroelastic model which, in turn, would be used to make accurate flutter margin projections seems more plausible. In any event, the increased accuracy in determining modal frequency and damping results will allow more precise extrapolations of these measured quantities to obtain flutter margin estimates.

The maximum likelihood algorithm requires multiple passes through a given test data record to obtain final convergence on estimated parameter values. The technique is computationally intensive, and compared to our current least-squares method, generally requires a 1 to 2 order of magnitude increase in computer arithmetic processing power for the timely determination of results. Use of this advanced analysis technique in on-line flight testing requires a high-speed computer with at least a half million words of central data memory. We consider our plans to implement this method on a Floating Point Systems 164 peripheral array processor to be a minimum capability configuration allowing us to handle flutter models in the 10 to 30-state range in an on-line processing environment. Larger models would be handled in a batch processing environment on the 164 array processor or dispatched to a supercomputer supporting test operations. Realization of this on-line processing goal is dependent on initializing the algorithm with aeroelastic models that enable convergence to be achieved quickly. Here our primary approach will be to use analytically derived engineering models precomputed for each anticipated test condition or, alternately, models determined at the previous test point in an incremental test build up.

6. REFERENCES

1. Perangelo, H. J. and Milordi, F. W.: "Flight Flutter Testing Technology at Grumman," presented at the NASA Symposium on Flutter Testing Techniques, Flight Research Center, Edwards, CA, Oct. 9–10, 1975.

2. Koenig, K.: "Flight Vibration Test Analysis - Methods, Theory, and Application," presented at the AIAA 2nd Flight Testing Conference Las Vegas, NV, Nov. 16–18, 1983.

3. Klein, V.: "Identification Evaluation Methods," AGARD Lecture Series No. 104 On Parameter Identification, AGARD-LSP-104, Oct. 1979, pp. 2-1 to 2-21.

4. Schiano, C. and Simpson, E. M.: "Grumman's Automated Telemetry System Past, Present and Future," presented at the AIAA 2nd Flight Testing Conference, Las Vegas, NV, Nov. 16–18, 1983.

5. Clark, W. B.: "Loads and Dynamics Program Record No. 81.1," Grumman Aerospace Corporation Internal Report, Oct. 1981.

6. Bryson, A. E. and Ho, Y. C.: "Applied Optimal Control," John Wiley and Sons, Inc., NY, 1975, pp. 348-377.

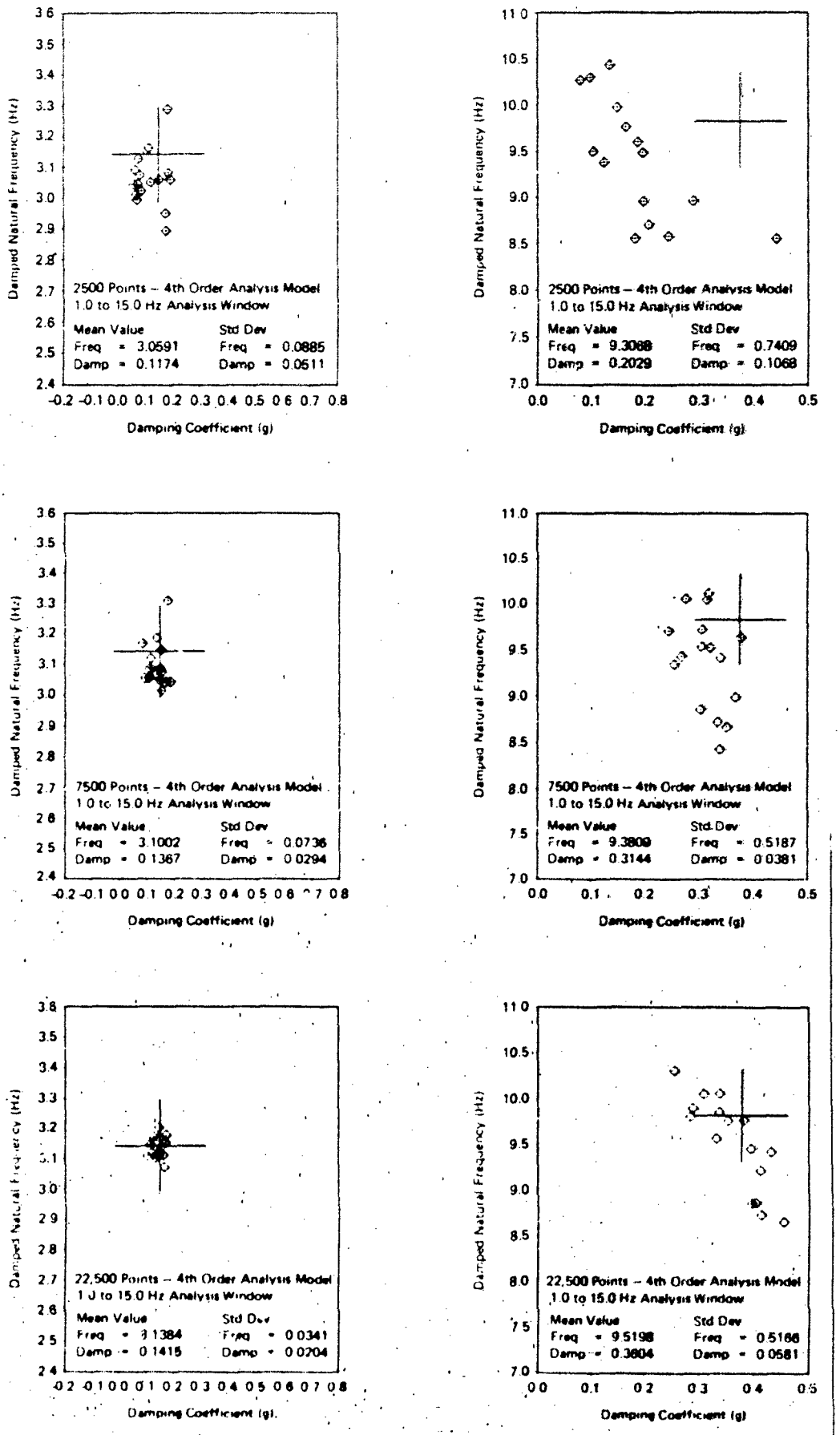

H66-0292-021B

Fig. 16. Scatter Plots of Least-Squares Results on Randomly Faulted Data

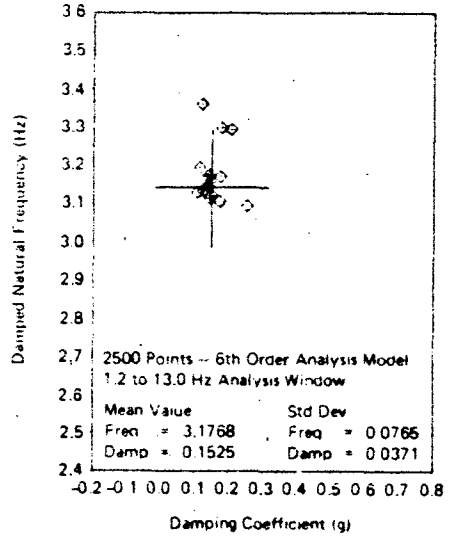
Damped Natural Frequency (Hz)
2500 Points – 6th Order Analysis Model
1.2 to 13.0 Hz Analysis Window
Mean Value
Freq = 3.1768
Damp = 0.1525
Std Dev
Freq = 0.0765
Damp = 0.0371
Damping Coefficient (g)

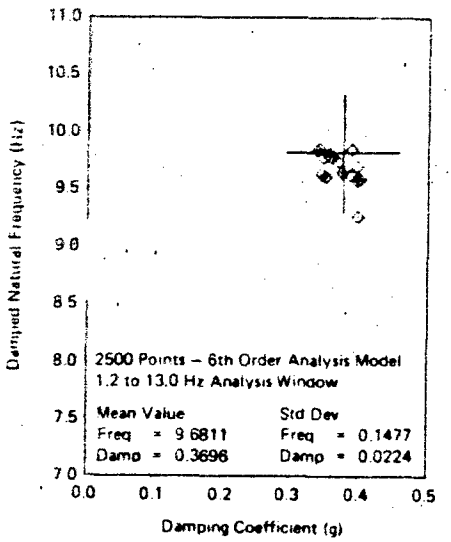
Damped Natural Frequency (Hz)
2500 Points – 6th Order Analysis Model
1.2 to 13.0 Hz Analysis Window
Mean Value
Freq = 9.6811
Damp = 0.3696
Std Dev
Freq = 0.1477
Damp = 0.0224
Damping Coefficient (g)

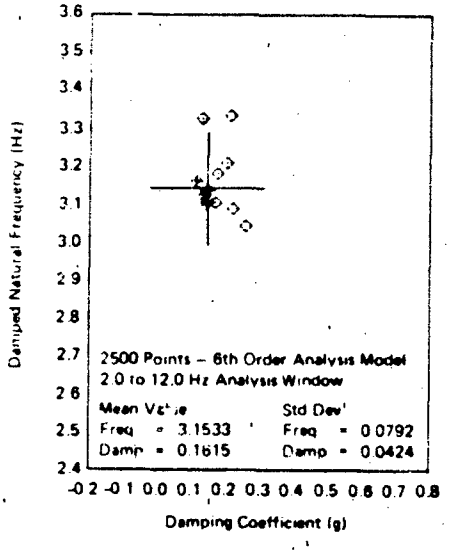
Damped Natural Frequency (Hz)
2500 Points – 6th Order Analysis Model
2.0 to 12.0 Hz Analysis Window
Mean Value
Freq = 3.1533
Damp = 0.1615
Std Dev
Freq = 0.0792
Damp = 0.0424
Damping Coefficient (g)

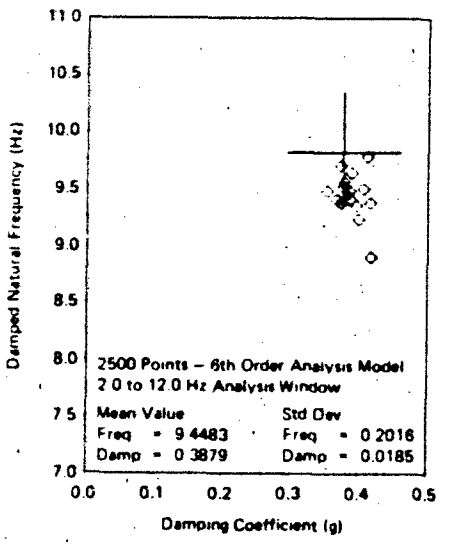
Damped Natural Frequency (Hz)
2500 Points – 6th Order Analysis Model
2.0 to 12.0 Hz Analysis Window
Mean Value
Freq = 9.4483
Damp = 0.3879
Std Dev
Freq = 0.2016
Damp = 0.0185
Damping Coefficient (g)

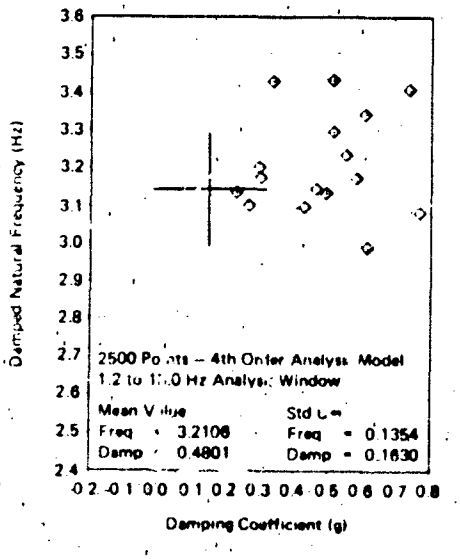
Damped Natural Frequency (Hz)
2500 Points – 4th Order Analysis Model
1.2 to 13.0 Hz Analysis Window
Mean Value
Freq = 3.2106
Damp = 0.4801
Std Dev
Freq = 0.1354
Damp = 0.1630
Damping Coefficient (g)

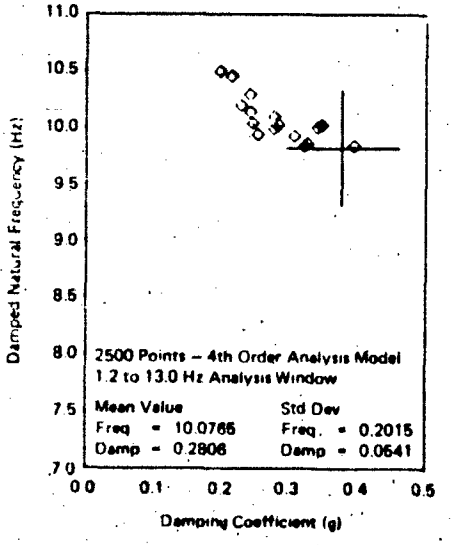
Damped Natural Frequency (Hz)
2500 Points – 4th Order Analysis Model
1.2 to 13.0 Hz Analysis Window
Mean Value
Freq = 10.0765
Damp = 0.2806
Std Dev
Freq = 0.2015
Damp = 0.0641
Damping Coefficient (g)

7. Russo, M. L., Richards, P. T. and Perangelo, H. J.: "Identification of Linear Flutter Models," presented at the AIAA 2nd Flight Testing Conference, Las Vegas, NV, Nov. 16–18, 1983.

8. Le May, J. L.: "Kalman Filtering," lecture notes for course Kalman Filtering-Engineering 881.38 offered by the University of California (Extension for Continuing Education), Los Angeles, CA, March 10–14, 1980.

A TECHNIQUE TO DETERMINE LIFT AND DRAG POLARS IN FLIGHT

A. KNAUS
HEAD OF DATA ANALYSIS
FLIGHT TEST DEPARTMENT
MESSERSCHMITT-BÖLKOW-BLOHM GMBH, 8 MUNICH 80
FEDERAL REPUBLIC OF GERMANY

SUMMARY

Performance trials of the European combat aircraft TORNADO have concentrated on the systematic measurement of lift and drag polars. Such polars have been successfully measured by means of well-adapted test instrumentation, a data reduction system, and a high calibration standard of the aircraft and engines. The use of a certain combination of steady-state and dynamic test maneuvers has resulted in a drastic reduction in the amount of flight time required to obtain sufficient data for the determination of the zero lift drag, induced drag characteristics and drag increments due to aircraft configuration changes. Flight test results are presented which demonstrate the advantage of the test technique utilized and the high data quality achieved.

NOMENCLATURE

A_7	= nozzle exit area calculated
A_j	= nozzle exit area measured
AX_D	= acceleration along flight path
AZ_L	= acceleration normal to flight path
AX_{NC}, AY_{NC}, AZ_{NC}	= acceleration corrected
C_D, C_L	= coefficient of drag and lift, respectively
C_G	= gross thrust coefficient
C_{DN}	= nozzle discharge coefficient
C.G.	= center of gravity
C_P	= specific heat value
D	= drag
D_R	= ram drag
EHV	= effective heating value
F_{EX}	= excess thrust
F_G	= gross thrust
F_{Gid}	= gross thrust ideal (calculated)
F_N	= net thrust
G	= enthalpy ($C_P \cdot T_T$)
g	= gravitational constant
K_1, K_2	= angle-of-attack calibration coefficients
L	= lift
MF_M	= main fuel mass flow
MF_R	= reheat fuel mass flow
M_T	= Mach=true Mach number
M_1	= air mass flow at engine entry
M_5	= gas mass flow at nozzle entry
M_7	= gas mass flow at nozzle exit

M_{BL} = bleed mass flow

N_H = high pressure spool speed

N_L = low pressure spool speed

n_z = load factor

Ps_o = ambient pressure

P_{mix} = mixed total pressure (from PT_4 + PT_{4LB})

P_j = total pressure at nozzle exit

PS_2 = static pressure HP-compressor exit

PS_{2LB} = static pressure bypass entry

PS_7 = static pressure at nozzle exit

PT_1 = total pressure at engine entry

PT_{2LB} = total pressure at bypass entry

PT_4 = total pressure at LP-turbine exit

PT_{4LB} = total pressure at bypass exit

PT_7 = total pressure at nozzle exit

POT = power off take

P = roll rate

q = pitch rate or dynamic pressure

r_x = angle of attack sensor x-axis distance to C.G.

r_y = angle of attack sensor y-axis distance to C.G.

S.L. = sea level

TS_7 = static temperature at nozzle exit

TT_{BL} = total temperature bleed outlet

TT_F = fuel temperature

TT_1 = free stream total temperature

TT_2 = total temperature HP-compressor exit

TT_{2LB} = total temperature bypass entry

TT_5 = mixed jet pipe entry temperature

TT_7 = total temperature at nozzle exit

V_T = true airspeed

V_7 = nozzle exhaust speed

W = weight

α_E = corrected true angle of attack

α_i = indicated angle of attack

β = angle of sideslip

γ = angle of flight path

ΔA_7 = nozzle area correction

ΔP = $P_{mix} - P_j$

η_C, η_R = burner efficiency

Λ = angle of wing sweep

σ = angle of engine installation

INTRODUCTION

The determination of the performance capability of a newly developed combat aircraft during flight testing is of great importance. The purpose of aircraft performance trials is to obtain characteristic performance data for the entire mission spectrum. These data are needed in order to compare flight test derived results with predicted data, to determine the performance capability of the aircraft, and to provide evidence of this capability to the customer.

As a rule, when a new aircraft project is being developed, the first phase of testing is carried out on prototypes with an airframe and a powerplant system which, in most cases, are not completely identical to those in the final production aircraft. For this reason, the accurate measurement of engine thrust and the establishment of the lift and drag polars should be given priority from the very beginning.

Thus, in the course of flight testing, the aerodynamic qualities of the airframe and the effectiveness of the power system can be determined and analyzed systematically. These considerations were of particular importance in the case of the European combat aircraft Tornado. On the one hand, flight testing on the newly developed RB 199 three-spool engine has been started simultaneously with aircraft testing. The result was that most of the aircraft performance trials had to be carried out with engines whose performance characteristics were not identical to those of production engine. On the other hand, the aerodynamic configuration of the first prototypes was not identical to that of the final production aircraft. Windtunnel tests had already revealed that various modifications had to be flight tested so as to optimize the airframe. Beyond that, a large number of different aircraft configurations (i.e. different wing sweeps, flap/slats settings, external stores) had to be tested within an extensive Mach, altitude, and normal acceleration envelope.

Therefore, the objective of Tornado performance trials was to determine the performance characteristics by means of an economic test method which ensures high-quality data, and to evaluate and analyze the test results within a short time period. This paper gives a general overview of the methods and techniques which were used to measure the Tornado lift and drag polars, and it also presents typical test results. The thrust-in-flight measurement method used in this context is briefly discussed.

TEST AIRCRAFT

The design of the two-seat Multi Role Combat Aircraft Tornado is characterized by its compact fuselage and shoulder mounted variable geometry wing, and its low taileron and relatively tall vertical fin. A three-view drawing of the airplane is shown in Fig. 1. The sweep range of the wing is 25° to 67° and can be manually controlled in flight. Lift augmentation for takeoff, landing and maneuvering is provided by full span leading-edge slats, double-slotted trailing-edge flaps, and Krüger flaps on the highly swept fixed wing gloves. Two speed brakes with an automatic blowback system are located on the upper side of the rear fuselage. A wide range of external stores can be carried on a total of seven pylons; three pylons under the fuselage and, under the movable wings, two swiveling pylons each. The air intake system consists of two horizontal, two dimensional variable geometry inlets with three ramps. Ploughshare shaped boundary-layer diverters seperate the intake from the fuselage side. An inlet throat bleed hood is located on the top of each intake for ramp boundary-layer control and inlet air bypass. Furthermore, two blow-in auxiliary doors are on the side of each intake in order to achieve high-pressure recovery under takeoff conditions.

The aircraft is powered by two RB199-34R engines, developed by the trinational consortium TURBO-UNION. The RB199 is a three-spool bypass engine, designed for high thrust under takeoff and combat conditions and for low fuel consumption in high subsonic flight at low altitudes. Fig. 2 shows a schematic cutaway view of the engine. The three-stage fan is driven by a two-stage low-pressure (LP) turbine. A three-stage intermediate-pressure (IP) compressor is driven via a seperate shaft by a single-stage IP-turbine, and the six-stage high-pressure (HP) compressor is driven by a single-stage HP-turbine. The reheat system combines a conventional turbojet burner with gutter flame stabilizers for the hot turbine efflux and a seperately fueled colander burner for the bypass flow. The variable, convergent exhaust nozzle consists of fourteen pairs of interlocking primary and secondary petals. The nozzle area varies from a minimum of 0.208 m^2 to 0.4 m^2 at maximum reheat. Bucket-type thrust reversers, developed to fulfill the requirements for extremely short landing distances, are mounted at the rear of the engine.

TEST EQUIPMENT

All test aircrafts involved in Tornado performance testing were equipped with flight test instrumentation of high quality which also contained parameters for stability/control and propulsion systems flight testing. The instrumentation system has the capability to record all data on magnetic tape and to telemeter it to the ground station, equipped with a data reduction system for real-time analysis.

The onboard data acquisition system consisted of a Pulse Code Modulation System (PCM) and a Frequency Modulation-Multiplex System (FM/FM) to record and transmit digital and/or analog signals. It also included units for signal conditions, filtering, and time-coding. The entire measuring chain of each individual performance parameter was calibrated and continuously monitored during the performance test phase in order to achieve the required test data accuracy. Particular emphasis was placed on the accurate measurement of:

- o total and static pressures, angle of attack and sideslip by means of a specially developed noseboom with wind vanes;
- o longitudinal, lateral, and normal acceleration using thermally controlled sensitive accelerometers which were accurately aligned and installed close to the center of gravity of the aircraft;
- o specific engine parameters such as pressures, temperatures, fuel flow etc., as shown in Fig. 2 which are required for the determination of engine thrust-in-flight.

Engine calibration data (for example, discharge coefficient, thrust coefficient, pressure loss in the afterburner tailpipe, etc.) used in conjunction with in-flight measured engine parameters for the calculation of engine mass flow and net thrust, were obtained from special component test beds or from Altitude Test Facilities (ATF). Engines used for performance trials (drag measurements) were generally calibrated in the AT-Facility at the National Gas Turbine Establishment (NGTE) at Pyestock, U.K.

BACKGROUND

During flight test, the lift and drag of the total aerodynamic force cannot be measured directly, however, they can be calculated from measurable quantities. This is illustrated below, showing the forces which act on the aircraft. The lift and drag can be expressed as follows (see also Fig. 3):

$$L = -F_G \sin(\alpha_T + \varepsilon) + (W/g).AZ_L$$

$$C_L = L/(S.q)$$

$$D = F_G \cdot \cos(\alpha_T + \varepsilon) \cdot \cos\beta_T + F_G \cdot \sin\beta_T - D_R \cdot \cos\beta_T + (W/g) \cdot AX_D$$

$$C_D = D/(S.q)$$

The engine installation angle ε and the wing reference area S are fixed, known geometric quantities. The dynamic pressure q can readily be obtained. It can be seen that lift and drag are dependent on the gross thrust F_G, the intake ram drag D_R, the aircraft weight W, the longitudinal acceleration AX_D, and the normal acceleration AZ_L as well as the actual angle of attack α and the angle of sideslip β. These remaining quantities are discussed in the following sections.

IN-FLIGHT THRUST DETERMINATION

The so called "thrust derived P_1/nozzle calibration"-method for engine performance and aircraft drag analysis was developed in cooperation with the engine manufacturer. This method is labelled as a "linked method" since the most important engine parameters i.e. gross thrust and air mass flow are determined at the same engine station, the nozzle exit plane.

Any pressure distortion induced by the intake and any temperature profile disturbance can be thereby eliminated as much as possible. Measurements made farthest downstream of the engine will usually give better results than those carried out just behind the fan. A further important point is, that the same engine respectively engine instrumentation have been used in flight as during ATF calibration in order to avoid any systematically errors. The engine gross thrust F_G and ram drag D_R are defined as follows:

$$F_G = F_{Gid} \cdot C_G \qquad D_R = M_1 \cdot V_T$$

Fig. 4 shows the principle of the method and the procedure for the gross thrust and mass flow determination. Using in-flight measured and estimated engine parameters (i.e. MF_M, MF_R, TT_1, TT_5, ect.) the massflow M_5 at the nozzle entry is calculated by a heat balance over the whole engine. Such a heat balance results in the following equations (also, see Fig. 5).

$$M_5(G_5-G_1) = EHV(MF_M \cdot \eta_C + MF_R \cdot \eta_R) - M_{BL}(G_1-G_{BL}) - POT$$

and the massflow at the engine face is

$$M_1 = M_5 + M_{BL} - (MF_M + MF_R)$$

With the nozzle discharge coefficient C_{DN} obtained from model tests a geometric nozzle area A_7 is determined and compared with the real measured nozzle area A_j.

Herewith any thermodynamic parameters in the nozzle exit plane and consequently an ideal gross thrust F_{Gid} and an ideal nozzle area A_{7id} are to be determined utilizing measured PMIX and the ΔP-calibration data. This comparison will usually show that both areas differ after this first step. Therefore a nozzle matching will be performed, i.e. the whole calculation loop for thrust and massflow will continue, after having corrected the calculated nozzle A_7 by a ΔA_7 term. This ΔA_7 value is obtained from another calibration curve $\Delta A_7/A_7$ which is a function of the corrected gas flow at jet pipe entry.

If A_7 and the real measured nozzle area A_j are identical, then gross thrust, net thrust and various engine performance parameters can finally determined. For the reheated engine conditions, the calculation of the static parameters in the nozzle exit plane including the reheat nozzle area require the determination of the reheat temperature and the fundamental pressure loss due to heating. In this case another calibration curve for the reheat efficiency $\eta_{Reheat} = f$ (reheat-temperature TT_7) is used. Again this characteristic is the result of Sea-Level-Test bed and ATF testing. The required max. capability curve for TT_7 and reheat efficiency have been evaluated from component test beds. The subsequent calculation steps are then the same as above.

Finally the in-flight engine thrust resulting from this method is adjusted to the defined Tornado thrust/drag bookkeeping system. This means that drag components such as subcritical spill drag and nozzle interference drag, which are functions of engine rating and flight condition, are accounted for within the thrust term (see Fig. 6). These drag items have been obtained from windtunnel tests with special intake and propulsion nozzle/afterbody models. Hereby the polars have been made completely independent of induced drag effects due to engine rating.

AIRCRAFT ACCELERATION MEASUREMENT

For use in the basic equations, the total inertia force must be split into components along and normal to the flight path (AX_D and AZ_L). The load factor and the excess thrust can be derived from:

$$n_z = AZ_L/g \qquad F_{ex} = AX_D \cdot (W/g)$$

Accelerations can be determined by two different methods:

- the "classic" TOTAL ENERGY METHOD for stabilized flight maneuvers, and
- the ACCELEROMETER METHOD mainly for dynamic flight maneuvers.

The TOTAL ENERGY METHOD makes use of pitot/static system indications only and gives the accelerations directly in the required lift/drag axis. AX_D is determined via the residual rate of change of altitude and speed (dH, dV_T) over the stabilized part (dt) of the maneuver:

$$AX_D = \frac{dV_T}{dt} + \frac{dH}{dt} \times \frac{g}{V_T}$$

The normal acceleration AZ_L is calculated via the flight-path angle γ, a rectilinear trajectory supposed:

$$AZ_L = g \cdot \cos\gamma$$

where γ is derived from

$$\sin\gamma = \frac{dH}{dt} \Big/ V_T$$

The "classic" maneuver for the application of this method is the steady level; however- to a certain extent - accelerations/decelerations and climbs/descents at constant rates can be evaluated as well. Excess thrust is determined with a high degree of accuracy.

he ACCELEROMETER METHOD uses the readings of an accelerometer package for the three ircraft axes. After a correction for cross-axis sensitivity, the measured accelerations ave to be transferred from the location of the sensors to the centre of gravity and then rom the body - into the aerodynamic (lift/drag) system of axes. The transformations were one by the use of standard equations which might be modified if the sensors measure in ny other than the body axes (for example in the geodetic system as with an inertial navigation platform). The resultant equations, as used in the data reduction, are given in ig. 7 in terms of AX_D and AZ_L.

NGLE-OF-ATTACK SIDESLIP MEASUREMENTS

he angle of attack was measured by a noseboom mounted wind vane or by a fuselage mounted ifferential pressure probe. A final accuracy of $\alpha_T = \pm 0.1$ deg. is mandatory and this equires a careful calibration which considers the following factors:

- o correction for local flow and upwash effects from in-flight calibration ($\alpha_p = K_1 + K_2 \cdot \alpha_i$)
- o pitch (roll) rate correction $\Delta\alpha_q = \arcsin (qr_x/V_T)$ $\Delta\alpha_r = \arcsin (pr_y/V_T)$
- o fuselage and noseboom bending due to air and inertia loads $\Delta\alpha_B$ (from static structural tests and in flight calibration)
- o correction due to inclined installation of the sensor ($\Delta\alpha_M$)

his finally leads to the true angle of attack for a given Mach number:

$$\alpha_T = K_1 + K_2 \cdot \alpha_i + \Delta\alpha_q + \Delta\alpha_r + \Delta\alpha_B + \Delta\alpha_M$$

n a similar way the sideslip can be determined; however, the main interest during lift/ rag measurements is a correct indication of a zero sideslip, as the test maneuver should e carried out at zero sideslip.

IRCRAFT MASS AND CENTER OF GRAVITY DETERMINATION

he actual gross weight (W) and center of gravity (C.G.) are calculated from the empty eight and the fuel contents in the individual tank groups. Aircraft empty mass and the orresponding C.G. were determined by weighing. The actual contents of the fuel tank roups was measured in-flight by fuel gauges which are calibrated for various attitude ngles on a special fuel rig. Furthermore the measured tank contents were checked indeendently by integrating the fuel flowmeter readouts over an entire flight. With this rocedure it is possible to determine the weight to within ± 50 kg.

EST TECHNIQUE

he need for a cost-effective test procedure and an accurate method for determining lift nd drag polars over a large angle-of-attack range at a const. Mach number requires the se of various dynamic maneuvers in combination with steady levels. The flight maneuvers hich were used in testing are tabulated and described in Fig. 8. Depending on the aircraft onfiguration and the Mach-range to be covered, the following maneuver sequence was performed.

RUISE, MANEUVER, AND HIGH-SPEED POLARS

After a steady level flight of 2 to 2.5 minutes duration, the range of angle of attack (corresponding to a load factor of 0g to 2g) about the trim point is covered by means of a roller coaster maneuver. After this maneuver the aircraft is stabilized briefly and then the range of greater incidence angle (corresponding to a load factor of 1g to maximum g) is tested by means of a wind up turn maneuver. Using this combination, it is possible to obtain the flight data for the entire incidence range within three to four minutes. Another advantage of this method is the chance of comparing continuously the results obtained from different types of flight maneuvers. Thus possible measuring errors (shifts, offsets) can be detected more easily and more quickly, and even small residual errors in the measurements or alignment of the accelerometers can be verified.

A test flight can cover a large number of such maneuver sequences when higher or lower test Mach numbers are joined by accelerations or decelerations, as shown in Fig. 9.

This test technique produces further test data and allows, in addition, the verification of the drag rise and the zero lift drag.

LOW-SPEED POLARS (TAKEOFF-LANDING CONFIGURATION)

In the range below Ma = 0.4 ACCELERATION-DECELERATION-ACCELERATION and SLOW-DOWN maneuvers were used instead of roller coaster or wind-up maneuvers because in this range Mach effects on the polars are negligible and the aircraft can be piloted better. Again these maneuvers are carried out after a steady level flight of 2 to 2.5 minutes duration. The ACCELERATION-DECELERATION-ACCELERATION maneuver is used for testing the range of angle of attack about the trim point and the SLOW-DOWN maneuver, for the range up to the maximum permissible angle of attack. Consequently, the entire polar can be flown within approximately five minutes.

Using this test method it was possible, for example in the course of TORNADO testing, to establish a complete set of subsonic polars within a one hour test flight. Without using dynamic test maneuvers, the flight time required to obtain test data even for a limited range of angle of attack would be at least four to five times greater. Furthermore, it is evident that conventional steady level maneuvers do not allow collection of enough data points for the determination of induced drag and zero lift drag characteristics, which are required for aircraft performance optimization and accurate performance prediction.

POST FLIGHT ANALYSIS AND PRACTICAL ASPECTS

The test data are processed, with the aid of a comprehensive computer software program. This software uses the airborne tape as test data source and performs all operations, calculations and corrections required to establish a polar. This degree of automation in data flow and data evaluation makes it possible to carry out the complete analysis of the measured polars within one day.

However, particular attention must be paid to the following problem areas in order to achieve the data accuracy and quality aimed for.

ANGLE OF ATTACK/ACCELEROMETER COMPLEX

The equations in Fig. 7 show that the accelerometer method requires a large number of parameter in order to calculate the acceleration (AX_D) along the flight path and this makes the method more sensitive then the total energy method. This problem area was investigated in detail within a sensitivity study. One of the results of this study is given in Fig. 10, which demonstrates the effect of an error in the angle of attack on a drag polar. For example, an error of ± 0.3° will alter the character of the polar completely and the induced drag will be off by about 6%.

Therefore a comprehensive check and calibration procedure, as shown in Fig. 11, was carried out during the polar measurements. This procedure included the following steps:

- Checks on the accelerometers in the laboratory and the accurate alignment of the installed accelerometer package with the aircraft axes. Any offsets or misalignments were recorded so as to include necessary corrections into the final polar determination.
- Accurate in-flight calibration of the angle of attack using different methods.

However, experience shows that despite this procedure, small residual errors may still be unaccounted for because in real life the accuracy in aligning the accelerometer package or calibrating the angle of attack in-flight is limited. Thus, a final in-flight check method was applied using steady state maneuvers as reference, i.e. existing residual accelerations during steady levels were determined via the total energy and the accelerometer method. The results obtained by the total energy method are regarded of better standard as residual accelerations can be determined very accurately via the rate of speed and altitude. Existing differences (ΔAX) to the results obtained by the accelerometer method can be expressed as a residual angle of attack error as follows.

$$\Delta\alpha_E = \Delta_{AX}$$

$$\Delta_{AX} = (AX_{D\ \text{TOTAL ENERGY}} - AX_{D\ \text{ACCELEROMETER}})$$

$$\Delta\alpha_E \approx \left[\left(\frac{dv}{dt} \cdot \frac{dH}{dt} \cdot \frac{g}{V_T}\right) - AX_D\right] \cdot \frac{180}{\pi}$$

This mathematical relation can be derived from the basic equation in Fig. 7 where, for the case of steady levels, $\beta \approx 0$, $n_z = 1$ and

$$\sin \alpha = AX_{NC} - AX_D$$

$$\Delta\alpha = \Delta_{AX}$$

Results of such in-flight checks are also shown in Fig. 11., where the true angle of attack α_T and the corrected angle of attack $\alpha_E = \alpha_T + \Delta\alpha_E$ are compared. The excellent agreement confirmes that in this ideal case no further correction is required for the final polar evaluation.

DATA FILTERING AND SMOOTHING

To a certain extent data filtering, either on-board (pre-sample filters) or within the test data evaluation software (digital filters), is necessary so as to avoid that critical measurements be affected by unwanted factors.

For example, the accelerations measured by accelerometers during a dynamic maneuver are of a very low frequence type. But appreciable signals coming through at much higher frequencies than those of interests can cause scatter in the data or biasing errors depending upon the sampling rate. Therefore for the Tornado polar measurements the sample rate for critical measurements such as accelerations, angle of attack, angular rates etc. have been set to 64 samp/sec and well adapted digital filters were used within the analysis software.

Furthermore, a curve fitting routine was applied to certain parameters, if derivatives were calculated. For precise measurements the angular acceleration was determined by differentiating the angular rate output of the rate gyros. The improvement in data quality which can be achieved by such a technique is demonstrated in Fig. 12, by means of a drag polar.

FLIGHT TECHNIQUE AND RECALL TECHNIQUE

Test data scatter and quality depends to a large extent on the precision the pilot has performed the maneuvers. This means, that during steady levels sudden pilot inputs to control airspeed or altitude changes should be avoided or alternatively the motion of his indicators must continue in the same direction in order to minimize possible hysteresis errors.

Dynamic maneuvers must be performed slowly and smoothly. Airspeed excursions should not exceed $\pm$ 0.01 to 0.02 Ma and the maximum pitch rates should be below 2°/sec. These conditions and consequently the quality of the test maneuvers were checked during the Tornado polar measurements by a specially developed recall system. This system enables the flight test engineer to selectively process maneuver packages during the test flight using telemetered data, whereby significant parameters, defined in advance, will be calculated. Thus, after the maneuver results are output in graphic form onto a display followed by a hard copy as demonstrated in Fig. 13 using a roller coaster maneuver. The criteria used in validating the maneuver, are in this case the evolution of the angle of attack, the airspeed, the normal acceleration and the lift coefficient.

TEST RESULTS

Typical flight test results obtained from the Tornado performance test program are presented and discussed in the following. All flight data were generally corrected to defined standard reference conditions in order to make test data (obtained from different flights) comparable among each other or with predictions. This data reduction procedure includes correction for altitude (Reynolds number), center of gravity position and power effects. However, test flights were normally performed close to the reference conditions to keep correction terms as small as possible.

REPEATABILITY OF TEST DATA

Fig. 14 and Fig. 15 show typical lift and drag polars for the cruise and takeoff/landing confiturations which were measured on three different test aircraft, however, with the same airframe standard as far as performance is concerned. For example, flight test data collected for a wing sweep of 67° at Ma = 0.7 fall within a scatterband of $\pm$ 1.5% in the case of lift and $\pm$ 3% in the case of drag (Fig. 14). This is a remarkable result, keeping in mind that:

- [illegible] standard were used
- the accuracy of the in-flight thrust is in the order of ± 2.5 ./. 3%
- the accuracy of the true angle of attack is not better than ± 0.1°

Furthermore, the results show excellent correlation between steady-state and dynamic test techniques. However, it must be emphasized that such an agreement can only be achieved if roller-coaster or wind-up turn maneuvers are performed slowly and smoothly and a certain angle-of-attack/accelerometer calibration standard, as discussed above, has been attained.

Comparable results have been achieved in the case of low-speed polars for different flap settings, as presented in Fig. 15. Again, test data obtained from STEADY LEVELS, ACCELERATION/DECELERATION maneuvers, and from SLOW-DOWNS agree very well. Stall test results from prototype aircraft A/C 02 (with special test equipments, i.e. antispin chute etc.) are also given in this figure. It is a matter of course that the data scatter will increase under stall conditions (pilot stick inputs due to wing rock, vibration, etc.). However, it was possible to define the maximum lift with a high reliability owing to the large quantity of test data derived from SLOW-DOWNS.

AIRFRAME/OPTIMIZATION

As already mentioned at the beginning, the test method, as outlined in this paper, was used for a number of performance investigations in order to measure the effect of aerodynamic changes on lift and drag. An example is given in Fig. 16. This figure shows the airplane zero lift drag variation with Mach number for prototype aircraft A/C 01, (unfavorable rear end) and for aircraft A/C 06 (improved afterbody shape and [illegible]). The zero lift drag at a given Mach number was determined from measured C_D versus C_L^2 curves, as shown in Fig. 14. In all cases the airplane induced drag characteristics were obtained from roller-coaster and wind-up turn maneuvers. The quality and quantity of these drag measurements give evidence to the overall drag change due to airframe modifications. It was possible, as shown in Fig. 16, to reduce the drag level of A/C 06 by about 8%, which was later confirmed by drag measurements on preseries aircraft A/C 11 as well as A/C 13.

COMPARISON WITH PREDICTIONS

Some representative comparisons between flight data and predictions follow. The predictions are based on wind-tunnel results which were adjusted from model-test to full-scale conditions. Fig. 17 shows subsonic and supersonic lift/drag polars at Ma = 0.7 for 25° wing sweep and at Ma = 0.9 and 1.42 for 67° wing sweep. Such polar measurements have been carried out for four different wing sweeps in 0.05 or 0.1 Mach increments within the entire flight envelope. This allows the accurate determination of drag variation with Mach number. Again the large quantity and high quality (low data scatter) of test data obtained from dynamic maneuvers permit an accurate assessment of the polar which would not be possible using steady-state maneuvers only. In general, comparison between flight test data and predictions have shown good agreement for all wing sweeps. Minor discrepancies were found in the lift and induced drag of the 25° wing. As indicated in Fig. 17, the flight measured lift is better in the post-linear range of the lift polar, while over a certain angle of attack range, a slightly steeper induced drag [illegible] obtained.

Fig. 18 presents the zero lift drag variation with Mach number. The CD_0 figures, at a given Mach number, were determined from the [illegible] curves, as given, for example in Fig. 17. After having established the [illegible] characteristic by dynamic maneuvers the zero lift drag in the supersonic region was [illegible] from accelerations with maximum reheat power, so as to obtain final drag measurements at defined reference conditions (open nozzle). The comparison shows excellent agreement in the subsonic and higher supersonic range. Flight data show a somewhat steeper drag rise in the transonic area, but lower drag in the low supersonic Mach range.

Fig. 19 shows typical results of store drag measurements for a heavy store configuration. The measured total aircraft drag as compared to the basic drag polar of the clean aircraft is given for the most interesting angle of attack range, on the left-hand side of Fig. 19. After both polars have been corrected to the same reference conditions, the difference between the two polars represents the drag increment due to external stores. Results from measurements at different Mach numbers are plotted on the right-hand side of Fig. 19 and are compared with predictions. In this case test data show a lower drag level but steeper drag rise conclusively proven by acceleration and deceleration maneuvers.

using test methods current in existence, it is possible to measure lift and drag polars accurately in-flight. The use of dynamic maneuvers allows a drastic reduction in flying time as well as the measurement of the induced drag and zero lift drag characteristics of an aircraft. This in turn, makes it feasible to verify in-flight, over the entire angle-of-attack range, the effects of aerodynamic modifications on lift and drag.

To achieve the indicated accuracies, high demands are placed on the flight test instrumentation, which must be specifically tailored to the task, as well as on the calibration standard of the engines involved in the thrust in-flight determination. It is self-evident that demands of this type necessitate certain expenditures. This aspect is therefore currently the subject of an intensive effort to further improve the cost effectiveness of the flight test of the future.

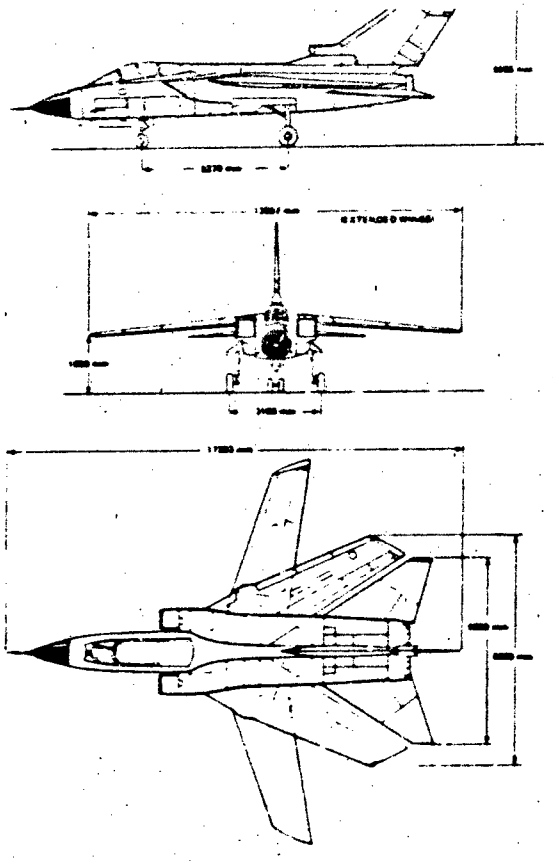

FIG.1: Three View Drawing Tornado

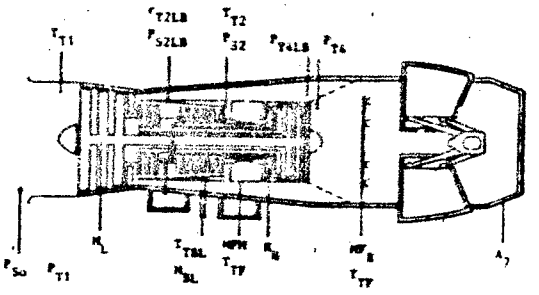

FIG. 2: Thrust In Flight Engine Instrumentation

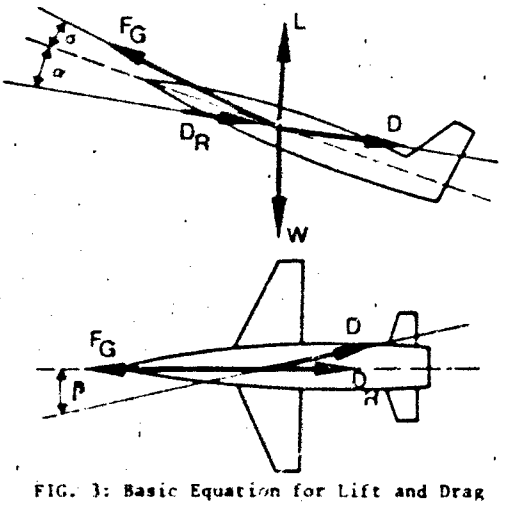

FIG. 3: Basic Equation for Lift and Drag

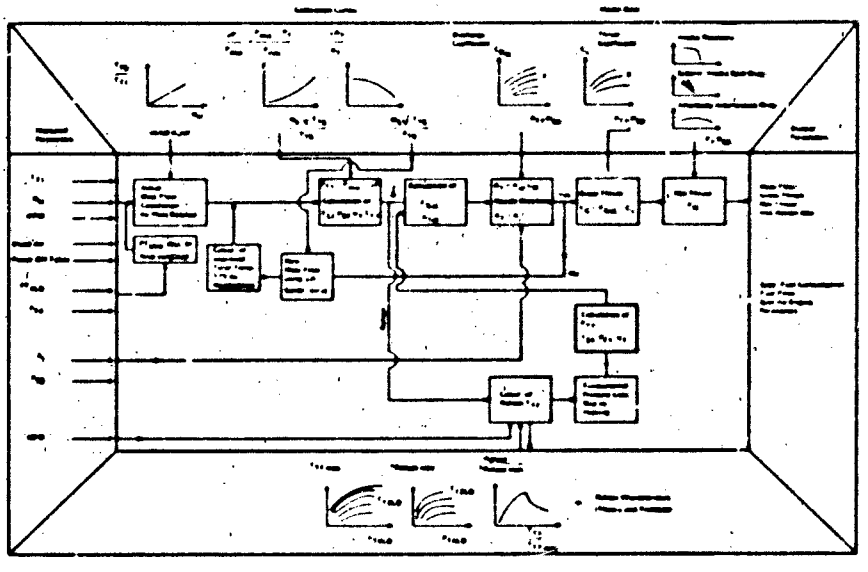

FIG. 4: Thrust Derived P_j/Nozzle Calibration Method

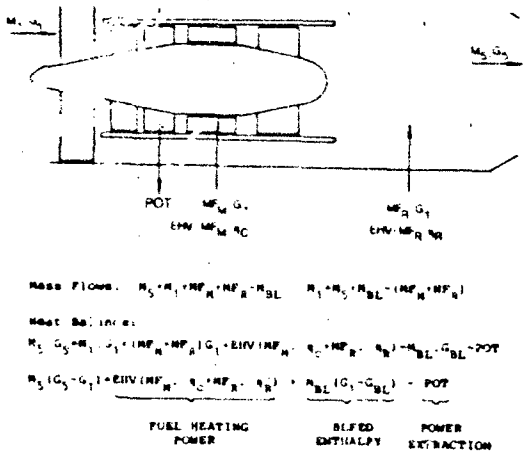

FIG. 5: Heat Balance Method

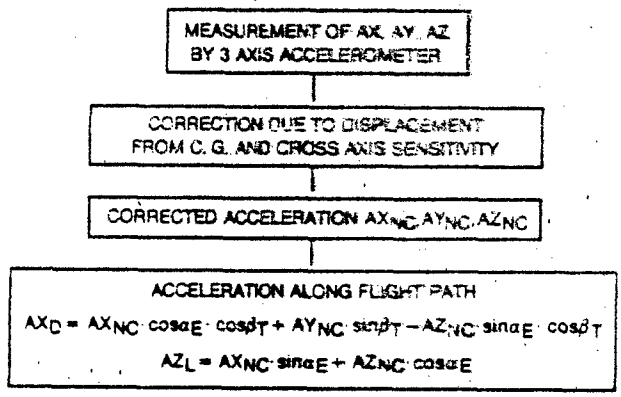

FIG. 7: Accelerometer Method

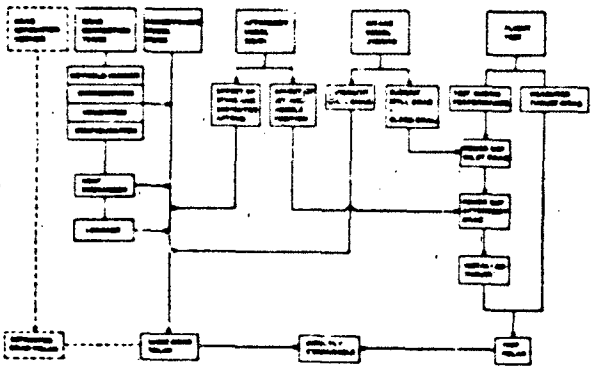

FIG. 6: Thrust/Drag Bookkeeping

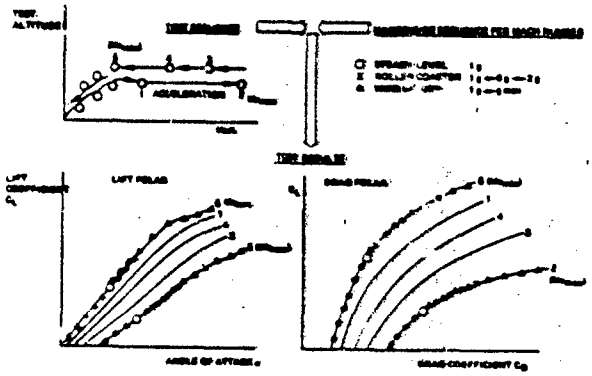

FIG. 9: Test Technique

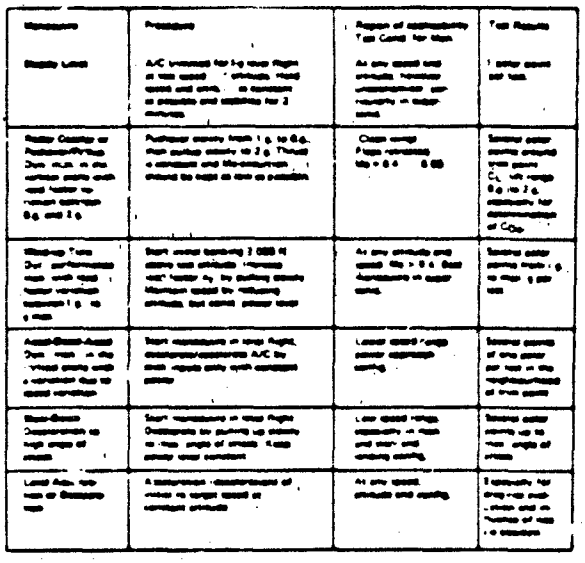

FIG. 8: Manoeuvre to evaluate Polars

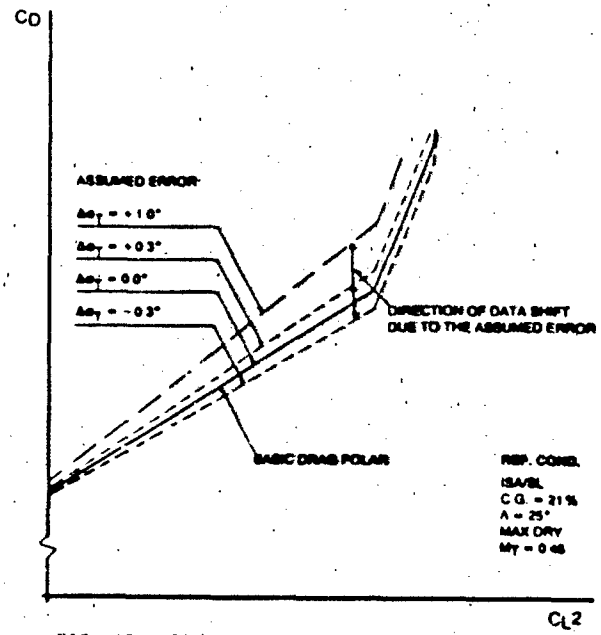

FIG. 10: Effect of Angle of Attack Accuracy on the Drag Polar

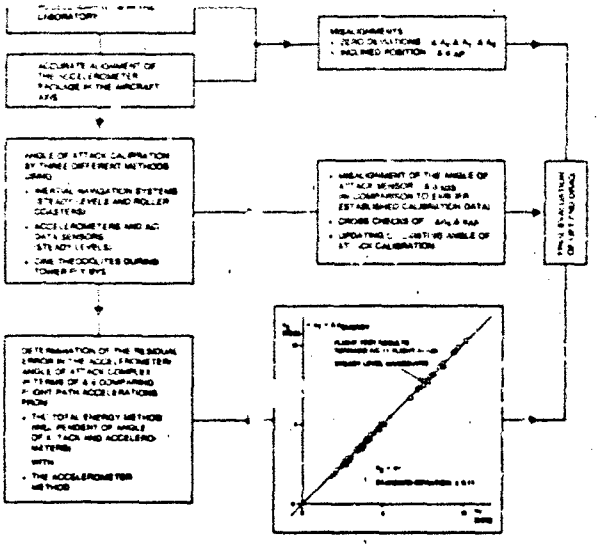

FIG. 11: Procedure of the Incidence/ Accelerometer Complex Calibration

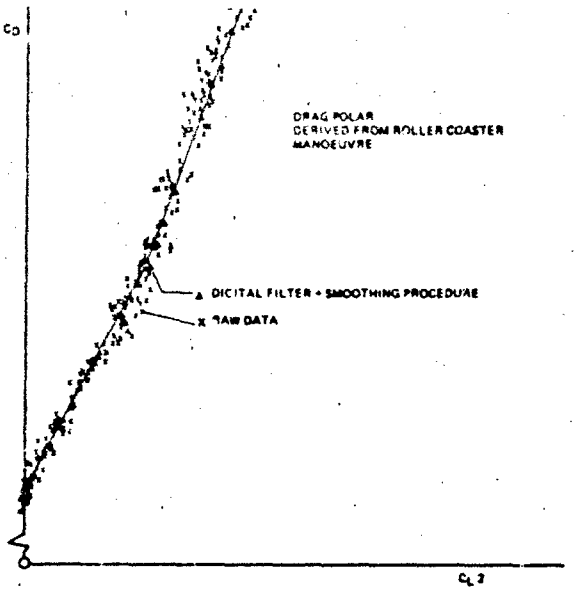

FIG. 12: Application of Digital Filter and Data Smoothing Procedure

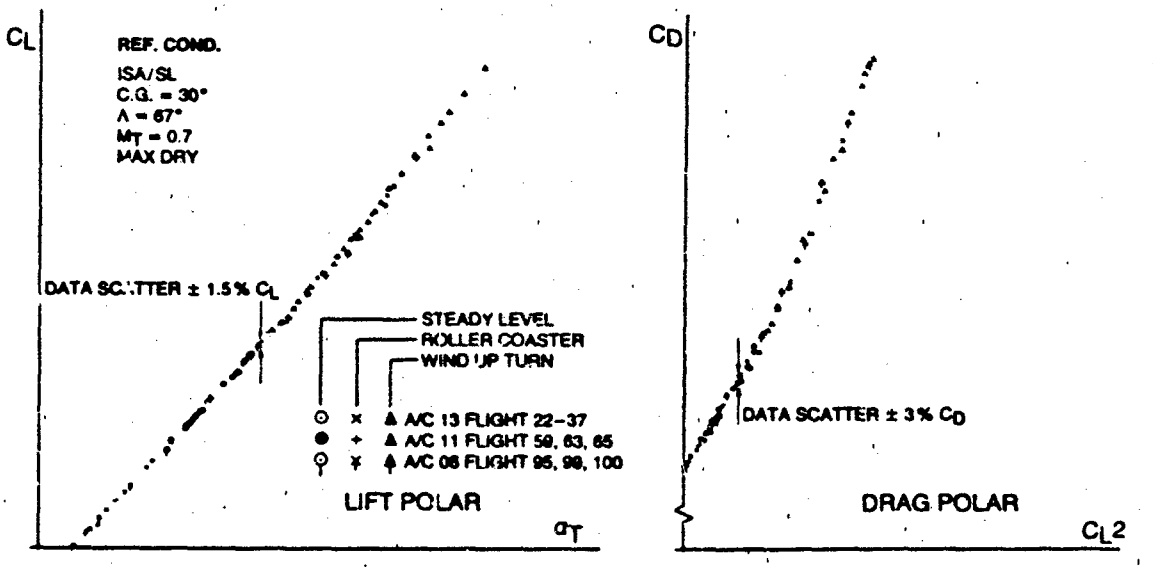

FIG. 14: Repeatability of Flight Test Data

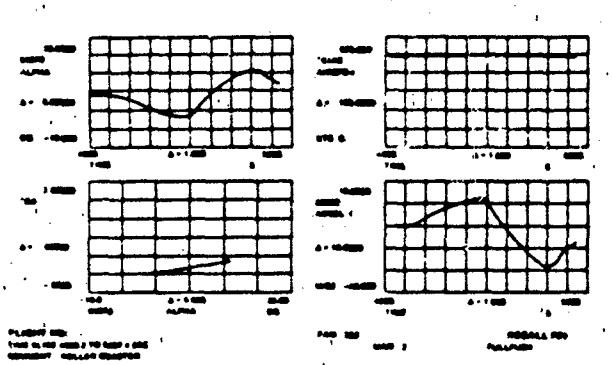

FIG. 13: Control of Flight Manoeuvre

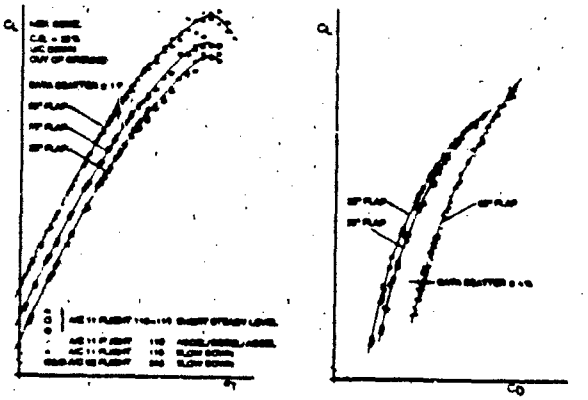

FIG. 15: Low Speed/High Lift Configuration

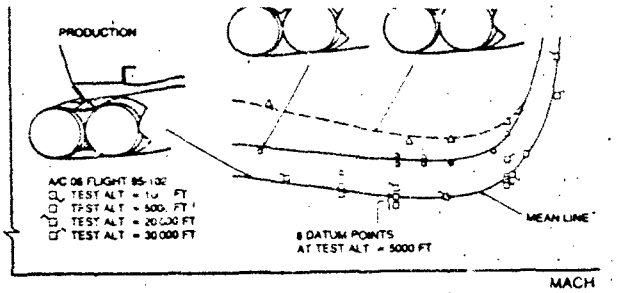

FIG. 16: Airframe Optimization

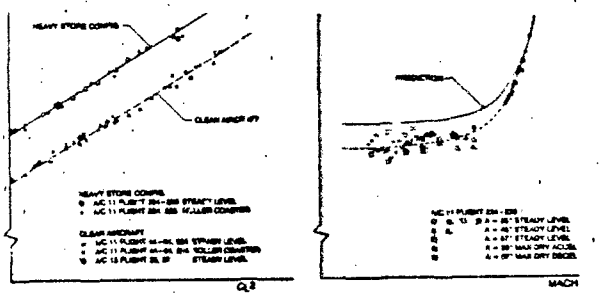

FIG. 19: External Store Drag

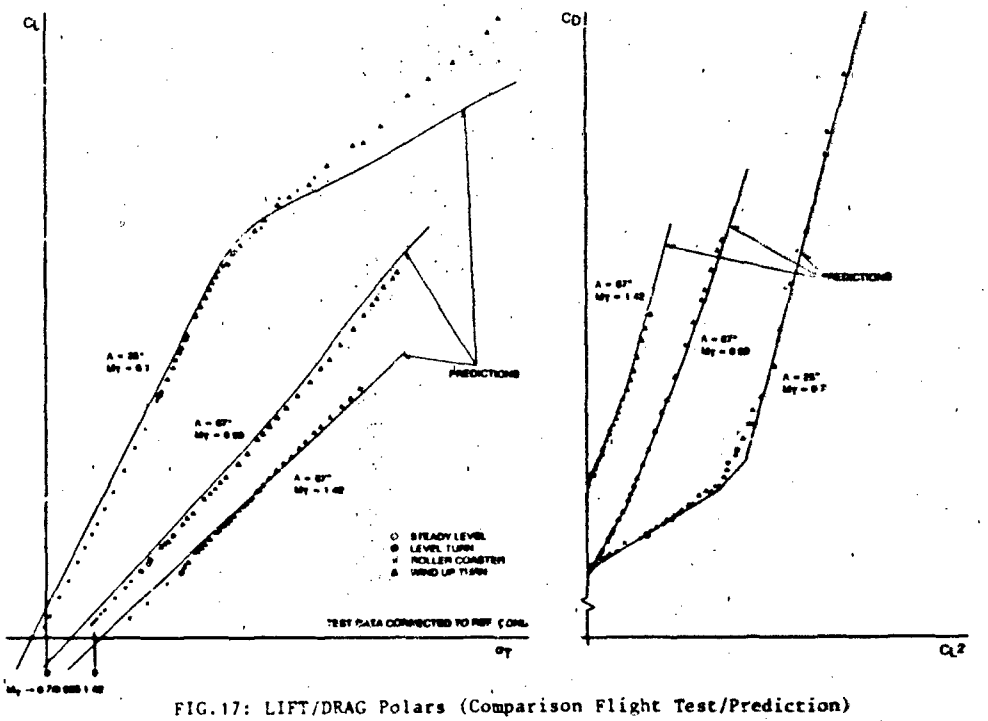

FIG. 17: LIFT/DRAG Polars (Comparison Flight Test/Prediction)

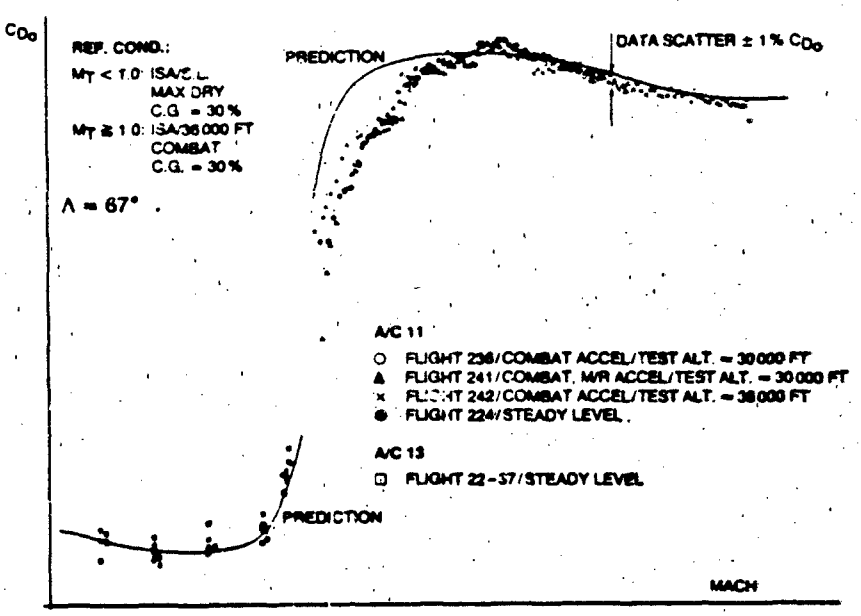

FIG. 18: Zero Lift Drag Variation with Mach

Air Force Wright Aeronautical Laboratories
Wright-Patterson AFB, Ohio 45433

ABSTRACT

The AFTI/F-16 Advanced Development Program, a joint USAF/USN/US Army/NASA effort with General Dynamics (GD), has modified an F-16A to be a testbed for evaluating new flight control related technologies. The program has presently completed its first phase of flight testing at NASA Dryden Flight Research Facility, Edwards AFB, CA. Some of the unique technologies being developed on this program are: a triplex digital fly-by-wire flight control system which operates asynchronously, an analog independent backup unit (IBU), eight separate digital task-tailored control laws, and six decoupled (six degrees-of-freedom) controller options. Included among these task-tailored modes are normal operation modes, air-to-air combat modes, and air-to-surface combat modes. One unique aspect of this program was the heavy involvement of the AFTI/F-16 Joint Test Force throughout the entire system development (pre-flight test) phase of this program. This forced early design consideration to be given to pilot-vehicle interface issues. Through the use of the GD Simulator, the test pilot became an integral part of the flight control law design. The AFTI/F-16 can be landed in possibly nine different sets of control laws including its normal digital mode, seven different sensor reconfiguration digital modes, and the analog IBU. Much concern surfaced prior to first flight as to how landable these different modes were; this resulted in all the landing modes being extensively tested on the GD Simulator, the Flight Dynamics Lab LAMARS, and the NT-33 Inflight Simulator. To date two of these modes, the normal mode and the IBU, have been flight tested on the AFTI/F-16 itself, and the flight test results were different from any of the simulators' predicted results. This has raised several issues on the use of simulators to accurately represent today's highly augmented fighter aircraft. This paper will discuss several flight test issues, how they were resolved, and their effect especially on the aircraft handling qualities. Specific topics which will be discussed are: the IBU, the effect of the asynchronous computer operation and system redundancy management has on the flight control laws and flight testing, and some handling qualities problems with combination coupled/decoupled control laws.

INTRODUCTION

The AFTI/F-16 Advanced Development Program is primarily oriented to the development, integration, and evaluation of new flight control technologies. The testbed used in this program is an FSD F-16A (Figure 1). In this aircraft the quad redundant analog flight control computer system was replaced with a triply redundant digital flight control computer system using three BDX-930 digital processors and a triply redundant analog independent backup unit. New control surfaces were attached to the aircraft and usage of existing control surfaces was changed to provide more capability and flexibility in the flight control law design and to allow limited six degree-of-freedom decoupled motion capability. The surfaces added to the aircraft were two vertical chin canards, which were attached below the engine inlet, to provide enhanced directional force and moment control and to provide drag modulation capability. The surface whose usage was changed was trailing edge flaps. In the F-16 these two surfaces are only used for roll control and as normal flaps in landing. In the AFTI/F-16, they are used additionally in maneuvering flight to enhance the onset and control of normal acceleration and to provide longitudinal decoupled flight control. This paper directs its attention to three major design issues which had an impact on the first phase of the program. These issues which will be discussed in the next three sections of this paper are a direct result of these system modifications. This paper addresses each issue, the tradeoffs, the results, and its impact in flight testing.

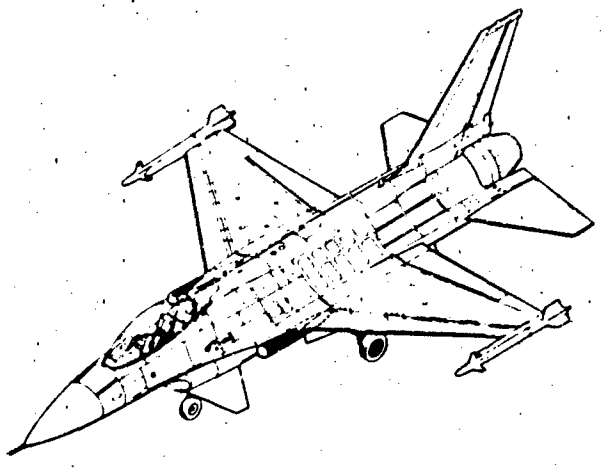

Figure 1 The AFTI/F-16

2. Reliability: DFCS failure rate resulting in loss of control of the aircraft will be less than 1 failure in every 10^7 flight hours.

3. Fail-Operation: the DFCS shall be fully operational (Operational State I as defined in MIL-F-9490D) after any first failure. After any second like failure, the control system will provide at least safe flight (Operational State III, MIL-F-9490D) with a probability of 0.95 being fully operational.

These requirements were to be met without reliance on an IBU. The primary reason for an IBU was to have a backup system which was independent of all the digital flight control software. This IBU was to be designed to allow for its removal after sufficient confidence was developed in the primary digital system. Also required was that the primary system and the IBU be designed so that the performance of the primary digital flight control system would not be affected by the removal of the IBU. The IBU alone would provide at least Level 3 flying qualities, as defined in MIL-F-8785B, throughout the flight envelope and at least Level 2 flying qualities in the landing phase.

Several pro/cons exist for having an analog independent backup for a digital flight control system. The basic reason for an IBU is to protect against unknown - unknowns in the digital software, especially generic software design errors. Due to an IBU being dissimilar redundancy, it also provides some protection against flight control EMI upsets. The presence of an IBU gives a definite increase in pilot and user - command confidence in flight testing a new digital flight control system. An IBU also increases the system loss-of-control reliability because it can survive some hardware failures.

Although the presence of an IBU has a lot of advantages, several disadvantages also exist. With an IBU, there will be increased system complexity which will result in increased cost. It will also be a source of additional flight control system failure points. The existance of an IBU can become a design "crutch" and be overrelied upon. An IBU can pose problems when there are no problems in the digital system: a nuisance automatic engagement and inadvertent or deliberate pilot engagements. The IBU may also require additional flight testing to clear its flight envelope. It might also mean additional pilot training to be proficient in the mode (assuming it is manually switchable from the cockpit).

To meet design requirements, the AFTI/F-16 program utilized a triplex analog IBU design. Since the digital flight control system is triplex, an analog card containing an IBU was located in each digital box. The IBU can be engaged through two methods. First a switch on the side-stick allowing the pilot to manually either engage or disengage the IBU. This gives the pilot the final authority to judge the health of the digital system. The second method of IBU engagement is by the digital system itself when it can no longer identify the last remaining good digital processor. In this case the IBU will automatically be engaged.

Early in the overall system design it was seen as beneficial to use the IBU when the redundancy management is unable to a high probability identify the last good remaining processor. The following scenario illustrates how the IBU can be used to improve the overall system safety. When no failure exists, the digital system uses the output of processor B to control the aircraft. (Processors A, B, and C are all compared to ensure B is good). If one processor has failed, the remaining two good processors will identify the sick processor and vote it off. The system will then use only the two good remaining processors. If a miscompare then occurs between the two remaining processors, they both go into self test with the anticipation that one will self test "GOOD" and the other "BAD". If this happens the aircraft flys home on the last good remaining processor (Figure 2). If both should test "GOOD", either processor could be chosen and safe operation should be assured. If both test "BAD" several options exist: one computer could be arbitrarily chosen (coin flip) to fly on, or the computer with the smallest output could be chosen (a small output is better than a hard over output). In any case, under these circumstances there is no guarantee of correctly choosing the last good remaining processor. On the AFTI/F-16 instead of arbitrarily choosing the last processor in this scenario, the system will automatically revert to IBU (Figure 3). Without an IBU, the redundancy management system would be forced to choose one of the last two processors to fly on. Some small risk exists that the incorrect processor would be chosen. The level of this risk is unknown since there are no known failures which would cause both processors to self test "BAD". This is clearly a case where the IBU is protecting against unknown - unknowns. Because this was a new flight control concept being developed and flight tested (digital, triplex, asynchronous design), it was felt to be more prudent to utilize the IBU. It should be noted that the reliability rate for loss-of-control (less than once every 10^7 flight hours) is still met even if the IBU is not in use in the above scenario.

From a control law standpoint, it was decided to make the IBU as simple as possible to keep the analog real estate small and keep the IBU as independent from hardware failures as possible. Under this criteria, the IBU design resulted in a system with three input paths (pitch, roll, yaw) and a single feedback path: pitch rate feedback which was the minimum necessary to maintain aircraft stability. In the roll and yaw axis no feedback was used even though the dutch roll characteristics were rather poor. The design resulted in a single gain system which had to have sufficient stability margins to be stable and still flyable from Mach 1.6 through touchdown speed. The critical region in determining the value of this gain was the low altitude/supersonic region. This resulted in forcing the gain to be low which caused the pitch damping at power approach airspeed to be low.

Prior to first flight of the AFTI/F-16 the IBU (named Original IBU) was evaluated in a power approach (PA) configuration on the NT-33A Inflight Simulator. While performing a PA task this IBU was given Level 3 flying qualities ratings with Cooper-Harper ratings of 8 to 9.5 in pitch and 4 to 5 in roll. The level 3 ratings were due to heavy, sluggish pitch response, a PIO tendency in high gain tasks, and heavy and extreme gust sensitivity in roll. At this point is was obvious a single gain IBU was not going to be sufficient to safely fly the aircraft throughout the entire flight envelope and still safely land it.

series of NT-33A tests and both found to have good level 2 handling qualities.

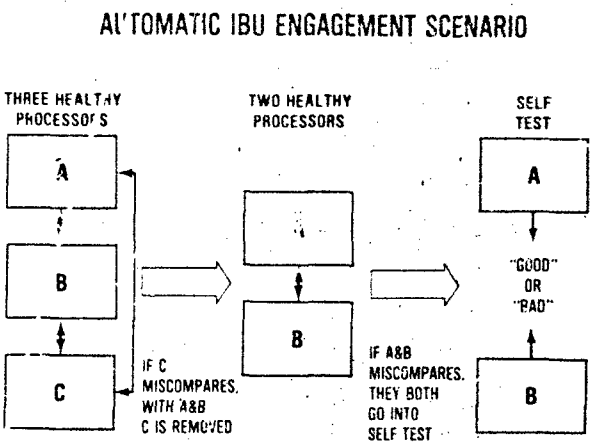

Figure 2 Failure Scenario

Figure 3 Result of Self Test

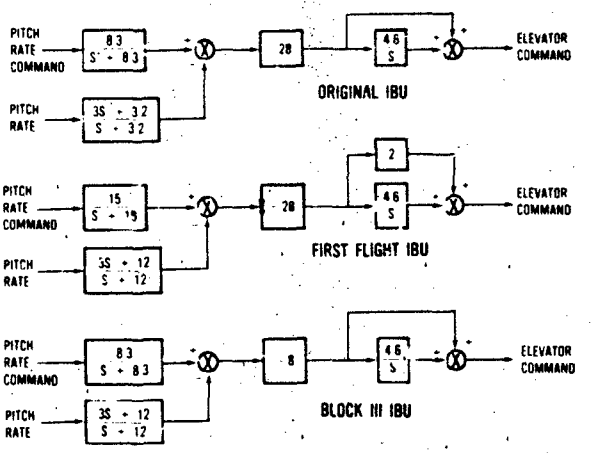

Figure 4 IBU Development History

As first flight date of the AFTI/F-16 approached, a major issue began to surface with respect to the intentional inflight usage of the IBU. Should the IBU be intentionally engaged inflight, how often, and in what flight conditions? The flight test community was definitely in favor of testing the IBU inflight and desired it very early in the program (second or third flight). The advantages of doing this would be to gain confidence in the IBU under controlled rather than last chance emergency conditions. Under this scenario, the IBU would be tested under benign flight conditions and there would be a healthy digital flight control system to immediately revert back to if the IBU flying qualities showed to be unsatisfactory. Since the NT-33A evaluated the flying qualities to be very close to Level 1, this did not seem to be too likely. From a redundancy/reliability standpoint the IBU is monitored for failure at all times, even while flying in a digital flight control mode. The IBU on the AFTI/F-16, being a triplex system, is fail-operative after first failure but has no protection against a second failure. The IBU hardware has a predicted mission reliability of less than $7X\ 10^{-6}$ failure per flight hour.

Historical data has not shown a very good track record concerning inflight engagements of flight control system backups. Aircraft such as the B-47, B-66, Tornado, and Concorde have mechanical backup systems for their primary flight control systems. In the B-47 and B-66 these mechanical systems were maintenance nightmares and were many times not well maintained. In the B-66, twice pilots switched to the mechanical system and found it inoperative. Neither pilot was able to switch back to the hydraulic (primary) system which resulted in loss of both aircraft.

Those in favor of engagement of the IBU inflight won and the IBU was first engaged during the third flight of the aircraft. All the pilots commented that the IBU had degraded flying qualities as compared to the Standard Normal Mode but that the flying qualities were sufficient as a backup mode. Pitch axis was very stable but possessed moderate to heavy stick forces. It had a lightly damped dutch roll which was excited by roll or yaw inputs. The IBU to date has been flown out to Mach 1.2. At that speed the pilot got into a lateral PIO once when he excited the dutch roll with a maximum rudder input.

The IBU is now routinely engaged during the course of flight testing. As the flight envelope is expanded, the IBU is now one of the first modes to be evaluated at each new flight condition. The philosophy is that the IBU will be tested for safe operations to give confidence in case of non-resettable automatic IBU engagement.

ISSUE: CONTROL LAW AND REDUNDANCY MANAGEMENT CO-EXISTING IN A DIGITAL ENVIRONMENT

A major objective of the AFTI/F-16 program was to develop and evaluate new concepts in flight control design. One of the major concepts being developed was that of multimode design containing task-tailored control laws. This implies a separate flight control mode be designed for each type of combat task to be flown (bombing, air-to-air gunnery, etc.). Also required with this control law structure was limited authority six degree-of-freedom decoupled set of flight control laws. Additionally required was separate reconfiguration modes which allow for continued flight after the loss of flight control sensors (pitch rate, roll rate, tec.). In other words, a very complex set of control laws was required to be developed. A second major concept being developed was a triplex, digital flight control computer system. This system was required to utilize software to the greatest extent possible to perform all control law and all redundancy management functions. Early in this program, some important decisions were made concerning the approach used to implement these concepts. At the time these decisions were made, it was felt their effect would not impact each other. As the design progressed from development to mechanization to flight testing, it became obvious these decisions were greatly intertwined and system adjustments were necessary to allow for harmonious system operation. One of these decisions was to operate the digital computers asynchronously with respect to time. The other decision was to design the control laws utilizing Linear Quadratic Synthesis (LQS).

Asynchronous digital computer operation implies that the individual clocks in each processor will operate independent of each other thus implying the time skew between each processor will not be controlled (Figure 5). Therefore each processor will receive its input data at different times and will complete the output surface computations at different times. Prior to making the decision to go asynchronous, a trade study was performed. Some of the main conclusions of this study were:

Synchronous Operation

Advantages:

1. Simpler Operational Flight Program (OFP) verification and testing.

2. Cross-channel monitor trip level at output selector/monitor plane can be set to a near zero value (a cross-channel difference can be used as a failure indication).

Disadvantages:

1. Sync function must be carefully designed so as not to introduce a single point failure possibility into the system.

2. Design is not inherently fault-tolerant. Unless special care is taken, a transient condition in one branch will in general result in a branch being temporarily disconnected.

Asynchronous Operation

Advantages:

1. More fault-tolerant since branches are not expected to be in exact agreement.

2. Insensitivity to short term electromagnetic interference effects is enhanced since data which is modified or in error is likely to be sensed in diverse portions of the redundancy management function.

Disadvantages:

1. Increased data acquisition speed requirement to prevent dynamic responses from being identified as faults at the output selector/monitor plane.

AFTI/F-16
ASYNCHRONOUS COMPUTER OPERATION

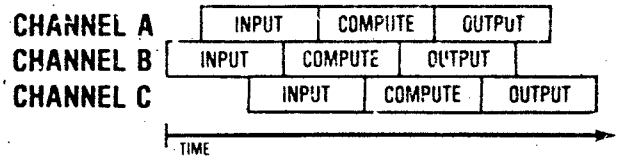

Figure 5 Time Skew

An equally risky approach was taken in using the LQS approach to the control law design. The control laws were developed for many point conditions in a batch computer mode utilizing a digital computer program called DIGICON. The goal in the control law design was to have a very quick responding system, both in pitch rate and onset of normal acceleration, and this system would provide gust alleviation and be relatively invariant to uncertainties in the airframe aerodynamic derivatives. To meet these design goals, a multi-state feedback system was designed which had very high gains on the forward path signals, especially the error signals between commanded response and actual aircraft response. The result of these high gains was a system that has very large amplitude and high frequency content in the output signal to the control surface actuators.

Within the digital flight control system, two major tasks are being performed during each frame: the flight control law computations and the redundancy management computations. Initial development of these two systems (control law versus redundancy management) was done separately; it was not until later in the preflight development phase of the program that the two systems were integrated together.

The redundancy management system is an integral part of any multiple computer system. The purpose of the redundancy management system is to ensure that the aircraft is always being flown by a healthy processor (s). One component of this system which highly interacts with the control laws is the output selector/monitor (S/M). The function of the output S/M is to compare the surface commands of all three processors to detect computational failures. Each processor has its own output S/M which compares all eight of its surface command outputs with those of the other two processors. If any processor's output (including itself) differs by more than a given percentage from the other processors, that computer output from that processor is identified as having possibly failed. If this condition persists for seven computational frames, that output from that processor is voted off-line. This given percentage is called the trip level and its purpose is to prevent a sick output of any processor from commanding an aircraft surface. In order to have early warning of a possible failure and prevent any aircraft failure transients, ideally this trip level would be set near zero percent difference. But this is impossible because of asynchronous nature of the system. This asynchronism will allow each processor to be time skewed from each other processor - each processor's output being different even for a perfectly healthy system (Figure 6).

The difficulty arises in determining an acceptable trip level which allows normal operation to continue in a time skewed environment and still identify output failures at a safe level. For a healthy system, three factors will affect the inter-channel difference between the outputs from the three processors: the time skew between the three processors, the change of the input signals (both commands and sensor inputs) in that time, and the control law gains and structure which amplify these differences. As stated above the desired size of this trip level is controlled by two opposing factors. The trip level must be large enough to allow for a normal interchannel difference due to the three factors listed above so it will not erroneously declare an output failure. Opposing this, the trip level must be small enough such that a real failure can be identified before it can produce a large (unsafe) aircraft transient when switching from a sick output to a healthy output. Although this non-zero trip level allows the system to be fault tolerant (it could possibly allow a small short term transient to pass through system without declaring a failure), a deficiency of this asynchronous system is its inability to always distinguish the difference between a time skewed output mis-compare and an actual failed output at a low threshold level.

When the total system was integrated initially the inability of the redundancy management system and the control laws to work in perfect harmony became obvious. Originally the output trip level was set at a constant value of 15% of full scale deflection of each given surface. When the total system was first tested on the simulator, it was found that large inputs, especially at moderate to high frequency, were exceeding this 15% trip level in the output S/M. At this point comparisons were made between the AFTI/F-16 control laws and those in the F-16. It was found in some cases that the gains in the AFTI/F-16 control laws were sometimes many times larger than equivalent gains in the F-16. Some suggested the AFTI/F-16 gains were unrealistically high. In any case these high gains generated by the LQS approach proved to be a real deficiency of that type of control law design.

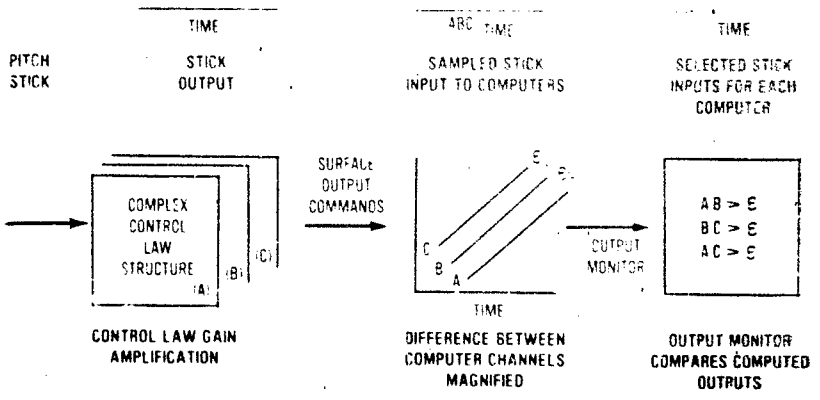

Figure 6 System Interaction

The LQS design methodology used on the AFTI/F-16 varied the gains in the forward path and feedback paths to satisfy a cost function and performance criteria. Unfortunately the method did not give the designer a sensitivity analysis of the effect of the gain on system performance. The end effect was the final design resulted in some very large gains which could have been reduced at a very small loss of performance. These large gains caused a lot of problems when integrated with entire system. They would produce a large amount of control surface activity which meant hinge moment limits were a bigger problem, more surface rate limiting, and large demands on the hydraulic system. The end result with respect to the redundancy management was that for maximum processor skews, a very small difference in input signal magnitude could result in very large differences at the output plane for non-failed conditions. Ultimately the gains had to be reduced to be more realistic and to coexist with the redundancy management. The lowering of the gains was not done without some penality; in some cases it resulted in reduced robustness of the aircraft response and possible degradation of aircraft handling qualities. The primary area this gain reduction occurred was the forward path to the elevator in all the flight control modes and the forward path to the trailing edge flaps in the decoupled control modes. The region of the flight envelope most affected by the gain reduction was the high altitude, low dynamic pressure areas. In this region, the sluggish performance of the basic airframe is masked by the very high gain control laws to achieve good tracking performance and improved handling qualities; therefore, the gain reduction had its greatest effect there. In general though, gains were reduced throughout the flight envelope. The effect of reducing the gains in the forward path to the elevator was a reduction of system bandwidth in the pitch response. The effect of reducing the gains in the forward path to the elevator was a reduction of system bandwidth in the pitch response. The effect of reducing the gains in the forward path to the trailing edge flaps was an increase in the impurity present in the decoupled control options. The end result was the control laws had to be changed from their optimal design to live in harmony with the redundancy management system.

The redundancy management system was also changed to be more compatible with the control laws. The constant 15% trip level was changed to be a variable trip level based on the rate of change of a specific output in its own processor. In most cases the trip level is 15% but it can reach as high as 30%. This change still provides the same level of protection against a real failure. If one processor has a failure forcing one of its outputs to increase at a high rate (thus increasing its trip level to 30%) the other two processors may still be using 15% for that output, thus voting it as failed as early as if all three processors were using 15%. Other changes also made to the redundancy management system because of the high gain control laws were to increase the rate at which some inputs are sampled and to increase the update rate of gain tables. These changes were necessary to prevent large, rapid spikes to propagate to the output S/M plane. Therefore, the end result was the redundancy management system also had to be modified to live in harmony with the control laws. This system adjustment, to make the control laws and redundancy management system work in harmony, was primarily performed on the simulator. During the flight testing phase (a total of 118 flights, 177 flight hours) only one inflight flight control system fault indication occurred which resulted in a control law gain adjustment.

As a result of the flight test program, several conclusions can be made concerning the operation of high gain control laws in an asynchronous computer environment. First (and most important), these two systems can be made to work together successfully. During the last two weeks of flight testing, the pilot was permitted to aggressively fly air-to-air and air-to-ground combat scenarios and the system performed flawlessly with zero flight control problems. The second conclusion is that there is an interdependency between the control laws and the redundancy management in an asynchronous computer system, and the two parts cannot be developed independent of one another. The smaller the control laws gains are or the faster the computer frame rate is, the less this will be a problem. On the AFTI/F-16, the computer processors have a frame length of approximately 16 milliseconds which allows the worst case skewing

With these gain restrictions, the control laws on the AFTI/F-16 were still sufficiently robust that they received Level 1 Cooper-Harper Handling Qualities Ratings in all the combat modes. These control laws were also determined to have improved handling qualities over the basic F-16 in all combat modes and in power approach and landing. Third, this asynchronous design proved to be very fault tolerant. During the flight testing phase, forty-one inflight flight control system fault indications occurred. The effect of these fault indications ranged from no loss of the system redundancy up to the loss of two channels of redundancy (i.e., flying on only one processor). In almost all these cases the system was resettable to a zero fault condition. In no case was there a degradation or change in the aircraft handling qualities due to a fault indication.

ISSUE: DECOUPLED CONTROL LAWS

The AFTI/F-16 digital flight control system contains eight primary task-tailored control law modes (Figure 7). These modes are full authority and are optimized for specific tasks such as air-to-air gunnery and air-to-surface bombing. For vernier, fine tracking adjustments, six decoupled control options were developed. These options include: in the longitudinal axis - pitch pointing, direct lift, and vertical translation (Figure 8); in the lateral - directional axis - yaw pointing, direct side force (also named wings level turn or flat turn), and lateral translation (Figure 9). (See Reference 1 for a description of these modes). These decoupled control options are superimposed on the primary control laws as a secondary means of precisely tracking a target in the final stages of a tracking solution.

AFTI/F-16 Multimode Flight Controller Commands

CONTROLLER	MULTIMODE			
	STD NORMAL	STD BOMBING	STD A/G	STD A/A
SIDE STICK (Pitch)	A_N COMMAND	A_N COMMAND	Q COMMAND	Q COMMAND
SIDE STICK (Roll)	ROLL RATE COM	ROLL RATE COM	ROLL RATE COM	ROLL RATE COM
RUDDER PEDAL	RUDDER DEFLECTION	FLAT TURN	FLAT TURN	FLAT TURN
THROTTLE (T$_{max}$)	NONE	NONE	NONE	NONE
	DECOUPLED	DECOUPLED	DECOUPLED	DECOUPLED
SIDE STICK (Pitch)	FPME*	FPME	PPME*	PPME
SIDE STICK (Roll)	ROLL RATE COM	ROLL RATE COM	ROLL RATE COM	ROLL RATE COM
RUDDER PEDAL	TRANSLATION	FLAT TURN	POINTING	POINTING
THROTTLE (T$_{max}$)	TRANSLATION	DIRECT LIFT	POINTING	POINTING

*FPME - FLIGHT PATH MANEUVER ENHANCEMENT
PPME - PITCH RATE MANEUVER ENHANCEMENT

Figure 7 AFTI/F-16 Flight Control Modes

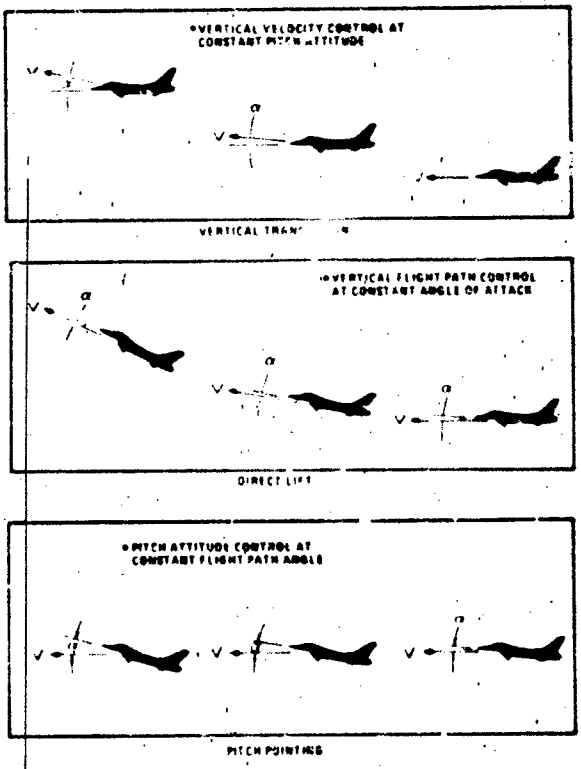

Figure 8 Longitudinal Decoupled Options

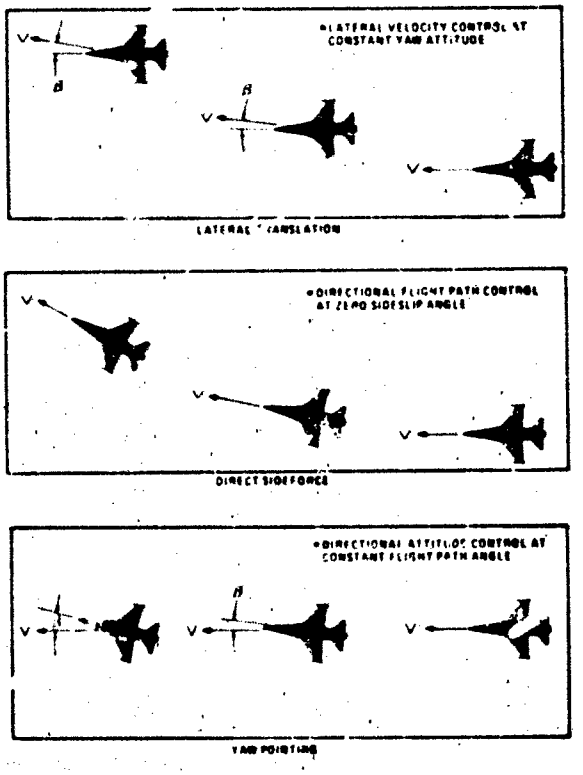

Figure 9 Lat-Dir Decoupled Options

flight control computer which was not an integral part of the primary analog quad redundant flight control system. This was to allow the aircraft to always, instantly revert back to its primary coupled control laws if the aircraft got into a problem area during the decoupled operation. Since the baseline F-16 feedback remained intact within the primary computer, specific feedbacks not desired for decoupled operation were cancelled by predicted open loop response signals from the auxiliary computer. Gain scheduling as a function of air data parameters provided operation of the decoupled options over a wide range of flight conditions.

In the AFTI/F-16 flight control system, the entire control law architecture was redesigned from the existing F-16 control laws. There was no requirement (nor need) to jury-rig the decoupled control system to an existing full authority control system as was done in the Fighter CCV program. Therefore two methods existed for integrating the limited authority decoupled control laws with the full authority system. The first method was the open loop approach similar to the Fighter CCV; the second method was the closed loop approach integrating the decoupled control laws with the entire control law structure and utilizing the multiple sensor feedbacks that were available. Being an advanced development program evaluating new aspects of integrated flight control technology, the latter approach was chosen.

In the AFTI/F-16 program, the first major decision to be made with respect to decoupled control was what type of controllers would be used to input decoupled commands. On the Fighter CCV, a miniature two-axis force controller was installed on top of the F-16 side stick controller for commanding the decoupled modes. As a pilot option, the rudder pedals could be used to input lateral-directional modes. The pilots found that this two-axis controller produced a lot of crosstalk with the coupled controller anytime a decoupled input was made. In other words, it was difficult to make a decoupled input without unintentionally deflecting the coupled (primary) side stick controller. The AFTI/F-16 chose to use separate controllers (not co-located) to command decoupled inputs. This was to prevent cross-talk or interference between controllers. Only two controllers were necessary to make all decoupled inputs. The pilot controller chosen for lateral-directional inputs was the rudder pedals. Flight testing showed the rudder pedals to be very natural for this task. For the longitudinal inputs, the throttle grip was modified to have a dual function as a throttle and as a decoupled motion controller. As a controller the throttle is twisted aft to command up motion and twisted forward to command down motion (Figure 10). Flight testing showed the twist throttle to have several problems. The pilot tended to put inadvertant twist throttle inputs in during high gain tracking tasks and high G-loading. If the twist throttle was held slightly out of detent, the trailing edge flaps would integrate to their limits, hence greatly increasing drag. Sometimes the pilot's first indication of an inadvertant input was the slowing of the aircraft or the onset of wing buffet. The second problem is the twist grip's harmony with the side stick controller. The pilots found it difficult to use the twist throttle and the pitch stick simultaneously to control the pitch axis. To use the throttle, the pilot generally had to freeze the pitch stick which tended to increase pilots overall workload.

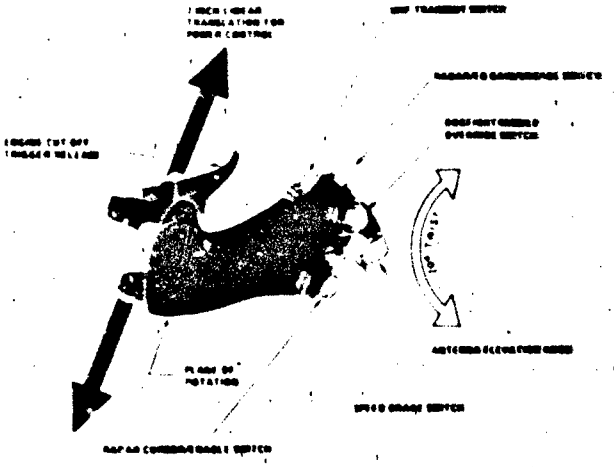

Figure 10 - Throttle Twist Grip

The utility of the decoupled control options is very dependent on their response being linear, predictable, free of large impurities, relatively quick, and of sufficient magnitude to be useful. It is not necessary for these control laws to be able to perform gross acquisition tasks, but they must be very effective at vernier tracking tasks to be useful. Results from the Fighter CCV program showed the highest payoff for these modes to be: pitch and yaw pointing for gunnery tasks; direct side force for air-to-air tracking, strafing and bombing; direct lift for defensive maneuvering to confuse an attacker; and lateral translation for strafing or landing in a crosswind. Vertical translation showed very little utility for task.

Below is a summary of results from flight testing the decoupled control options on the AFTI/F-16. This summary includes what each controller commanded, authority levels used by the pilots, and the option's primary utility.

- For flat turn, the rudder pedal commands an acceleration. The average maximum authority used by the pilots was 0.5 G's (Figure 11). Of the six modes evaluated, this mode was found to be the most useful for reducing the time to a firing solution on a combat target. Flat turn was found ideal in air-to-surface

found that turn was [illegible] power
ing errors the lateral accelerations produced by the flat turn (0.7 to 1.0 G's side force) was objectionable to the pilots. For these large errors, the pilots found conventional banking was best for the acquisition task and flat turn best for removing the final tracking error.

● For direct lift, the twist throttle commands an acceleration. The average maximum authority used by the pilots was 0.7 G's. Although the response to the twist throttle input was smooth, linear and predictable, direct lift did not show great utility since the pitch stick also provided precise flight path control for air-to-ground tasks.

● For pitch and yaw pointing, the twist throttle and rudder pedal command an angular rate. The average maximum authority used for pitch pointing was 3.0 degrees; yaw pointing was 3.5 degrees. The pointing modes were initially programmed to be used in air-to-air combat and strafing. But after some initial flight testing, the pilots discovered they preferred controlling flight path (flat turn, direct lift) rather than weapon line pointing for the strafing task. Pitch pointing was found useful in tracking a cooperative air-to-air target aircraft, but for a jinking target, pitch pointing's utility greatly diminished because of its limited authority and speed. As with direct lift, the pitch stick could track as well as pitch pointing thereby further diminishing its need. Yaw pointing's utility was slightly better, but it was only good for small lateral corrections. When maximum pointing angles were commanded, roll coupling was sometimes a problem. All the pilots commented they would have preferred commanding pointing angle rather than pointing rate for both pointing modes.

● For vertical and lateral translation, the twist throttle and rudder pedal commands an acceleration. In close formation flying the pilots felt these modes actually increased their workload over conventional techniques. This was possibly due to these modes being acceleration command systems which forced the pilot to provide lead compensation to precisely position the aircraft. All the pilots stated the modes would have had more utility if they were velocity command systems.

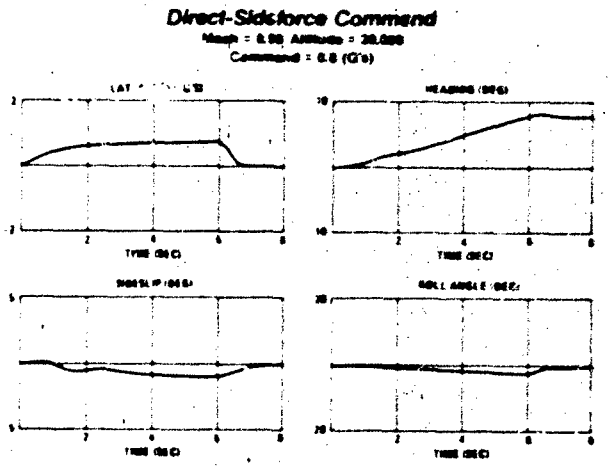

Figure 11. Flat Turn Time History

Purity of the decoupled responses became an issue as the mode designs began to finalize. With the open loop system used on the Fighter CCV, the purity level was a function of how accurately the designer could predict the aerodynamic forces produced by each control surface. In the closed loop system, the designer's ability to feedback the correct variables will provide the primary influence on mode purity. As an example, in the direct side force mode the rudder pedal input is a lateral acceleration command. The lateral acceleration error passes a proportional plus integral network then commands a canard surface deflection. To maintain zero sideslip angle, sideslip rate feedback is passed through a proportional plus integral network then commands a rudder surface deflection. The difficulty occurs in the ability to accurately measure (or calculate) sideslip rate. The ideal way to calculate sideslip rate would be to use sideslip angle. Unfortunately, no location on the aircraft could be found from which a sideslip angle probe worked accurately at all flight conditions. As a result, sideslip rate was calculated by using yaw rate, lateral acceleration, and a small roll rate component to compensate for any angle-of-attack. Without there being sideslip angle feedback, any steady state sideslip that exists at the beginning of a direct side force maneuver will never be washed out during the maneuver. Also for very slow command inputs, the yaw rate can be so low that the yaw rate sensor is ineffective in measuring it, thus, sideslip angular error will build up.

Flight testing, though, showed that the mode purity was not nearly as critical as originally thought. There appeared to be a purity threshold above which further improvement had no effect on pilot acceptability or task performance. For pitch pointing and yaw pointing modes, the impurities were generally proverse in the form of acceleration in the direction of the pointing angle. It seemed that the impurities could be fairly large, especially air-to-air, and have no effect on pilot performance. During strafing, though, the down acceleration impurity associated with down pitch pointing was rather objectionable. For vertical and lateral translation, the impurities were in the form of aircraft rotation and the amount of acceptable impurity was very task dependent. If the task was formation flying or aerial refueling, a little impurity can make the pilot very nervous. Any other tasks where collision avoidance is not an issue, the impurities were not important. Proverse rotational impurity was less disorienting than adverse. For direct lift,

the vertical tail. Therefore, flat turn purity may be primarily dictated by structural strength rather than pilot performance.

These were just a few of the problems encountered while trying to integrate decoupled/coupled flight control laws into one system. This program has demonstrated that decoupled control laws, especially flat turn, can be used to improve weapon system effectiveness.

CONCLUSIONS

As a result of these design issues, several conclusions can be made:

1. An IBC is effective in improving user confidence while flight testing a new complex digital flight control system. An IBC also provides a safeguard against generic software failures.

2. An asynchronous computer system works; the redundancy management system for asynchronous operation can live in harmony with high gain control laws but their designs will be interdependent on one another. This asynchronous computer system (as tested on the AFTI/F-16) is a highly fault tolerant system.

3. Of the six decoupled control law options tested, flat turn is the most effective in reducing time-to-null weapon line tracking error relative to conventional tracking methods. The rudder pedals are ideal for controlling flat turn and 0.5 G's is its optimum authority limit.

EPILOGUE

The AFTI/F-16, after completion of all system modifications, began its flight test phase in July 1982. The flight testing was successfully completed in July 1983 at which time Phase I of the program (Digital Flight Control System Phase) was concluded and aircraft modifications for Phase II of the program (Automated Maneuvering Attack System Phase) began. In this second phase of the program, the aircraft will be tested in a much harsher environment of low altitude, automatic weapon delivery. In this environment good flight control system reliability and high pilot confidence in the system is essential to successfully achieve program goals. The ability of the aircraft to maneuver precisely and aggressively and to accurately deliver weapons in a high-G environment is also an important factor in the second phase of this program. To allow the AFTI/F-16 program to reach its goal these issues and many others had to be (and will have to be) successfully resolved.

REFERENCES

1. Van Vliet, B.W., Barfield, A.F., and Anderson, D.C., "AFTI/F-16 Advanced Multimode Control System Design for Task-Tailored Operation," AIAA Paper 81-1707, Aug 81.

AIRCRAFT TESTS IN THE CLEARANCE PROGRAM FOR THE USE OF A COMBAT AIRCRAFT FROM A RUNWAY AFTER DAMAGE REPAIR

Wolfgang Seidel
Flight Test Department
MESSERSCHMITT-BÖLKOW-BLOHM GMBH
Airplane Division
P.O. Box 801160
D-8000 München 80 W-Germany

Abstract

The requirements to the repair quality of a damaged runway depend highly on the design capabilities and the strength of an aircraft and its undercarriage, and it is quite obvious that, regardless of the repair technique, low repair quality will save valuable time to the reopening of a damaged runway for use.

This makes accurate knowledge of the behaviour of the aircraft on non-flat surfaces necessary and it is standard practice to develop a computer model of the aircraft and its undercarriage for analytical coverage of all operational cases. This analytical model requires comprehensive verification in tests and since the development of a service clearance by test alone due to the vast number of possible initial conditions is impossible, it is rather this verification, where the test work has to concentrate on.
The tests are additionally necessary to optimize pilot techniques for the use of the aircraft under such conditions with minimum risk.

The paper describes tests, which have been performed with a combat aircraft on a runway, where mat repair has been simulated. A description is given of the test setup, and the reasons for the selection of test configurations and test cases are discussed. Test instrumentation, data acquisition and data processing are briefly described and a part of the paper is devoted to the test techniques, which have been used to meet predetermined test conditions.

Examples of test results are presented and compared with predictions. A discussion of unpredicted results highlites the need for accurate test performance.

The paper concludes with an outlook to desirable improvements in measuring techniques and pilot supporting test equipment.

possibility of extensive bomb damage has to be taken into account. The repair technique to such expectable damage is in continous development and promising results have been accomplished recently with prefabricated concrete blocks replacing the ordinary runway after cutout of the damaged surface and fill in of the craters.

Standard procedure for fast repair however still is to cover the graded and filled craters with repair mats. Large stocks of such mats are available on most of the NATO airfields. The result of all such repairs will always be a field with uneven surface and of reduced length.

Much effort has been put into the definition of design criteria for undercarriages to be compatible with such uneven strips in addition to the definition of the semi-prepaired runway type of NACA TN 4303.

It is obvious, that regardless of runway repair technique, low repair quality will save valuable time to the reopening of a damaged runway for use.

The accurate knowledge of the behaviour of the aircraft on non flat surface is therefore the prime task of the designer and it is standard practice, to develop a computer model of the aircraft and its undercarriage for analytical coverage of all operational cases. This analytical model requires comprehensive verification in tests, and since the development of a service clearance by test alone due to the vast number of possible initial conditions is impossible, it is rather this verification, where the test work has to concentrate on. The tests are additionally necessary in order to optimize pilot techniques for the use of the aircraft under such conditions at minimum risk.

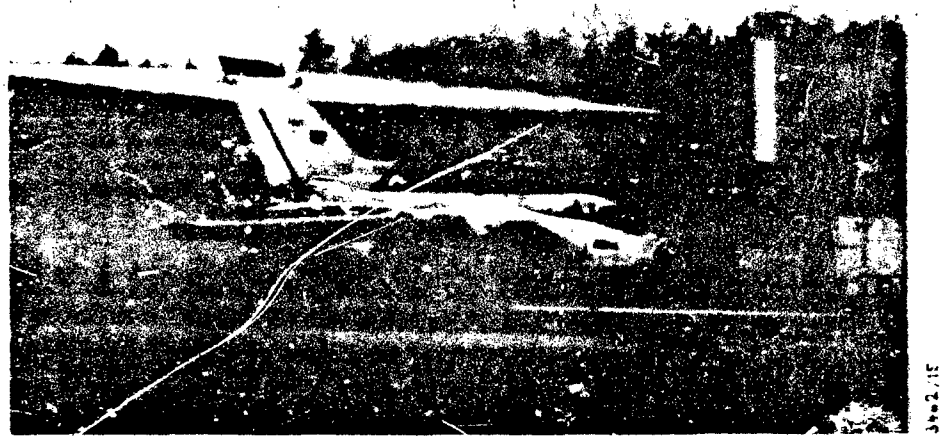

FIG. 1 TORNADO MULTI ROLE COMBAT AIRCRAFT IN MAX. DRY T/R DECELERATION AFTER LANDING

2. Planning the TORNADO Repaired Runway Test Program

In the development of the TORNADO (a multi role, sweepable wing combat aircraft of the 15 tons class, with two engines and with integrated thrust reverser, Fig. 1), semiprepared runway (NACA TN 4303, Fig. 2) capability in a limited mass envelope was adopted as design philosophy of the undercarriage in addition to the maximum sinkrate criterion.

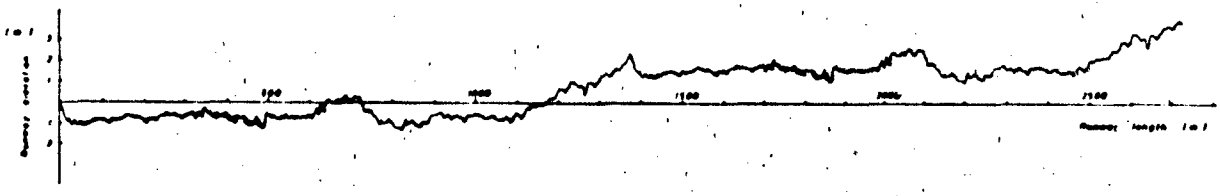

FIG. 2 NACA TN 4303 SEMIPREPARED RUNWAY PROFILE

and with Class 60 mats which are [illegible]

After this redefinition, a test program was planned which aimed equally at the verification and improvement of the analytical model and at the verification of pilots techniques in handling the aircraft at a repaired strip.

This test program was divided into two phases:

Phase 1: An initial program with tests on a flat surface, on which ideal repair with one or two AM2-mats was simulated. In this program, and to cover the differences between AM2 and Class 60 mats, also traversion of a single half sized Standard Class 60 mat was included.
In this first block of tests, no test points were included, for which according to analytical predictions (with the initial computer model) loads in excess of 80% of limit would have to be expected.

Phase 2: With the improvements of the analytical model from the results of the first test phase, a second test phase was planned in which a reduced however analytically defined degree of repair quality was adopted as test basis and in which, contrary to Phase 1, dynamic preconditions are included.

So far, only the tests of phase 1 have been completed.

Although the verification of the computer model does not necessarily require the inclusion of all operational cases in the test program, this inclusion helps to verify the separate influental parameters and is in any case required to cover all conditions for the verification of pilots handling techniques.

The typical a/c conditions under which traversions of repaired runway or taxiway sections are possible can be distinguished in dependence from the aircraft mass as follows:

Aircraft going out with takeoff-mass

1. Steady rolling during taxiing and limited to taxi speed
2. Deceleration during taxiing at low speed with brakes (no reverse thrust)
3. Acceleration during take off-roll covering all speeds up to lift off (RTO-excluded)

Aircraft coming in with landing mass

1. Landing impact with lift dump, including derotation
2. Deceleration during landing roll at high speed with thrust reverser, but no braking
3. Deceleration during landing roll at low speed or during taxiing (with braking but no reverse thrust)
4. Steady rolling during taxiing at taxi speed
5. Deceleration during landing roll with thrust reverser and braking (all speeds - short-field case)

All the above conditions were included in the test program of phase 1.

As mentioned earlier, no test cases were included for which loads higher than 80% of limit were predicted. This goal required a careful buildup in the test program because enough examples exist that an adverse combination of incorrectly accomplished initial conditions may rapidly lead to excessive loads up to failure .

In this buildup program the results had to be continously compared to predictions and corrections had to be made where necessary.

Since the predictions had suggested, that critical loads will only occur from multiple mat traversions, the program was started with the traversion of a single mat with various speeds and for both a/c test masses. For the verification of the handling properties from the asymmetric loads due to the traversion of the mat with only one main undercarriage leg, such traversions were included as well.

The trials were continued with double mats with variable distance and with mat distance adjusted to the conditions for adverse mat spacing in the different speed ranges and for the two test masses.

Comparative runs over a half size UK class 60 mat were planned with the a/c in landing configuration to conclude the phase I test program.

3. Preparation of the test aircraft

3.1 Aircraft standard

As long as the Repaired Runway Test Program is done during the development time of the aircraft, there is always the availability of a prototype aircraft, which for development flight test reasons has basic flight test instrumentation. There may however, be shortcomings in the use of prototype aircraft for such a program either, that important structural or undercarriage properties, influencing the dynamic behaviour may have been changed in production aircraft or that increased strength in production aircraft without change of dynamic properties may yield larger safety margins. Although the verification of the analytical model could be done with a prototype aircraft for a prototype-model with subsequent analytical coverage of the differences, as much production standard properties should be provided as possible.

In the TORNADO test program and for phase 1 prototype P01 was used. Main and nose undercarriage have been of improved prototype standard with performance characteristics representative of series standard (except for recoil damping of the nose undercarriage) . Elastically, the prototype a/c is sufficiently similar to the production type and the differences ar covered in the dynamic response analysis.

Aircraft mass, and c. g. have been adjusted to the requirements for series aircraft and the remaining differences in the inertia values of the rigid aircraft are covered in the analysis.

3.2 Flight test instrumentation and data acquisition

The primary flight test instrumentation in such a program consists of parameters for the determination of the undercarriage behaviour, that is the determination of loads, strokes, and if possible of the internal pressure conditions in airspring and damping oleos.

An important is the determination of the rigid body aircraft motions from the traversions as well as from pilots inputs as braking, steering or control surface inputs. Engine and thrust reverser power settings need to be measured as well as buildup and magnitude of brake pressures.

Depending on the type of aircraft, dynamic loads in the wings or of stores as response to the a/c motions from traversions may become critical and need therefore test instrumentation.

The a/c used in the trials had as the first prototype aircraft a comprehensive handling instrumentation. Measured were the a/c c. g. longitudinal and angular accelerations in all 3 axes and pitch, roll and yaw rates.
All pilots inputs, as stick or pedal positions were available as well as all the relevant control surface positions including spoilers for lift dump initiation.

The special instrumentation for the undercarriage responses consisted of calibrated straingauge instrumentation for the determination of longitudinal, side and vertical forces as acting on the wheels of all three legs. All three undercarriage legs were also instrumentad to measure shock absorber stroke position and airspring nitrogen pressure.

Fig. 3 shows the undercarriage loads straingauge locations.

For the verification of the dynamic response calculation the elastic movements of wings, fuselage and wing mounted stores were measured with accelerometers.

All measured parameters were recorded onboard via PCM, with adequate sampling rate. All loads parameters were recorded with 128 samples/sec and in parallel for the verification of peak loads via the FM multiplex system (200 Hz handwidth).

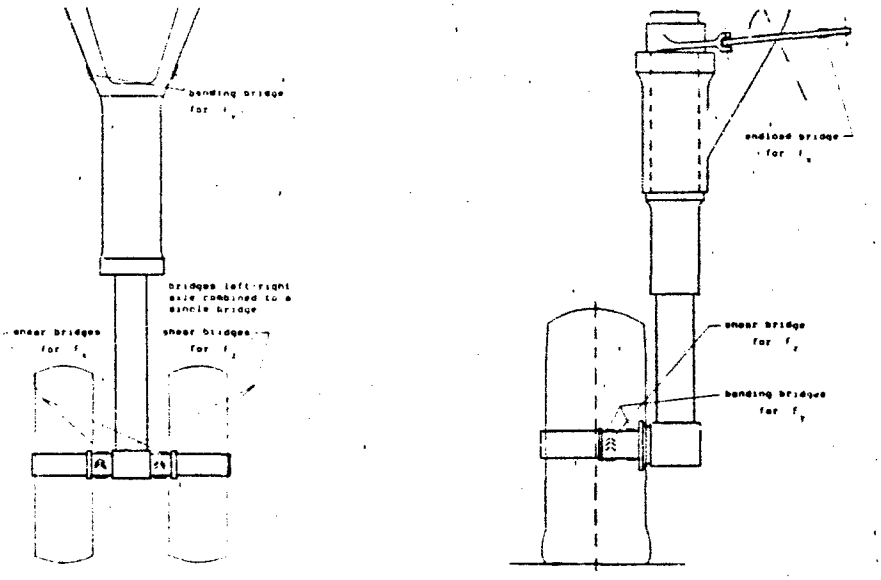

FIG. 3 UNDERCARRIAGE STRAINGAUGE INSTALLATION

The PCM data-stream was telemetered to the ground station for quasi-on line evaluation. This was helpful, to decide upon correct performance of a test point for the continuation of the program, as well as for the correct functioning of the flight test instrumentation.

3.3 On-board test speed indication

A dial instrument was installed in the cockpit in optimum view of the pilot, which was connected to the wheelspeed generator of the antiskid-system of one main undercarriage leg. This simple instrument provided in connection with the accurate traversion speed determination from tape switches in front of the mats a valuable aid to the pilot for accurate test speed adjustment.

3.4 Maintenance and servicing

Special consideration was given to have the test aircraft as close to the required status as possible in particular with respect to the undercarriage properties. Damping fluid and nitrogen fillings have been adjusted in accordance with the official filling procedures prior to commencing the tests.

4. Test site and Test setup

4.1 General remarks

It is quite obvious, that a test program, which is planned to cover the wide range of conditions as described earlier will require a considerable number of testruns, both to cover the different test conditions as well as the repetition of testruns due to the inadvertent scatter in the test performance.

Such a program will certainly last for at least a few weeks and it cannot be assumed, that the test setup, e. g. the runway repair mats with the associated test equipment is compatible with a normal use of an airfield for flight operations.

Most test centers have two runways available so that frequent installation and removal of test equipment or change of test location during the test program can be avoided by closing one runway for the trials.

from preceding takeoff conditions.)

Such cases can be

° Requirements to lower tire temperatures than at best can be reached in a taxirun in particular at high a/c mass and

° Requirements to shock absorber initial temperatures which may in case of a taxitrial not be representative of those in high speed cases after a landing.

The choice of the mat position along a closed runway or taxiway has to take into account the required distance for acceleration and stabilization of the test condition, but priority must always be given to an adequate runout length under consideration of failures of deceleration aids.

The experience with the TORNADO trials has shown, that another important parameter in the choice of a test site is the quality of the surface at the envisaged test site because unwanted responses to local surface irregularities will interfere with the intended responses to the different test parameters. Runways are not by far as smooth as they look and a survey of the surface profile at the test site should therefore be done definitely before the final mat location is chosen.

4.2 Test site for the TORNADO trials

The test center of Manching has the opportunity of two separate runways, one with 10 000ft and the other with 8 000ft standard length. This made the closure of the 8 000ft (north) RWY possible for the trials. This RWY does not have a longitudinal slope but a lateral slope of 1.5° both sides down from the runway centerline. Therefore the mats had to be put on only one side of the runway and the left side of RWY direction 25 was chosen. The associated light drift off of the aircraft had to be corrected by the pilot. The small difference in vertical load from the bank angle is within the accuracy of the measurements and was therefore neglected in the comparison with predictions. Fig. 4 shows the single mat on the left half of the runway.

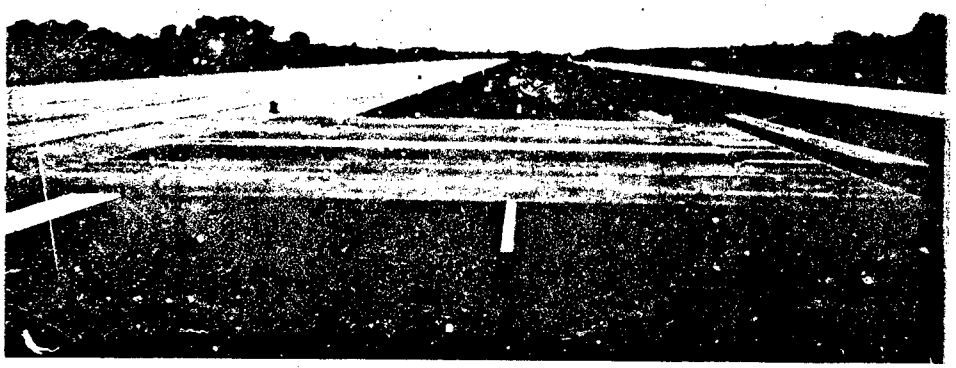

FIG. 4 SINGLE AM-2 MAT ON THE RUNWAY

The optimum compromise-position of the mats for acceleration and deceleration was initially selected with the forward end of the (fixed) second mat at 200 meters in front of the mid of the runway leaving an acceleration distance of 1290 meters out of the east overrun and 1420 meters runout length to the barrier + 504 meters overrun.

Unexpected undercarriage loads responses and poor correlation with prediction in the first trials triggered a surface quality survey across the mats at the initial location and this survey revealed an irregularity in the runway surface right at the location of the main (second) mat and in the area behind. This irregularity consisted of a depression about 15meters long and with its lowest point about 3.5 cm below the average surface in front of the depression and followed by a rise to about 1.5 cm above the average in front of the depression.

FIG. 5 RUNWAY DEPRESSION AT THE SELECTED TEST SITE

Fig. 5 shows the result of that surface survey. After this discovery, the mats were pulled back and relocated finally 70 meters in front of the initial position in a reasonably flat area. Fig. 6 shows the final mat location and the surface around.

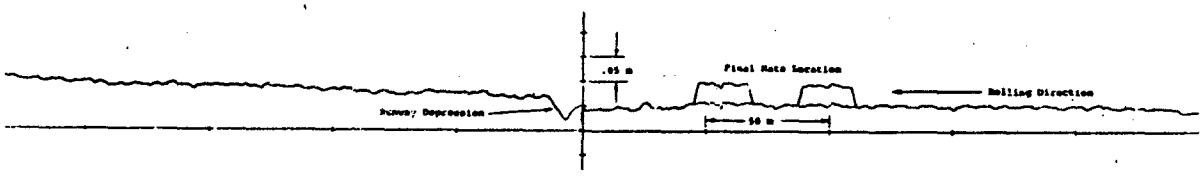

FIG. 6 FINAL MAT LOCATION ON A FLAT RUNWAY SECTION

For the orientation of the pilot, an auxiliary centerline in the middle of the left RWY half was applied and distance lines were painted across the runway every 100 meters to the test reference line, as which the forward end of the single or second mat was defined. These lines had large number plates on the RWY shoulders for the pilot.
In the area, where runup positions for acceleration runs were planned, that is 300 m to 50 m to the reference line, these 100 m distance lines were subdivided by 20 meter lines at the side for accurate brake release positioning.

During the acceleration runs, and all other runs, which required pilots action at a certain position of the runway e. g. brake release, brake initiation, thrust reverser deployment or nosewheel touch down, this runway position was identified to the pilot by parking a motorcar next to the shoulder of the runway at this very location.

Since the a/c had a comprehensive flight test instrumentation which permitted quantitative determination of all test parameters, the medium speed onboard and runway movie cameras, which had been provided were installed rather for the identification of unexpected behaviour of the a/c than for quantitative verification of the test performance.

Exact traversion speed of the mats was determined by means of 2 sets of tape switches, one in front of each mat.

As most important ground equipment, there was equipment to measure tire bead temperatures and equipment for cooling of tires and of brakes.

Warmup of the tires from deformation energy and heat dissipation from the brakes was also checked by measuring tire inflation pressure after each run and after cooling. In most cases, main u/c wheels were replaced with cold tires after 2 test-runs and the removed wheels were used again after cooloff later in the program.

5. Test performance and typical results

5.1 Single mat

Since predictions suggested, that critical loads will only occur from multiple mat traversions and in order to generate the first a/c responses for comparison with predictions, the first set of traversion was done as steady state traversion across a single mat with various traversion speeds and with the two test weights (take off and landing mass).
For the verification of the handling properties from the asymmetric loads due to the traversion of the mat with only one main undercarriage leg such traversions were included as well.

All these trials were done from accelerated runs, they did not pose any problem for the pilot. The pilot hardly recognized the traversion and the unsymmetric traversion could be easily controlled.

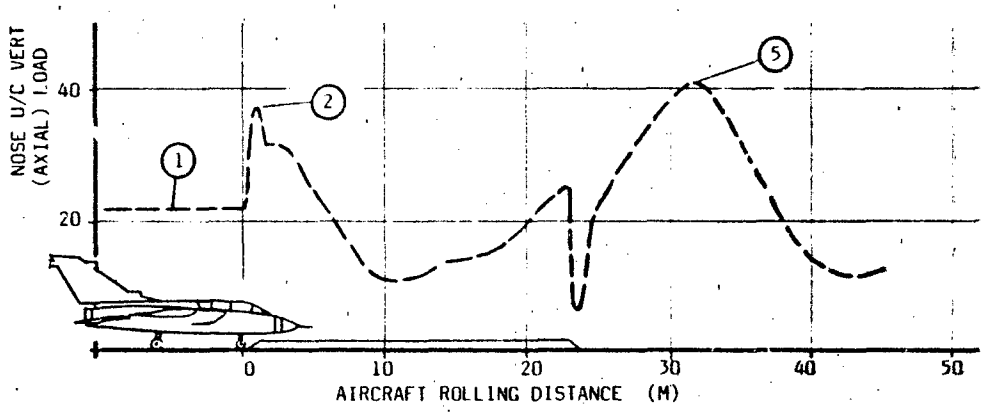

FIG. 7 TYPICAL NOSE U/C LOADS FROM A 60 KTS TRAVERSION OF A SINGLE AM-2 MAT

Fig. 7 shows a typical example of vertical u/c response loads from a single mat traversion at constant speed. The most important loads are those generated when the wheel goes up the front ramp onto the mat and the "dynamic overswing", which is caused by dynamic compression of the relevant undercarriage leg from the a/c mass oscillating with the u/c spring stiffness after leaving the mat again.

As function of speed and u/c spring stiffness (nose/main) there may also be dynamic loads generated on the mat higher than the load from the front ramp.

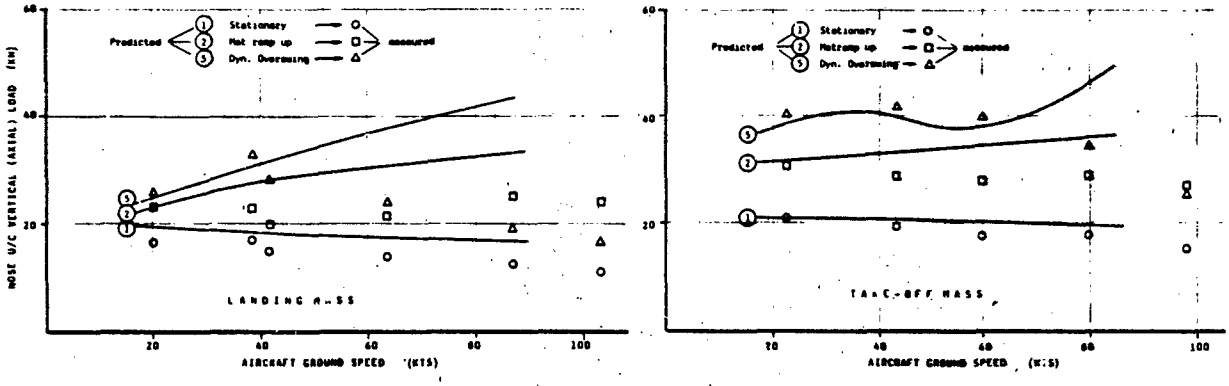

FIG. 8 PREDICTED AND MEASURED NOSE U/C LOADS FROM TAXYING A SINGLE AM-2 MAT

Fig. 8 shows the predicted loads on the nose u/c for mean initial load and the two defined loads "ramp up" and "dynamic overswing" as function of forward speed and for the two relevant a/c weights.

The measured results from the single mat traversions show

1. an increasing deviation in the stationary load on the nose u/c from prediction with increasing speed and
2. a wide scatter in the results for the dynamic overswing.

As result from 1. the aerodynamic pitching moment in the model was adjusted to the measured results and from 2. the scatter in the dynamic overswing led to the discovery of the runway depression as described before.

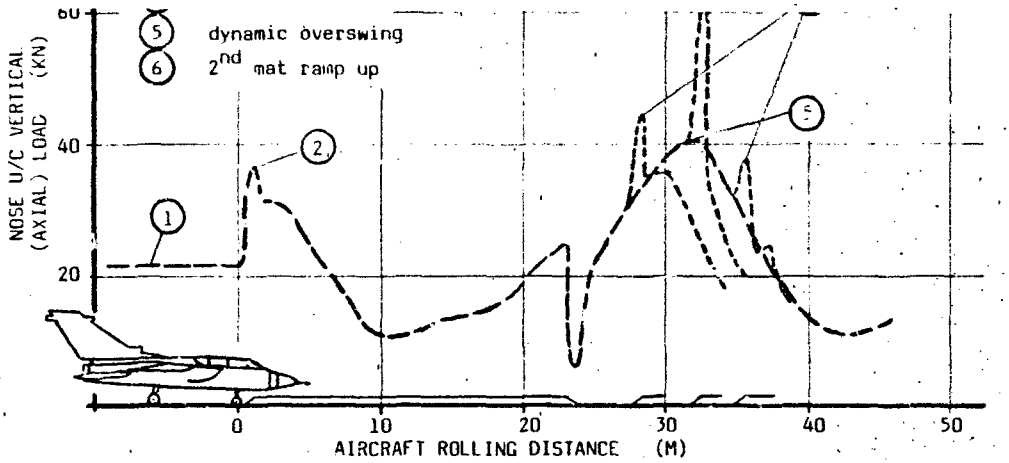

FIG. 9 TYPICAL NOSE U/C LOADS RESPONSES ON THE RAMP OF A SECOND MAT

If the runway damage makes it necessary to place mats in close proximity, the response of the first mat will dictate the initial condition for the encounter with the following mat. Fig. 9 shows a typical example of possible combinations and the mat distance where the ramp of the second mat coincides with the location of the dynamic overswing is called the adverse mat spacing. It varies with a/c weight, forward speed and stationary precondition and analyses had been performed for the prediction of the adverse mat spacing for the two a/c masses and for the different initial conditions. These analyses showed, that both for main and nose u/c and for a wide range of initial conditions, the adverse mat spacing in the medium speed range 30....80 kts lies between 8 and 14 meters.

Figs. 10 and 11 show the calculated adverse mat spacings for different speeds and for the different initial conditions.

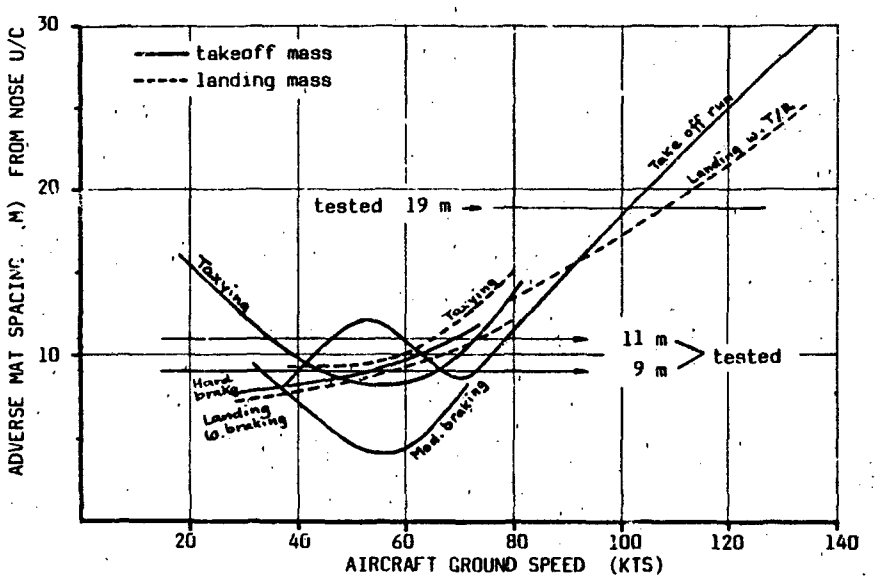

FIG. 10 CALCULATED ADVERSE MAT SPACING FROM NOSE U/C LOADS

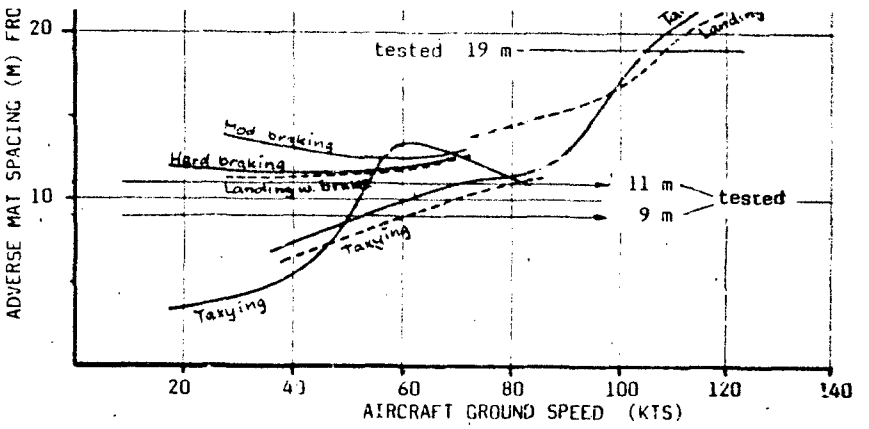

FIG. 11 CALCULATED ADVERSE MAT SPACING FROM MAIN U/C LOADS

Although mat spacings of less than 10 meters are unlikely, because at lower damage distances, mats or parts of it would be combined to a single (longer) mat, covering the entire local damaged area mat spacings of 9 and 11 meters were selected for the trials in the low and medium speed range. For the coverage of the high speed cases 19 meters distance were chosen.

Constant speed traversions

For the constant speed traversions which were performed in the speed range of 35 to 70kts ground speed for both a/c masses, acceleration distance was selected such, that sufficient time for a/c speed stabilization and for steady initial condition was available without using long taxi distances to avoid unwanted tire heating. Best results were reached with short max dry power accelerations and stabilization distances of 150....300meters. Typical traversion speed deviation was around one kt, from aim speed with biggest deviation of 4 kts in a 40kts case.

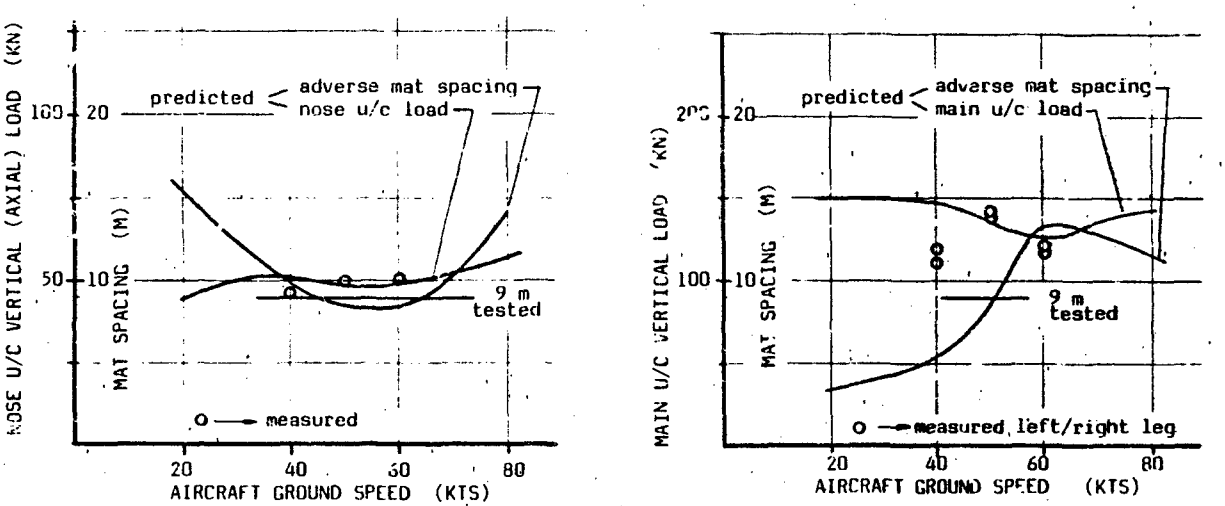

FIG. 12 PREDICTED AND MEASURED U/C PEAK LOADS ON THE RAMP OF THE SECOND MAT WITH 9 M SPACING

with 9 m spacing in comparison to prediction. The figure shows good agreement between measured and predicted load at the speed where 9 m distance is predicted as adverse spacing and reduced loads (main u/c) at speeds where the predicted adverse mat spacing is different from the tested 9 m.

Take off acceleration runs

For the heavy weight acceleration runs, the a/c was positioned at a distance to the mats, which after brake release with max reheat power setting would result in a mat traversion with the intended speed. With this procedure, the real speed was within 3kts of the intended.

This procedure however, produced an aircraft response which, although being typical, was not compatible with the intention of the test, i. e. monitoring the test progress by comparing the results with the predictions.

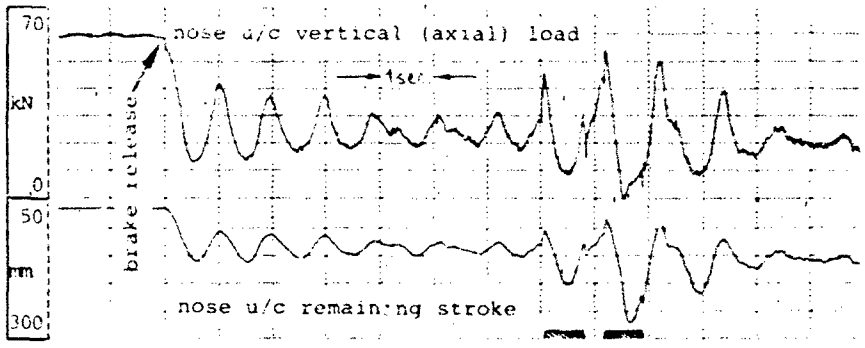

FIG. 13 NOSE U/C LOADS OSCILLATIONS FROM BRAKE RELEASE AT HIGH POWER SETTING

As is shown on Fig. 13 the nose u/c vertical loads variations from the a/c pitch oscillations after brake release had in particular in the cases with short distances to the mats (aiming at low traversion speed) at the time of the mat traversion not sufficiently damped off as to generate steady state initial conditions for the traversion of the mats.

The predictions however assumed steady state initial conditions also in the accelerated or braked runs. Therefore, the accelerations procedure was changed later such, that in the cases up to 80 kts traversion speed, a controlled engine acceleration to max reheat from idle was done after brake release, within a given time, for higher traversion speeds (larger distance to the mats), the engines were simply slammed to max reheat after brake release.

With this procedure, speed scatter with ± 5kts against intended speed was higher than in the standard acceleration runs, but a/c oscillations interfering with the mats traversions could be adequately avoided as is visible in Fig. 14.

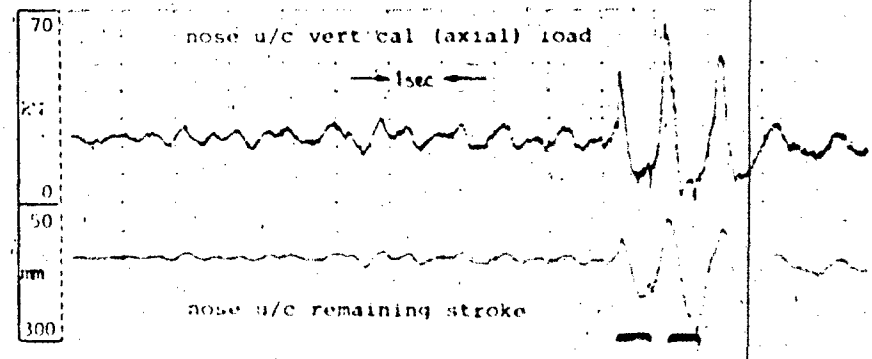

FIG. 14 AVOIDANCE OF NOSE U/C LOADS OSCILLATIONS BY CHANGED ACCELERATION PROCEDURE

which was predicted as unimportant, in the relevant speed range. Fig. 15 shows the time histories of the nose u/c vertical load in the two heavy weight take off runs with 104.7 kts and 103.6 kts at the ramp of the second mat (19 m spacing).

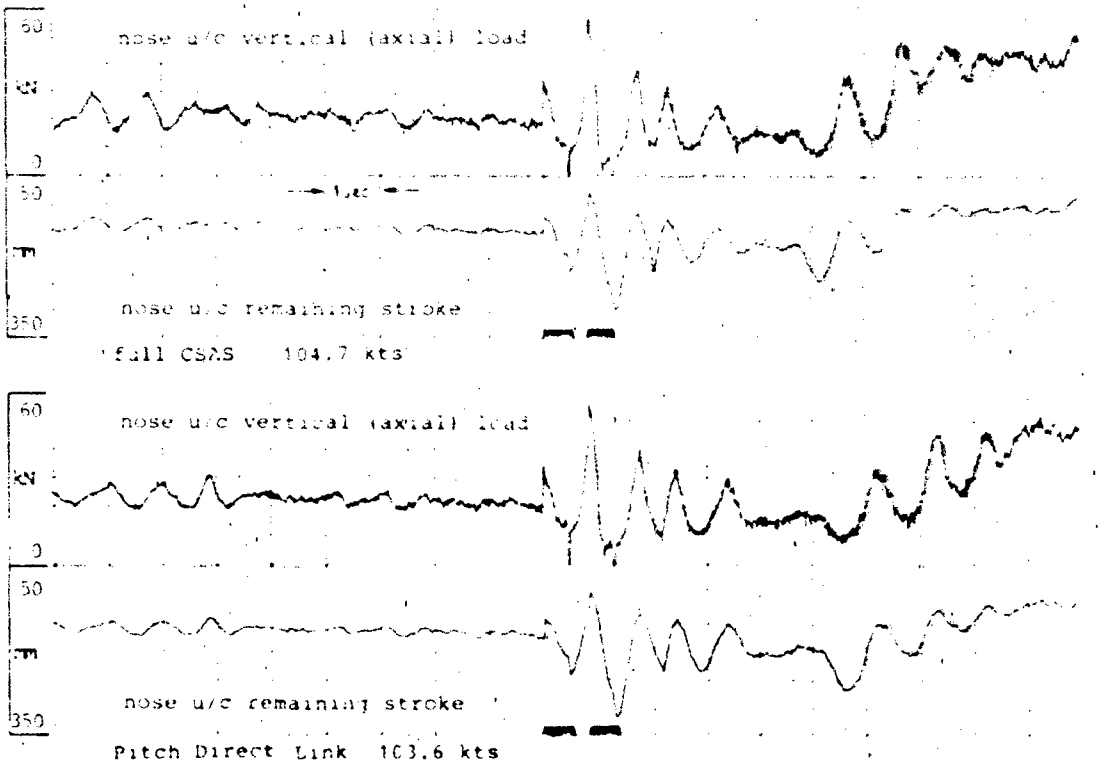

FIG. 15 COMPARATIVE TAKE-OFF RUNS WITH AND WITHOUT CSAS OPERATIVE

The time histories not only show no visible influence from the CSAS but also a good repeatability of test performance with almost identical output data.

Braked test runs

The widest scatter in test performance was in the braked runs and a special technique had to be developed to come to acceptable results.

At first, moderate braking and slow buildup of brake power (to avoid pitch oscillations) had to be trained by the pilot.

The best results were reached, when the pilot watched the cockpit brake pressure indication and increased the brake pressure to a predetermined level within a given time.
Fig. 16 and 17 show a comparison of an early testrun and of one after some training. The improvement is evident.

Initial speed before brake onset was stabilized high enough to give sufficient deceleration [illegible] for the decay of any dynamics from brake onset before crossing the mats, but low enough to avoid long deceleration distances with an associated wide scatter of traversion speed from slightly different brake application.

The location of brake onset in the stabilized speed run with reference to the mats was indicated at the runway side with a parked motorcar and the passing of the motorcar was reported to the pilot by the navigator, so that the pilot could concentrate on the stabilization of the a/c and on the braking and crossing event. This technique proved helpful especially at higher speeds and in the testruns with reverse thrust application, where there was high workload on the pilot from a/c and engine handling.

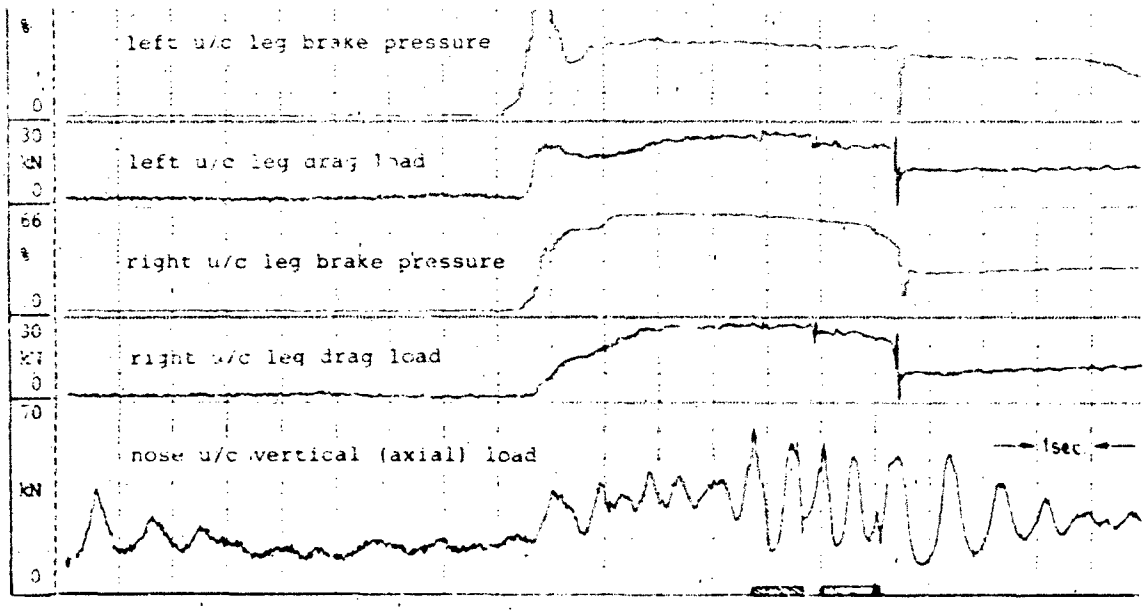

FIG. 16 UNSATISFACTORY BRAKE APPLICATION IN A BRAKED TEST RUN

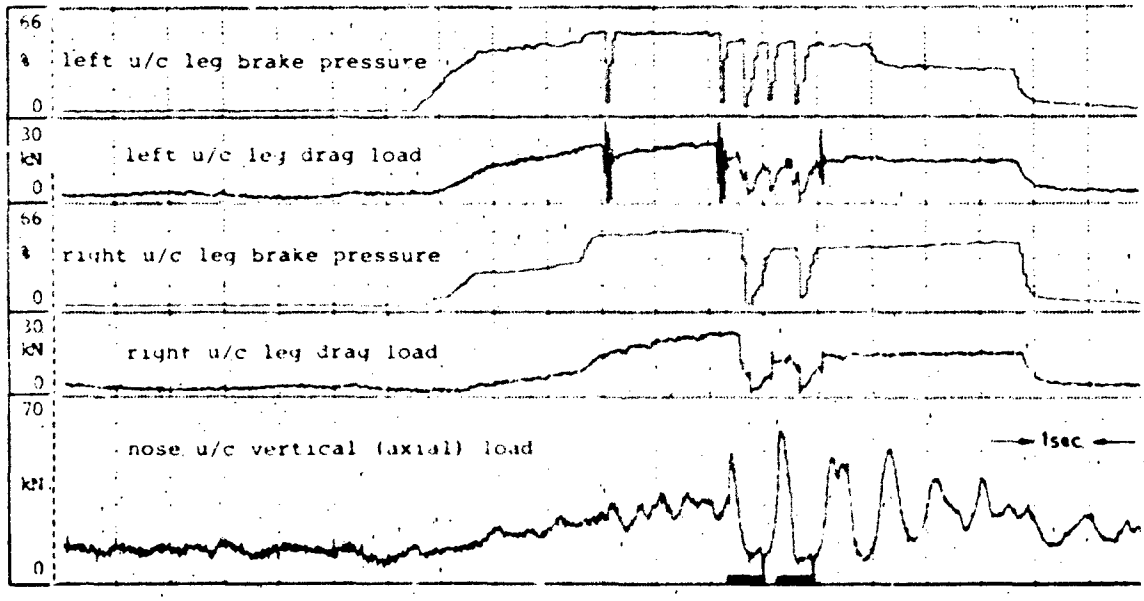

FIG. 17 RESULTS OF IMPROVED BRAKING TECHNIQUE

Landing runs with thrust reverser

The highest nose u/c loads had been predicted for landing runs with max dry thrust reverser because the reverse thrust produces a nose down pitching moment on the a/c.

Fig. 18 shows the predicted nose u/c axial load vs. speed when going up the ramp of the second mat at adverse distance. The figure also shows, which adverse distance is associated with which speed.

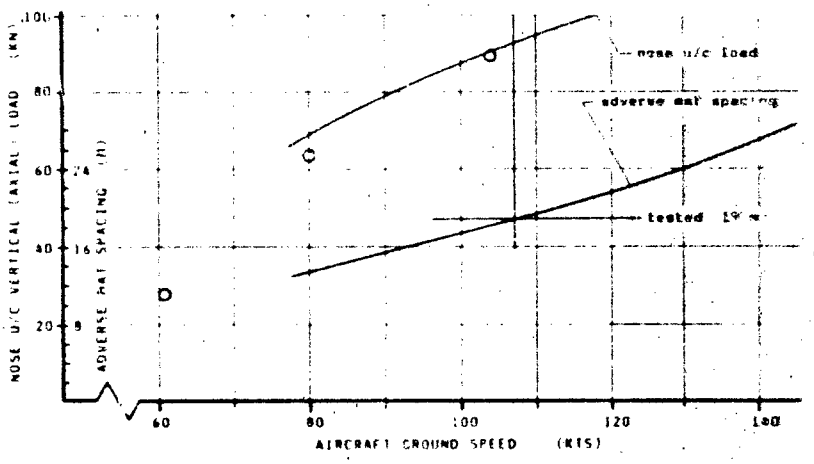

FIG. 18 NOSE U/C VERTICAL (AXIAL) LOAD ON THE 2ND MAT RAMP IN MAX DRY T/R DECELERATION AFTER LANDING

A direct comparison of the time histories of runs with 60 to 117kts traversion speed with 19 meters mat spacing on Fig. 19 shows the increase in dynamic load with traversion speed.

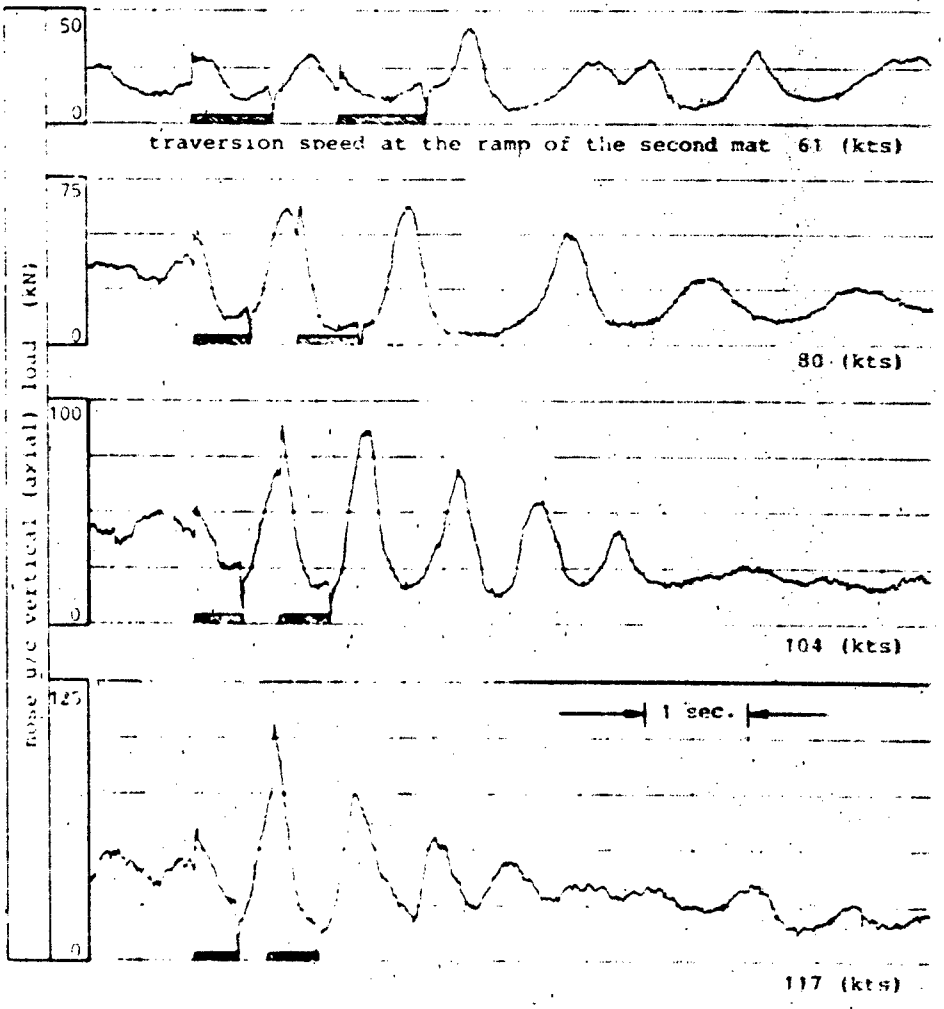

FIG. 19 NOSE U/C LOADS IN MAX DRY REVERSE THRUST DECELERATION RUNS (LANDING) MASS

critical area by inaccurate test performance.

An interesting experience in the high speed runs with thrust reverser is the pilots complaint about the narrow strip. The pilot had the impression, that with reverse thrust, which produces yaw motions of the aircraft, he had difficulties to stay on the narrow strip. The evaluation of the onboard films of the test however showed, that although there was some yaw motion of the a/c, the a/c did not deviate more than 1 m left and right from test centerline leaving ample space for safety.

6. Use of the test results

Although not subject of the paper, the consequences of the test program in respect to the validation of the computer model shall be shortly mentioned.

The basic computer model was updated

1. in the ground effect aerodynamic pitching moment and

2. in the incremental nose down pitching moment from max dry reverse thrust from the data generated in the trials.

Additionally the nose u/c recoil damping was changed to the value for the used prototype u/c.

With the updated model a number of tested runs was recalculated with inclusion of additional boundary conditions as follows:

1. measured runway surface irregularities
2. ground wind and direction
3. actual taileron position during the test
4. momentary mass data of the a/c (mass; c. g. inertia)
5. braking drag as measured
6. mat ramp profile as measured in situ

As an example of such a recalculation, Fig. 20 shows the comparison between measured and recalculated nose u/c axial load from the landing deceleration run with max dry reverse thrust, which had generated the highest nose u/c load during the test program.

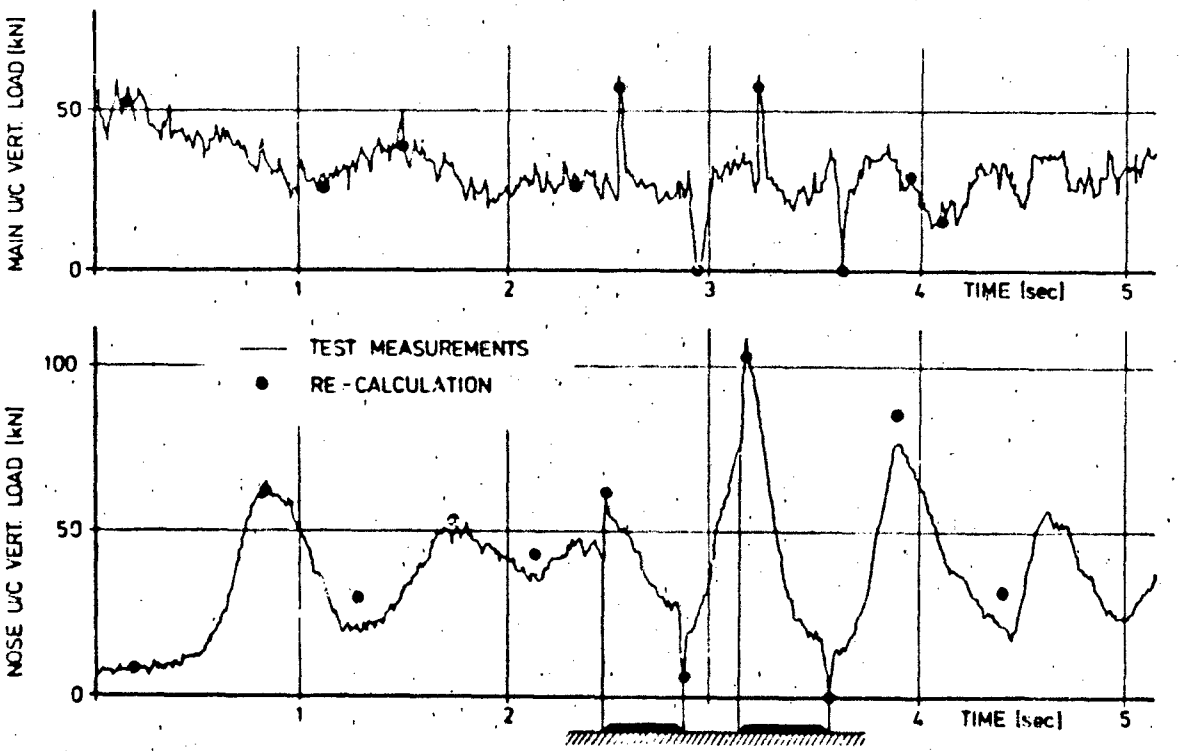

FIG. 20 MAX. DECELERATION LANDING RUN AND RESULTS OF RECALCULATION WITH THE UPDATED COMPUTER MODEL

7. Conclusion

Although the final verification of the computer model is done by the recalculation of real test cases, the aim of such a test program must be to as accurately as possible meet given test conditions in order to:

1. give clearance for the continuation of the test program by immediate comparison of measured data with prediction

2. cover the whole range of conditions for the separation of influental parameters as it is the basis for the test program

3. discover situations wher a/c handling qualities make it difficult for the pilot to control the a/c as required for the avoidance of adverse combinations of initial conditions, which might lead to excessive loads.

From the experience of this test program, improvements in testing technique can be thought of in the area of braking, to better control buildup and size of brake power by a semiautomatic device in the brake system and possibly an externally triggered brake onset from a runway positioned device.

From the measuring techniques, more information would be welcome about the internal processes in shock absorbers, i. e. airspring and damping chambers including a determination of piston friction. Also a measurement of the rolling radius of the tires under all tested conditions is on the list of desirable additional information.

The recalculation of tested cases and the good agreement with the measured results nevertheless show, that in case of TORNADO a high standard computer model exists as basis for test phase II and further clearance work.

Acknowledgement

The author expresses thanks to the company's loads analysis department and in particular to Herr G. Kempf for the contribution to this paper from the analysis side.

THE HANDLING AND PERFORMANCE TRIALS NEEDED TO CLEAR AN AIRCRAFT TO ACT AS A RECEIVER DURING AIR-TO-AIR REFUELLING

by

J Bradley
Aeroplane & Armament Experimental Establishment
Boscombe Down, Salisbury, Wiltshire SP4 0JF

SUMMARY

A brief description is given of the AAR equipment and techniques presently used in the RAF. The handling and performance tests needed to clear a new receiver type are described, together with some of the results obtained when large transport aircraft are used in the receiver role.

1 The events of 1982 stimulated great efforts to enhance the air-to-air refuelling (AAR) capability of the Royal Air Force. Prior to the Falklands conflict the RAF had one dedicated tanker, the Victor K2, and from it 9 types of aircraft were cleared to refuel. By the end of 1982 the Vulcan and Hercules had been converted to the tanker role and 10 types of aircraft cleared to receive from each of them; in addition, exploratory trials had taken place to assess the KC 10 and Tristar as candidates for the strategic tanker aircraft. By the end of 1983 the VC 10 K2 was in Service as a tanker and 9 types of aircraft had been cleared to refuel from it. Later this year the VC 10 K3 and Tristar tankers will be introduced and this will involve a heavy programme of receiver clearances.

2 The Aeroplane and Armament Experimental Establishment (A&AEE) has been intimately connected with this effort. It has been found difficult for industry test pilots to maintain AAR receiving practice and in consequence A&AEE pilots have flown on all the receiving tests of each type, and the Establishment is therefore well placed to comment on the testing of aircraft in this role.

3 Most UK aircraft used for AAR are equipped with probe and drogue equipment developed by Flight Refuelling Ltd. The dispensing gear consists of either the Mk 20 or Mk 32 pod, designed for underwing mounting on the tanker, or the Mk 17 Hose Drum Unit, HDU, which is mounted in the fuselage. The principal characteristics of each unit are shown in Figure 1. When used with the usual high speed drogue an AAR speed range of between 230 kn and 320 kn EAS should be available (subject to the limitations specific to the tanker aircraft). The low speed drogue fitted to the Hercules tanker allows a speed range between 180 and 250 kn EAS to be used. Although the three refuelling systems are engineered in different ways they must all be capable of satisfying the following requirements relating to receiver handling.

a At the minimum airspeed the drogue must offer a resistance of at least 200 lbf to ensure that the probe will latch. At the maximum airspeed and receiver closure rate (12 ft/sec) the drogue must not offer such a high resistance thatprobe damage results.

b Sufficient torque must be applied to the hose drum so that when the receiver probe has engaged in the drogue and the receiver moves forward relative to the tanker the hose winds in smoothly at a rate of up to 12 ft/sec without allowing hose oscillations to develop.

c The receiver pilot must be provided with information regarding how much hose is extended so that he can maintain an optimum position.

d In the event of an emergency disconnect being required the drum will be braked when the wind out velocity exceeds 5 ft/sec; this will then allow the probe to part company from the drogue when the 'pull out' force of about 600 lbf is exceeded, without the hose first having to be fully extended.

e A system of signal lights (red, amber and green) must be incorporated to provide unambiguous information to the receiver pilot by day or night.

4 A brief description of a typical refuelling manoeuvre will serve to illustrate the procedures that are presently employed in the RAF. The receiver aircraft will join with the tanker in the echelon position; the tanker hose will be fully trailed. When cleared astern by the tanker pilot, the receiver pilot will position his aircraft some 50 to 100 feet astern of, and below, the drogue with which he is going to make contact. In going from the 'echelon' to the 'astern' position the receiver must allow sufficient room to pass below the vortex system of the tanker wing. When cleared by the tanker pilot to make contact the receiver will advance up the line of the hose at an overtaking speed of 3-4 kn. This is based mainly on visual estimates of the closure rate. As the receiver closes, the flow field from the tanker will begin to influence it more strongly; buffet and noise levels may increase, more power

been created by the tanker pilot, and the drogue is [illegible] power increment is applied to re-establish the overtaking speed and the probe is flown into contact with the drogue. This can be achieved in several ways and is dependent largely on tanker/receiver type and pilot preference. As a general rule the pilot should concentrate on using visualreferences on the tanker to hold a steady approach up the line of the hose in the final seconds until contact is made. Unless the pilot is very experienced he should resist the temptation to focus his attention on flying the probe tip into the drogue, since this invariably results in a late correction which can lead to overcontrolling and the risk of probe damage caused by the hose 'whipping'. However on some aircraft types a second crew member can usefully assist the pilot, by calling for any small corrections required, while the pilot maintains his references on the tanker. In the event of contact being missed the receiver should move back to the stabilised position and another attempt be started from there.

5 If the contact has been successful the receiver will then continue to close on the tanker, possibly requiring additional power to do so since the drag of the drogue is now largely borne by the receiver (the tanker pilot will have had to make a corresponding small power reduction to maintain target speed). Fuel transfer begins automatically when about 7 feet of hose has been pushed back on to the drum. The receiver will continue to close on the tanker until about 40 to 50 feet of hose remain extended in the case of the Mk 17 HDU or 35 to 40 feet for the pod equipments. This amount of hose extended gives a safe separation between the two aircraft, but will allow some latitude for the receiver to fall back without extending the hose fully and breaking contact. The amount of hose extended can be gauged from coloured marking bands around the hose or, on some tankers, by noting the position of the hose serving carriage. The optimum position can be flown throughout the refuelling by maintaining the correct vertical and lateral position with the aid of line up markings and other visual references on the tanker such that the section of hose immediately in front of the drogue is aligned with the probe. Any sharp change of angle at the coupling indicates that unnecessary bending strain is being exerted on the probe due to the receiver being incorrectly positioned. When in the refuelling position the receiver can follow the tanker in turns (provided there is sufficient power available) and in descents. The tanker captain should, whenever possible, signal his intention and make smooth entries to and from such manoeuvres. The tanker is usually flown under autopilot control. At the conclusion of refuelling the receiver pilot will normally make a small power reduction and retreat slowly down the line of the hose until reaching the full trail position, when the probe will pull out of the drogue. An emergency disconnect can be achieved by making a rapid power reduction/airbrake extension in the receiver, promoting a separation rate in excess of 5 ft/sec in which case the emergency brake on the drum will act and allow the probe to pull out of the drogue without the hose being fully extended.

6 From the foregoing it can be seen that the AAR manoeuvre requires considerable piloting skill, visual contact with the tanker, and reasonably smooth air to avoid an unsteady drogue. With these criteria satisfied AAR can be attempted by day or night, but it is not possible to guarantee success. In normal circumstances all AAR operations are planned so that a failure to refuel results in nothing more serious than a diversion. All probes should have a 'weak link' at the tip so that in the event of an excessive loads being applied it breaks off, the tip being retained in the drogue. No further structural damage should be sustained.

7 When A&AEE is tasked to clear a new receiver with a specified tanker, the process begins with a consideration of the following aspects.

a Physical Clearances: Scale diagrams of the two aircraft are compared to ensure that safe separation can be maintained. No hard and fast criteria are laid down but flight trials will only be proceeded with if the aircrew are satisfied with the clearances, and, in particular, that an emergency disconnect will not require excessive attention to avoid a collision with the tanker. In general the physical constraints make it possible to refuel only fighter and ground attack aircraft from wing stations.

b The flight envelope within which the tanker may dispense fuel is compared with the flight envelope of the receiver. Airspeed calibrations must be taken into account and the two envelopes overlapped to determine where AAR can be attempted. A diagram showing the AAR capability of two tanker types is given in Figure 2. It can be seen that there is a significant difference in the minimum speeds of the two types which must be taken into account when planning mutual AAR trials. (It has been the practice to regard the minimum speed for the combination as being that where at least 1.2 'G' can be achieved by either aircraft without encountering buffet or other pre-stall symptoms. This gives a reasonable manoeuvre capability and allows turns with up to 30° bank to be undertaken). Also shown in Figure 2 is the maximum permitted speed for a turbo prop transport which is required to receive from both the above tankers. The refuelling envelope available is much larger from Tanker A than from Tanker B.

ii Are the refuelling drills satisfactory and can the C of G limits be respected readily?

iii Does the receiver fuel system allow contact to be made without any fuel flowing if the pilot wishes to practice only training contacts?

iv What is the maximum engine power rating to be used in the AAR role? How will the crew ensure that the limits are respected? Are the engines surge prone?

v Is the aircraft suitable for flying in close formation? For instance can the pilot (or copilot) fly the aircraft, manipulate the throttles/airbrakes and trim the aircraft satisfactorily? If not, how will the duties be split?

vi Are the pitot/static sources likely to be affected by the drogue wake?

vii Are there any devices that need to be inhibited in case they should operate incorrectly in the disturbed airflow behind the drogue eg angle of attack sensors that might trigger a stick pusher?

viii If the aircraft is fitted with autostabilisers or a flight control system what facilities should be selected for the AAR role? What levels of degraded operation and failure states should be investigated?

ix Are there any items mounted on the fuselage, adjacent to the probe, that might be susceptible to damage by the drogue and which, if damaged could cause a hazard eg an antenna that could be ingested by an engine?

8 Normally the objective of the flight trials programme will be to clear as wide an AAR envelope for the tanker and receiver combination as is possible. This will require exploration of the maximum speeds and maximum altitudes (for which both aircraft will probably have to be at lightweight), maximum airspeed and Mach no, the effect of operating both aircraft at up to maximum weight and any handling changes caused by operating the receiver at the extremes of C of G position. It is also likely that night AAR will need to be demonstrated. For receiver aircraft that can carry external stores the most adverse configuration should be demonstrated. For all initial contacts between a tanker and new receiver type a chase aircraft should be available so that a video record can be obtained in case any unexpected behaviour warrants subsequent analysis.

9 The flight programme will commence with an initial exploration of the receiver behaviour when flying in representative positions behind the tanker with the tanker hose wound in. This will be done at moderate speed, altitude and weight, where the receiver will have plenty of power and manoeuvre capability in hand. In addition to exploring the positions likely to be encountered during a good approach and contact, the receiver pilot will also ensure that the handling remains acceptable when displaced from the correct position. The tanker will then extend the hose and, the receiver will make the first contacts with the drogue. At one speed and altitude a typical test programme would be as follows;

a Make contact with the drogue, move into the optimum refuelling position and assess the flying qualities of the receiver for several minutes. Performance measurements can be made.

b Displace the receiver from the optimum position (with the hose still attached). Explore the handling within a 'cone' of about 15° around the optimum position, if this is possible.

c Move closer to the tanker and make an assessment at the closest position that is likely to be encountered.

d In the optimum refuelling position follow the tanker into and out of left and right turns at bank angles of up to 30° if possible.

e Follow the tanker into a descent at a rate of up to about 500 ft/min. (This simulates a manoeuvre that may be necessary if a receiver becomes power limited during a large fuel transfer; a descent or 'toboggan' may be the only way to remain in contact).

f Break contact in the normal way by gently backing off from the tanker until, at full extension, the hose disconnects.

programme will then be concerned with extending the AAR envelope. The rate of progress depends on the difficulties encountered and the flexibility available for varying the loadings of the tanker and receiver aircraft. Usually 3 to 4 receiver sorties are necessary to complete the programme and explore the flight envelope fully. On occasions it has been possible to test several receivers during the course of one tanker sortie. This is economical but requires subtle arrangement of the programme to achieve all the objectives.

11 A&AEE philosophy on testing failure cases has been to assess whether or not refuelling can be achieved when either the tanker or receiver has sustained a failure prior to making contact. To date this has consisted of examining refuelling with one engine shut down on multi engine aircraft and assessing the effects of a simulated autostabiliser failure. The object has been to give advice to the Service so that a pilot who has sustained such a failure can make a judgement as to whether or not refuelling should be attempted. The transport aircraft now being introduced into Service have high levels of system redundancy, and are capable of being despatched with a variety of passive failures present. It is worth debating whether the extent of AAR testing should be extended to cover some of these cases. The consequences of a failure occurring while in contact with the tanker have not been tested in flight. Any system failure in the tanker or receiver that causes a transient excursion of the flight path is obviously a hazard to aircraft in close formation. The risk can be minimised by conscientious monitoring of the flying controls by the tanker crew (as the tanker is normally flown with the autopilot engaged). The presence of the weak link in the probe tip should also ensure hose separation from the receiver if either aircraft suffers a disturbance that results in the hose becoming seriously mis-aligned with the probe.

12 AAR is essentially similar to flying in formation, but the receiver pilot must fly his aircraft in a position, relative to the tanker, that is dictated by the hose trailing characteristics. If this puts the receiver in unsteady airflow the pilot has to compensate as best he can. When conducting an AAR handling assessment the criteria of acceptable or unacceptable behaviour, is at present, almost exclusively the qualitative judgement of the assessing pilots. The test engineer can produce quantification of the relevant parameters but, often, they serve only to explain why a pilot should find the handling 'easy' or 'difficult'. It is hoped that, from the wide range of experience that has been gained recently, it might be possible to determine numerical criteria that relate to pilot opinion and which might be applicable to future trials. The A&AEE trials have shown that all the aircraft types tested have the potential to be AAR receivers from the various tankers. While problems have been experienced by some aircraft at various points in the flight envelope none has proven universally unacceptable on handling or performance grounds. Some specific items of interest are given in the following paragraphs.

13 AIRFRAME BUFFET Airframe buffet is nearly always present to a greater or lesser extent. Usually, from a handling point of view, it has not been judged limiting. When tests were made in a Hercules behind the Tristar and KC 10 the buffet experienced on the centreline station was much reduced when the tanker's centre engine was throttled back but, in contrast, the buffet experienced in a Hercules behind the VC 10 K2 was not reduced by throttling the two inboard engines of the tanker. On the centreline refuelling station buffet levels can nearly always be reduced by flying lower but this may involve a risk of probe breakage. This is one reason why a high mounted probe is beneficial compared to a low mounted one; the receiver aircraft can be lower relative to the tanker wake. On some receiver types the noise level in the cockpit increased markedly at higher airspeed, presumably because of the wake from the drogue interacting with the airflow around the nose of the aircraft.

14 ENGINE HANDLING AAR can demand large engine power variations to make and then maintain contact with the tanker. For a transport aircraft this can represent a very different pattern of power usage from that envisaged during initial certification. Also it is necessary for the pilot, not the engineer, to manipulate the throttles. Figure 3 shows the parameters recorded on on engine of a VC 10 K2 while operating as a receiver. These were chosen as being fairly representative of the power excursions that may be used during AAR on a large receiver aircraft while maintaining station in the refuelling position. In general, from handling considerations, the engines of receiver aircraft appear not to be affected by the disturbed airflow environment. An exception to this occurred during trials with the VC 10 K2 as a receiver from the Victor K2 tanker. Engine 'pop' surges were experienced on several occasions, even when power demand was steady. No obvious pattern of circumstances in which these surges occurred could be detected and the results are still being investigated. When the same VC 10 K2 was flown as a receiver from another VC 10 K2 tanker no surging was experienced during the entire programme. When the VC 10 K2 was operated as a receiver at high altitude it was found almost impossible to respect the low pressure compressor speed limits. Whereas in the transport role, engine power changes at altitude tended

altitude and speed. The pilot was then free to manipulate the throttles up to the limit imposed by the new stops without the risk of exceeding the maximum compressor speed.

15 A problem experienced on some fast jet aircraft is the need to use reheat to obtain a high altitude refuelling capability. On the Phantom it was found necessary to run one engine in reheat and then modulate the thrust on the other engine which was operating in the dry power range. This was the only practicable way to circumvent the step change of thrust produced by going from maximum 'dry' power to the minimum reheat setting. In other circumstances relatively low power settings may be needed and this can introduce different problems. When the Buccaneer attempted to refuel from a Hercules tanker at low altitude both engines were operating at reduced power settings where the engine response was unacceptably slow. It was found necessary to extend the airbrakes partially, to increase the drag so that the engines were operating at a higher power setting with faster response characteristics.

16 LATERAL CONTROL POWER When a receiver approaches a wing refuelling station it usually experiences a rolling moment towards the tanker fuselage. On most fast jet aircraft this can be trimmed out without use of excessive roll control. During trials to explore the likely capability of aircraft to refuel from the strategic tanker, a Hercules made an approach to a Tristar starboard wing station (no refuelling equipment was fitted but the wing was marked to indicate where a refuelling pod might be fitted). As the receiver approached the refuelling position it was necessary to apply progressively more right aileron and rudder. Eventually, at a point still behind the tanker and well short of the drogue position that would be achieved with existing pod equipments, full aileron travel was required to hold the wings level. The investigation was terminated and it was concluded that, all other considerations aside, the handling characteristics of the Hercules were not acceptable for wing station refuelling. This test was repeated at higher speeds with two large turbojet receivers; in both cases large amounts of aileron and rudder deflection were necessary to hold a simulated refuelling position, and it was not thought that wing station clearances would be practicable.

17 LATERAL AND DIRECTIONAL BEHAVIOUR With several large receiver aircraft there has been a tendency for yaw oscillations to occur when approaching the drogue. Normally it has been possible to counteract this by use of rudder and the characteristic has not proved to be a serious handling problem. However during early trials with 'Nimrod' variants behind the Victor K2 the handling was judged to be unacceptable because an undamped yawing oscillation developed with a period of about 8 seconds. It was found necessary to alter the behaviour by modifying the yaw damper demand produced by aileron movement. This modification, together with an effective increase of fin area (necessary to compensate for the de-stabilising effect of the probe) produced acceptable handling characteristics for AAR.

18 ASYMMETRIC BEHAVIOUR To date there have been no significant handling problems due to asymmetric thrust when attempting to refuel a multi engine receiver with one engine shut down. However the loss of thrust has resulted in a marked reduction of the available AAR envelope. On some fast jet aircraft it was found necessary to use reheat on the remaining engine to overcome the performance deficiency and this has introduced problems in formating with the tanker. When refuelling a Phantom from a Hercules tanker at low airspeed, the single engine had to be in full reheat. Thrust was thus held constant and the drag modulated by airbrake operation to maintain station.

19 LONGITUDINAL CHARACTERISTICS Marked changes of trim, in pitch, are a feature of all receiver aircraft when moving from the astern position through to the refuel position. Unless a column or yoke mounted electric trim switch is incorporated, then difficulty in retrimming can be experienced. This has been a deficiency of some transport aircraft being used in the AAR role, where high out of trim forces can be experienced and the pilot has to contain these single handed while retrimming with the other hand. Another handling problem that has been experienced by some large receiver aircraft has been a tendency to enter a short period pitch oscillation when making contact or when in the refuelling position. Both the VC 10 and Victor have exhibited this tendency. During recent trials a VC 10 K2 was found to be prone to such pitch oscillations when acting as a receiver from another VC 10 K2 tanker. However despite this, the overall handling characteristics were judged to be satisfactory by the pilots when refuelling at speeds up to the maximum at which the tanker was permitted to fly. When the same aircraft was flown as a receiver, but with a Victor K2 acting as tanker the pitching oscillation was more pronounced. Handling became difficult at

behind the Victor. The data was recorded from a fuselage mounted vane and serve to show the increased unsteadiness of the flow at that position.

b The increased amplitude of the normal acceleration excursions recorded when flying behind the Victor which was associated with larger elevator movements; these also required greater control forces to be exerted by the pilot.

c The marked differences in elevator and tailplane angle required to trim the aircraft under similar airspeed, height and loading conditions. This was probably due to the higher span loading of the VC 10 tanker causing a more intense downwash field than behind the Victor.

Figure 5 shows a comparison of the short period longitudinal characteristics of the VC 10 K2 when refuelling behind a Victor K2 at 250 kn and 310 kn IAS. At the lower speed the handling was judged to be relatively easy whereas at 310 kn, as indicated previously, it was markedly more difficult. Even at the lower speed the oscillatory nature of the normal acceleration record is apparent, but the period is appreciably longer (3.8 seconds) than at the higher speed (2.3 seconds). Also, at the lower speed, the incidence vane fluctuations are smaller.

20 At present the criteria for acceptable longitudinal handling characteristics of a receiver aircraft behind a tanker are not well understood. It seems that if a large receiver is prone to develop a short period pitching oscillation, then as the airspeed increases the period of the oscillation gets shorter. A study of the record of normal acceleration, measured at the C of G, indicates that it might be possible to develop pilot opinion plots based on the frequency of the oscillation and the amplitude of the normal acceleration excursions. These possibilities are still being examined. It is interesting to speculate on how the receiver might be made less susceptible to the short period oscillation. The introduction of a pitch auto- stabiliser might be a solution. On large aircraft that have been converted from other roles, it is possible that the high values of stick force/g lead to an unnecessarily high piloting workload when attempting AAR; the pilot might be better able to control the aircraft if the elevator forces could be made significantly smaller. There is certainly some incentive to try and improve the handling in this respect in order to give the maximum possible AAR speeds and, perhaps more importantly, to reduce the 'g' excursions and the associated fatigue damage that may be sustained by the receiver aircraft. Oscillatory behaviour in pitch is not confined to large aircraft. Several fast jets exhibit a similar tendency when refuelling from both the centreline and wing stations.

21 PERFORMANCE Operation as an AAR receiver may require a considerable increase in power to make contact with the drogue and then to maintain the refuelling position. This can reduce the available AAR envelope significantly, particularly when a large performance disparity exists already, ie a turboprop receiver and turbojet tanker. It is postulated that the drag increase occurs due to:

a The receiver flying in the tanker downwash field. This can be equated to the extra power needed to maintain level flight when in the presence of a down draft;

b An increase in induced drag caused by the receiver's spanwise loading distribution being changed because of operating in the tanker wake; and

c A proportion of the drag of the drogue being borne by the receiver. (For the high speed drogue at 300 kn EAS this can amount to 1,100 lbf).

22 It was found possible to express the Hercules performance as a receiver in the form of a graph of apparent drag coefficient (C_D) plotted against C_L^2. (The term 'apparent C_D' has been coined because it can be argued that the drag coefficient of the receiver, as defined in the conventional way, cannot have altered because it is flying in the wake of another aircraft). This is shown in Figure 6 for the Hercules receiver behind a Hercules tanker and in Figure 7 for the Hercules receiver behind a widebody tanker. The Hercules performance in free air is shown for comparison. Behind both tanker types the increase in apparent drag coefficient indicates the very significant power increases needed to act as a receiver. This is particularly noticeable behind the widebody tanker where the drag was effectively doubled when in the normal refuelling position, even without drogue drag being considered. (These data were acquired during feasibility testing of the widebody aircraft, and representative refuelling equipment was not fitted). Figure 7 also shows the reduction in drag that could be obtained by flying some 10 to 15 feet lower than the estimated normal refuelling position. It is interesting to compare the Hercules performance as a receiver behind various tankers with which it has been tested. The results are shown in Figure 8. The two wide bodied aircraft tested as potential

while Figure 6 clearly shows the much higher apparent drag coefficient when the receiver was flown behind a widebody (span loading 2100 to 2600 lbf/ft) compared to behind a Hercules tanker (span loading 750 to 1300 lbf/ft) it is apparent that the Vulcan tanker still produced a higher apparent drag coefficient in the receiver than did the Victor tanker despite the similarity in span loading (1100 to 1600 lbf/ft). It is assumed that, in the former case, the tanker wake caused a more adverse lift distribution across the receiver wing producing a greater induced drag factor. The variations in weight of a given tanker type have not produced consistent measurable changes in the apparent drag coefficient of the receiver. It might be expected that a light tanker would produce a smaller downwash velocity, at a given speed, than when it was heavy, and that this would show up as reduction in the apparent drag coefficient of the receiver. No such effect could be measured except possibly at very high C_L values (see Figure 6).

23 It has been found that, if a receiver has insufficient performance to make or maintain contact with the tanker, it may be possible to compensate for the thrust deficiency by performing AAR in a descent. This is known as 'tobogganing'. A&AEE has made and maintained contact during descents of rates of up to 1000 ft/min without difficulty. The performance benefits have to be weighed against the operational disadvantages of having to descend from the selected flight level and the risk of cloud and turbulence being encountered in the descent. However, for certain tanker/receiver combinations the 'toboggan' is the only practicable way of achieving a refuelling.

24 RECEIVER CLEARANCES BY 'READ ACROSS' With the proliferation of tankers and receivers it might be asked if it is strictly necessary to re-test each receiver behind a new tanker, if it already has a clearance from another tanker type. 'Read across' clearances have already been given to a limited extent, because on certain fast jet receivers the trials were made on one mark of aircraft and the results read across to other marks. It is proposed to extend this philosophy for the clearances of certain fast jet aircraft behind the VC 10 K3 tanker which is due into Service later this year. The VC 10 K3 is a 'stretched' version of the K2, with a slightly different wing planform and engine alignment. It is intended to test only three fast jet aircraft, including the type whose handling was found to be most critical with the K2 tanker. If the results on these three show similarity of behaviour behind the two tankers then it is likely that 'read across' clearances will be recommended for other fast jets to refuel from the K3. At present there appear to be detailed reasons why each of the large receivers will have to be re-tested behind the K3, but it is hoped that the extent of the test programme for each type can be considerably reduced.

25 When an aircraft is converted to the AAR receiver role a number of structural and 'lifeing' issues should be considered particularly so in the case of large aircraft. For instance;

a Does the general level of buffeting felt in the aircraft imply a reduction in fatigue life of components, particularly in the tail area?

b Does the oscillatory pitching motion exemplified in Figures 4 and 5 lead to excessive fatigue consumption?

c Could changes in spanwise lift distribution, from that associated with flying in clear air, lead to accelerated wing fatigue?

d The pattern of engine power usage may be very different from that used in the original role of the aircraft. Frequent variations in engine power will occur when the engine is already running at a high average power setting as the pilot tries to hold station with the tanker. Figure 3 shows the pattern of engine power demanded during a typical refuelling manoeuvre. Mention of engine surges has already been made, but even if the obvious engine distress associated with an audible surge is not apparent, can the sort of incidence fluctuations shown in Figures 4 and 5 induce high compressor stress?

One thing is certain; most of the aircraft now used in the receiver role are likely to continue in Service for many years and specialist attention should be addressed to the long term airworthiness issues mentioned above.

of flying an operational aircraft for th type of training, the fatigue damage incurred may be considerable. With the RAF's commitment to AAR for a major part of its fixed wing fleet it might prove economical to introduce AAR into the training syllabus at an earlier stage. For instance a modification to fit dummy probes (ie not plumbed into the fuel system) on to some of the Hawk fleet would allow training contacts to be made and the basic competence in the manoeuvre to be acquired. The cost of conversion and continuation training on some of the operational aircraft might then be reduced significantly by using a moving base simulator, able to reproduce realistic handling characteristics, motion and visual cues. Despite the high initial cost of such a facility the overall saving throughout the service life of the tanker fleet might be considerable.

	MK 17 HOSE DRUM UNIT (H.D.U.)	MK 20 POD	MK 32 POD
MAXIMUM FLOW RATE	4400 lb/min	2000 lb/min	3000 lb/min
HOSE BORE	3"	1½"	2"
HOSE LENGTH EXTENDED	81'	50'	54'

FIG 1

CHARACTERISTICS OF FUEL DISPENSING EQUIPMENTS.

RECEIVING / TANKING CAPABILITY AT 90% MAX. A.U.W. FOR :-

TANKER A ———

TANKER B - - - - -

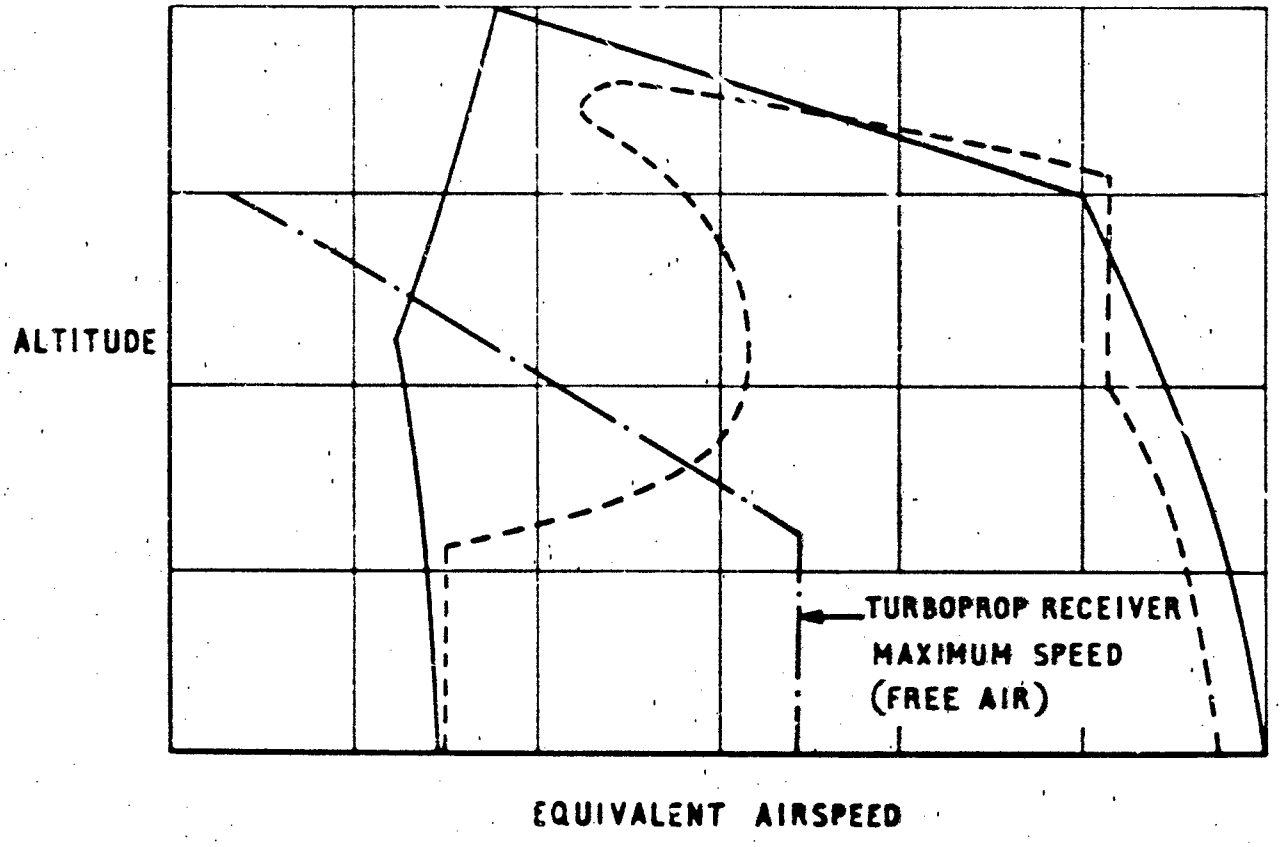

FIG. 2

FLIGHT ENVELOPE COMPATIBILITY FOR A.A.R.

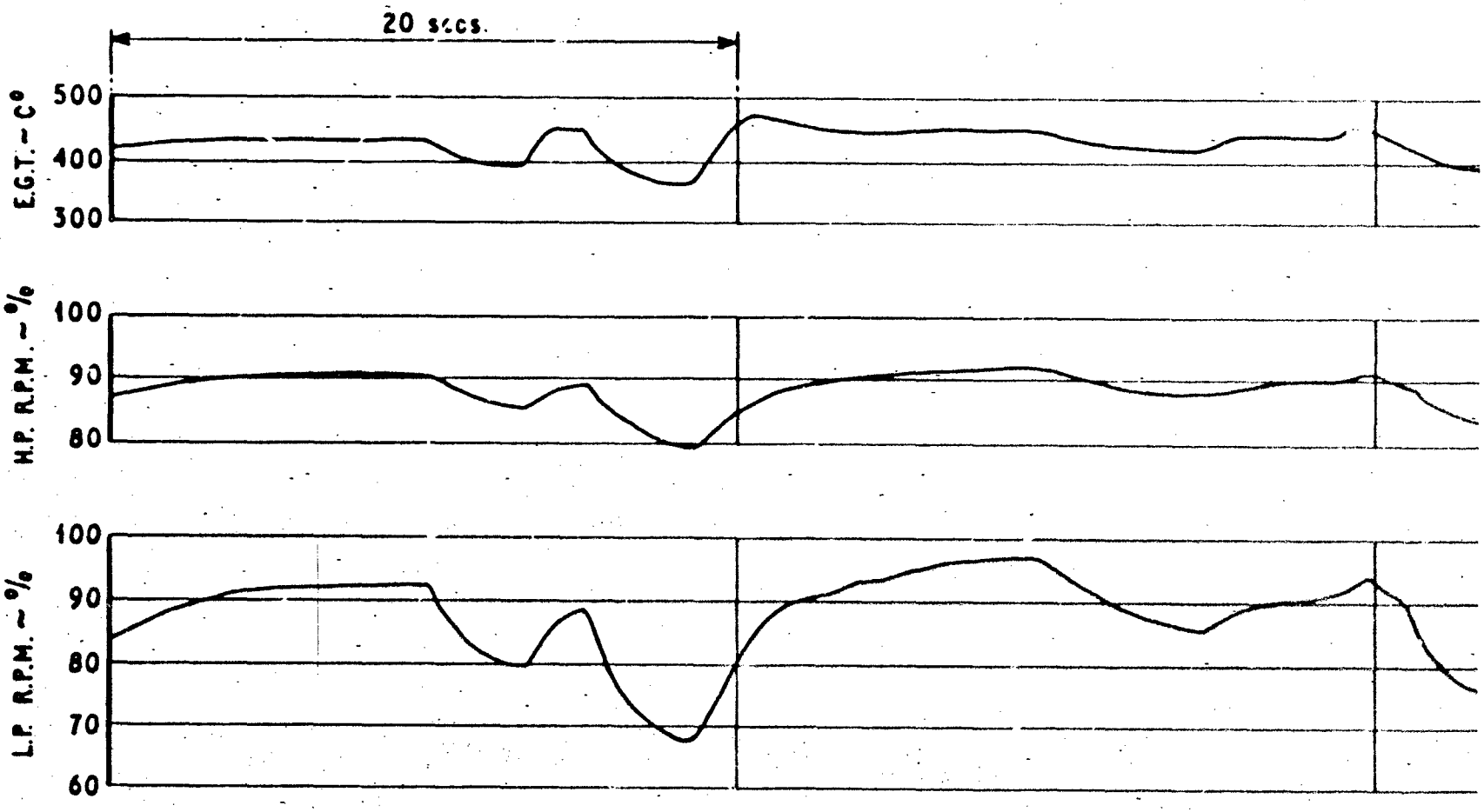

FIG. 3

ENGINE POWER VARIATION DURING A.A.R. VC 10 K2 ~ 35.000 ft. 245 kn I.A.S.

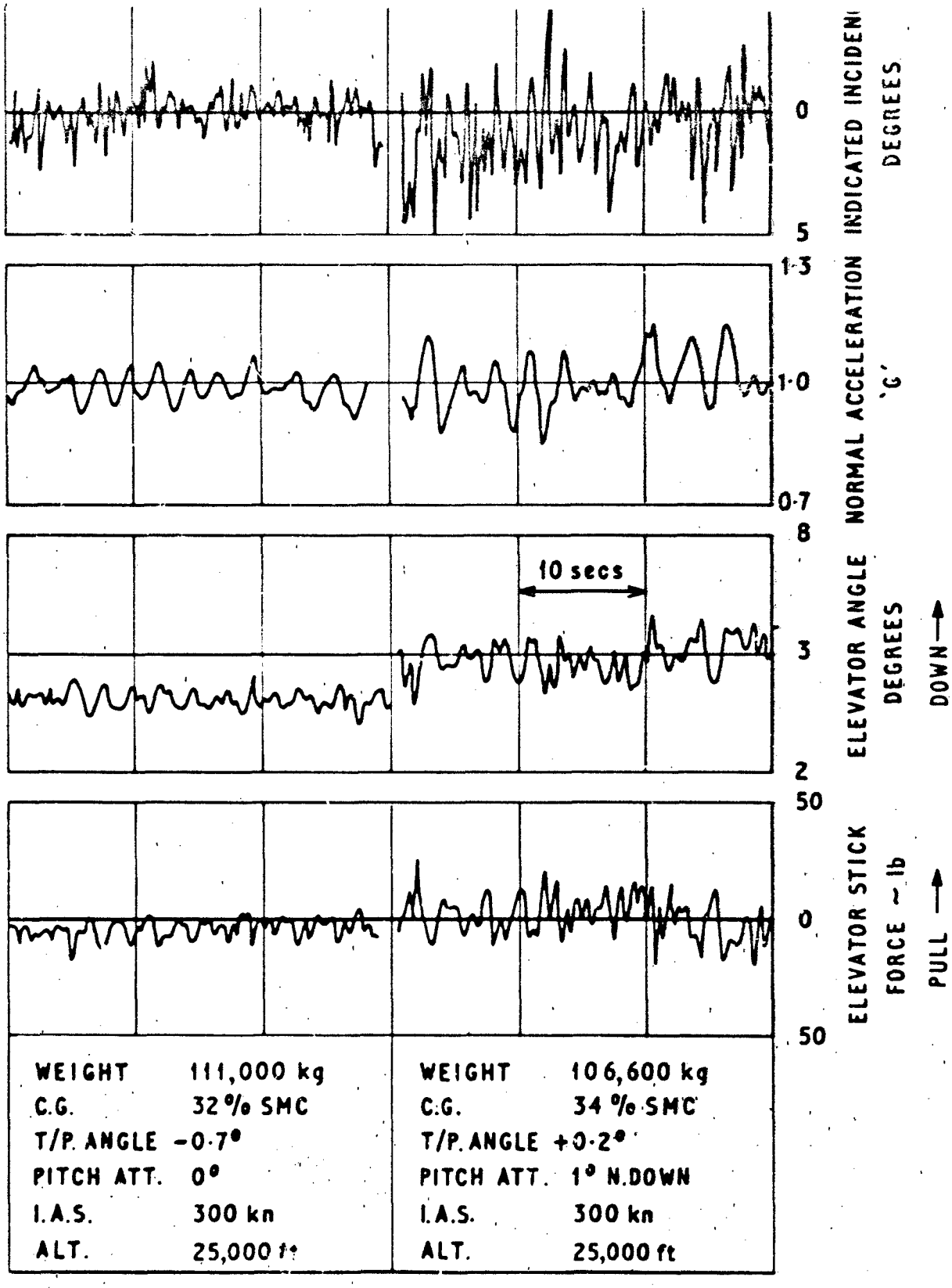

FIG. 4

COMPARATIVE TIME HISTORIES OF VC 10 K2 REFUELLING BEHIND TWO TYPES OF TANKER UNDER SIMILAR FLIGHT CONDITIONS.

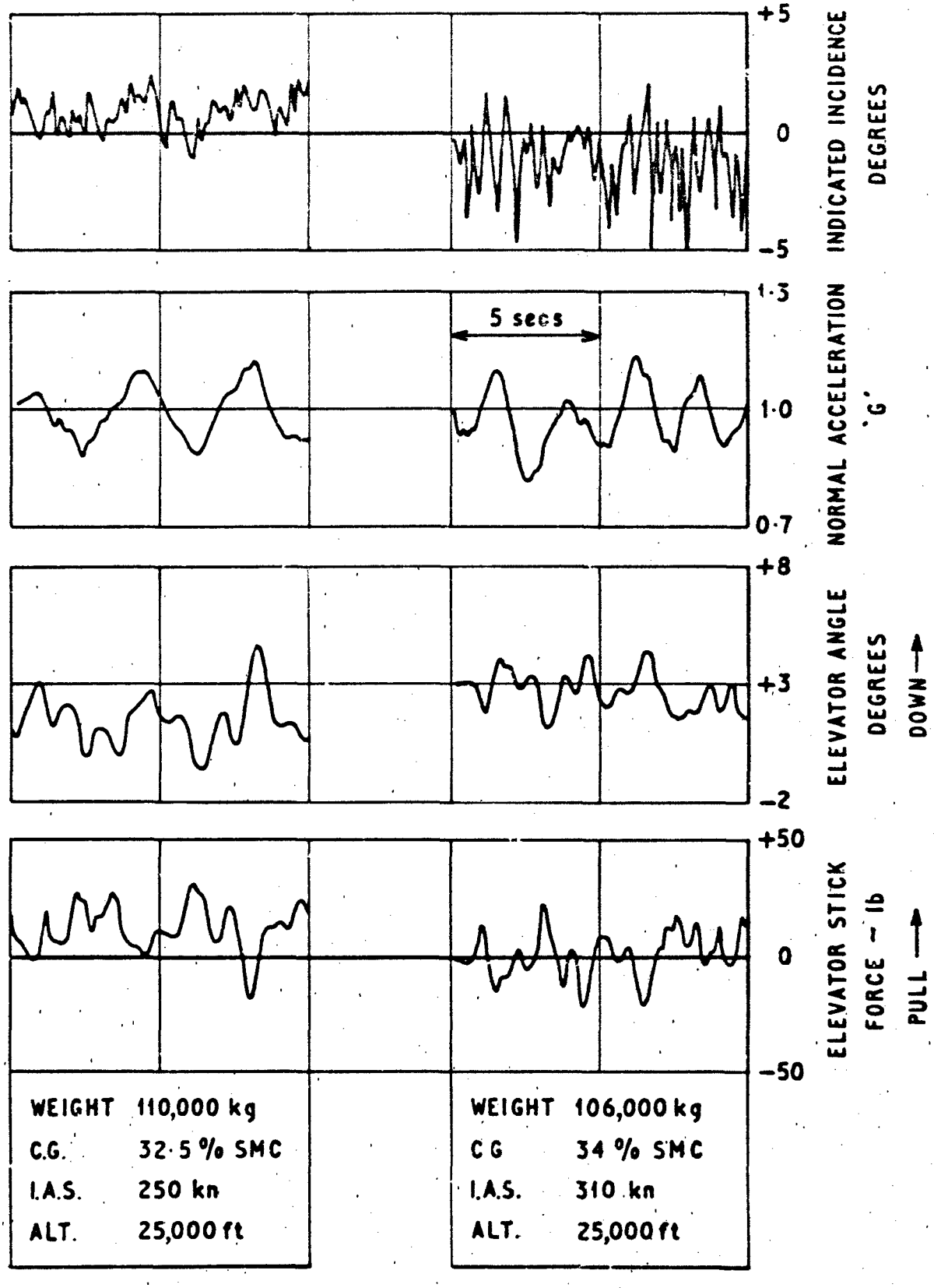

COMPARATIVE TIME HISTORIES OF VC 10 K2 REFUELLING FROM A VICTOR K2 AT DIFFERENT SPEEDS.

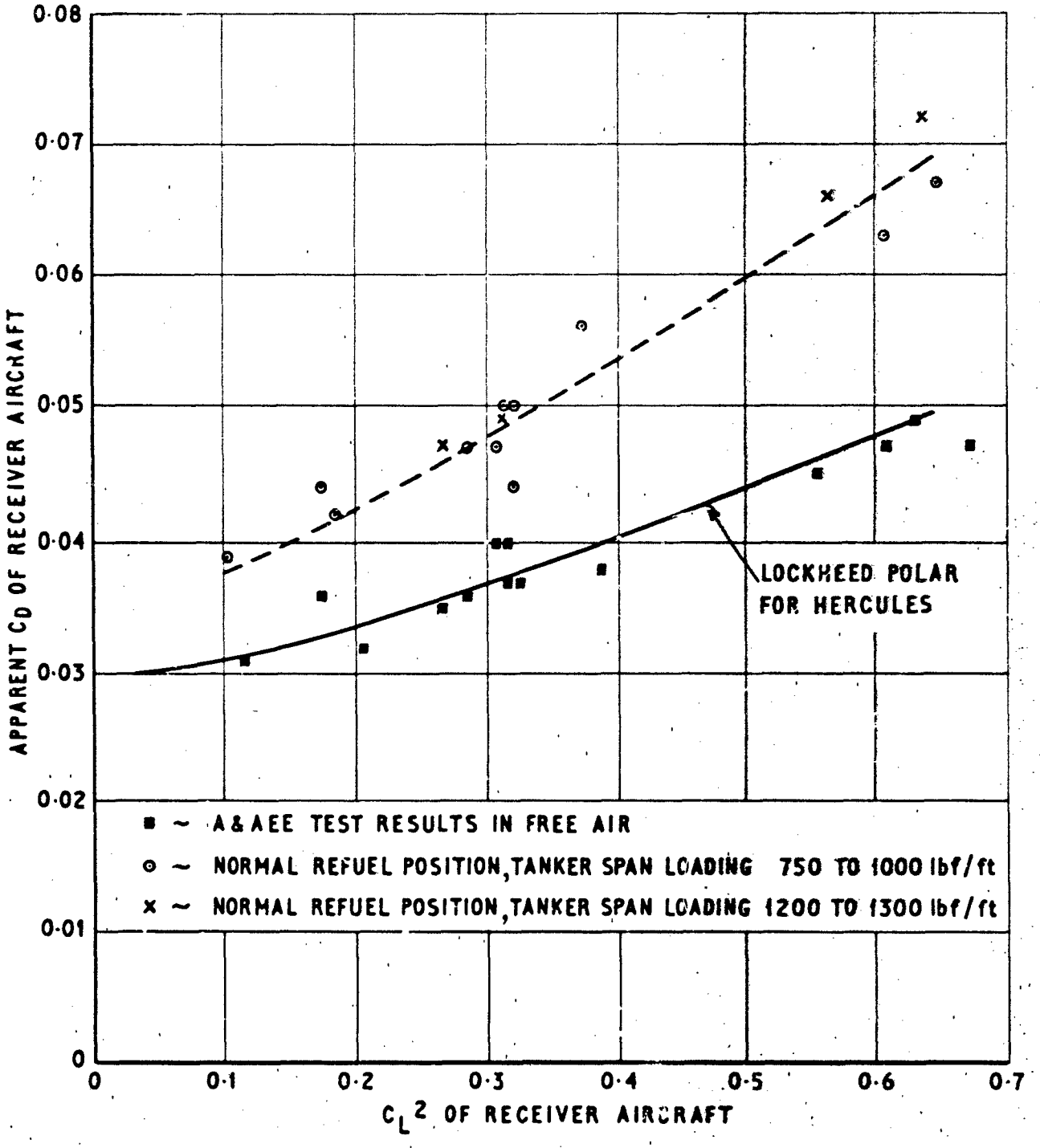

HERCULES C MK 1 ~ PERFORMANCE AS A RECEIVER AIRCRAFT BEHIND A HERCULES C MK 1 TANKER AND IN FREE AIR.

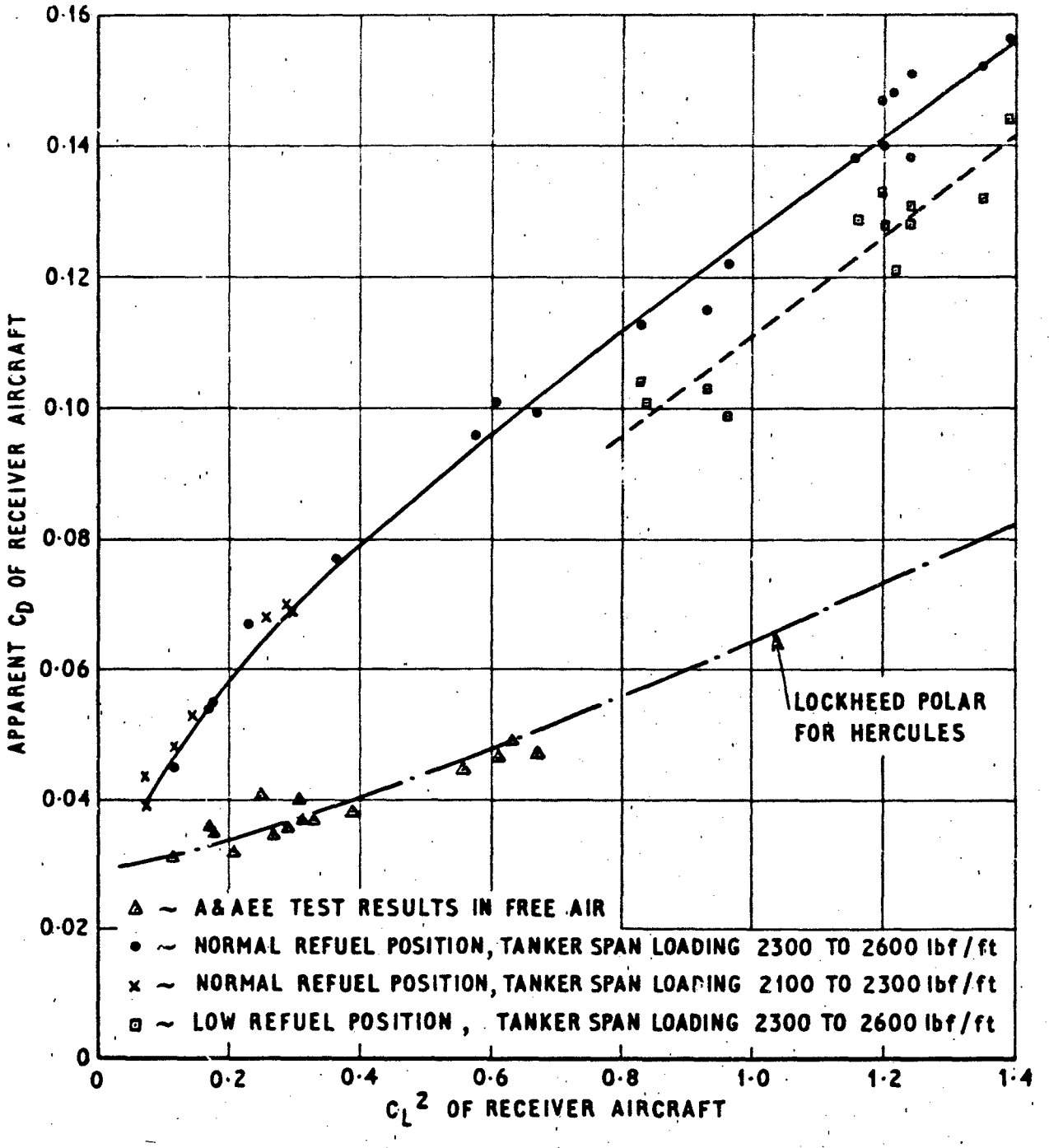

HERCULES C MK 1 ~ PERFORMANCE AS A SIMULATED RECEIVER AIRCRAFT BEHIND A WIDEBODY TANKER AND IN FREE AIR.

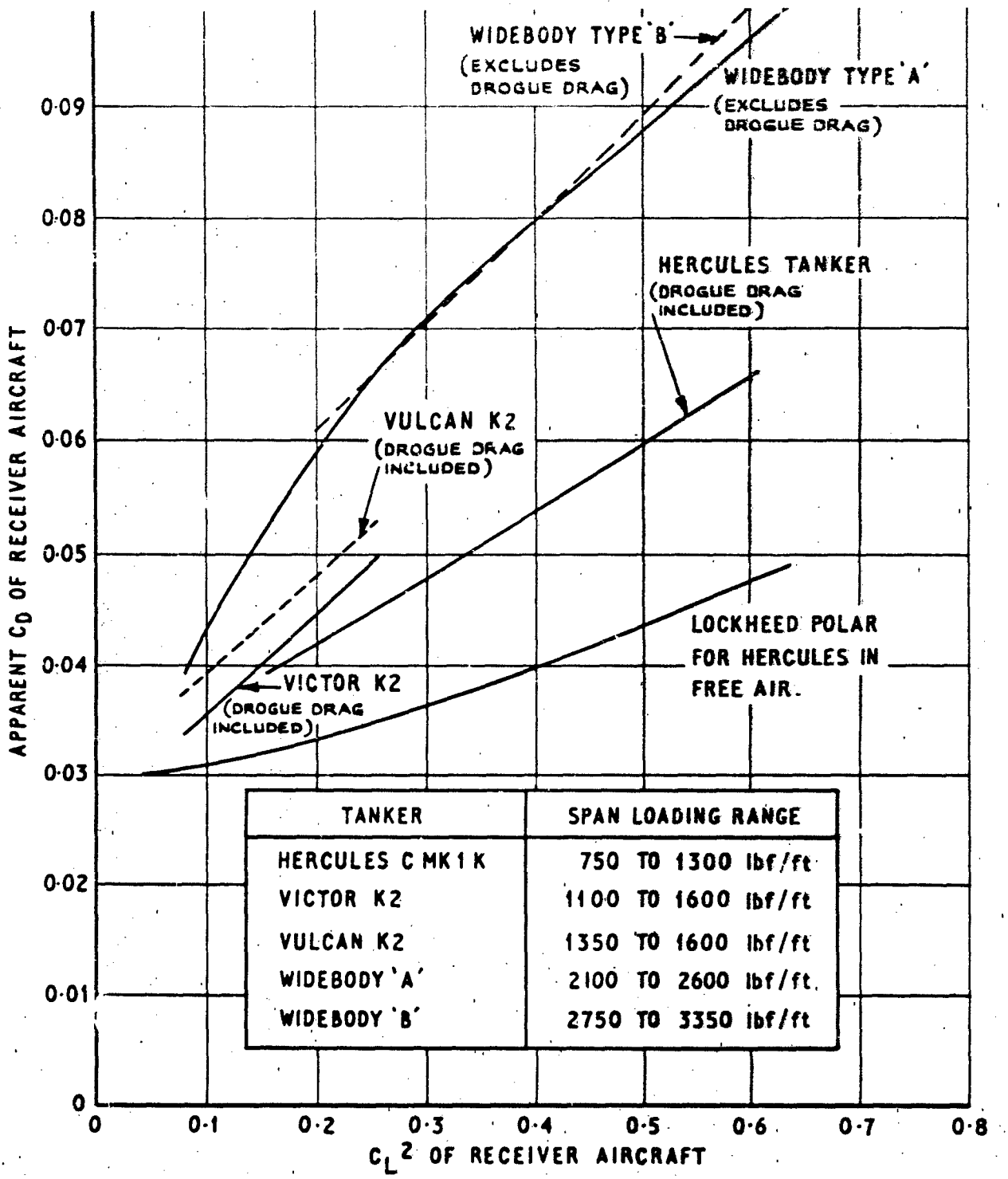

TANKER	SPAN LOADING RANGE
HERCULES C MK 1 K	750 TO 1300 lbf/ft
VICTOR K2	1100 TO 1600 lbf/ft
VULCAN K2	1350 TO 1600 lbf/ft
WIDEBODY 'A'	2100 TO 2600 lbf/ft.
WIDEBODY 'B'	2750 TO 3350 lbf/ft

HERCULES C MK 1 ~ PERFORMANCE AS AN A.A.R. RECEIVER WITH VARIOUS TANKERS ~ NORMAL REFUELLING POSITION.

R. F. Stokes and J. C. Smith
Royal Aircraft Establishment
Farnborough
Hampshire
GU14 6TD
United Kingdom

SUMMARY

Aircraft dead-reckoning navigation systems present particular problems in their assessment, and diagnosis in development where a continuous measurement of their error pattern is required. The inherent accuracy of modern inertial and Doppler equipment is such that there are few direct methods of measuring the system errors to the required precision.

The need for long range, long duration flights over both land and sea with a continuous high accuracy reference has led to the development by RAE of an integrated navigation system in which the outputs of a number of inertial navigation systems are recorded in parallel with those of Doppler radar, DME, Decca, Loran C and Omega. The recorded data is processed post-flight in a Kalman filter which is used to estimate the inertial system errors. The final reference is formed by compensating the inertial outputs for these errors and has the properties of high accuracy, low noise, and continuous availability.

Although simple in concept, the implementation of such a scheme is complex. The major problem lies in constructing suitable mathematical models of the various equipments, and the technique of pre-processing is described. The second difficult area is that of obtaining the statistical information regarding the performance of the equipments in a form suitable for inclusion in the models.

Although the reference is produced off-line the techniques can be implemented on-line.

1 INTRODUCTION

1.1 History

Work on reference systems for evaluating navigation equipment for aircraft started at RAE Farnborough at least as early as the mid-1950s. At that time the Inertial Navigator (IN) for a guided bomb was being developed and the navigation of the aircraft to the target used a combination of the weapon IN, Doppler radar and position fixing. An output of the navigation process was a calibration of the weapon IN.

Development of this sytem included flight trials in RAE and A&AEE aircraft using the Decca Navigator chains in Southern England for position reference. The same method was used in the development of the IN intended for the TSR2 which took place in 1960/63. On these trials an early airborne digital computer on board the trials aircraft enabled Decca, Doppler and the IN information to be recorded and processed in flight in a form suitable for post flight analysis using a ground digital computer. This technique formed the basis for producing the reference navigation system which has been used for all our subsequent trials. The production of a position, velocity and attitude reference system for trials of inertial and other navigation systems has formed a major objective for RAE work on integrated navigation since that time.

Through the late 1960s and the 1970s UK IN systems for Harrier, Phantom, Tornado and Jaguar were developed, with RAE playing a major role in the trials of development systems, diagnosis of error sources and the accuracy assessment for operational use. As time progressed the equipments grew more and more accurate and it became increasingly difficult to provide reference data of greater accuracy than the systems under test. This has led to more and more sophisticated techniques being used, and the addition of other navigation aids, such as DME, Loran and Omega, into the mix.

The most stringent accuracy requirements came with the development of IN systems for maritime patrol aircraft in the late 1970s. Here it was necessary to know the position of the trials aircraft to a few tens of yards, at any time in a sortie of several hours duration, and at any place - including low level, over the sea, several hundred miles from the coast. This was needed in order to investigate the subtle effects of flight manoeuvres on the accuracy of the IN systems under operational conditions.

1.2 Early developments of the reference system

As mentioned above, the early trials of IN used the Decca Navigator as a position reference. When the systems under development had accuracies of five to ten miles per

twice per minute along with the readings of the Deccometers. After flight the Decca readings were processed to give the Decca version of aircraft position, also in latitude and longitude, and the two versions compared.

A plot of latitude and longitude differences as a function of latitude and longitude enabled the main errors in the Doppler system to be determined, viz the heading error, bias and drift error, and scale factor error. The effects of these errors could then be calculated for each recorded time, and the Doppler position corrected. The resulting position had low noise (due to the integration process used on Doppler velocity information) and the long term accuracy of the Decca.

This technique proved adequate when flight trials could be based on simple profiles, mostly straight legs along the Decca bisectors. However in 1964 a new generation of IN arrived. The accuracy of these systems approached one nautical mile per hour, and the intended operation meant that flights of longer duration and range had to be flown. Decca was no longer suitable as the sole position level data source as the aircraft had to be operated in regions outside the Decca cover. For operational reasons the optimum trials route was from Boscombe Down via Shannon to Argentia in Newfoundland. Loran C was used as the position reference over the North Atlantic with Decca at each end of the route. The IN itself provided the most accurate heading information, so this was used for the Doppler/heading based position calculations.

Data processing was done in stages. In flight the Doppler/heading system gave one version of position, the Decca and/or Loran C a second version, and the IN itself a third version. All the data was recorded twice per minute on punched paper tape. Post flight this was processed to provide plots of the differences in latitude and longitude between the various systems as functions of time, and these plots were smoothed by curve fitting using a least squares method.

The IN error plot was often used to correct the position data obtained from Doppler and the radio aids. For example it was found that Loran C had a systematic error which was a function of position and grew to significant levels near Newfoundland. This was detected by the IN error plot having a form unlike typical IN errors, and being consistent from flight to flight. This form of error could be allowed for and was incorporated into the analysis on subsequent stages of data processing to produce the aircraft datum position.

1.3 The modern system

In the 1970s IN equipment had developed to the stage where current datum methods were no longer accurate enough. The only radio aid with sufficient accuracy for our purposes was DME, used in a range/range mode. However DME is a relatively short range aid and it was necessary to modify trials routes to give sufficient cover. One or two exercises were carried out in the USA in order to obtain sufficiently long flight paths for trials purposes. At this time the aircraft were fitted with commercial IN which were incorporated into the datum system, and enabled a reference to be obtained during the periods of flight when radio data was not available. This was done by mathematically modelling the IN errors and correcting for them using the information from the periods when external data was available.

As may be appreciated the process of obtaining reference positions for any particular flight was long winded and very labour intensive, since vast amounts of computation was needed, with human interpretation of the results at most stages. In order to automate the process Kalman filter techniques were developed. This involved designing accurate mathematical models of all the navigation systems employed in the reference system, and devising means whereby faulty data could be eliminated before the results were applied to the filter.

These techniques have been developed over the past five years or so and have found application in the most recent work, that associated with the development and assessment of an IN system for maritime patrol aircraft applications.

2 KALMAN FILTERING

The term Kalman filtering is used somewhat loosely in this paper and is intended to cover techniques descended from the original work by Kalman rather than a direct implementation of his original ideas.

2.1 Advantages of Kalman filtering

The Kalman filter algorithms are very suitable for any application where data has to be processed and results provided in real time, because the incoming data is used sequentially and then discarded. The results present in the Kalman filter at any time reflect the nett total of all information received to date. Thus the 'best' answer is continuously available and there is no requirement for the storage of input data from earlier times.

heading.

A further consequence of the form of the Kalman filter algorithm is that data from various sensors can be accepted intermittently and yet still be used in an optimal way. For example, the Doppler ground speed data could be used asynchronously from the drift angle values, and the DME fixes taken at yet other times.

The data from individual sensors are, to a large extent, processed independently of each other, and so it is relatively easy to change the manner in which the inputs from one sensor are treated without affecting the processing of data from other sensors.

As with all good things there is a price to be paid, and in the Kalman filter this is manifest in the requirement for a detailed knowledge of the characteristics of the individual sensors.

2.2 Assumptions

The basic principles of the Kalman filter are based on a number of assumptions:

(1) The process to be modelled in the Kalman filter can be adequately represented by the values of a set of coefficients.

(2) The values of the coefficients at a future time can be predicted from their values at an earlier time and a knowledge of the dynamics of the process. These dynamics have to be reduced to a set of linear differential equations.

(3) The statistical properties of these coefficients are known.

(4) It is possible to measure the value of some combination of the coefficients.

(5) The uncertainty of the measurement quantities are known.

The Kalman filter algorithms then provide a sequential recursive procedure for determining values for the coefficients that are statistically optimum in the sense that they have minimum probable error.

2.3 Kalman filter procedure

The steps in the Kalman filter procedure are as follows:

(1) Assuming a set of values for the coefficients or state elements of the system at some time t, the values of the state at some future time $t + dt$ are predicted.

(2) Using the known statistical properties of the state elements, their uncertainties at time $t + dt$ are also predicted.

(3) The value and probable error of some measurable combination of the state elements is then also predicted.

(4) An observation is made of this measurement quantity, with the observation having a known uncertainty. The difference between the predicted and observed values of the measurement quantity is used to adjust the values of the state elements. The Kalman filter equations yield optimum weighting factors that are used to distribute the difference between the various state elements.

(5) The estimate of the uncertainties is also adjusted to take account of the fact that extra information has also been added to the estimates of the elements, thus reducing their uncertainty.

In the case of the Navigation Reference System the generalised form of the Kalman filter takes the form of the block diagram shown in Fig 1. The state elements are the set of error sources sufficient to characterise the errors in the outputs of the various navigation sensors being used. The prediction process is carried out by mechanising a set of linear differential equations, with time varying coefficients, that describe the behaviour of the error sources in the absence of external disturbances.

2.4 Prerequisities of the filter

There are two aspects of a navigation system's behaviour that it is vital to understand before the system can be successfully incorporated into the Kalman filter. The dynamics of the error propagation must be modelled, as a set of linear differential equations, with sufficient precision to enable the predicted error values to be calculated with acceptable accuracy. In addition the statistics of the system errors have to be known, together with the statistics of any approximations that have been made in the dynamic model. It is often a major task to obtain the information needed to formulate these models, particularly the statistical ones. It can involve analytical studies, and detailed analysis of flight trials results. Often special flights have to be conducted

The RAE system has been built around the data from an IN which provides the basic outputs of position, velocity, attitude and heading. The Kalman filter is used to estimate the errors in the IN data by comparing it with the outputs of a number of other navigation systems. The various sensors are modelled in terms of their errors in order to simplify the prediction process and reduce the computational load.

Because of the fundamental importance of the deterministic and statistical error models, these have always been derived from, or verified against, flight trials data. In practice the error sources included as state elements do not fully describe the behaviour of a given system because of practical limitations on the number of state elements and a lack of knowledge of the precise details of the error dynamics. An attempt is made to compensate for this by extensive modelling of the uncertainties in the prediction and measurement processes.

It has been found that the processing of the data from individual sensors can best be split into two stages, with a stage of data conditioning or preprocessing being applied before the data is fed to the main Kalman filter.

3.1 Preprocessing

The preprocessing of data from individual sensors serves to reduce the total computing task and simplifies the software design. Three main functions are undertaken:

(1) The incoming sensor data is checked for consistency and reasonableness. Much of this function is easier to perform in the preprocessing because data can be taken at a much higher rate than would be possible in the Kalman filter, although the cross checking of data between systems is best left until the filter.

(2) The outputs of individual sensors are corrected for predictable errors, given the knowledge of the aircraft trajectory from the Kalman filter output and inputs from the operator concerning the conduct of the flight and other environmental data. Examples of these corrections would be lag compensation of outputs of sensors with a low frequency response, and compensation of Doppler ground speed and drift angle for the errors produced when flying over water.

(3) The outputs of some sensors can be averaged to provide inputs to the filter that can be represented by a reduced set of state elements. For example the multiple range position lines available from each Omega ground station can be reduced to a single range value. The error statistics used in the uncertainty prediction and measurement processes are often computed as a function of the flight profile, or of some secondary output from the sensor such as signal to noise ratio.

3.2 Features of the filter

The use of preprocessing techniques makes it possible to use a relatively simple set of error sources for the Kalman filter state vector with considerable benefits in terms of reduced computation. The prediction and measurement processes are mechanised in terms of errors and are linearised with respect to the aircraft trajectory as defined by the output of the integrated navigation system. The Kalman filter makes optimum use of the fixes from any combination of sensors and data rates, and there are further checks on the consistency of the input data before a measurement is used to update the filter's estimate of the individual system errors. This is most important because the filter has a long memory and can be upset for a long period by the inclusion of inconsistent measurements.

A mechanisation of the Kalman filter equations has been used that has been shown to have very good numerical stability, and this has meant that few problems have been experienced in this area where considerable difficulties have been experienced in some other applications.

The general form of the integrated navigation system is shown in Fig 2, with the Kalman filter box containing the elements shown in Fig 1.

4 REFERENCE DATA

Reference data is required for two basic types of trial, which have rather different requirements. Assessment trials require the best absolute accuracy from the reference data, while error source identification requires the data to be free from errors of a similar form to those of the system under test. Because the errors of a navigation system are frequently dependent upon the flight profile, a wide variety of routes have to be flown. This produces a requirement for a reference system with very broad capabilities.

Full three dimensional reference data at position, velocity, and orientation level (nine parameters in all) is needed so that the behaviour of any of the test system's

wide coverage required.

The approach to obtaining the required reference data has been based upon using multiple IN to provide the basic nine parameters. The data from IN has very low noise and a good frequency response, it is however subject to a build up of errors with time and manoeuvre. These errors can be corrected by mixing the inertial data with fixes from radio navigation aids having good long-term accuracy. The aids used for position fixes are Decca, DME, Loran C, Omega, and ground based tracking radar; while velocity fixes are obtained from a Doppler radar velocity sensor.

4.1 Inertial Navigator

Examples of the position and velocity errors of an IN are shown in Figs 3 and 4. The main features of interest are the characteristic periods of oscillation whose amplitude and phase change only slowly with time and aircraft manoeuvres. The observed errors are due to a multitude of sources within the IN, some of which are substantially constant over a number of flights and others of which change from flight to flight or even during the course of one flight. The preprocessing can be used to correct for the result of any error sources that are identified as being constant over a number of flights, and the filter is used to estimate the errors that change. The Kalman filter uses 10 state elements to characterise the IN.

The preprocessing scheme contains a very comprehensive model for predicting the statistics of the IN error states as a function of the aircraft trajectory and uses some 28 statistical error coefficients. These statistical coefficients allow for the changes in the values of the error states due to causes such as acceleration dependent gyro drifts, scale factor errors, and component misalignments.

4.2 DME

Fig 5 shows a typical set of errors in DME range data. The most significant features of these errors are:

(1) The noisy nature of the fixes compared with the smooth position data that is obtained from the IN.

(2) For the data from any one beacon, apart from the noise, the errors are of the form of a slowly changing bias.

(3) The bias can change significantly from one beacon to another.

DME errors are modelled in the Kalman filter as a bias on the DME range readings, with the process statistics set to acknowledge that the bias can change slowly with time. The DME data is used in the filter by forming as a measurement quantity the difference between the observed DME range and the equivalent quantity predicted from the IN position corrected by the Kalman filter's estimate of the IN position errors.

In order to minimise the number of errors being estimated by the filter, only one DME range bias is modelled for each DME receiver. When the receiver is tuned to a new beacon the bias estimate and its uncertainty are reset. The values of bias and uncertainty for the old beacon are preserved, so that if that beacon should be retuned later in the flight, the filter estimates can be reset incorporating the information gained earlier in the flight.

There is little true preprocessing done on the DME range data, other than to check its validity. If a particular beacon is found to give a consistent bias over a number of flights, then this bias is removed before the data is fed to the Kalman filter. The DME data is ignored when the aircraft is very close to, or very distant from a beacon, because the assumptions of a slowly changing bias error tend not to be valid under these conditions.

A rather special case of preprocessing arises with the treatment of the position data for the DME beacons, and also for the ground stations of the other radio fixing aids. In order to fully realise the potential accuracy of the integrated navigation system it is necessary to ensure that all position data used is referenced to the same geodetic datum. Frequently, the latitude and longitudes of navigation beacons are quoted with respect to the geodetic datum of the country in which the ground station is sited. For any particular flight, a single datum has to be selected, and all position data is transformed to be with respect to the one datum.

4.3 Decca and Loran C

It may seem surprising, but there are many similarities between the significant characteristics of DME and those of Decca and Loran C, if the data from the latter two aids is considered in terms of their hyperbolic position lines, rather than as a

the DME data. The Decca position line data is handled in the filter in an exactly analogous way to that used for the DME data, except that the readings are ignored when the aircraft is very close to either master or slave station, and the distant data is rejected on the basis of the width of the Decca zones.

Errors from a Loran C position line are similar to those of Decca. However the data has a new feature compared with the other radio aids, in the discontinuities associated with the 10 microsecond jumps in the output of the Loran receiver. The 10 microsecond jumps can be detected by comparing the observed Loran reading with the equivalent values predicted from the corrected IN positions, and then corrected before the data is passed to the filter. Loran C errors are modelled as a bias that changes only very slowly. Their uncertainty is a function of whether ground or sky wave are being tracked, and of the number of 10 microsecond corrections being applied.

4.4 Tracking radar

The use of data from ground based tracking radar presents a rather different set of problems compared with the other fixing aids. This is because the fixes are much more accurate, and so the estimation of their biases is less significant.

However, because these fixes are given such a high weighting in the filter, it is most important to ensure that the probable error of the measurement quantities are estimated correctly. This is the main task of the preprocessing of the radar data. The fixes are used in terms of the range and bearing from the radar, and a number of factors are used in predicting their probable errors:

(1) The elevation of the radar beam is important because it is very often close to grazing incidence with the surface of the earth.

(2) The actual bearing can also be significant because of the varying terrain surrounding the radar head.

(3) The magnitude of range is significant if the aircraft is not fitted with a transponder.

(4) The accuracies are such that the quantising of digital data and the timing delays associated with the ground and airborne recording systems can introduce significant uncertainties that are a function of the relative positions and velocities of the aircraft and radar.

4.5 Doppler radar

At first sight the errors of Doppler, when operating over the sea, seem very large. This is illustrated in Fig 7. There are large fluctuations in error between successive data points, coupled with large biases that alter with changes in aircraft position and heading. The errors can be largely corrected using a number of stages of preprocessing to correct for deterministic error sources. These error sources are:

(1) Lags in the Doppler information due to its mechanisation which appear as errors in ground speed and drift angle when the aircraft is manoeuvring.

(2) Errors due to distortion of the Doppler spectrum when flying over water.

(3) The effect of the motion of the sea surface.

The IN gives a very good measure of the aircraft manoeuvres and this information can be used to correct for lag induced errors.

Motion of the sea surface can be predicted from knowledge of surface wind. When the aircraft is flying at low altitude, say below 2000 feet, the velocity from the integrated system can be used to measure the wind at the aircraft and this vector can be reduced to sea level to give the surface wind that can be used in the correction algorithms. The accuracy of the corrections vary with the conditions of surface wind and aircraft manoeuvre and the knowledge of these conditions can be used to calculate the uncertainty of the Doppler ground speed and drift angle data at each time.

Fig 8 gives an example of the reduction in Doppler errors produced by the preprocessing.

The residual Doppler errors are represented by four error sources in the Kalman filter, viz Doppler scale factor, drift angle bias, and residual sea motion errors north and east. The changing uncertainties of these four error sources are modelled by the terms calculated in the preprocessing. The Doppler data is introduced into the Kalman filter via two measurement quantities formed as the difference between the filter and the Doppler's indications of ground speed and drift angle.

and longitude derived from a combination of data from a number of ground stations, or the number of position lines with respect to the individual ground stations.

Typical examples of the errors in the latitude and longitude data from Omega are shown in Fig 9. The most significant error characteristics are the short term variations coupled with quite long period changes which have a small mean value. Over a long period, these characteristics are complementary to the errors of an IN, except that both systems have errors with oscillatory periods of about 24 hours.

The errors of either type of Omega output are modelled in the filter as a slowly changing bias. The choice between outputs is a difficult trade-off between accuracy, redundancy, and computing load. The latitude and longitude outputs require the smaller computing power because only two error states are needed, but it is hard to predict the probable rate of change of bias because the positions are derived from an ever changing combination of individual position lines. At the other extreme, the individual position lines - up to 25 of them - much more closely meet the assumptions implicit in the error model, but would impose a heavy computing burden.

Two methods of using Omega/VLF data have been examined: firstly, the use of the latitude and longitude outputs in a straightforward manner; secondly, the use of position line data with preprocessing to combine a number of lines and to calculate their likely uncertainties.

This latter preprocessing is another interesting example of how the technique can be used to reduce the size of the filter. The data from each ground station is available as a reading of the range between the aircraft and station measured on each of the transmitted frequencies. Since each of these multiple range measurements is made along a very similar propagation path, it is reasonable to form a single average range measurement to each ground station. The uncertainty of the average range may be calculated from a number of factors: the observed signal to noise ratio gives an indication of the quality of the individual range measurements; the aircraft position plus time and date enables the form of the propagation path to be determined, and from this the uncertainty in the propagation corrections may be calculated.

5 OFF-LINE PROCESSING

All of the features discussed so far are appropriate to an integrated navigation system that is required to produce its results in real time. The creation of reference data for flight trials is a special case in that the maximum accuracy is not required until after the flight. Under these conditions another convenient feature of the Kalman filter algorithms can be used to enhance the accuracy of the final results. Because the propagation equations are linear, the filter can easily be made to run backwards with respect to time to produce a new set of estimates of the IN's errors. Thus at any time we have estimates of the IN errors based on all the information available before that time and an independent estimate derived from all of the information available after that time. The uncertainty of each of these estimates is also available. Thus the two versions can be merged to give a single best estimate based on all of the available information. This technique of forward-backward filtering is especially beneficial for preserving accuracy in areas with poor fixing aid coverage.

6 REFERENCE SYSTEM ACCURACY

The reference data produced by the process described above has all of the desired characteristics stated at the start, and its overall accuracy, when operating without the benefit of fixes from tracking radar may be summarised as follows:

(1) Reference position accuracy 0.07 nautical miles (130 m) rms.

(2) Reference velocity accuracy 0.3 knots (0.15 m/s) rms.

(3) Heading accuracy 0.05 deg rms.

These errors were measured by comparing the results obtained with and without the radar fixes being included. In any given area the accuracy will depend upon the coverage available from the fixing aids and the behaviour of the IN which is itself influenced by the manoeuvres being performed.

It should be noted that the data processing techniques employed to produce the reference system provide a ready means for examining the behaviour of every navigation system used on the flight. The results thus obtained are used to continually refine and update the parameters of the models for each system, and the Kalman filter mechanisation provides a very convenient mechanism whereby this new knowledge can be incorporated for future flights; usually by amendments to the preprocessing corrections or to the calculation of the various uncertainties.

7 LESSONS LEARNED

The Kalman filter approach really does work and its use is justified by its ability to handle diverse and intermittent data and the ease with which it can accommodate

The price to be paid is in the detailed knowledge required of the characteristics of the individual sensors. This knowledge has led to a more informed use of the data from the sensors and has had wider application than just the integrated systems, in that it has assisted the general improvement of the individual sensors.

If integrated navigation techniques are to be applied more widely there is a need for the flight trials of individual equipments to produce more pertinent data as a matter of course. Too often it has been found that past trials have not produced information in a form appropriate to integrated navigation applications and it has been necessary to conduct special trials to gather the required data. It is highly desirable that future equipment trials should consider the possible use of the equipments in integrated systems and attempt to gather the appropriate basic information.

8 ACKNOWLEDGMENTS

The authors would like to acknowledge the contribution made to the work by their associates, particularly those outside the immediate group at RAE. Firstly Navigation and Radio Division at A&AEE, Boscombe Down, with whom they have worked from the earliest days on trials of navigation equipment, secondly the Racal-Decca Group who have developed models for Doppler to be incorporated in the filter and preprocessing algorithms, and lastly Stephen Howe Ltd who have done much of the general implementation of the Kalman filter. Stephen Howe are providing A&AEE with a version of the RAE integrated navigation software which will be used by Boscombe for future navigation trials.

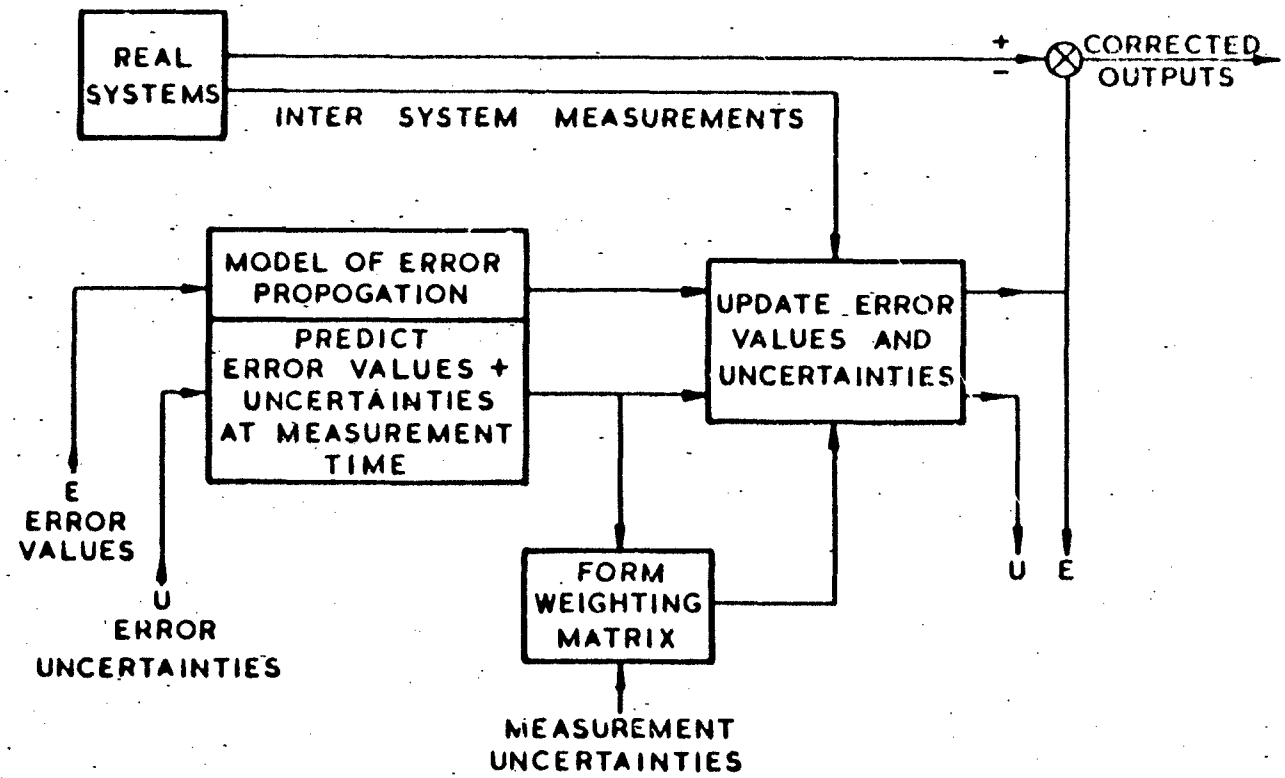

PRINCIPLES OF THE KALMAN FILTER

FIG 1

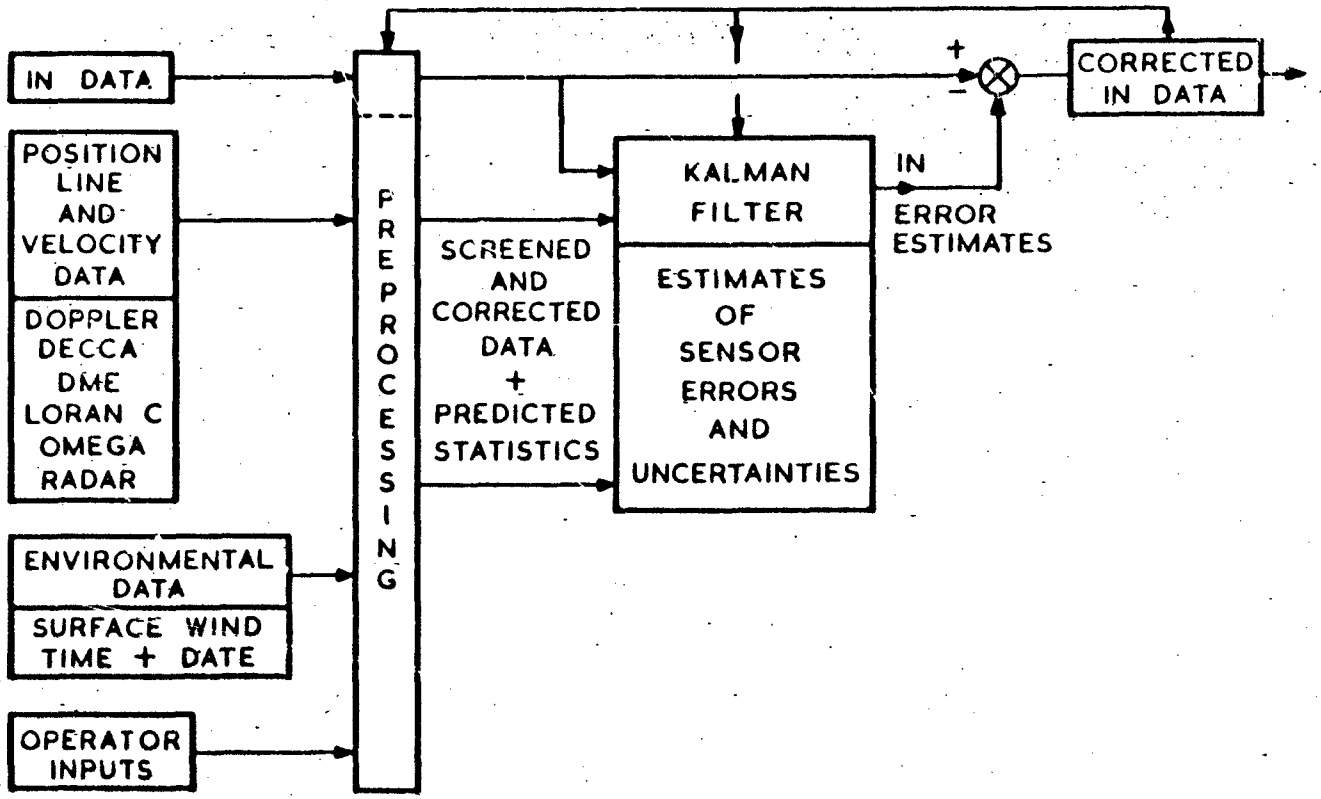

FORM OF THE INTEGRATED NAVIGATION SYSTEM

FIG 2

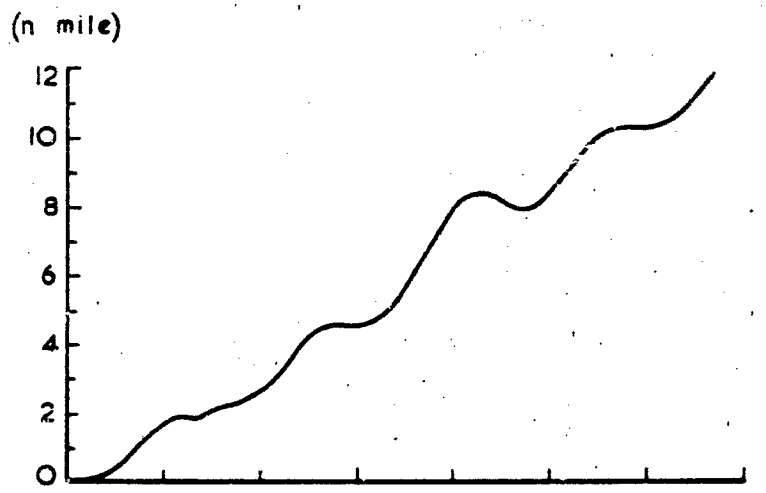

NORTH POSITION ERROR

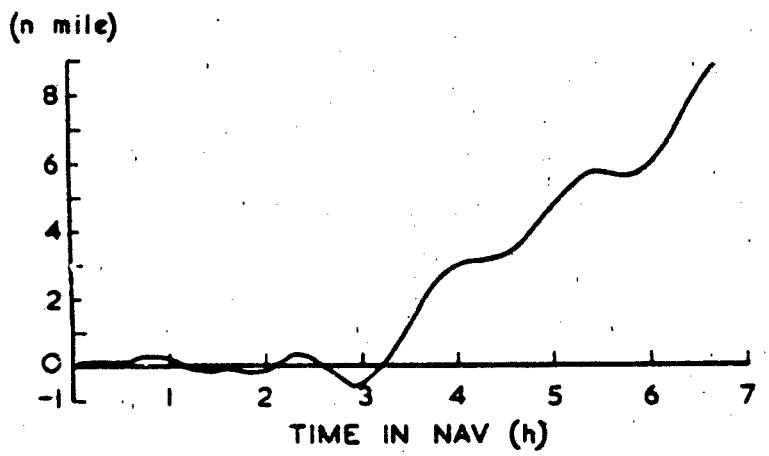

EAST POSITION ERROR

TYPICAL INERTIAL NAVIGATOR POSITION ERRORS

FIG 3

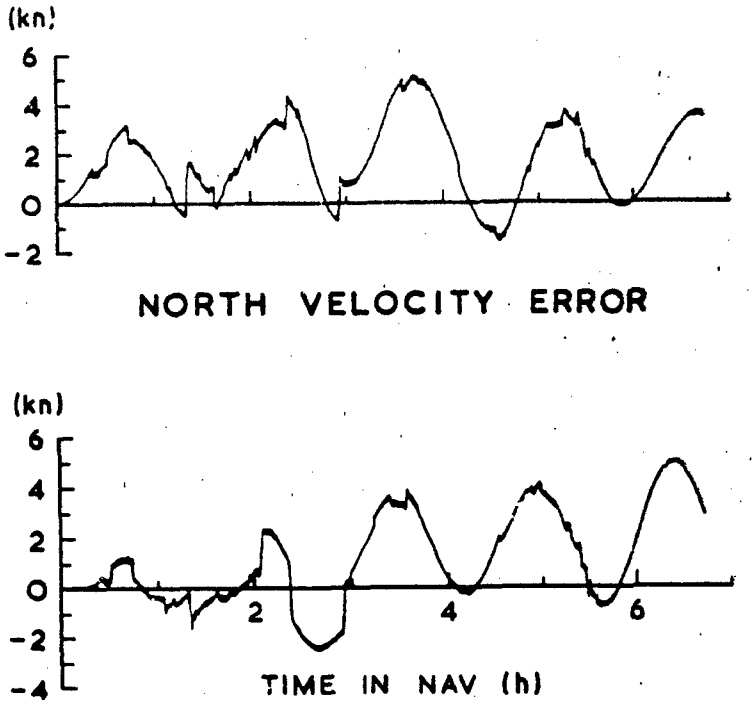

TYPICAL INERTIAL NAVIGATOR VELOCITY ERRORS

FIG 4

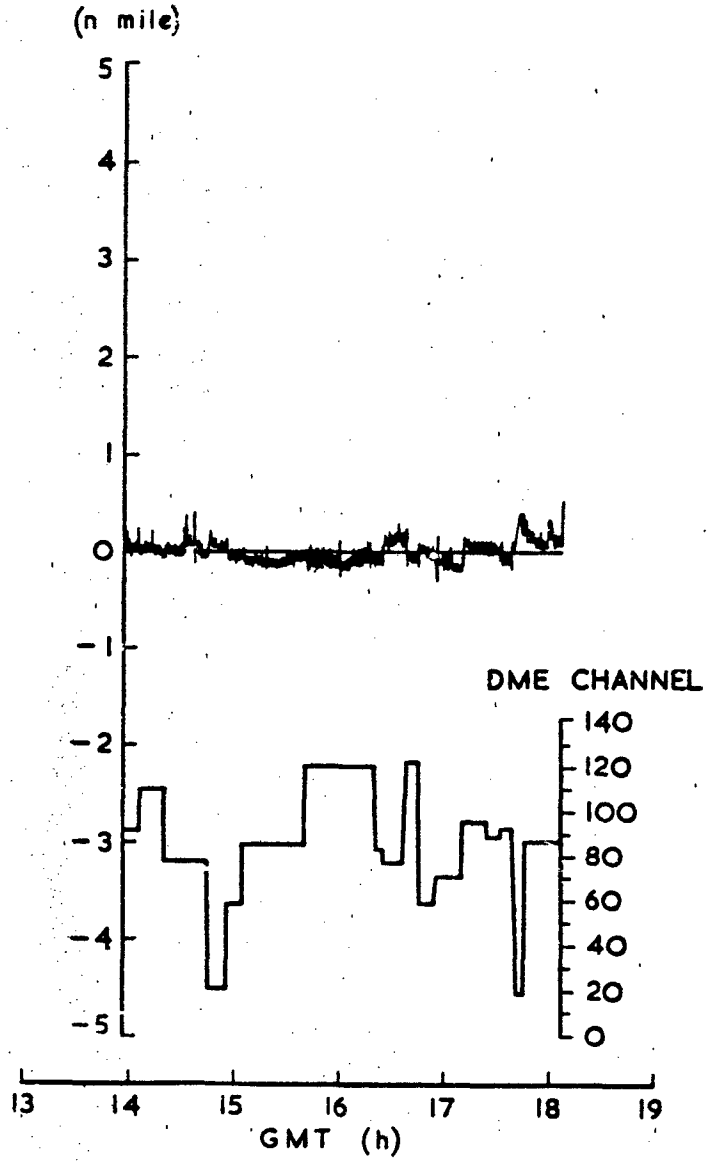

TYPICAL DME RANGE ERRORS

FIG 5

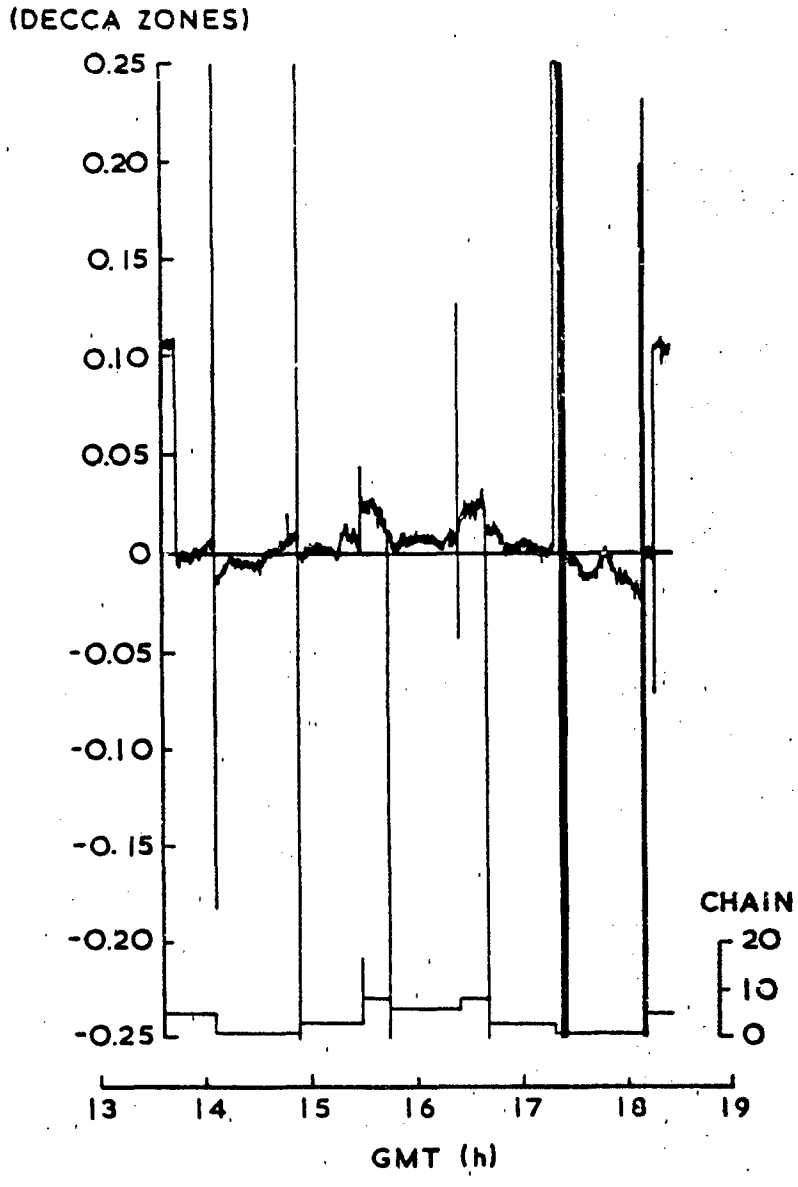

TYPICAL DECCA NAVIGATOR PHASE ERRORS

FIG 6

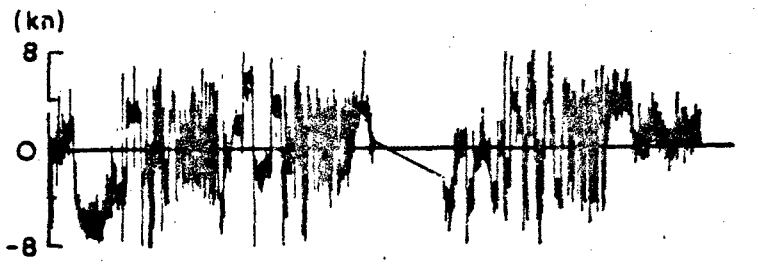

GROUND SPEED ERROR

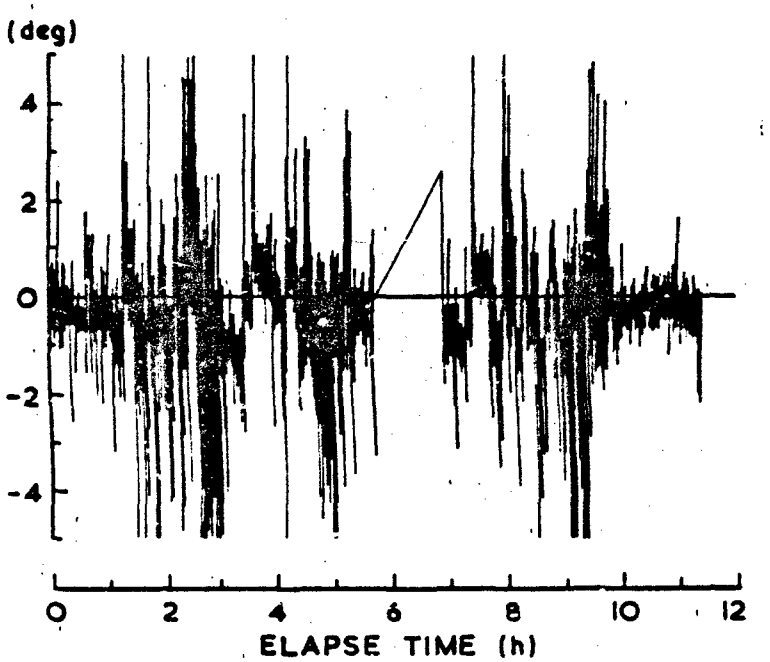

DRIFT ANGLE ERROR

TYPICAL RAW DOPPLER ERRORS

FIG 7

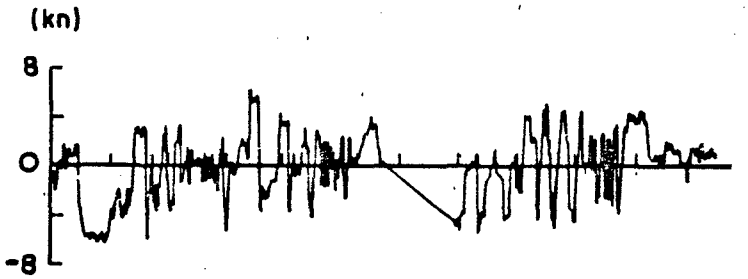

RAW GROUND SPEED ERROR

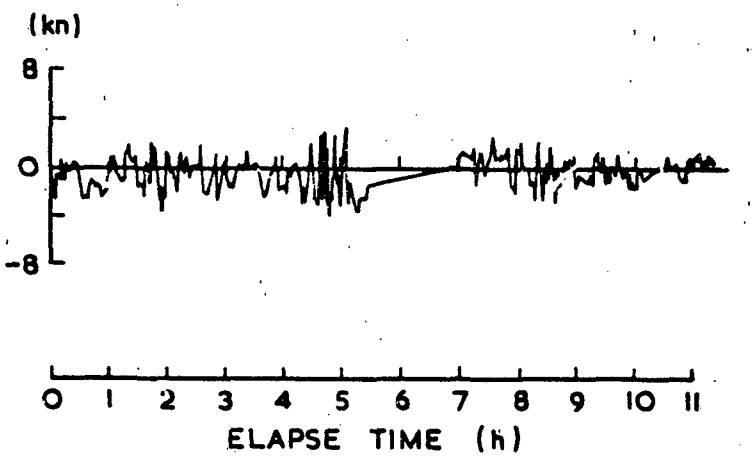

PREPROCESSED GROUND SPEED ERROR

RESULTS OF DOPPLER DATA PREPROCESSING

FIG 8

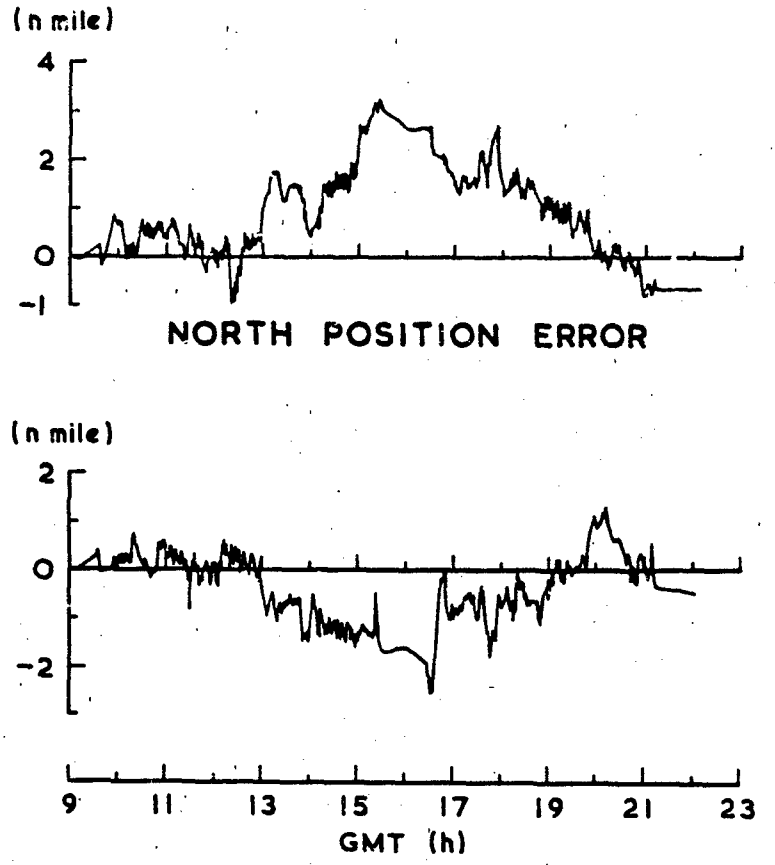

TYPICAL OMEGA POSITION ERRORS

FIG 9

R. Carabelli
Combat Aircraft Group - Flight Test Department

R. Pelissero
Avionic Systems and Equipments Group

of Aeritalia S.A.I.p.A., 10072 Caselle Torinese, Italy

SUMMARY

Extensive autopilot system performance evaluations have been conducted at Aeritalia Flight Test Centre in Caselle on TORNADO Prototype 05 and 09.

The experience made, though objectives were only marginally inclusive of System development, gave the opportunity to be faced with a set of problems usually affecting earlier prototype systems assessment.

Several problems affecting equipments, control laws, system integration (hardware and software) were discovered and studied.

The activity took advantage from various computing and simulation facilities i.e. a digital processor to analyse data from fast data transmission lines and an avionic integration rig with real-time closed-loop simulation capability.

Lessons learnt are herein reported, with enough details to represent, we hope, a valuable reference also for readers not familiar with the projects we are writing about.

New facilities tailored to cover as much as possible of weapon system testing needs are being developed to cope with requirements from oncoming projects relying upon more advanced technologies.

Trends for next trials conduct are discussed outlining engineering activities and ground facilities needs i.e. simulation and system rig, required to support flight testing of prototype avionic systems.

1. INTRODUCTION

Tornado autopilot test flights carried out by Aeritalia were confined to investigate about performance compliance to system specification requirements when operating in the so-called "Basic & Cruise Modes" and with external stores complement to the basic aircraft configuration i.e. only stores suspension system fitted.
That implied flying in a limited number of external store configurations having potential to clear the full configurations tree Tornado has to operate with.
A joint effort of Flight Test and System Design Engineering has been necessary to overcome some problems, not all of technical nature, we had to struggle with.

Next paragraphs describe problems, solutions found and what we are doing in preparation of a new weapon system development i.e. the AM-X tactical fighter.

Before going through all that some words need to be spent to illustrate the systems we will discuss about.

Few words are necessary for Tornado, weight of papers dealing with it probably being in excess of aircraft gross weight. Tornado (Fig. 1) has a variety of aerodynamically different configurations resulting by the combination of wing sweeps and external stores that may be fitted to underfuselage and underwing attachment points.

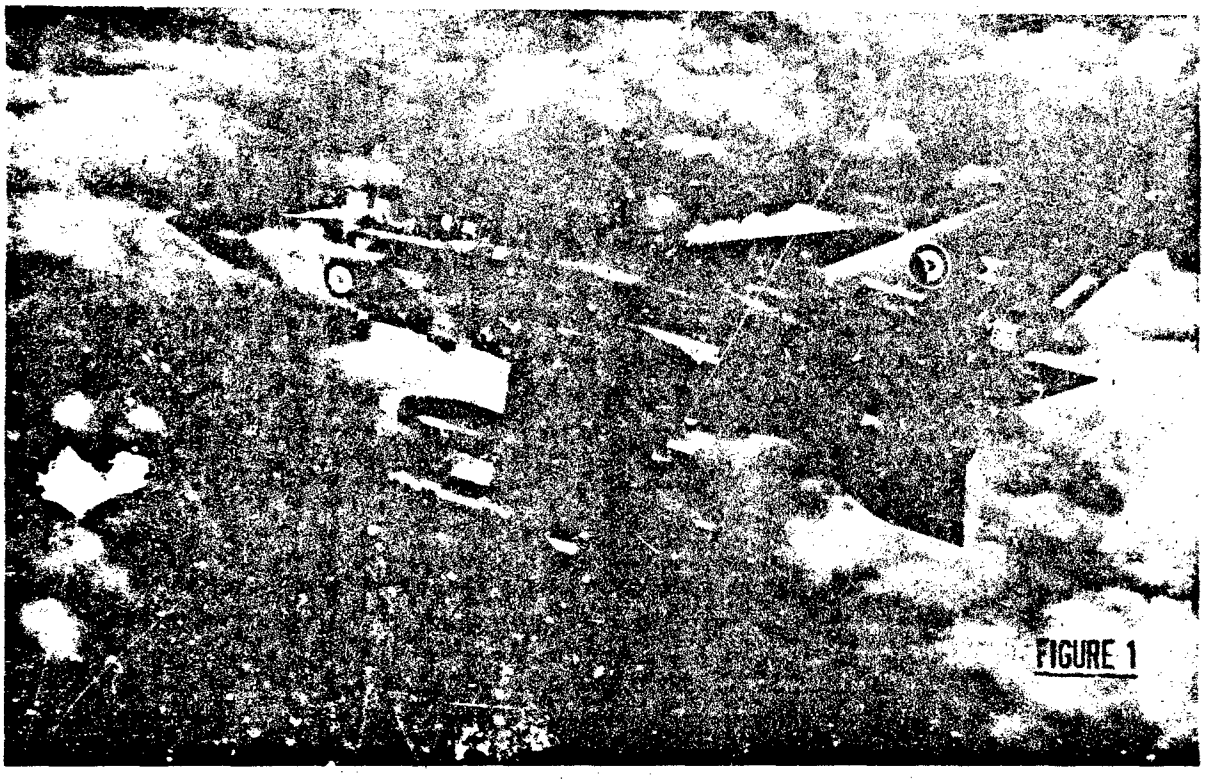

FIGURE 1

This, in addition to its large flight envelope and significant centre of gravity excursions resulting from fuel consumption and weapons release, asks for suitable response of the autopilot system which may be operated in the following modes during cruise flights : attitude /heading acquisition, track acquisition, baro-attitude hold, autothrottle.

During cruise modes operation the autopilot is interfaced with the following equipments i.e.

- Command and Stability Augmentation System (CSAS)
- Inertial Navigator (IN)
- Secondary Attitude and Heading Reference (SAHR)
- Air Data Computer (ADC)
- Main Computer (MC)
- Horizontal Situation Indicator (HSI)
- Attitude Director Indicator (ADI)
- Head-up Display (HUD)

HUD and ADI receive AFDS signals, CSAS receives/provides signals from/to Autopilot; all the other Systems can be considered as Autopilot data sources (Fig.2).

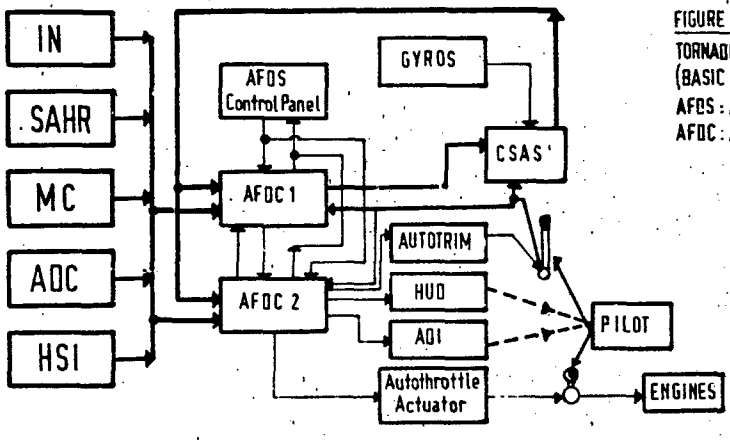

FIGURE 2
TORNADO AUTOMATIC FLIGHT CONTROL LOOP
(BASIC AND CRUISE MODES)
AFDS : Autopilot and Flight Director System
AFDC : Autopilot and Flight Director Computer

Today's state-of-the-art for avionic systems design emphasizes the integration via time multiplexing of digital data buses with a general trend to adopt the MIL-STD-1553b as the common standard.
This design solution implies that all the signals are converted to the digital standard format before their transmission.
As a consequence the bus deals with just one kind of signal and always with the same.

Using the above mentioned technique it is possible to design a great variety of avionic system structures, each of them characterized by a different level of data bus integration.

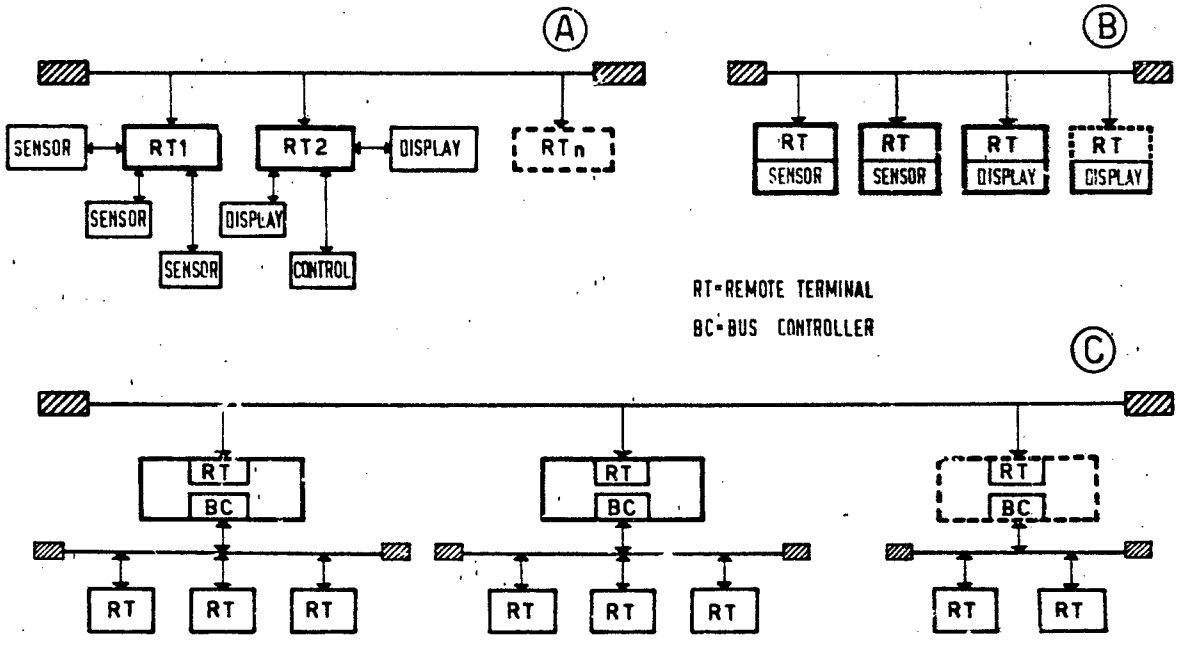

FIGURE 3 - DATA BUS SYSTEM STRUCTURE

In this solution the digital data bus allows the interconnection of a limited number of remote terminals tasked to act as concentrators of the traffic to/from the various sensors and displays.

This type of structure asks for great complexity of the remote terminals because of the need to convert a lot of different signals to/from the digital data bus. In addition this solution is characterized by heavy data traffic on the bus because each remote terminal needs to be filled with all the data related to all the equipments that are connected to it.

The next step is a system where every equipment gains access to the digital data bus by means of its own remote terminal and where a centralized bus controller performs the integration of system sensors and displays by sending through the bus a proper sequence of command words (Fig. 3b).

The main feature of such a data bus structure is its high level of flexibility : whichever modification to the system lay-out and/or data exchange is easily handled by changing the sequence of the command words.

Normally each equipment does not require a great deal of data to be exchanged with the remaining of the system. This situation especially happens when enough computational capability is embedded in the equipment itself.

However, the traffic of course increases with the number of the equipments connected to the data bus.

tasks (navigation, weapon aiming, etc.) are to be performed by a centralized computer, it is obvious that this equipment is the prime candidate as bus controller.

This kind of solution was adopted for the avionic system of the next project knocking at the door i.e. that is the AM-X aircraft (Fig.4), resulting by a joint effort of Aeritalia and Aermacchi for Italy and Embraer for Brazil. Redundancy criteria require duplication of bus controller, bus terminals and digital data bus to meet safety and reliability requirements.

The most complex theoretically achievable solution, that can be chosen when the bus load becomes too high or when a more distributed architecture is required, is obtained applying the same structure concept to a subsystem level architecture (Fig. 3c).

In this case it is necessary to design a hierarchical network where a bus controller/processor performs the integration among the different equipments of a subsystem and is at its turn a remote terminal with respect to a higher level bus, which collects data from different subsystem processors.

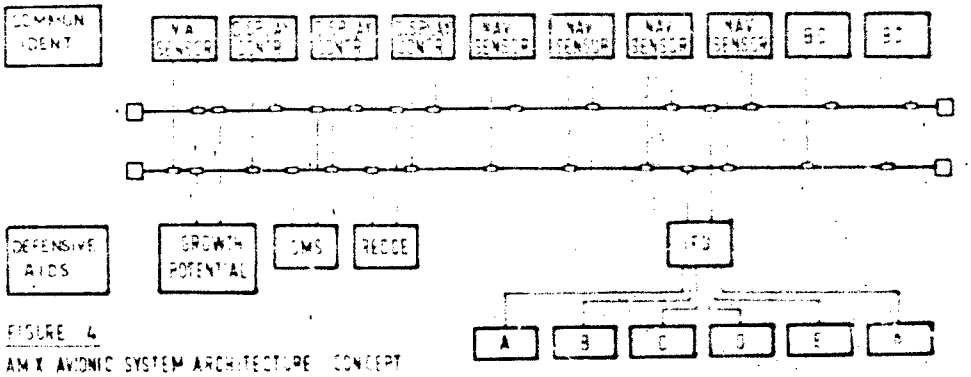

FIGURE 4
AM-X AVIONIC SYSTEM ARCHITECTURE CONCEPT

This means that in a typical avionic system each subsystem function is performed by a group of items having their own bus controller/processor (navigation subsystem function with Inertial Navigators, Radio Navigators, Navigation Processor/Bus Controller and Flight Controls Subsystem function with gyro package, actuators, pilot's commands, Flight Control Processor/Bus Controller). All these processor/bus controllers, as previously mentioned, are interconnected via a higher level bus which of course has its own bus controller (e.g. a System Monitor Processor or Pilot Display Processor). Using such an architecture each subsystem data bus can be tailored to its own needs and in particular it may be possible to overcome all the integrity problems related to the application of MIL-STD-1553b to the Flight Controls/Autopilot systems.

The integrity requirement for the flight control subsystem can be met using a triplex system as redundant buses allow error correction in addition to error/failure identification.

In this case the test instrumentation has to be dedicated to the particular subsystem as a remote terminal to be inserted in a further data bus subsystem which collects all the data from all the test-dedicated remote terminals.

The use of a remote terminal for test instrumentation together with the data bus monitor passive function is required to allow monitor of parameters normally not available on the data bus as intermediate results of iterative calculations.

Let's conclude our diversion on data bus techniques by considering some implications we feel worth to note :

- for the aforementioned hierarchical structures and in general for all the remote terminals having access to/from different data buses, problems exist about bus controllers synchronization and delays among data from different sources.
- The bus structure allows the availability in a single point of all the information exchanged at any time. Therefore, data collection to evaluate performances and every kind of test results becomes quite easy, provided that a device able to pick up the traffic and to identify data to be captured is available.
  At this point, data identification is made possible by knowledge of the command word defining the message and of the data position within the message.

the limitation to 15 of the number of subaddresses for each equipment.

2. FLIGHT TEST INSTRUMENTATION

The flight test engineering discipline was born together with the possibility to instrument an aircraft and record aboard in some way what picked up by the transducers.

Subsequently, generations of aircraft have seen extensive application of this practice together with that, quite similar in principle, of tapping equipment aboard.

Tapping practice has seen extensive application on Tornado together with milking of digital computers information content.
In autopilot performance assessment direct access to main computer and autopilot computer data has been realized by onboard recording of data transmission line serial digital stream. However, tapping i.e. picking up of internal information in equipments originally not designed for, was also necessary.

Tornado's autopilot has two digital computers (AFDC 1 & 2) self-monitored except for a crossfeed of command inputs to the CSAS subject to level comparison. A DAC/ADC interface makes Autopilot/CSAS inputs exchange possible, the CSAS being an analogue system.

During autopilot development, tapping of the interface in the analogue section was necessary to pick up internal signals when investigating about more frequent than expected system drop outs.

This facility was present also in the autopilot/CSAS interface fitted to Aeritalia's prototype aircraft, with of course, all protections any system tapping is required to have by design.

Protection some time fails and it did indeed.

One of the control inputs from autopilot to the lateral CSAS was affected by voltage level error induced by a faulted FTI module used in picking up the signal at the tapping point with a couple of consequences.

One was benign being self-revealing as autopilot drop-outs occurred when the system commanded the airplane to roll.
The other was deceitful because when the difference between Computer 1 and 2 signals stood below the threshold of the monitor it could not trip and the consolidated signals in input to the CSAS had a level equal to the average of the correct and the wrong one. The second was logically a nasty case for people involved in system performance evaluation.
Next Fig. 5 shows the two cases experienced.

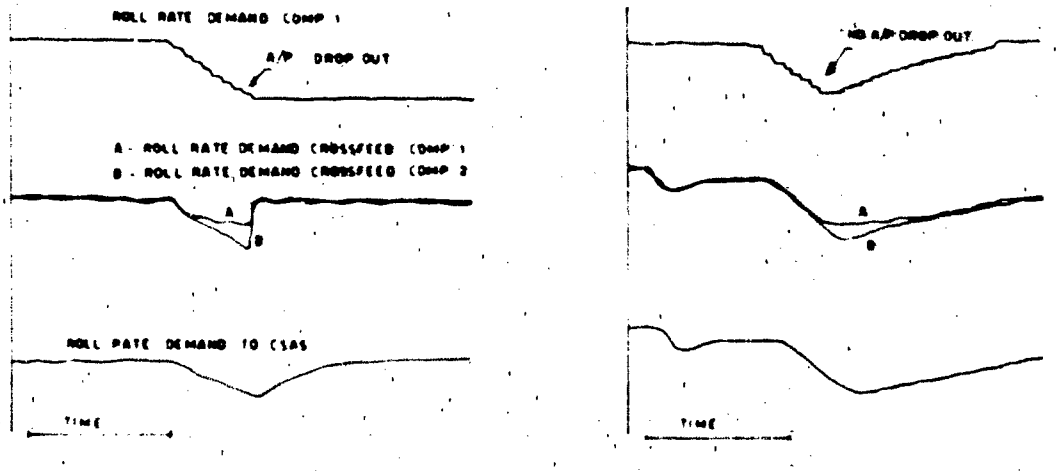

FIGURE 5 - AFDC 1 AND 2 INPUTS TO LATERAL CSAS

due consideration must be given to integrity when potentially impaired, looking for different solutions if the technology adopted makes them applicable.

The AM-X Avionic System has given us a good chance to apply this concept. Writing the specifications for the flight test data pulse code modulating (PCM) and recording system request has been made of a MIL-STD-1553b data bus transformer-coupling-type stubbing to allow either all the dual redundant bus traffic recording or, via the PCM subsystem, select and record only those messages on the buses pertaining to equipments involved in the test being carried out.

This method of stubbing has been chosen in accordance with MIL-STD-1553b Appendix point 10.5 recommendation to provide "the benefits of DC isolation, increased common mode protection, a doubling of effective stub impedance, and fault isolation for the entire stub and terminal".

In some cases the PCM subsystem may assume the role of effective buses remote terminal which means that when directly addressed it will extract data then transmit a status word back to the controller.

In all the above cases buses trilevel signals are converted into binary by an interface electronics and their logical sum sent to the tape recorder as a pseudo single bus signal in serial digital format.

Binary form adopted is bi-phase modulation which does represent further protection against mismatch between bus line and flight test equipments.

A scheme of the data recording system of the AM-X is shown in Fig.6.

To make the PCM subsystem working as a remote terminal of the avionic system a modification is necessary into the bus controller i.e. the main computer software.

Though relatively simple in principle, as recommended at point 10.2 of MIL-STD-1553b Appendix, it can represent the gap errors may steal through into the software with potential nasty consequences. Use of such a facility will therefore be limited to those cases where benefits in return largely pay for the risk taken.

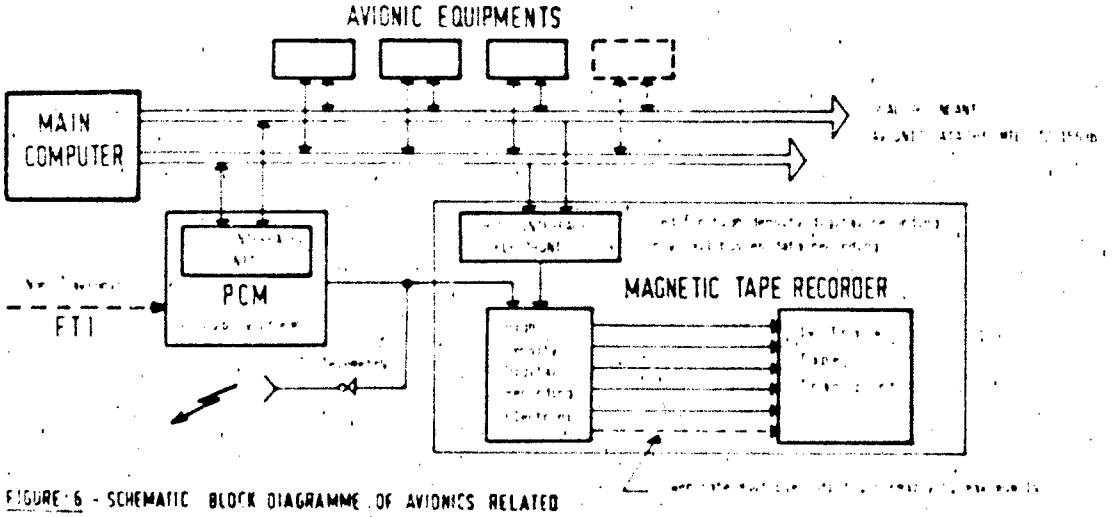

FIGURE 6 - SCHEMATIC BLOCK DIAGRAMME OF AVIONICS RELATED FLIGHT TEST DATA RECORDING SYSTEM

now progressively getting 100% operability assuming first flying of AM-X 01 as ultimate date for having software and control room hardware availability at the standard required by flight test engineering (Fig. 7). Facilities more comprehensive description is given in Ref. 1.

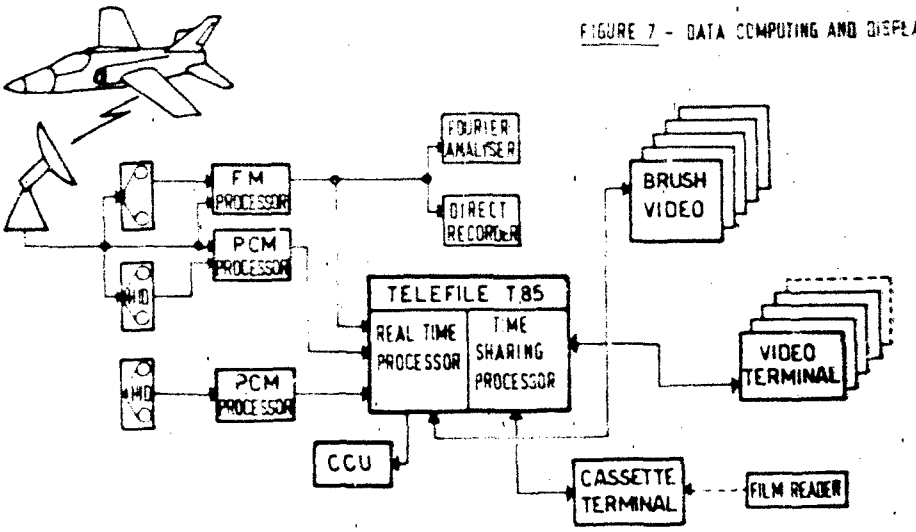

FIGURE 7 - DATA COMPUTING AND DISPLAYING SYSTEM

Telemetry data may be stored on high density tapes (HID) and, in parallel, processed for real time displaying and to allow quasi-real-time data analysis. At the same time, data from previous flights may be also processed by the second PCM processor and analyses conducted using the time sharing computer partition.

Most of the avionic tests data analyses not requiring extensive statistical computations may be performed in quasi-real-time from computer video terminals working on telemetry data stored in a temporary computer memory.

In the case of avionic system dedicated tests, data from the PCM subsystem and sent to ground via telemetry (Fig.6) allow quasi-real-time data processing (Fig. 8) being inclusive of both 1553b bus autopilot system related data and also non-avionic data as necessary to identify from different source, aircraft motion and flight conditions.

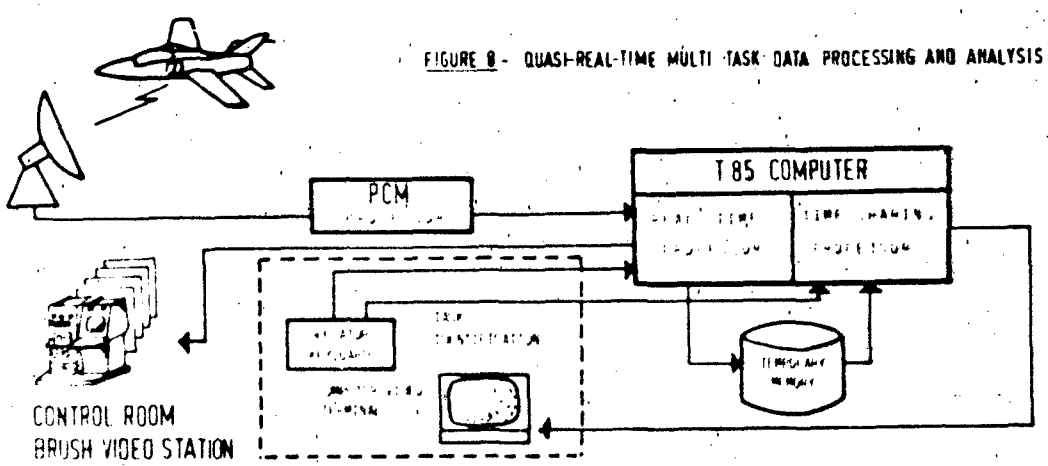

FIGURE 8 - QUASI-REAL-TIME MULTI TASK DATA PROCESSING AND ANALYSIS

development phases of the Tornado aircraft (Ref. 2).

Due to the specific tasks to be performed, every rig was set up differently to obtain the required capabilities.
Starting from the purpose of providing the capability to perform avionic system integration, very efficient and flexible facilities were arranged to cover a lot of different activities.

In particular when automatic flight control system, like Tornado autopilot, are to be considered, it is necessary to use a facility allowing real time simulation with the hardware in the loop in order to reproduce the real behaviour of the system.

A closed loop system in fact allows to perform efficiently and cost effectively all the activities related to the testing objective of proving, in conjunction with flight trials activity, the performance and the hardware/software integrity of the automatic flight control system under normal and abnormal operating conditions.

To cover some involvements in automatic flight controls area, the AIT Tornado rig system, that initially was just used as a flight back-up rig, was improved with the capability to perform real time closed loop testing.

The present AIT Closed Loop System is based on three items : avionic integration rig, data handling computer and simulation computer.

The behaviour of the real control loop (see Fig. 2), is reproduced by fitting the avionic rig with AFDS, sensors, MC, displays, control panels and closing the loop through software models of CSAS and aircraft dynamics (Fig. 9).

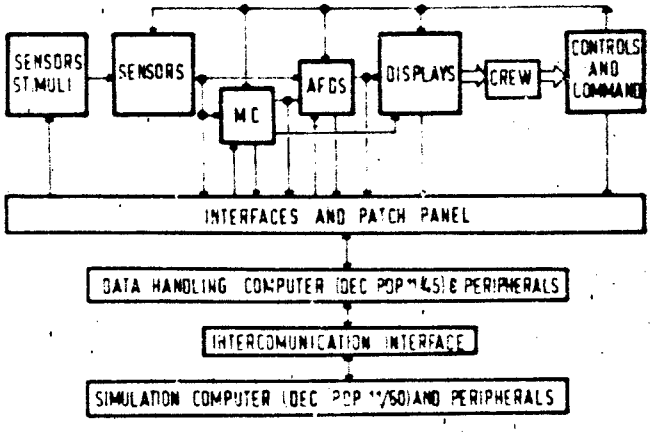

FIGURE 9 – CLOSED LOOP SYSTEM SET UP

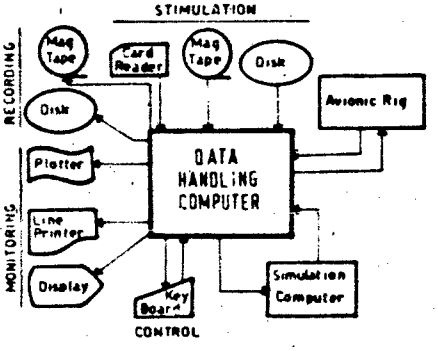

FIGURE 10 – CLOASS REAL TIME FUNCTIONS

The avionic equipments are connected as on the aircraft, and their input/output signal flow is controlled by the data handling computer via a dedicated software system, some special interfaces and through dedicated patch panels.

The operators can use the various control panels/keyboards and a dedicated hardware/software system representative of stick, trim and throttle functions.

The two computers are connected physically via a standard high speed communication interface and logically by two jobs operating respectively on the data handling computer and on the simulation computer.

The operational data flow in the systems is fulfilled according to the following steps :

- The output signals of the various equipments are acquired by the data handling computer and sent to the simulation computer.
- These data are used as input signals for the software models by the simulation computer which computes the equipments inputs to be sent to the data handling computer.
- These computation results are used by the data handling computer to stimulate the equipments that so produce new data to be acquired.

A real time monitoring of this process is accomplished by aircraft displays, measurement devices, video terminal, line printer and plotter.

able to handle the various kind of signals used within the female avionic system i.e. serial digital, parallel digital, binary coded decimal, synchro, discrete, analogue.

The closed loop system makes use of special software on both the computers.

The data handling computer is provided with the so called Closed Loop Data Acquisition and Stimulation System (CLDASS) which was developed by AIT starting from the Data Acquisition and Simulation System (DASS) designed by MBB, with AIT contribution, for open loop testing purposes (hardware/software integration, system investigation, flight back-up, support for avionic system charges).

The real time functions (Fig. 10) are :

- recording on magnetic tape and/or disk
- monitoring on video display or line printer and/or plotter
- dynamic stimulation
- substitution of serial digital data
- data transmission to the simulation computer
- event processing and subsequent action
- on line commands (for control, test, monitoring and stimulation)

Monitoring, recording, stimulation and substitution functions apply both to the avionic rig data and to the stimulation computer data.

The off-line functions allow to replay the recorded data on line printer/video display (alphanumerically) or on plotter (graphically) and to make use of all the necessary utilities.

The simulation computer is provided with a real time simulation program and with two utility systems : the aerodynamic data handling programs and the test preparation interactive program.

These systems were designed and developed with the purpose that some limits of the machine (speed and word length) should not affect the ability to perform real time testing and that, at the same time, the computer should be utilized at the maximum of its hardware capabilities. During the project, in fact, the strongest constraints were :

- the need that the simulation program running time is such to maintain the global cycle time at a value enabling a realistic operation
- the address limitation of a 16 bit computer just allowing 32 K words program when overlay techniques can not be used for time consuming reasons.

The aerodynamic data handling programs system allows the aerodynamic data management with the capability of selecting desired portion of the flight envelope; its functions are :

- data selection in accordance with the test to be performed
- data generation in accordance with the aircraft configuration
- data interpolation for intermediate situations

The test preparation interactive program provides all the data/information necessary to the test; its functions are :

- selected data formatting
- trim conditions computation
- fixed parameters computation
- logic commands interpretation and formatting

The real time simulation program contains the software models of all the non avionic items like aircraft dynamics, engine, CSAS, environmental conditions, and also of some avionic sensors, so that the use of either real or simulated sensors is allowed.

The program, which was developed using computer oriented real time techniques, allows :

- starting phase
- avionic data acquisition from data handling computer
- avionic data conversion into floating point format
- environmental conditions computation
- CSAS and actuators output computation
- dynamics equations integration
- engine parameters computation
- sensors output computation
- sensors stimuli computation

The Closed Loop System allows testing of all the relevant functions with very high level of flexibility and accuracy.

In particular it makes possible to :

- display and test all the subsystem functions and logics against specification
- detect incompatibilities or failures at any level
- study and verify corrective actions
- anticipate the system in-flight behaviour
- reproduce in-flight situations
- produce results for the flight clearances
- perform training activities

Before starting test activities the facility itself has to be validated comparing the obtained outputs with the various off-line simulation results, the development flight simulator data and, as a final step, the flight trials traces.

Fig. 11 shows a comparison between rig and flight test results.

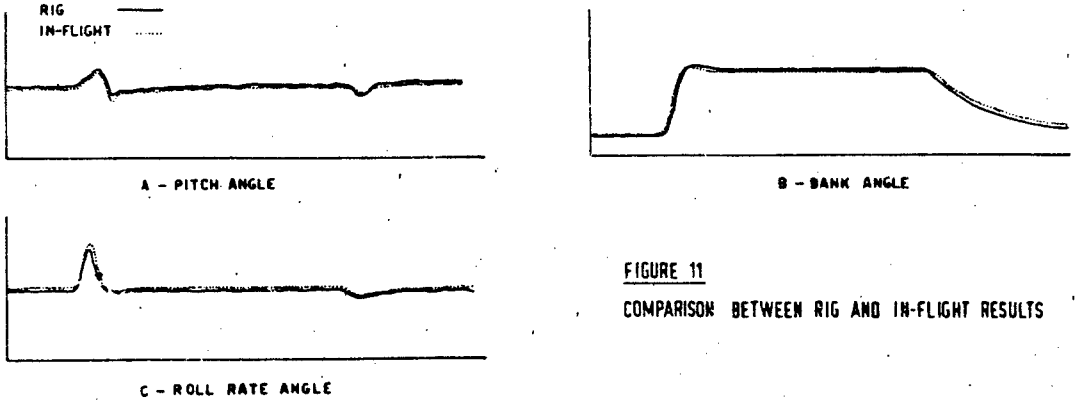

FIGURE 11

COMPARISON BETWEEN RIG AND IN-FLIGHT RESULTS

The facility gives the opportunity to perform a software confidence testing on the program implemented within the autopilot computers, checking the correct implementation of :

- control laws and failure logics
- limits, thresholds, switches and selectors

and simulating mishandling actions and various types of external malfunctions including lack of sensors and of power supplies. The performance analysis tests extend the investigations covering as largely as possible the complete flight envelope and including several aircraft configurations. The purpose of performance evaluation, which corresponds to software validation, is to control whether the specification is met or, in other words, whether the software is working as expected.

The performances and the hardware/software integrity are to be proven not only under normal operating conditions but also in abnormal situations.

The main objective of failure analysis tests is to check the failures detection by AFDS and the aircraft recovery, analysing failures effects on the system functions and on the aircraft motion.

Lane failures, interface failures and component failures are to be examined :

- lane failures include open and short circuit
- interface failures include power fails, hardovers and signal specific variations (failure to zero, step failure, failure to last value, ramp failure)

In addition checks on sensor data tolerance, mishandling operations and disengage characteristics are to be carried out. Rig testing is of course performed in parallel with flight trials : the need of a comparison between flight test results and real time simulation makes the permanent Closed Loop System support essential during the various phases of development and in-service.

This support extends from answering the test pilots questions to reproducing strange in-flight occurrences.

° Performance prediction and evaluation
° Interface failures effect testing
° Read across between real and simulated flights
° Training activities

The autopilot modes performance has been evaluated considering the operating mission requirements in all their complexity. This is carried out by examining in addition to the typical autopilot and aircraft dynamics parameters, also additional ones not outlined within the autopilot specification but of relevance in respect to the evaluation of the system operational effectiveness. For instance, the rapidity of certain manoeuvres e.g.: maximum bank angle achievement in heading acquisition mode or zero bank angle achievement after the desired heading has been acquired, does represent a valuable information to assess the suitability to the mission success of the various autopilot modes.

The facility has been continuously used as a valid support to the flight trials : every phoenomenum encountered in flight was examined reproducing the same conditions to discover its cause. The investigations are often let easier to be made by the possibility of obtaining dynamically transfer functions between two internal points of the system provided they are accessible.

The manual controls implemented on the Aeritalia rig system allow to drive the aircraft and so to test also flight performances.

The avionic system integration concepts which applied to the Tornado programme are still considered valid and applicable.
So, as far as the ground test activity on the rig is concerned, also for today's/future applications (like the AM-X programme) the same capabilities required and used during Tornado development phase are considered necessary.

Within the AM-X programme Aeritalia are responsible for the avionic system development and integration, therefore rig facilities must be able to adequately cover every involved equipment/subsystem area and to allow any kind of necessary/envisaged activity be performed.

Tasks to be performed are :

- testing of system/subsystem functions
- performance prediction and evaluation
- software verification and validation
- testing of failures effect
- reproduction of in-flight situations
- study and verification of corrective actions
- production of results for flight clearances
- performance of training activities

To allow the above mentioned tasks completion the facility must be provided, as previously seen, with a bench to fit actual avionic equipments as on the aircraft and with an external computing system as required by all the real time and off line functions generation.

The real time functions shall allow :

- recording on proper supports
- monitoring on displays/plotters
- dynamic stimulation
- event processing and subsequent action
- on-line commands
- generation of failures/disturbances
- simulation of the aircraft dynamics
- simulation of all the necessary non avionic items

The off line functions shall allow to replay the recorded data on proper devices and to use the various utilities (both for signals handling and for initial data generation).

In addition to the functions already required for the Tornado there is need of special interfaces allowing data transmission between the avionic bus and the external computing system.

In the AM-X case in fact also data on the MIL-STD-1553b bus are to be managed by the rig facility in addition to more conventional types of signals (analogues, discretes, synchro).
During the preparation of the avionic bench it is always very important to maintain the wiring arrangement as similar as possible to the aircraft one.

lure detection, avionic equipment stimulation and performance evaluation/verification.

The need to have interfaces dedicated to the signal transmission/acquisition of the chosen digital data bus imposes to use computer machines having particular features.

The configuration of the external computing system must be therefore conceived taking into account a lot of considerations about the various exigencies.

Considering the present computer technology it was decided to arrange a facility based on a single computer able to perform both the functions of signals handling and of simulation.

So it was necessary to search for a computer provided not only with particular features in terms of memory and speed, but also with an architecture oriented to solve real time problems and able to accept every kind of interfaces.

The basic requirements to be satisfied were :

- maximum use of commercial hardware and software products
- use of a commercial real time oriented operating system
- use of high order languages to develop the rig software
- capability of managing the MIL-STD-1553b data bus traffic
- very high performances in terms of throughput and bandwidth

The Gould-Sel 32/87 computer resulted to be the machine suitable to satisfy in the best way the various requirements.

Concluding on the rig facility, to monitor at system level the data flow on the avionic bus a serial bus analyzer needs to be provided. Some differences in the testing with respect to Tornado are inevitable because of the bus structure of the avionic system.

For example in Tornado the failure analysis was hardware oriented, while in the AM-X is mainly related to the bus data traffic management.

Typical problems are the system dead lock (i.e. a system crash without restart capability), error propagation on all the equipments of the bus after data corruption in the memory of whichever Remote Terminal.

The testing of such a structure must be considered simpler than in the previous projects due to the fact that it is possible to maintain the failure condition under control by means of the dedicated monitors and the special computer interfaces.

In this case we have to test only the software because even the hardware failures produce as primary effect the loss of the information on the bus. After the failure the system recovery with the related bus re-configuration must be verified.

However it must be noted that just for this recovery capability, that was not present in the Tornado, an absolute repetition capability is not allowed due to the fact that the phoenomena under consideration are probabilistic.

All what above implies reduction of instrumentation and interfaces with respect to similar activities on traditional problems.

Test units and test procedures can be made standard because identical functions can be tested in identical way.
The rig facility, at present under development, envisaged for the AM-X avionic system is composed by a bench allowing the installation of all the avionic equipment as in the aircraft and by a SEL computer provided with all the peripherals and interfaces necessary to cope with all data handling and reproduction requirements (see Fig. 12).

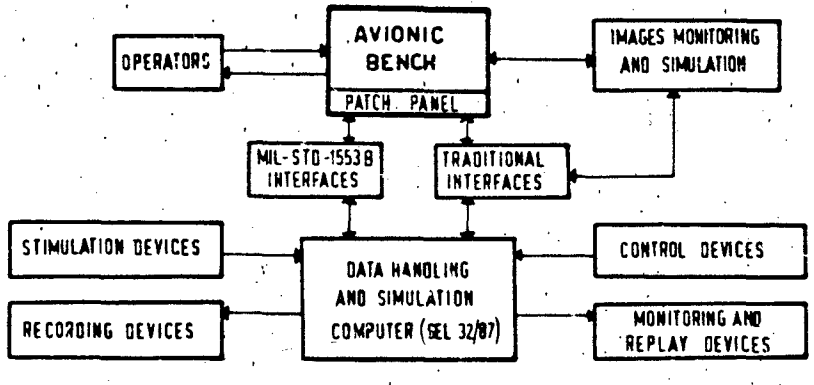

FIGURE 12
AVIONIC INTEGRATION RIG BLOCK DIAGRAM (AM-X)

First, the system had not to have development problems unresolved.

Second, close cooperation had to be maintained with the system design responsible Company (MBB) and with Customers' representative who actively participated to tests planning, data analysis, reporting and finally to flight operations by providing aircrew for those flights aiming to investigate more on system operability than on Specification compliance.

It was a nice experience indeed, requiring appropriate equilibrium between contractual rigour as Panavia partners and objectivity as part of the joint evaluation team.

We are glad to say that when compromizes had to be reached it was always after counterparts mutual agreement, though difficult to reach under some circumstances, and full evidence of problems found.

Early tests were with "clean" configured airplane i.e. no stores on pylons, to check autopilot integration with aircraft 09 equipments making also a preliminary assessment of performances before moving to extensive investigation with external stores carried.

Software implemented in the autopilot computers we got was a new standard claimed to be validated having been successfully tested during a few shakedown flights after extensive computer simulation investigation.

After looking at differences existing between new and old software standard, in-flight checks were specifically addressed to investigate those parts of the flight envelope where differences were expected to get more evidence.

One check consisted in flying the airplane at altitude/speed/wing sweep values at which the old software was limiting the maximum bank angle achievable in turn to lower angles with basic autopilot modes i.e. attitude hold, engaged.

Test evidence was achieved about failing of the autopilot to maintain the reference pitch attitude during turns because of a lack of pitch compensation signal expected to be proportional to the bank angle signal. Flight traces shown in Fig. 13 indicate a continuous pitch down from roll attitude hold engage till baro-altitude mode engage when bank angle reduces consistently with lower limit scheduled for "cruise modes" operation.

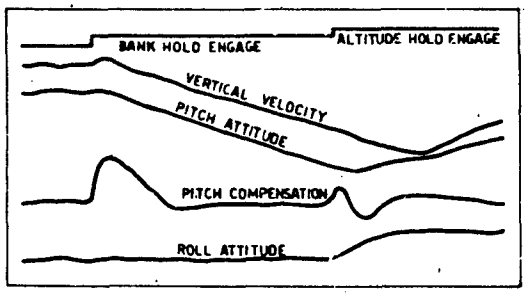

FIGURE 13 - AIRCRAFT PITCHING DOWN WITH PITCH-ROLL ATTITUDE MODES ENGAGED

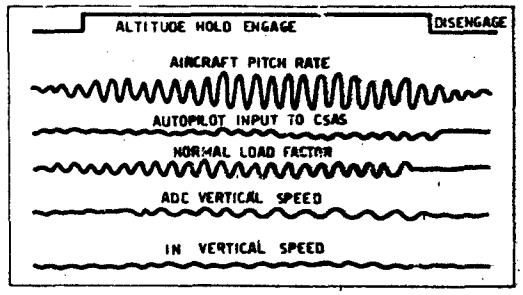

FIGURE 14 - LIMIT CYCLE WITH BARO-ALTITUDE MODE ENGAGED

Reporting was made to system design engineering and an investigation carried out taking advantage of the support consortium's avionic integration rigs could provide.

Origin of the problem, as quickly identified, was an undue limiting of the pitch compensation signal with bank angle, occurring because of a partial software modification from previous standard.

The consequence was an annoying limited capacity of the airplane to performe fully productive test flights for a certain time, software modifications taking many days, not hours, to be introduced.

Experience made had both negative and positive aspects which is worth to note having general validity i.e. not attributable to a specific team or organization.

tly increase especially when series hardware standard is used because of lower flexibility and huge paper work often required.

What aforementioned justifies worries expressed at the end of paragraph 2 about main computer software changes as required to ease in-flight data recording.

On the positive side there was :

- the quick and productive response avionic integration rigs gave in finding out mistake location.
  This advantage has been fully appreciated leading to require, as mandatory, similar support in next flight development programmes.

The basic philosophy adopted when selecting aircraft store configurations for test flying, was to keep all those which had shown some peculiarity during handling qualities and performance dedicated trials e.g. reduced stability margins or higher drag.

There was a good reason to do that because, as almost inevitably as in all projects requiring special autopilots to be developed, the system design had to be frozen before the availability of aerodynamic data set fully matched to flight data.

The most troublesome operational external stores configuration ever flown on Tornado consists of large fuel tanks underwing on inboard pylons and small stores on the outboard in addition.

Large fuel tanks cause larger than predicted longitudinal stability margin reduction at high subsonic Mach number the CSAS can barely cope to. Closing the autopilot outer loop on a marginally stable inner one we all were conscious to beware of lack of stability, due to the fact that the autopilot stability margin might have been eroded to an extent larger than expected.

Flight tests with baro-altitude mode selected indicated this was the mode actually affected by loss of stability to a level causing concern about system ability to match Specification requirements. The phenomenon observed was quiet taking about 30 sec from mode engage to get its maximum evidence and consisted of a limit cycle with $\pm$ 0.4 'g' normal load factor excursion (Fig. 14) which is too much indeed for "cruise" flying.

An agreement on the interpretation of the phenomenon found was not easy to achieve in this case.

Staying on the technical aspect of the matter both ADC and Pitot-Static system got attention because of significant discrepancies existing between IN and ADC vertical speed measurements during the oscillatory motion. Otherwise, the ADC is fed by the Pitot-Static system which closes the loop with the aircraft dynamics. Therefore, also this system was subject to investigation.

The investigation was initially conducted taking care of the nature of the problem that in principle might be twofold.
In fact, the limit cycle could be related to a lack of stability caused either by inadequacy of gain/phase margin as provided by design (when actual system components and related tolerances were used) or by components with dynamic characteristics worse than expected.

As shown in next Fig. 15 both circumstances occurred.

Airplane's inherent stability is lower than predicted flight test experience has shown.

Therefore design gain/phase margins fail to compensate being tailored to fairly better bare airplane.

Otherwise, also equipments in the loop may be contributing to further degrade the overall stability once the oscillation starts.

Next Figure 16 relates to the overall ADC/Pitot-Static system altitude error calculation based on flight data at the frequency at which the oscillation occurred. In the calculation reference is made to actual sensor altitude change as resulting from pitch motion transducers i.e. gyros and accelerometers.

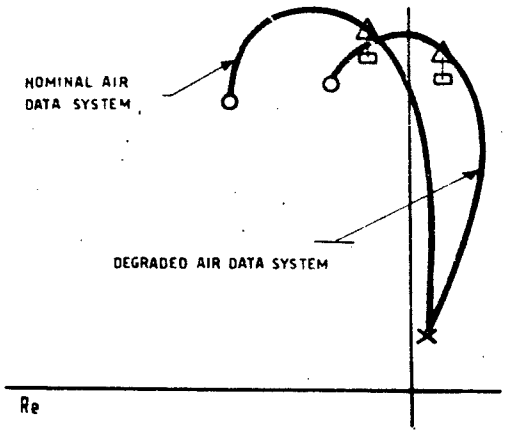

□ - AUTOPILOT NOMINAL GAIN

FIGURE 15

ROOT-LOCI SHOWING STABILITY LACK WHEN FLIGHT MATCHED AERODYNAMICS AND TOLERANCE ARE USED

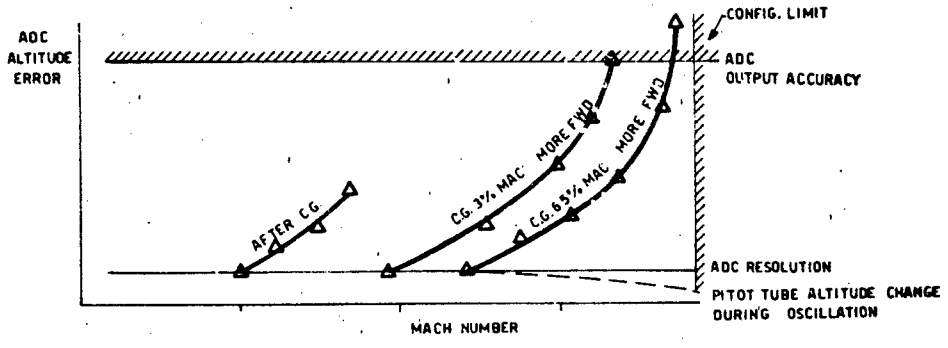

FIGURE 16

ADC/PITOT STATIC SYSTEM ALTITUDE ERROR

Data shown indicate the ADC error increases when the oscillation amplitude increases with negligible effect on it attributable to the Mach number effect.

Oscillations onset was found repeatable and depending on stability margin available i.e. manoeuvre point and centre of gravity (C.G.) relative position. By consequence, start of the oscillation could be obtained at different Mach Numbers flying different C.G.s.

Some consideration can be made on this kind of experience with a couple of recommendations:

- when evaluating autopilot performances flight test engineers must be always minded that an airplane i.e. a vehicle moving through and thanks to the air and carrying a human being, is under testing.
  If an approach has to be recommended it is more along with a handling qualities path rather than an avionic one.
  In any case a background in control systems design and technology is highly desirable.
- Conflicts between counterparts in charge of different responsibilities are almost inevitable.
  Perfect solutions are in God's hands but steps forward are easier when a minimum of background commonality exists between people approaching a given problem, though from different stand point, and use of validated tools accepted by all parties mutually agreed e.g. simulation facilities and models.

Final settlement of the dispute was made easier by the lucky circumstances of contemporary verification of what in the above recommendations.

All three are expected to get substantial benefits from previous training of flight test engineers by use of the flight simulator to get feeling about airplane, stability and control systems, autopilot dynamics.

Pilots should be asked to check first on the simulator the flight test programme proposed and flight test engineers to make their assessments in an environment which closely resembles that of the flight.

In our opinion this represents a mature approach to the flight test phase also from design engineering side who accept "foreigners" be in touch with their own "baby".

In parallel system designers should carry out their activity on the avionic rig which has capacity, ad described in para 4, either to "dialogue" with a "soft" airplane model to set up control loop gains and filters or to accept actual "bird" traces for trouble-shooting once flight testing has started.

The large number of different external store configurations AM-X is expected to fly does justify an approach to the test programme allowing to minimize the number of flight necessary.

Actual tests should be limited, as usual, to a number of key configurations with potential to provide clearances, either by analogy or because of greater criticality, to all those in the inventory the Contract claims. Despite of that the number of flights required to assess autopilot/avionics performance remains high and any further flight simulator use to reduce it is seen with benevolence.

How this goal can be achieved is barely and idea at the moment, based on the well known potential any good simulation system has to replace for specific purposes the actual airplane. Since many years ago simulators have been accepted in the training role. Time has come for Customers to accept also Specification requirements compliance demonstrations by simulation in some cases.

Autopilot performance demonstrations as part of autopilot development flying fits very well to the purpose, external world cues playing a less critical role than in other tasks.

With autopilot hardware available, airplane mathematical model matched to flight data and sensors dynamics adequately represented the simulator may represent a powerful tool to save money, its degree of representativity of the actual airplane behaviour during automated flight being very high as shown in previous para 4.

Looking forward to the oncoming activity a couple of recommendations are thought necessary.

A) The first is to write down a system performance specification fully consistent with system characteristics and phisical world.

B) The second is to make Customer's representative fully aware of the methods and evaluation criteria going to be used in flight test results analysis.

Point A) e B) contents are in tight connections and both only apparently trivial. Many specifications are written in some parts regardless of testing needs and constraints quite simply because people in charge of it has no experience in this field and often too much under pressure to look for support where this experience may be found.

In addition, specifications are written in an early phase of the programme, when equipments /systems are still on paper.

Changes almost inevitably come in, making contractual documents in some points inconsistent with hardware/software as actually provided by Contractors.

Finally, when statistical evaluation is necessary as it is for avionic equipments and autopilots as well, performance figures should always be given together with an appendix stating in full detail how the actual performance has to be derived from test data.

Autopilot performance evaluation test flights have been the last phase of a process in which participation to design, development and production were the preliminary steps. Closing the loop we got the opportunity to focus attention on simple but fundamental concepts flight test engineers should never forget :

- whatever item is tested it is on an airplane and we must know how it flies i.e. make your selves familiar with flight mechanics principles and control systems technique.

- Avionic systems technology is evolving quite rapidly.
  Also flight test instrumentation and computing facilities must evolve at the same rate to make dialogue feasible.
  Money spent may be recovered by a clever test programme conduct.

- Flight test engineers cannot longer live on the other side of the hill. Design engineers must be flanked, and where applicable, same language and tools used to ease reciprocal undestanding i.e. mathematical modelling and flight simulation.

New facilities implemented for AM-X Programme support and data bus related problems have been shortly illustrated and discussed. Much is expected in terms of faster data handling from the investment made, much is also expected in terms of knowledge enhancement about onboard data management as required to face future aircraft generation testing.

8. REFERENCES

1) AIAA-83-2744
   "Evolution in Flight Test Techniques Application at Aeritalia"
   by G.Ferretti and R.Carabelli - Aeritalia SAIpA, 10072 Caselle Torinese, Italy

2) AGARD CONFERENCE PROCEEDINGS N° 330
   "Tornado Flight Control Software Validation : Methodology and Tools"
   by R.Pelissero - Aeritalia SAIpA, 10072 Caselle Torinese, Italy

by

Alan H Roscoe
Royal Aircraft Establishment
Clapham
Bedford MK41 6AE

SUMMARY

The importance of being able to assess pilot workload in real flight is generally acknowledged by people concerned with cockpit design and operational efficiency and safety. Currently, the most used and probably most reliable methods of estimating levels of workload in flight are those based on some form of subjective reporting by experienced test pilots. But subjective opinions are susceptible to bias and to pre-conceived ideas and so the use of a second and more objective measure to augment these opinions would seem to offer distinct advantages.

This paper describes the way in which a pilot's heart rate can be recorded to support, or occasionally question, his subjective rating of workload. A small number of examples from RAE Bedford trials are presented to illustrate the technique, and a short description is given of the BAe 146 Crew Complement Certification exercise. Finally, a current flight experiment to compare heart rate levels and workload ratings in a more scientific manner is described. The rationale for using heart rate in this way is discussed briefly.

INTRODUCTION

Whether one is attempting to optimise workload levels on the flight deck of a civil airliner to improve safety, or to reduce workload in the cockpit of a combat aircraft to improve mission effectiveness, it is important to be able to assess workload in flight.

First of all in any paper devoted to assessing pilot workload it is clearly desirable to define what is meant by the term, for even a brief survey of the literature highlights the confusion that exists. Although there are several definitions they tend to be vague and to vary according to the disciplines and interests of their authors. It is possible, however, to place most of these definitions into one of two broad conceptual groups, those that are related to the demands of the flight tasks - input load, and those that are associated with the response to those demands - operator effort. Of course, there is a fundamental difference between these two groups each of which has its devotees. A confliction like this is difficult, if not impossible, to resolve and so it is not surprising that there is no general agreement on what is meant by the term pilot workload.

For the sake of completeness it is worth pointing out that a small number of people would argue for a third conceptual group containing interpretations of workload based on work results - or performance. Although it is an important attribute of workload it is suggested that performance per se should not be considered as the basis for working definitions. Nevertheless, whatever interpretation is used when assessing workload it is still essential to define and monitor performance.

Designers of aircraft cockpits and flight decks find it convenient to think of workload in terms of the task. In this way they can predict levels of workload for different flight tasks and operational situations by using data derived from various types of task and time analysis in mock-ups and simulators. (1), (2) (3). Levels or indices of theoretical workload (perhaps more appropriately termed 'task load'), usually expressed as a function of time required and time available, are extremely valuable in the design stage but, eventually, levels of actual workload will need to be assessed in real flight.

In this paper workload is considered to be related to effort - an interpretation which appears to be consistent with the views of more than 80% of professional pilots (4). It is also an interpretation that agrees well with the influence on the piloting task of such individual factors as natural ability, training and experience, physical fitness, age, and the individual response to stress. Cooper and Harper (5), in the introduction to their handling qualities rating scale, suggested a definition of pilot workload which, in a slightly modified form, seems to be most appropriate: Pilot workload is the integrated mental and physical effort required to satisfy the perceived demands of a specified flight task.

At present the most used and probably the most reliable methods for assessing workload in flight are based on some form of subjective reporting by experienced test pilots. Unfortunately, subjective opinions are susceptible to bias and pre-conceived ideas and so there are clear theoretical advantages in using more objective techniques to assess pilot workload. Among the many techniques studied are those based on measuring physiological variables; but the method of choice must be non-intrusive as well as being compatible with flight safety. Heart rate, which satisfies these criteria, is relatively simple to record and the discrete nature of the signal allows various forms of analysis to be carried out with ease. Moreover, the use of a physiological variable to assess workload fits in well with a concept that allows for the individual nature of piloting skill.

types [6], it was decided to reduce ... those flight trials where assessing workload is important.

This paper describes examples taken from a number of flight trials where this method of assessing workload has proved to be of some value

METHODOLOGY

The technique used at Bedford for recording heart rate in flight is based on the electrocardiograph (ECG). Amplified ECG signals, detected by means of two disposable electrodes applied to the pilot's chest, are recorded in analogue form on magnetic tape along with speech and various aircraft parameters. In the first instance heart rate is plotted out in beat-to-beat form together with the ECG 'R' wave - the basic signal, (Fig 6 is an example); subsequently mean rates for consecutive 30 sec epochs are plotted against time, these are found to be most useful (Fig 2 is an example). Mean heart rate values for particular flight manoeuvres, tasks, or sub-tasks may be calculated as required.

Initially pilot opinions of workload were given in a relatively unstructured descriptive manner but the need for some form of rating scale soon became obvious. After much trial and error, and with the help of numerous comments and criticisms from test pilots, a ten-point scale using the concept of spare capacity was developed (Fig 1). The overall design is based on the Cooper-Harper Handling Qualities Rating Scale (5), familiar to Bedford test pilots and sometimes used previously, though mistakenly, to rate workload (7).

The scale is not linear and probably lacks sensitivity at the lower end but is readily accepted by most pilots who have found it easy to use without the need to always refer to the decision tree. Half ratings are allowed within each decision branch and tend to be used frequently; originally it was decided not to permit the use of half ratings between the decision branches but the occasional difficulty of deciding between the last two branches, (in effect between ratings 3 and 4) was resolved by accepting a rating of 3½. Pilots seem to find it much easier to rate a flight task if it is short and well defined.

Most of the flight trials of interest from the point of view of workload have involved the take-off or the approach and landing, two tasks that are well defined and where performance can usually be monitored by on-board instrumentation and by airfield-sited kinetheodolites or radar.

Heart rates and opinion ratings indicate only relative differences in workload so that it is helpful to have some form of datum for purposes of comparison. Although it is not always possible to compare heart rate responses for different experimental variables during the same sortie, or even under similar flight conditions, the advantages of doing so are obvious.

The individual nature of heart rate responses makes it necessary, especially when dealing with small numbers of pilots, for each pilot to be considered as his own control. This restriction, together with the high cost of operating research aircraft, usually makes it impossible to obtain enough data for worthwhile statistical analysis. Nevertheless, obvious trends in heart rate changes together with pilot ratings can provide valuable and reliable indications of differences in workload levels.

EXAMPLES

The brief examples presented in this section have been selected from different flight trials to demonstrate the practical use of recording pilots' heart rates as a means of augmenting their subjective assessments of workload.

Heart rate was first recorded routinely during a series of flight trials to evaluate different types of reduced-noise landing approaches (8), (9). The first two trials used a HS 748 Andover twin turbo-prop transport to compare simple-segment steep approaches with gradients of 6°, 7½° and 9°, and, later two-segment approaches of 7½° changing to 3° at 200 ft, with conventional 3° approaches. There was generally good agreement between the project pilots' heart rates and their subjective estimates of workload; and in the case of the single-segment steep approach also with expected levels of difficulty - the workload being expected to increase with steeper approach paths and higher rates of descent. Figs 2 and 3 are examples of overall mean heart rate plots (different pilots). Interestingly, despite their relatively low heart rate responses the project pilots initially rated the workload for the two-segment approaches as high. It later transpired that these two pilots had instinctively disliked the idea of changing from a steep gradient - with the higher rate of descent - to a normal gradient at 200 ft. After their first sortie they modified their views and then consistently rated the 7½°/3° approaches as being as easy as, if not easier than, the normal 3° approaches. This example highlights the fact that subjective assessments may be biased by allowing instincts and misconceptions to influence judgement. It also illustrates the advantage of using heart rate to augment - or sometimes to question - subjective assessments of workload.

Similar heart rate responses during a later trial using a BAC VC-10 four-jet transport to evaluate 5°/3° two-segment approaches (with a transition height of 500 ft)

benefits of direct lift control (DLC) fitted to a BAC 1-11(10). Fig 5 shows overall mean rates for one of the three project pilots recorded during 3° and 6° approaches flown with and without DLC. It can be seen that the only appreciable reduction in heart rate with DLC occurred during the glide slope acquisition and early part of the 6° approaches. But glide slope performance was significantly better during all DLC approaches and all three pilots reported lower workload with DLC. Although heart rate did not appear to discriminate between the two experimental conditions, nor did it agree entirely with pilot opinion, it is worth noting that performance improved which suggests that pilots increased their effort without being aware of it.

These examples are typical of flight trials in which workload levels for different degrees of task difficulty can be compared with some forms of datum or with each other. Perhaps a well designed rating scale would have proved useful for assessing workload in these instances but where direct comparison is not possible such a scale becomes almost essential.

The final version of the Bedford rating scale was introduced during the HS Harrier ski-jump take-off trials (10). Fig 6 shows a typical beat-to-beat heart rate plot recorded during a ski-jump take-off - rated at 4. This can be compared with Fig 7 which was recorded from the same pilot during his first ski-jump take-off - rated at 6. There was good overall agreement between heart rate responses and workload ratings in demonstrating that workload levels for these ramp take-offs are no higher than those for conventional short take-offs from a runway.

During a more recent series of flights to Evaluate Economic Category 3 landings - consisting of autopilot approaches to a 50 ft or 60 ft decision height (depending on aircraft type) ending in a manual landing - pilots' heart rates and workload ratings were recorded (11). Fig 8 is of a typical heart rate plot indicating the increase in workload as decision height is neared and manual control assumed for the landing. The scatter diagram (Fig 9) illustrates graphically the relationship between 32 heart rate responses and workload ratings in real fog for the senior project pilot.

These brief accounts of in-flight workload assessment at Bedford are offered solely as examples of the way in which the technique of recording pilot's heart rates to supplement their subjective opinions has been developed and used in practice. More detailed reports of individual trials have been published elsewhere (see references).

BAe 146 WORKLOAD CERTIFICATION

A short description of the use of this technique in the certification of a new passenger transport aircraft - the British Aerospace 146 four-jet feederliner - is relevant.

Following a long, and sometimes acrimonious, debate between pilot unions on the one hand and operators and manufacturers on the other, on whether jet transport aircraft can be flown safely by two pilots President Reagan attempted to resolve the controversy by establishing a Task Force to examine the question impartially(12). The President's Task Force on Aircraft Crew Complement, which reported in July 1981, identified flight deck workload analysis and measurement as a major issue and pointed out that the only generally accepted method for evaluating workload at present is task/time-line analysis based on a comparison with previous aircraft and flight deck designs. It was suggested that this method, supplemented by improved subjective methods by suitably qualified pilots, should offer the best means for demonstrating compliance with FAA complement criteria for new aircraft (FAR 25 1523 Appendix D).

In the United Kingdom the CAA has adopted the Joint Airworthiness Requirements (JARs) which include a direct reproduction of FAA 25 1523 (as JAR 25 1523). British Aerospace elected to use a combination of techniques to assess workload in the BAe 146 - the first aircraft to be certified under JARs -during only one evaluation exercise. The basis for evaluation was a mini-airline exercise of the type already performed by Boeing - for the 757 and 767, McDonnell-Douglas - with the DC9-80, and Airbus - with the A300 FF. In late 1982 three teams of two pilots each flew consecutive three-day intensive flight schedules around a circuit of three major high intensity airfields, with crew duty hours considerably in excess of those allowed by the CAA for passenger carrying operations. Crew workload was assessed by means of subjective estimates from the pilots and flight observer (using a rating scale and post-flight questionnaire) and by recording heart rate; flight deck activity and performance - including error counts - were monitored by video cameras situated on the flight deck.

Heart rate was recorded continuously from before pre-start checks to after shut-down checks. Isolation pre-amplifiers situated on the cockpit floor fed the ECG signal, as pulses, to a Hewlett Packard 9826A computer. Heart rate in beat-to-beat format was displayed in real time on the computer's in-built CRT and then plotted out by a HP 2763 graphic printer. Each plot - or frame - was for 300 sec of heart rate plus a 60 sec plot in a negative direction, ie from the previous frame. Fig 10 shows a typical frame (recorded during a take-off from Amsterdam).

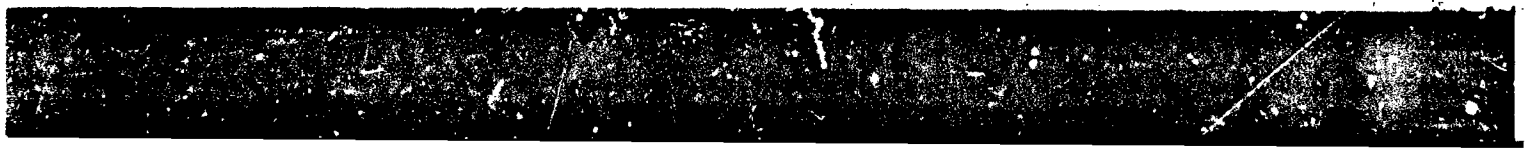

determined plan - on the heart rate plot (fig 10). Pilots were instructed in the use of the rating scale before the exercise started and, in particular, were asked to consider the load during the previous 30 sec. Ratings were requested frequently during high workload phases of flight such as the take-off and departure, the approach and landing, and when simulated in-flight failure occurred; during the cruise ratings were requested less frequently.

As the main reason for recording heart rate was to augment subjective assessments of workload, mean rates for the 30 sec proceeding each set of ratings were calculated and then collated with those ratings. Results for the high workload phases were of particular interest; fig 11 shows plots of heart rate (30 sec) and of ratings from a handling pilot and from a flight observer recorded during a take-off and departure from Hatfield (A) and during an approach and landing at Amsterdam (B).

Overall there was reasonably good agreement between heart rates and workload ratings, but there were a number of exceptions which were probably due partly to inexperience with the rating scale and partly to rating the instantaneous level of workload rather than the level experienced during the previous 30 seconds. For example, whereas fig 10 shows quite good agreement fig 11 shows some disagreement between the two different pilot's heart rates and their ratings recorded during a take-off and departure at Amsterdam (A) and an approach and landing at London (B); it is interesting that the flight observers' ratings showed better agreement with the pilot's heart rates.

In addition to relating heart rate with subjective ratings each beat-to-beat plot was examined for unduly high heart rates that may have suggested inappropriately high levels of workload; for rapid changes in rate indicating sudden changes in workload; and, in the absence of changes in overall rate, for suppression of heart rate variability consistent with increased mental load.

RELATIONSHIP BETWEEN HEART RATES AND WORKLOAD RATINGS

The use of heart rate to augment pilot's subjective opinions of workload prompts the question: how good is the relationship between the two measures? It is a question that should really have been examined in more detail some years ago, but now, after previous plans failed to materialise, a more scientific study is underway at Bedford. The experiment involves four short but well defined flight tasks, (generating theoretically markedly different levels of difficulty) being flown in a BAe 125 twin-jet 'business' aircraft by several pilots. The sequence of tasks - to be flown within laid down performance limits - consists of :

1 A 360° turn in 2 min at constant altitude, IAS, and rate of turn.

2 A 360° turn in 2 min with a simultaneous loss of 2000 ft in altitude at a constant IAS and rate of turn.

3 A 360° turn in 2 min with a simultaneous 2000 ft altitude loss followed by a reverse 360° turn in 2 min with a simultaneous gain of 2000 ft at a constant IAS and rate of turn.

4 A 360° turn in 2 min with a simultaneous altitude loss of 2000 ft and speed reduction of 100 kts.

The subject pilot's heart rate is monitored throughout and he is also asked to rate each task, or if he desires each sub-task, using the ten-point workload rating scale referred to earlier (Fig 1).

It was originally intended that the experiment would follow a design based on the Latin square with each pilot flying the sequence four times in different order. In practice, partly because the aeroplane is available only on an 'opportunity' basis and partly because more pilots have offered to participate, the sequence is now flown in the most convenient order at the time; but with the first task to be flown being repeated at the end of the sequence.

Performance was measured during the first few flights but as it became clear that pilots were striving to achieve there best performance anyway, and as it was proving difficult to apply error scores to heart rates and ratings, subsequent sequences have not been measured.

All subject pilots are highly experienced but those not current on the aeroplane are given at least 30 mins familiarisation before being asked to rate the tasks; similarly, pilots unfamiliar with the rating scale are given a full briefing beforehand.

Todate 11 pilots have flown a total of 14 sequences and results show an extremely good relationship between their mean heart rates and their workload ratings for 5 pilots, reasonably good agreement for another, and no agreement at all for one pilot. This latter finding is in accord with previous observations on individual responses that occasionally a pilot's heart rate, whilst responding qualitatively with expected changes in workload,

There is now substantial evidence to suggest that during normal but demanding flight heart rate responses in experienced pilots are determined almost entirely by their workload, so it is interesting to speculate on the neuro-physiological mechanisms that are likely to be involved. Rarely is the heart rate change due to the influence of physical activity or to environmental stressors which in normal flight are quite low, although higher rates recorded from pilots in the manual control loop suggest that increased neuro-muscular activity of some form may play a part.

Piloting an aeroplane, especially during the more difficult manoeuvres, requires the brain to collect, filter and process information quickly, to exercise judgement and make decisions, and to initiate rapid and appropriate actions. This neurological activity - which must have been essential for the survival of primitive man - is associated with a state of preparedness sometimes known as arousal. Furthermore, there is experimental evidence that increased arousal, up to a moderate level, enhances a person's capacity for complex skills
and thus improves performance (13). It has been suggested by several people that the relationship between performance and arousal can be described by an inverted 'U'-shaped curve - though there is only meagre evidence in support (14). Nevertheless, a theoretical relationship of this type has a particular attraction in the context of flying as there is evidence that both under- and over-arousal have preceded landing accidents where performance was clearly below an acceptable level.

There is also some experimental evidence that a similar inverted 'U'-shaped function describes the relationship between performance and task demands (15); and it has been suggested that levels of arousal are determined by task characteristics or demands, by how the individual perceives the situation, and by how he responds to his environment (16). So one can speculate that a pilot is more likely to produce an adequate - if not optimum - level of performance by matching his level of arousal to the perceived difficulty of the flight task. The result will depend largely on his training and experience although if the task is a novel one, as happens often in test flying, a significant element of empiricism must be involved. Of course, the level of arousal should be high enough for the task itself and also high enough to allow for the unexpected; for example, an engine failure on take-off may require extremely rapid and appropriate actions.

On occasions at Bedford, it has been obvious from the sudden increase in heart rate after the start of a manoeuvre that a pilot had failed to anticipate the difficulties of the task and 'set' his arousal accordingly. Conversely, high heart rates have been recorded when there was an element of uncertainty about the task; this was particularly noticeable for the novel 'ski-jump' take-offs and for a pilot's first approach and manual landing in fog. At such times there has been a tendency for heart rate levels to disagree occasionally with workload ratings.

Support for these speculations is provided by experimental evidence showing that appropriate pathways in the brain and central nervous system do exist. The concept of arousal is an oversimplification of complex neuro-physiological mechanisms but it is functional and, providing it is not confused with emotion, it explains the relationship between a pilot's workload and his heart rate in a convenient manner.

The use of physiological variables to indicate levels of workload has been viewed with suspicion by many people and the use of only one variable - such as heart rate - has been criticised in particular. However, many of these criticisms have been based on the results of laboratory and flight simulator experiments where quite often the task and the levels of workload were unrealisitic.

It can be argued that in using heart rate to augment pilots' subjective ratings two variables are being used; but it is questionable whether they are really separate measures - the relationship, already discussed, between perceived difficulty of the task, arousal, and heart rate precluding true independence; although, as the actual neurological mechanisms are uncertain the possibility of conscious unawareness must exist.

Heart rate and subjective ratings are relatively coarse measures - a fact which is often criticised by scientists accustomed to using more precise measuring techniques. But when one considers the individual variations in the different aspects of skill between pilots, and even within the same pilot from time to time, the search for minor differences in workload may be unrealistic in real-world conditions. It is also worth noting that expected differences in workload may be more theoretical than real and so before deciding whether heart rate or subjective ratings can differentiate between workload levels it is important to be sure that there is in fact a real difference (10).

Experience at Bedford has shown that when a pilot is in the control loop, or is expecting to enter the loop, and when the flight task is reasonably demanding, heart rate will usually identify meaningful changes or differences in workload. When the task is relatively undemanding or when the pilot is in a purely monitoring role, as happens frequently in the new generation of civil transport aircraft, heart rate alone may not discriminate between small differences in workload - although subjective ratings may well do so. Assessment of cognitive activity of this type is more difficult but often, in

Monitoring heart rate during flight seems to be readily accepted by pilots; Bedford test pilots have co-operated to the extent of applying their own electrodes and preparing recording equipment for flight on many occasions. The heart rate data are often studied with interest by the pilots who find their results helpful in recalling various aspects of the sortie.

In its final form the workload rating scale has been generally welcomed by pilots who find it relatively easy to use in practice - even, surprisingly, after the briefest of introductions. Recently the rating scale has been used quite effectively to assess workload on the Boeing 737 by airline pilots unfamiliar with the technique. These favourable observations are probably due to the use of a definition of workload accepted by pilots and to basing the scale on the idea of spare capacity.

The experiment to examine the relationship between heart rates and workload ratings has so far produced some encouraging results. The reasons for the poor agreement for one pilot in this series, and a small number of pilots during flight trials, are not known. Are the heart rate responses at fault? or are the subjective assessments unreliable? At times some pilots tend to give a rating of the instantaneous workload when asked rather than to consider the workload level over the previous period or task. A pilot may misinterpret the demands of the task - this is a recognised cause of aircraft accidents; or perhaps the physiological mechanisms involved in tuning the arousal level are at fault.

In the BAe 146 certification exercise there was a reasonable level of agreement between heart rates and ratings but inconsistencies and anomalies did occur, although neither ratings nor heart rate levels suggested unusually high workload. In this trial and in others anomalies and inconsistencies in heart rate responses and workload ratings have been resolved by discussion with the pilots and re-analysis of the data in most instances. For example, several inconsistencies could be traced to rating instantaneous workload rather than that for the previous 30 sec. It was interesting to note that on several occasions a flight observer's ratings agreed more closely with the pilot's heart rate than did his own ratings (fig 11).

Such observations underline the need to use at least three pilots when assessing workload.

CONCLUSIONS

So far evidence supports strongly the use of the methodology described above in the practical assessment of workload in flight; but experience has underlined the need for the following points to be born in mind:

it is important to use a well designed rating scale which is easy to use and fully understood by pilots;

such ratings are increased in value by recording the pilot's heart rate;

heart rate responses are idiosyncratic and so each pilot should be used as his own control;

to a large extent the same applies to subjective ratings;

neither heart rate responses nor ratings are absolute measures of workload.

In the long term a more sophisticated, reliable and sensitive measure of workload may be developed, but it is suggested that for the time being the use of a techinque based on the one described in this paper is worth contemplating.

AFFTC-TR-82-5 254-274 1982.

2 E L Brown, G Stone, W E Pearce. Improved Cockpits Through Flight Crew Workload Measurement. Paper presented to Second Advanced Aircrew Display Symposium. Naval Air Test Centre Patuxent River 1975.

3 R T White. Task Analysis Methods. A Review of Development Techniques for Analysing Mental Workload in Multiple-task Situations. McDonnell Douglas Corporation Report No MDC J 5291 1971.

4 G A Ellis, A H Roscoe. The Airline Pilot's View of Flight Deck Workload: A Preliminary Study Using a Questionnaire. Royal Aircraft Establishment Technical Memorandum FS(B) 455 1982.

5 G E Cooper, R P Harper. The Use of Pilot Rating in the Evaluation of Aircraft Handling Qualities. NASA Technical Note 5153 Washington DC 1969.

6 A H Roscoe. Use of Pilot Heart Rate Measurement in Flight Evaluation. Aviat Space Environ. Med 47 86-90 1976.

7 G A Ellis. Subjective Assessment Pilot Opinion Measurements. In: Assessing Pilot Workload Ed. Roscoe A H. AGARDograph AG-233 AGARD Paris 1978.

8 A H Roscoe. Heart Rate Monitoring of Pilots During Steep Gradient Approaches. Aviat. Space Environ. Med 46 1410-1415 1975.

9 A H Roscoe. Pilot Workload During Steep Gradient Approaches In: Conference Proceedings No 212 Aircraft Operational Experience and its Impact on Safety and Survivability. AGARD Paris 1976.

10 A H Roscoe. Handling Qualities, Workload, and Heart Rate In: Survey of Methods to Assess Workload Eds. B O Hartman and R E McKenzie. AGARDograph No 246 AGARD Paris 1979.

11 A H Roscoe. Pilot Workload and Economic Category 3 Landings In: Conference Preprints. Aerospace Medical Association Annual Scientific Meeting 1980.

12 J L McLucas, P J Drinkwater, H W Leak. Report of the President's Task Force on Aircraft Crew Complement. Washington DC 1981.

13 E Duffy. Activation and Behaviour. J Wiley and Sons New York 1962.

14 A T Welford. Arousal, Channel Capacity and Decision. Nature 194 365-366 1962.

15 A T Welford. Stress and Performance. Ergonomics 16 567-580 1973.

16 D Kahneman. Attention and Effort. Prentice-Hall Inc Englewood Cliffe 1973.

17 H J G Zwaga. Psycholphysiological Reaction to Mental Tasks - Effort or Stress. Ergonomics 16 61-67 1973.

PILOT WORKLOAD RATING SCALE
(for a specified piloting task)

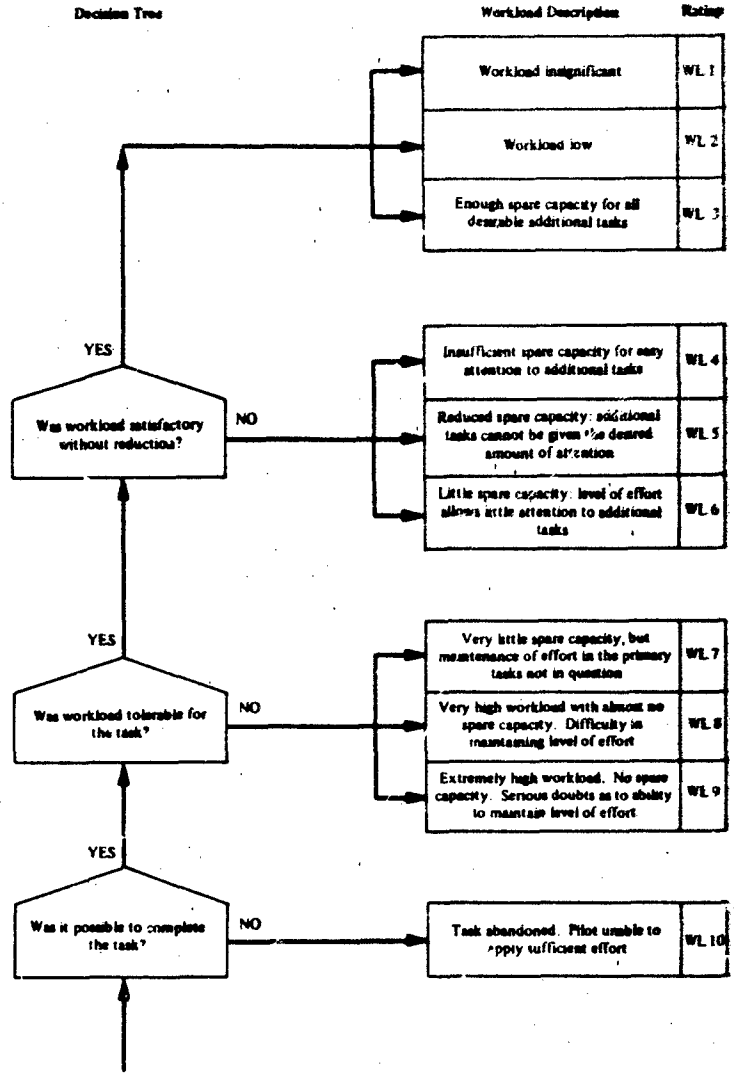

Fig 1 Pilot Workload Rating Scale

The pilot starts his decision-making process at the bottom left corner of the 'decision tree'.

The workload being assessed is that involved inthe execution of the primary task. The pilot will almost certainly be performing additional tasks, but the effort expended on them must be included as part of his spare capacity.

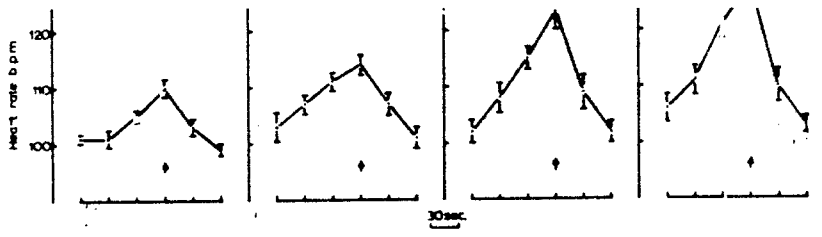

Fig 2 Overall mean 30 sec heart rates (±SEM) for four statistically designed sorties of single-segment experimental noise abatement approaches in an HS 748 Andover - one pilot. The arrows indicate the epochs centred on the touchdown.

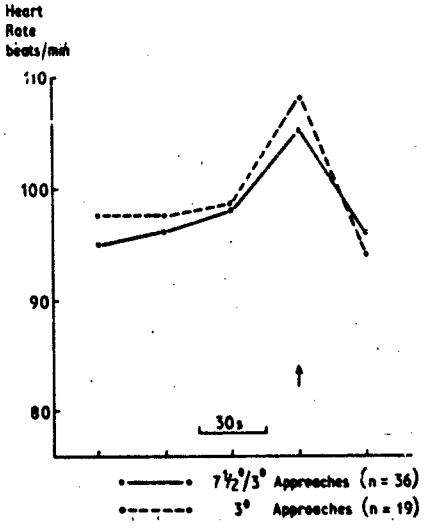

Fig 3 Overall mean 30 sec heart rates for 7½°/3° two-segment approaches and for conventional 3° approaches in an HS 748 Andover - one pilot. The arrow indicates the touchdown epoch.

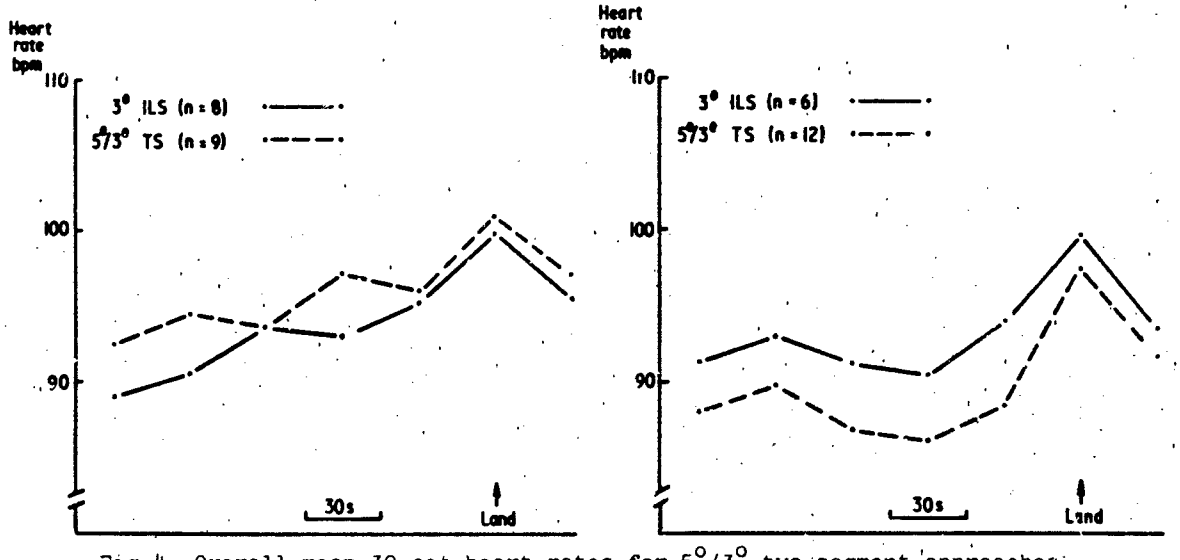

Fig 4 Overall mean 30 sec heart rates for 5°/3° two-segment approaches and for conventional 3° approaches in a VC-10 - two pilots. The arrows indicate the touchdown epoch.

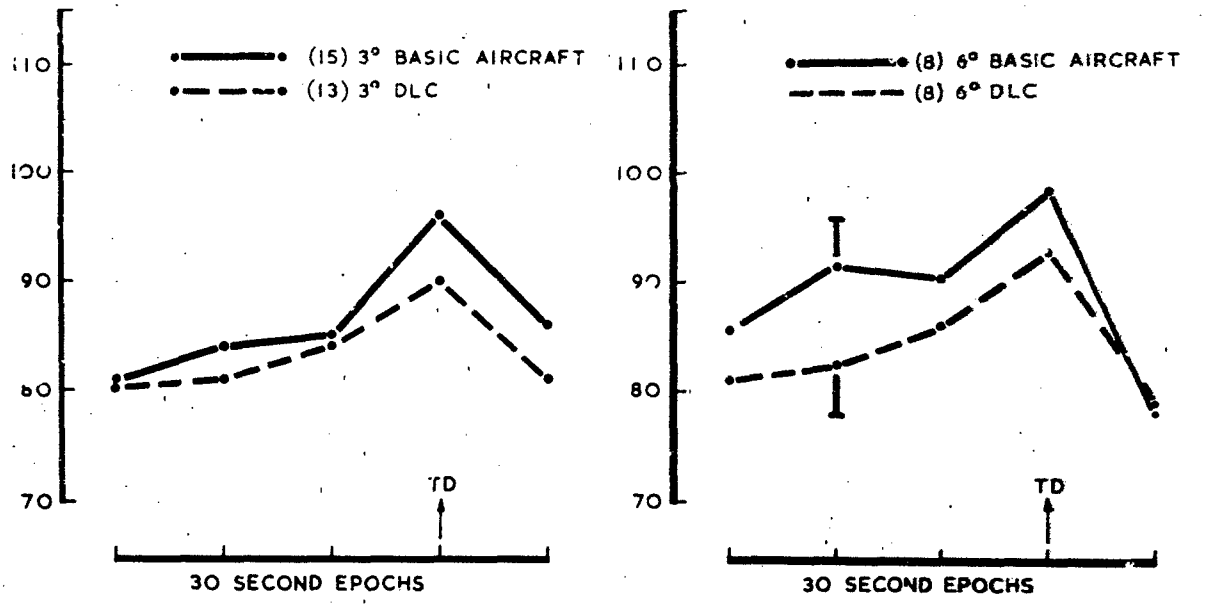

Fig 5 Overall mean 30 sec heart rates for 3° and 6° approaches and landings flown with and without DLC in a BAC 1-11 - one pilot.

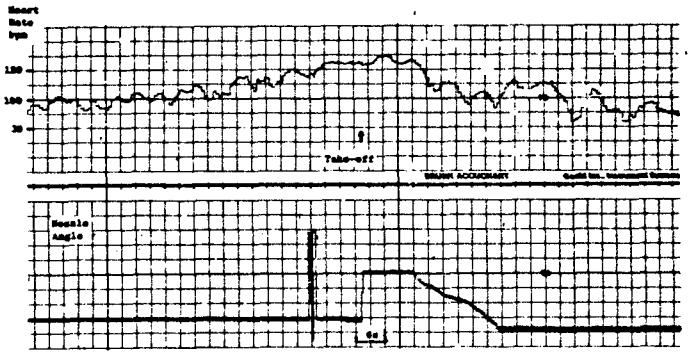

Fig 6 Typical beat-to-beat heart rate and nozzle angle traces recorded during a ski-jump take-off in an HS Harrier. (Note the rapid downwards rotation of engine thrust (upwards in the trace) as the aircraft left the ramp (arrow) followed by the gradual rearwards rotation (downwards in the trace) as speed was increased.)

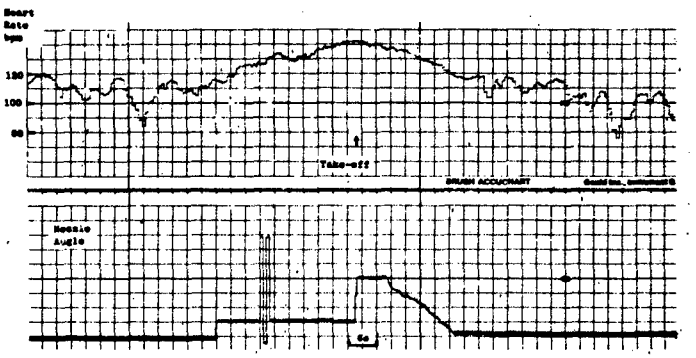

Fig 7 Beat-to-beat heart rate and nozzle angle recorded during the first ski-jump take-off by this pilot - the same pilot as in Fig 6.

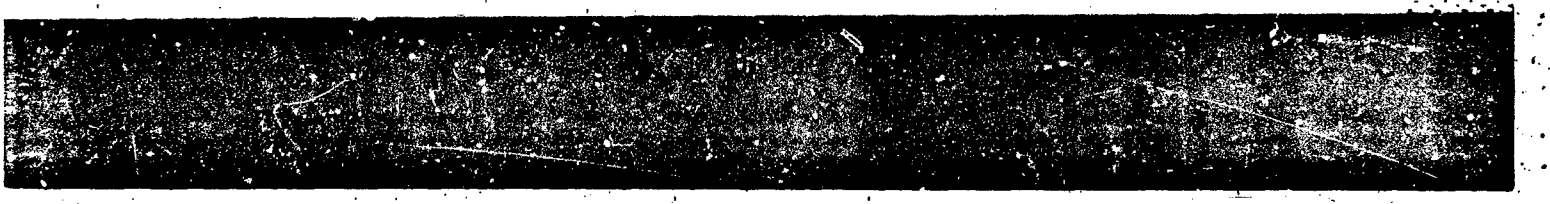

Fig 8 Typical beat-to-beat heart rates (P1 and P2) recorded during an autopilot approach and manual landing in fog (RVR 200 m) BAC 1-11.

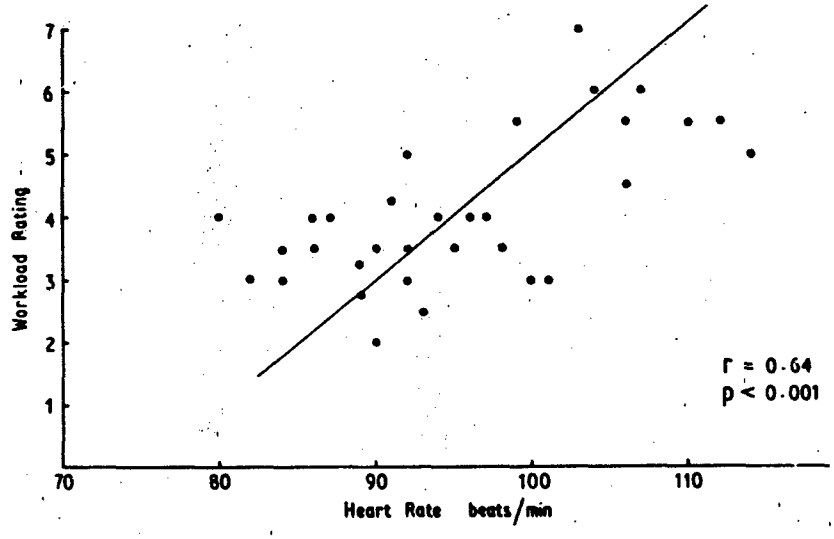

Fig 9 One pilot's heart rate responses and workload ratings for manual landings in fog.

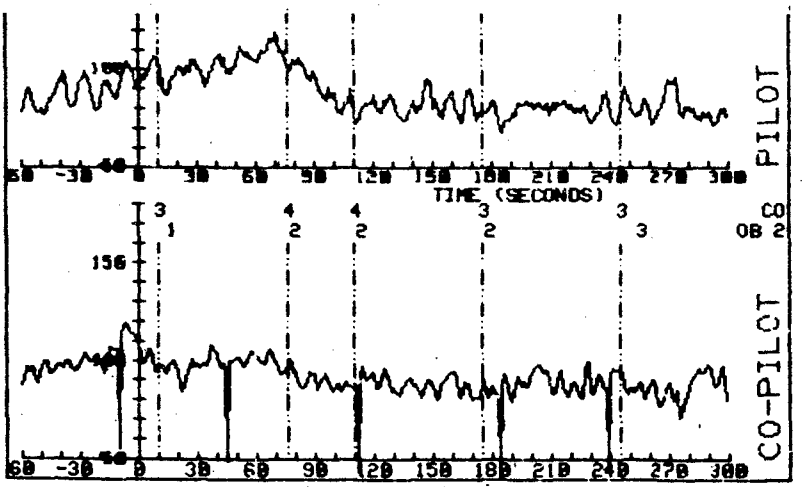

Fig 10 Example of beat-to-beat heart rate plots and workload ratings from the BAe 146 certification programme. (Recorded during a take-off from Amsterdam.)

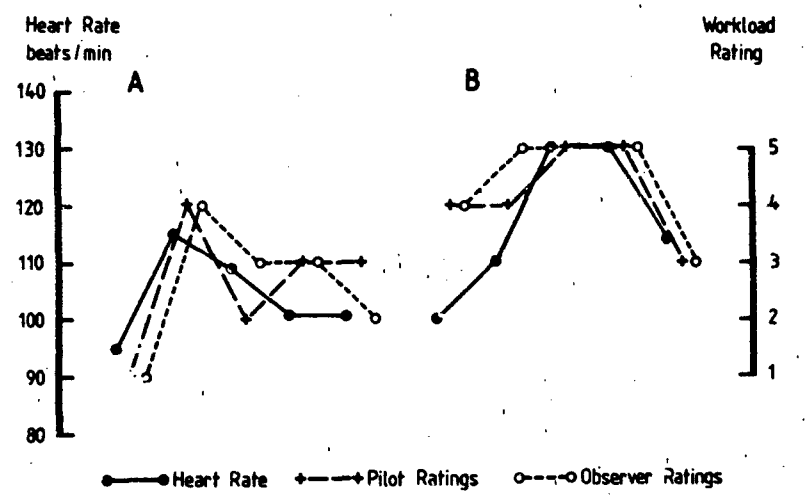

Fig 11 Plots of man heart rate responses (30 sec) and of workload ratings from the handling pilot and flight observer - BAE 146.
A - Take-off and departure from Hatfield.
B - Approach and landing at Amsterdam.

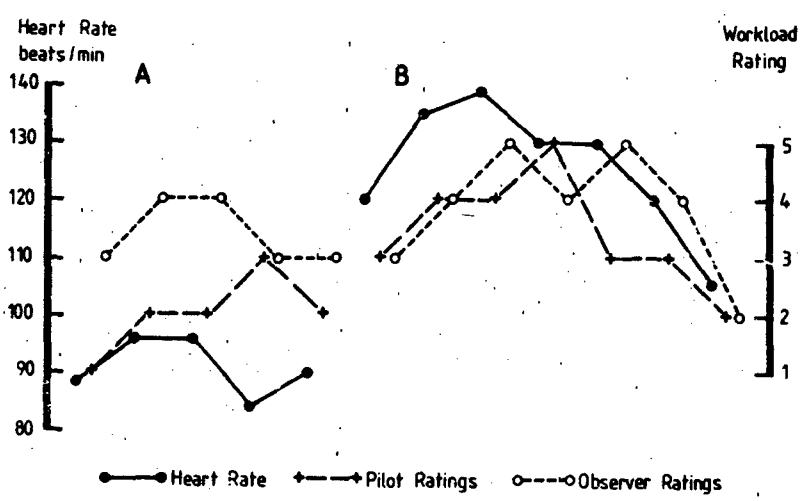

Fig 12 Plots of mean heart rate responses (30 sec) and of workload ratings from the handling pilot and flight observer - BAe 146.
A - Take-off and departure from Amsterdam.
B - Approach and landing at London.

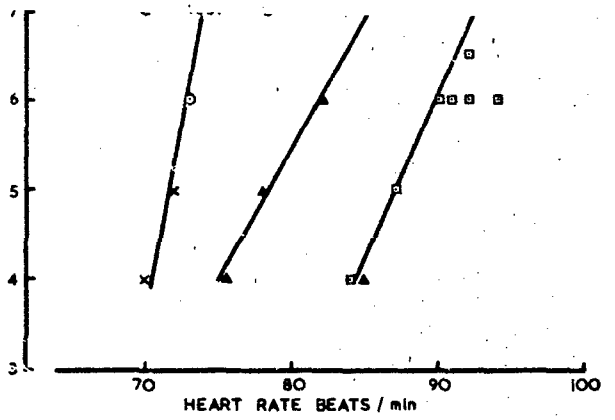

Fig 13 Heart rate responses and workload ratings for four pilots. HS 125.

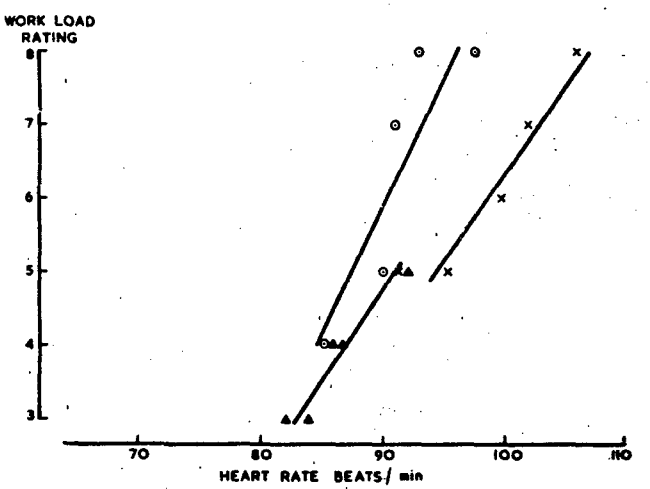

Fig 14 Heart rate responses and workload ratings for three pilots. HS 125.

Systems Engineering Test Directorate
Naval Air Test Center
Patuxent River, Maryland 20670

SUMMARY:

In this paper I will show how the judicious use of simulation in support of flight test can be used to leverage the flight test available in many programs to more adequately cover the complex test requirements of modern systems. The simulation facility I will describe is designed around the multiplex data bus structure found in all modern U.S. aircraft. This architecture makes the simulation problem easier but is not a necessary condition for the application of these techniques to support flight test. However, for non-multiplex bus systems the simulation is by nature more single purpose and the difficulty in changing the simulation facility from one aircraft type to another is greatly increased. We at the Naval Air Test Center are committed to the use of simulation to support the flight test requirements for all current and future Navy aircraft. We use the facility today to support F/A-18 and AV-8B avionics system testing. The facility is being expanded to also support flight system and flight control computer testing for the F/A-18, AV-8B, F-4S, F-14, and X-29 aircraft. It is our opinion that the use of simulation to supplement flight test offers the only hope for being able to adequately test todays highly complex and highly integrated weapons systems within the level of test assets expected to be available in future programs.

BACKGROUND:

At the Naval Air Test Center we are responsible for the Test and Evaluation (T&E) of new Naval aircraft. This includes testing of both the airframe, engine, and flying qualities, and the integrated airborne weapons system. As technology has advanced over the past decade, especially in aircraft weapons systems, we shared the same problem that plague T&E communities throughout the world. Namely, how to adequately test these increasingly complex systems within the constraints imposed by program schedules and asset availability.

This problem became critical with the advent of the new, U.S. Navy, F/A-18 fighter attack aircraft. This aircraft, designed by the McDonnell Aircraft Corporation, is intended to perform both the fighter and light attack missions of the U.S. Navy through the 1990's. It also represents a quantum increase in system complexity over previous tactical Naval aircraft. This increase in complexity is a direct result of the aplication of advances in digital system technology to the design of the F/A-18 weapons system. The aircraft system is designed around a federated collection of independent processing elements connected over three separate MIL-STD-1553 multiplex data buses (Figure 1). Each of these processing elements contains substantial software or firmware. When viewed as a single system, this large collection of software and firmware represents a complexity level that far exceeds that of previous tactical Naval aircraft.

The dilemma we faced in testing the F/A-18 was how to adequately test this complexity within the constraints imposed on us by the realities of the program. Figure 2 qualitatively gives a historical presentation of this problem. If the amount of software in a system and thus the complexity is used as a metric against which to judge test requirements for a particular system, then the historical increases in system complexity have been matched by corresponding increases in the testing required to adequately test and evaluate these systems. At the same time, the individual test requirements, as well as the cost of consumables necessary to perform a test, have increased individual test costs. The result, as figure 2 shows, is a rapid escallation in the total resources necessary to adequately test a modern weapons system using conventional flight test techniques. At the same time, normal program and fiscal constraints have held the assets available to a typical test program relatively constant over time. The result is an increasing gap between the amount of conventional testing required to adequately characterize a system and the test assets actually available. Without alternate test approaches to fill this gap, systems that have not been completely tested will be introduced into operation and hidden inadequacies will be discovered when they can least afford to be, during operational use.

We recognized this problem at the advent of the F/A-18 program and found what has come to be an increasingly common solution. Namely, the use of simulation in support of flight test to fill this gap between test requirements and test asset availability. The idea is to apply system simulation techniques to increase the amount of valid test data obtained from a given amount of flight testing. The strategy is to use conventional flight test to validate the results of a simulation at a particular point in the aircraft weapon envelope. Then to use the simulation to determine the performance of a particular system throughout its total operational envelope. If questionable

In addition, the use of the simulation allows the tester to concentrate available flight testing in portions of the operational envelope where problems are expected rather than first having to use flight test to discover these problem areas.

THE SIMULATION SYSTEM

Once we had decided on the need to provide some type of simulation support for the F/A-18 weapons system test program we were faced with the problem of designing a system to supply this support. Our design, which resulted in a facility called the Tactical Avionics and Software Test and Evaluation Facility (TASTEF), was based on the architecture of the F/A-18 system. We recognized this system, the first of a number of Navy systems to be based on the MIL-STD-1553 data bus, was a precursor of future weapons systems designs. As a result we designed a simulation system that was compatible with not only the specific F/A-18 weapons system but that would also be compatible with the whole new generation of multiplex bus oriented aircraft systems

The basic design philosophy is shown in figures 3a and 3b. Any MIL-STD-1553 bus oriented system can be represented by a simplified block diagram similar to that shown in figure 3a. The system consists of a single bus controller, in this case the Fire Control Computer (FCC), which communicates over the MIL-STD-1553 bus with a number of remote terminals which are the other elements in the weapons system. Our approach was to use standard, general purpose, computers, along with specially designed interface hardware, to simulate this system in a very general way. Figure 3b shows how this can be done for the simplified system shown in figure 3a. In this example the FCC is assumed to be both the primary weapons system computer as well as the MIL-STD-1553 bus controller. The general purpose computers are connected to the MIL-STD-1553 bus through specially designed interfaces. The computers are also provided a data sharing path between each other through a multiport memory system. This multiport memory system provides a single physical segment of memory that simultaneously appears to be logically local to each of the processors in the facility. It also provides an interrupt capability between processors in the facility that can be used to control the timing and execution of the simulation. One more element is required to complete the facility. This is a multiprocessor executive program used to synchronize and control the execution of the simulation processors.

With this hardware and executive software in place the facility can be used to simulate virtually any MIL-STD-1553 bus oriented system. The simplified diagram of the system, shown in figure 3b, illustrates how this is done for a typical aircraft weapons system. Each of the avionics subsystems in the aircraft is modeled in software in the general purpose computers. In addition, the actual aircraft Fire Control Program (FCP) is loaded in the avionics FCC in the facility. When the FCP is running, the only connection between the FCC and the aircraft is through the MIL-STD-1553 data bus. The models of the aircraft avionics subsystems in the simulation computers are designed to provide responses to the FCC computer over the MIL-STD-1553 bus that are identical to those in the real aircraft. As a result, once the FCC and the avionics subsystem models are running, the data environment the FCC experiences is identical to that in the real aircraft during flight. One other class of simulation software is required to supply the avionics subsystem models with the other environmental data required by the FCC. This class includes models of the airframe dynamics, the atmosphere, the earth, and any other external data required by the simulation such as target models and communication data link models.

In operation the system is very simple. The environmental models calculate the state of the simulation including all the environmental data required by the sensor models. The sensor models use this environmental data to develop the various responses required by the FCC computer during the next computation cycle. The interfaces between the simulation computers and the MIL-STD-1553 buses are used by the avionics subsystem models to transfer these data, in the proper format, on command to the FCC. An example of how the FCC obtains and places information on the aircraft Head Up Display (HUD) will illustrate this operation. First, the aircraft and atmosphere models calculate the dynamic and static pressure currently experienced by the aircraft. These values are placed in the multiport memory for use by the avionics subsystem models in the simulation. In this example the Air Data Computer (ADC) model takes these values and reformats them for transmission to the FCC. These values are transmitted to the FCC when, acting as the bus controller, the FCC requests the particular MIL-STD-1553 message from the ADC containing this information. Once the FCC receives these data from the ADC model it can compute the aircraft airspeed. When the computation is complete the FCC transmits special messages to the model simulating the controls and displays subsystem of the aircraft to command the display system to draw the proper airspeed information on the HUD. The key point is that all the data on the MIL-STD-1553 data bus is identical in all respects to that the FCC would see during actual flight operations. Since the MIL-STD-1553 data path is the only connection between the FCC and the real aircraft and since the data on this bus is identical in the simulation to that in an aircraft in flight the FCC is effectively fooled into thinking it is in flight. As a result the computational performance of the FCC in the simulation is identical to its computational performance during flight. Thus, tests performed on the FCC software in the simulation accurately reflect the in flight performance of the system and can be used to supplement flight test data.

software in the airplane. The process of insuring the simulation accurately reflects the true aircraft performance is referred to as validation. In the type of simulation I have described, the validation effort is minimized by the structured nature of the simulation. The only interfaces that have to be validated are the data paths between the avionics subsystem models and the FCC. The limited amount of data passed between these systems makes this a simpler task than it might appear on the surface. In the case of the F/A-18, the contractor had developed a multiplex bus list that completely defined all the data messages between the FCC and the various avionics systems in the aircraft. In developing the simulations of the avionics subsystems this list of the bus messages was used to define the MIL-STD-1553 input/output structure of each of the models. This helped to guarantee the models in the simulation would accurately reflect the performance of the aircraft hardware. There was, however, one final test required to complete the validation of the simulation. In this test the performance of the weapons system was measured during flight test. A duplicate test was then performed in the simulation and the performance of the simulated system was also measured. The simulation was considered validated when the performance and operation of the simulation matched the performance and operation of the actual aircraft.

The simulation architecture shown in figure 3b is considerably simpler than the architecture of the F/A-18 avionics system shown in figure 2. This difference in complexity, however, is completely accomodated within the general simulation architecture I have described. In the actual F/A-18 simulation all three MIL-STD-1553 buses were present along with both of the FCC's from the airplane. Figure 4 shows a wiring diagram of the facility configured for F/A-18 testing. As you will note this is an exact analog of the actual aircraft system architecture shown in figure 2. The F/A-18 multiplex bus data information, obtained from the prime contractor, was used in the development of all the avionics subsystem models. In addition, after the simulation was complete and running, the operation of the simulation in a number of conditions was compared with the operation of the aircraft in flight to validate the simulation.

TYPES OF TESTS PERFORMED

The types of tests which can be performed using a simulation similar to the one I have just described are even more varied than those which can be performed on the aircraft itself. They can, however, be broken into two general classes. The first are tests on the software contained in the FCC. In this case the only actual hardware required in the simulation are the FCC's. Models of the remainder of the avionics subsystems are used to provide data to the FCC on the MIL-STD-1553 multiplex bus. The simulation, under computer control, flys the simulated weapons system through a number of flight scenarios and measures the performance of the FCC software in each of these scenarios. I will describe more of these tests in detail and how they are performed in the next section.

The second class of tests involves testing the software, and in some cases the hardware, operation of avionics other than the FCC. In this type of testing, the model of a particular piece of avionics is replaced by the actual equipment. In the simulation the interface between the avionics models and the MIL-STD-1553 data bus is identical to the real hardware. As a result the only actions necessary to include real hardware in the simulation are to terminate the model of the hardware and plug the actual equipment into the MIL-STD-1553 bus in the facility. The only problem is that any equipment included in the facility in this way must also be provided simulated external stimuli that replicate those it would sense while installed in the aircraft. An example of a system that can be provided reasonable stimuli of this type is the Stores Management Set (SMS) in the F/A-18. The SMS is the weapons release and control system for the F/A-18. In addition to the MIL-STD-1553 data bus, it only connects to the weapons release and weapons control systems in the airplane. The computational requirement necessary to simulate these external systems and provide the correct stimuli to the SMS are rather modest and well within the state-of-the-art. This is in contrast to the F/A-18 radar hardware which could also be easily connected to the simulation but which would require very extensive and expensive advances in the state-of-the-art in stimulation equipment to provide an electromagnetic environment that completely replicated flight conditions.

FIRE CONTROL COMPUTER SOFTWARE TESTING

In this section I will describe a number of the tests that have been performed on the F/A-18 FCC software in the TASTEP. I will first give a relatively detailed example of how a particular series of tests, air-to-ground ballistic accuracy and sensitivities, were performed. In the remainder of the section I will present a series of shorter descriptions of other types of tests performed in a similar manner.

The F/A-18, as most modern attack aircraft, has a number of automatic and semi-automatic air-to-ground weapon delivery modes. A typical test performed on this type of system is to evaluate its accuracy. This evaluation can be obtained from flight test by delivering a statistically significant sample of weapons at a target in a particular release condition and recording the distance between each weapon impact point and the aircraft aim point. The result of this series of tests is an estimate of the weapons system accuracy for the particular weapon used at the particular flight

A simulation, such as the one described in the first part of this paper, can be used to extrapolate a relatively small amount of flight test weapon system performance data to estimate the performance of the weapon delivery system over the entire delivery envelope for all weapons carried on the aircraft. The first step in this process is to obtain flight test data that records the performance of the weapon delivery system for a particular weapon and delivery condition. The next step is to obtain similar data from the simulation for the same weapon at exactly the same weapon release condition. The simulation is validated by comparing these two sets of data and making sure they are the same within the measurement accuracy of the flight test data. This validation process may, and often will, involve modifications and corrections to the simulation and simulation models to make them more completely representative of the actual hardware.

The validated simulation is used to expand the system accuracy estimates throughout the weapon delivery envelope for all weapons carried on the aircraft. The model of the SMS is initialized to indicate to the FCC that the aircraft is loaded with the weapon type for which the system accuracy is to be evaluated. In addition, a driver program is developed that will automatically fly the aircraft simulation through a number of weapon delivery profiles. This driver program is set up to automatically step through a complete family of possible release delivery profiles by incrementing dive angle, airspeed, wind condition and release altitude. A final set of simulation test software is also developed to extract the FCC performance in each of the simulated weapon delivery runs. This software can either capture the computed release point from the simulation or extract the expected down range and cross range travel for the weapon from the FCC during the weapon delivery run. These extracted data are the FCC's estimate of the impact point of a weapon released at the point in the delivery profile where the data were extracted. The accuracy of the FCC's prediction is determined by using the release point as the initial condition and then running a validated ballistic model of the particular weapon selected from these initial conditions to the ground. The accuracy or performance of the FCC at the particular release condition is established by comparing the FCC predicted impact point with the impact point established using a validated ballistic simulation.

This process can be extended to provide system accuracy sensitivity data that could not be extracted using flight test alone. To do this the simulation is first run using perfect models of all the avionics sensor subsystems that provide input to the FCC weapon delivery calculations. With these data as a baseline various levels of sensor errors are introduced into each of the sensor simulation models. The FCC predicted solutions with and without a particular level of sensor error are compared to determine the sensitivity of the weapon delivery algorithm used in the FCC to errors in the aircraft sensors.

Another result of using the simulation to extend the flight test results is that the initial validation of the simulation provides what we, at the Naval Air Test Center, refer to as a closure analysis of the weapon delivery system. A key element in the simulation validation process is to make sure that the operation of the simulation matches that of the aircraft. This is done by comparing flight test data with data produced running an equivalent test on the simulation. Ordinarily, the sensor models in the simulation are initially modeled as perfect sensors that return error free data to the FCC. In a real aircraft this is never precisely the case. There are radar ranging errors, altimeter lag and position errors, and INS velocity errors. These errors contribute to the accuracy of the weapon delivery system measured in flight test. As a part of the validation effort, data are collected during the flight test to determine the levels of sensor error present in the aircraft systems. In the validation process these error levels are inserted into the sensor models before comparing the simulation test results with flight test results. Once a match has been achieved between the simulation and the flight test data it is possible to evaluate the contribution of each of the sensor subsystem errors to the overall system accuracy. This closure analysis is valuable because it highlights the most significant contributors to system error and provides management with the information necessary to determine the most cost effective improvements to the system.

In the previous paragraphs I have covered in detail how simulation can be used to extend the data available from flight test to completely characterize air-to-ground weapon delivery software. The same approach can be used to evaluate the performance of the other software elements in the FCC. Typical examples include system modeing and backup capability, air-to-air weapon delivery software, navigation functions, and break-x cueing.

The first and simplest types of tests are the evaluation of system modeing and backup capability. Once the operation of the simulation has been validated it provides a convenient tool for doing all the types of "what if" tests that need to be performed to make sure the system will operate properly under all conditions. Pilots and or engineers can use the simulation to subject the system to all combinations of switch closures, mode selections and subsystem failures. They do this to minimize the chances that there is any combination of commands that can be given to the system under any circumstances that will cause the system to operate improperly. An additional result of this type of testing is that it provides indepth training to both pilots and engineers on the system opeation. This is important in testing modern, highly complex, aircraft

the system tests a short period of time is greatly reduced. Thus, in addition to the data collection advantages, the simulation also provides pilots with a vehicle to become refamiliar with the system before embarking on highly complex and expensive flight tests. In our experience at NAVAIRTESTCEN this ability to refamiliarize pilots briefly complex tests in the simulation has reduced the number of tests that have to be repeated due to coordination problems and pilot error.

A similar type of testing can also be performed to verify the proper operation of many of the functions of the navigation software. In these cases, pilots and engineers "fly" the simulated aircraft through a number of navigation oriented flights and verify proper operation of the navigation systems. These include proper handling of waypoint information, proper steering commands to selected destinations and proper operation of the system at all latitudes and longitudes.

Testing the air-to-air software is similar to testing air-to-ground software. Again the simulation must be validated using flight test data from several air-to-air tests. Once this is done, the simulation can be used to extrapolate the performance of the air-to-air system over the entire range of the weapon envelope. A typical test is to evaluate the accuracy of the Launch Acceptable Region (LAR) calculation in the FCC. This is the calculation that is made to determine the maximum and minimum ranges for the weapon selected at the current target-shooter geometry. Usually the system designer develops a curve fit model to approximate the performance of an actual missile in making this calculation. The potential problem is that this curve fit will not exactly match the performance of the missile and the system will tell the pilot he is in range of the target when he is not or that he is out of range of the target when he really is in range. The validated simulation is used to evaluate this system by writing a driver program to step through a multiparameter family of target-shooter geometries varying such things as shooter altitude, target altitude, shooter velocity, target velocity, and shooter-target aspect angle. At each individual condition the FCC estimate of missile maximum and minimum range is extracted from the simulation. A validated 6 degree-of-freedom simulation of the actual missile is then used to check the accuracy of these extracted solutions. The particular target-shooter geometry is setup and a simulated missile is fired at the target. Simulated missiles are fired for a number of ranges until the maximum and minimum ranges that the simulated missile hits the target are determined. These ranges, which are the best estimates of the actual missile performance, are compared with the FCC generated solutions to assess the accuracy of the LAR calculations in the FCC.

Evaluation of the FCC computation of break-x cueing is another example of using the simulation to extend flight test data and, in this case, improve test safety. The F/A-18 FCC computes a minimum safe altitude depending on the current conditions of the aircraft. When the pilot goes below this altitude in a dive the system alerts him by flashing a break-x cue on the HUD. This cue is timed so that if the pilot executes a specified pullout maneuver when the cue starts he will miss the ground by some specified distance during the pullout. To test this system, flight test data is obtained at some relatively shallow dive angle and used to verify that the operation of the break-x cueing in the simulation matches the operation in the airplane. When this validation is complete the simulation is used to extend the evaluation of the break-x cue over all airspeeds and dive angles. A driver program is developed to fly the simulation through a dive pullout maneuver. The driver program also is designed to step the simulation through the complete envelope of dive angle and airspeed possibilities for the airplane. This program starts the simulation in a dive at some altitude above the break-x altitude. It then flys the airplane through a straight path dive until it determines the FCC has initiated the break-x cue. At this point it forces the airplane to fly through the specified pullout maneuver that was used to define the break-x performance. During the pullout maneuver the program constantly monitors the distance between the simulated aircraft and the ground. The minimum value of this distance is used to verify the operation of the break-x software.

OTHER HARDWARE/SOFTWARE EVALUATIONS

In addition to using the TASTEF to evaluate the FCC software we have also used it to verify the proper operation of other avionics subsystems. Normally these subsystems are removed from the aircraft and connected directly to the MIL-STD-1553 data bus in the facility. These systems are then also provided with external stimulations to replicate the total signal environment of the subsystem in the airplane. In the case of the F/A-18 the most novel and successful application has been using the SMS. As it turned out, the method used to integrate this avionics hardware into the simulation was unusual and as far as I know unique. Instead of simply using the SMS hardware out of the airplane and plugging it into the simulation along with other required stimulation hardware and software, we were able to connect the simulation to a fully integrated aircraft system including an SMS. As a result we were able to test not only the SMS computer hardware and software, but also the encoders, decoders, cables, and auxiliary hardware.

The structured architecture of MIL-STD-1553 bus oriented systems makes the potential of plugging a simulation directly into a fully integrated aircraft extremely attractive. The only thing that must be done is to find a way to connect the simulation bus to the aircraft bus and then not execute the simulation models of hardware that will be active in the airplane. Figure 5 shows schematically how this was done for the F/A-18 system.

of the rest of the avionics subsystems were used to complete the entire weapons system. As a result the SMS was fooled into thinking that it was in flight in an actual aircraft. This was necessary to be able to put the SMS through its complete paces in a ground test environment. The problem is that the F/A-18 system is too intelligent and when it is sitting on the ground with zero velocity and zero altitude it knows it is on the ground. As a result, the F/A-18 system will not perform all the weapons release sequences it would in flight. However, once the simulation and the airplane systems were connected, the models of the Air Data Computer (ADC) and INS provided simulated flight data to the FCC and SMS which made these systems believe the aircraft was in flight. As a result the SMS and FCC could be made to perform all release sequences on the ground exactly as if they were in flight.

In order to set up this type of an operation the first problem was how to connect the simulation to the airplane. In the case of the F/A-18, it turns out that this was easier than anyone would have imagined possible. On the right side of the airplane, immediately available under a removable panel, is a small box with a single cannon plug entering it. This box is the termination for the two data buses in the airplane. All that is required to connect the simulation to the airplane is to disconnect this one cannon plug from the bus termination box and plug it into a connector that connects to the simulation.

Before describing the testing that was performed on the SMS using this setup I would like to digress and discuss the impact of this method of testing. The connection between the simulation and the aircraft is extremely quick and simple. Additionally, making this connection in no way disturbs the flight worthy condition of the airplane. The impact is that production configured aircraft could be used without modification to conduct tests of this type. The rapidity and ease with which the connection is made means that these production aircraft would only be required for a very short period of time during the actual testing. After the tests were finished the simulation could be disconnected from the airplane, the airplane buses reterminated in the aircraft and the plane flown away. This opens a new and as yet relatively unexplored set of test assets that can be made available to a program on a relative low cost and non-interference basis. In addition the connection of the simulation to the aircraft in this way indicates a potential for turning the aircraft itself into a training simulator.

Getting back to the SMS tests, once the aircraft system was connected to the simulation it was possible to exercise the SMS in every mode that it could operate during flight. The purpose of the testing was to verify proper operation of the SMS under all possible loading configurations and release modes for the aircraft. To do this a series of driver programs were developed that would fly the simulation through a weapon release profile. A test matrix was developed that included representative samples of all the loading configurations for all the weapons carried on the aircraft. Each loading configuration was tested by telling the SMS that the particular configuration was on the airplane and flying the airplane through a release profile. Stripcharts were used to record the SMS commands to the Cartridge Actuation Devices (CAD's) in the racks as well as to arming solenoids and electric fuzes. After each simulated release, the stripcharts were analyzed to verify that the proper commands had been sent to the weapon suspension equipment. The results of these tests did point to several problem areas in the initial SMS software including incorrect electric fuzing options for several weapons and incorrect weapon release operation for long strings of bombs. Admittedly, these are not severe safety of flight problems. However, they are the type of problems that any test activity should discover before sending an aircraft to operational use.

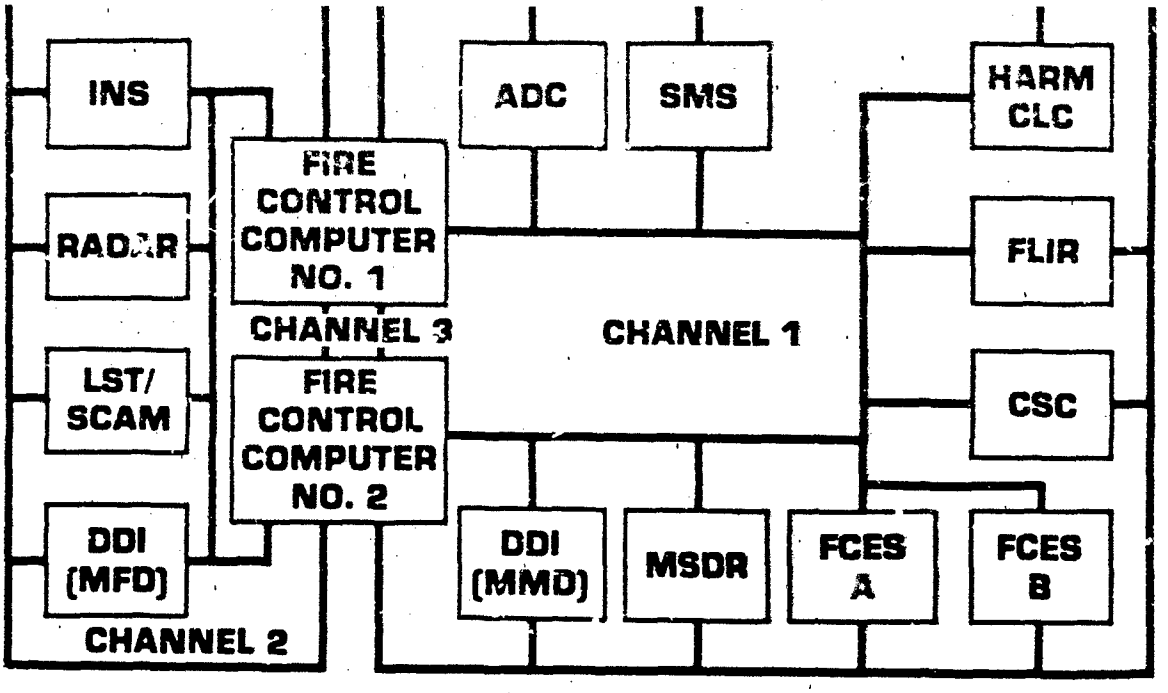

F/A-18 AVIONICS MULTIPLEX BUS SYSTEM

FIGURE 1

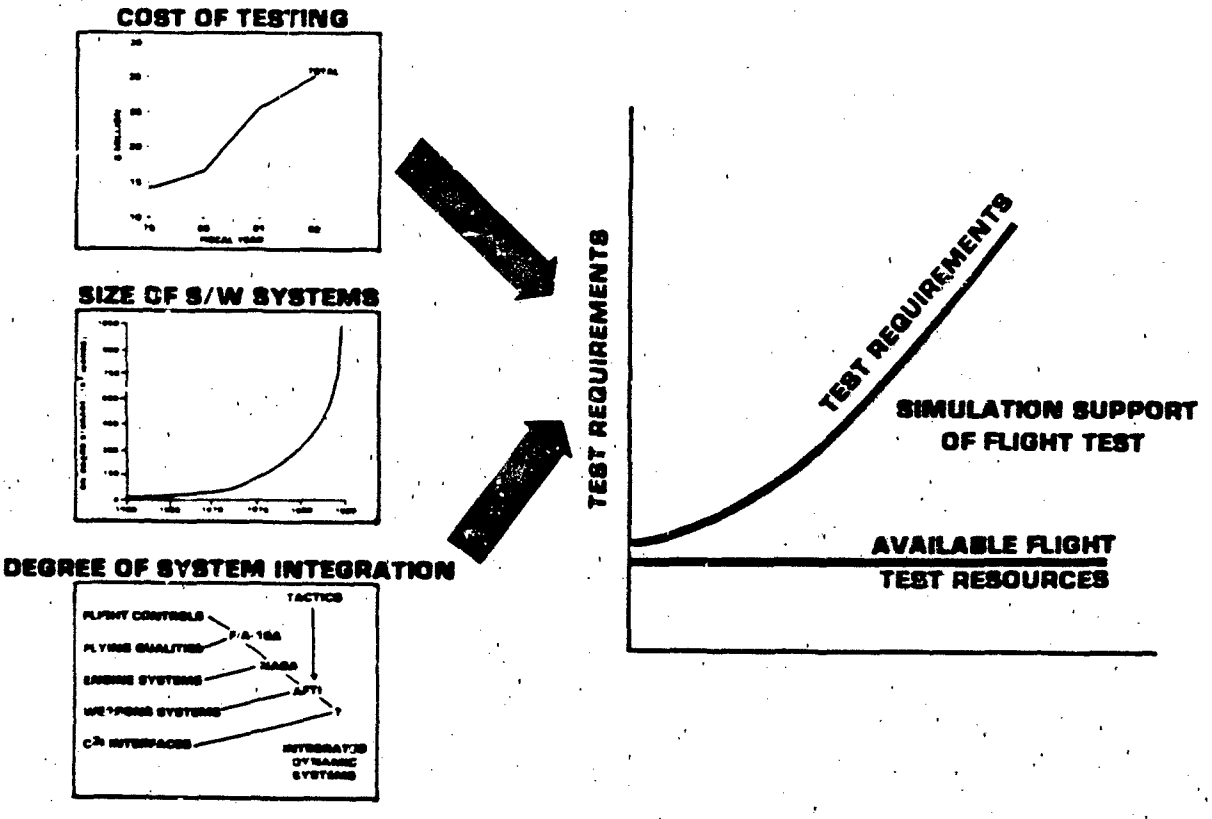

PROBLEMS FACING MODERN AVIONICS SYSTEM TESTERS

FIGURE 2

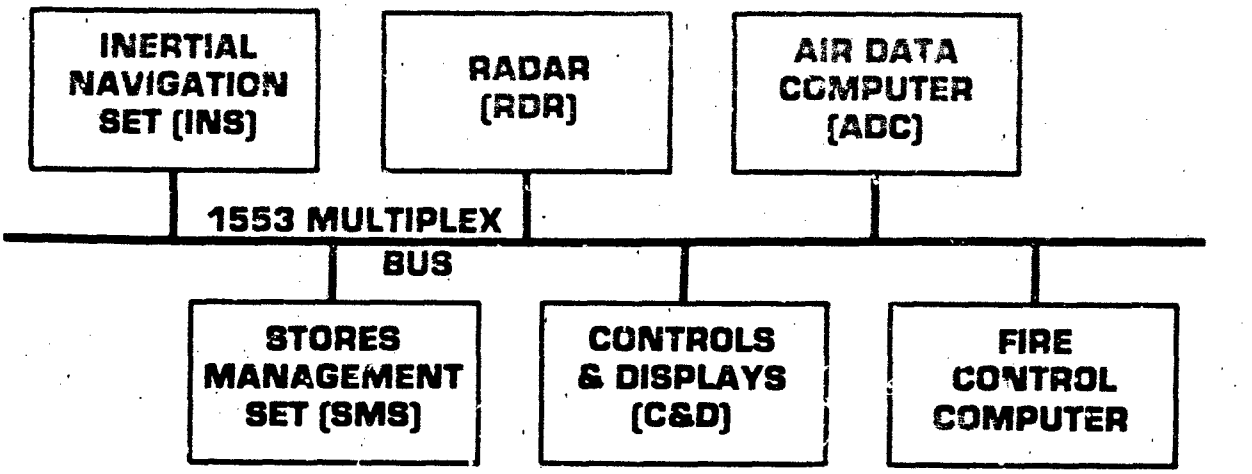

SIMPLIFIED MIL-STD 1553 WEAPONS SYSTEM

FIGURE 3A

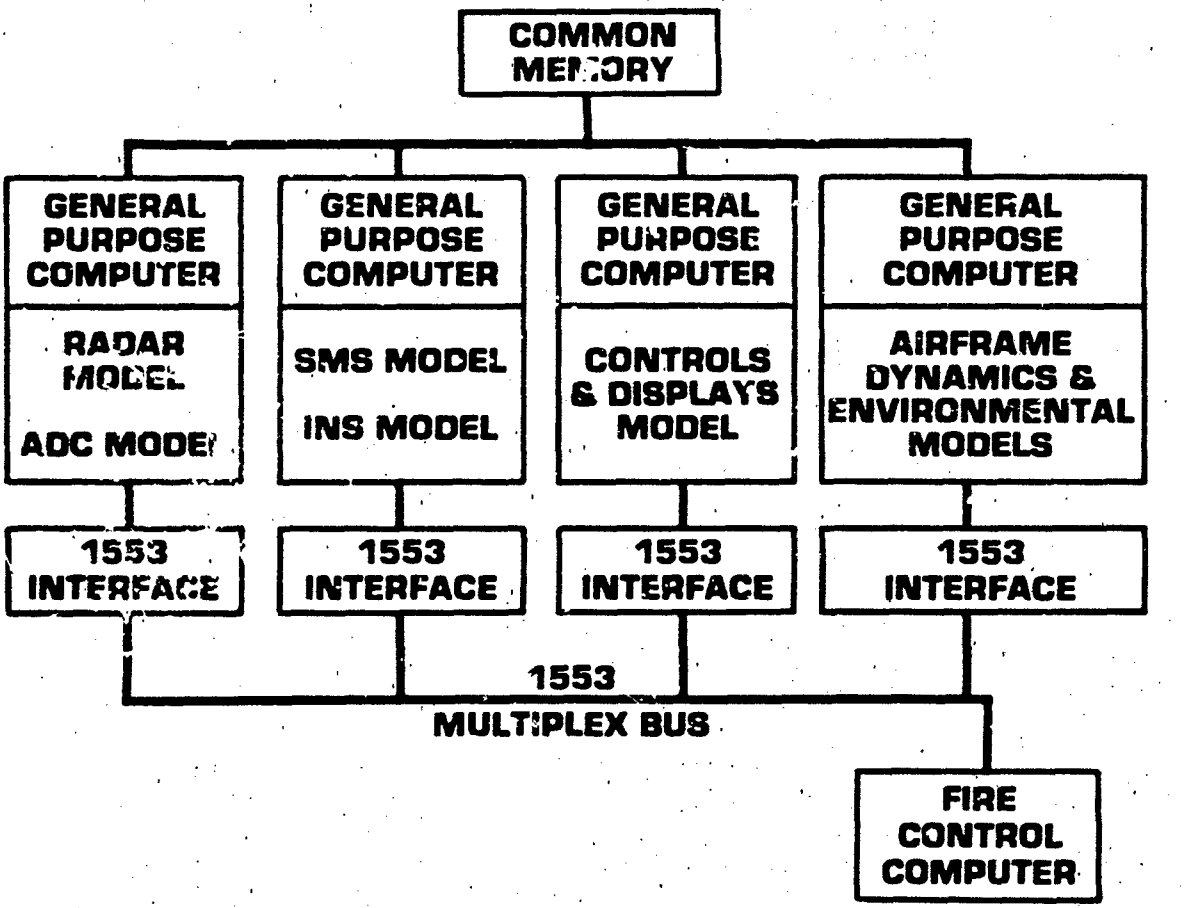

SIMULATION ARCHITECTURE FOR A SIMPLIFIED WEAPONS SYSTEM

FIGURE 3B

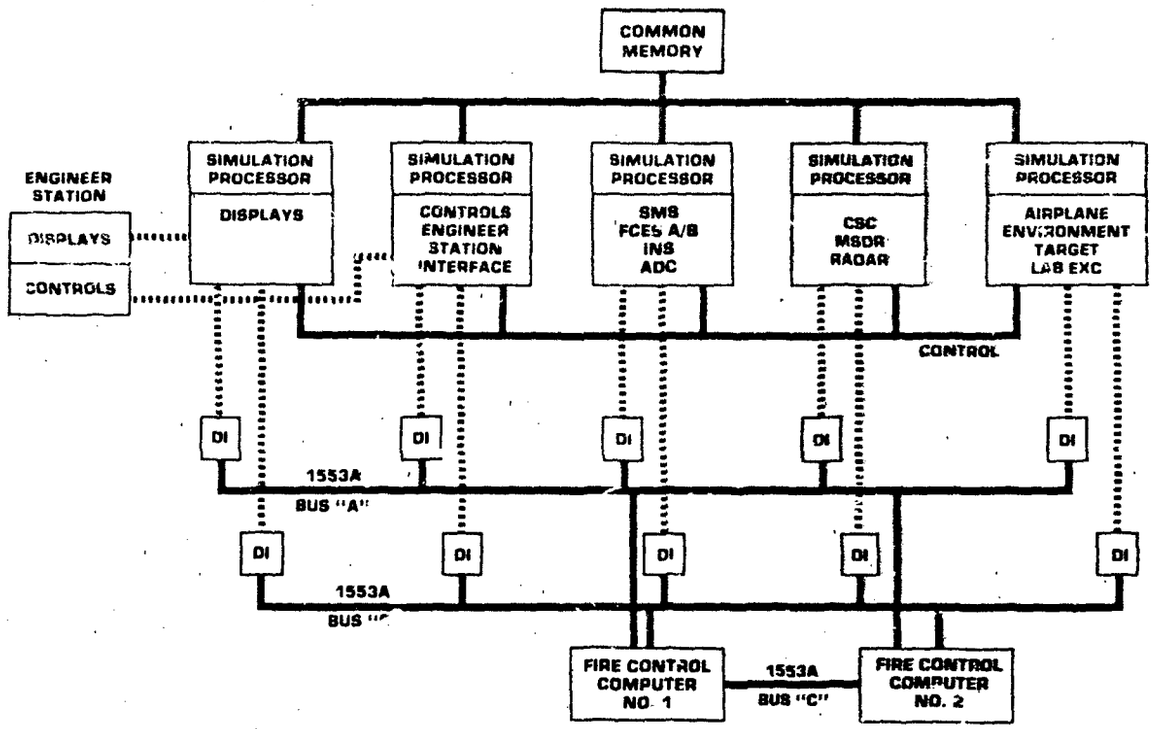

F/A-18 AVIONICS SYSTEM SIMULATION ARCHITECTURE

FIGURE 4

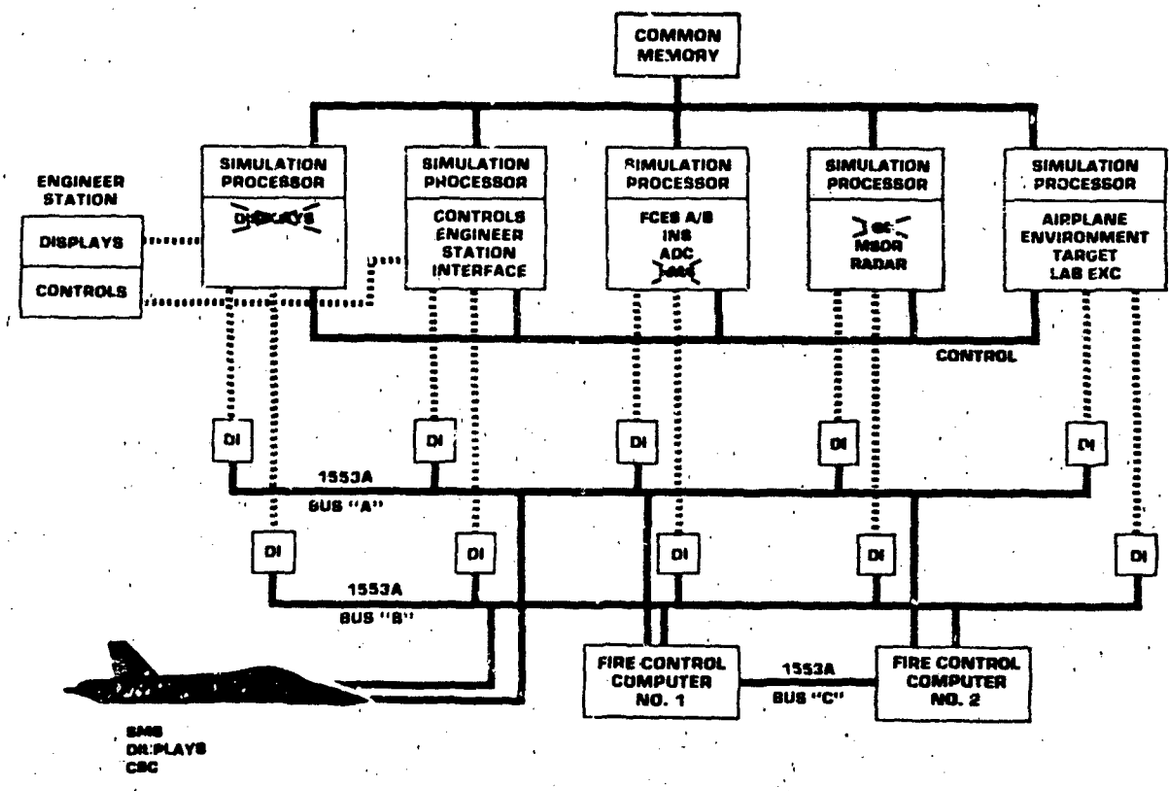

AIRCRAFT IN THE LOOP SIMULATION ARCHITECTURE

FIGURE 5

FLIGHT TEST TECHNIQUES EMPLOYED IN THE NIMROD MR MK 2 WEAPON SYSTEM PERFORMANCE TRIALS

by

Squadron Leader L M Dutton
Aeroplane & Armament Experimental Establishment
Boscombe Down, Salisbury, SP4 0JF, UK

SUMMARY

The Nimrod MR Mk 2 represents a large step forward in Anti Submarine Warfare (ASW) technology. The aircraft operators therefore need to know not only how accurately the new systems and sensors work, but also the best ways in which to use the overall system as a fighting machine. A&AEE Boscombe Down and the RAF Central Tactics and Trials Organisation therefore joined forces to assess the ASW performance of the Nimrod in as near an operational environment as possible.

The paper shows how the potential accuracy of the Nimrod's ASW systems had to be matched by the precision of trials data collection, in the air and both on and below the sea surface. To gain such precision, the aircraft were extensively instrumented and the majority of the trials were conducted at the Atlantic Undersea Test and Evaluation Centre (AUTEC) Range at Andros Island in the Bahamas.

The paper continues by explaining how the trials analysis technique had to match the variety of combinations of the data which were needed to make a statement on overall system performance.

The paper concludes by looking to the future in the Nimrod trials programme and shows how forward trials planning is drawing heavily on experience gained so far.

1 INTRODUCTION

1.1 The Nimrod MR Mk 2 aircraft, which entered squadron service with the Royal Air Force in 1979, is a complex, digital computer based, weapon system. Early trials by A&AEE Boscombe Down cleared the aircraft's systems as safe to operate, and verified that the equipment gave "sensible" information. The trials also gave a limited statement of sub-system and sensor performance. However, it was recognised early in the development of the aircraft that the complexity of the interactions between the overall system, its operators and the operational environment would make it difficult to provide a simple description of the performance of the overall system in analytical terms. Consequently, immediately following the Controller of Aircraft Release (CA Release) trials, a trials phase was begun which attempted to measure the performance of the overall weapon system in as near an operational environment as possible. This phase was entitled the Weapon System Performance Trials (WSPT).

1.2 Any WSPT results are clearly dependent upon the system configuration standards at the time of the trials and consequently any changes to hardware or software could significantly affect performance statements. The WSPT must therefore be seen as an on-going trials requirement which will continue, in one form or another, throughout the in-service life of the aircraft, because software, and to a lesser extent hardware, will continually be updated, developed and improved in an effort to match the operational squadrons' requirements.

1.3 Because of the continuing requirement for system performance trials, future trial aims and techniques will necessarily need to develop alongside the system. However, there are some underlying simple common principles in the trials methodology to-date which have proved successful, and should provide a sound foundation for future trials planning.

1.4 The aim of this paper is therefore to state these simple principles and explain in some detail how they have been used to good effect during the Nimrod WSPT to-date.

2 THE SYSTEM UNDER TEST When the Maritime Reconnaissance (MR) Nimrod was upgraded from Mk 1 to Mk 2 status, the major improvements were in the sensors and tactical sub-systems. Extensive use was made of digital data processing to improve the radar, acoustic and Electronic Support Measures (ESM) sensor systems; and for the first time these sensors were linked directly to the central tactical computer. Before we consider the integrated system, it is worth considering each sub-system in turn.

FIGURE 1:
Twin AQS °01
Acoustic Data
Processing Suite

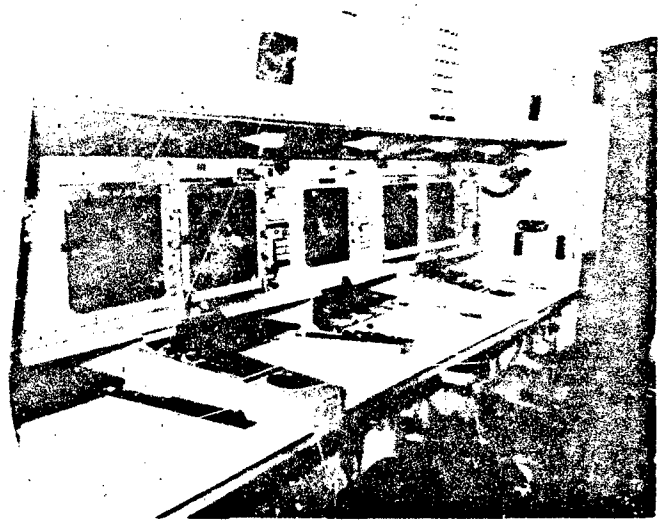

FIGURE 2:
Searchwater Radar

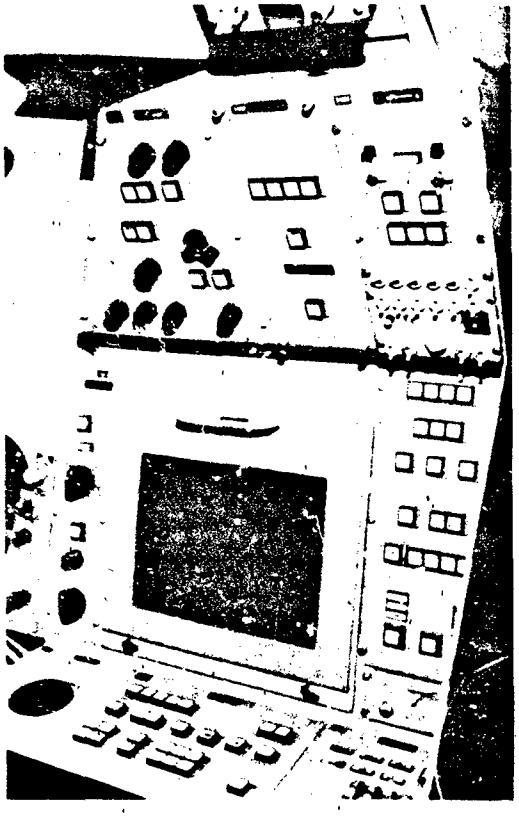

FIGURE 3:
Loral 1017A ESM

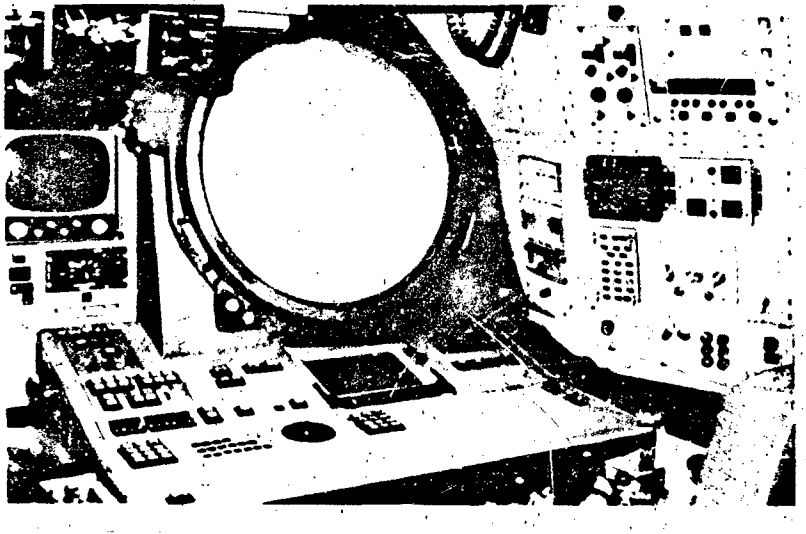

FIGURE 4:
Central Tactical
System

2.1 THE AQS 901 ACOUSTIC PROCESSORS Figure 1 shows the twin Marconi AQS 901 acoustic processing suite. Each AQS 901 has two Video Display Units (VDUs) and two Hard Copy Units (HCUs) on either of which acoustic data is presented to the operator. Between the two systems is situated a co-ordinators station at which a dedicated VDU is situated with an associated control keyboard. The AQS 901s can be operated either singly or as a combined system. Each AQS 901 is controlled by a GEC/Marconi 920 Advanced Tactical Computer (ATC) and can process data from a variety of active and passive sonobuoys. From data displayed to the operator, the crew are able to detect and classify acoustic targets and obtain range and bearing information which can be passed directly to the central tactical computing system.

2.2 THE SEARCHWATER RADAR Figure 2 shows the Thorn-EMI Electronics Searchwater Radar. The radar is controlled by a Ferranti 1600D digital computer and offers multiple target tracking and an identification capability which allows the outline of targets to be studied, even at long range. The radar was specifically designed for the maritime role and gives high detection and tracking performance, even in high sea states. The system incorporates IFF to aid classification and also has air-to-air and weather modes. Targets of interest and their associated data can be passed directly to the central tactical computing system.

2.3 THE LORAL 1017A ESM Figure 3 shows the Loral 1017A Electronic Support Measures (ESM) equipment. The system, which has an extremely wide RF bandwidth, works on the agile superhet principle and is controlled by a GEC-Marconi 920 ATC and a TI 2520 digital computer. The ESM gives the crew radar warning, classification and DF facilities throughout the RF passband, and is capable of passing all relevant data to the central tactical computing system.

2.4 THE CENTRAL TACTICAL SYSTEM Figure 4 shows the central tactical computing system (CTS). The system is capable of taking inputs from the aircraft's sensors, including the AQS 901s, the Searchwater and ESM. The system has its own 920 ATC digital computer and is used to database and display the tactical information. Also, by adding information from the navigation system, the tactical navigator is then able to use the CTS to aid his tactical management of the overall aircraft weapon system.

2.5 THE INTEGRATED SYSTEM The 4 sub-systems discussed above are connected together as a complex tactical data system. The overall system is summarised in Figure 5. This system represents the majority of the aircraft systems under test in the WSPT. Points worthy of note are, firstly that there is no overall control by a single software program, each sub-system is under the control of a host program.

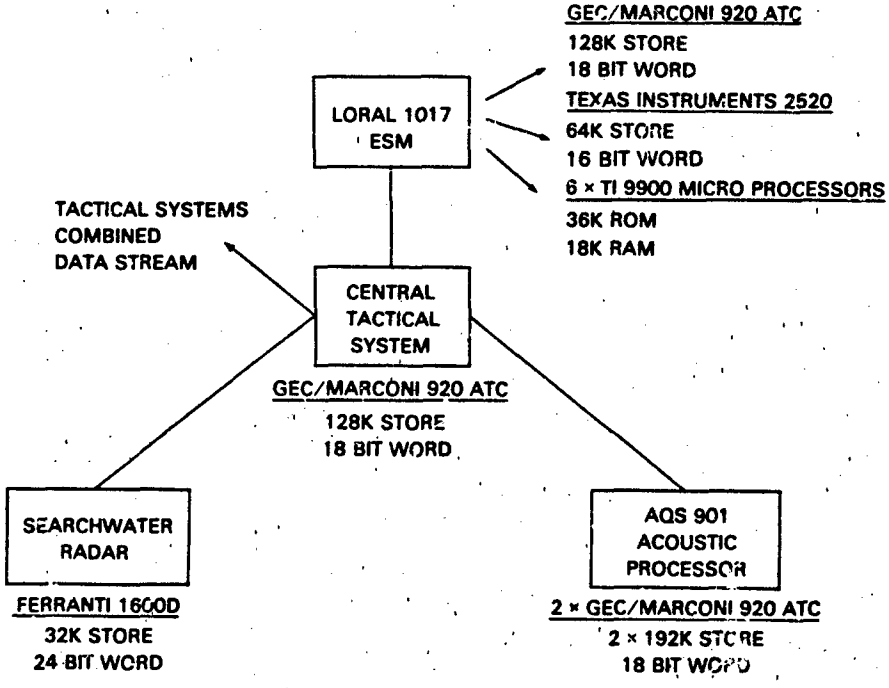

FIGURE 5 - NIMROD MR MK 2 - MAIN TACTICAL COMPUTING LAYOUT

Secondly, the interfaces between the sub-systems impose an extra layer of difficulty on system trials because if any faults were to emerge, it is possible that the fault could be rooted in one system, yet show up in another. Thirdly, the programs in the 4 sub-systems are updated when required and not all at the same time, thus controlling the interface compatibilities is a complex problem. This last point also had trials relevance in that any trial results would only be valid for their corresponding sub-systems' software standard. In summary, the trials team recognised that the Nimrod Mk 2's tactical computing systems were extremely complicated both individually and as an integrated weapon system. In order to measure and understand the operation of such a system, the trials would need to be of equal or perhaps greater complexity.

3 TRIALS PHILOSOPHY

3.1 THE DIVISION OF EFFORT The trials needed to measure the performance of the aircraft in its many maritime roles. Because of the large amount of effort involved, the trials activity was divided between A&AEE and the Royal Air Force's Central Tactics and Trials Organisation (CTTO). A&AEE's work revolved around the aircraft's Anti-Submarine Warfare (ASW) role. This paper deals only with those trials methods employed in A&AEE trials.

3.2 ACCURACY REQUIREMENTS The systems under test contain complex computer algorithms and are capable of high accuracy both as sensors and tracking systems. If there were to be any confidence in the trials results, extremely accurate datums would have to be employed when measuring system errors. Traditional open ocean type trials were sufficient for many of the trial aims, particularly in the early days of the trials, but datum accuracies in the open ocean were not high enough to enable position and time to be correlated sufficiently well for detailed performance measurement. An instrumented range was therefore necessary where both the aircraft, buoys, submarine and any other maritime vehicles could be continuously tracked to extremely high orders of accuracy, and where time could be accurately related to all trials events.

3.3 THE TRIALS ENVIRONMENT The first trials undertaken were those on the acoustic processing system. In order to measure the performance of the system, it was necessary to compare the system's estimates of target parameters derived from the acoustic properties of the target and environment, with actual conditions. Clearly this task could only be carried out with any confidence if the acoustic properties of both the target and the environment were at best under full control or at worst fully understood by the trials team. Such a requirement again pointed towards the need for the detailed trials work to take place on an underwater range, under closely controlled conditions. Such an argument would also justify the need for trials on the ESM system to take place on a closely controlled range, though in that case it would be the RF environment which would need to be fully understood or controlled.

3.4 INSTRUMENTATION Instrumentation in the Nimrod's operational fit is sparse. There are 2 tape recorders, used to record data streams from various systems in order to provide data of operational relevance for post flight analysis. Such operationally-orientated instrumentation facilities needed to be supplemented, not only to record extra data from the aircraft's data streams, but also to record dedicated trials data which was generated by purpose built instrumentation. Much of the special instrumentation was provided to ensure extremely accurate time synchronisation between all the systems within the aircraft and also between the aircraft and the Range computers. Also, with much of the data being presented to the crew on video screens, it was possible to fit video recorders to record actual data, as presented to the operator. In summary the instrumentation suite was extensive, but essential if the full performance of the overall system was to be analysed in minute detail.

3.5 TRIALS ANALYSIS It was recognised at an early stage that the trials would need to be extremely complex if they were to measure the performance of such a complicated system. It was also recognised that some performance characteristics would be subtle in their effect and so would require an equal or greater subtlety of analysis if effects were to be isolated. In recognition of the large analysis effort which would be necessary, the trials team contained several scientists whose activities were dedicated to the analysis tasks, and Air Force trials officers were assigned to systems of their own professional specialisation. Also, the team acquired a GEC 4070 mini-computer which was also dedicated to the analysis of MR Nimrod trials. The trials team of 12 people represented a large team by A&AEE standards but was absolutely essential for trials on a system of such complexity.

4 CONTROL OF THE ENVIRONMENT At the outset of the trials it was agreed that highly accurate, well calibrated ranges were probably the only environments in which there would be a chance of obtaining data under very closely controlled conditions. Such knowledge about, and control of, the environment would be essential if the effects of system and environment were ever to be separated in the analysis of the trials. For trialling of the acoustics, radar and central tactical systems, the range chosen was the Atlantic Undersea Test and Evaluation Centre (AUTEC) Range at Andros Island in the Bahamas. The Range is controlled by the US Navy but the UK is a frequent range user. The geographic layout of the AUTEC Ranges is shown at Figure 6.

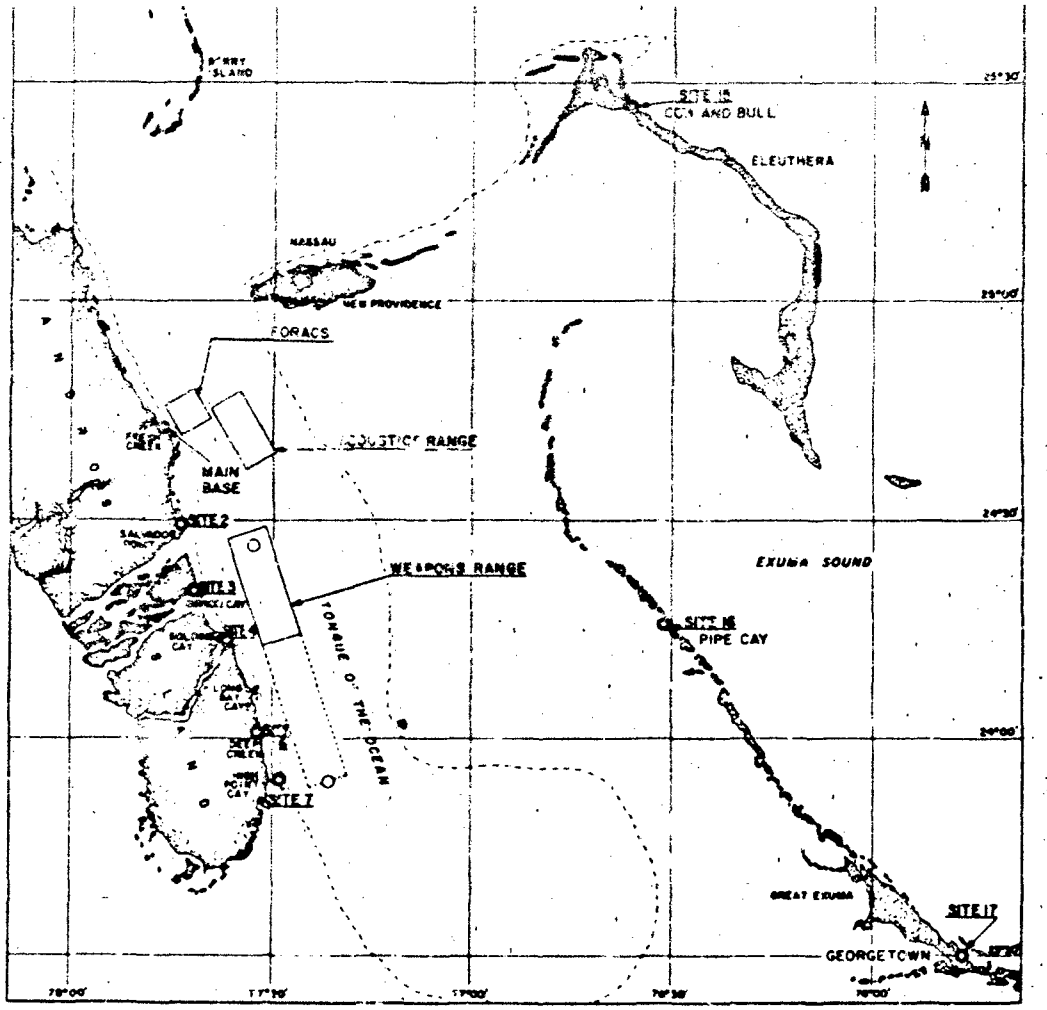

FIGURE 6 - AREA MAP - AUTEC RANGES

The system performance trialling took place in the Weapons Range, which is a 3-D underwater and in-air tracking range, situated close to the eastern coast of Andros Island. Despite its proximity to land, the range water is, on average, 800 fathoms deep, thus enabling deep water scenarios to be trialled, under the close tracking, control and supervision of the range.

4.1 CONTROL OF THE UNDERWATER ACOUSTIC ENVIRONEMNT

4.1.1 THE SUBMARINE For the trials, the target submarine was fitted with a noise generator, capable of emitting a variety of acoustic frequencies, controllable in acoustic power output and frequency stability. The acoustic power "polar plot" of this system was then carefully measured on an underwater acoustic range. Thus the submarine used in the trial was a calibrated and controllable sound source.

4.1.2 AMBIENT ACOUSTIC NOISE. The Autec Ranges are surrounded, on 3 sides, by extremely shallow water, hence there is no acoustic noise generated by heavy transiting surface traffic, other than Range users. Therefore, acoustic interference is light. The sources of such interference are easily indentified and can be catered for in trials analysis. Thus in the analysis, effects caused by system and environment could be measured and separated.

4.1.3 BATHYTHERMAL MEASUREMENTS Water conditions have a marked effect upon any acoustic system's performance. Detailed knowledge of the acoustic conditions is therefore essential for any credible analysis of acoustic trials. During trial serials the Range, surface units and the aircraft were able to take frequent bathythermal soundings for use in the analysis.

...concept problem was that of time synchronising the activities of the target submarine and the aircraft. This was particularly difficult since the submerged target was not in radio contact with the aircraft and hence synchronisation of action could only be achieved by the strictest adherence to timing schedules and the meticulous recording of times of significant events. Timing accuracies of 1 second were aimed for when timing occurences such as the submarine's masts breaking the water line.

5 DATUM REQUIREMENTS

5.1 TIME SYNCHRONISATION With data being collected both in the aircraft and on the range, it was essential that the two data sources should be time synchronised. Time synchronisation procedures using manual events and time 'mark' calls on V/UHF would only have provided a 1 to 2 second accuracy of time lock. This was considered inadequate since the aircraft travels 400 feet or so every second and any time lock error would result in a large and unknown data offset between the range and the aircraft. The trials team considered that 40 feet would be the maximum alalowable error on aircraft data due to time offsets and a technique which would ensure time locking to an accuracy of $^{1}/_{10}$ second or better was therefore specified. In retrospect, this figure was fortunate choice since it equals the tactical system computer cycle time. So, if time synchronisation could be achieved within a CTS computer cycle, the aircraft and Range data would be synchronised to $^{1}/_{10}$ sec at the worst, and probably to a smaller figure.

5.2 TRACKING DATUM Detailed knowledge of the trial vehicles' relative and absolute positions is essential for trials which intend to separate the constituent errors of any weapon system. Trials at the AUTEC Ranges presented a new problem to the trials team, because although the AUTEC standard facilities could track both the aircraft and the submarine very accurately, the sonobuoys, which drift at the mercy of wind and tide, could not be tracked by the Range facilities. Continuous knowledge of sonobuoy position is clearly essential because the buoy is the link between the aircraft and submarine and an integral part of the system under test. A new approach was therefore needed, since tracking the buoys during previous trials had not been found possible, with any level of accuracy.

5.2.1 TRACKING THE AIRCRAFT One of the trial aims was to separate the constituent errors of the aircraft's attack error budget. In order to do this it was necessary to study the behaviour of the aircraft at critical stages in its tactical operation. The aircraft's navigation system was subject to system drift and therefore not accurate enough to provide the level of position accuracy required. The aircraft was therefore tracked by Range tracking radars throughout the trials. Exceptional positional accuracy was obtained by using an I-band radar tracking transponder on the aircraft. It was therefore possible to measure navigation system drift and accurate attack geometries.

5.2.2 TRACKING THE SUBMARINE Obtaining an accurate submarine datum track is one of the most difficult parts of maritime trials. Such tracking facilities are only available on a very small number of underwater tracking ranges. On the AUTEC Weapons Range, the undersea range floor is covered with tracking hydrophones, and the trial submarine is fitted with an acoustic transponder or pinger. By measuring the time difference, by which the transponder's pings arrive at the hydrophones, the submarine can be tracked in position and speed in 3 dimensions. Very high data rates are possible and an extremely accurate submarine datum plot can be obtained.

5.2.3 SONOBUOY TRACKING The WSPT included trials which used new types of directional and ranging sonobuoys. It was considered particularly important that the performance of the buoys should be measured accurately. This detailed knowledge would then be a baseline against which system performance statements could be made. In order to make accurate measurements of buoy bearing or range errors it was necessary to track both the submarine and sonobuoy throughout a trial serial. This was the first time that maritime trials had tracked the sonobuoys as it was previously considered too difficult. However, Figure 7 is a graphic justification of the absolute necessity for buoy tracking if any credible statement is to be made on bearing or range errors. The figure shows the progress of 3 sonobuoys during the period that the submarine transited from the start of the track shown, to the finish. If the buoy drifts had not been accounted for, then buoy bearing or range error distributions would clearly have been meaningless.

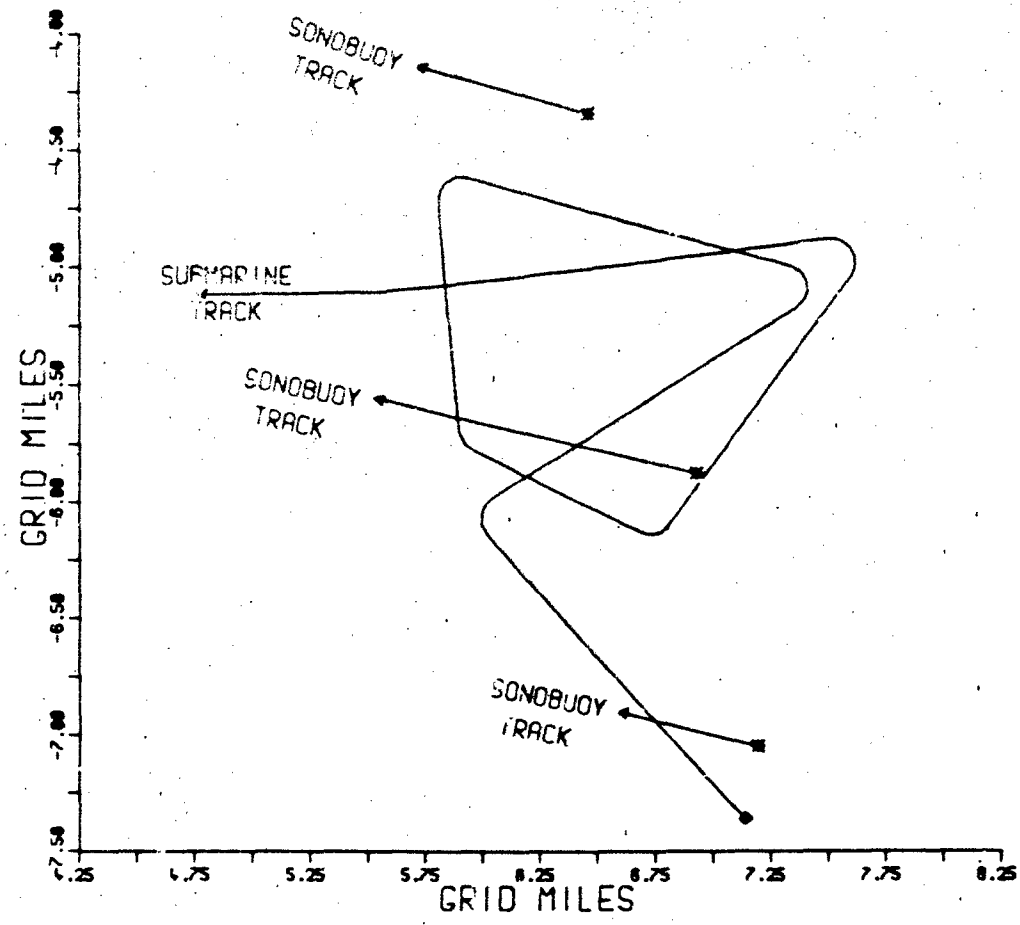

FIGURE 7 - WSTT SERIAL SUBMARINE AND SONOBUOYS SURFACE DATUM PLOT

Because the AUTEC Range has very limited sonobuoy tracking capabilities, a sonobuoy tracking technique was developed which involved the aircraft flying overhead the buoys and taking photographs as it passed through the on-top. Once the buoy was identified on the film the buoys position in the picture was carefully measured. Then, with knowledge of aircraft datum position, aircraft pitch, roll, heading and height, an accurate sonobuoy position could be calculated. By flying successive photographic on-tops, the buoy drift vector could be deduced. Figure 8 shows the print-out of one such plot where 4 photographs were obtained out of the 6 on tops which followed the drop. Sometimes, for a variety of reasons, such as sea glint, high bank angle, etc, it was possible that the buoy could not be seen on the photograph. However, in such cases the aircraft's position at on-top gave a close approximation to the buoy position.

Once the buoy drift vector was computed the trials analysis programs were able to compute datum ranges or bearings with great accuracy for exact times when the acoustic system's estimates were made.

6 INSTRUMENTATION

6.1 TIME SYNCHRONISATION

6.1.1 THE SYSTEM USED The AUTEC Range had the facility to transmit Range master time on V/UHF using IRIG-B century coded format. Special aircraft instrumentation was built to decode the Range time signals and, on the full minute synchronise the aircraft's master time code generator (TCG) with Range time. Typically, synchronisations were accurate to 1-3 milliseconds. The aircraft's computers were then synchronised to the TCC via a specially built link which provided extremely fast time data transfer to the tactical system via a high level interrupt. It was this interrupt servicing which set the final accuracy figure of $^{1}/_{10}$ sec or better on the overall accuracy of the time synchronisation system.

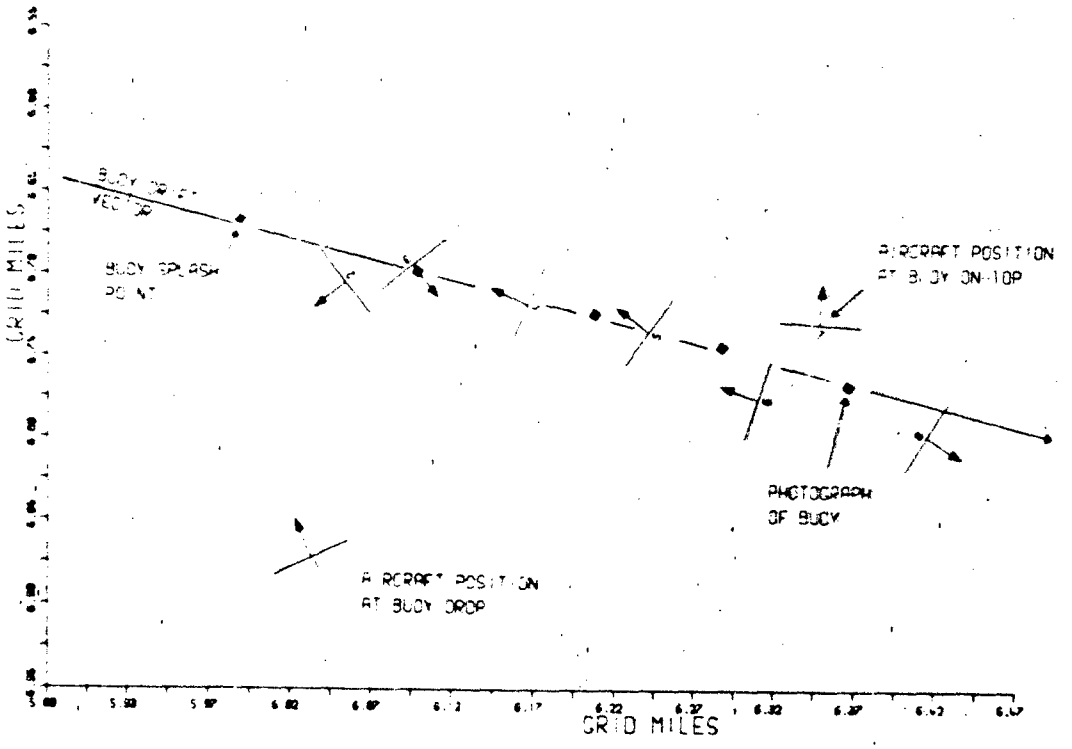

FIGURE 8 - CALCULATION OF SONOBUOY DRIFT VECTOR BY PHOTOGRAPHIC ON-TOP METHOD

6.1.2 TONE EVENTS Within each serial there were usually around 20-30 events which were extremely significant for trials purposes. Such events could be buoy on-tops, attacks, sensor mode changes etc. The aircraft was fitted with a tone generation system which could be triggered either manually or in some cases automatically by tactical systems. At the event, a 1 KHz tone lasting 1 second was transmitted to the Range. On reception of the tone, the Range computers automatically output snapshots of data for the event time. This facility was particularly useful for quick-look analysis and also gave trial managers quick reference to critical areas of data.

6.2 DATA RECORDING

6.2.1 INSTRUMENTATION RECORDERS The aircraft's main instrumentation recorder was a 14 track Wideband-2 AMPEX tape recorder. This recorder was used to record the various tactical data streams, the various navigational data streams, tone-events, IRIG-B time, intercom and V/UHF radios. The trials also used the aircraft's operational recorders, which not only provided a limitied back-up facility for the main instrumentation recorder but also recorded raw acoustic data from some of the sonobuoys. Because the operational recorders do not record raw acoustic data from all the buoys in use, a further Wideband-2 AMPEX recorder was fitted to enable recording of raw acoustic data from all buoys used in the trials. Paragraph 7.1 explains why this data was required.

6.2.2 RECORDING RADAR DATA One of the main problems with radar trials was that of separating the performance of the radar and the operator. To assist the trials officer's task, a video tape recorder was used to record the radar screen throughout the trials period so that post-flight, the operator's assessment was compared with the recording, which could be examined in some detail.

6.2.3 KEYING ACTIONS All the 4 major sub-systems under test have keyboards and switches which provide the control interface between the equipment and the operator. Fortunately for the trials team, the equipment incorporated records of keying and switching actions in their data streams. Such information was of great value, and in the analysis phase frequently helped resolve conflicting data records.

6.2.4 HAND-HELD TAPE RECORDERS During early trials, the trials officers had noticed a problem peculiar to working on systems where most of the information output to a crew member was on video displays. The trials team found that if they looked away whilst recording data on paper, they were unable to follow dynamic changes in the data and much information was lost. For this reason, the trials

it was possible to make detailed notes from the playback of the tapes.

6.2.5 HAND-HELD CAMERAS There were times during the trials when the entire contents of video screens were required, more particularly when the data needed subjective appraisal. For this purpose the trials team used hand-held cameras. 35 mm cameras were generally used to provide data for post-flight analysis, but polaroid cameras were extremely useful for instant reference to data during the trials sortie.

6.2.6 WRITTEN NOTES Despite all the high technology data recording systems, the trials officers still made copious notes as the trials progressed. The notes were, however, more skeleton notes than the detailed type necessary when automatic data recording is not employed.

6.3 VERTICAL CAMERAS Paragraph 5.2.3 describes the technique by which sonobuoys were photographed using vertical cameras in order to calculate buoy drift vectors. The cameras were F135 twin spool cameras using Kodak Ektachrome colour reversal film. The cameras were extensively modified for trials purposes. As the aircraft flew close to the on-top position of a sonobuoy, the camera was switched on. As the film passed through the camera, 3 fibre optic leads printed time codes onto the film at 1 Hz, 10 Hz and 100 Hz. As the aircraft passed through the on-top position, the buoy homer registered the on-top event and passed an event pulse to the instrumentation and to the camera interface. On receipt of the pulse at the camera, an extra fibre optic lead marked the film at the event time. The time code then stopped and the event time was printed out in alpha-numeric form on the film, using the 4 fibre optic leads. From the time track it was thus possible to deduce the exact time of the event time and the camera shutter time of the picture containing the buoy image. The on-top event marker on the film also focussed attention in the most likely area for finding the very small image of the sonobuoy.

7 ANALYSIS FACILITIES

7.1 DATA REPLAY It is possible for the aircraft's acoustic processing system to process the acoustic data, from the sonobuoys, in several ways. When flying on range, the acoustic data is processed in one mode, and then because the raw sonobuoy data is recorded, it is possible to re-process the data in another or perhaps several other modes post-flight. By adopting this technique, the various modes of processing can be compared directly since all other factors are exactly the same between processing modes. This is particularly important because small changes in oceanographic conditions can have quite large effects on system performance. However, replay from raw data is not quite as straightforward as it may seem, and a replay interface is required. The interface contains bit-synchronisers and de-flutter buffers, plus time synchronisation devices to ensure that the data presented to the AQS 901 acoustic processor is of exactly the same quality as that generated in flight. The full system is shown diagramatically at Figure 9. The figure shows data being replayed on a 28-track tape recorder, and being immediately split into two paths, one for digitally-coded data and one for analogue. Analogue data is relatively easy to deal with, and can be passed directly to the replay system, whereas digital data has to pass through the bit synchroniser and de-flutter buffers to ensure perfect timing of the data. The figure shows the two possible replay configurations, one where the aircraft may be used as a full replay system and the other where dedicated rigs are used. The rig method tends to be used for the more clinical analysis scenarios, whereas the aircraft can be used with all systems running to provide full data bus loadings and more complex scenarios. Either system generates data tapes which provide flight-quality data. The replay system is an extremely powerful trials facility, and can be used to measure the effects of any aircraft system change. The aircraft's hardware and software are subject to continual change and improvement, and relative performance measurements are possible using the replay system on "benchmark" runs with standard and well understood data. It is this sort of long term testing capability which makes the replay system an extremely cost-effective trials facility.

7.2 DATA ANALYSIS

7.2.1 ANALYSIS TASK OUTLINE In outline, the data analysis first merged data from several sources (the Range, instrumentation and various aircraft systems) and secondly, calculated system performance. Data from the aircraft came mainly from the 14-track instrumentation tape which contained various data streams and an accurate time reference. Data from the AUTEC Range was time, position and velocity for all the trial vehicles, recorded at 1-second intervals. In addition, data from the sonobuoy photographic analysis was included. In the 1982 trials, 21 sorties were planned, each of 7 hours data collection time. It was therefore clear that making the best use of all the data gathered would be a substantial task. Reliance on automated data analysis by digital computer was therefore essential.

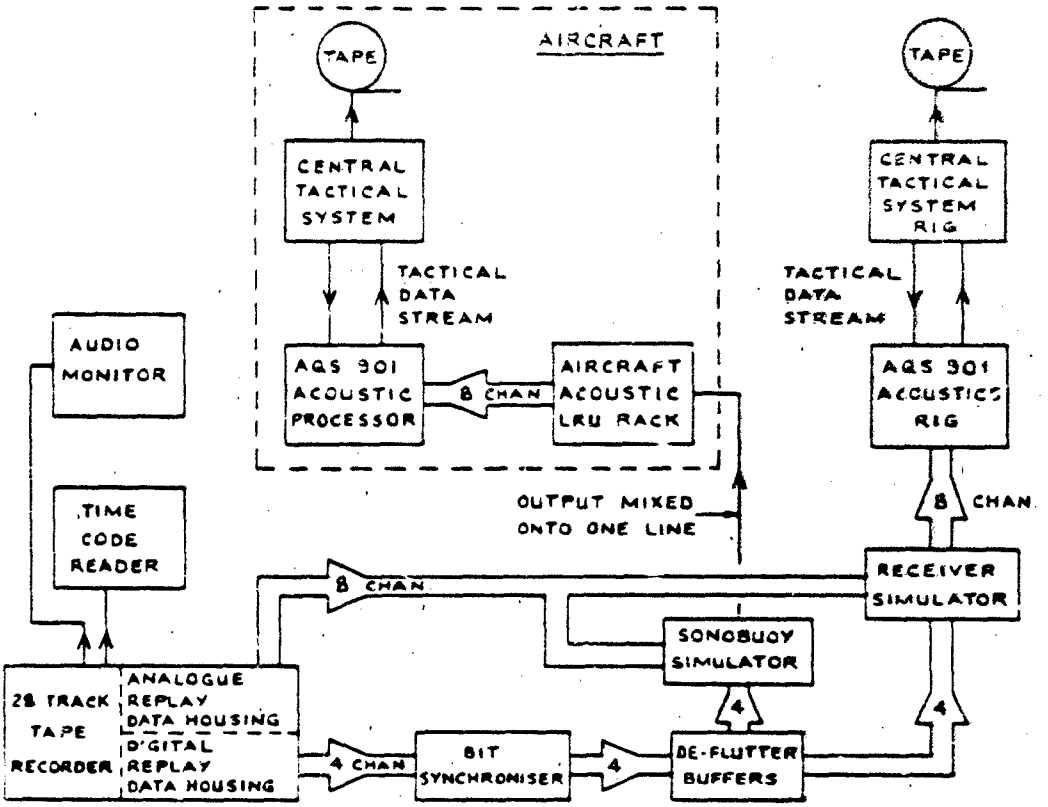

FIGURE 9 - NIMROD MR MK 2 ACOUSTIC SYSTEM TRIALS REPLAY FACILITY

7.2.2 ANALYSIS DATA STRUCTURE When preparing the data structure and programs for the analysis of the WSPT, the trials team was faced with a major problem. With around two years of preparation time, there was ample time to prepare the analysis software. However, the systems under test were new and their performance, although understood in principle, were only broadly understood in detail. It was expected that such a large and complex overall system would exhibit not only its planned characteristics, but also some emergent properties due to unforseen feedback loops within the system, possible faults or even non-standard operating methods. Analysis techniques were needed therefore which gave the trials officers flexibility in their analysis approach. Certainly, standard statistical error calculating and plotting routines would be necessary but it was recognised at an early stage that the most difficult job would be that of compiling the lists of data from which the error and behaviour statistics would be generated. The trials were expected to generate vast quantities of data, some of which would be needed in many analyses and some which would be used in one type of analysis only. Similarly, it was forseen that much data would be rejected for a variety of reasons, as is normal in trials of this nature. For the above reasons, a database format was chosen for the trial data. The pre-trial activity was therefore concentrated in the production of programs which would merge, sift and smooth data in order to produce several databases. Each database would contain data relating to a general trials area, for example: data from one type of sonobuoy. Routines were prepared which allowed the trials officers swift access to the databases, ease of editing capabilities and abilities to compute and plot error statistics on specified parts of the database under analysis. Figure 10 shows the data flows in constructing some of the databases. Pre-trial activity centred on the programs shown in the figure, which is shown to give some idea of the complexity of the task necessary to generate the databases.

the 2 km of film, searching for the sonobuoys, to calculate their drift vecotrs. Once that tedious task was completed the database generation proceeded swiftly. As expected, much data was rejected for many reasons and the data generated many questions. The main task of the analysis team at this stage was to write the application programs necessary to get to the roots of the unexpected questions. The analysis flexibility and rapid access to data provided by the database has proved the technique worthwhile and will be used again on similar trials in the future.

7.3.4 ANALYSIS COMPUTING CAPACITY The computing facility at A&AEE used in the analysis of the Nimrod trials is a GEC 4070 system. The major benefit of this computer is that it is the same system as used by the research, development and operational agencies within the Nimrod MR Mk 2 project. Software used by all the agencies is therefore compatible.

8 FUTURE TRIALS

8.1 SYSTEM UPDATES Trials activity will continue for some time in the manner described in this paper. This is because there will be a continuous trickle of new software and hardware, the purpose of which is to improve the aircraft's capability in line with a continuously refined requirement by the Royal Air Force. Return visits to the AUTEC Ranges are already planned to cover those scenarios which cannot be examined under replay conditions. In particular new types of sonobuoy will be studied and new geometries will be investigated. Also, because during replay, the effects of aircraft dynamics on the overall weapon system cannot be studied, these areas of trialling are rightly left until visits to instrumented ranges such as AUTEC.

8.2 TRIALS ON THE LORAL 1017A ESM Trials on the Loral 1017A ESM are underway, but not at such an advanced stage as Acoustics/CTS trials. It is interesting that the principles underlying the planning and execution of the Accustics/CTS trials are equally valid for the ESM/CTS trials. Much effort has gone into identifying what is felt to be the best way of controlling the trials environment for the ESM. Because of the nature of the equipment, the wide RF spectrum involved and the long-range receiving capability, no single trials environment would cover all the trials requirements. In the event, 3 controlled environments have been identified, the sum of which should enable a detailed performance trial to be carried out. Again, the Ranges and facilities necessary are in the United States, as no comparable facilities have been identified in Europe.

8.2.1 THE CHESAPEAKE BAY ELECTRONIC WARFARE TEST RANGE (CTR) The CTR, operated by the US Navy at Patuxent River, Maryland has the ability to track the aircraft throughout its period on range, and to illuminate the aircraft with a variety of radars whose transmission parameters can be controlled and changed to give adequate RF coverage across the passband of the equipment under test. The aircraft, at various distances from the transmitters will analyse the CTR radars in a very dense RF environment, bearing in mind that the East Coast of the USA has an extremely large number of radars, both military and civil. This sector of the trials therefore provides calibrated emitters and aircraft tracking in a dense RF environment.

8.2.2 ELECTRONIC WARFARE INSTRUMENTED TEST LABORATORY (EWISTL) The EWISTL, also at Patuxent River would be the next logical step in the EW trials. The broad operating performance data and DF accuracy would have been ascertained on the CTR phase, and this data would provide calibration data for a simulator interface at EWISTL. The EWISTL computers would then be able to generate EW scenarios, pass the data through the calibrated interface and then in through the aerials for processing by the aircraft's ESM system. The configuration outline of the EWISTL facilities are shown in Figure 11.

Such laboratory conditions represent almost total control of the environment: the aircraft and simulator are housed in an RF screened hangar so electro-magnetic interference should be minimal (but not zero). The main advantage of such a facility is that scenarios can be generated, ranging from a single pulse to a complete tactical mission with other ships, aircraft or whatever is desired. The (exact) same scenario will be run as many times as required on different software standards to optimise the flight programs. Once the equipment's performance is understood in detail, then the other tactical systems will be switched on and their interface links opened. This is an important step because the ESM has the capacity to generate and pass very large quantities of data to the CTS. The ESM/CTS joint systems, once connected will then be the subject of a joint trial to assess overall system performance with the environment under full control.

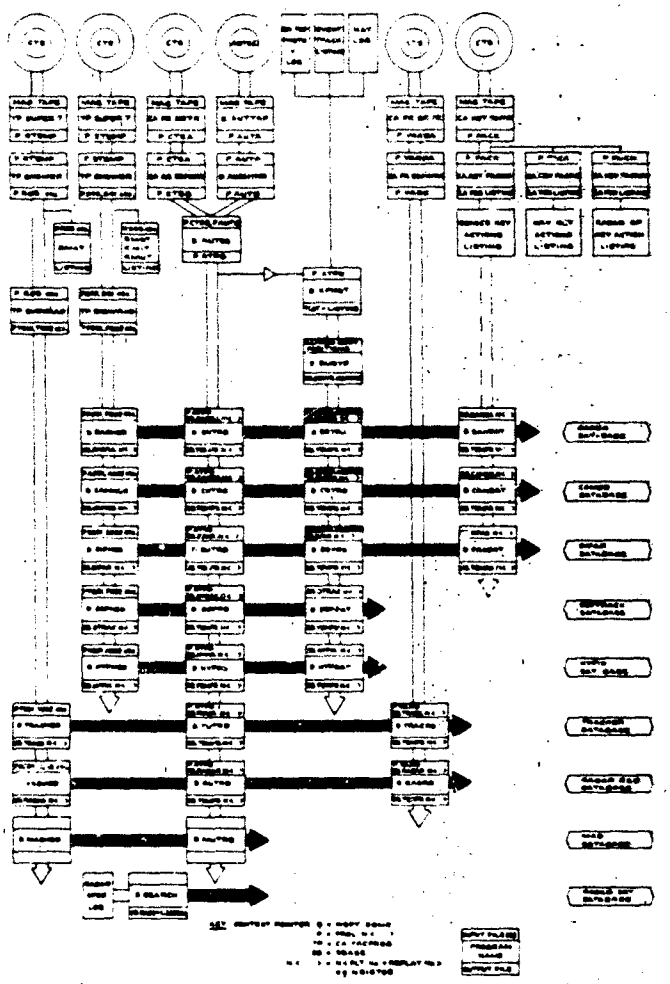

FIGURE 10 - ANALYSIS DATAFLOW FOR DATABASE GENERATION

8.2.3 EW TRIALS AT AUTEC The third controlled environment for EW trials will be the AUTEC Ranges. The Ranges at AUTEC can be regarded in much the same way as the CTR trials phase, but with a much quieter RF environment. Because of the relatively small number of non-range radars, it will be possible to obtain, before the trials, details of their transmission parameters, thus giving the trials team a fuller knowledge of the RF environment than at CTR. The ESM will then be able to use the calibrated AUTEC emitters as radars for the EW trial. The main benefit of using AUTEC, however, is that the aircraft will be conducting further acoustics/CTS/Radar trials at the same time. All interfaces will be opened and the data loading will be varied to check ESM performance under various loads on data busses.

8.3 NEW INSTRUMENTATION We have already discussed the necessity of a first-class instrumentation system when trialling a system as complex as that of the Nimrod. Much of the instrumentation used in trials to date has been that initially used in the development phase of the aircraft's systems. Now that the aircraft's systems are fully developed a new integrated instrumentation system is in the process of being built which will combine and record all the aircraft's tactical data streams. The new instrumentation system is known as the Maritime Data Acquisition System (MARDAS) and can be fitted in a front-line aircraft in a few days. MARDAS is shown diagramatically in Figure 12. The system is being designed and built at A&AEE and will be used to support trials for at least the next 10 years.

The system is controlled by a microprocessor which interrogates the various input data streams and compiles a 1600 bit per inch computer-compatible tape (CCT) in flight. By generating CCTs in flight, the analysis can start immediately on landing and thus give an enhanced trials management facility. This system will run in tandem with VTRs for the ESM and Searchwater and raw data recorders for the acoustic systems.

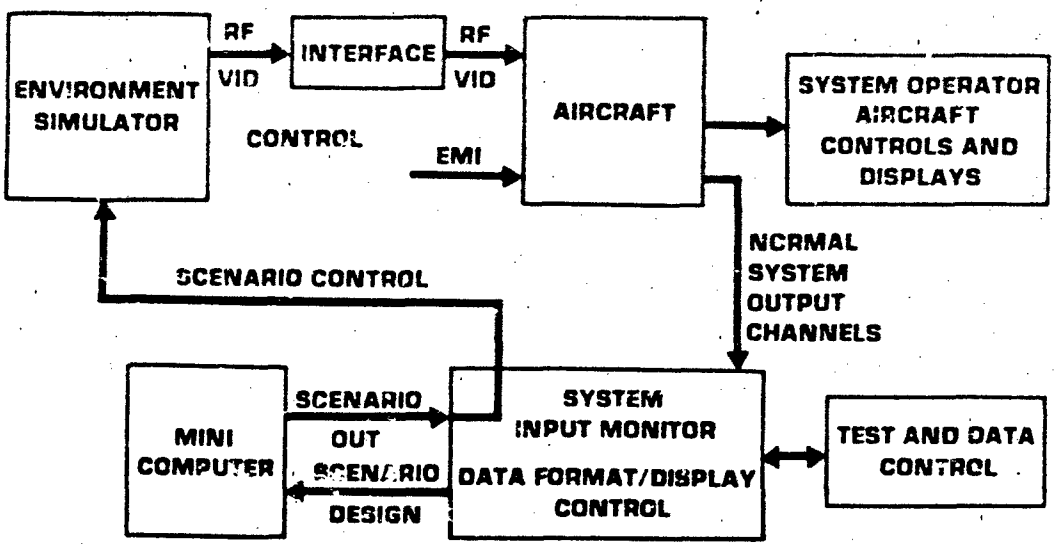

FIGURE 11 - EWISTL CONFIGURATION

9 CONCLUSION The Nimrod MR Mk 2's systems demanded a high level of complexity in the trials methods used to measure their performance. The areas of greatest trials concern were firstly the control and understanding of the sensor's environments, secondly the high accuracy datum requirements in time, position and velocity, third the extensive suite of instrumentation necessary to record all the data and finally the extensive analysis task generated by the trials. Each of the areas of concern contained some methods or techniques never before employed in A&AEE trials. The techniques overall were successful and the future trials programme is drawing heavily on experience gained so far.

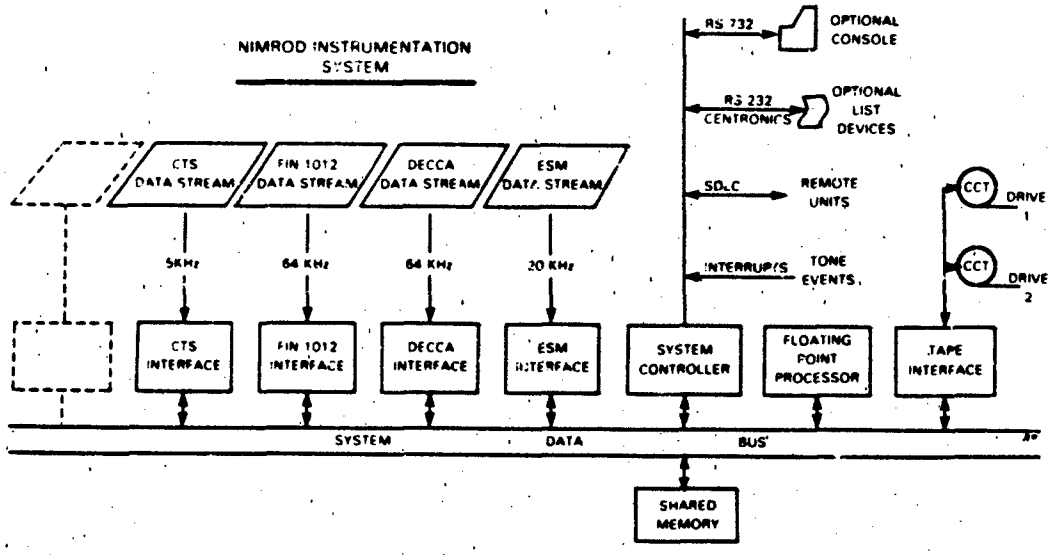

FIGURE 12 - THE MARDAS INSTRUMENTATION SYSTEM

F-16 AND A-10 DIFFRACTION OPTICS HEAD UP DISPLAY (HUD) FLIGHT TEST EVALUATION

Hans-Georg P. Wurfel
6520 TEST GROUP/ENVA
Air Force Flight Test Center (AFFTC)
Edwards AFB California 93523

ABSTRACT

Advances in Avionic Systems and Display Technologies that provide a night attack capability require an approach to testing that is markedly different from the classical flight test approach. Improvements in computers, sensors and cockpit displays have dictated innovative test planning to insure that all integrated system performance requirements are fully addressed.

The introduction of Wide Field-of-View (WFOV) diffraction optics Head up Displays (HUDs) provide potentially more capability than has been previously available. A direct head-up, pilot-to-real-world interface via video raster and stroke written symbology permits low level maneuvering flight at night and provides at least a survivable capability. Integration of the WFOV HUD with the F-16 and A-10 aircraft provides a potentially useful capability that could make single seat night attack a realistic and effective alternative.

This paper examines the major planning activities and test results of the F-16 and A-10 HUD evaluations and provides a synopsis of relevant test procedures and test techniques applicable to HUD testing in general and night video raster testing in particular. The unique test requirements and safety aspects of night attack system testing are also addressed and lessons learned are documented.

INTRODUCTION

This paper presents the results of the flight tests to verify the performance usability and acceptability of the F-16 and A-10 Wide Field-of-View (WFOV) Head up Displays (HUDs) manufactured by Marconi Avionics Limited, Rochester, Kent, England. The tests were conducted at the Air Force Flight Test Center (AFFTC), Edwards Air Force Base, California, from 12 August 1982 through 17 January 1983 (for the F-16), and 5 November 1982 through 8 March 1983 (for the A-10). The F-16 test effort involved 107 test sorties for a total of 118.4 flight hours and the A-10 program encompassed 45 test sorties and 58.2 flight hours.

The primary objectives of the flight test programs were to verify that the WFOV HUDs were functionally equivalent to the production HUDs installed in the F-16A/B and A-10A aircraft. For the purposes of these evaluations, functional equivalency was defined as:

> "The condition whereby the capabilities of the WFOV HUD, evaluated over all functional areas, are equal to or exceed the total capabilities of the current HUD."

Secondary objectives were to evaluate the capabilities of the WFOV HUDs to display a Forward Looking Infrared (FLIR) video source. These efforts included an evaluation of the pilot's ability to interface with the HUD and to qualitatively determine the performance of the HUDs in the video raster mode.

BACKGROUND

In late 1980, Headquarters, Air Force Systems Command (AFSC) initiated a program to evaluate various avionic systems applicable to the night attack mission. The Quick Look Review of Night Attack Systems program, was designed to expose evaluation pilots to a wide spectrum of night attack systems, so as to permit them to make a comprehensive evaluation of the avionics requirements for the night attack mission. The quick look test effort provided an opportunity to consolidate Air Force experience with specific weapons system and extrapolate this information to a common viewpoint. This information was then made available to aid the Air Force in making critical decisions concerning avionics and workload trade-offs in the night attack arena.

The quick look evaluation encompassed the six different aircraft and seven simulators shown in Table 1. The program spanned the spectrum of night attack avionics and, in some cases, specific avionics systems were examined in several design schemes. The "hands-on" epxerience of the test team members was also supplemented by discussions with operators who routinely used the equipment in their night operations.

The results of the Quick Look evaluation verified the effectiveness of some specific night attack avionic systems and confirmed the importance of the Head up Display (HUD) in particular. The ability to overlay flight and weapons information on a wide angle electro-optical video presentations and provide that information to the pilot via a Head up Display was determined to provide a significant advantage for conducting effective night attack operations.

TABLE 1 SUMMARY OF QUICK LOOK REVIEW AIRCRAFT AND SIMULATORS

AIRCRAFT	CHARACTERISTICS	SIMULATORS	CHARACTERISTICS
YA-7E	BEST EXAMPLE OF SINGLE SEAT NIGHT ATTACK AVIONICS AND INTEGRATION	F-16 LOW ALTITUDE NAVIGATION AND TARGETING INFRARED FOR NIGHT (LANTIRN)	PROPOSED CONFIGURATION
AC-130	CURRENT NIGHT ATTACK AVIONICS	F-15 STRIKE EAGLE	POTENTIAL TWO SEAT ALL WEATHER
HH-53 PAVE LOW	AVIONICS USED IN NIGHT LOW ALTITUDE OPERATIONS (INCLUDES NIGHT VISION GOGGLES)	F/A-18 HORNET	NAVY SINGLE SEAT NIGHT ATTACK
RF-4C, ARN-101 PAVE TACK	SOPHISTICATED NAVIGATION SYSTEM INTEGRATED WITH RADAR AND FORWARD LOOKING INFRARED	MARTIN MARIETTA SYSTEM TEST LAB (STL)	MAJOR SOURCE OF FREVIOUS NIGHT ATTACK RESEARCH
F-111D	MULTI-FUNCTION DISPLAYS AND SOPHISTICATED NAVIGATION SYSTEM	CREW STATION DESIGN FACILITY (CSDF)	PROPOSED AIR FORCE SIMULATOR FOR LANTIRN
F-111F PAVE TACK	SOPHISTICATED NAVIGATION SYSTEM WITH INTEGRATED FORWARD LOOKING INFRARED	DIGITAL AVIONICS INFORMATION SYSTEM (DAIS)	RESEARCH VEHICLE FOR ADVANCED COMPUTER INTEGRATION
		HUMAN RESOURCE LABORATORY (HRL)	F-16/A-10 SIMULATOR WITH COMPUTER GENERATED SCENES

The F-16 and A-10 Wide Field-of-View Head up Displays (WFOV HUDs) (Figure 1), were specifically designed to provide these capabilities. Built by Marconi Avionics of Rochester, Kent, England, the WFOV HUDs incorporate diffraction optical techniques to provide a wide angle video raster image to the pilot that corresponds one-to-one with the normal daytime scene. Because the image seen by the pilot relates directly to what he is accustomed to seeing by day, he can continue to use his normal day low flying visual cues and techniques at night and thus increase safety while considerably reducing his workload.

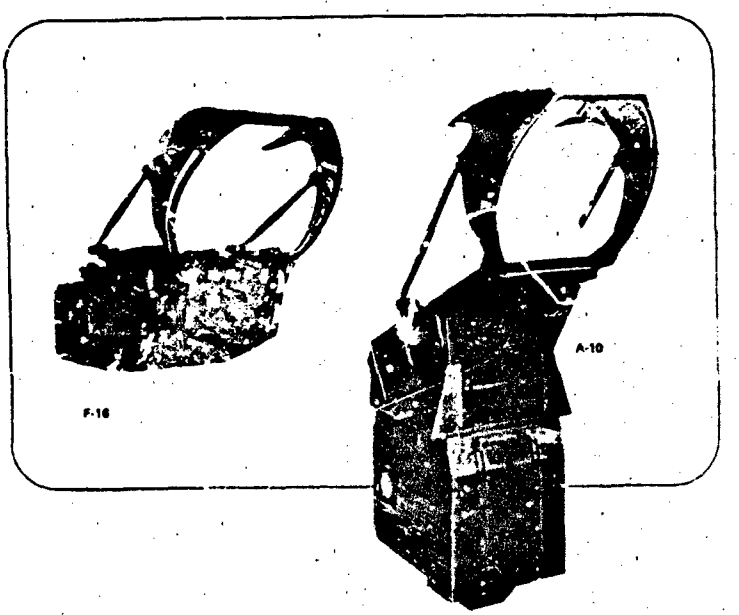

FIGURE 1 F-16 (LEFT) AND A-10 (RIGHT) WIDE FIELD-OF-VIEW HEAD UP DISPLAYS (HUDs).

F-16:

In Early 1980 the United States Air Force and General Dynamics initiated the F-16C/D, Block 25, Multinational Staged Improvement Program (MSIP). Divided into three stages (I, II, III), this program involves a series of changes to be integrated into the F-16 airframe and systems which would facilitate the introduction of various advanced avionics and systems.

Specifically, some of the additions to the F-16 as a result of these modifications include: The improved Westinghouse APG-66 radar; the modified AN/APN-22 Radar Altimeter; an increased capacity environmental control system; and expanded core avionics computer; and Advanced Central Interface Unit (ACIU); multi-function displays, upfront Communicatins, Navigation and Identification (CNI) equipment and the LANTIRN Navigation Pod, Targeting Pod and a Wide Field-of-View Head up Display.

The incorporation of the MSIP modifications essentially rebuilds the F-16 avionics suite and provides for a significant development potential for increasing the aircrafts multirole capabilities. The increased avionics capabilities are mirrored in the instrument presentations (Figure 2).

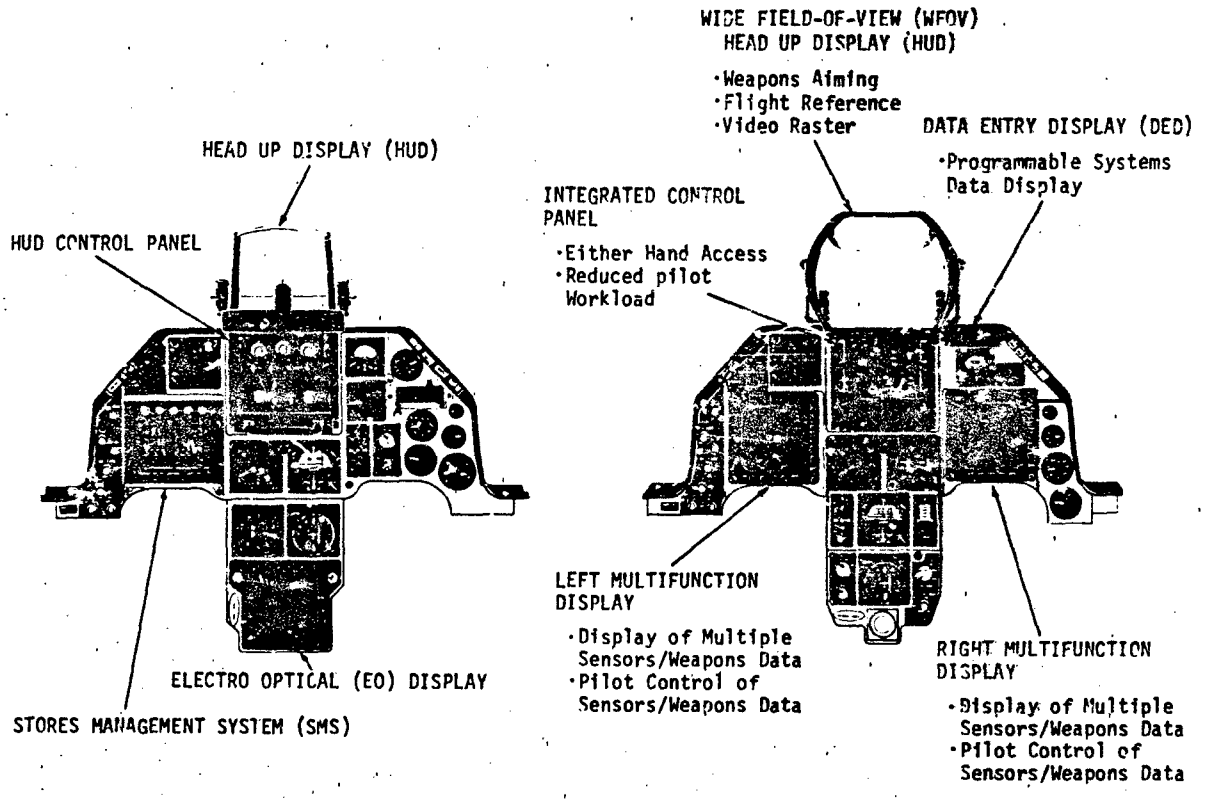

FIGURE 2 F-16 INSTRUMENT PANEL CONFIGURATION PRE- AND POST- MULTINATIONAL STAGED IMPROVEMENT PROGRAM (MSIP) INCORPORATION INCLUDING THE WIDE FIELD-OF-VIEW HEAD UP DISPLAY.

A-10:

The A-10 is also being upgraded to significantly increase the aircraft's effectiveness specifically in the night attack, first pass scenario. The total system is envisioned as utilizing pod capabilities to provide the necessary low level terrain following and target cueing aids that are not a part of the basic aircraft avionics. The A-10 Integrated Navigational System (INS) which utilizes digital multiplex techniques, provides the necessary interface system that allows for integration of Advanced Avionics with a minimum of aircraft modification.

As part of the A-10 capability upgrade, a noticable change to the aircraft configuration is the addition of the WFOV HUD in the cockpit (Figure 3). Designed as a replacement for the production KAISER HUD, the WFOV HUD can provide the pilot with a video raster presentation as well as the necessary flight, navigation and targeting information for effective utilization of the aircraft in the night attack arena.

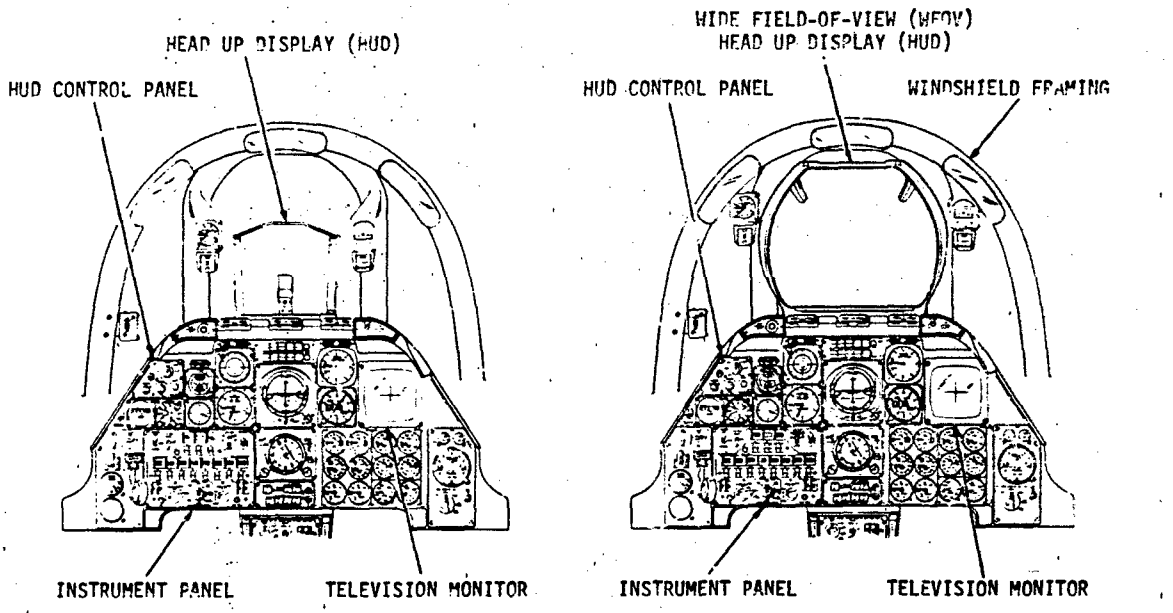

FIGURE 3 A-10 INSTRUMENT PANEL CONFIGURATION PRE- AND POST- LANTIRN SYSTEM INCORPORATION INCLUDING THE WIDE FIELD-OF-VIEW HEAD UP DISPLAY.

TEST AND EVALUATION

GENERAL

Following the test objectives, system description and method of test, the specific test results for each HUD (F-16 and A-10) are presented in detail. Human factors data and qualitative pilot comments together with engineering analysis are also included. The test effort was structured to evaluate each HUD independently. An integrated system level performance evaluation was not considered a part of these tests.

TEST OBJECTIVES

The specific objectives of the Wide Field-of-View Head up Display (WFOV HUD) flight test programs were: 1) to verify that the WFOV HUDs were functionally equivalent to the production HUDs currently installed in the F-16 and A-10 aircraft and 2) to provide an early evaluation of the HUDs video raster capability.

TEST LIMITATIONS

The F-16B aircraft used for the evaluation was a production Block 15 aircraft specifically modified for the test program. The Wide Field-of-View Head up Display, designed for the Block 25, Multinational Staged Improvement Program (MSIP) aircraft only, was modified to be compatible with this aircraft as shown in Figure 4.

A Texas Instruments/General Dynamics Forward Looking Infrared (FLIR) pod was used for the video raster evaluation. As implemented on the F-16, the interface between the aircraft and the pod was limited to a video raster display only without stroke-written symbology overlayed. In order to demonstrate the raster capability in time to support the production decision, these limitations were deemed acceptable and the flight tests were conducted with this configuration.

For the A-10 WFOV HUD evaluation, the Texas Instruments/General Dynamics FLIR pod was again used as the video raster source. Pod control functions (FLIR power, polarity, gain and level, etc.) were operated by using existing cockpit switches and controls.

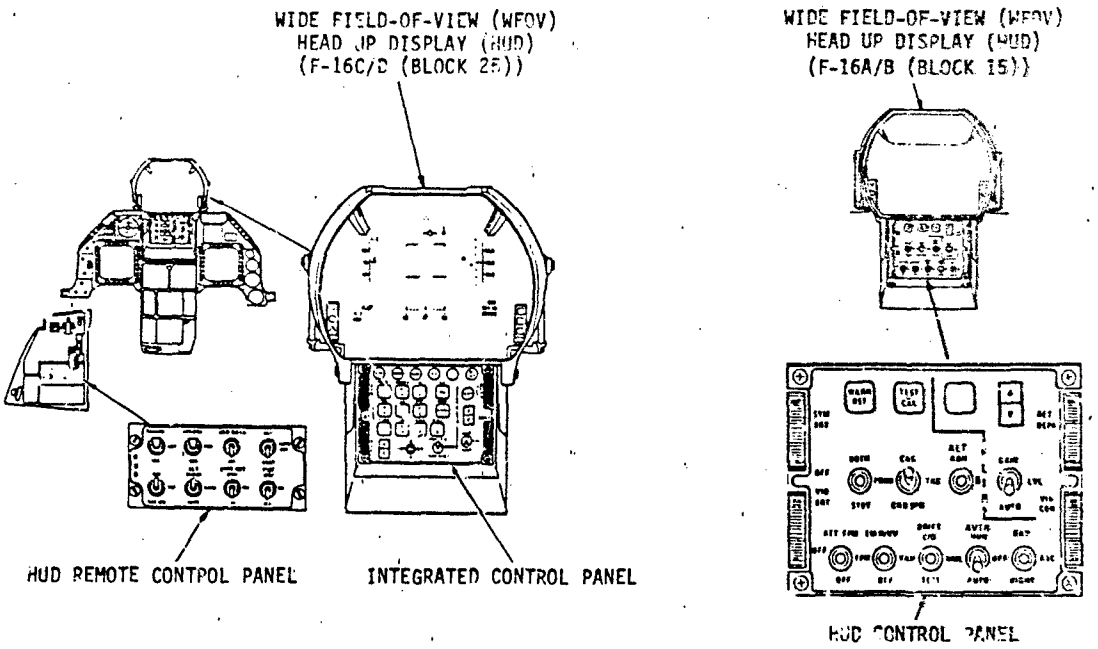

FIGURE 4 PROPOSED F-16 BLOCK 25 (MSIP) PRODUCTION CONFIGURATION (LEFT) AND THE TEST UNIQUE CONFIGURATION UTILIZED DURING THE FLIGHT TEST EVALUATION (RIGHT).

TEST ITEM DESCRIPTION

Aircraft:

F-16.

F-16B, USAF serial number 80-0635, was a production Block 15 aircraft modified with a reprogrammed Fire Control Computer (FCC), Central Interface Unit (CIU), and Fire Control Radar (FCR) computer. Additionally, the aircraft was modified to carry the Quick Reaction Instrumentation Package (QRIP) (for recording Mil-Std-1553B data traffic) and an Airborne Video Tape Recorder (AVTR) capable of providing two hours of video and audio recording.

A-10.

A-10A, USAF serial number 81-0945, was a production aircraft structually and electronically modified to accept the WFOV HUD. The modification provided for the installation of the HUD in an aircraft equipped with an Inertial Navigation System (INS) and a Cockpit Television Sensor (CTVS)/Airborne Video Tape Recorder (AVTR).

Hud:

The F-16 and A-10 WFOV HUDs (Figure 5) were electronic and optical devices designed and built by Marconi Avionics, Rochester, Kent England. They processed data and projected weapons delivery and flight information in symbolic form on a combining glass assembly located in the pilot's forward field-of-view. The HUDs provided for stroke-written symbology for day and night operation, and a wide-angle video raster display for night operation. The raster display was compatible with RS-170 (MOD) standard video. The HUD's used diffraction optics techniques to obtain a wide angle field-of-view. The raster display and diffraction optics were the most significant differences from the production HUDs. The F-16 WFOV HUD consisted of two Line Replaceable Units (LRU's): the Display Unit (DU) and the Electronics Unit (EU). The A-10 WFOV HUD had a hard LRU in the form of a remote control panel.

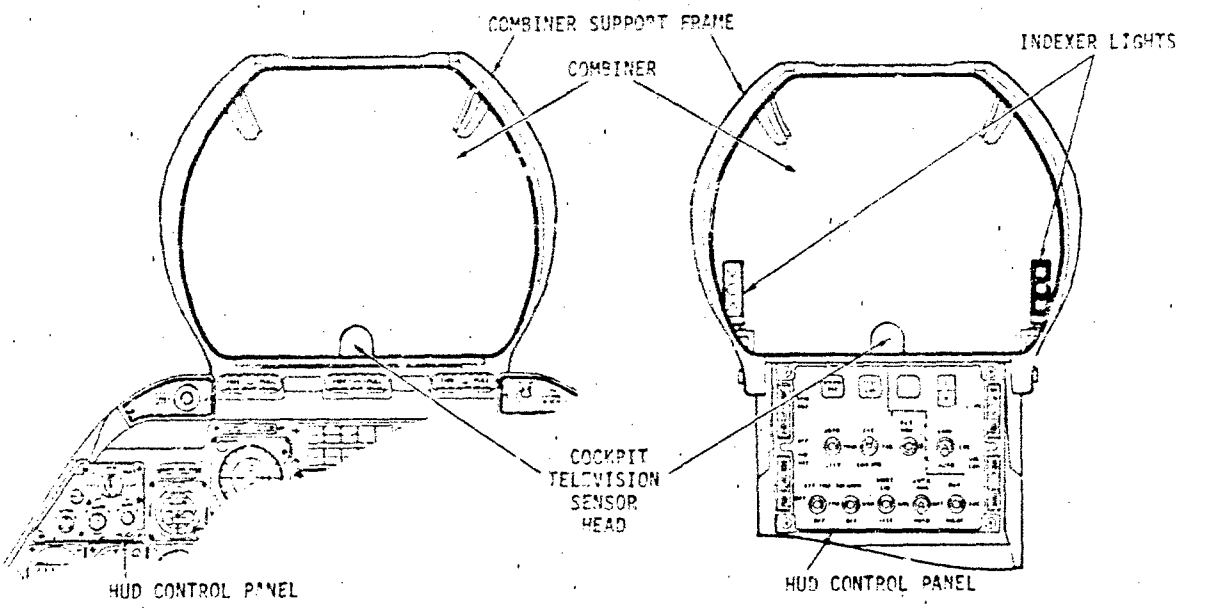

FIGURE 5 A-10 (LEFT) AND F-16 (RIGHT) WIDE FIELD-OF-VIEW HEAD UP DISPLAY

Display Unit (DU) (F-16 and A-10).

The Display Unit was mounted in the pilots forward Field-of-View above the glareshield. It contained a high brightness Cathode Ray Tube (CRT), an optical module, an automatic brightness sensor, associated electronics for signal interface compatibility, and a combining glass assembly with its associated support structure. It also contained a standby reticle generator to provide an independent standby sighting capability in case of total electronic unit failure. In the night environment, the DU could display video raster in addition to stroke symbology.

The F-16 HUD provided the pilot with an Instantaneous Field-of-View (IFOV), (i.e., seen by both eyes simultaneously) of 18.0 degrees vertical by 30.0 degrees horizontal (Figure 6). The Total Field-of-View (TFOV) was 20.0 degrees vertical by 30.0 degrees horizontal. This compares with an IFOV of 9.1 degrees vertical by 13.4 degrees horizontal and a TFOV of 20.0 degrees vertical by 20.0 degrees horizontal in the present production HUD.

The A-10 WFOV HUD provided the pilot with an IFOV of 19.0 degrees vertical by 30.0 degrees horizontal. This differs from the F-16 WFOV HUD (Figure 6) by being 1.0 degree larger in the vertical axis (from +3.0 degrees to -16.0 degrees from the horizontal datum) and the same in the horizontal axis. The TFOV of 20.0 degrees vertical by 30.0 degrees horizontal was the same as the F-16 WFOV HUD. These values are significantly larger than the 14.0 degrees vertical by 10.0 degrees horizontal TFOV in the A-10 production KAISER HUD.

Both the F-16 and A-10 HUDs contained mounting provisions for a cockpit television sensor (CTVS). The CTVs was a Charged Couple Device (CCD) electro optical imaging system which produced a composite video (television) output. It consisted of a video sensor head mounted forward of the combiner glass assembly pointed out over the nose of the aircraft and an electronic unit which was mounted in a remote location. The CTVS raster was electronically overlayed with symbology before being recorded by the AVTR.

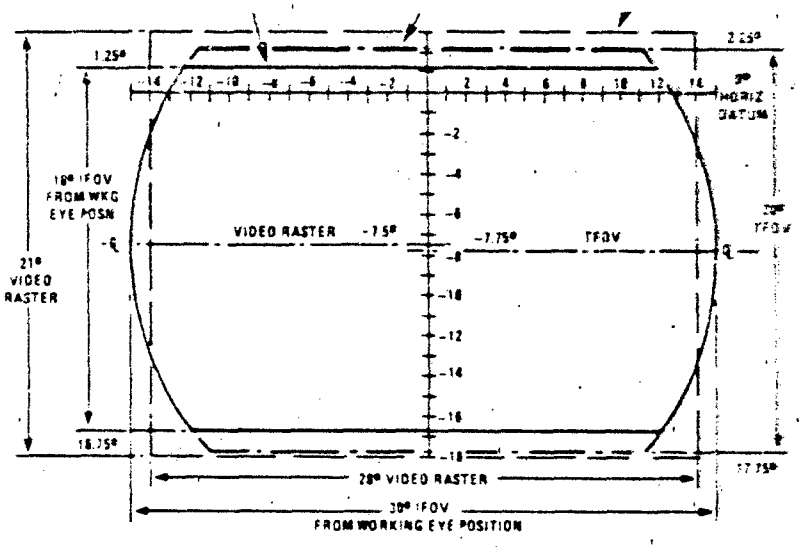

FIGURE 6 F-16 WIDE FIELD-OF-VIEW HEAD UP DISPLAY SPECIFICATION FIELDS-OF-VIEW.

Electronic Unit (EU) (F-16 and A-10).

The electronic units were located forward of the DU in the Electronics bay (F-16) or in the cockpit area (A-10). The EU contained the low voltage power supply, symbol generator, scan converter, digital computer and synchronization signals associated with the HUD interface requirements. Symbol generation, weapons aiming computations and parameter input scaling were performed by the dedicated digital computer. The symbology presented to the pilots was essentially the same as the symbology of the present HUDs. Figure 7 show typical F-16 and A-10 WPOV HUD symbology.

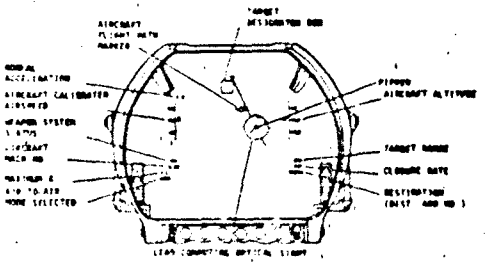

F-16 AIR-TO-AIR SYMBOLOGY

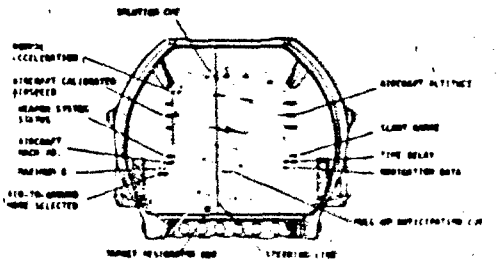

F-16 AIR-TO-GROUND SYMBOLOGY

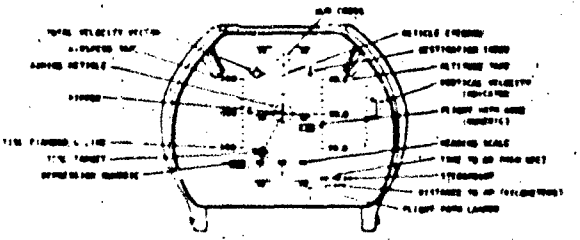

A-10 AIR-TO-GROUND SYMBOLOGY

FIGURE 7 TYPICAL F-16 (TOP) AND A-10 (BOTTOM) HEAD UP DISPLAY SYMBOLOGY.

the upper left control panel and provided the necessary controls for the operation of the HUD. There were five controls on the panel which operated symbol brightness, mode select, reticle depression, option select and a non-functional radar altimeter.

Forward Looking Infrared (FLIR) Pod:

The General Dynamics/Texas Instruments FLIR Pod was used as the video source for the raster evaluations. The pod contained a modified Texas Instruments AN/AAQ-9 FLIR, which was repackaged into an existing pod and mounted on the left inlet station of the F-16 (Figure 8) and wing station number 4 of the A-10 for the tests. The optics for the FLIR were modified to provide a 21-degree vertical by 18-degree horizontal Field-of-View that was compatible with the HUD. The FLIR was a fixed installation and provided no look-into-turn or lead-into-turn features. The pod weighed 135 pounds (297.5 kg) and was 72 inches (182.8 cm) in length and 14 inches (35.6 cm) in diameter.

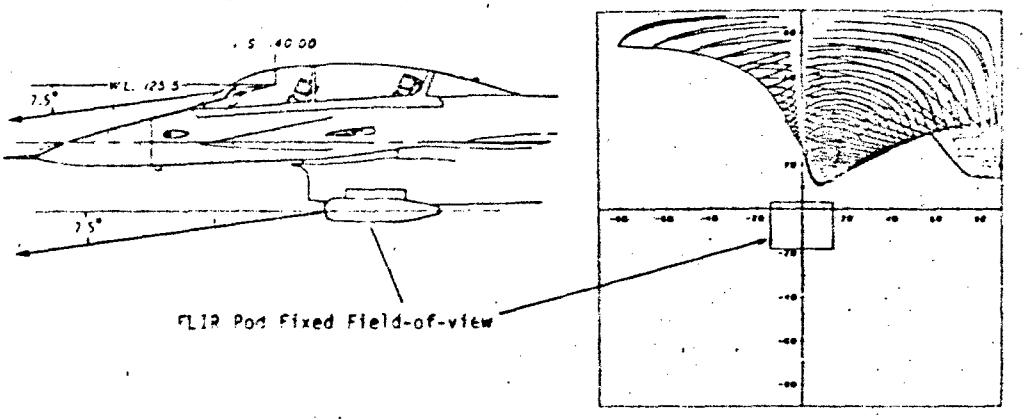

FIGURE 8 F-16 FORWARD LOOKING INFRARED (FLIR) POD FIELD-OF-VIEW.

METHOD OF EVALUATION

The HUD evaluations were based on pilot debriefings and responses to questionaires. The questionaires were developed for the evaluation of the HUD's in the following areas:

1. Optical - included issues such as field-of-view, depth perception, distortion, color changes, transmissivity, head motion box, symbology brightness, reflections and sunspots. For the video raster flights, the additional areas evaluated included raster brightness, scene discrimination and real-world registration.

2. Mechanical - addressed such items as visibility, scene blockage and controls/switches.

3. Symbology - included symbol generation and mechanization.

Pilots flew the F-16 and A-10 aircraft under a variety of flight conditions for each set of tasks, e.g., navigation: day and night, overcast, bright sunlight. During post-flight debriefings, data were collected on each of the HUD characteristics for the particular conditions evaluated. The criteria for assigning these ratings and determining the performance of the WFOV HUDs is presented in Table 2.

Table 2 HUD EVALUATION CRITERIA

Rating	Meaning
Excellent	WFOV HUD enhances the baseline (F-16 or A-10) production HUD capability.
Satisfactory	Equivalent to baseline capability.
Marginal	Not equivalent to baseline capability, but acceptable.
Unsatisfactory	Not equivalent to baseline capability and unacceptable.

The potential acceptability of the F-16 WFOV HUD by the users was a significant concern during the evaluations. To provide as broad a spectrum of user inputs as possible, four

weapons, air-to-air maneuvers, instrument approaches, VFR patterns, and landings.

In an attempt to quantify the results of these evaluations, a HUD rating scale (Figure 9) was developed to provide an objective indication of how the users perceived the F-16 WFOV HUD.

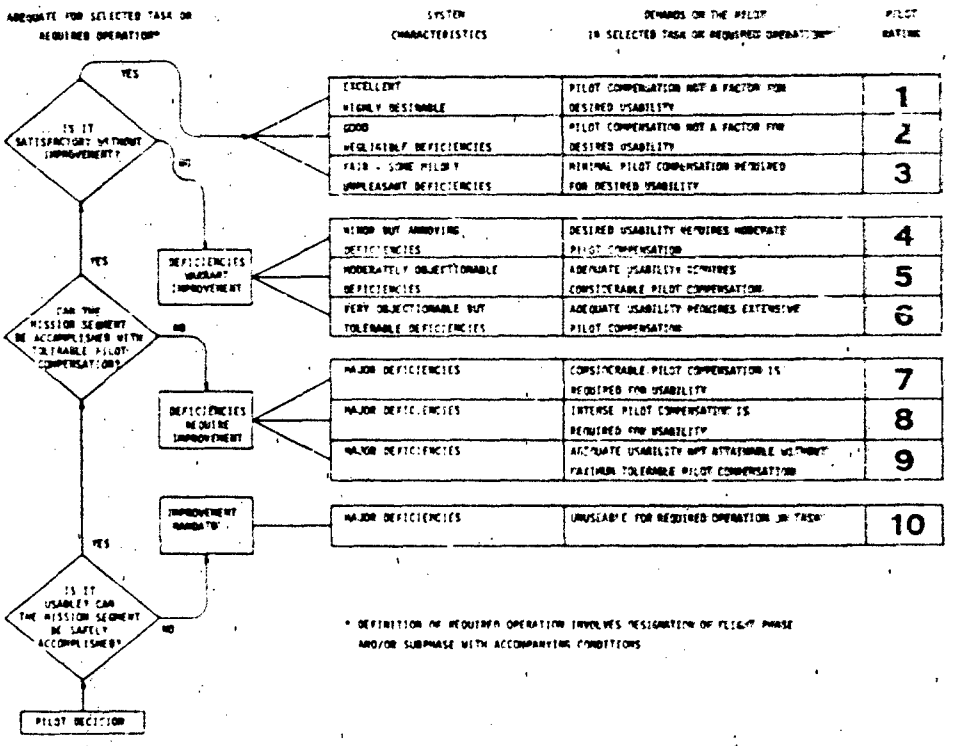

FIGURE 9 HEAD UP DISPLAY RATING SCALE.

Prior to commencing flight tests with the WFOV HUD, pilots were asked to rate the production HUD such that a performance baseline could be established. This baseline performance rating provided a direct production HUD to WFOV HUD comparison on which the functional equivalency evaluation was based.

TEST RESULTS

F-16:

Day Operations.

The greater Instantaneous and Total Fields-of-View (IFOV and TFOV) provided by the WFOV HUD, were favored by all the pilots who flew the aircraft. However, because of the deficiencies listed below, the advantages of the WFOV HUD were negated.

There were many pilot reports of a reduction in depth perception and other optical deficiencies. The magnitude and effect of these difficulties varied with the different canopy and HUD optical systems tested. The depth perception effects ranged from the HUD being reported unsafe for low level or weapons delivery events, to pilots touching down earlier than expected during landings.

Several pilots also reported was an apparent dual imaging anomaly. While focusing on the target, two sets of symbology were often viewed. Likewise, when focusing on the symbology, two targets were seen. This deficiency was particularly noted during simulated air-to-air combat and air-to-ground weapons deliveries.

The reduction of depth perception, early touchdown and dual imaging were initially thought to be related to some HUD optical characteristic. An in-depth analysis of the F-16 canopy (both Block 15 and 25), the HUD, and the canopy/HUD combination was conducted in an attempt to pinpoint the primary cause and gain some insight into the HUD and canopy interactions. The participants in the analysis included Aeronautical Systems Division (ASD), Marconi Avionics, General Dynamics and AFFTC personnel. The findings indicated that the effects were caused by a canopy induced decollimation of the outside world which was noticeable primarily because of the large Binocular Instantaneous Field-of-View (BIFOV) of the WFOV HUD (20.0 degrees horizontal by 18 degrees vertical). Figure 10 graphically illustrates this effect. This situation existed with all of the limited number of F-16 canopies and WFOV HUDs tested.

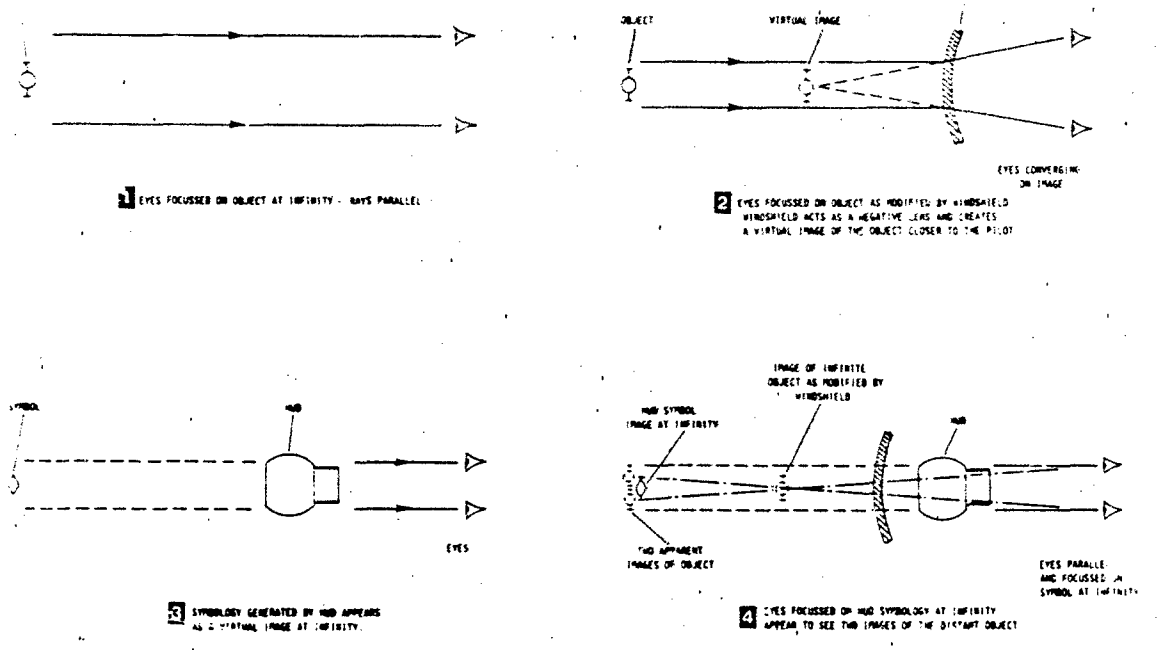

1 EYES FOCUSSED ON OBJECT AT INFINITY - RAYS PARALLEL

2 EYES FOCUSSED ON OBJECT AS MODIFIED BY WINDSHIELD
WINDSHIELD ACTS AS A NEGATIVE LENS AND CREATES A VIRTUAL IMAGE OF THE OBJECT CLOSER TO THE PILOT

3 SYMBOLOGY GENERATED BY HUD APPEARS AS A VIRTUAL IMAGE AT INFINITY

4 EYES FOCUSSED ON HUD SYMBOLOGY AT INFINITY APPEAR TO SEE TWO IMAGES OF THE DISTANT OBJECT

FIGURE 10 F-16 WIDE FIELD-OF-VIEW HEAD UP DISPLAY DECOLLIMATION EFFECT.

The narrow BIFOV of the production HUD (5.0 degrees horizontal, by 9.0 degrees vertical) was too small to make the decollimation effect readily apparent. It is expected that dual imaging and a reduction in depth perception will exist whenever a HUD with a large BIFOV is coupled with this type of canopy. The proposed Marconi Avionics fix involved determining the range of canopy decollimation over a large number of canopies and decollimating the HUD optics to a comparable mean value. This approach was never incorporated for the flight test evaluation.

The color changes and transmissivity of the HUD were rated marginal by the majority of the pilots. There were two or three colors present in the HUD at all times. In general, the bottom of the combiner had a pink shade with the top of the eyebrow area being a darker rose color. Light reflections, depending on their incident angle, often caused a green halo and green glare across the entire lower half of the combiner which was extremely distracting to the pilot.

Several pilots reported reduced transmissivity which caused an apparent reduction of visual acquisition ranges of airborne targets. Also noted when flying low level under overcast weather conditions, was an apparent darkening of the visual scene which made it difficult to distinguish detailed terrain features. The initial pilot response was to continually look around the HUD to monitor their flight path, terrain clearance, and to visually acquire targets. The dark appearance of the combining glass relative to background illumination gave the impression of having considerably reduced transmissivity. This anomaly was further exaggerated by the pink tint of the HUD which is a by-product of the diffraction grating technique on which the WFOV HUD optics are based.

Removing the gelatin from the upper one-third of the rear hologram to increase the overall transmissivity resulted in a cut-off line and added two more additional color changes to the HUD and was a further noticeable distraction to the pilots. In lieu of cutting the holographic gelatin, Marconi proposed leaving the gelatin but gradually fading the hologram toward the top of the combiner. This approach seemed workable but was never incorporated for flight testing.

The pink and rose-colored tints, the green halo, internal reflections, and the non-uniformity of the color changes tended to reduce the pilot's perception of the true world. With the Block 15 production HUD, pilots often tended to acquire targets outside of the HUD and then transfer to the HUD for weapons aiming and flight information. The WFOV HUD allowed tracking targets longer in the FOV but the apparent reduction in real-world transmissivity along with color mismatching and internal reflections caused a loss of visual acquisition range. Having to look through three combiner elements in the upper third of the HUD only exaggerated this deficiency and reduced the overall pilot acceptance of this HUD configuration.

The eye motion box was considered too restrictive by the pilots for several reasons and was rated unsatisfactory. The eye position stipulated in the HUD specification and for which the HUD optics were designed was not located at the eye position from which most pilots flew the aircraft. Figure 11 shows the allowable eye motion box and the design and working eye positions. The eye motion box defines the allowable head

Dynamics and AFFTC personnel. The data obtained during this study are presented in Figure 12. Eye positions were plotted while pilots seated themselves at their normal, relaxed aft, and alert forward positions. As shown by Figure 12, the average for all three positions was noticably forward of the specification values.

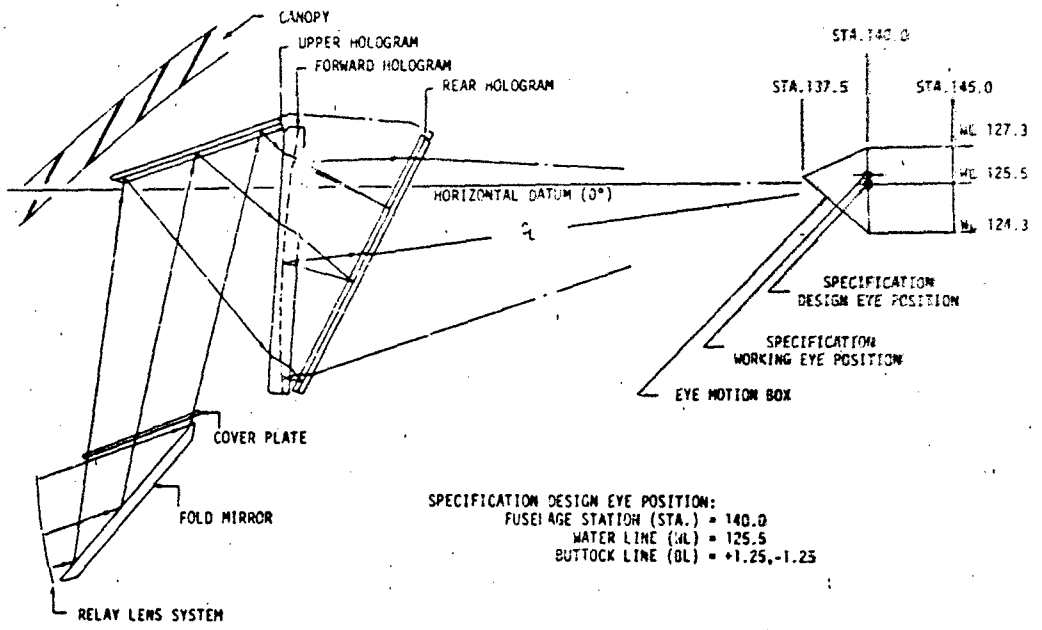

FIGURE 11 F-16 SPECIFICATION DESIGN EYE POSITION AND HEAD MOTION BOX.

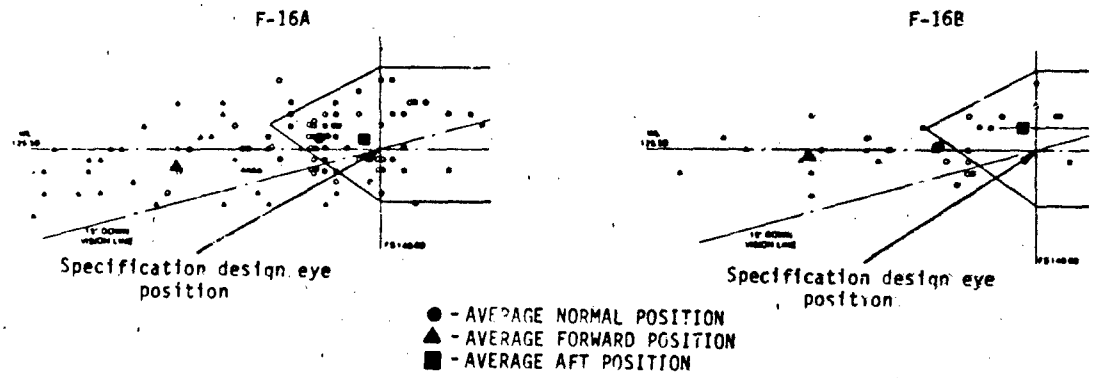

FIGURE 12 RESULTS OF F-16A (LEFT) AND F-16B (RIGHT) PILOT EYE POSITION STUDY.

An additional consequence of being outside and forward of the eye motion box resulted in the combiner halo, green glow and some of the interal HUD reflections previously discussed. Ground test verified that with proper eye positioning some, but not all, of those deficiencies could be alleviated.

The results of the eye motion box study was incorporated into the F-16 HUD Prime Item Development (PID) specification. Verification of the HUD design eye position proved to be of paramount importance during this HUD test and can have a significant effect on diffraction optic HUD flight test evaluations.

Symbology brightness was rated marginal. The symbology was controlled by an intensity control wheel as a function of two manual or one automatic brightness modes (DAY, NIGHT, and AUTO). When using the AUTO mode, the display brightness did not accurately compensate for changing ambient light or background conditions. The AUTO position also caused some fluctuations in symbology intensity under certain ambient light conditions. When operating the DAY mode, the range of brightness control was satisfactory; however, one setting was not adequate to maintain the symbology at a comfortable level. The intensity had to be continuously adjusted because of sun angle, clouds or terrain background brightness changes.

cockpit area in front of the HUD combiner were also evident at various lighting conditions. These reflections included the CTVS sensor, canopy placards, and the depression area in front of the CTVS sensor head. Different colored flight cards were tried, but no color eliminated the reflections completely. Because the reflections caused significant pilot distractions during mission critical tasks, the HUD's performance was rated unsatisfactory.

Sunspots were observed on nearly all daytime flights when the sun was not totally obscured by clouds. The most distracting sunspots were collimated which caused extremely bright, circular images approximately 25 milradians (MR) in diameter. These types of sunspots washed out HUD symbology and made it difficult to see through the HUD. A second type of sunspot was caused by reflections of the sun from canopy, pilots' helmet visor, or other reflective surfaces into the HUD. These types were not nearly as intense as the collimated sunspots and were normally 10 to 15 MR in diameter. There were up to five such sunspots on the HUD at one time. The number and intensity of sunspots caused significant pilot distractions and the HUD was rated unsatisfactory for that reason.

Visibility, had the optical deficiencies not been present, was rated excellent. The HUD allowed a better view over the nose of the aircraft and the increased width was a significant improvement over the "porthole" effect of the production HUD.

The sides of the HUD and the upper combiner support arms (see Figure 5) caused some scene blockage which required significant pilot head movements during target acquisition and attack. As shown in Figure 5, the Angle of Attack (AOA) indexer and nosewheel steering/air refueling status lights caused some scene blockage. Pilots consistently found themselves moving their head around in an attempt to compensate for the bulky structure. This detracted from the overall HUD performance. The bulk of the combiner frame, the support arms, and the presence of the indexer lights contributed to the pilots' rating the HUD marginal with respect to scene blockage.

The controls and switches on the control panel were also rated marginal by most pilots. Control sensitivity, feel, sense, linearity and response degraded the ability of the pilots to operate the HUD. The thumbwheels were considered too flimsy with insufficient friction for optimum actuation and the symbology intensity control required approximately two-thirds total travel for any symbology to appear. During daytime operations, the symbology intensity was controllable by only the last one-third of the control movement.

The video raster control was located directly under the symbology control, and if the raster control was not on the OFF position, symbology could not be displayed. It was impossible to tell if the raster control was off unless it was physically checked. The stripe on the thumbwheel was misplaced and did not line up with the OFF label when it was off.

There were numerous deficiencies noted in the symbology. Improperly placed symbology, jitter, blanking, poorly defined or missing symbols, etc., were all deficiencies contributing to an unsatisfactory rating.

Due to high frequency noise, the symbology was often fuzzy and hard to distinguish. The Flight Path Marker (FPM) and pitch ladders jittered excessively, especially during ground operations. The symbology in the lower right portion of the HUD was also observed to jitter excessively and symbology often blanked intermittently in the top 10 percent of the FOV.

Those were but a few of the numerous software deficiencies documented during the test program. The software anomalies accounted for approximately 60 percent of the deficiencies identified and resulted in an unsatisfactory rating for symbology generation.

To verify symbology placement, a series of ground tests were scheduled. The composition of these tests was based on tests that were found valuable during similar efforts on other F-16, F-15, and A-10 programs. In particular, the F-16 canopy/WFOV HUD combination required that special attention be given to the canopy correction algorithms used to correct symbology placement relative to the outside world as seen by the pilot and the CTVS camera system.

Target displacement tests had previously been conducted at the General Dynamics, Ft Worth facility. Using a still photographic digitizing procedure, the General Dynamics tests provided the canopy eye position and CTVS correction coefficients which were used during the test program. The AFFTC ground tests, used a video digitizing process, and were intended to verify the coefficients and also to verify the algorithm.

The diffraction optical techniques used with the WFOV configuration precluded the use of a camera for direct viewing of the outside world. The CTVS sensor head was therefore required to be mounted forward of the HUD combiner and the symbology was then electronically interlaced with the forward field-of-view. Prior to interlacing the symbology, canopy corrections were applied to the symbology to compensate for outside world distortions.

algorithm not being evaluated. The ground tests were originally scheduled prior to the start of flight testing and included a complete HUD and canopy optical evaluation. Lack of suitable test equipment and clearly defined test procedures at that time required postponing these tests to a later date where they were only partially accomplished. The availability of these data early in the test program would have saved considerable flight test time and would have provided substantiating data for some of the anomalies noted later in the program.

Night Operations.

The night evaluation did not expose any significant findings not already identified. FOV, depth perception, image distortion, transmissivity and eye motion box comments were very similar.

One color change deficiency not identified during the day operations was the pilot's inability to accurately judge glide slope information from the Visual Approach Slope Indicator (VASI) lights. When on the glide slope, the normal red-over-white VASI indicators appeared red-over-pink because of the HUD's pink tint. Loss of this important cue at night significantly increased the pilot's reliance on instruments and vision outside of the HUD's FOV.

The AUTO brightness mode was also unusable at night, being too bright and causing fluctuations in symbology intensity. The NIGHT mode was also deemed inadequate since the lowest intensity setting was too bright for night operations.

Reflections were less noticeable at night than during day operations. Some reflections of the cockpit console lights were noted on the left and right edges of the HUD but were not considered objectionable. During night air refuelings, pilots had no difficulty with reflections when in the contact position. However, when moving into or away from the contact position, reflections in the HUD from the KC-135 tanker lights were considered a distraction. Also when flying with a moon from one-half to full conditions, reflections or "moon spots" appeared just as sunspots had during day operations and the HUD was rated marginal.

The symbology also produced one deficiency not seen in the day. When symbols were at or near the edges of the FOV, they would often flash or sparkle at a greatly increased brightness level and were extremely distracting to the pilot. This flashing symbology made the HUD unsatisfactory at night.

A summary of the evaluation is presented in Table 3. The significant deficiencies included: a lack of depth perception/distortion, head motion box, reflections, sunspots, and symbology. A summary of the user evaluation is presented in Table 4.

TABLE 3 SUMMARY OF F-16 WFOV HUD FUNCTIONAL EQUIVALENCY EVALUATION

CHARACTERISTICS	RATING	
	DAY	NIGHT
OPTICAL:		
FIELD-OF-VIEW	EXCELLENT	EXCELLENT
DEPTH PERCEPTION/DISTORTION	UNSATISFACTORY	UNSATISFACTORY
COLOR CHANGES/TRANSMISSIVITY	MARGINAL	MARGINAL
HEAD MOTION BOX	UNSATISFACTORY	UNSATISFACTORY
SYMBOLOGY BRIGHTNESS	MARGINAL	MARGINAL
REFLECTIONS	UNSATISFACTORY	MARGINAL
SUNSPOTS	UNSATISFACTORY	N/A
MECHANICAL:		
VISIBILITY	EXCELLENT	EXCELLENT
SCENE BLOCKAGE	MARGINAL	MARGINAL
CONTROLS/SWITCHES	MARGINAL	MARGINAL
SYMBOLOGY:		
SYMBOL GENERATION	UNSATISFACTORY	UNSATISFACTORY
MECHANIZATION	SATISFACTORY	SATISFACTORY

TABLE 4 SUMMARY OF F-16 USER EVALUATION

MISSION FUNCTION	PILOT #												CONSENSUS		
	#1			#2			#3			#4					
	PRODUCTION	WFOV		PRODUCTION	WFOV		PRODUCTION	WFOV		PRODUCTION	WFOV		PRODUCTION	WFOV	
		DAY	NIGHT		DAY	NIGHT		DAY	NIGHT		DAY	NIGHT		DAY	NIGHT
GROUND OPERATIONS	1	1	1	3	4	3	2	4	4	2	3	2	2	3	3
TAKE-OFF	2	3	1	4	4	4	2	5	4	2	3	1	2	4	3
VFR NAVIGATION	2	3	1	4	4	-	2	4	4	2	3	2	2	3	2
WEAPONS DELIVERY (BOX PATTERN)	3	6	2	3	5	5	2	10	10	3	4	4	3	6	5
LOW LEVEL NAVIGATION	2	4	-	4	5	5	4	5	10	2	6	2	3	5	5
TACTICAL WEAPONS DELIVERY	3	6	-	3	5	-	5	10	-	3	6	-	3	6	-
A/A WEAPONS	4	8	-	4	5	-	6	10	-	2	8	-	4	8	-
A/A MANEUVERS	3	3	-	3	6	-	4	8	-	2	8	-	3	7	-
INSTRUMENT APPROACHES	5	3	1	4	4	4	5	2	5	2	2	2	4	3	3
VFR PATTERNS	2	2	1	3	4	4	2	2	5	2	2	2	2	2	3
LANDING	4	2	1	3	4	4	2	2	2	2	2	2	3	2	2

NOTE: NUMERIC VALUES BASED ON HUD RATING SCALE

When compared to the production F-16 HUD within the criteria established, the WFOV HUD was determined not to be functionally equivalent. It was recommended to the program office that the WFOV HUD not be considered for fleetwide incorporation into the F-16 C/D aircraft in its present hardware and software configuration.

Video Raster.

Three night evaluation flights utilizing the WFOV HUD were flown. All of the flights were limited to FLIR video only with no symbology overlayed. Additionally, the FLIR was locked in the Automatic Contrast Enhancement (ACE) mode for a majority of the airborne evaluations allowing only a cursory look at the manual gain and level control functions.

Overall, the IFOV and TFOV provided by the HUD were impressive, and the HUD provided excellent FLIR video. Pilots found that with only slight head motions left and right, a complete view of the entire FLIR video picture could be obtained. None of the comments pertinent to previously described head motion box anomalies were observed during these flights. However, there was no symbology present on the video scene which the pilots could compare to daytime observations.

There were three distinct edges to the FLIR video (top, bottom and right side) but the left side had a green band along its entire length which 'bled' into the video approximately 3 to 5 degrees. There were also two wavy lines through the video which were present only during one of the flights. These two features were somewhat distracting to the pilots and detracted from the overall uniformity of the video display.

The HUD provided good apparent depth perception, especially over undulating terrain. Over relatively flat terrain with no distinctive vertical features, a definite degradation in depth perception was evident. Overall, a very realistic image of the real world was attainable.

There were no canopy/cockpit reflections from the FLIR video on the HUD, and no halo effect or reflections were observed by the pilot or by the rear cockpit observer looking forward.

The range of video brightness/contrast control appeared adequate to achieve an optimum FLIR picture. During low altitude acquisition runs on IR targets, detection ranges steadily increased with system familiarity and operator technique. Once the FLIR gain and level were set in manual, or when using the ACE mode, adjustments were required only to the video brightness to achieve a satisfactory FLIR video.

Real-world registration was rated satisfactory; however, two points are worthy of mention. Point light sources in a high ambient light environment appeared to show through the FLIR imagery and appeared to the pilot as add-ons, i.e., the lights were superimposed on the FLIR video. One pilot found viewing these lights through the HUD and canopy gave coincidental results while a second pilot felt there was some parallax error between real-world lights and FLIR imagery. Secondly, FLIR video over highly lighted areas was virtually invisible. The outside ground lights showed in the HUD as they were in the real world through the canopy but only small pieces of FLIR imagery were present. Overall, the outside light made for a significantly washed out FLIR presentation. This phenomena did not restrict pilot usability of the HUD, and on transitioning to an unlighted background, the pilot was again presented with a satisfactory FLIR picture.

All three evaluation pilots found the controls and switch operations to be satisfactory. In the ACE mode, the pilot was able to control brightness and contrast while maintaining good gray scale definition. In the manual mode, small adjustments of video brightness were easily accomplished.

System limitations did not permit an evaluation of FLIR video with HUD symbology overlayed. This is an area which requires extensive evaluation to ascertain the impact (if any) of HUD symbology on FLIR video quality and the effect on pilot interpretation. The FLIR video raster flights demonstrated the general raster capability of the HUD; however, further testing of the WFOV HUD with video raster and stroke written symbology was recommended to quantify and define the HUD's total system capabilities.

A-10:

Day Operations.

The greater field-of-view provided by the WFOV HUD was favored by all of the A-10 pilots on the test team. The wide field-of-view significantly improved forward visibility and reduced or completely eliminated any tendency of the pilots to look around the HUD. This feature was deemed an appreciable advantage over the present KAISER HUD.

Unlike the F-16, there were no depth perception or optical distortion difficulties reported. Depth perception was "normal" and comparable to the present HUD, with no obvious differences noted. There were no apparent distortions of the outside world when viewed through the WFOV HUD and the flat plate windshield. The visual scene and the symbology were reported as being clear, concise and in true perspective.

The head motion box, although rated satisfactory, was considered somewhat restrictive. As with the F-16, the eye position stipulated in the HUD specification was not located at the eye position from which most pilots flew the aircraft. Figure 13 shows the design and pilots eye positions and the head motion box. Most of the pilots flew the aircraft from a position which placed their eyes two to three inches forward of the design eye point. This situation was not as critical as the F-16 eye motion box due to a substantial portion of the A-10 head motion box being forward of the design eye position. Proper seat positioning and experience partially compensated for this limitation.

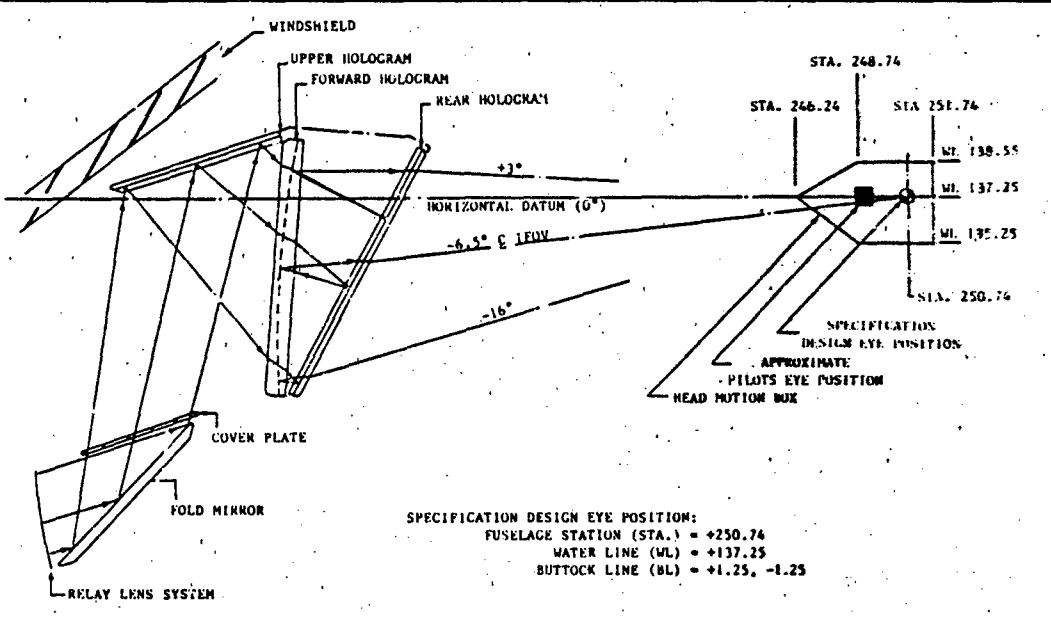

FIGURE 13 A-10 SPECIFICATION DESIGN EYE POSITION AND HEAD MOTION BOX.

The transmissivity of the HUD was rated satisfactory although there was a discernable difference in the amount of light transmitted through the WFOV HUD, the difference was not objectionable and the pilots felt that it did not affect their ability to acquire and maintain visual situation awareness.

The slight pink tint of the HUD in and of itself was not considered objectionable. Light reflections, depending on their incident angle, sometimes also caused a green tint along with the pink tint. These colorations were not noticed by the pilots during high gain tasks and pilots reported they could see through the combiner easily and not be distracted.

Symbology brightness was rated satisfactory. The symbology was controlled by a ganged knob which operated two manual and one automatic brightness modes (DAY, NIGHT, and AUTO). When utilizing the AUTO mode the display brightness did not accurately compensate for different aerial and terrain background. When operating in the DAY mode the range of brightness control was considered satisfactory. The overall rating for symbology brightness was based on the results obtained in the DAY mode.

Pilot reports on internal reflections in the HUD ranged from "no reflections seen" to "everything in the cockpit reflected on the HUD" with the majority of the pilots reporting reflections of flight cards and maps laying on their legs. In an effort to alleviate this problem, pink flight cards were used and pilots generally agreed that the pink cards were reflected less than the white but were still visible and annoying. The reflections were most evident when the cockpit was subjected to intense front lighting. When compared to the production HUD, the WFOV HUD's performance relative to reflections was rated marginal.

Sun reflections were also observed on a number of daytime flights. Again comments were wide ranging from "no sunspots noted" to "reflections of the sun in the HUD were persistent at all times". The consensus was that although there were some sunspots visible, they only appeared with the sun at high angles relative to the aircraft. The approximate sunspot "cone of occurrence" was observed when the sun was within 10 degrees of HUD vertical. This cone was slightly larger than the one existing in the present KAISER HUD. The sunspot effect degraded the WFOV HUD and therefore the pilots rated the HUD marginal in this area.

Visibility through the HUD and scene blockage were considered excellent and satisfactory respectively. Being considerably wider than the present HUD, the WFOV HUD allowed a better view over the nose of the aircraft and intruded less into the prime vision area. The combiner support was in line with the front windshield frame permitting an unbroken view through the front windshield. Pilots could occasionally produce some scene blockage but this required extreme pilot head movements.

Controls and switches on the HUD control panel were determined to be marginal from several aspects. Control sensitivity, feel, switch shape, arrangement, and spacing, were objectionable and resulted in a degraded ability to operate the HUD. The addition of steps on the rotary switches would have provided the necessary control feedback.

Various deficiencies in the symbology were noted. The display of non-specification symbols, jitter, poorly defined symbols, and some symbol blinking were often identified as problems or anomalies and resulted in an overall rating of unsatisfactory for symbology generation. The pilots were able to adapt to these deficiencies; however, time to read and understand the displays was increased and mission performance was degraded.

During the evaluation, pilots witnessed several cases of a momentary loss of symbology. This blanking was noted particularly during gun firing and multiple "G" pull-ups. The blanking did not persist for any significant length of time, was never predictable, and was not diagnosed. Symbology blinking was also observed on the Heading and altitude scale numerics. As heading or altitude scale numerics would enter or leave the scale, the numbers would often momentarily blink.

Deficiencies were also identified which resulted in the symbology mechanization being rated marginal. A particular porblem in this area was the steering tadpole. On several occasions the steering symbol would seem to disappear from the HUD FOV. Actually, the symbol was still on the display; having only moved to the outer edge of the HUD where it was not easily seen. There were two reasons for this: 1) the symbol was horizon stabilized and was routinely limited on the display FOV during high positive or negative pitch angles, and 2) the range of movement for the symbol was too large and pilots would lose it at the extremes of travel. By moving the head around, the symbol could be located. This was considered unacceptable and increased the workload significantly. This deficiency could have been easily remedied by limiting this symbol's range of travel.

Display clutter, particularly in the gunnery and bombing modes, degraded the overall usability of the WFOV HUD. Symbology displayed when approaching a target was often cluttered by having the pipper, pitch line, flight path marker and symbols obscuring each other. Also, multiple images of the 0 degree pitch reference line, which appeared as three lines with the top line breaking away from the other two were reported. In one instance, the aiming pipper also appeared to be composed of multiple images. If the symbol brightness were turned down to an uncomfortable low level the

ghost images would disappear. These two observations, however, were not noted by the majority of pilots.

Nighttime Operations.

The night evaluation of the HUD did not expose any significant findings not already identified. Field-of-view, depth perception/distortion, color changes/ transmissivity and head motion box comments remained unchanged.

One deficiency originally identified during the day evaluation produced a completely different characteristic at night. The AUTO brightness mode, which caused no significant symbology brightness change during the day, caused erratic brightness changes during the night flights which made this mode unusable. The NIGHT mode proved to be adequate and the DAY mode was usable at night although it was slightly too bright.

Reflections were significantly less noticeable at night compared to day operations. Reflections of interior cockpit panels, flight cards, etc., were observed but were considered less distracting than those observed during the day. The most conspicuous night reflections experienced were from the emergency (thunderstorm) flood light which greatly increased the interior cockpit illumination. The predominant reflections reported when using these lights include the arms, hands, aircraft console panels, and flight cards. During simulated attacks under aerial flares and ground illuminated targets, some reflections were observed but were not reported as being objectionable. During aerial refueling, the tail mounted flood lights on the KC-135 tanker illuminated the cockpit interior and caused some reflections on the HUD. However, the flood light was not required for in-flight refueling of the A-10 and, once extinguished, cockpit reflections during refueling were eliminated. Night reflections in the HUD were minimal and the HUD was rated satisfactory.

Several night flights were flown with the moon present at one half to near full conditions. Moon reflections were reported when the moon was at a high angle to the HUD, however, these moon reflections were weak and not objectionable.

The HUD control panel had an additional deficiency noted during the night operations. The control panel back-lighting was considered satisfactory but the knobs were not shape coded and did not provide sufficient tactile identification.

Data from the air-to-ground gunnery and bombing missions were analyzed to determine if there were any significant degradations to the accuracy of the A-10 by the addition of the WFOV HUD. The findings indicte that the existing air-to-ground capability of the A-10 was not degraded by the addition of the WFOV HUD. The HUD appeared to portray the correct aiming solutions for gunnery and bombing tasks but the results provided only an intuitive feel for the contribution of the HUD to the A-10's accuracy performance. Quantitative flight test of the WFOV HUD in the air-to-ground gunnery and bombing modes is yet to be conducted.

Table 5 tabulates the results of the functional equivalency evaluation. When compared to the production A-10 HUD within the criteria established, the WFOV HUD was determined to be functionally equivalent.

TABLE 5 SUMMARY OF A-10 WFOV HUD FUNCTIONAL EQUIVALENCY EVALUATION

CHARACTERISTICS	RATING	
	DAY	NIGHT
OPTICAL:		
FIELD-OF-VIEW	EXCELLENT	EXCELLENT
DEPTH PERCEPTION/DISTORTION	SATISFACTORY	SATISFACTORY
COLOR CHANGES/TRANSMISSIVITY	SATISFACTORY	SATISFACTORY
HEAD MOTION BOX	SATISFACTORY	SATISFACTORY
SYMBOLOGY BRIGHTNESS	SATISFACTORY	SATISFACTORY
REFLECTIONS	MARGINAL	SATISFACTORY
SUNSPOTS	MARGINAL	N/A
MECHANICAL:		
VISIBILITY	EXCELLENT	EXCELLENT
SCENE BLOCKAGE	SATISFACTORY	SATISFACTORY
CONTROLS/SWITCHES	MARGINAL	MARGINAL
SYMBOLOGY:		
SYMBOL GENERATION	UNSATISFACTORY	UNSATISFACTORY
MECHANIZATION	MARGINAL	MARGINAL

Video Raster:

The video raster capability of the WFOV HUD was demonstrated during two night flights with the General Dynamics/Texas Instruments FLIR pod. The flights were flown over a variety of terrain types and included several approaches and landings. Two WFOV HUD systems were flown to evaluate any differences as a result of different hardware/software combinations.

The greater FOV provided by the HUD enhanced the video raster capability. The improved FOV was very helpful in terrain avoidance. There was no hesitancy to maneuver the aircraft and the FOV was sufficient for low level terrain avoidance and terrain following tasks.

Recognition of objects seen on the display was marginal. While flying at 2,000 feet above ground level (AGL) pilots could barely discriminate large vehicles (trucks and buses) at very short slant ranges and smaller vehicles (cars) were reported as being difficult, if not impossible, to reslove. Terrain features (large trees, ridges, etc.), could be identified sufficiently to perform navigation tasks but ground attacks with the tested system were only marginally possible and thus the system was rated inadequate.

The simultaneous stroke written symbology and video raster presentation were very good. The display had some minor raster distortion around the edges but was reported to be insignificant and acceptable. The FLIR picture and real-world registration were estimated to be within two milliradians (mr) of each other. Problems of imaging, that of the real-world bleeding through the video raster picture, were not seen. There was no discernable mismatch when viewing the real-world through the HUD and there were no problems with any double images.

The prototype switches and non-operationally integrated system controls made FLIR adjustments very difficult. Pilots were required to look into the cockpit when making these adjustments. During high workload situations tuning the display, adjusting contrast, brightness and gain levels, was considered too time consuming and increased the likelihood of errors.

Display brightness and symbology were judged to be adequate. An adequate range of brightness was available and the symbology was clear and crisp. Since the symbology background was the FLIR picture, background intensity changes would occasionally require compensating symbol brightness changes. This was an annoyance which could be tolerated.

No reflections of cockpit lighting on the HUD were reported while video raster was being displayed. With the white cockpit lighting "on" and adjusted to a comfortable level, reflections were minimal. Approaches and landings to a brightly lighted runway produced no noticeable reflections.

There was no significant degradation of the FLIR video picture in banks up to 30 degrees. FLIR "blooming" (washout) in turns over 15 degrees had been looked for since the effect had been noted during the F-16 video evaluation. Modifications to the FLIR pod by Texas Instruments after the F-16 flights, apparently prevented a recurrence of this effect during the A-10 flights. This feature significantly improved the maneuvering capability of the aircraft.

Because of the altitudes at which these flights were conducted (2,000 feet AGL), no depth perception difficulties were expected or reported. During the approach and landing phases of the flights, no difficulties were experienced in judging range or altitude using the video raster presentation.

The A-10 FLIR video raster flights further demonstrated the raster capability of the WFOV HUD. Follow-on flight testing of the WFOV HUD with video raster was recommended to the program office to substantiate the HUD's capabilities and further define its characteristics.

CONCLUSION

The results of these evaluations were briefed to the F-16 and A-10 program offices in January 1983 and March 1983 respectively. The failure of the WFOV HUD to demonstrate functional equivalency with the production F-16 HUD was an area that had significant ramifications to the F-16C/D (MSIP) production schedules. The final decisions relative to this program was two-fold: 1) The MSIP HUD reverted to a wide-angle conventional (WAC) optics HUD and 2) the WFOV HUD optical module was to be redesigned and further testing with this new configuration was to be continued.

The Marconi Avionics Wide Angle Conventional (WAC) HUD (Figure 14) has essentially the same form, fit and function as the WFOV HUD with the primary difference being in the optical module. Where the WFOV HUD used diffraction optical techniques for a wide field-of-view, the WAC HUD uses conventional optics to obtain a significantly larger field-of-view than the present production HUD. The HUD provides the pilot with an IFOV of 13.45 degrees vertical by 20.0 degrees horizontal. The TFOV of 25.0 degrees vertical and horizontal is the largest possible using this optical technique and given the F-16 cockpit configuration and sizing limitations. The first flight test articles are expected to be available in the April-May 1984 time frame.

The findings of the WFOV HUD test program identified various areas that were deficient with that particular HUD configuration. An improperly defined head motion box, a larger than desired optical combiner frome, transmissivity losses, canopy/HUD decollimation effects and internal HUD reflections were major areas that required correction before this HUD could be considered acceptable for incorporation into operational aircraft.

In early 1983, Marconi Avionics initiated work on a redesigned optical module for the WFOV HUD to correct these anomalies and substantially improve the overall acceptance of this HUD (Figure 14). The new configuration is designed to alleviate all of the previously identified anomalies including the canopy decollimation effect which is improved by decollimating the HUD to a mean value determined from a production canopy survey. The use of a single piece cast combiner frame in lieu of the three piece supported combiner is also expected to substantially reduce the scene blockage effect that was deemed unacceptable with the previous configuration.

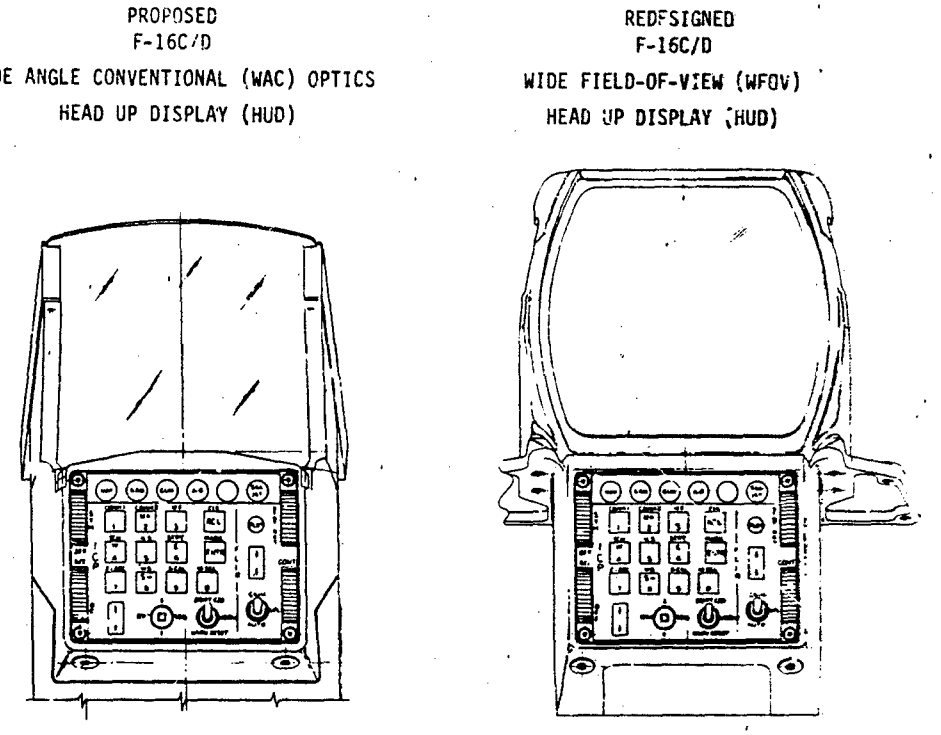

FIGURE 14 PROPOSED F-16C/D WIDE ANGLE CONVENTIONAL (WAC) OPTICS HEAD UP DISPLAY (LEFT) AND REDESIGNED WIDE FIELD-OF-VIEW HEAD UP DISPLAY (RIGHT).

Flight testing of this new configuration began in November 1983 and is on-going at this time. The availability of an MSIP configured F-16 for this test program also allows the reconfigured WFOV HUD to be tested in a fully integrated configuration and should result in a more meaningful test of the WFOV HUD.

The incorporation of the WFOV HUD into production A-10 aircraft is still undetermined. The decision to fit the A-10 with WFOV HUDs was not as critical as the F-16 decision since the HUD can be retrofitted to the aircraft and does not require the total integration as was the case for the F-16.

The development of the WFOV HUD has opened a new frontier in both design technology and test and evaluation techniques. As with any new state-of-the-art system, the initial technical application exhibited some undesirable characteristics that detracted from the overall performance. Much to the credit of both the contractor and Air Force Test and Evaluation community, most of the shortcomings have been identified and are being corrected during the current phase of the WFOV HUD development. The potential demonstrated by the WFOV HUD indicates it will have a major, favorable impact on the next generation of free world combat aircraft.

Helmut Bothe

and

Kurt Klein

Deutsche Forschungs- und Versuchsanstalt
für Luft- und Raumfahrt (DFVLR)
Institut für Flugführung
3300 Braunschweig
Germany

Electronic Support Measurement Systems (ESM) and Systems for Electronic Counter Measures (ECM) of military aircraft require antennas for signal transmission and reception. The coverage of these antennas is an important parameter in the effectiveness of the systems. As the radiation patterns of aircraft antennas are interfered to a hight degree by the structure and configuration of the aircraft, flight tests are conducted in order to prove the coverage of the above-mentioned systems. In addition, the accuracy of ESM systems, which measure the direction of arrival of an incoming radio frequency signal on board, is mostly influenced by the characteristics of the receiving antennas and hence has to be determined in flight too.

The Institut of Flight Guidance of DFVLR has developed a system which covers the aforesaid requirements. It consists of 3 subsystems :

- a ground emitter system illuminating the target up to frequencies of 18 GHz,
- an on-board receiving system, which detects the signals received by the antennas of the system under test
- a data acquisition and transmission system, which transfers on-board and ground data to a digital computer for quick-look and data processing.

The basic system philosophy is illustrated in Fig. 1. An on-board ESM-System measures the direction of arrival of a ground transmitted radio frequency signal, denoted by ϕ_D, e.g. with respect to the roll axis of the aircraft. Taking bearings from different known positions of the flight path, the position of the ground station can be computed for reconnaissance purposes. The accuracy of this computation depends on the accuracy of the navig... equipment of the aircraft and the accuracy of the ESM-System determining ϕ_D.

For test purposes, as in Fig. 1 illustrate, the direction of arrival angle ϕ_D can be computed, if the heading angle ψ and the position dependent angle β are known, by

$$\phi_D = 180° - \beta - \psi \qquad \text{Eq. 1}$$

The heading angle ψ is usually measured by an on-board gyro or platform system. The position dependent angle β is picked up in the ground station, if the antenna system is tracking the aircraft, as $\beta = 360° - \rho$, ρ being the tracking angle of the antenna. Necessary corrections due to altitude and antenna elevation variations are discussed below.

At last, the direction of arrival output signal of the ESM-System is compared to the angle computed by the test system and the error is plotted. The angular accuracy of the measuring system has to be considerably higher than the accuracy of the ESM- System.

A complete 360° angular coverage of an ESM-System is usually performed by a number of different on-board antenna arrangements, each covering a certain sector of the total angular range (Fig. 2). In order to evaluate all individual sectors and transitions from one sector to the next one the aircraft has to perform a complete 360° turn during a test flight.

Moreover, the performance of the ESM-System's receiving antennas may vary with respect to the depression angle illustrated in Fig. 3. To discover this influence, test flights in different proper selected altitudes and distances have to be performed, in the corse of which the altitude of the aircraft has to be taken into account too.

An ECM System detects incoming radio frequency signals in order to warn the pilot of being tracked by a ground or missile radar and to transmit appropriate jamming signals. To achieve an adequate near spherical coverage of the receiving and transmitting system usually several antennas are installed on board the aircraft, and the directional sensitivity of these antennas have to be tested to assure the required coverage.

The basic coverage test method is very similar to the ESM-System test configurati... shown in Fig. 1. Just the direction of arrival ϕ_D is replaced by the aspect angle ϕ_A. In addition the distance d between the ground station and the aircraft has to b...

aircraft have to be taken into account.
Due to the fact, that ϕ_A and ϕ_E are measured in an aircraft oriented coordinate system and the other parameters in a ground based system, the necessary coordinate transformation leads to complicated equations. If the earth curvature is neglected (0.09° for 10 km distance, summing up linearly) in the range of interest, we get as given in Ref. 1:

$$\phi_A = \tan^{-1} \frac{A_y}{A_x} \qquad \text{Eq. 2}$$

$$\phi_E = \tan^{-1} \frac{-A_z}{A_x^2 + A_y^2} \qquad \text{Eq. 3}$$

where

$$A_x = -\cos\rho_E \cos(\phi-\rho_A)\cos\delta - \sin\rho_E \sin\delta$$

$$A_y = \cos\rho_E (\sin(\phi-\rho_A)\cos\varphi - \cos(\phi-\rho_A) \sin\delta \sin\varphi) + \sin\rho_E \cos\delta \sin\varphi$$

$$A_z = -\cos\rho_E (\cos(\phi-\rho_A)\cos\delta \cos\varphi + \sin(\phi-\rho_A) \sin\varphi) + \sin\rho_E \cos\delta \cos\varphi$$

Distance correction of received power level is derived from the transmission equation of the air-ground propagation channel. If logarithmic units of measure are used this expression after Ref. 1 becomes:

$$G_R = P_R - P_T - G_T - G_M + L + 20\log d + 20\log f + 2.45 \text{ dB} \qquad \text{Eq. 4}$$

It is

G_R = gain of receiving antenna in dB
P_R = input power of receiver in dB_m (dB above 1 m W)
P_T = output power of transmitter in dB_m (dB above 1 W)
G_T = gain of transmitting antenna in dB
G_M = gain of reflecting ground in dB
L = line losses (between power measuring terminals and antennas) in dB
d = distance between transmitting and receiving antenna in km
f = transmitting frequency in MHz

After all necessary calculations with respect to Eq. 2, 3 and 4 are completed, the gain of the antenna under test can be plotted as a function of the horizontal or vertical aspect angle

Usually the ECM-Receiver is not fit for measuring the received power level. Therefore a special wide-band power level measuring device with high input sensitivity had to be developed, being able to replace the ECM-Equipment also physically during the flight tests. Further details follow below.

Attitude parameters are derived from a gyro or platform system on-board the aircraft. Position parameters are detached from an on-board radio navigation system and the ground antenna tracking system. All on-board derived data is transmitted to the ground station via a telemetry link. A high precision telemetry ground tracking antenna traces the aircraft automatically.

The high gain ground emitter antenna illuminating the aircraft is slaved to the telemetry antenna.

Real time calculation is done by a digital processor. The processor output supplies aspect angle, coverage for ECM-Systems, angular accuracy for ESM-Systems, as well as flight path parameters in analog voltages for graphic presentation.

Angular accuracy and coverage are plotted in polar coordinates. During flight tests these printouts are a main decision element for continuing the flight test program.

estal carrying the parabolic antennas, which can be mounted atop the roof of the container. So the ground station is fully mobile and can be transported by air, ship or truck to any place in the world. In order to prevent damages during transportation all racks inside the container are shock and vibration isolated from the container structure.

The arrangement used for ESM-measurements is illustrated in Fig. 4, the upper part of which illustrates a synthesizer, as main RF-signal source, a modulator, a frequency multiplier and a power amplifier. The power amplifier has to be adapted to the allocated frequency band. Different octave band travelling wave amplifiers (TWTA) with an output power up to 20 W and for higher frequencies up to 100 W are available. Feed antennas - in most cases horns - installed in the parabolic dish have to be interchanged as well in order to meet the desired frequency band and polarization. This antenna system is slaved to the automatic tracking system called Monotrac, which receives telemetry data from the aircraft under test.

Monotrac is a fully automatic tracking system, but it is recommended to monitor the automatic tracking as interferences by ground reflections may cause the system to lose bearing. A dipole feed system arranged in the focus of the 3 meter parabolic dish of the high gain antenna detects the direction of the incoming RF signal. A resulting error signal is fed through the receivers as well as the telemetry signal. In a control unit control signals are set up from the error voltages steering the motor drives in both axes. The unit can operate in different modes, separately selectable for both axes. So, the pedestal may be slaved by computer data or the position or the turning speed can be adjusted manually. In addition a TV monitoring system is mounted aside the parabolic antenna to pick up and be sure to correctly track the aircraft on direct path. The second transmitting antenna illuminating the target is slaved electrically or mechanically to the Monotrac antenna. By this the tracking system guarantees, besides an uninterrupted data link, also proper illumination of the aircraft by the test emitter.

The video output of the receiver system is connected to a PCM decoder and magnetic tape recorder. The PCM decoder restores and interfaces the data to a computer. Quick-look presentation of the measurement results, including plotted raw data and flight path, is possible by using the computer and appropriate software. In addition selected data channels may be routed directly from the PCM device to a strip chart recorder.

For off-line evaluation the received data as well as ground derived data like tracking angles, encoded by a PCM device, is recorded on magnetic tape. To guarantee error-free recordings for evaluation later on reproduce control is done by an oscilloscope in combination with an universal PCM decommutator.

In addition to these data processing devices a time code generator synchronized by radio station DCF77 is used for data identification on the magnetic tape. With regard to the hazardous high RF signal strength radiated it is very important to limit the illuminated surrounding area especially at low tracking angles. So, not to endanger people a small computer monitores the radiation angles and in case of unwanted directions reduces the RF signal power automatically.

To handle and control flights the flight test engineers can use VHF/UHF-transceivers and telephone which are installed in the container too. If there is no briefing and maintenance room available a second container is supplied. Fig. 5 gives an overall view of the described ground station including telemetry antenna (the large dish) and the mechanically slaved source antenna illuminating the target.

A special test receiver for the measurement of ECM antenna coverage had to be designed and prepared, small enough to be installed within an original ECM-pod. Due to the broad required frequency band the tuner section has been split into two separate signal paths (Fig. 6). A double superheterodyne prinziple with special quartz stabilized local oscillators has been provided in order to permit small IF bandwidth filters, which increase the over-all sensitivity.

Two separate demodulators detect the amplified incoming signal. The FM-discriminator detects extraneous interferences from other stations eventually radiating within the same frequency band. The dynamic range of the AM demodulator covering 80 dB in amplitude enables operation within a large distance range of the aircraft under test and the ground station. Moreover, the adaption to various on board installations, including antenna and cable attenuation, is enhanced. Because of frequency management limitations only a few discrete frequencies are usable for antenna measurements. So, fixed filters and local oscillators are provided to reduce size, weight and engineering effort of the receiver.

In ESM applications the ground station has been sucessfully used as well. Usually the error of the DOA-angle (Direction Of Arrival) is plotted in relation to the correct angle. The distinct sectors originate from the different antennas causing overlapping regions, and the correction tables in the computer utilities of the ESM equipment. Different regions of quality are demonstrated in Fig. 8. Depending on the accuracy of the ESM-system under test, the full scale of the error reading has to be adapted.

Summarized, the specification data of the test system developed by DFVLR are listed in Tab. 1. Constructing on available telemetry and in-flight antenna calibration equipment for VHF and UHF applications, it was possible to realize the ground station within a short time. On the other hand the special receiver design required about 20 months due to the long delivery time of the RF components. The future tasks are to increase the accuracy of measurement data, and to improve and transfer the existing software to a new generation of computing equipment.

References

|1| Bothe, H.
Macdonald, D.
"Determination of Antenna Patterns and Radar Reflection Characteristics of Aircraft",
AGARD-AG-300-Vol. in Prep.

|2| Klein, K.
"Ein SHF-Feldstärkemeßempfänger für die Antennenvermessung im Fluge",
DFVLR-Institut für Flugführung,
Internal Rep. 112-82/05, Braunschweig, Germany, 1982

|3| Klein, K.
"Mobile Bodenmeßstation zur Überprüfung der Genauigkeit von SHF-Bordpeileinrichtungen",
DFVLR-Institut für Flugführung,
Internal Rep. 112-82/21, Braunschweig, Germany, 1982

|4| Klein, K.
"Telemetrieeinsatz bei der Erprobung von ESM-Gerät",
in: Bericht über die 11. Sitzung des TAK; BWB FE V 3,
Koblenz, Germany, 1981

Acknowledgement

The authors wish to acknowledge the assistance of G.-J. Barth and N. Döler during the development and test of the system.

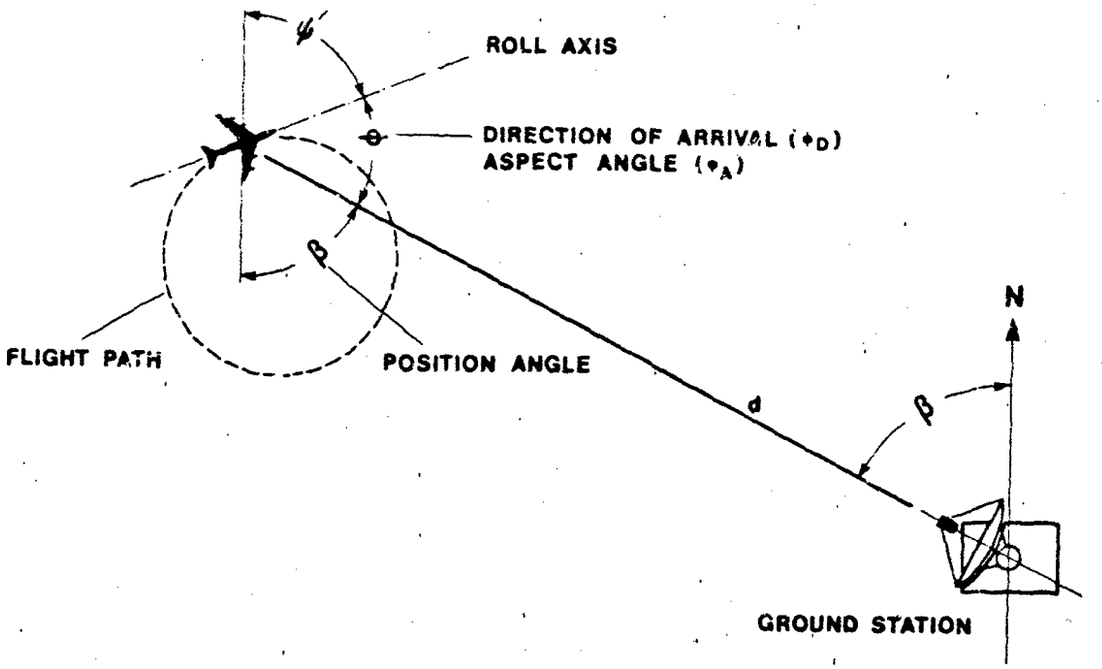

Fig. 1: Basic System Philosophy

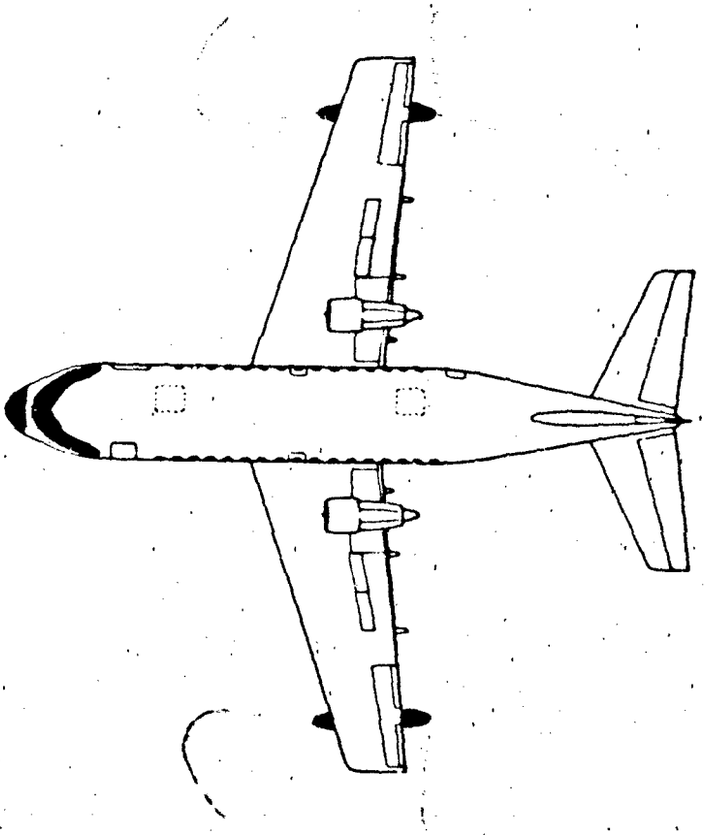

Fig. 2: Coverage of Angular Range

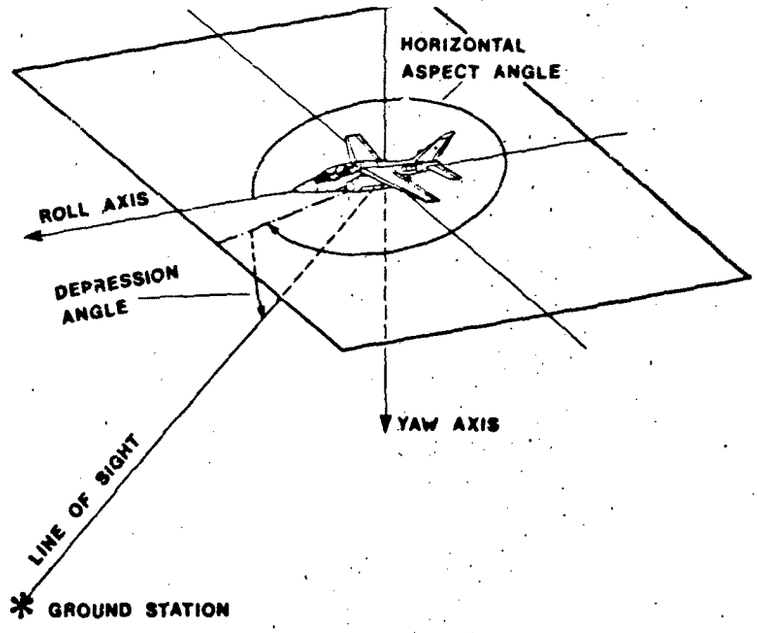

Fig. 3: Illustration of Horizontal Aspect and Depression Angles

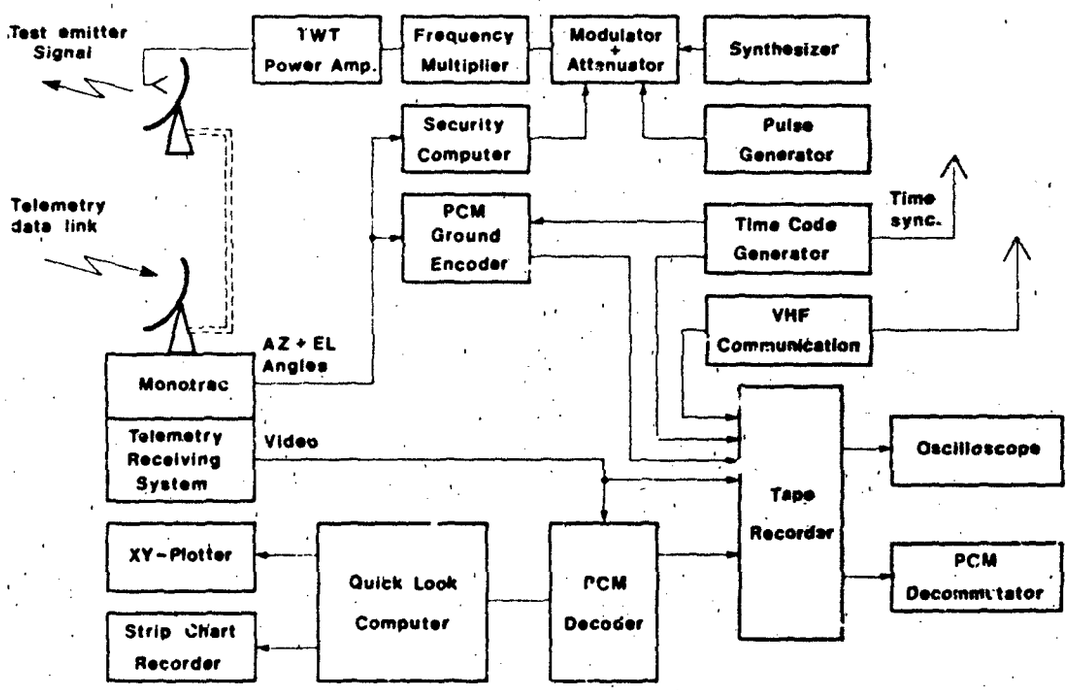

Fig. 4: DFVLR SHF-Ground-Station

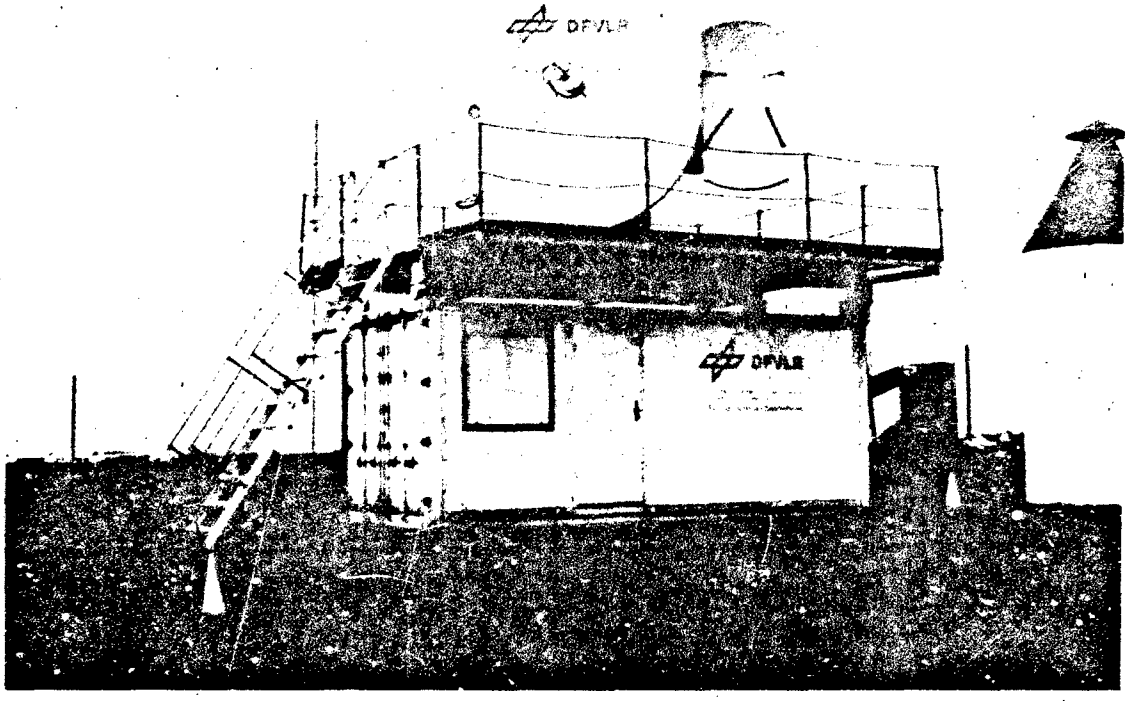

Fig. 5: Ground Station Container and Antenna Systems

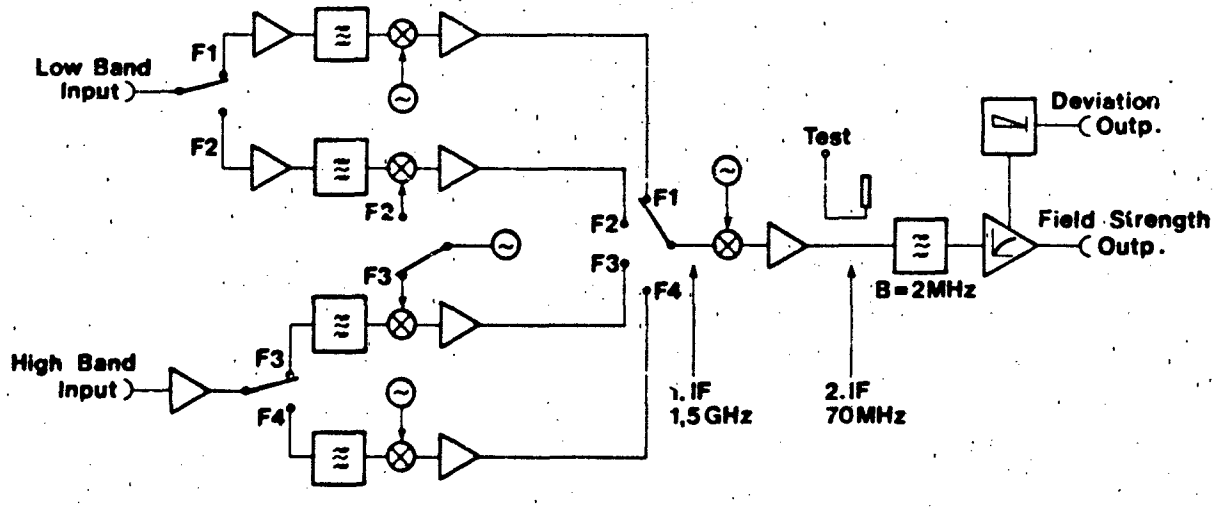

Fig. 6: Block Diagram AIF-SHF-Receiver E103

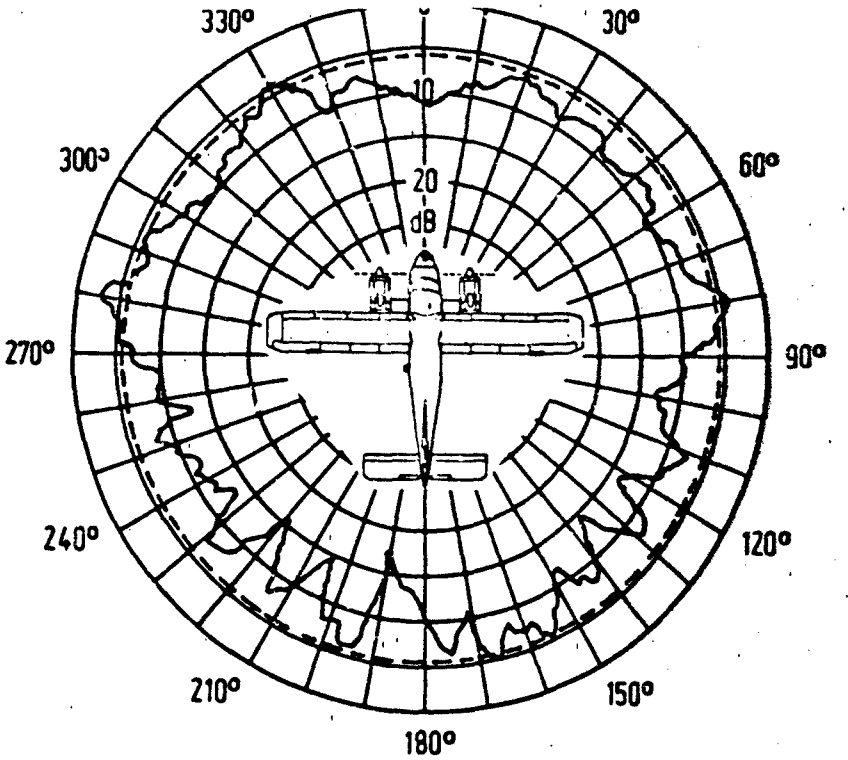

Fig. 7: Antenna Radiation Pattern
Aircraft: DO28, Type of Antenna: Monopole
Frequency: 1.5 GHz, Bank Angle: 0±3 Deg.
Ref. Pattern: - - - Monopole

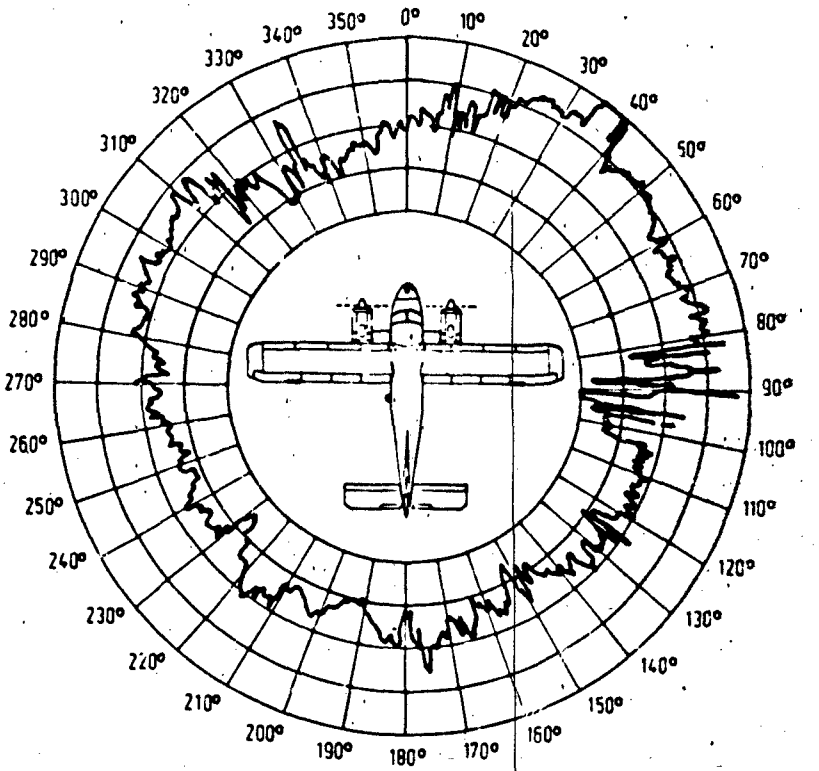

Fig. 8: Simulated typical ESM-DOA Error

a) Test Emitter:

Frequency Range	UHF - 18 GHz
Antenna	Parabolic Dish with Horn Feeds
Transmitter	Synthesizer, Quartz stabilized
Output Power	20W (<8 GHz); 100W (>8 GHz)

b) Telemetry:

RF-Receiver	Monopulse Tracking System (MONOTRAC)
Demodulator	FM
Frequency	E (L) or D (S)-Band
Accuracy	0.3 Deg. (RMS)
Decommutator	FM, PCM
Bit Rates	(≤ 0.5 Mbit/s)
Recording	Intermediate Magnetic Tape Recorder (IRIG)

c) Computer:

CPU	HP 2100; PDP 11/24
Interfaces	ADC; DAC; DMA; Parallel in, Out
Peripherals	Printer; Plotter; Tape Reader; Magnetic Tape

d) Accessories:

Time Code	Generator (DCF77-Receiver controlled); Reader
Recorder	Strip Chart Recorder
Communication	VHF-Communication System, Interbase Communication, RF-Receiver
Test	RF-Power Meter; RF-Spectrum-Analyser; RF-Attenuators; DVM; CRT

e) System Design:

Equipment Installation and Laboratory	20' ISO-Std. Container Air Conditioned
Pedestal Mounting	20' Container Platform

FLIGHT TEST TECHNIQUES USED FOR PROOF OF STRUCTURAL INTEGRITY OF TORNADO WHEN CARRYING EXTERNAL STORES

by

M. PEHL and F.J. RUDOLPH
Messerschmitt-Bölkow-Blohm GMBH
Unternehmensbereich Flugzeuge
Postfach 801160
D-8000 München 80, W-Germany

E. BERTOLINA and A. IPPOLITO
AERITALIA-Società Aerospaziale Italiana
Gruppo Velivoli da Combattimento
C.so Marche, 41
10146 TORINO - Italy

SUMMARY

The multirole characteristic of TORNADO results in an almost universal capability to carry an array of existing stores in every conceivable combination, within different operational flight envelopes.
In order to verify the structural integrity of the aircraft when carrying stores, a comprehensive flight loads survey programme was set up to validate the store aerodynamics used for the design of pylon attachments to the main structure, the pylons, the ERU's and the store structure.
Preliminary indications of store loads measurements have been given in a paper presented at the 61st FMP Symposium in 1982. This common AIT and MBB paper gives now a description of the overall stores flight test programme including the instrumentation and calibration procedures, the flight test techniques and a presentation of the to date available data.
Finally an explanation of the most significant problems occurred during this task will be pointed out.

1. DESCRIPTION OF TORNADO

The main feature of the design of TORNADO has been a high weapon loading capability and high speed low level attack mission resulting in a compact fuselage and shoulder mounted sweep wing, which can be varied between 25 and 68 degrees (see Fig. 1). Lift augmentation for take-off, landing and manoeuvering is provided by full-span leading edge slats, double slotted trailing edge flaps and Krueger flaps at the highly swept inner fixed wing (nib).
TORNADO is equipped with a total of seven pylons, three under fuselage (two shoulder plus one centreline station) and two swiveling pylons (I/B and O/B station) underneath each movable wing.
The streamwise orientation of these pylons during sweeping is automatically achieved by a rod system, which is fixed at the fuselage, connecting both the wing pylons.

2. WEAPON CAPABILITY

The multirole concept requires the capability to carry a wide range of external stores in different combinations according to the purpose of the mission (see Fig. 2): fuel tanks for long range, air-to-air, air-to-ground and antiship missiles to provide adequate defence and attack performing, dispenser and a variety of bombs depending on the mission target, electronic counter measure pods to improve the aircraft defensive capability, reconaissance pod for photographic survey. In addition, the operational capability to manoeuvre under loaded conditions for self defence without having to jettison the stores allowing the mission target, is granted.
The basic TORNADO was developed with a carriage system including MACE ERU's; a subsequent change of FRG and IT Air Forces requirements due to the need to carry MW-1, NATO weapons and conventional stores without exchange of adapters/ERU's for the different configurations, has imposed the study of a new system with revised fuselage pylons and ERU's (see Fig. 3).
In the following, the main features of the MACE (Minimum Area Crutchless Equipment) (see Fig. 4), and the MWCS (Multi Weapon Carriage System) (see Fig. 5), will be briefly summarized:

MACE :

- Internal swaybracing system by means of a dual nib hook saddle/lug arrangement using automatic wedges and additional saddle location spigots.
- Manual closing of the hooks.
- Reaction of applied store loads:
  Z - forces by hooks and wedges
  X and Y - forces by saddle location spigots.

MWCS :

- Independent, self-adjusting semi-automatic external crutcharm mechanism consisting of an upper stiff arm (swaybrace) and lower flexible arm (springarm).
- Automatic closing of the hooks.

reaction of applied store loads.

Z - forces by hooks and crutcharms.

Y - forces by crutcharms and lug/ERU interaction.

X - forces by the lugs into the main body via lug pocket.

The carriage capability, spread over 13 attachment points for MACE and 15 for MWCS is practically the same for the two systems for almost the complete series of stores; specific features are the Twin Store Carriers for the MACE System and, for MWCS, the MW-1 and the Quadruple Store Carrier especially developed for palletized low drag weapon carriage under fuselage (see Fig. 3).

3. DESIGN LOADS CRITERIA AND PURPOSE OF FLIGHT MEASUREMENTS ON EXTERNAL STORES.

The aircraft components design is derived from the requirements of the MIL-A-8860 specification series. Despite of existing AvP 970 and Air 2004E, MIL-A-8861 is the main basis for the performance of response calculations. Except for so called "exotic manoeuvres" (post stall) where realistic operational manoeuvre simulations are performed, to day's common practice is to perform the MIL "Strength Manoeuvres" using 5 to 6 degrees of freedom programmes including:

- All non linearities in the response equations and flexible aircraft aerodynamics.

- Control systems laws and force dependent actuator models.

- Flexible component aerodynamics for loads monitoring.

For the adaption of external stores, the rapid rolling manoeuvres are of special interest representing most design critical conditions.
The definition of the store loads is complicated by the variable wing geometry with its adjustable sweep positions (25°, 45°, 68°) which greatly affects the following characteristics:

A/C responses :

the aerodynamic and inertia characteristics are highly influenced by the wing sweep angle (pratically 3 aircraft).

Store aerodynamics :

the aerodynamic coefficients for under wing mounted stores are a function of sweep angle, with additional mutual variable interferences between fuselage and wing stores.

Elastic effects :

elastic interaction between I/B and O/B mounted stores due to control line flexibility.

In the preliminary design phase the aerodynamic derivatives for the aircraft and components are derived from theory and early W/T measurements. This data base is continuously updated in the following design phases, especially during early prototype flying. An improvement of aircraft aerodynamics is expected from the parameter identification process using the results of:

- data gathering flights (stick jerks, yaw doublets, partial rolls) up to:

- rapid rolling manoeuvres (box car rolls) where the overall aircraft calculation model including local dynamic effects is checked and updated.

Concerning the calculation model for component loads, especially the stores, it is necessary to check the W/T measurements in flight in order to cover realistic conditions for Re-number, shock boundary layer interactions, scale and transonic interference effects etc.
MIL-A-8871 is requiring a variety of in flight measurements in order to cover these effects for structural design.
It has turned out to be acceptable practice to update the calculation models with "lets say" uncritical manoeuvres and to demonstrate structural integrity by ground tests and calculation.

4. CONCEPT OF INSTRUMENTATION

In the overall TORNADO structural flight test programme one prototype has been devoted to comprehensive loads measurements.
The aircraft was specifically instrumented to reach this target, and in addition it was equipped with a full primary structure instrumentation to monitor the loads interactions due to the presence of stores.
Thus wing sectional and taileron loads were measured while the loads on the movable control surfaces were obtained instrumenting the actuators.

The main investigation was done during MACE system flight testing producing the evidence of aircraft capability to carry selected stores in the full flight envelope.
During MWCS system testing, being the programme peculiarily dedicated to investigate store suspension loads, store total loads and pylon attachements behaviour, only some check parameters have been recorded again for cross checking purpose with MACE.
The aircraft was also provided with a full standard instrumentation to allow complete correlation between measured loads and flight parameters: aerodynamic configuration parameters (wing sweep, high lift-manoeuvering devices), flight parameters (Mach number, speed, altitude), aircraft attitude (incidence, sideslip and bank angles), aircraft response parameters (linear accelerations, angular rates and accelerations), control surfaces positions (spoiler, taileron, rudder deflections).

4.1 STORE ATTACHMENT INSTRUMENTATION

Different instrumentation concepts were adopted for MACE and MWCS systems programme.
MACE flight testing covered the aircraft development, and therefore the investigation of underwing stores/wing structure interactions was the main purpose.
Right I/B and O/B wing pylons have been fully instrumented and tested.
An attempt was also made to obtain loads indications from under fuselage carried stores, first instrumenting the shoulder adapter and then a specifically developed dummy ERU. Some acceptable results for design conditions check were obtained just with the dummy MACE ERU.
In contrary to MACE, MWCS testing programme was planned not only to measure store loads, but in particular to assess the static and dynamic behaviour of the EDO ERU's and their components, still under development, and to verify their capability to carry the proper stores within the required flight envelope, proving the operational validity of this new concept of ERU.
To cover all these aspects it has been decided to use a standard ERU, even if this choice has caused considerable time spent in a specific instrumentation study and development, to overcome the problems due to redundant load paths, possible poor signal levels and sensitivities highly dependant on the preload values on hooks and springarms and interaction between single loads. Since the MWCS is now the standard store carriage system of TORNADO for FRG and IT, the relevant activities will be deeply discussed giving only comparisons with MACE when necessary.

4.2 MWCS INSTRUMENTATION CRITERIA

The under-fuselage adapter spigots and the ERU's installed in the design critical stations have been straingauged.
The criteria, adopted for the flight loads survey, included :
1. the measurement of the attachment loads (spigots) of the shoulder and of the centreline pylons to the fuselage thus obtaining the load distribution into the fuselage for heavy store carriage (MW-1, QSC).
2. the measurement of the attachment stores loads on Ejection Release Units (ERU's) in the following locations:

- left wing O/B pylon (14" LMERU)
- right wing I/B pylon (30" HMERU)
- centreline adapter (30"/14" HMERU)
- right shoulder adapter (14" fwd LMERU and 30" HMERU).

Fig. 6 illustrates the positions of the instrumented store racks in respect to the entire capability of the aircraft.
Some considerations about the load carrying structures of the adapter spigots and ERU's are useful to clarify instrumentation criteria.

Fuselage-Pylon Attachment

Each shoulder adapter (pylon) is suspended under the fuselage by two main spigots carrying vertical and side load as well as rolling moment and two auxiliary spigots at the forward and aft sections carrying only vertical and side loads (Fig. 7). The longitudinal load is principally reacted by the aft main spigot, the forward main spigot carries just some longitudinal load by friction in a sliding bearing.
The centreline adapter is suspended on two main spigots carrying simultaneously all loads except longitudinal, which is only reacted by the aft spigot. The centreline adapter has an equipment box attached to the rear end, which is suspended by a separate spigot not carrying loads from stores and therefore not instrumented. Tables 1 shows the summary of the spigot instrumentation.

EDO ERU's

The unique feature of the EDO-ERU's is the separation of the crutcharms into two components: the springarm for the maintaining of store suspension pretension and the swaybrace for the carriage of the higher loads. With this feature, and with a set of movable wedges, an automatic crutcharm closure mechanism is provided. Fig. 8 shows the principle of the movable crutcharms.

The attachment loads paths can be described as follows:

Fx : From the lugs into the main body via the lug pocket.
Fy : From the lugs as side force into the hook (HMERU) or into the lug pocket (LMERU) plus side component of the crutcharm normal load.
Fz : Sum of hook loads and crutcharm vertical components.
Mx : Rolling moment from crutcharm normal loads.
My : Pitching moment from Fz of forward and aft hooks and crutcharms.
Mz : Yawing moment from lug-side loads and from the crutcharm side-components
Fy : Yaw Spigot.
The yaw spigot is only used for heavy store carriage on fuselage adapters. It is fitted outside of the HMERU and reacts against the adapter 0.828 m in front of ERU centre line, to support a contribution of the store side force and yawing moment.

With this load paths description, a straingauge instrumentation was developed as described in Table 2 taking into account the small design differences between LMERU's and HMERU's which in a few areas made a different instrumentation method necessary. No reasonable instrumentation was found for the determination of the longitudinal load.

4.3 MACE INSTRUMENTATION CRITERIA

With the assumption that in the MACE version the store measurements have been considered as relevant contribution to the aircraft structure qualification, the instrumentation for stores measurements was mainly dedicated to the interface areas between the pylons and the main structure.
Underwing pylons spigots were instrumented to measure total loads from store and pylon contributions; straingauges full bridges were installed on the spigot to allow the rolling and pitching moments measurements; the yawing moment was measured by a straingauge at the pylon turning rod.
An attempt was also made to measure the pylon forces although difficulties have been encountered for a reasonable straingauge instrumentation at the pylon structure. The loads outputs during flight testing were very poor despite of acceptable results during on rig and on aircraft calibrations.
Therefore, for the specific purpose of the aircraft qualification, the measurements of the three moments were satisfactorily used, being the most significant loads of the particular structure of the spigot.
Some detailed picture about these measurements and the relevant matching are in Fig. 9.1, 9.2 and 9.3.

5. DETAILED INSTRUMENTATION PROCEDURE

5.1 GENERAL ON INSTRUMENTATION TECHNIQUE

Apart from the specific problems which will be detailed later, general considerations have been applied in the instrumentation definition:

- In order to prevent output drift due to ambient temperature influences, the straingauge bridges have been bonded as complete 4 arm bridges and whenever possible with 4 active arms.
  In the cases when only two active arms have been possible (end-load parameters) the bridge completion was made with the 2 inactive arms bonded on the same material in the vicinity of the active gauges.

- Straingauge bending bridges whenever possible have been prefered to shear bridges in order to obtain increased electrical output voltages and measuring sensitivity.
  Straingauge shear bridges have been bonded on typical shear sections present on different components, e.g. main spigot bolt. On the other hand, shear parameters have also been fitted as alternative to bending parameters with respect to cross influence suppression or improvement of signal linearity.

- Cross influence on a straingauge output, if evident, has been compensated by computer processing. Electrical combinations of two bridges signals under reciprocal cross influence, have not been considered in the basic instrumentation plannings. This technique asks for duplication of straingauge parameters and for linearity of the signal outputs. In addition due to limited space on spigots, hooks, lugs, ERU housings, redundant bondings and wirings wouldn't have been possible.

- In all cases, 350 Ohm foil straingauges producing reasonable bridge outputs have been fitted.

5.2 DETAILS ON SPIGOTS STRAINGAUGING

Use of straingauge technique asks for loads carrying structures which reach limit loads at optimum strain. Such a preferable feature, however, is missing in an adapter main spigot. The dimensions in section A-A, Fig.10, are in excess for the highest X, Y and Z-load case providing poor strains, since the strength of the highest inflight rolling moment has to be covered. Useful straingauge sensitivities,

however, have been obtained to measure X and Y forces emaciating the spigot material in section A-A. A reduction of rolling moment capability as consequence, could be accepted, since the flight load survey is performed in a limited envelope.
After this modification, realized on all main spigots, two straingauge shear bridges have been bonded for X and Y-force measurements.
The straingauge location for the Z-force parameters (Fig.11), has been shifted to the spigot bolt. By a machined segment cut-off, this bolt got two vertical planes on which two straingauge shear bridges have been bonded in the sections between spigot and adapter bearing. At a combined Z-force and rolling moment application the Z-force reaction is obtained from the sum of the two calibrated output signals, the rolling moment from the difference. All main spigot bolts have been straingauged according to this procedure.
Fig. 12 shows an instrumented shoulder forward auxiliary spigot which is designed to carry Y and Z-force. The Y-force parameter has been straingauged to pick up the compression strain from a side force when the adapter is compressed against the upper spigot fork, i.e. at a side force to right the left part of the fork is stressed due to compression, whilst the right part is not influenced. An endload parameter has been straingauged on the spigot rod, to measure Z-force.
In analogy the auxiliary spigot aft of a shoulder adapter has been straingauged. The straingauged spigot components are presented in Table 1.

5.3 DETAILS ON ERU STRAINGAUGING

A straingauge shear bridge has been fitted on the 14" and 30" hooks, as shown on Fig.13, to determine the Z-force.
The HMERU side walls, which reacts with the store lug, have been selected to bond a straingauge bending bridge for side force measurement, while the side force parameter of a LMERU has been obtained by means of a straingauge shear bridge installed on the store lug base. Straingauge bending bridges have been bonded on springarms and swaybraces to measure compression forces against the swivels. (Fig. 14).
A summary of ERU's instrumentation characteristic is provided in Table 2.

6. CALIBRATION PROCEDURE

6.1 GENERAL APPROACH

Application of straingauge technique, to measure forces on load carrying structures requires a careful calibration of the parameter voltage outputs.
The approach to useful spigots and ERU's calibration has been done in different steps:

- Laboratory checks have been carried out to optimize straingauge locations on complex components(main spigots, hooks).

- Due to the direct method used to obtain the total forces and moments from the ERU load paths, the components have been calibrated off A/C, using rigs for statically determined force applications.
  In analogy, the spigots have been calibrated off A/C, to obtain the load outputs directly. After this procedure the calibration equations have been put into the computer for load processing during a subsequent on A/C calibration.
  Known loads,off A/C, have been applied up to limit load to verify the calibration slopes with respect to nonlinearity and cross influence.

- Following the off A/C calibration of structural components an on A/C calibration has been performed applying single loads and actual load combinations. Since the total store and spigot loads are already specified by the calibration equations from the step above, the significance of this "in situ" calibration is based on a check to verify the applicability of these defined equations for the actual system now statically undetermined and to demonstrate fully capable flight test instrumentation and consistency of the total load outputs obtained by computer processing. The validity of the software data processing is consequently the reason of the this last calibration step; in cases of deviations between measured and applied loads, corrections of the calibration equations can be retrospectively made.
  Calibration loads have been applied via a dummy store in steps of 20% up to 60% of limit load.

6.2 DETAILS ON OFF A/C CALIBRATION

The straingauge bending bridges of the springarms and swaybraces have been calibrated together in one cycle to obtain compression force.
A typical calibration slope of the springarm and swaybrace output against applied load as well as the crutcharm slope, derived from the springarm and swaybrace slopes, is given in Fig. 15. The foreward and rear hooks have been simultaneously calibrated applying a Z-load via the dummy store. Since the crutcharms are open, the dummy store is statically determined suspended on the two hooks at known Z-forces.

on LMERU and HMERU simulating the geometry of different stores.

6.3 DETAILS OF ON A/C CALIBRATION

As already mentioned the on A/C calibration is considered an imperative requirement to complete satisfactorily the whole exercise.
The A/C has been fixed on a support frame by means of the nose and main landing gear locked hydraulically and mechanically at their maximum extension to prevent movements of the A/C under loading and provide maximum clearances to install loading devices under the fuselage.
Flight standard pylons were suspended and the dummy store fitted in several stations to check the following loading combination cases:

X-force, to check the main spigot response along longitudinal axis
Z-force
Z-force and pitching moment in combination
Combined Y-force and Rolling moment, with and without yawing moment superimposed
Combined X and Z force.
Combined Y and Z-force.

The parameter outputs have been recorded on airborne magnetic tape using the signals conditioning as for in-flight testing.
First the signal outputs have been checked with respect to polarity, linearity, sensitivity, and cross signals thus to verify the elaborated component forces.
The subsequent check has dealed with the assessment of measured store total loads with the known applied ones. For the symmetrical loading cases good agreement has been obtained with the measured store total loads. Only small cross signals to the lateral outputs have been revealed within the error limits.
Concerning the lateral loading cases, the errors of the measured forces in comparison with the applied force combinations could be assessed as follows: side force and yawing moment revealed errors within the tolerances, rolling moment error could be neglected, vertical force and pitching moment presented errors, due to cross influence, marginally beyond tolerances. The reason for these errors has been attributed to the friction between the store and ERU interface. The neglection of this effect was considered acceptable because it was assumed for the flight trials, that during the quasi static loads-manoeuvres the vibration environment of the store-ERU interface would provide sufficient dynamic load to settle major preloads from friction. This fact was proven in a few comparative trials where potential friction was avoided by special means, e.g. teflon layer between the swivels and the store surface.
Major investigations have been done to check the spigot loads at adapters suspended on the fuselage. Since each shoulder adapter is statically undetermined, being suspended on four spigot points, and therefore the load distribution is not available from geometric relations against the single applied load, only the sum of spigot reaction loads can be checked.
With this criterion the measured spigot loads distribution has been verified. Adequate agreement with theoretical spigot loads distribution has been found at higher loading levels. At lower calibration loads, friction, e.g. rubber sealing between adapter and fuselage, has influenced the spigot side loads and rolling moments. For this reason a removal of rubber sealing has been considered but rejected to avoid undesirable aerodynamic flow around the adapter during the flight load survey. Reasonable corrections have been made in the spigot equations of the software at low load outputs.

7. FLIGHT TEST PROGRAMME CRITERIA

The flight test programme is performed for selected store configurations.
The choice has been made to cover the most design critical stores in respect to aerodynamic and inertia characteristics.
Different phases of the flight loads trials are identified as Flight Loads Survey with subsequent built up and demonstrations and finally Rapid Rolling.
The FLS aim is the gathering of the information necessary to assess the incidence and the sideslip dependence of the aerodynamic coefficients in the widest range of these two parameters and in the most significant region of the flight envelopes with the inclusion of the control of Mach influence and Mach/altitude effects on aerolastic behaviour of the structure.
For these aspects it is very important to note that the final results are depending on the flexibility of: wing, pylon-wing or pylon-fuselage interfaces, ERU and store. For the underwing pylons, the control-line stiffness has to be considered. The load factor range is well inside the limits in order to allow flying without necessity of clearance work between the flights.

- Asymmetric manoeuvres as steady heading sideslip to explore the sideslip influence on the aerodynamic coefficients.

These manoeuvres are required to be performed as slow as possible, in order to be very close to a quasi steady manoeuvre and to allow the aerodynamic field clean from transient phenomena.
In addition to this requirements, other characteristics as the Mach number constance, the minimum values of roll rate and/or acceleration together with the minimum bank angle during the steady heading sideslip, are necessary to define the manoeuvre as acceptable and useful for the subsequent matching work. The compliance with the above requirements cannot be always satisfied considering that the handling qualities of the aircraft, optimized on the clean configuration, are strongly affected by the presence of the external stores. The increase of drag produces a significant decrease of the flight speed during the manoeuvre and the pilot induced engine adjustement to balance increased drag often is not sufficient to maintain the aircraft into the very small Mach/speed tolerance required for the whole manoeuvre, especially when flying at the boundary of the operational envelopes with heavy stores.
For this reason different testing techniques, strictly depending on the stores configurations have been applied.
A comparison between two standard Roller Coaster manoeuvres performed with MACE (light configuration) and MwCS (heavy configuration) is shown in Fig. 16. As it can be seen, for the light configuration it is easier to maintain the Mach in the tolerance range during the manoeuvre, while the heavy configuration requires a steeper load factor slope in the pull-up to comply with the same requirement: the high pitch acceleration which is associated in this phase, being present for a reduced time and being negligeable for the store inertia calculation, is not considered significant.
After the matching work performed considering the FLS results, built up and demonstration phases can follow and then the Rapid Rolling program takes over.

8. FLIGHT TEST PROCEDURES

Two conditions have to be considered in the use of straingauge measuring technique: adequate sensitivity and electrical output balancing.
The first condition has to ensure that the sensitivity of each single parameter is correct and no instrumentation failure occurs. The second one has to ensure, that the bridge outputs under unloaded or definite static conditions on ground are well known, that is, either zero or constant, to have correctly operative load equations. Although any effort is made to reach and maintain the last condition, it is often not possible to avoid signal outputs unbalancing because of signal conditioning characteristics.
For these reasons, a "pre-flight datum check" is used to correct for a reference value, the shifts of each straingauge bridge response as in analogy is done to wind off values recorded before W/T testing.
The loads measured at this reference time are compared with theoretically known loads associated to the aircraft configuration.
The defined correction terms are automatically applied to the measured loads at all flight time so that the resultants are the total loads in absolute quantities. A "post-flight datum check" is also used to compare again the corrected total loads with the known ones to monitor the outputs drifts which could have occurred during the flight.
An appreciable contribution to speed up the validity check of the measured loads, has been ensured by an ad-hoc performed manoeuvre at the beginning and at the end of each flight at the same flight conditions. Then, this so called standard manoeuvre, allows the evaluation of manoeuvre loads in standard flight conditions for which accurate predictions could be also provided for comparison. With this procedure, an adequate degree of confidence can be reached in reliability concerning the accuracy of the load measurements throughout the flyings; on the other hand, possible signal responses and malfunctioning of the parameters can be discovered in time.

9. REAL TIME MONITORING

Data transmission via telemetry link was also made to increase the aircraft structural safety when approaching potentially dangerous test conditions and, obviously, to allow a quick-look data analysis. In addition, real time monitoring permitted to check the correct execution of manoeuvres and the functioning of peculiar instrumentation or to informe the pilot for a manoeuvre repetition in case it has not been satisfactorily performed.
Therefore the monitoring reduced the flight time required to complete the flight programme and granted a better quality of F.T. results.
For flight safety reasons, mainly the ERU wedge movements in parallel to crutcharms pretension, have been monitored throughout the F.L.S.
Fig. 17 shows how the pretension was influenced by vibrations induced by dynamic longitudinal pilot's stick manoeuvres and the improvement reached testing a new ERU standard.

rate (typically 8 s.p.s.), to get an acceptable compromise between the aircraft data acquisition capability and test requirements.
In this way, more than hundred signals S.G.'s outputs were recorded.
Most of flight mechanic parameters have been recorded at a higer sampling rate (typically 16 or 32 s.p.s.), but a reduction to 8 s.p.s. was made for the correlation with the loads.
The requirements for dynamic loads investigations have been covered increasing the sampling rate for relevant parameters and in particular recording and telemetering signals in FM/FM multiplexing.

10.2 DATA PROCESSING

In the MACE and mainly in the MWCS flight load programme, considerable efforts have been devoted to develope a universal software for proper processing, data handling and load analysis. This software, used for both on aircraft calibration check and flight data analysis, has been a leading factor for the succesful performance of the exercise. In order to produce loads data for the different aircraft configurations in a suitable form for the subsequent analysis, several significant factors must be considered:

- The high number of parameters to be analytically combined together.
- The straingauge outputs with different characteristics to compute the loads from linear terms or terms up to third order covering the nonlinearities.
- Ground datum correction terms.
- The flight parameters for correlation with the loads.
- The computation of inertia loads for the subsequent derivation of aerodynamic loads.

Now what to do to reach this ambitious target? The answer has been the harmonization of such a relevant number of data in a series of computation modules, correlated together, in which homogeneous data block are processed.
As it can be seen from the data processing flow-chart (Fig.18), the input parameters are extracted from the secondary tape on the basis of engineering requirements (parameters, run time inputs, slices interested, options, etc.).
When appropriate modules have been selected and made operative, the total loads are calculated using the relevant calibration equations and the "Data Base" containing geometric store data, store configurations, ground datum correction terms, etc. In this way, the acting loads, are computed from instrumented ERU's or adapter and pylon spigots parameters in a series of modules.
The computation of the loads at the H.M.ERU reference point, is presented as example of the working process of a single module, which calculates the intermediate forces (Fig. 19) on springarms, swaybraces, crutcharms, hooks, side walls and yaw spigot giving the store total loads.
The first step of the ERU load processing, consists of the crutcharm load computation which involves some problem due to the series connection of an elastic and a stiff element. According to the crutcharm feature, the springarm induces preloads to centre the store, whilst the swaybrace arm reacts the higher loads due to the store rolling moment with the two arms in contact.
As presented in Fig.15 , the response of the swaybrace parameter is subject to a cross over effect when the springarm is only compressed. On the other hand, the springarm gives also a response beyond the kink point at which the gap between springarm and swaybracearm is closed. The algorithm of the crutcharm load, considers only the contribution of the linear springarm slope up to the kink point; at the loading conditions with both arms in contact, the maximum springarm load is kept constant and added to the swaybracearm load. For this reason, the unbalance of the swaybrace slope has been eliminated respectively shifted to zero voltage output at zero loading condition. As far as the springarm is only compressed, the carry over effect to the swaybrace parameter output is irrelevant. But the maximum carry over output, indicated at the kink point, must be continously subtracted from the swaybrace output to measure the resultant force of the two arms correctly. The sum of the two elements, is the crutcharm load.
This algorithm is given by proper coefficients taking the advantage that the kink point can be easily adjusted, if the springarm setting varies from one flight to another.
The identification of the conditions in which the crutcharm gap is closed and consequently the kink point of the springarm calibration curve is reached, is a decisive factor on the accuracy of the final loads computation.
A small variation of this reference point in respect to actual operational conditions at which the calibration equations are referred, generates an error on the crutcharm loads computation, that multiplied perhaps for 4 crutcharms, could invalidate the measurements.

calculation of the store rolling moment. The module flow chart (Fig. 20) shows the development of the described activities.
Other software development was required to correctly measure the spigot total loads. As already pointed out, the spigots have been predominantly instrumented to asses the load distributions into the fuselage main structure when heavy stores are carried. A software module was prepared for store loads determination via the spigots, which withstand, beside the store loads, the adapter loads and constraint forces. Being the latter produced by the adapter deflection due to the fuselage bending, a correction term must be introduced to obtain the store loads. Since the fuselage bending depends rather on the aircraft manouvering condition more than on the carried store, the spigots loads were recorded during a dedicated flight with only the fuselage adapters fitted. The interesting spigots constraint forces were derived and reduced to analytical correction terms, following this way:

- analyze the spigot loads from flight measurements with adapters fitted only
- neglect the aerodynamic load contribution of the adapters in the vertical plane
- subtract the inertial spigot load contribution due to the adapter weight from the spigot total loads
- define correction terms for the constraint forces in respect to the main variables (load factor, wing sweep, manoeuvring devices positions, Mach number and airspeed).

10.3 INERTIA LOADS COMPUTATION

The verification of aerodynamic store loads trends is the final goal of flight load survey and this requires the separation of the inertia loads from the measured total loads,at each measuring reference point.
These inertia loads, due to the motion of the aircraft, have been computed by means of the Euler equations introducing three linear accelerations, three angular rates and three angular accelerations, measured at aircraft c.g. package, and referred to the c.g. of the stores and then transferred to the ERU's and spigots points (Fig.21). Three angular accelerometers have been used for the angular accelerations measurement to improve the accuracy of inertia calculation. Fixed data as store mass, inertias and coordinates are stored in the file.
This simplified method, avoiding the need of a full set of sensors at the centre of gravity of each relevant store, has been considered acceptable because the peculiar characteristics of quasi static performed manoeuvres allow the assumption of a rigid motion of the stores with the aircraft.
The technique of "Ground Datum Load" correction, has been also applied for inertia load computation.

10.4 DATA PRESENTATION

The characteristics of the speed and flexibility of the software gives the availability of a full set of data for a detailed analysis in a short time after flight, improving the possibility to check the validity of the results or to find out instrumentation malfunctions (Fig. 22).
Due to the instrumentation response characteristics and to the complexity of the data processing, the direct comparison of first flight test data with the prediction in a number of cases, allowed the clarification of some phenomenon, not identified or not well simulated during the calibration, such as kink point definition for refined crutcharm load computation and the need to improve the measurements, asking for additional check calibration. With this approach the flight load measurements have been updated for a better agreement with predictions, although not fully applicable predictions were discovered.
An example of software adjustment and computation improvement is shown in Fig.23. The final flight test data are presented in several forms: time histories, tabulations and mainly cross plots of measured loads in respect to significant flight variables, for an immediate use.
Then a selection of total, inertial and aerodynamic data are copied on magnetic tape and transferred to final analysis for the production of matched aerodynamic data set.

11. MATCHING

11.1 PROCEDURE

As results of the above mentioned activities, a great number of information is available for analysis: as already reported, the measurements are presented in form of total, inertia and aerodynamic loads, and as first step of the data reduction process, the results are organized in order to have all the manoeuvres with comparable measurements range, packed together giving an immediate view of the available data.
After that, a fine selection of the data is performed applying tolerances on the most significant parameters in order to avoid wide scatter of the data with consequent poor homogeneity of the results:

In order to minimize the undesired effects, the applied tolerances (as reference only for a general discussion while some particular case can lay outside) are:

- Roll Rate : ± 5 deg/sec.
- Mach number : from ± 0.01 up to ± 0.025 depending on the specific case.
- Incidence angle : during steady heading sideslips, the maximum variation allowed of incidence is ± 1.5 degs
- Sideslip angle : during nominally symmetric manoeuvres, the maximum values of ß allowed is ± 0.3 degs.

The aerodynamic forces and moments are then adimensionalyzed into coefficient form and plotted against incidence and sideslip: using these plots, the comparison with Wind Tunnel data, reduced and presented for the same parameters range, is performed.
The incidence and sideslip effects are verified in terms of slope and intercept variation in the available range of informations.
In this way, the proper corrective values for slope and intercept are established and the relevant changes to basic data can be applied: extrapolations to maximum values are performed.
This last part of the process is conducted in a semi-automatic way in order to control, when engineering judgements is required, the computer extrapolation avoiding the presentation of unacceptable results.
On the bases of the achieved experience, mainly during the MACE activities, it appears very important for the matching, the consideration of the possible effects induced on results by the accuracy of the measurements; in the presentation of the results, the influence of these effect will be pointed out and commented.
Figs. 24.1 to 24.20 are showing the correlation between the wind tunnel and in flight measured aerodynamic coefficients for a selected typical underwing (Chaff Dispenser) and underfuselage (Sub Tank) mounted store.
Going more into detail the Flight Test data reduction was performed, applying the tolerances mentioned before, by means of a linear and non linear regression method introducing a statistical precision interval of 1σ (including 2/3 of the measured points) centered on the mean value of the coefficients.
It must be pointed out that the results presented, are only the first evaluations without any data precision consideration (W/T, FT) in order to get an overview about the available informations, to sort out malfunctions, and to reveal correlation problems.
This for example the scatter of the actual flight data, is a first indication of the accuracy of the measurements. Of course there is no precise accuracy measure because of the impossibility to establish "true values" (relative validity). That means all aerodynamic coefficients from any source are by nature only estimates.
Now some preliminary indications could be done about the flight testing results. Referring to Fig. 24.1-24.20 noticeable agreement has been found for moments with some uncertainty in the very sensivite yawing moment.
Generally a drift occurs on force measurements especially for the side force, which can be recalculated from the excellent Rolling moment.
The slope of the side force against the variables α and ß instead correlates with the W/T measurements.
Major deviations have been observed between in flight and WT measured vertical force coefficients particular for the under fuselage mounted tank.
The vertical loading of the tank at this station is small and within the tolerance band explaining the wide scatter of the test results.
This aerodynamic force is of minor importance, because the vertical design load is dominated by the inertia.

11.2 ACCURACY OF MEASUREMENTS

For the final data reduction of the FLS results, engineering judgment, the oldest measure for estimating reliability, must be applied to weigh all available information about the accuracy of the inflight and W/T measured aerodynamic coefficients. Considerations about the applicable tolerances will be given in the following:

- Differences between the maximum applied calibration loads (50-60% limit load see para 7.) and the measured outputs have been amounted to less than 5% but depending on the complexity of the algorithm, the number of parameters needed, and on appropriate application of correction terms and procedures during data processing. The actual tolerances are higher due to the specific steady manoeuvres producing a store load level of about 20% of the design based on R.R. manoeuvres.

- The influence of aeroelastic effects on the inflight coefficients will be checked by evaluating the test results as a function of altitude.
  Different store positioning due to asymmetric wedge engagement should be separated.

- Additional attention must be paid to the tolerances for the fundamental aircraft instrumentation systems.

- The maximum allowed tolerances of the nominal flight loads survey conditions as already given, must be applied for the data reduction.

- All relevant corrections concerning flow conditions, Reynold effects, balance output tolerances have to be introduced into the W/T measured aerodynamic store coefficients.

All these available relevant information about these tolerances will be taken into account to calculate data precision bands for the inflight and W/T measured coefficients ensuring a correct matching. The final results, a modified aerodynamic store set, used together with responses newly calculated with flight matched aircraft aerodynamics (from handling and rapid rolling step by step testing), allows the redefinition of the maximum load levels checking and providing the structural capability of the aircraft when carrying external stores for the entire operational envelopes (Fig. 25).

12. CONCLUDING REMARKS

Even if the MWCS-flight test programme is not yet completed, the experience gained during the first evaluation of the results, confirms the reliability of that philosophy choosen. The main advantages are:

- The possibility to check the static and dynamic behavior of the standard ERU's under actual conditions.

- To set important contributions for the ERU's development (mainly wedge design improvement).

- To reveal unexpected load distributions concerning the underfuselage pylon spigots.

- To produce final clearances for the aircraft with stores based on reliable flight matched aerodynamic coefficients data set, as proven by the first analyzed results.

- To improve the cross reading possibility for the clearance of similar store configurations.

- To have available an important tool for any future clearance work on the adaption of new stores.

13. REFERENCES

1. TORNADO FLIGHT LOAD SURVEY
   by : D.W.Altham, J.Nuscheler, D.K.Potter, W.Seidel.

2. COMPARISON OF FLIGHT LOADS MEASUREMENTS RESULTS AND PREDICTION FOR TORNADO
   by : J.R.J.Dovey, G.Moretti.

3. GROUND AND FLIGHT TEST TECHNIQUES USED FOR PROOF OF STRUCTURAL INTEGRITY OF THE TORNADO COMBAT AIRCRAFT
   by : K.Knauer.

4. A TECHNIQUE TO DETERMINE LIFT AND DRAG POLARS IN FLIGHT
   by : A.Knauss.

			L/H	C/L	R/H	
1	Auxiliary Spigot FWD	y compr. z endload	Fy Fz		Fy Fz	
2	Main Spigot FWD	x shear y shear	Fx Fy	Fy	Fx Fy	
2a	Spigot Bolt FWD I/B O/B	z shear) z shear)	Fz Mx	Fz Mx	Fz Mx	combined via computer
3	Main Spigot AFT	x shear y shear	Fx Fy	Fx Fy	Fx Fy	
3a	Spigot Bolt I/B O/B	z shear) z shear)	Fz Mx	Fz Mx	Fz Mx	combined via computer
4	Auxiliary Spigot AFT	y compr. z endload	Fy Fz		Fy Fz	

Tab. 1 TABLE OF STRAINGAUGED SPIGOT COMPONENTS

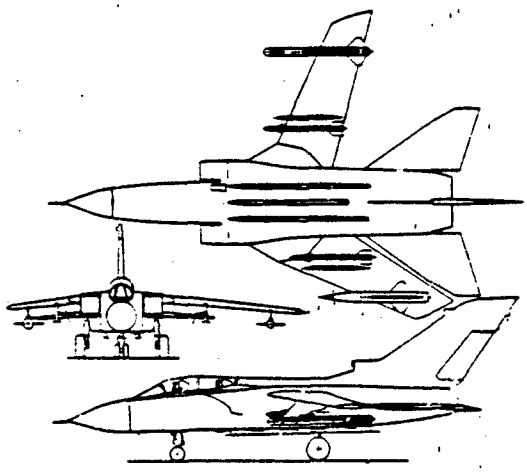

E.R.U. Component	Kind of Bridge	Elaborated Force Component	Remarks
Spring FWD right	Bending	F-compression	
Sway brace FWD right	"	"	
Spring FWD left	"	"	
Sway brace FWD left	"	"	
Spring AFT right	"	"	
Sway brace AFT right	"	"	
Spring AFT left	"	"	
Sway brace AFT left	"	"	
Hook FWD	Shear	Fz tension	
Hook AFT	"	"	
Sear FWD	Endload	" "	Hook back up perm.
Sear AFT	"	" "	" " " "
Side wall FWD	Bending	Fy	For MHERU only
Side wall AFT	"	Fy	" " "
Lug FWD	Shear	Fy	For LHERU only
Lug AFT	"	Fy	" " "
Yaw Spigot	"	Fy	For heavy store only on C/L or R/SH

Tab. 2 TABLE OF STRAINGAUGED ERU COMPONENTS

Fig. 1 THREE VIEW DRAWING OF TORNADO

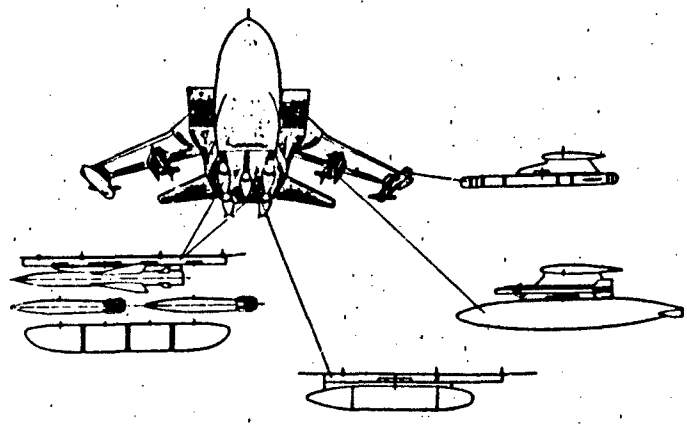

Fig. 2 TORNADO-MWCS EXAMPLE OF WEAPON CAPABILITY

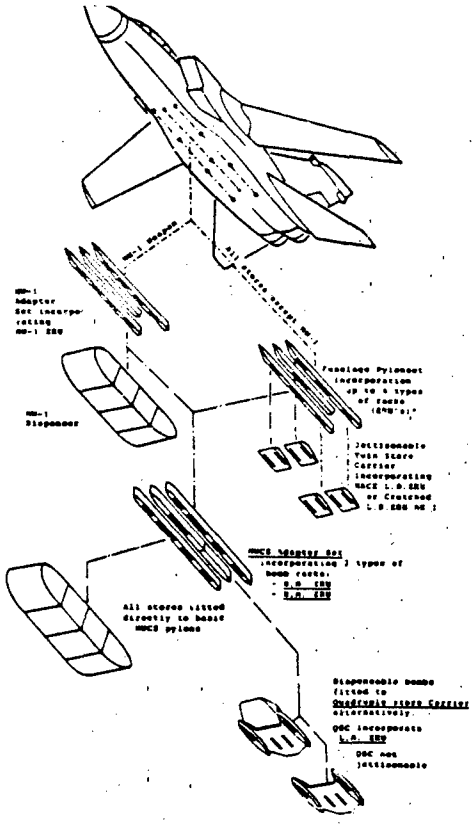

Fig. 3 TORNADO HISTORICAL DEVELOPMENT OF UNDERFUSELAGE ADAPTERS

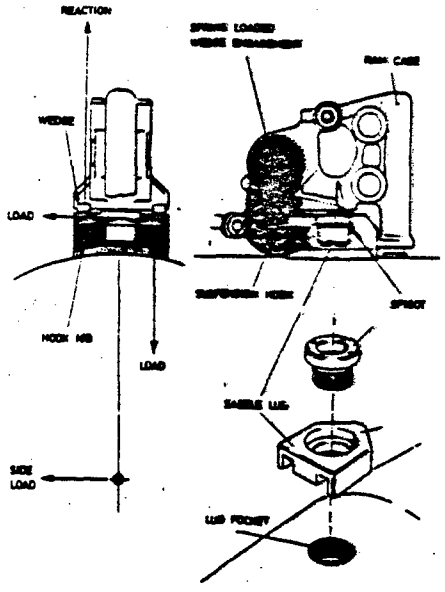

Fig. 4 PRINCIPLE OF RACE SYSTEM

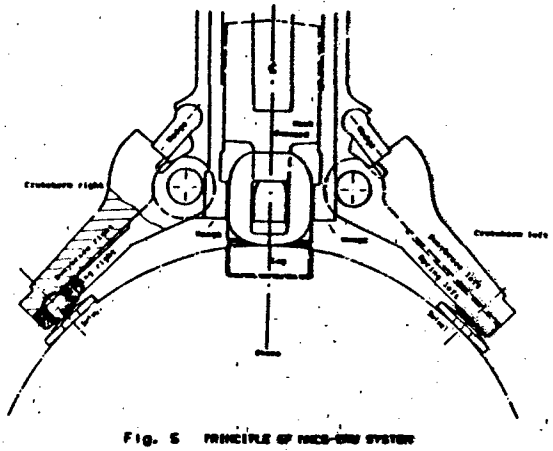

Fig. 5 PRINCIPLE OF RACS-DRU SYSTEM

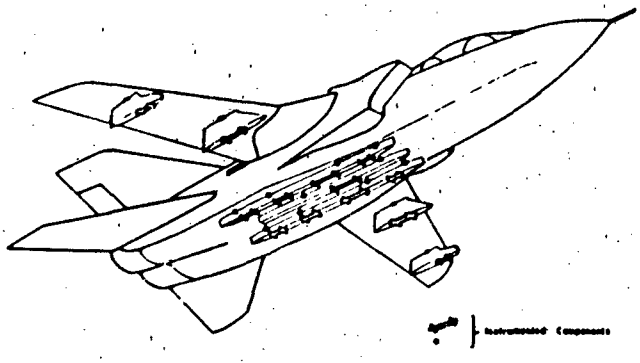

Fig. 6 RACS-INSTRUMENTED DRU's AND ADAPTER SPIGOTS

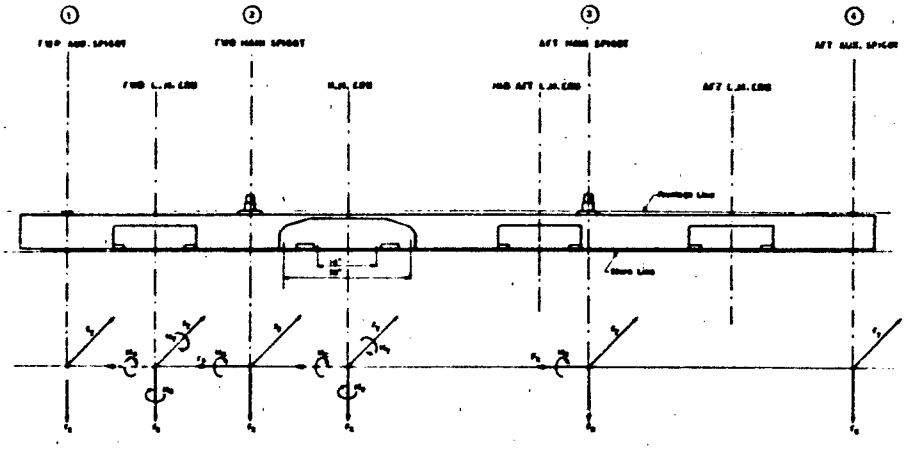

Fig. 7 RIGHT SHOULDER PYLON-SPIGOTS AND ERU's LOCATION IN RESPECT TO MEASURED LOADS COMPONENTS

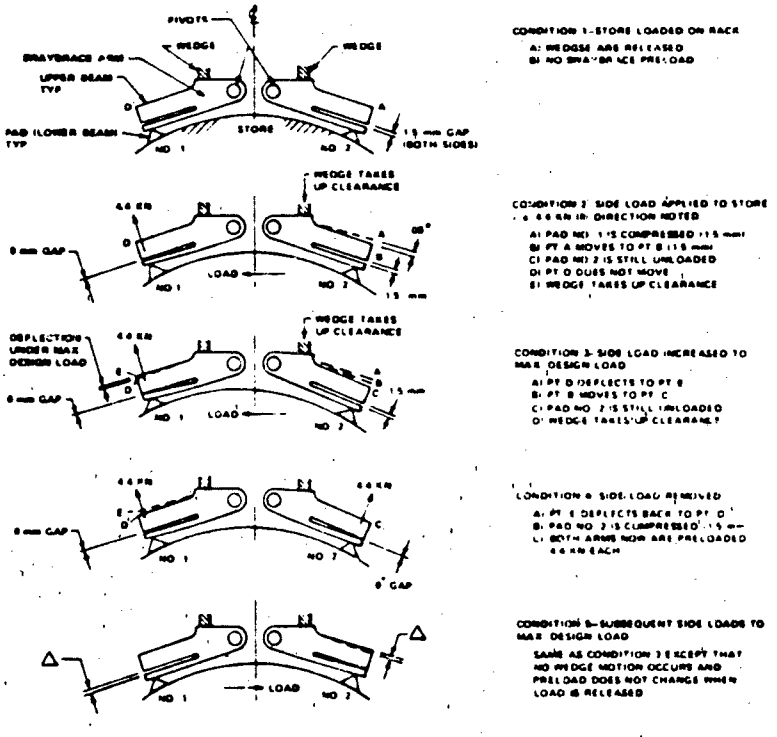

Fig. 8 PRINCIPLE OF MOVABLE CRUTCHARMS OF THE MWCS-ERU's

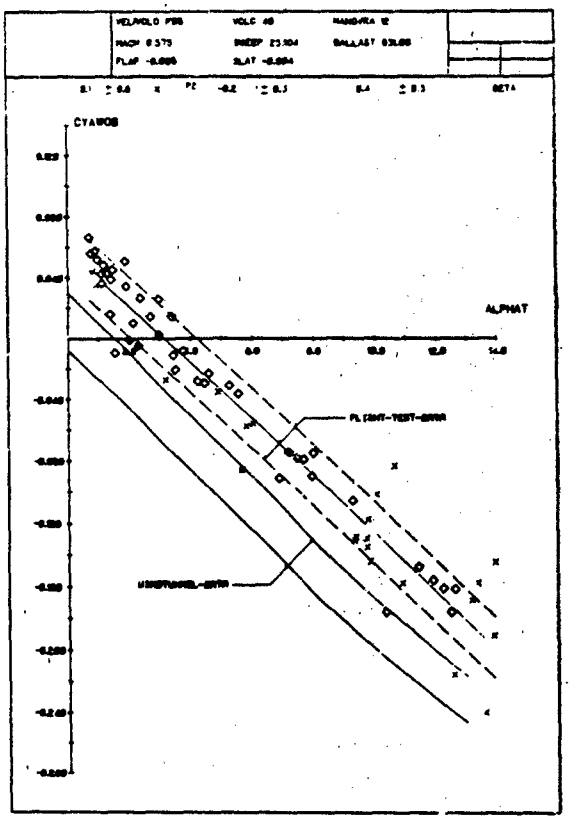

Fig. 9.1 MACE-COMPARISON OF FT-/WT MEAS. YAW MOM. AT O/B PYLON SPIGOT

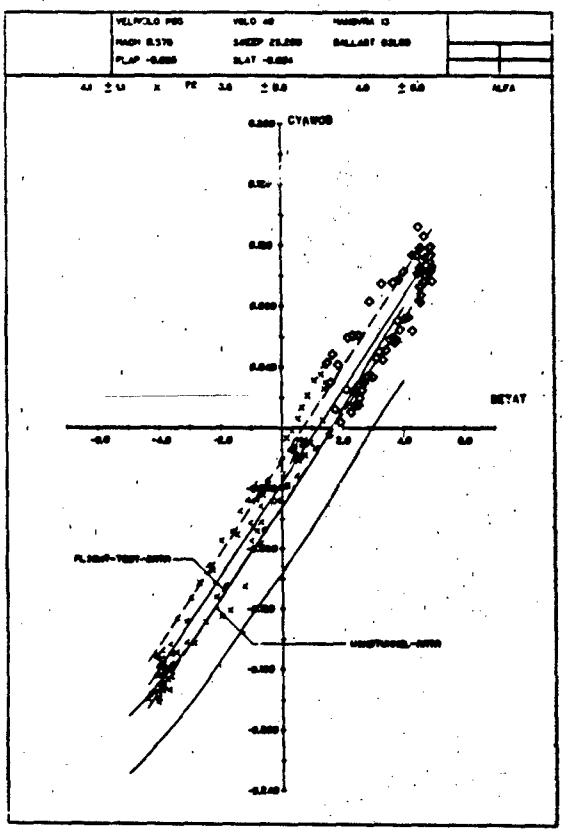

Fig. 9.2 MACE-COMPARISON OF FT-WT MEAS. YAW-MOM. AT O/B PYLON SPIGOT

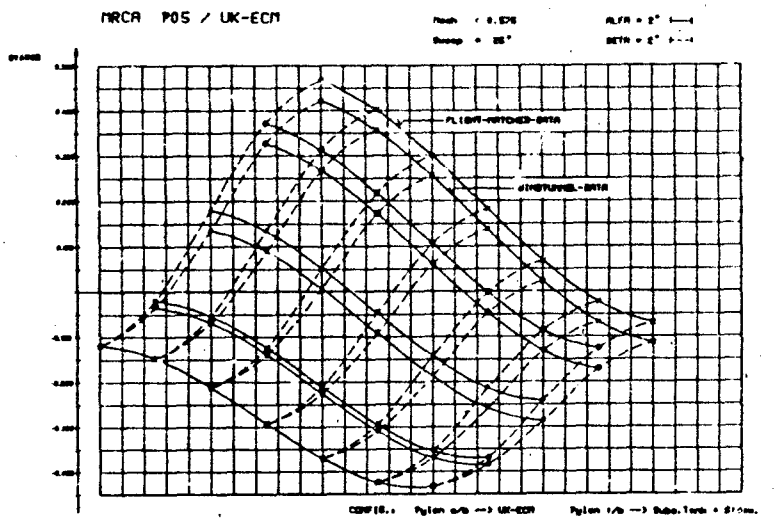

Fig. 9.3 MACE-FINAL FLIGHT MATCHED YAW-MOMENT COEF. AT O/B PYLON SPIGOT

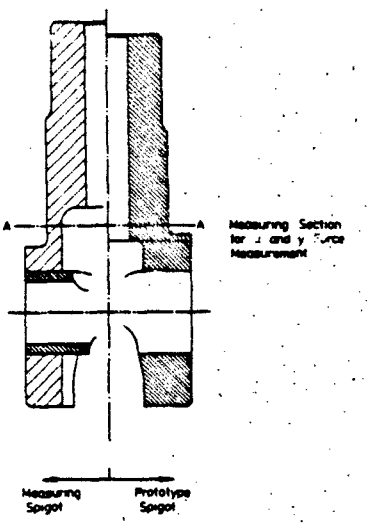

Fig.10 COMPARISON BETWEEN MEASURING SPIGOT AND PROTOTYP SPIGOT

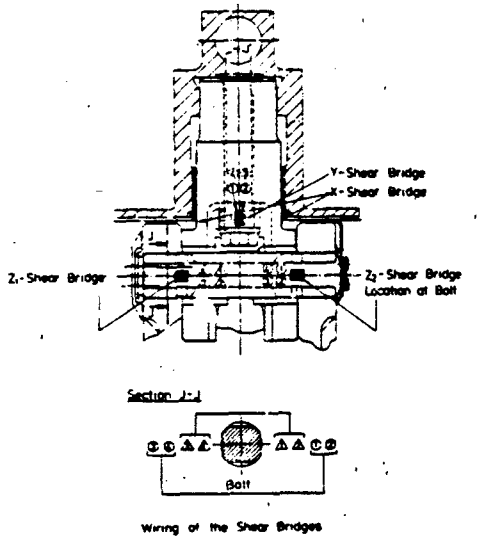

Fig.11 STRAINGAUGING OF FWD SPIGOT AND BOLT (SHOULDER ADAPTER)

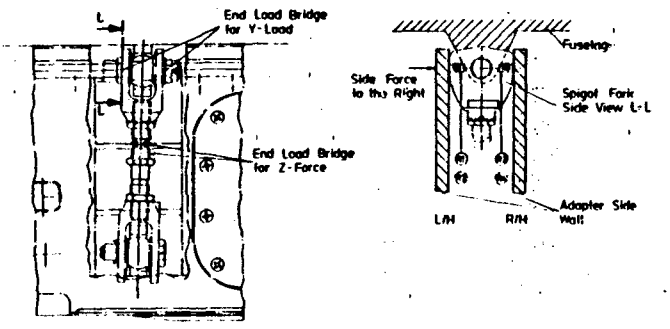

Fig.12 STRAINGAUGE AUXILIARY SPIGOT FWD (SHOULDER ADAPTER)

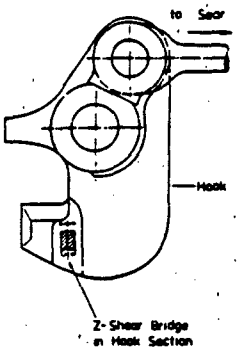

Fig.13 STRAINGAUGING LH-ERU HOOK

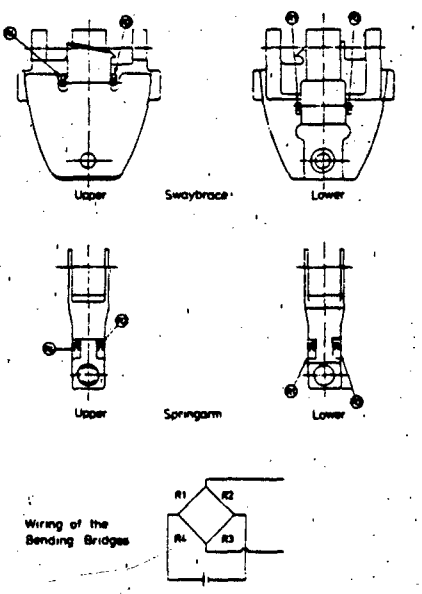

Fig.14 STRAINGAUGING RH-ERU, SPRINGARM AND SWAYBRACE

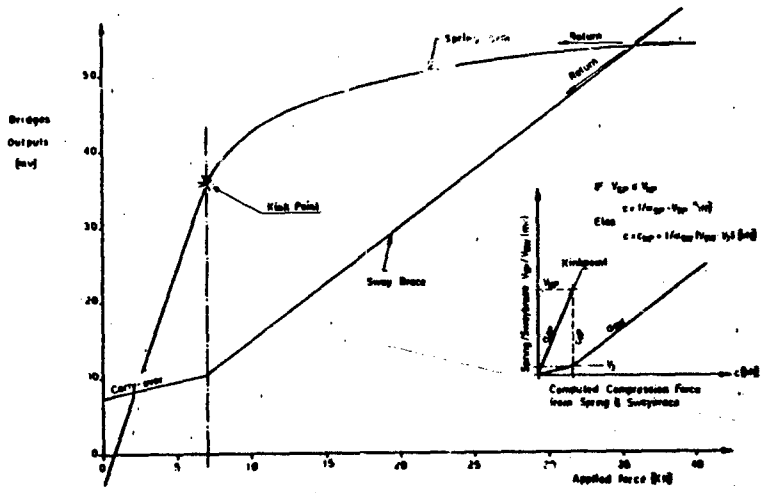

Fig. 15 ERU SPRINGARM/CRUTCHARM BRIDGE RESPONSE AND LOAD COMPUTATION

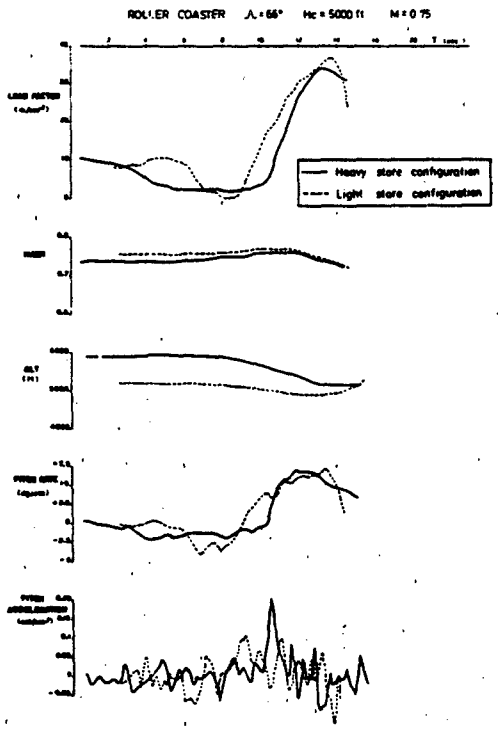

Fig. 16 SYMMETRIC MANOEUVRE-FLIGHT TESTING TECHNIQUE

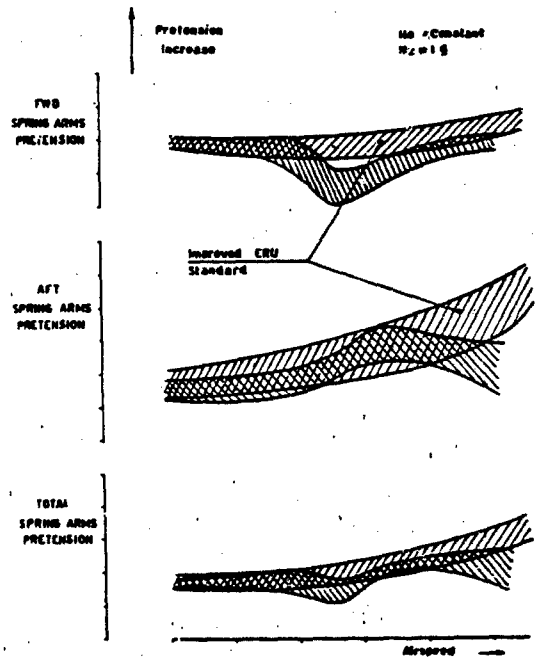

Fig. 17 14° LM-ERU SPRING ARMS PRETENSION INVESTIGATION

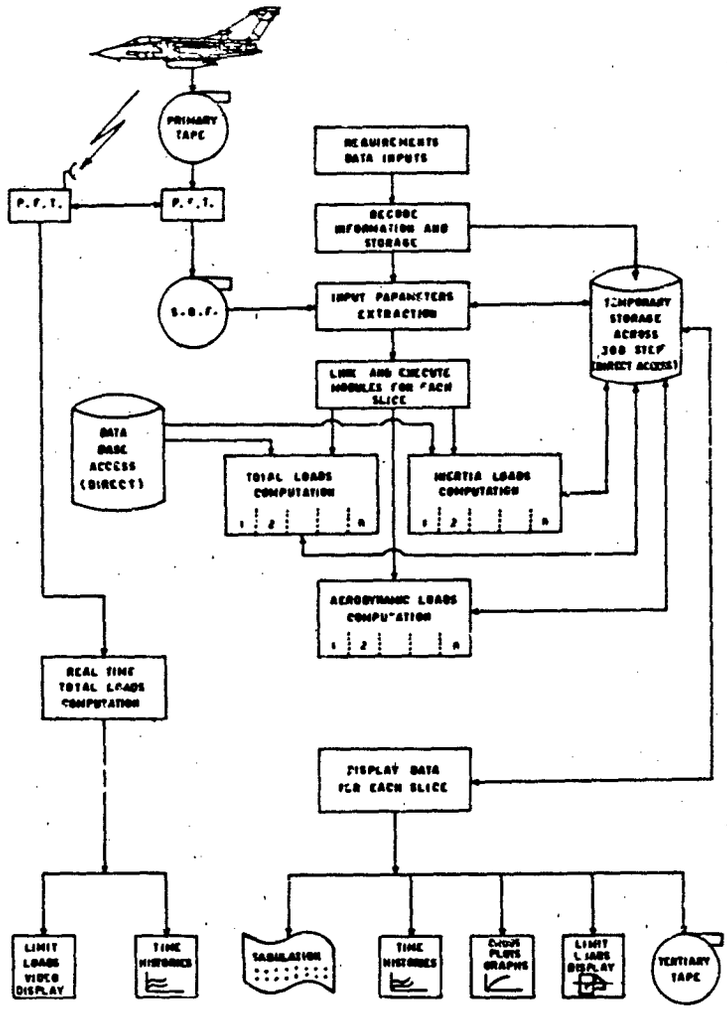

Fig. 18 FLIGHT TEST DATA PROCESSING

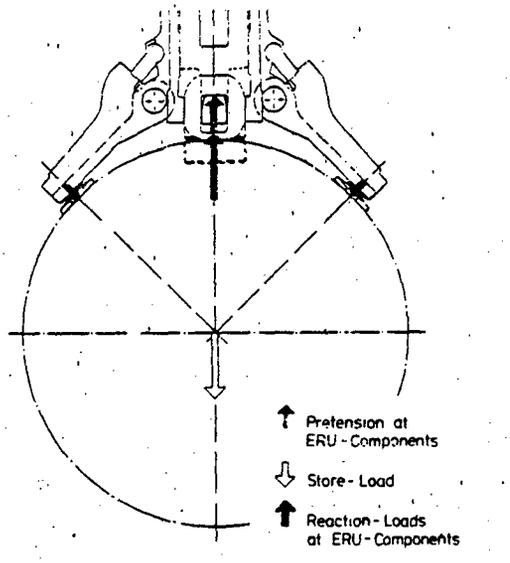

Fig. 19 PRINCIPLE OF REACTION-LOAD OF ERU-COMPONENTS

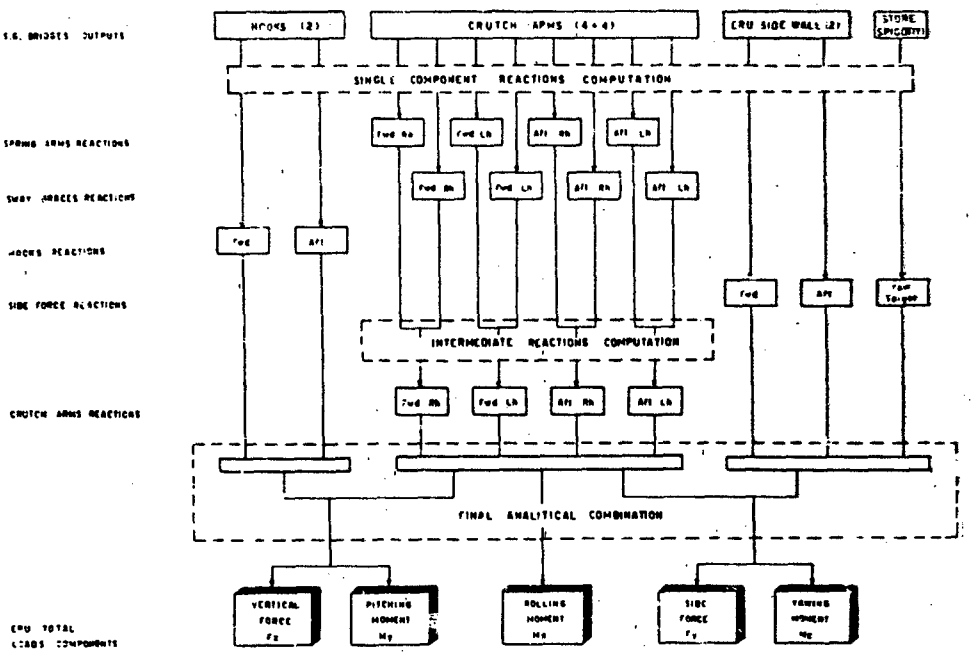

Fig.20 30° HM-ERU TOTAL LOADS COMPONENTS CALCULATION

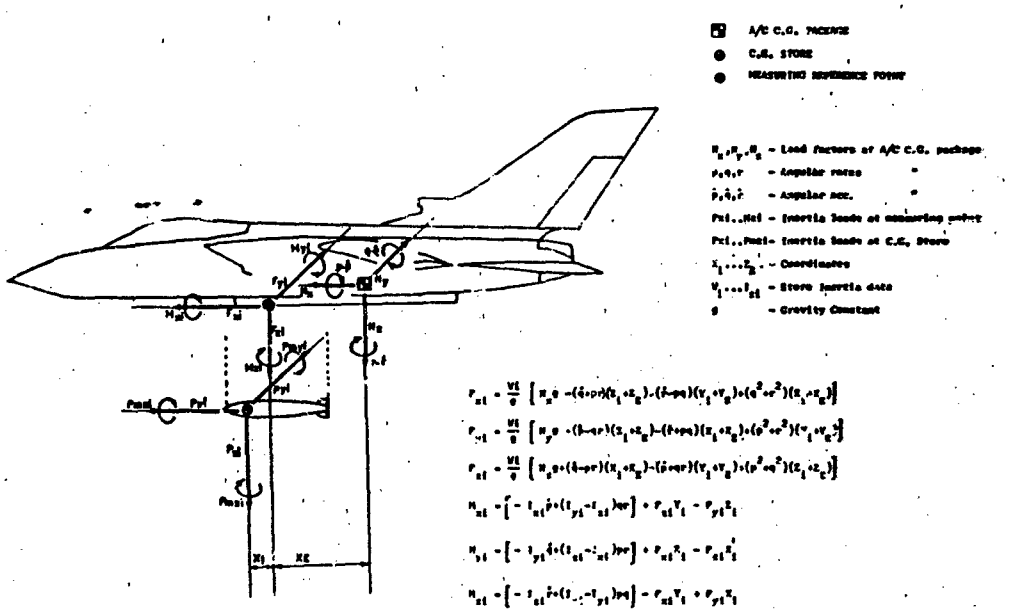

$$F_{x1} = \frac{W_1}{g}\left[n_x g - (\dot{q}+pr)(Z_1+Z_0) - (\dot{r}-pq)(Y_1+Y_0) + (q^2+r^2)(X_1+X_0)\right]$$

$$F_{y1} = \frac{W_1}{g}\left[n_y g - (\dot{r}-qr)(X_1+X_0) - (\dot{p}+rq)(Z_1+Z_0) + (r^2+p^2)(Y_1+Y_0)\right]$$

$$F_{z1} = \frac{W_1}{g}\left[n_z g + (\dot{q}+pr)(X_1+X_0) - (\dot{p}-qr)(Y_1+Y_0) + (p^2+q^2)(Z_1+Z_0)\right]$$

$$M_{x1} = \left[-I_{x1}\dot{p} + (I_{y1}-I_{z1})qr\right] + F_{z1}Y_1 - F_{y1}Z_1$$

$$M_{y1} = \left[-I_{y1}\dot{q} + (I_{z1}-I_{x1})pr\right] + F_{x1}Z_1 - F_{z1}X_1$$

$$M_{z1} = \left[-I_{z1}\dot{r} + (I_{x1}-I_{y1})pq\right] - F_{x1}Y_1 + F_{y1}X_1$$

Fig.21 INERTIA LOADS COMPUTATION AT MEASURING POINT

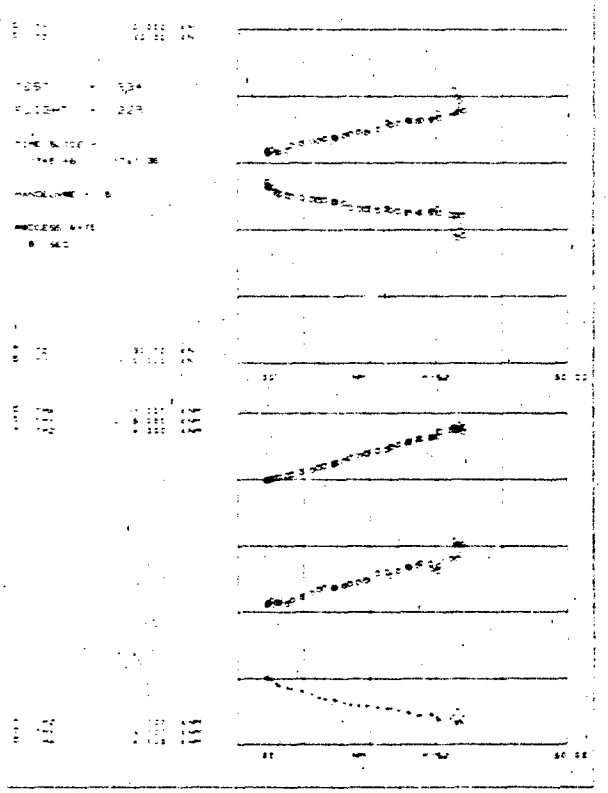

Fig.22 EXAMPLE OF FLIGHT TEST DATA PRESENTATION

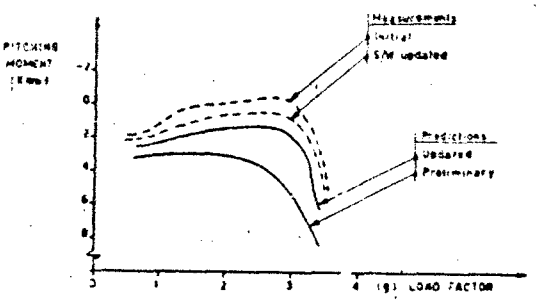

Fig.23 HM-ERU I/B WING PYLON
IMPROVEMENT OF MEASUREMENTS AND PREDICTIONS

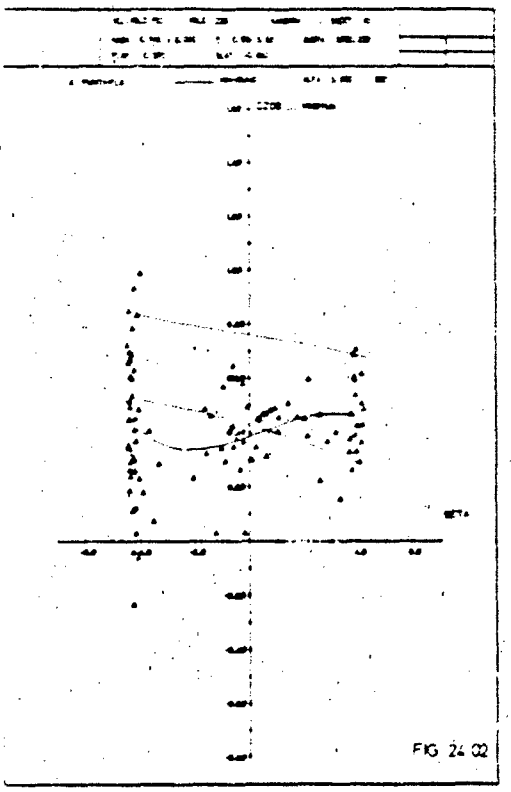

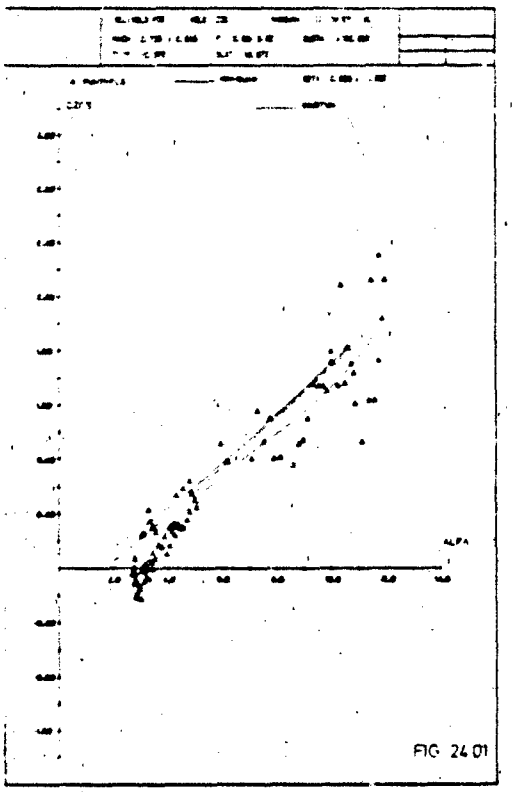

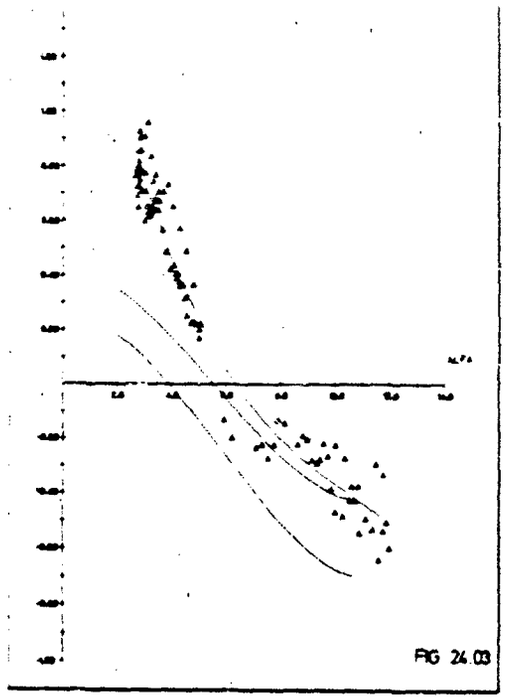

FIG 24.03

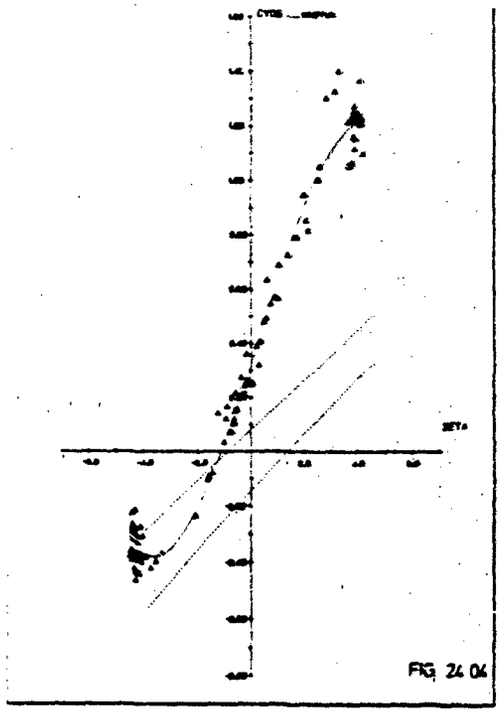

FIG 24.04

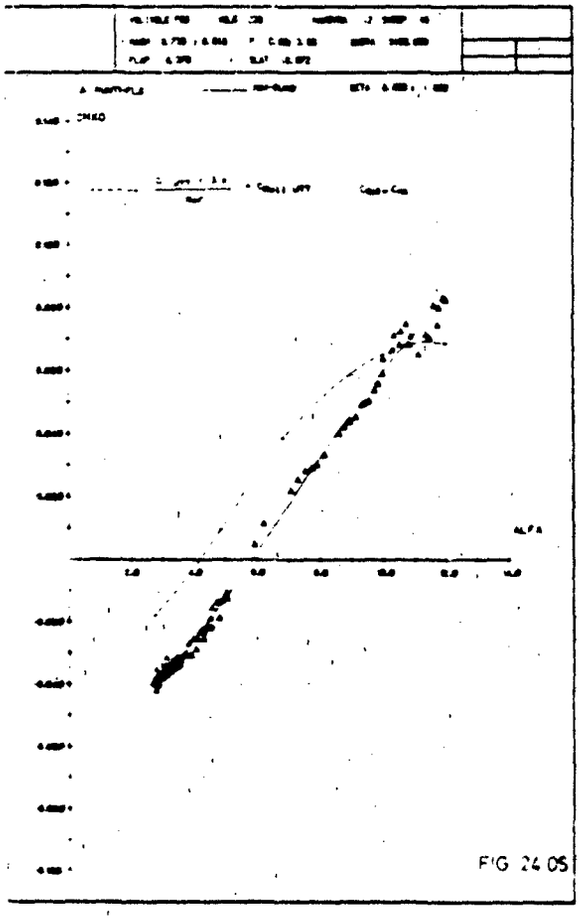

FIG 24.05

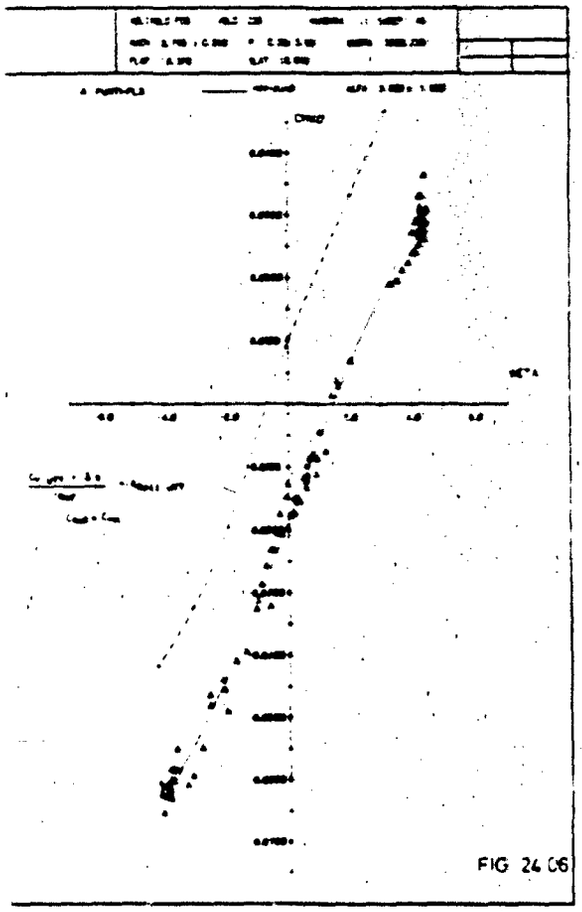

FIG 24.06

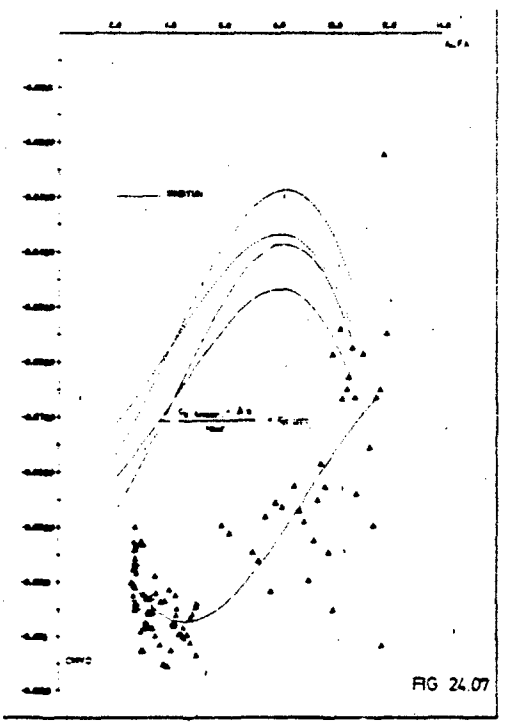

FIG 24.07

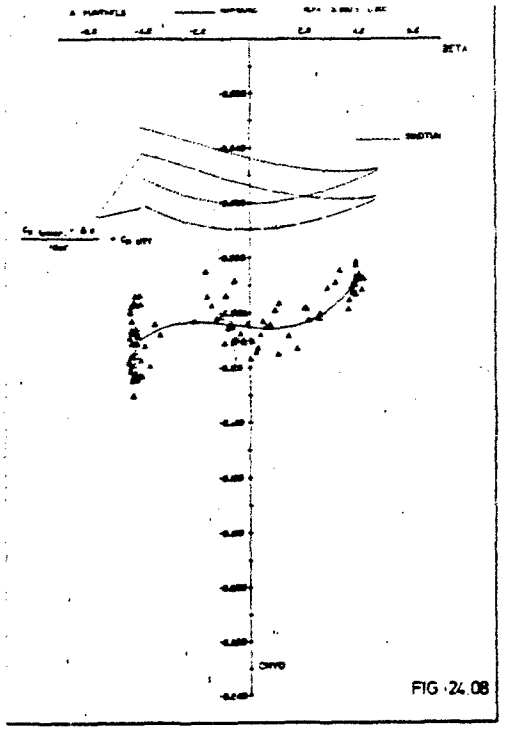

FIG 24.08

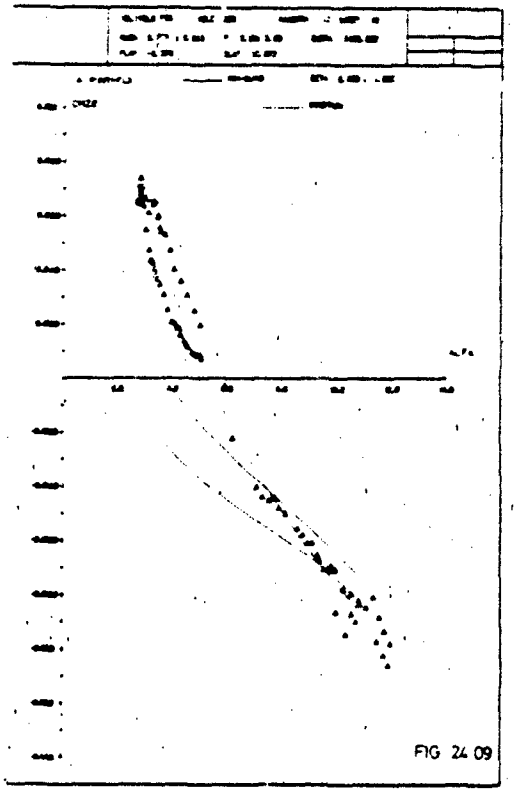

FIG 24.09

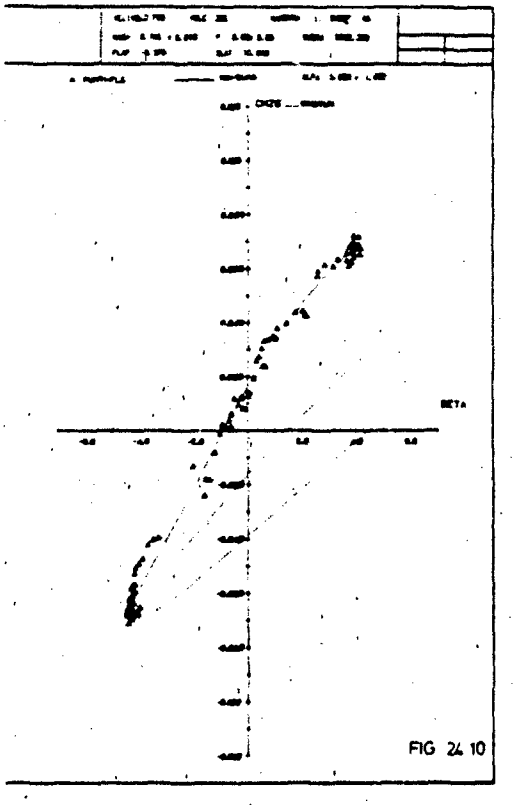

FIG 24.10

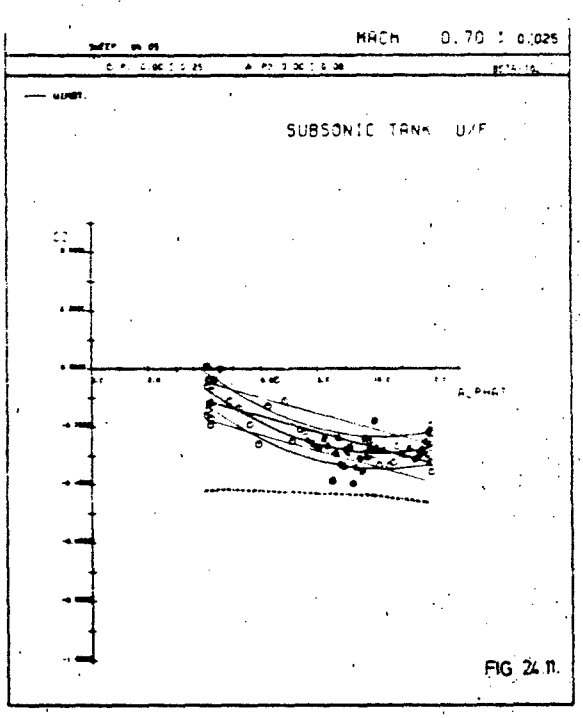

FIG. 24.11.

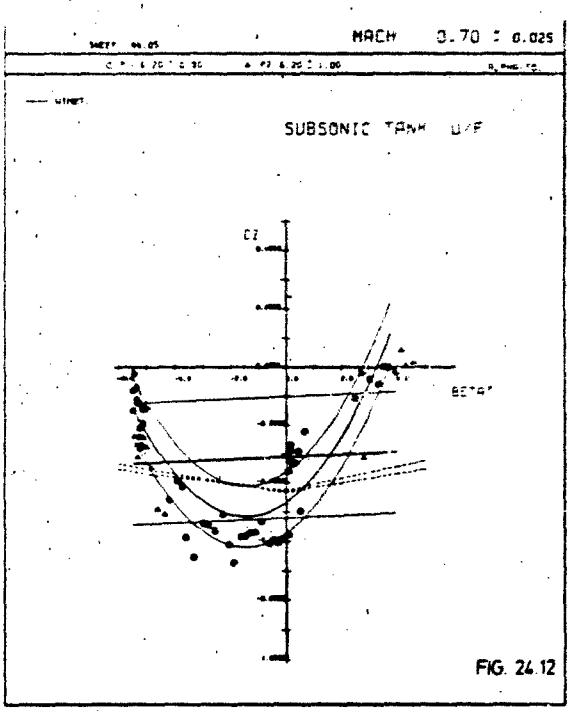

FIG. 24.12

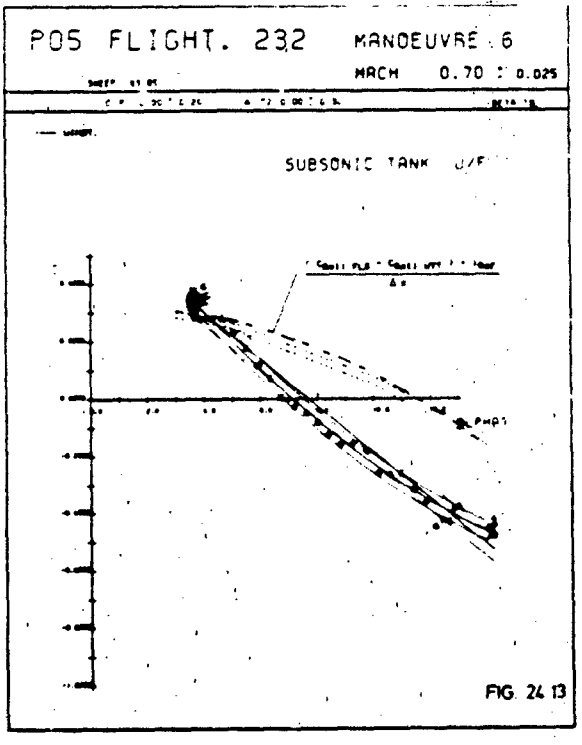

FIG. 24.13

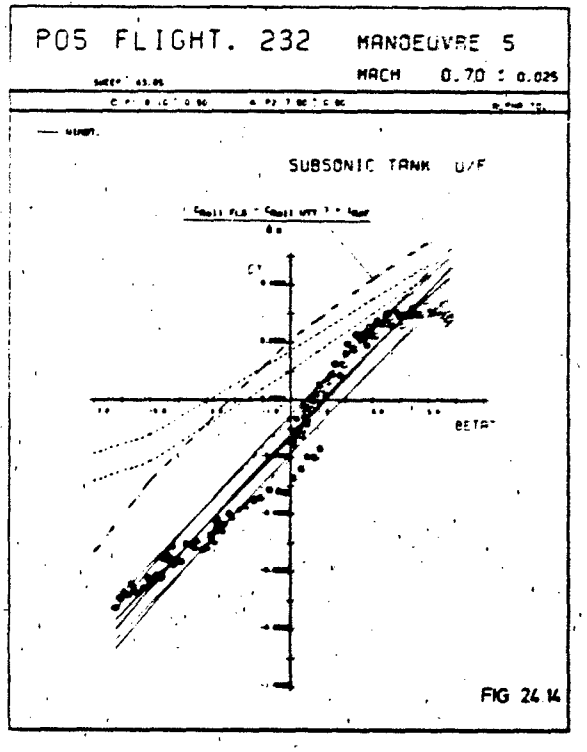

FIG 24.14

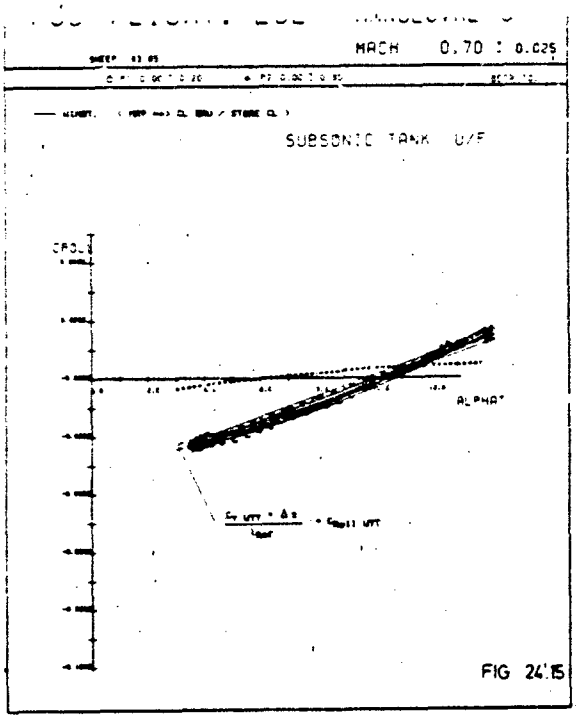

FIG 24.15

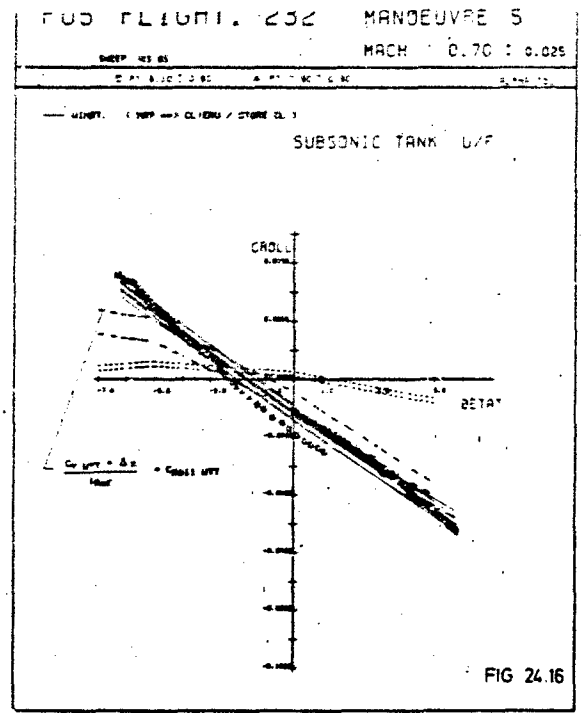

FIG 24.16

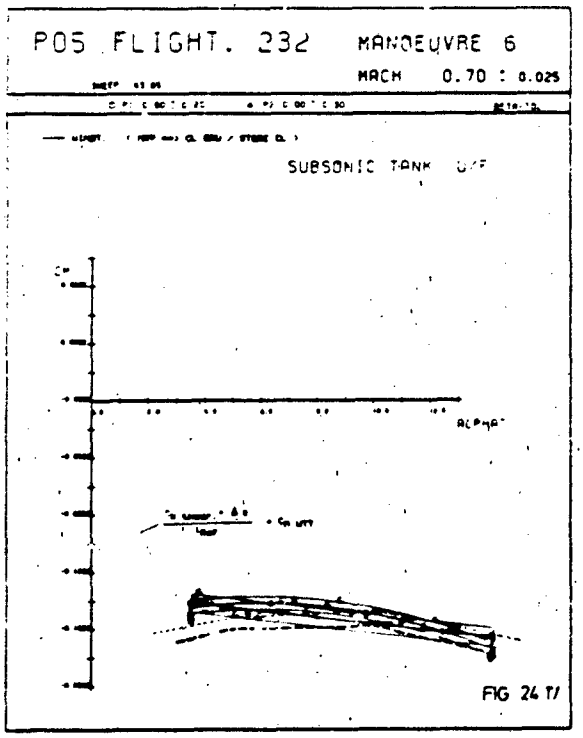

FIG 24.17

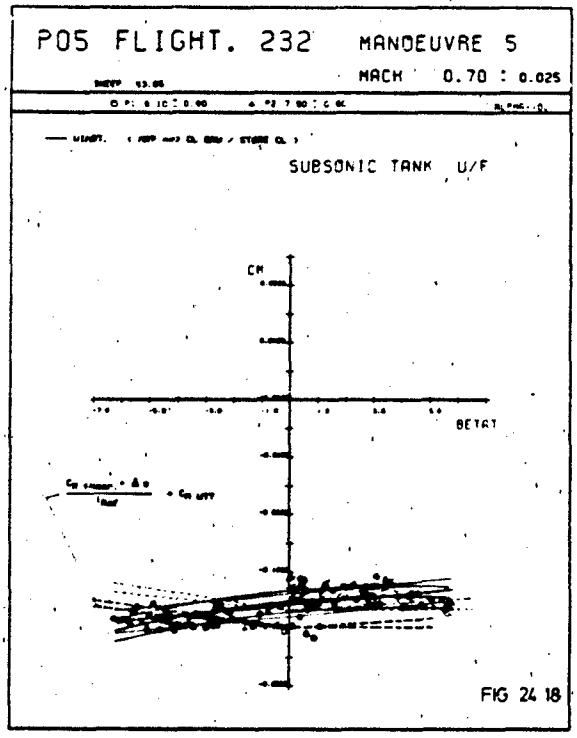

FIG 24.18

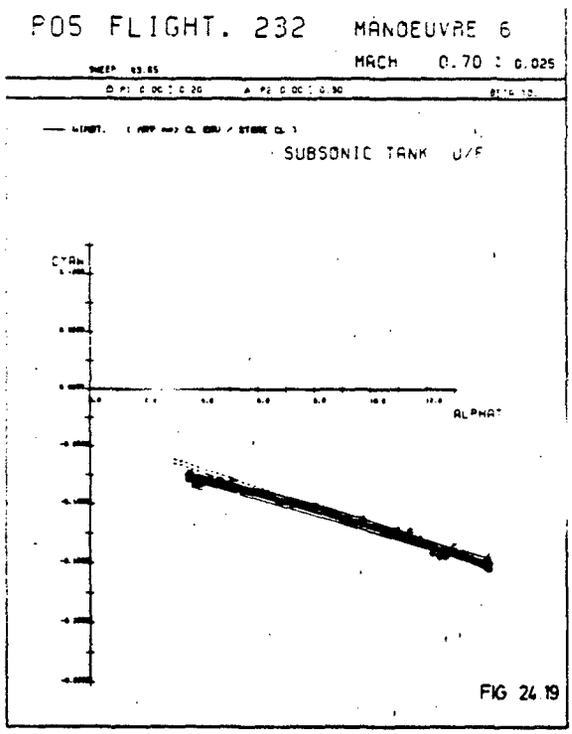

FIG 24.19

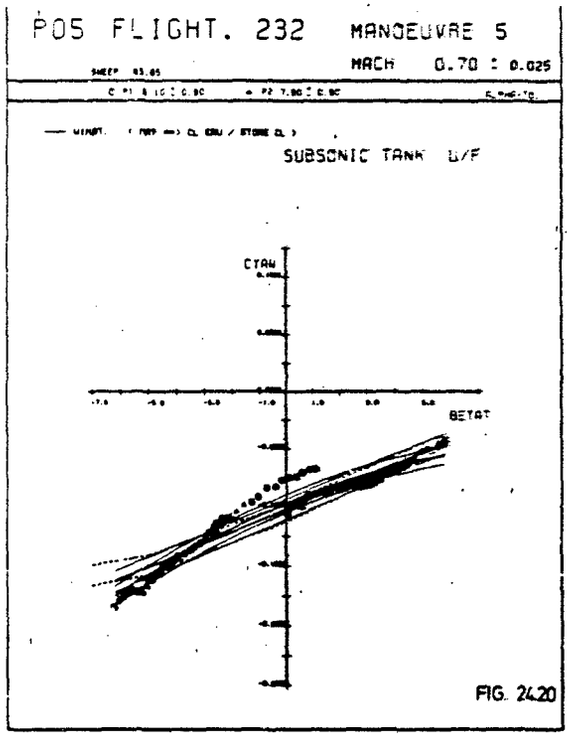

FIG. 24.20

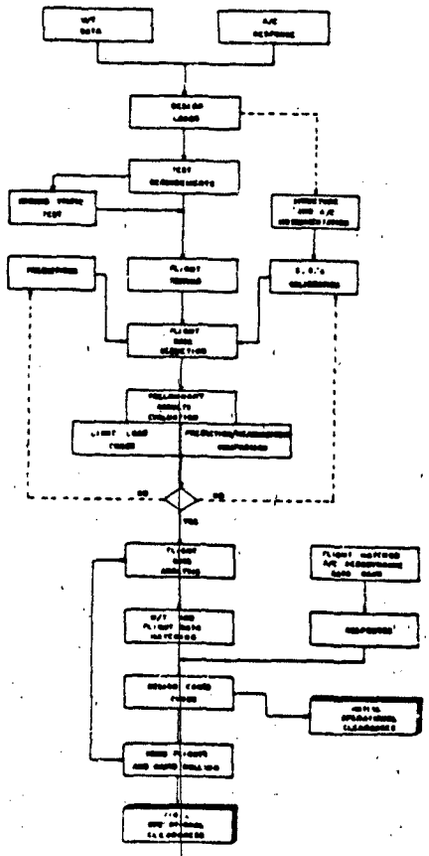

Fig. 25 GENERAL PROCEDURE FOR OPERATIONAL CLEARANCES RELEASE

CONDUITE ET SURVEILLANCE DES ESSAIS EN VOL

EN TEMPS REEL

Bertrand SCHERRER
Chef du Service Méthodes et Moyens d'Essais
Centre d'Essais en Vol - Base d'Essais d'Istres
13128 ISTRES-AIR - FRANCE

RESUME

La Base d'Istres du Centre d'Essais en Vol est principalement responsable de l'exécution des essais de performances, de structure et de propulsion. Située dans le sud de la France, au centre d'une région plate, cette Base Aérienne bénéficie d'un climat très favorable. Si l'on ajoute à cela la possibilité d'une très grande longueur d'envol et d'atterrissage, étendue jusqu'à 6 kilomètres par les prolongements de la piste, ceci explique l'affectation de la Base d'Essais aux essais les plus dangereux comme ceux de vrille, d'extension du domaine de vol, les essais d'extinction et rallumages moteur, de flottement, etc.. Un effort spécial a été consacré, à Istres, à la mise en place de moyens et dispositifs destinés à améliorer l'efficacité et la sécurité de tels essais, en particulier ceux ne pouvant être répétés sans accroître les risques potentiels. La description porte sur l'infrastructure Mesures utilisée, incluant la télémesure, la trajectographie, le centre de calcul, la présentation des informations qui permettent de diriger et de surveiller plusieurs essais en cours d'exécution, simultanément. Cette présentation donne des exemples d'utilisation de ces moyens.

1 - GENERALITES

Présenter quelques uns des moyens d'essais du Centre d'Essais en Vol rend opportun le rappel succinct des missions de cet Etablissement et la description sommaire de son organisation. Cette présentation permettra notamment d'expliquer le partage d'activité entre les trois Bases d'Essais principales.

1,1 - Les missions du Centre d'Essais en Vol

Des textes qui les définissent il ne sera retenu que ce qui peut être utile à l'exposé, à savoir que le Centre d'Essais en Vol (C.E.V.) est l'Expert Essais en vol des Services Officiels.

Ce rôle signifie plus précisément :

- que le C.E.V. intervient dans l'évaluation de tous les matériels aéronautiques résultant de programmes aéronautiques pilotés par l'Etat. L'importance relative des programmes destinés à couvrir des besoins des Armées explique que le C.E.V. soit un Etablissement rattaché à une Direction Technique dépendant, sous l'autorité d'une Délégation Générale à l'Armement, du Ministère de la Défense.
- que l'existence, au sein de l'Administration, d'un Etablissement qui dispose des moyens en personnels et matériels ayant la capacité d'assurer l'évaluation en vol de matériels aéronautiques, donne au C.E.V. la possibilité et la mission de participer au processus de certification des matériels aériens civils.

Ces deux aspects de la mission d'Expert Essais en vol des Services Officiels peuvent être résumés en disant que le C.E.V. est appelé à connaître tous les matériels aéronautiques qui impliquent une responsabilité de l'Etat agissant, soit à titre de promoteur et/ou acquéreur, soit en tant que puissance publique responsable de la sécurité des citoyens.

Le terme de "matériels aéronautiques" a été volontairement utilisé pour indiquer qu'il ne s'agit pas uniquement d'évaluation d'aéronefs complets mais que les propulseurs, les équipements aéronautiques et les armements aéroportés peuvent faire l'objet d'essais en vol et qu'ils peuvent impliquer, dans ce cas, l'utilisation d'aéronefs déjà expérimentés adaptés à des fonctions de bancs d'essais.

A cette mission de base, il convient de citer, parmi les autres responsabilités du Centre d'Essais en Vol :

- la mise en oeuvre de moyens d'infrastructure d'essais en vol au profit de tiers et, en particulier des Services Essais en vol des Constructeurs (Contrôle de la circulation aérienne d'essais et de réception, trajectographie, réception télémesure.....).
- la formation des personnels spécialistes des essais tant pour ses propres besoins que pour ceux de l'industrie et des organismes civils et militaires, français et étrangers.

Ce large domaine d'activité qui requiert, selon la nature des essais et des matériels essayés, un environnement spécifique, a conduit le C.E.V. à répartir ses essais entre 3 Bases d'Essais principales (Brétigny, dans la région parisienne, Cazaux sur le littoral atlantique et Istres à proximité du littoral méditerranéen).

1,2 - Les missions de la Base d'Essais d'Istres

Au titre de la mission principale du Centre d'Essais en Vol, la Base d'Essais d'Istres est chargée

- des essais de performances, de qualité de vol et, occasionnellement, d'essais de structure des avions.(1)
- des essais de propulseurs d'aéronefs.
- des essais de simulation à l'aide de banc volant ou de moyens sol.

Au titre des autres missions évoquées au § précédent, la Base d'Essais en Vol d'Istres fournit aux essais en vol des Constructeurs un certain nombre de prestations : contrôle circulation aérienne, trajectographie, réception télémesure dont la part la plus importante est fournie aux services installés sur la Base : Avions Marcel Dassault - Bréguet Aviation (AMD-BA) et Société Nationale d'Etudes et de Construction de Moteurs d'Aviation (SNECMA).

Elle a également, depuis 1962, la responsabilité de la formation des Navigants d'Essais assurée au sein de l'Ecole du Personnel Navigant d'Essais et de Réception.

Les raisons qui ont conduit l'Administration à investir la plate-forme d'Istres ont été, à l'origine, directement liées aux programmes aéronautiques de l'immédiat après-guerre qui a vu, avec la relance de l'aéronautique française, la naissance d'un nombre très important de prototypes. L'exploration de larges domaines de vol impliquant l'incursion dans le domaine supersonique avec des moteurs de fiabilité relative et de performances modestes, rendait particulièrement attractif un site d'essais disposant d'une longue piste aux approches dégagées coiffée d'un ciel bleu permettant le retour à vue d'un aéronef ayant un incident de propulsion.

Ces facilités aéronautiques n'ont pas perdu de leur intérêt mais elles ne sont plus exclusives et les essais d'avions et de moteurs exigent, du fait de l'évolution des techniques et des aéronefs, que le site d'essais dispose d'une infrastructure en moyens d'essais au sol dont les composants peuvent être classés en quatre catégories :

- moyens d'équipement d'aérodrome,
- moyens de contrôle de la circulation aérienne,
- moyens de simulation,
- moyens de mesure au sol.

2 - L'INFRASTRUCTURE EN MOYENS DE MESURE DE LA BASE D'ESSAIS D'ISTRES

2,1 - Organisation générale

INFRASTRUCTURE MOYENS DE MESURE

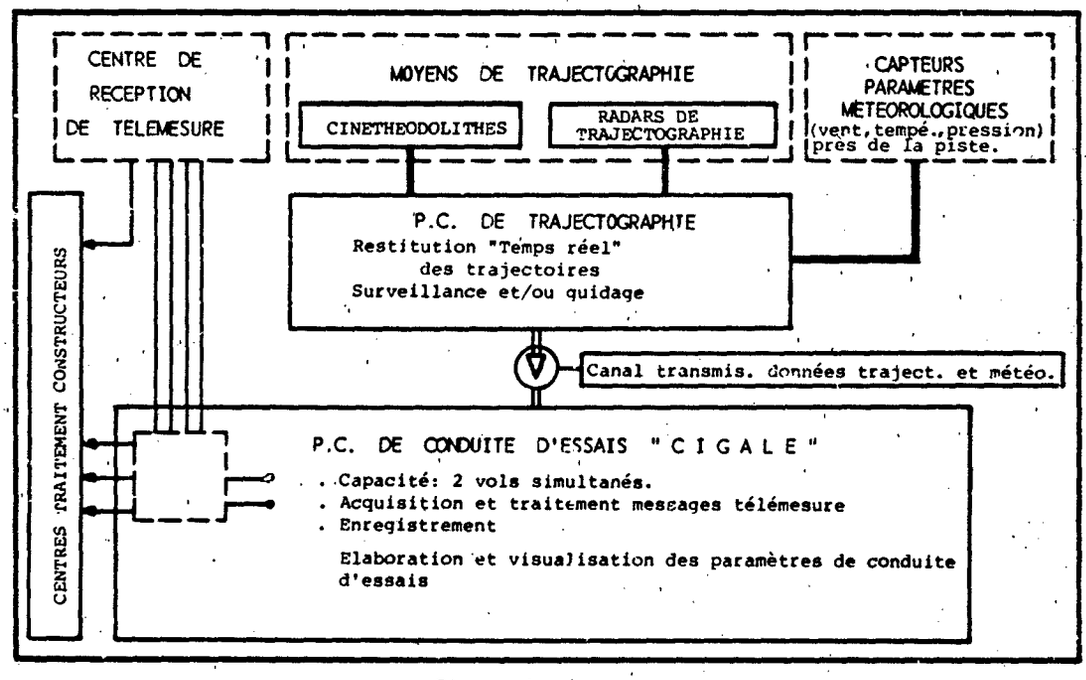

Figure 1

(1) - La Base d'Essais d'Istres participe également aux essais d'intégration des systèmes sur Avions d'Armes et aux essais d'évaluation globale des Avions d'Armes (prototypes et avions de développement).

les deux conceptions suivantes :

- l'une vise à minimiser la dépendance de l'aéronef en essai, pendant les vols, vis à vis d'une infrastructure. L'installation d'essais embarquée a donc, non seulement la capacité d'acquérir les paramètres requis pour l'exécution du programme d'essais, mais aussi de les enregistrer à bord et de visualiser directement ou après traitement informatique, ceux qui sont nécessaires à l'équipage pour la conduite de l'essai.
- l'autre, qui s'apparente beaucoup plus aux méthodes imposées par les essais d'engins, tend au contraire à faire largement appel à des moyens de mesure sol dont l'activation est indispensable à l'exécution des vols d'essais.

La nature des activités essais de la Base d'Istres, fortement marquée par les essais d'Avions d'Armes et la convergence des choix du C.E.V. et des Constructeurs pour donner une large place à la conduite d'Essais temps réel, ont rendu nécessaire l'implantation d'une infrastructure en moyens de Mesure dont l'organisation générale est donnée sur la figure 1.

On notera que les informations issues des moyens de trajectographie et des capteurs de paramètres météorologiques caractérisant l'environnement de la piste, sont regroupées et traitées au niveau d'un Poste Central (P.C.) qui dispose de sorties Temps Réel et qui permet la surveillance de trajectoires et/ou le guidage. Ces informations peuvent, en tant que de besoin, être transmises au P.C. de conduite d'Essais "CIGALE" ou au Centre de Traitement Temps Réel des Avions Marcel Dassault - Bréguet Aviation.

Cette architecture donne une bonne souplesse à l'exécution des vols puisque les centres Temps Réel peuvent travailler au profit d'avions différents ou, au contraire, être interconnectés de tell manière que les P.C. de conduite d'Essais reçoivent les informations trajectographiques des avions qui les intéressent.

2,2 - Les moyens de trajectographie et leur P.C.

On constate, sur la figure 2, que le système de trajectographie (installé en 1974) comporte deux types de moyens :

- des cinéthéodolites,
- des radars.

Les premiers sont destinés à couvrir les trajectoires associées aux phases de décollage, atterrissage ou approche.

Les radars (un en installation fixe, l'autre en installation mobile) prolongent jusqu'à l'horizon optique, l'étendue de mesure du système.

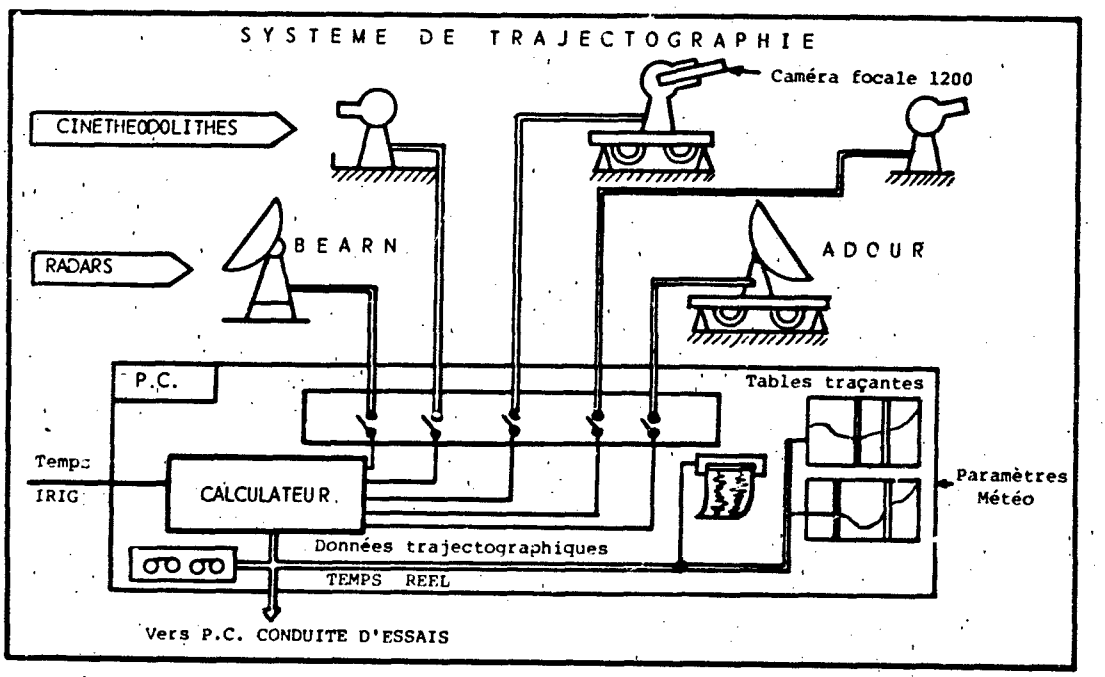

Figure 2

Les cinéthéodolites à sortie numérique (codage des angles à 19 bits) utilisent une partie des ressources d'un calculateur associé au système. Cette capacité, qui permet de sortir en temps réel des résultats bruts, sans correction des écarts de poursuite, donne avec des opérateurs entraînés, une qualité de poursuite et donc une précision de résultats qui est jugée suffisante pour 60 % des trajectoires traitées. Pour les autres cas, un traitement différé réalisé à partir de l'exploitation des films, permet d'introduire l'écartométrie et de tirer toute la précision dont sont capables les cinéthéodolites. On notera qu'à l'un des trois cinéthéodolites, est associée une caméra longue focale (f = 1200 mm) essentiellement destinée au suivi des essais de vrilles. Le choix de cette solution a été motivé par les possibilités d'interdésignation d'objectifs que permet le système. En cas d'essais de vrilles, un radar et le cinéthéodolite avec caméra longue focale sont activés : le pointage de la plate-forme cinéthéodolite porteuse de la caméra vrille est réalisé à l'aide du radar et l'opérateur du cinéthéodolite n'en reprend le pilotage manuel qu'au lancement de la vrille, solution qui garantit l'acquisition de l'avion.

- Le radar fixe est un radar BEARN à exploration conique travaillant en bande C avec aérien de Ø 4 m.
- Le radar mobile est un radar ADOUR (même bande de fréquence).

On observera que l'organisation du système rend possible le suivi de deux essais ou deux avions différents avec 1 ou 2 ou 3 cinéthéodolites et 1 radar, ou de faire participer à la poursuite d'un même aéronef ces mêmes moyens. Il est également possible d'utiliser simultanément les deux radars.

Le P.C. est équipé de moyens de visualisation qui permettent le suivi, le contrôle et le guidage sur trajectroires prédéterminées à partir de deux tables traçantes qui seront, à moyen terme, remplacées par des consoles cathodiques polychromes.

Les résultats de trajectographie cinéthéodolites ou radar sont également assemblés en un message série qui regroupe les informations brutes données par les moyens de trajectographie et les coordonnées calculées au niveau du P.C. de trajectographie. Le message est acheminé vers le P.C. de conduite d'Essais CIGALE et/ou vers le Centre de Traitement Temps Réel des essais en vol AMD-BA (Avions Marcel Dassault-Bréguet Aviation).

',3 - Le P.C. de conduite d'Essais "CIGALE"

',3,1 - Généralités

Quelques rappels historiques permettront de situer la génèse de ce Centre.

Le Centre d'Essais s'est intéressé, de longue date, à l'utilisation de la télémesure puisqu'en 957, après une évaluation des différents matériels français, il fixait son choix, pour les essais d'aéonefs, sur un équipement développé par l'O.N.E.R.A. (1) et fabriqué sous licence par la S.F.I.M. (2). vant d'adopter l'emploi d'un matériel valable aussi bien pour les engins que pour les aéronefs et fondé ur le stadard IRIG. L'expérience amorcée occasionnellement sur certains prototypes d'avions d'armes des nnées 60 s'est rapidement systématisée.

Par ailleurs, la pénétration sur le marché de l'informatique de calculateurs de conduite de processus a permis d'étendre le champ d'utilisation et d'aborder la conduite d'essais avec traitement temps éel.

L'expérience acquise dans la première décennie d'utilisation de la télémesure avait mis en évidence n gain pour la sécurité dans les essais d'aéronefs (tout particulièrement pour les aéronefs à équipage estreint - mono ou biplace). L'introduction du Traitement Temps Réel a confirmé et amplifié cet acquis t a permis, en outre, de démontrer son intérêt pour la validation des phases d'essais.

écurité

La participation au déroulement de l'essai de personnels au sol disposant d'informations provenant e l'avion, est particulièrement bénéfique dans trois cas :

surveillance de paramètres en évolution qui sortent du champ d'observation ou de sensation de l'équipage ou dont la surveillance est rendue difficile en raison d'une charge de travail passagèrement élevée.

surveillance de paramètres et contrôle de manoeuvres effectuées dans des essais ou des phases de vol particulièrement perturbées et éprouvantes pour le pilote (vrilles, limites de manoeuvres, essais temps chaud....).

assistance en cas d'incident ou d'accident, assistance pouvant aller jusqu'à l'ordre d'évacuation.

ualité des essais et des résultats

Le contrôle Temps Réel des paramètres significatifs permet de vérifier la qualité de l'exécution e l'essai et de s'assurer que les conditions nécessaires à l'obtention des résultats sont respectées. es enregistrements effectués au sol, qui serviront de bases de données pour l'exploitation différée es essais, sont donc validés.

Sur une échelle de temps plus longue, le Temps Réel supprime certains écueils du dépouillement différé. La procédure de recueil de données à partir d'enregistrements à bord a conduit fréquemment, dans les

1) Office National d'Etudes et de Recherches Aérospatiales.
2) Société de Fabrication d'Instruments de Mesure.

Centres d'Essais, à l'exécution de vols produisant une masse d'informations enregistrées sur une période donnée très nettement supérieure à la capacité d'exploitation des moyens de traitement sur une période de même durée. Cette situation, qui occasionnait des reports d'exploitation, pouvait en outre se solder par le constat que le fonctionnement de certaines chaînes de mesure essentielles ne correspondait pas à ce qui était attendu et que les modifications apportées depuis à l'installation de mesure ou à l'aéronef ne permettaient plus de retrouver un état susceptible d'apporter la vérification nécessaire. L'exploitation en temps réel présente donc l'intérêt de réaliser constamment l'équilibre entre l'exécution des vols et la capacité de dépouillement.

La conception de CIGALE a donc été fondée sur le traitement Temps Réel. Elle a intégré, en outre, uelques caractéristiques complémentaires.

La notion de P.C. de conduite d'essai. Elle constitue une extension du concept de station de réception de télémesure qui rend l'installation perméable à la prise en compte de données provenant d'autres moyens d'essais.

La flexibilité d'emploi imposée par la diversité des activités de la Base d'Essais d'Istres. Cette flexibilité devant permettre les mises en oeuvre successives rapides au profit de besoins essentiellement variables quant à la nature et au volume des messages de données à traiter et quant à la spécificité des informations à donner aux conducteurs d'essais.

Cette caractéristique a conduit à plusieurs options conditionnant l'architecture technique de la tation.

Introduction, dans le système, d'un "répartiteur programmable" dont la fonction essentielle est de réaliser rapidement l'affectation des moyens de conditionnement du signal et leur adaptation.

Utilisation de consoles cathodiques polychromes pour la visualisation des informations spécifiques.

,3,2 - Réalisation dans sa version originale.

La figure 3 met en évidence l'organisation générale du P.C. dans laquelle on distinguera 3 parties istinctes qui groupent, respectivement :

la salle de conditionnement des signaux de mesure.

la salle des moyens informatiques.

.B. - L'alvéole centrale regroupe les moyens utilisés pour l'exploitation différée qui, comme tels, ne participent pas aux processus de conduite d'essais en temps réel.

les salles de conduite d'essais dont 2 seulement doivent être prises en considération (la S.E. 3 est une salle dont le niveau d'équipement en fait une station simple, sans informatique, utilisable, soit en secours de S.E. 1 ou 2, soit pour des essais simples).

Une description sommaire de chacune e ces parties permettra d'en indiquer es principales caractéristiques et les onctions (voir figure 4, page 19-6).

CIGALE - IMPLANTATION DES MATERIELS

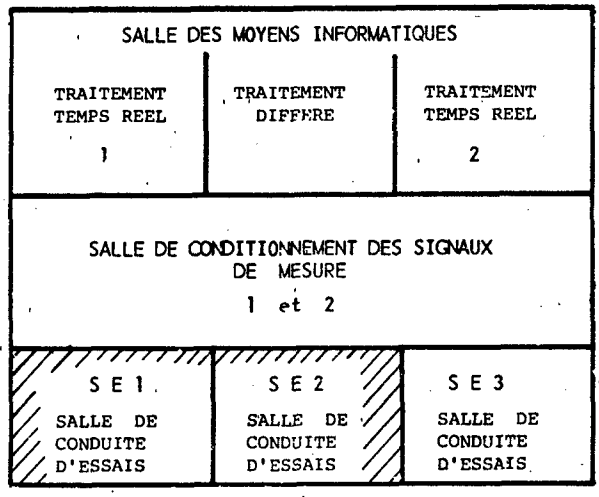

Figure 3

,3,2,1 - Salle de conditionnement des signaux

On a dit que la flexibilité d'emploi était un des objectifs auxquels le .C. devait satisfaire. Il était donc nportant de rendre l'équipement capable e minimiser les temps morts de changements de configuration lorsque l'activité impose d'enchaîner des ols d'aéronefs dont les types d'installation de mesure et la nature de l'essai sont très différents. ..: vol de vrilles d'un avion léger suivi d'un vol d'essai d'avion d'armes.

Cette flexibilité est assurée par l'association :

d'équipements qui permettent de traiter des messages de nature hétérogène allant du message de télémesure entièrement analogique avec un maximum de 18 voies, au message entièrement numérique en passant par les configurations hybrides comprenant un message numérique et des voies analogiques continues ou PAM.

et d'un répartiteur programmable dont les fonctions vont être succinctement décrites.

Cet équipement assure la connexion entre :

les éléments qui constituent les sources d'information :

- multiplex télémesure en provenance du centre de réception SIERRA ou de récepteurs locaux (solution qui était utilisée à l'époque où l'emploi de canaux de transmission était possible sur la bande de fréquence UHF).
- temps universel coordonné.
- enregsitrements magnétiques dans les cas de traitement en différé.
- moyens de contrôle ou d'étalonnage pour les vérifications.

les équipements de démodulation des sous-porteuses (discriminateurs à fréquences fixes ou discriminateurs universels) et/ou de synchronisation PAM ou PCM.

certains moyens de visualisation directe :

- indicateur à lecture directe,
- enregistreur graphique,
- écran cathodique multitraces pour les voies PAM.

Le répartiteur a une seconde fonction qui lui permet d'assurer la mise en configuration de ceux s équipements qui sont programmables par des ordres transmis sous forme de mots de 16 bits (discriminateurs universels et moyens de synchronisation PAM et PCM).

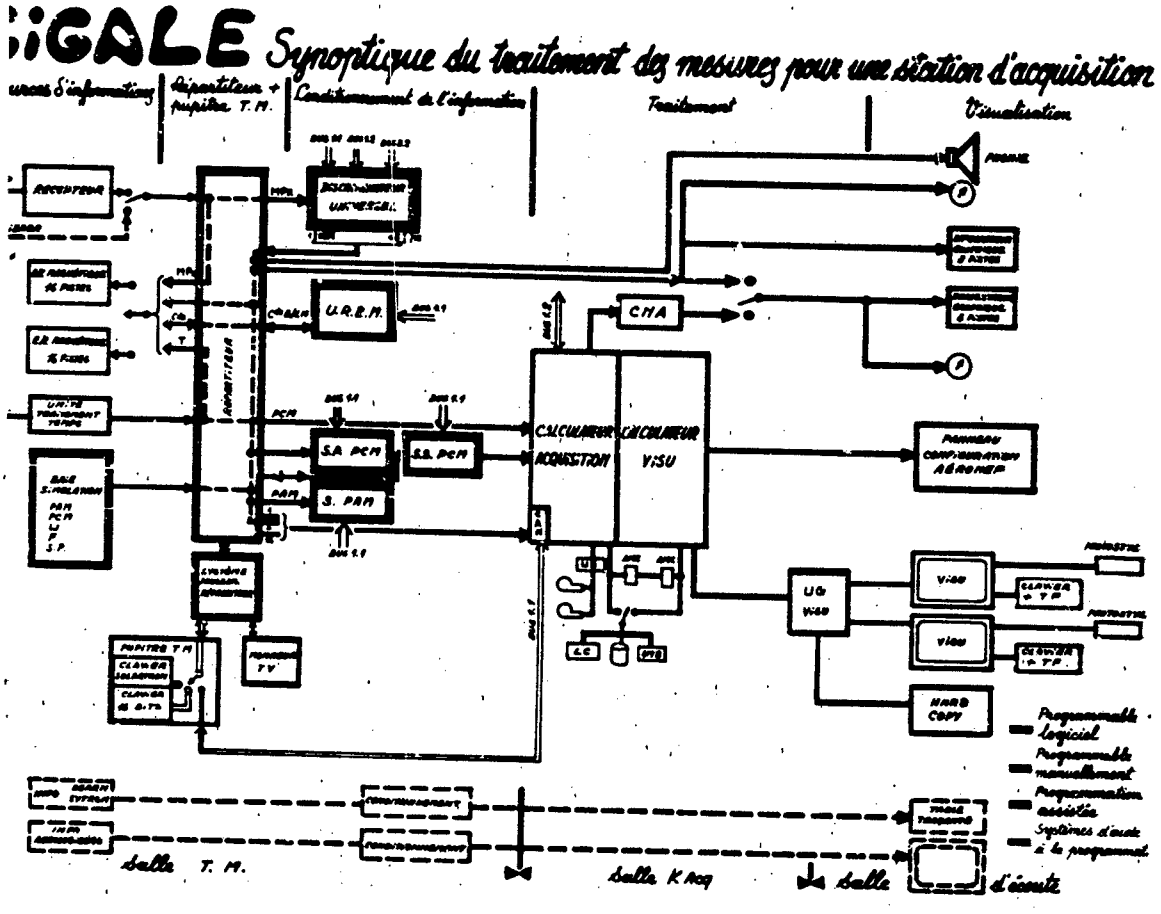

Figure 4

anisation

Dans sa fonction "connecteur", le répartiteur programmable est constitué d'une matrice à relais x 72) divisée en 9 zônes de 16 sous-zônes, chaque sous-zône comportant 36 connexions.

Les relais (environ 1000 dans la version actuelle) sont commandés par une logique de décodage dont ordres sont constitués de mots de 16 bits provenant :

soit du calculateur d'acquisition associé à chacune des 2 "filières" de traitement,

soit d'un système de programmation et de visualisation géré par un calculateur inclus dans le répartiteur.

Ces dispositifs caractérisent les deux modes de conditionnement d'une filière de traitement qui, on seulement réalisent les connexions, mais assurent également la mise en configuration des matériels rogrammables : discriminateurs, synchronisateurs PAM ou PCM, moyens de simulation.

ode automatique

C'est en principe le mode normal qui permet les mises en configuration rapides. Au moyen d'un logiiel spécifique, l'opération comporte en fait deux étapes :

la mise en configuration proprement dite commandée par le calculateur d'acquisition,

la vérification de la configuration affichée.

ode manuel assisté

A l'aide du système de programmation et de visualisation.

L'opérateur de la Salle de conditionnement des informations a la possibilité de commander le déroulement d'un programme pilotant le système qui fournit, à chaque étape, une visualisation sur l'écran ssociée à son pupitre. La mise en configuration du répartiteur peut être réalisée en mode conversationel en sélectionnant, à l'aide d'un clavier à 16 touches banalisées, l'une des 9 zônes de la matrice du épartiteur puis une des 16 sous-zônes de la zône retenue et enfin l'exécution ou la suppression des conexions possibles dans cette sous-zône.

L'opérateur a également la possibilité de sélectionner trois autres fonctions :

la visualisation sur écran de 16 paramètres issus de message télémesure en binaire, en décimal ou en octal, sans introduction d'étalonnage,

la visu dite "RESUMEE" qui donne sur l'écran une présentation explicite de la liste des connexions établies,

la programmation des discriminateurs universels.

Les opérations à effectuer apparaissent en séquence dans la zône commentaire de la visualisation ur l'écran du pupitre opérateur.

Ce "mode manuel assisté" permet d'effectuer, soit une mise en configuration sans le recours au alculateur d'acquisition, soit une modification temporaire de l'état affiché en "mode automatique". Au ode manuel assisté s'ajoute, le cas échéant, un mode purement manuel ; la programmation des équipements tant faite, soit par les touches de commande sur faces avant de chaque équipement, soit par l'envoi des ots de 16 bits de commandes sur les baies de programmation par l'intermédiaire d'un clavier spécifique e 16 touches au pupitre opérateur.

,3,2,2 - Les moyens informatiques

La figure 4 donne un synoptique de la chaîne d'acquisition et de visualisation associée à une alle de conduite d'essais. On observe que cet ensemble est constitué de deux mini-ordinateurs de 16 bits, ype MITRA, interconnectés par une liaison canal type AMC.

Le premier calculateur (initialement MITRA 15/35 puis MITRA 125, modèle plus puissant) exécute 'acquisition des informations télémesurées (ou enregistrées), la mise en grandeur physique de tous les aramètres, le calcul de paramètres élaborés à partir de paramètres exprimés en grandeur physique (X, VC, , centrage, masse, etc....), le stockage de tous ces paramètres sur bande magnétique, la fabrication 'une table de résultats destinés au calculateur de gestion de visualisation, l'édition d'un listage it "Historique de vol".

Le deuxième calculateur (MITRA 15/35 - 32 kmots) reçoit la table de résultats émise par le calculateur d'acquisition, envoie sur écran les paramètres faisant l'objet d'une surveillance relative à des aleurs de consigne et pilote, à travers une unité de gestion spécialisée, les 2 consoles polychromes.

,3,2,3 - Salles de conduite d'essais

La configuration des deux salles de conduite d'essais S.E./1 et S.E./2 est identique. Elle a subi, près une première phase au cours de laquelle les postes de travail principaux étaient séparés, un reroupement au niveau d'un pupitre principal (figure 5).

L'équipement des Salles de Conduite d'Essais comprend :

deux consoles polychromes graphiques,

une console monochrome alphanumérique donnant la liste et la valeur des paramètres qui sortent du domaine de surveillance prédéterminé, cette surveillance s'exerçant sur 48 paramètres,

des indicateurs à lecture directe dont l'information provient, soit directement de la sortie des discriminateurs de télémesure, soit du calculateur d'acquisition par l'intermédiaire de convertisseurs numériques analogiques.

SALLE DE CONDUITE D'ESSAIS

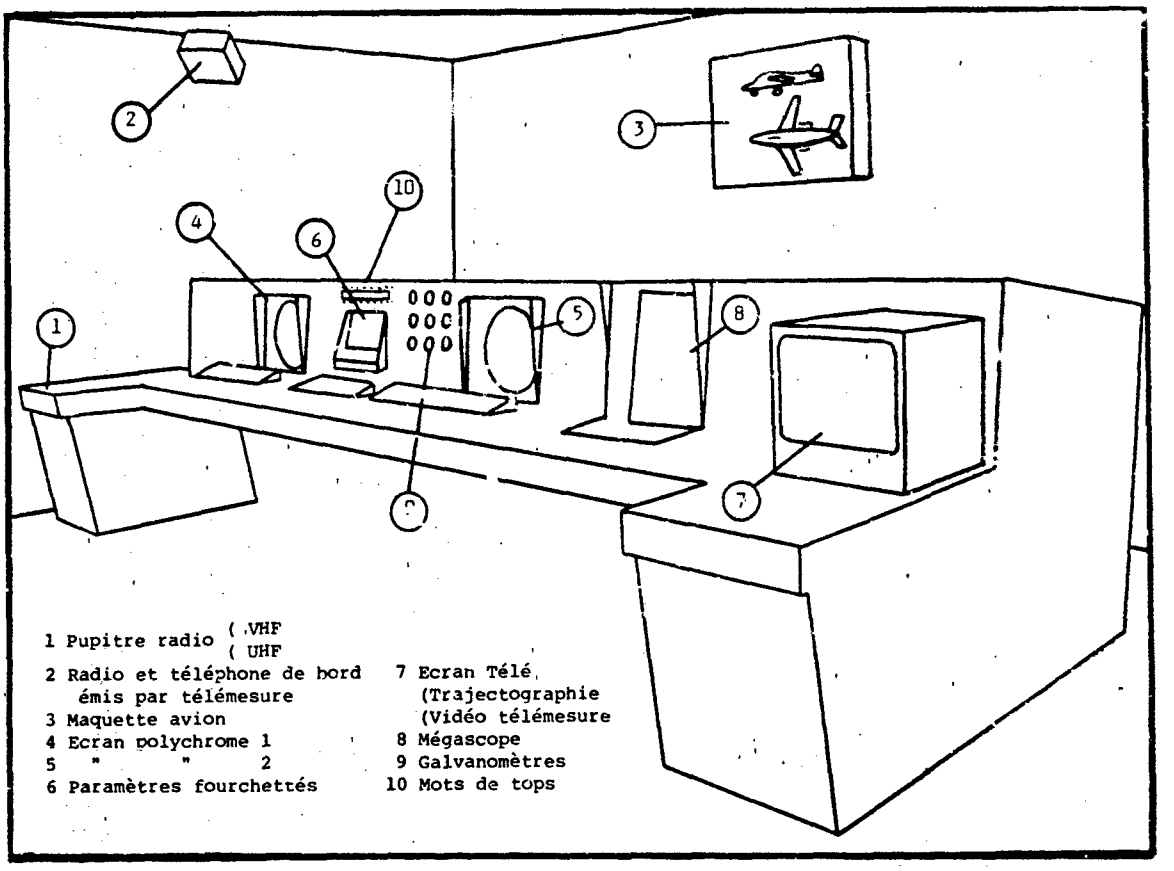

Figure 5

ORGANISATION DU DECOUPAGE DE L'ECRAN
POUR LA PRESENTATION D'UNE "PLANCHE" DE VISUALISATION

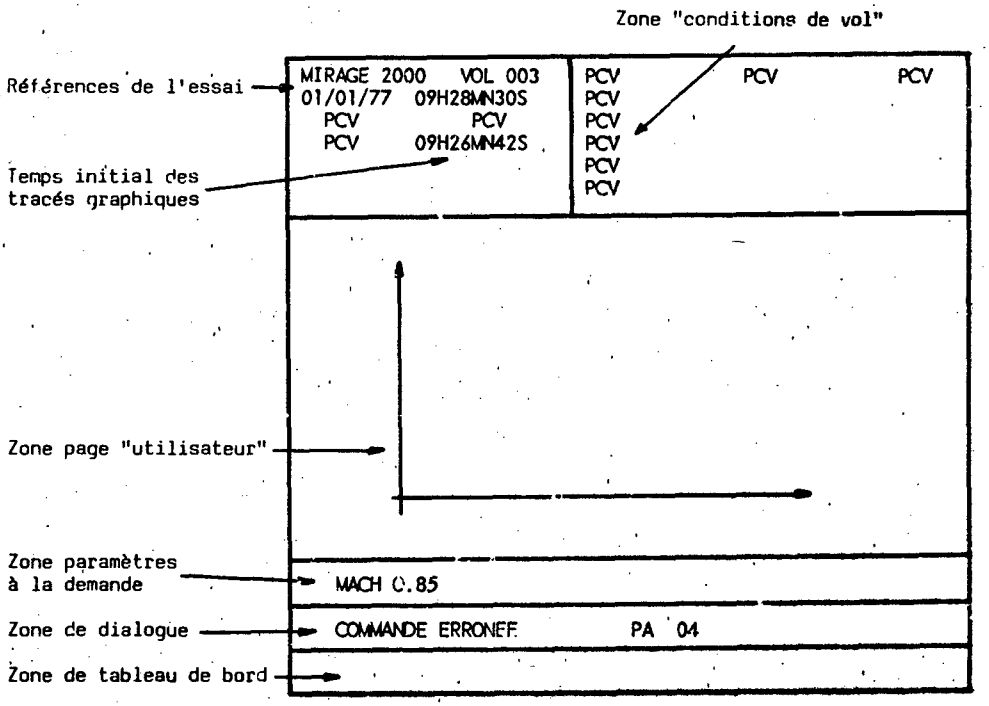

Figure 6

Toutes les figurations sont présentées de manière identique à ce qui est donné sur la figure 6.

Dans la partie supérieure, un "cartouche d'identification" qui donne les renseignements relatifs à l'essai, au numéro de vol et aux conditions de vol du moment. La partie médiane est réservée au graphe significatif de la phase d'essai. La partie inférieure peut être utilisée sur appel sélectif pour la figuration alphanumérique de six paramètres.

Avant un essai, l'ingénieur responsable sélectionne, dans une bibliothèque comprenant plus de 100 types de graphes, appelés "pages", celles qui pourront lui être utiles pendant les vols qu'il conduira et auxquelles les personnels à poste pourront faire appel à leur convenance, pour la visualisation, sur l'une ou l'autre des consoles graphiques.

Trois exemples sont donnés ci-après. Cette présentation ne peut prétendre à un caractère exhaustif mais vise simplement à concrétiser quelques unes des manières selon lesquelles des informations de conduite ou de surveillance des essais en temps réel peuvent être présentées.

Pige grilles

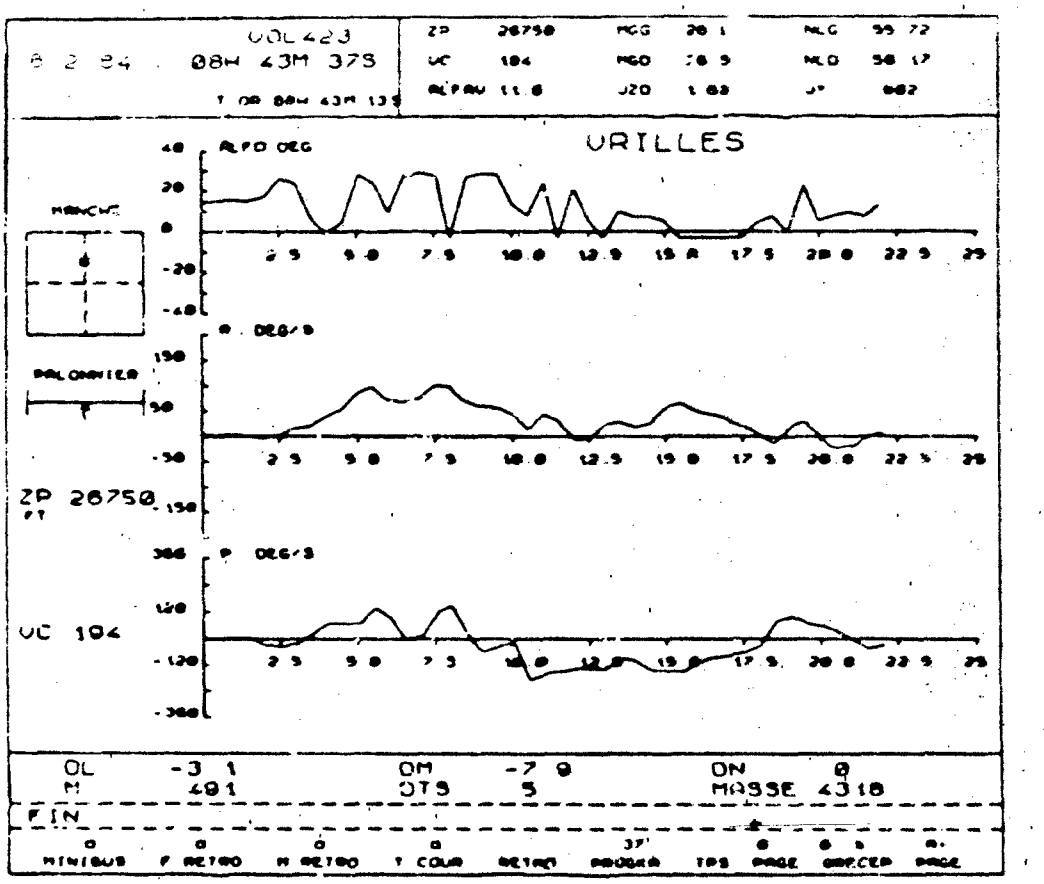

Figure 7

La partie du graphe spécifique comprend deux zones distinctes :

- à gauche

[illegible] simple et facile à appréhender des positions des commandes, où doivent deux informations [illegible] et la [illegible]

de l'engagement.

Cette présentation concentre dans le champ d'observation du conducteur d'essais, les paramètres qui permettent les opérations suivantes :

- validation de la procédure d'engagement prévue par observation de la partie gauche,
- contrôle par le suivi des paramètres f (t) partie droite qu'il s'agit bien d'une vrille et non d'un autotonneau,
- contrôle de la nature de la vrille (ventre ou dos),
- contrôle de l'application des consignes de sortie (partie gauche),
- contrôle de la sortie de vrille,
- surveillance de l'altitude qui passe en rouge dans la zône d'alerte puis en clignotement lorsque l'ordre d'évacuation doit être donné.

N.B.: Le comportement du moteur est généralement suivi sur l'autre console disposant d'une "page" spécifique moteur (s).

Page "Marges de manoeuvre"

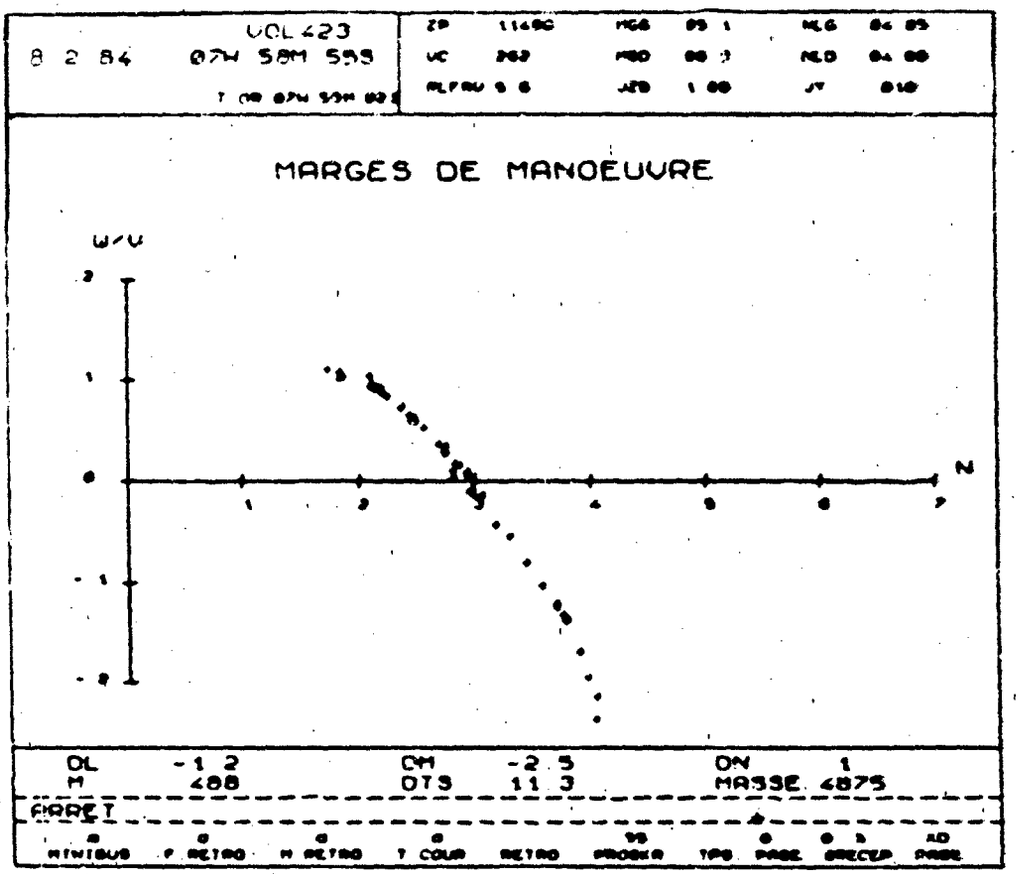

Figure 8

Cette planche permet la visualisation de l'évolution de ce que l'on appelle habituellement "l'accélération totale" ou "pente totale"

$$\frac{W}{W} = Jx \cos\alpha - Jz \sin\alpha$$

Le point de marge correspondant à une "accélération totale" nulle, on obtient la valeur de la marge à l'intersection du trace avec l'axe des abscisses.

Le facteur de charge ainsi déterminé doit être accompagné des conditions de vol à cet instant. On dispose pour cela du cartouche supérieur gauche qui visualise les valeurs de paramètres prédéterminés et du cartouche situé au dessous du tracé, à l'interieur duquel on peut faire apparaitre jusqu'à six parametres au choix du conducteur d'essai.

Cet ensemble de valeurs (Masse, Centrage, Altitude, Mach, Régime, Is - Iso) permet de reporter le point obtenu dans un abaque existant ou de transcrire facilement le résultat dans des conditions nominales.

Page "Basses vitesses"

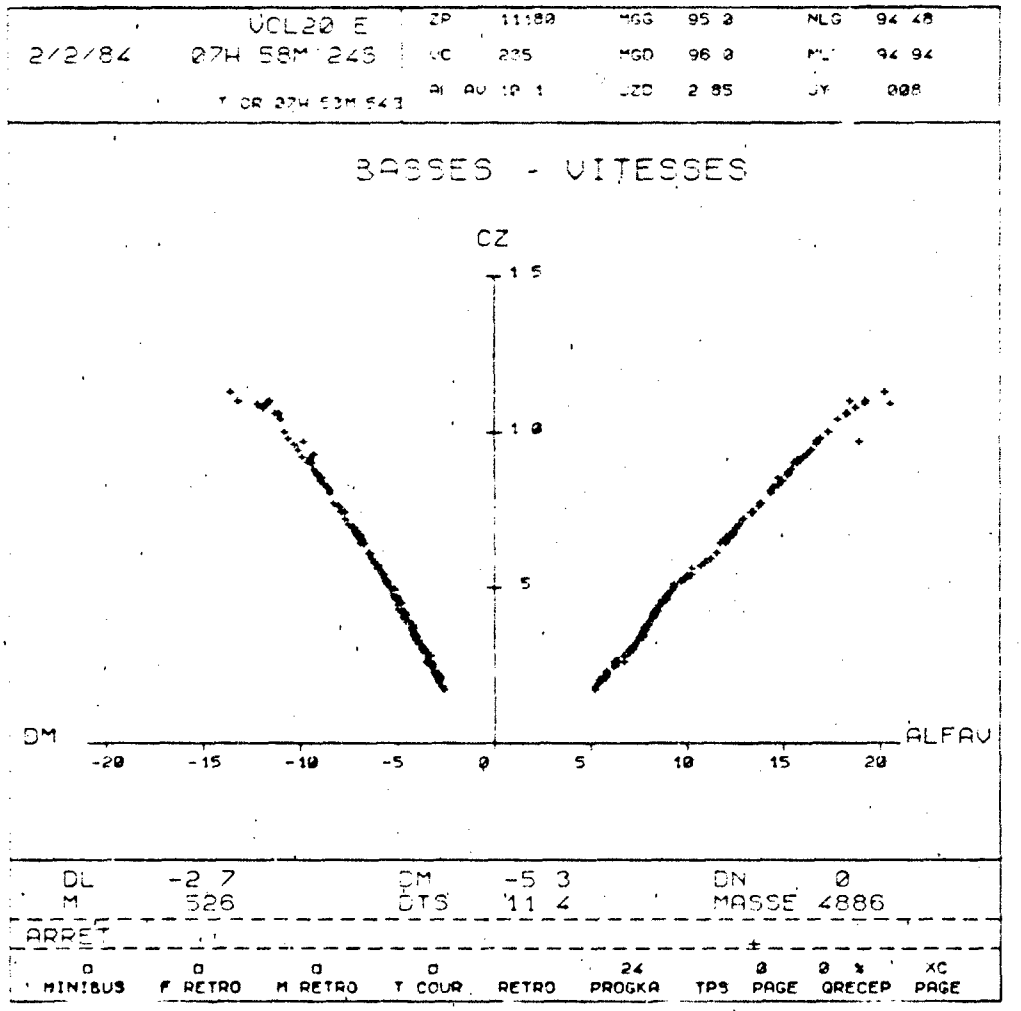

Figure 9

Elle représente l'évolution du coefficient de portance Cz en fonction de l'incidence d'une part et [illegible] de la gouverne de profondeur d'autre part.

[illegible] au cours d'une décélération à n = 1 on peut déterminer la correspondance entre ces valeurs et notamment les valeurs limites obtenues au moment du décrochage.

Il s'agit donc d'une planche de contrôle d'exécution des manoeuvres demandées et de surveillance [illegible] du vol.

MODIFICATIONS APPORTEES AUX SALLES DE CONDUITE D'ESSAIS

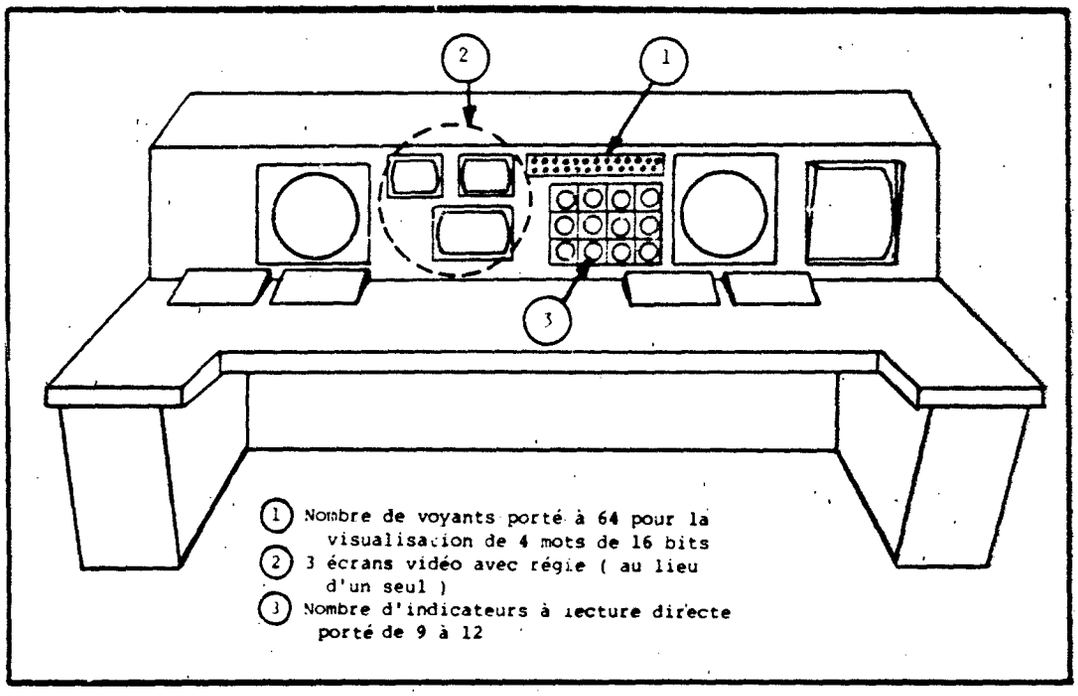

Figure 10

- Le pupitre principal a été doté d'un bandeau de 64 voyants permettant de figurer l'état binaire de 4 mots de 16 bits.
- A l'équipement "vidéo" initial, réservé aux paramètres "fourchettés" a été adjoint une régie TV qui permet de distribuer sur deux écrans monochromes supplémentaires :
  - soit les images provenant ou d'une caméra embarquée dont le message est transmis par un canal télémesure ou d'une caméra d'observation des parkings qui apporte d'utiles renseignements sur l'état de préparation de l'avion avant la mise en route,
  - soit la localisation de l'avion et son altitude à partir des données issues du PC de trajectographie,
  - soit 20 paramètres avion sous forme alphanumérique.
- La capacité du panneau d'indicateurs à lecture directe a été portée de 9 à 12.

L'augmentation du nombre d'indicateurs à lecture directe, associés à la visualisation de 20 paramètres alphanumériques, a été réalisée pour les raisons suivantes :

- donner aux Conducteurs d'essais une information résiduelle, simple mais suffisante au niveau de la sécurité de l'essai, en cas de défaillance en cours de vol des moyens informatiques ou de visualisation élaborée.
- permettre la visualisation de ces paramètres dits "paramètres de sécurité" avec un délai de présentation inférieur à celui qu'introduit la chaîne de traitement gérant la visualisation élaborée.

Pour répondre au besoin, la modification imposait que les paramètres prélevés dans le message télémesure ne transitent pas par les moyens informatiques principaux. La solution retenue a consisté à utiliser les ressources du calculateur intégré dans le répartiteur programmable. On a vu, au paragraphe précédent, que ce calculateur disposait, dès l'origine, d'un logiciel permettant de décommuter des paramètres et de les visualiser sous forme d'indication en alphanumérique, en binaire, décimal ou octal.

Cet ensemble de traitement a été modifié de manière à pouvoir assurer la décommutation de 32 paramètres issus de messages PCM - IRIG ou DANIEL, de les exprimer en unités de grandeurs physiques par un traitement simple ($ax + b$ ou $\frac{a}{x} + b$) et de les transmettre en salle de conduite d'essais (20 en alphanumérique + 12 analogiques). L'extension a conduit à modifier l'équipement informatique du répartiteur en associant au calculateur une unité de disquette qui permet de regrouper, pour un même avion, les fichiers de connexion, les fichiers de décommutation et d'étalonnages des 32 paramètres de "sécurité".

configuration sont assurées sur le répartiteur en mode manuel assisté. Elles sont ensuite transférées sur le calculateur d'acquisition de manière à ce que les mises en configuration répétitives soient faites en mode automatique. Cette tâche s'ajoutait à celles qui doivent être faites, avant chaque vol, au niveau des calculateurs d'acquisition et de visualisation et parmi lesquelles la constitution du fichier représentatif des pages de visualisation représente l'opération la plus lourde. Le transfert des opérations de mise en configuration sur une disquette associée au calculateur du répartiteur, permet de réaliser les tâches en parallèle et de réduire le délai d'enchaînement des vols relatifs à des avions différents qui est passé de 20 - 30 minutes à 10 minutes.

2,3,4 - Transformation en cours

L'opération la plus importante porte, actuellement, sur la rénovation des moyens informatiques. Elle a été rendue nécessaire par les limitations du système actuel qui se traduisent par l'impossibilité de traiter en temps réel des messages numériques supérieurs à 4000 mots/seconde. Cette limitation devient de plus en plus incompatible avec les besoins des essais de systèmes d'armes qui rendent nécessaire l'emploi de messages à cadence beaucoup plus importante.

Le C.E.V. a donc engagé une procédure qui conduira à remplacer les 2 x 2 MITRA de CIGALE par 2 GOULD-SEL 3287/90. L'un de ces calculateurs a été livré en Novembre 1983 et sa mise en service opérationnel est prévue pour le 3ème trimestre 1984.

Ce changement permettra d'augmenter, dans un rapport significatif, la puissance de traitement et de calcul temps réel.

Il permettra, en outre, de remédier au défaut de l'installation actuelle qui, du fait de sa structure (calculateurs d'acquisition et de visualisation en série) introduit systématiquement un retard de 1 à 2 secondes à la visualisation des paramètres élaborés sur les consoles polychromes. Avec les nouveaux calculateurs, ce retard sera compatible avec les besoins que l'expérience permet de situer à la valeur maximale de 0,5 seconde et la cadence de rafraîchissement des informations graphiques sera de 20 par seconde.

Cette modification sera complétée par deux opérations de moindre importance qui participeront à l'amélioration du système :

- changement de système de gestion de visualisation polychrome (CONCEPT 60) permettant une vitesse de traitement plus grande et des traitements plus souples et plus spécifiques,
- couplage, à chaque SEL 3287, d'une imprimante électrostatique pour le tracé de paramètres pendant les vols.

---

by

Jean Costard
Chef du Département Moyens de Mesure et Essais
Avions Marcel Dassault - Breguet Aviation
B.P. 28
13801 Istres Cedex, France

I - ACTIVITES DES ESSAIS EN VOL AMD-BA

1 - LES AVIONS EN DEVELOPPEMENT

Nous avons actuellement 13 familles différentes d'avions sur lesquels nous poursuivons des essais de développement.

MIRAGE III Monoplace et biplace
Avec des développements système d'armes (MIRAGE 5).

MIRAGE III NG — Le MIRAGE III à commandes de vol électriques et avec système d'armes évolué.

MIRAGE IV — Bombardier nucléaire avec une rénovation du système d'armes pour emporter le missile ASMP.

SUPER-ETENDARD — Modernisation de la structure (hypersustentation) du moteur et du système d'armes de l'avion ETENDARD embarqué de la marine.

MIRAGE F1 Monoplace et biplace
Avec de nombreuses versions export et la version reconnaissance F1 CR.

JAGUAR — Développement des configurations de charges externes.

ALPHA-JET — Avec des versions nouvelles, attaque à système d'armes digital et nouveaux moteurs.

MIRAGE 2000 Monoplace et biplace
Notre avion de pointe actuel dans diverses versions.

ATLANTIQUE ATL 2 — Rénovation du système d'armes des ATLANTIQUE MK 1.

FALCON 10 et 100
FALCON 20 et 200 — Qui a donné les versions GUARDIAN (USA) et GARDIAN (France).

FALCON 50
FALCON 900

En plus des avions en production, nous avons toujours un avion prototype.
Dans le passé récent, c'était le MIRAGE 4000 et nous préparons l'ACX qui accroîtra nos connaissances pour l'étude et le développement de nouvelles technologies.

2 - LES ESSAIS DE RESPONSABILITE AMD-BA

Pour ces avions, les moyens mis en oeuvre nous ont permis d'assumer de larges responsabilités dans les différentes mises au point.

. Mises au point cellule

- Domaines de vol de l'avion lisse et avec les différentes charges externes à l'intérieur desquels on contrôle :
  . les vibrations (flutter)
  . les efforts
  . les qualités de vol avec les limitations en incidence.
- Performances
- Adaptation moteur
- Commandes de vol
- Circuits
- Des essais spéciaux du type hautes incidences, vrilles, adaptation moteur, entrées d'air, systèmes d'arrêt (freins, crosse, parachute, barrière d'arrêt).
- Certifications d'avions civils.

Ce sont ces mises au point qui constituent actuellement le principal de nos activités.

. Essais d'intégration des contre-mesures.

. Essais d'armement

. Séparation d'armement ou de bidons.
. Tirs réels avec des bombes étalonnées pour contrôle de la précision.
. Tirs canons.

La mise au point de l'armement lui-même n'est pas de notre responsabilité, mais nous avons à effectuer les essais d'adaptation à l'avion.

Notre responsabilité du système d'armes s'étend aux essais d'armement.

. Essais de Reconnaissance

3 - AVIONS EN ESSAIS

Les travaux des Essais en Vol sur un avion s'échelonnent au minimum sur une période de trois ans :

. La définition des programmes et des mesures nécessaires.
. La réalisation des liasses électriques et approvisionnement des matériels.
. Montage de l'avion et de son installation.

. Puis les essais en vol.
Sur cette période, nous travaillons sur 80 à 90 avions différents et nous avons en ligne de vol simultanément 40 à 50 avions.

Actuellement on peut citer :

	PERIODE 1983/1986	VOLS MARS/84
. MIRAGE III - versions 5 et NG.	5	3
. MIRAGE IV P	2	2
. SUPER ETENDARD	3	1
. MIRAGE F1	17	8
. JAGUAR	5	2
. ALPHA-JET	7	3
. MIRAGE 2000	25	14
. ATLANTIQUE ATL 2	2	2
. Avions civils.	14	8
. ACX	1	

4 - BASES D'ESSAIS

Nous avons 3 bases d'essais.

ISTRES qui est la base principale pour les essais en vol,

. Mise au point cellule
. Emports de charges extérieures
. Certifications.
. Essais des systèmes d'armes en vol
. Essais de compatibilités radio-électriques (EMC-EMI) en chambre anéchoïde et en vol.

BRETIGNY : Centre principal pour les essais de systèmes d'armes. Essais au sol sur des bancs stimulables et quelques essais en vol système d'armes ou reconnaissance.

CAZAUX Essais d'armement.

On y élabore les prévisions qui serviront aux contrôles rapides sur les bases d'essais.
On peut effectuer des exploitations fines avec des ordinateurs puissants et faire la comparaison avec les prévisions de calculs et essais en soufflerie.
Une itération permettra l'élaboration de nouvelles bases de calcul.

5 - EFFECTIF HUMAINS

Le total des effectifs des 3 bases d'essais est de 1259 personnes.

. dont 226 ingénieurs
. 15 pilotes Essais et Réception dont 11 plus particulièrement Essais.

Mon service, chargé de la définition et mise en oeuvre des mesures embarquées, de la définition et installations des moyens d'exploitation au sol, est de 110 personnes.

. 8 Informaticiens ont créé tous les logiciels et en assurent l'évolution.

6 - ORGANISATION, MOYENS DEVELOPPES

Nous pensons que ces quelques chiffres démontrent déjà que nous avons obtenu une bonne efficacité dans nos essais. Elle a été rendue possible par l'organisation de notre travail, les moyens mis en oeuvre, et une certaine discipline dans le choix des matériels qui évite des mises au point répétées et permet de concentrer nos moyens humains sur des évolutions payantes.

Notre organisation est basée sur le travail en petites équipes avec des moyens légers permettant de les répartir à l'endroit géographique le mieux adapté. Parallèlement nous avons mis en place des liaisons rapides entre nos centres d'essais et le bureau d'études à ST. CLOUD. Nos ensembles informatiques sont compatibles.

Ces moyens développés sont basés sur :

. Acquisition et traitement de la télémesure en temps réel (ISTRES/CAZAUX)

. Bancs de systèmes d'armes stimulables par ordinateur (BRETIGNY).

. Essais de compatibilité radio-électriques (BRETIGNY-ISTRES).

II - ACQUISITION ET TRAITEMENT DE LA TELEMESURE EN TEMPS REEL

1 - AVANTAGES DU TEMPS REEL

Les essais en vol sont la dernière étape de la validation et certification d'un nouveau système avion. Il faut des centaines et fréquemment des milliers d'heures de vol pour qualifier complètement un avion de transport ou un avion de combat avec son grand nombre de configurations de charges extérieures.
A titre indicatif, nous avons ouvert sur le MIRAGE F1 environ 1450 configurations différentes et sur MIRAGE 2000 plus de 500 sont déjà programmées.

Le nombre de paramètres enregistrés peut varier de 100 pour des programmes d'essais simples, à plus de 1.000 (cas du MIRAGE 2000).
Pour traiter ce gros montant de données, la condition nécessaire du succès est un système d'acquisition et d'analyse temps réel efficace.

Dès le début des enregistrements magnétiques notre philosophie d'essais a été principalement orientée sur la télémesure.

Notre expérience significative en la matière date de 1969. Deux accidents nous ont montré à cette époque :

. la nécessité d'une surveillance en temps réel,
. qu'il fallait développer des moyens qui n'existaient pas dans le monde, en particulier du point de vue flutter,
. qu'il ne fallait pas négliger les vols d'essais dits de "routine".

LES MULTIPLES AVANTAGES DU TRAITEMENT TEMPS REELS SONT LES SUIVANTS :

1.1 - Sécurité du vol

En dehors d'incidents, dont on ne peut savoir s'ils auraient pu devenir plus critiques sans cette surveillance, nos efforts dans ce domaine et l'investissement ont été largement remboursés le jour où nous avons assisté un pilote qui avait eu un malaise en vol sur MIRAGE 2000.

Dans une ambiance plus sereine, l'équipe au sol peut conseiller efficacement le pilote dans les différentes manipulations à effectuer, en particulier pour les essais de système d'armes. On peut vérifier si la qualité de l'essai est bonne pour l'exploitation ultérieure et éventuellement le reprendre.

1.3 - Diminution des temps d'exploitation

Les résultats acquis en temps réel peuvent même permettre d'effectuer plus d'essais dans un vol. C'est en particulier le cas pour les essais hautes incidences et vrilles.

1.4 - Contrôle permanent de l'avion et de son installation de mesure pendant le vol.

A la fin du vol, le personnel de piste doit pouvoir intervenir avec le minimum de recherches sur les équipements en panne.

Le contrôle de toute l'installation de mesure, après le vol, demanderait un délai prohibitif.

1.5 - Intégration complète de l'équipe d'essais et des équipementiers au suivi du vol.

La disponibilité de résultats d'exploitation clairs rend plus efficace le débriefing avec le pilote à la fin du vol.

1.6 - Ces différents points permettent de diminuer le nombre de vols et d'augmenter la cadence

2 - DESCRIPTION DU SYSTEME D'ISTRES

Les signaux télémesurés sont reçus par le centre de réception SIERRA, mis en oeuvre par le CEV. Les antennes à grand gain et très directionnelles sont asservies à l'avion. Leur réception en bande E (2300 Mhz) est transposée en bande A (230 Mhz). Le combineur de diversité permet de sélectionner la meilleure réception et la transmission s'effectue par câble à notre salle de télémesure. Ce signal multiplex est directement enregistré sur bande magnétique à titre de sauvegarde et permettant un play-back en cas d'anomalie dans le traitement temps réel.

Pour le traitement en ligne, un ensemble de discriminateurs permet de séparer les différentes voies du multiplex avant de les transmettre à l'ordinateur et à la salle d'écoute.

. Avant d'entrer dans l'ordinateur, les signaux analogiques sont numérisés et les voies commutées PCM ou PAM sont traitées par des synchronisateurs. Les entrées/sorties de l'ordinateur sont implantées très près de la source des informations pour éviter des dégradations en ligne.

. Les informations continues et les informations analogiques obtenues, après décommutation des voies commutées, sont transmises à la salle d'écoute.

La salle de télémesure peut recevoir les informations de trois vols simultanés et tout le système, y compris l'ordinateur et la salle d'écoute, peut être reprogrammé en cinq minutes pour un autre avion.

Trois GOULD SEL 32/7780 sont disponibles dans la salle ordinateurs pour l'acquisition avec chacun 1 Méga octets de mémoire centrale.

Un des ordinateurs est équipé d'un ARRAY-PROCESSEUR AP 120 B pour effectuer les traitements de vibration avec analyse modale pour la surveillance du flutter.

On peut donc effectuer trois vols simultanés temps réel ou deux vols, si l'un d'eux comprend des essais de domaine, qui mobilisent deux ordinateurs.

Les données de vol sont converties en grandeur physique en utilisant un fichier d'étalonnage stocké sur disque.

D'autres calculs temps réel sont effectués systématiquement, permettant d'introduire les corrections anémométriques dans les calculs d'altitude, vitesse, Mach, d'étalonnage débit mètres dans le calcul du débit, de calculer la masse, le centrage, des coefficients aérodynamiques simples, l'incidence vrai etc...

Toutes ces informations sont stockées pendant tout le vol sur des bandes magnétiques à haute densité.

Notre capacité d'acquisition a toujours été le résultat d'un compromis entre le nombre d'informations nécessaires et les possibilités de traitement et visualisation temps réel.

Parmi ces sorties de résultats :

. Un listage de 90 informations élaborées toutes les quatre secondes est effectué en salle ordinateur pour être disponible au débriefing après le vol.

. Trois sorties analogiques sont transmises à la salle d'écoute, ainsi qu'un mot de 16 bits permettant de signaler des dépassements de limites avec la visualisation automatique des valeurs des paramètres pendant ce dépassement.

. La conduite des traitements optionnels et des sorties de résultats s'effectue directement de la salle d'écoute.

. L'équipe d'essais peut avoir accès à toutes les valeurs calculées sur des écrans sous plusieurs formes :

- Listages types d'ensembles de données préparés à l'avance
- Tracés - fonction du temps ou sous forme X, Y
- Listages de paramètres à la demande
- Présentation de l'attitude de l'avion, position des gouvernes, altitude vitesse dans le cas d'essais à haute incidence.

Le contenu présenté sur les écrans peut être copié sur traceur électrostatique. Compte-tenu de toutes ces informations, la capacité temps réel est de 8000 données par seconde .

En salle d'écoute, l'équipe d'essais a également accès à toutes les données brutes avant traitement sous forme de galvanomètres, mots tops, mégascope pour les vibrations, scopes avec présentation du type bar-graphes, écran vidéo.

Entre deux salles d'écoute. une salle permet la surveillance du flutter avec un analyseur temps réel donnant 2 spectres et la possibilité de traiter sur le troisième ordinateur toutes les vibrations transmises avec la présentation dès la fin d'un essai de tous les spectres et un peu plus tard d'analyses plus complètes permettant de tracer pendant le vol l'évolution des fréquences et amortissements.

Exploitation en temps différé

L'exploitation n'est pas limité au traitement temps réel.

Des tracés et des exploitations plus complètes sont effectués après les vols et de nuit. Un quatrième ordinateur permet également ce type d'exploitation, avec des mélanges de bandes. Il est utilisé aussi par nos informaticiens pour faire évoluer nos logiciels.Les logiciels acquis sont une accumulation de travail depuis 1977.

Les résultats stockés sur bande peuvent être copiés et envoyés au centre de SAINT-CLOUD pour la comparaison des résultats avec des modèles mathématiques complexes qui nécessitent une installation plus importante.

Une fois les données mises en forme pour ces exploitations, elles sont également accessibles par les ingénieurs d'ISTRES par l'intermédiaire d'un terminal lourd relié par ligne téléphonique avec l'ordinateur de SAINT-CLOUD.

3 - CAZAUX

Nous avons à CAZAUX un système temps réel de caractéristiques identiques à un des ensembles d'ISTRES.

III - ESSAIS DE SYSTEMES D'ARMES

1 - PRINCIPE ET MOYENS

Notre expérience dans ce domaine date de 10 ans.

L'arrivée de calculateurs numériques embarqués a permis de faire évoluer les systèmes d'armes par l'intégration de différents équipements dialogant par bus numérique.

L'augmentation de la complexité et les difficultés, que l'on pourrait avoir dans les recherches de responsabilité entre les équipementiers et le maître d'oeuvre de l'intégration, nous ont conduit à concevoir une nouvelle méthode d'essais.

Cette méthode a permis de rendre les essais au banc significatifs diminuant de façon importante les vols d'essais sur avion d'arme.

Les moyens de développement d'un système d'armes comprennent :

. La simulation avec des modèles mathématiques et des simulateurs permettant de contrôler la pilotabilité du système et définir le choix des figurations.
. Des bancs de test de génération électrique
. Des avions de servitudes spécialisés.
. Des bancs d'intégration avec éventuellement une plate-forme radar ou missile.
. Un avion de servitude intégration du S.N.A.
. Une maquette radio électrique avec cage de Faraday associée.
. Une chambre anéchoïde
. Les avions d'essais prototypes ou tête de série.

Comme pour les essais avions, les moyens ont été répartis dans les différents centres :

SAINT CLOUD : Etudes, simulations

BRETIGNY : Bancs d'intégration, avions de servitude CEV, cage de Faraday, maquette radio-électrique, avion d'intégration.

ISTRES : Centre de simulation au CEV.
Petite simulation pour les figurations aux essais en vol AMD-BA.
Les essais en vol.
Les essais en chambre anéchoïde.

CAZAUX : Tirs de qualification.

Un système de Navigation et d'Attaque est composé :

. D'un ensemble de capteurs comprenant par exemple centrale gyroscopique, plate-forme inertielle, centrale aérodynamique, doppler, radar air-air et air-sol, télémètre, ECM.
. D'organes de calcul pour la navigation, l'attaque, les contre-mesures.
. Au poste pilote, le pilote dispose d'organes de commande et de dialogues (panneau de contrôle de navigation, panneau de contrôle et sélection d'armements) et de visualisations sous forme de viseur tête haute, écrans cathodiques, Map display, ECM, instruments de pilotage.
. Les armements.
. Tous ces ensembles dialoguent entre eux.
. Ces équipements sont montés préalablement aux vols, sur un banc d'intégration de manière à optimiser les performances de l'ensemble.

On peut travailler de deux manières :

. Statiquement
. Dynamiquement (stimulation)

C'est cette dernière méthode qui a été développée par AMD-BA.

Les essais statiques permettent :

. d'adapter et contrôler les performances des interfaces des systèmes,
. de contrôler la sensibilité à la génération électrique,
. contrôler les performances des équipements,
. vérifier la sensibilité des sorties des paramètres vers les visualisations pilote,
. contrôler les logiques de pannes,
. débugger les software.

Mais ils sont limités :

. Seulement quelques problèmes d'interfaçage peuvent être appréhendés.

. Les fonctionnements dynamiques ne pouvaient être vus que plus tard en vol. Il s'agit de problèmes de filtrage, d'extrapolations de lois, de bruit, de précision dynamique.

D'autres problèmes étaient rencontrés en vol

. Les anomalies rencontrées en vol étaient difficilement analysables.
Elles auraient demandé l'enregistrement d'un trop grand nombre de paramètres pour avoir le paramètre clé.

. L'interprétation de certains phénomènes peut être difficile pour le pilote en vol.

. Il est très difficile de reproduire la même configuration d'essais et chaque modification redemanderait le même essais dans un nouveau vol.

La stimulation :

La stimulation permet de rejouer une phase de vol en réinjectant dans le système des informations capteurs cohérentes préalablement enregistrées en vol. On entre dans le système des paramètres pris assez loin en amont de façon à en limiter le nombre et la fréquence d'échantillonnage.

L'ordinateur de stimulation est un GOULD SEL 32/77-80 homogène avec les ordinateurs d'acquisition temps réel.

A partir des données enregistrées sur bandes, il effectue interpolations et le cadencement nécessaire pour reconstituer à travers la baie de stimulation les informations capteurs avec les mêmes caractéristiques qu'en vol.

Sur ces phases stimulées on a donc les mêmes visualisations qu'en vol et on peut changer les fonctions.

Le banc est instrumenté et l'ordinateur, pendant la phase de stimulation, fait l'acquisition sur disque des données. Elles seront ensuite traitées et tracées.

La stimulation peut-être effectuée au début de définition par des bandes types ou des simulations provenant des simulateurs ou calculateur d'étude ; ensuite par des bandes provenant d'un autre avion ayant enregistré des capteurs équivalents et enfin par l'avion d'essai.

Ce moyen permet d'avoir un outil très puissant pour mettre au point les systèmes indépendemment de l'avion et réduit ainsi le nombre de vols.

La compréhension des problèmes rencontrés en vol est simplifiée.
Il est possible de rejouer la phase de vol intéressée avec les équipements du banc et entuellement de l'avion avec une possibilité d'instrumentation plus aisée.

Il est très facile de valider les modifications au banc avec toujours le même essais. particulier, on peut valider les modifications des logiciels des équipements en regardant s conséquences sur le reste du système.
L'évaluation des performances en mode normal et en mode dégradé (radio sonde au lieu de dar ...) peut-être faite aisément au banc avec le même essai d'où, de nouveau, la diminution s vols. On peut également comparer les performances des algorithmes complexes dans les équipe- nts par rapport à un algorithme absolu sur ordinateur.

L'installation de mesure de l'avion d'essais montée au banc dans la phase préliminaire ermet de diminuer les temps de mise au point sur avions (nécessité d'avoir un dialogue réel sur is pour valider les interfaces numériques).

Compte-tenu des résultats obtenus et la facilité apportée aux équipementiers pour leurs ses au point, nous avons pu reporter notre principe plus en amont dans les équipements timulation de la centrale aérodynamique, de la plate-forme inertielle, du radar au niveau de n bus interne).

En dehors des gains de temps et de vols, ce moyen nous a donné la possibilité d'offrir à is clients des systèmes adaptés à leurs besoins.

Nous avons finalement, avec la même structure avion, des modèles qui sont très diffé- nts par leurs armements et leurs logiciels, ce qui explique le nombre d'avions en essais et le mbre de bancs.
Actuellement, nous avons 12 bancs stimulables avec 3 ordinateurs SEL 32/77-80 et MITRA 125.

URES ESSAIS EN VOL

Pour les essais en vol nous appliquons aux essais de système d'armes les mêmes procédures e pour les essais cellule. C'est-à-dire télémesure, procédures temps réel.

On ajoute ainsi aux gains apportés par les bancs ceux apportés par le temps réel, en rticulier la transmission vidéo des informations synthétisées sur la tête haute pilote est très ile pour la conduite de l'essai.
D'autre part, cette volonté d'exploitation temps réel, qui a apporté des contraintes dans s définitions des mesures effectuées, est très payante.
Il a fallu faire évoluer de front les systèmes d'acquisition embarqués et l'exploitation. s points importants apportés sont les suivants :

lange sur un message unique des informations sans rythme propre (paramètres analogiques assiques) et des informations ayant un rythme propre (informations bus).

éation d'un format PCM adapté à ce type d'exploitation (format DANIEL) permettant une quisition plus rapide et une datation fine des informations ce qui est nécessaire pour la imulation.

ogrammation du système d'acquisition embarqué par l'ordinateur d'exploitation qui possède tous s fichiers des informations bus. On évite en plus les erreurs de transmission d'informations i se traduiraient par une nouvelle numérisation.

s cadences d'acquisition temps réels étaient de :
00 mots par seconde en 1975,
00 " " " en 1978,
00 " " " en 1981.

tte contrainte, de cadence relativement faible, oblige les ingénieurs à bien réfléchir sur les soins en sélectionnant les paramètres qui sont nécessaires à la stimulation et leurs cadences.

us avons réussi ainsi de très bonnes mises au point. On évite la tentation de tout enregistrer priori, ce qui se traduirait par des augmentations de moyens et d'énergie sans résultats ngibles.

ur permettre des stimulations plus en amont dans les équipements et armements, nous sommes ligés d'enregistrer maintenant d'autres messages PCM sur magnétique embarqué. Ces exploitations temps différé sont réalisées avec les programmes temps réel pour éviter les travaux de giciels. Ce point pourra évidemment évoluer au fur et à mesure des disponibilités des ogrammeurs.

dehors de ces généralités, on peut citer d'autres points importants qui se traduisent par des minutions de coût et augmentation de l'efficacité.

5 - Rigueur dans les définitions.

Il s'agit d'éviter au maximum les mises au point inutiles.
Nos stations d'exploitation sont réalisées par une seule équipe et toutes identiques.

Une bonne rigueur dans les définitions et choix de matériels embarqués a permis d'entrer les chaines complètes de mesure sur ordinateur qui centralise les modifications. Le dessin des liasses sur ordinateur a divisé par trois nos heures d'étude (22 liasses complètes effectuées en 1982, 17 en 1983 sans compter les avions plus simples à courte période d'essais). Nos temps de mise au point sur avion ont été également diminués dans le même rapport.

6 - Utilisation de systèmes éclatés qui améliorent l'évolutionnabilité et diminuent les poids de câblage. Il permettent également d'associer des ensembles d'acquisition utilisés depuis 15 ans (matériels du MIRAGE G 8 et de l'ALPHA-JET encore montés sur MIRAGE 2000) dont nous avons une bonne expérience à des unités plus récentes suivant les besoins. On limite à chaque fois les risques de mise au point.

- ESSAIS DE COMPATIBILITE RADIO-ELECTRIQUES (EMC-EMI)

Ces essais permettent de vérifier l'aptitude des équipements à fonctionner dans l'environnement électromagnétique et de définir les actions correctives éventuelles (modifications des équipements ou du câblage avion).

Ils sont effectués :

. sur maquette grillagée pour les essais d'implantation d'antennes et les mesures de découplage dans notre usine de Villaroche.

. sur maquette radio-électrique et en cage de Faraday à BRETIGNY.

. sur avion, dans notre chambre anéchoïde d'ISTRES en particulier (notamment pour les hyperfréquences : radar et contre-mesures).

Il est à noter l'importance croissante :

. des essais en cage de Faraday sur équipements individuels (identification de la signature électromagnétique) et sur sous systèmes. En effet, l'évolution technologique (développement du numérique, courants de commande de plus en plus faible ...) conduit à une plus grande sensibilité aux parasites.

. en chambre anéchoïde, notamment pour les contre-mesures avec l'avion complet en ligne de vol. Cette chambre permet de mettre en configuration de vol (avec les circuits avion alimentés) tous nos avions (mis à part L'ATLANTIQUE). Ses dimensions sont :

- 20 m. de large
- 28 m. de profondeur
- 13 m. de haut

Soit un volume de 7280 m2.

- MOYENS INFORMATIQUES DISPONIBLES AUX ESSAIS EN VOL

HISTORIQUE

1969 - ISTRES	2 salles d'écoute temps réel 1600 mots/s	2 IBM 1800 Mémoires 2 x 48 Koct.interne 1,5 Moct. disque
1974 - VILLAROCHE	1 banc stimulable	1 SEL 85 Mém. 128 Koct interne 24 Moct disque
1978 - ISTRES	2 salles d'écoute temps réel 2000 mots/s	2 SEL 32/55 Mémoires 2 x 256 Koct interne 80 Moct disque + IAP 120 B.
- BRETIGNY	4 bancs stimulables	1 SEL 85 Mém. 192 Koct interne 24 Moct disque
		1 SEL 85 224 Koct interne 2 x 24 Moct disque
1979 - ISTRES	2 salles d'écoute temps réel 4000 mots/s	3 SEL 32/75 Mém. 384 Koct interne 3 x 80 Moct disque

BRETIGNY	5 bancs stimulables	2 SEL 85
	Dessins C.A.O à TOULOUSE	
1980 - ISTRES	2 salles temps réel 8000 mots/s	3 SEL 32/75 (+IPU+WCS)+ 1 AP 120B Mém. 512 Koct interne 4 x 80 Moct disque
	Simulation des visualisations pilote Liaison SEL/32 --→ Ordinateurs SAINT-CLOUD	
BRETIGNY	7 bancs stimulables	2 SEL 85 256 Koct interne 4 x 24 Moct disque
BRETIGNY		1 MITRA 125 512 Koct interne 50 Moct disque
1981 - ISTRES	2 salles temps réel	3 SEL 32/75
CAZAUX	1 salle temps réel 8000 mots/s	1 SEL 32/77 +IPU+WCS Mém. 512 Koct interne 2 x 80 Moct disque
BRETIGNY	9 bancs stimulables	1 SEL 32/77 +IPU+WCS 512 Koct interne 80 Moct disque
		2 SEL 85 1 MITRA 125
1983 - ISTRES	3 salles temps réel 8000 mots/s	3 SEL 32/7780 +1 AP 120 B 3 x 1 Moct interne 6 x 80 Moct disque
	Simulations pilote	1 SEL 32/7780
	Liaison SEL 32 --→ SAINT-CLOUD TSO --→ SAINT-CLOUD	
	1 station mobile télémesure 1 station mobile télémesure avec exploitation	1 SEL 32/2750 Mém. 1 Moct interne 2 x 80 Moct disque
CAZAUX	1 salle temps réel	1 SEL 32/7780 1 Moct interne 2 x 80 Moct disque
BRETIGNY	10 bancs stimulables	2 SEL 32/7780 1 Moct interne 2 x 80 Moct disque 2 x 300 Moct disque
		1 SEL 85 1 MITRA 125
CONFIGURATION 1984		
ISTRES	3 salles d'écoute temps réel 8000 mots/s	3 SEL 32/7780 +1AP 120 B Mém. 3 x 1 Moct interne 6 x 80 Moct disque
		1 SEL 32/8780 4 Moct interne 2 x 675 Moct disque x 1 AP 5025
	1 station mobile télémesure 1 station mobile télémesure + exploitation	1 SEL 32/2750 1 Moct interne 2 x 80 Moct disque
	Simulation	1 SEL 32/6780 1 SEL 32/9750
	Liaison SAINT-CLOUD terminal avec 2 consoles TSO	

Dessins C.A.O avec 2 consoles.

CAZAUX	1 salle temps réel	1 SEL 32/7780 1 Moct interne 2 x 80 Moct disque
BRETIGNY	12 bancs stimulables	3 SEL 32/7780 1,5 Moct interne 2 x 80 Moct disque 4 x 300 Moct disque
		1 MITRA 125 512 Koct interne 2 x 50 Moct disque

Dessins C.A.O 2 consoles.

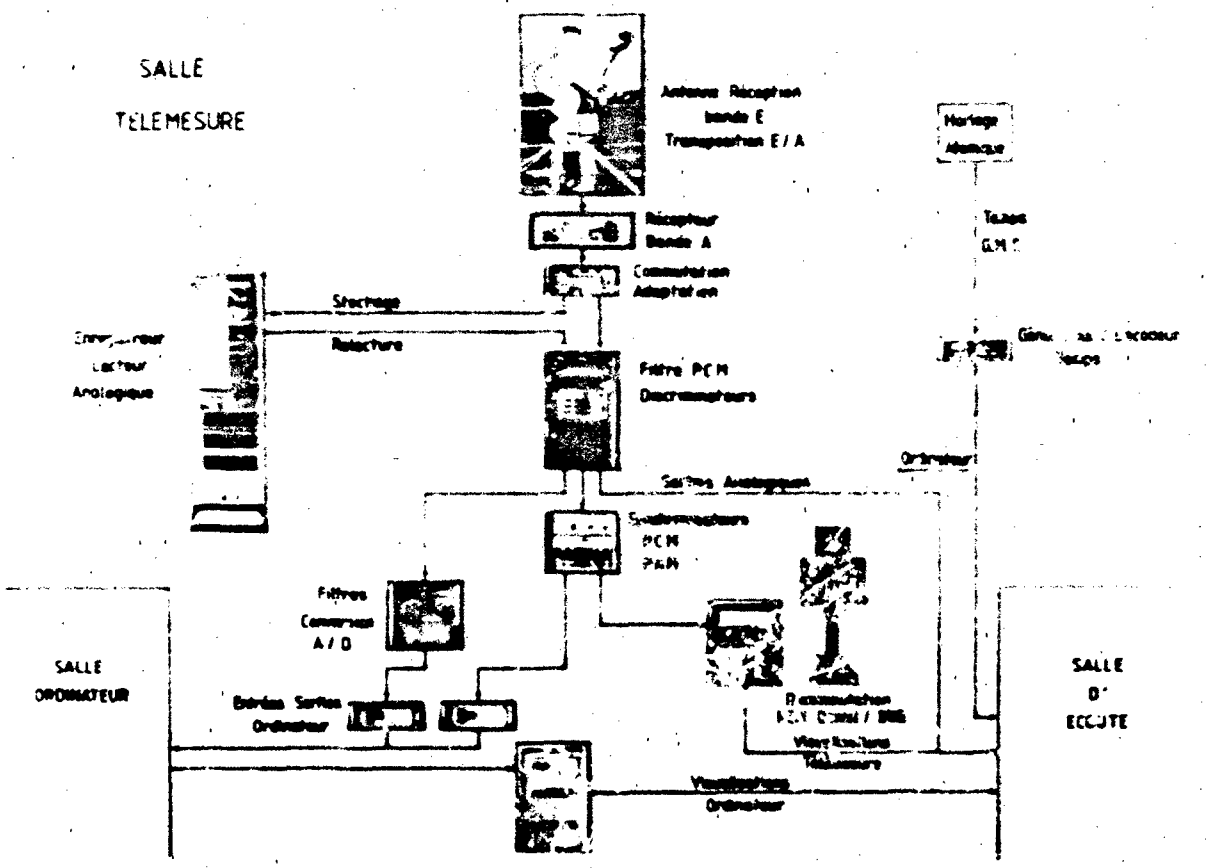

Figure 1

PRINCIPE DE LA STIMULATION

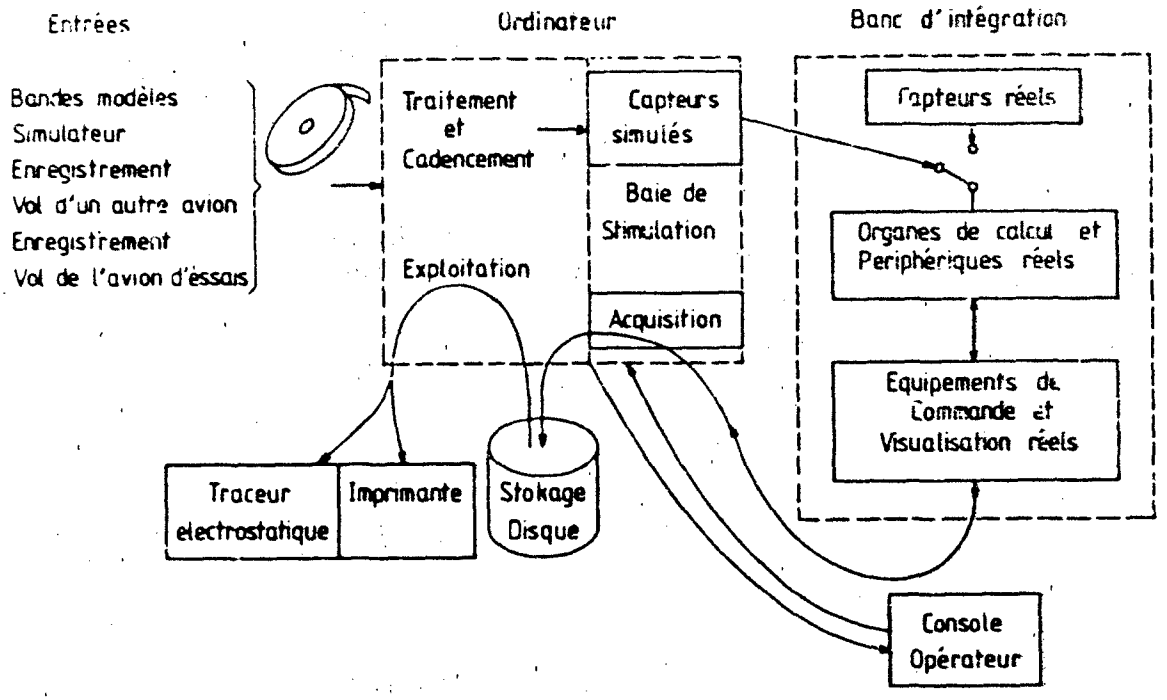

Figure 2

ACQUISITION DES MESURES A BORD

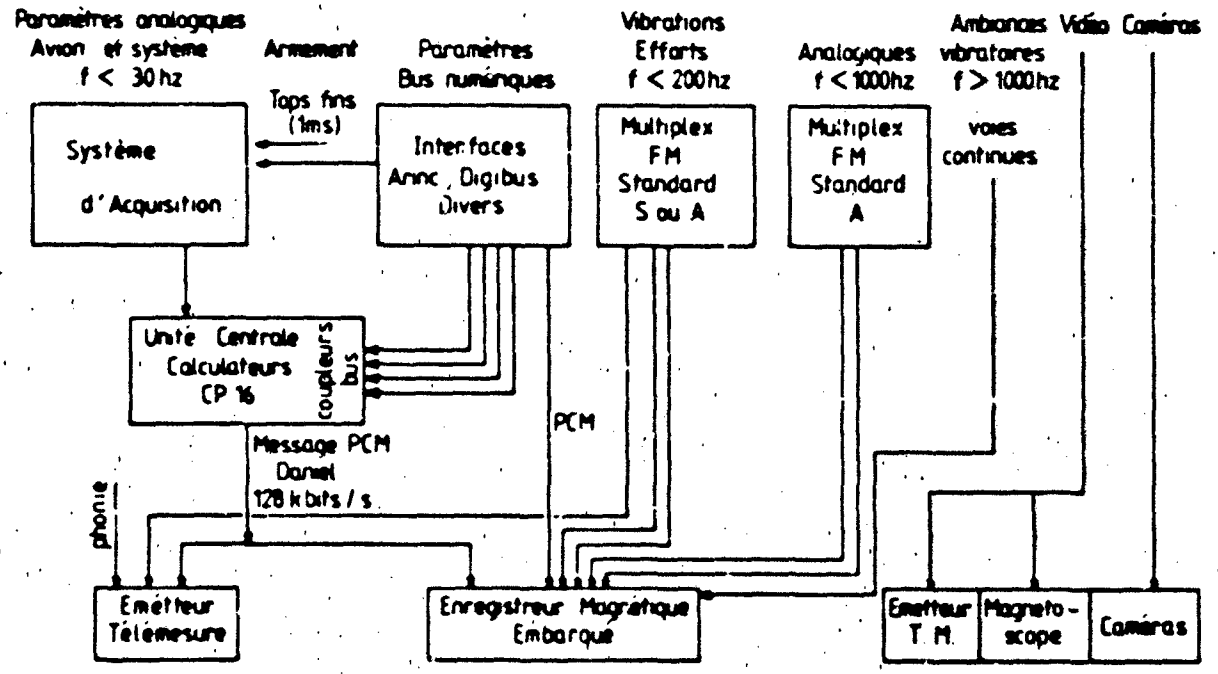

Figure 3

SYNOPTIQUE DE L'INSTALLATION DE MESURE EMBARQUEE

pour mesures mixtes Avion / Système d'armes

DANIEL

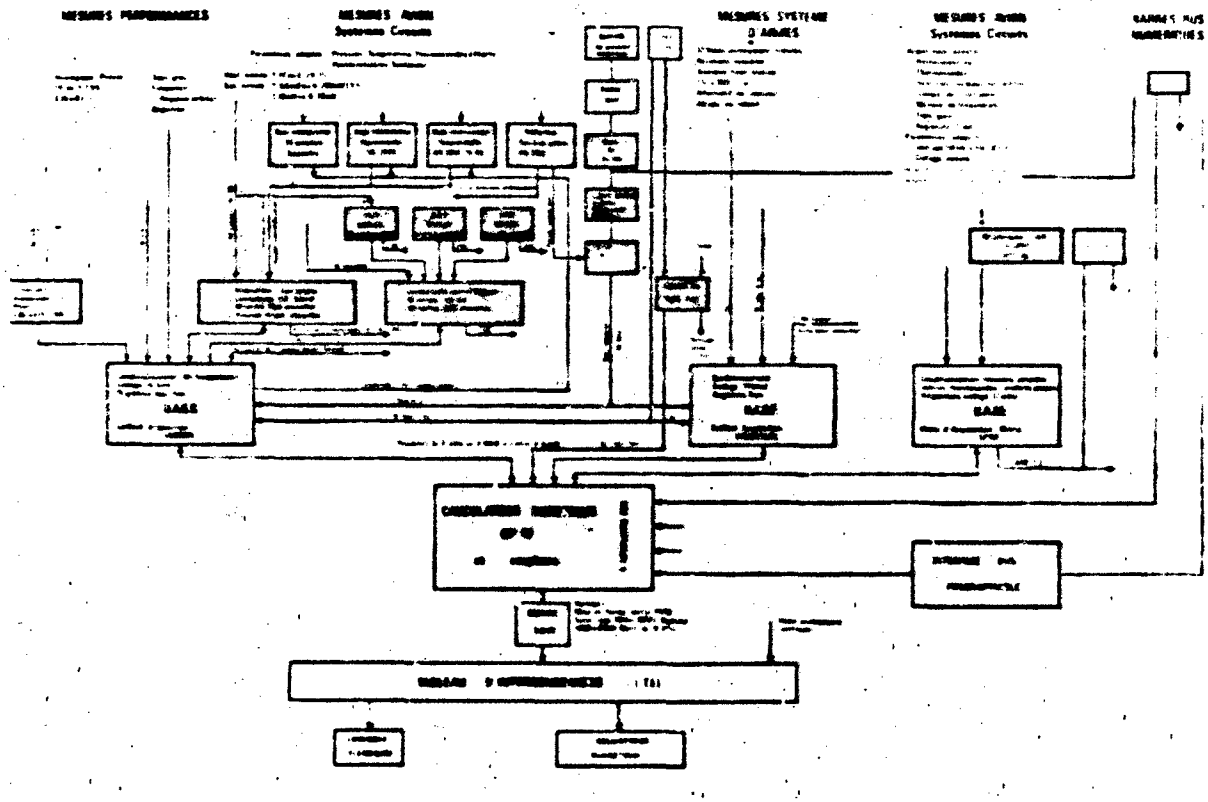

Figure 4

REAL TIME TESTING — THE NEXT GENERATION

James D. Dinkel
Grumman Aerospace Corporation
Calverton, NY 11933

SUMMARY

Grumman Aerospace has used real time testing since 1950. It took a giant step forward with the addition of on-line processing when the Automated Telemetry System (ATS) went on line in 1970. Through two generations of testing capability, the ATS has provided flight test engineers with the capability to acquire and process data and analyze the answers obtained during a test operation. To increase this capability for the more demanding requirements of the future, a New Display and Control System (NDCS) is being developed. When the NDCS is fully operational in 1986, the ATS will move into the next generation of real time testing. This paper will describe the requirements set for the new system and the design developed to meet them.

INTRODUCTION

Since 1970, Grumman has been using extensive real time/on-line processing during flight testing. From the highly successful F-14 development program to the present day, Grumman's ATS has reduced flight test development time and cost through:

- Improved testing efficiency
  - Fewer test points required
  - Fewer contingency flights
  - Immediate validation of maneuver
  - Assured quality of instrumentation and data
- Enhanced productivity
  - More test points per flight hour
  - Faster envelope expansion
    - o Flutter
    - o Loads
    - o Stability and Control
    - o Inlet Compatibility
  - More test time per flight
  - Use of alternative objectives
  - Fewer flight aborts
- Accelerated turnaround
  - Higher flight rate
  - Complete data analysis for critical decisions
  - Fewer flights, less required maintenance.

In addition, flight safety has been enhanced by automatic limit checking of measured parameters.

The ATS has been continually updated over the past 13 years to maintain its capability and is now in its second generation. However, it is evident that major changes are required to meet the increasing demands of complex future test requirements. This paper will discuss past ATS performance and what changes are being made to provide a superior real time testing capability at Grumman.

PAST GENERATION

The first generation of real time testing at Grumman was conceived in 1955 and became operational in 1970. This ATS system (Fig. 1) consisted of a complement of hardware and software subsystems which, combined with a central processor, formed the integrated system capability required to perform real time/on-line flight test analysis. The prime objective was to provide real-time answers (not just raw data) to flight test questions through interactive data processing of telemetered test data.

Using extensive computer control and sophisticated interfaces between subsystems, the system provided data services in real-time. In the past, these answers were not available until days after a test flight. The proven hardware and software characteristics of this facility promoted the successful and timely completion of a flight test program because it displayed engineering computations in an understandable format. In addition, it eliminated data turnaround constraints and allowed for on-line modification of flight plans.

The value of real-time testing has been proven many times. Grumman has documented three specific areas where ATS has improved the performance of flight test operations.

- A flight director, at his console, has access to the computational power of one of the largest scientific digital computers of the industry through an alphanumerical keyboard, function keys, and a video display. He may request, in real-time, processed data such as performance and Mach Number calculations and receive the test data immediately. During flight test operations, the system also monitors limit violations and reports them as they occur.
- The "man-in-the-loop" concept allows adaptive flight testing. The engineer can react to presented data by modifying the test plans based on actual results. Responses have ranged from extreme caution to unprecedented envelope expansion

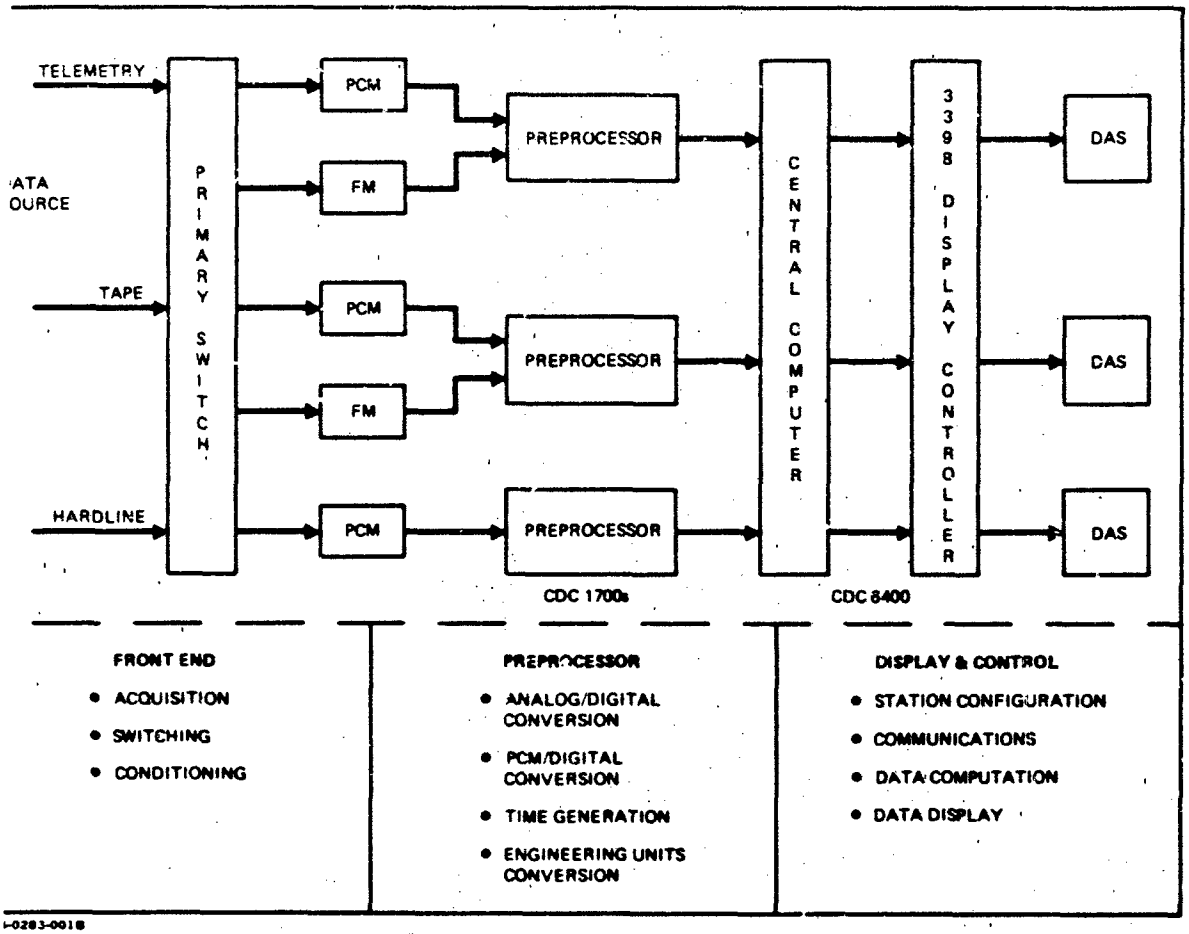

Fig. 1 ATS -Original Flight Test System

- The extensive CRT graphics capability allows the flight test analyst to work with "answers" in a variety of formats versus the tabulated engineering units data previously obtained.

ESENT GENERATION

We entered the second generation in 1976 with the introduction of a new software operating system — System Tele-OPE™ 340. Under this system, the ATS was reduced from three data streams to two primarily because of declining flight t activity as well as increased productivity of the new system. Tele-SCOPE™ 340, a superset of the former standard Con-l Data Corporation SCOPE software, provided extensive multiprogramming and multiprocessing capabilities. This translated o enhanced compectional capabilities which allowed the real time analyst to:

- Look up data from large tabulated data files
- Process non-real-time critical calculations in a deferred mode which allows calculations to be performed at whatever rate is required to complete them. This eliminates the need to keep up with the incoming stream of raw data, while supplying answers in a near real time environment
- Increase core storage for analysis programs
- Create output data files which could be sent to an off-line printer during or after the flight. These files could also be used as input to other programs
- Intermaneuver processing so that calculations could be made between test points using data accumulated from the previous test point.

All of these changes translated into more timely and accurate data and provided the flight test analyst with real time answers uch were previously available only in the batch processing environment.

The operational enhancements provided by Tele-SCOPE 340 included the ability to initialize and prepare for execution up to computer programs prior to flight, as compared to only one previously. This feature also shortened the time needed to itch from one program to another from over 2 minutes to under 30 seconds. In addition, Tele-SCOPE 340 created a data file mprised of all the raw data passed from the preprocessor to the central computer. This recall file permitted data previously oked at during real time to be reprocessed by the same or a completely different program.

Later additions to the second generation system included a heads-up display of flight conditions and priority parameter out of nits, and television displays of the runway and flight line.

XT GENERATION

he next generation ATS will begin in the second quarter of 1986 when the fully operational NDCS comes on-line. Fig. 2 tains the highlights of the NDCS development schedule. The initial portion of the schedule involved establishing design re- rements which will be discussed next.

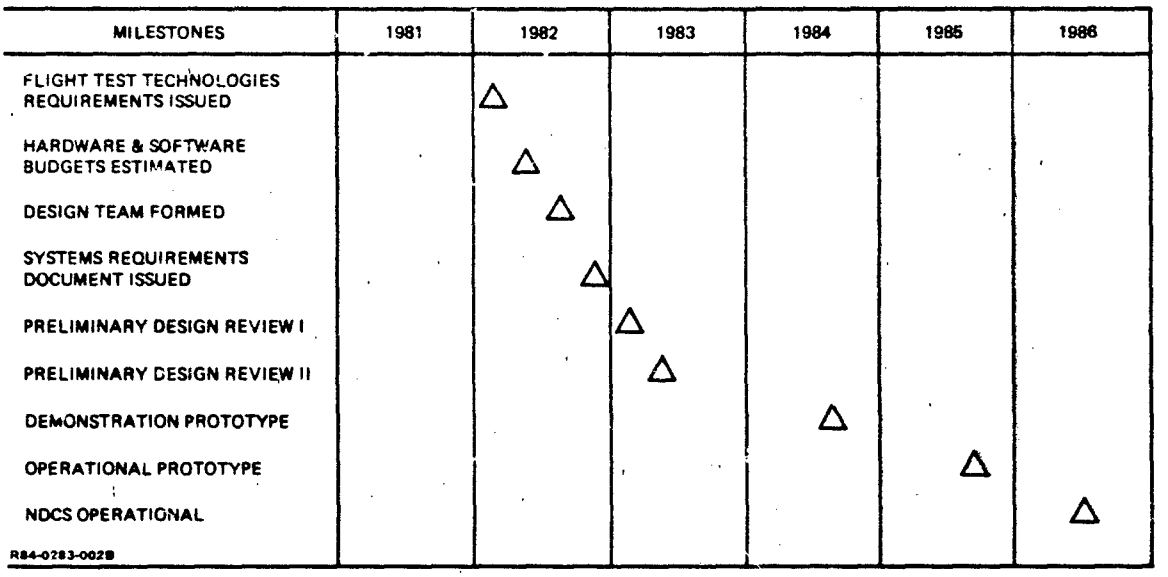

Fig. 2 Highlights of the NDCS Development Schedule

tem Requirements

irumman recognized in the late 1970s that major ATS subsystems required upgrading and/or replacement to be viable into 1980s. After careful technical analysis, management established the preprocessing subsystem as first priority. The processor replacement was completed when a new Advanced Telemetry Preprocessor (ATP), designed by Grumman Data tems, went on-line in July of 1982. Although the preprocessing subsystem was replaced first, the display and central com- r subsystems were by no means ignored. Since the late 1970s, scores of meetings have been held at many organizational ls to establish the general broad requirements that the replacement/upgrade had to address.

spite of the numerous software and hardware modifications made to the ATS over the years, the Flight Test Department ved that the "real time/on line" test productivity had materially degraded since the period of peak F-14 developmental ac- ty and the use of the ATS for systems flight testing had not materialized. The fundamental problem was that, while we were roving the flow of digits through the processing loop, we were not materially enhancing the quantity or quality of the wers presented to the flight test engineers. Among the most significant causes for this were:

- The basic display system design (i.e., only one Data Analysis Station (DAS) per stream)
- Complexity of applications software vis-a-vis available computational capability
- Inability of the system to respond rapidly to even minor changes in the applications software
- Limited (to non-existent) data base display capability
- Unsatisfactory hardcopy facilities
- Crowded physical arrangement
- Signal breakup and noise requiring processing from A/C tape.

hese factors forced the test engineers to rely more on post flight processing for their answers, and to depend on strip chart e displays for the real time (safety of flight oriented) testing.

dditionally, the existing system still had two single points of failure that could stop all real time test operations — the cen- computer and the 3398 Display Controller. While the ATP, per se, would not significantly alter the above deficiencies, its itecture would, when combined with a more capable Display and Control System replacement, allow an opportunity to rse this unacceptable trend.

o remedy this problem the Flight Test Department issued, in April 1982, a set of requirements for a NDCS which was in- led to improve real time/on-line test productivity by allowing the test engineers to complete their answer acquisition tasks ng the flight. The highlights of these requirements are:

- The display subsystem consists (initially) of two independent streams each consisting of two DASs and one Test Conductor Station with either or both DASs from one stream capable of being independently assigned to the other stream. Four strip chart recorders, available for the display of 32 raw parameters, may be individually assigned to either stream
- The initial system must be expandable to three streams with three Test Conductor Stations and up to 12 DASs (nominally four per stream), with any eight assignable to one stream
- The DASs must be capable of performing computations and display functions and have sufficient local storage capability to store aircraft envelopes, previous flight data fairings, and selected data from previous flights and/or baseline engineering analysis data as well as local recall and system/user files

Each of the DASs must be independent, and capable of operating on the same data (as any other DAS supporting the same real time input) with different programs, or different data (in the same real time stream) with different programs
The computational capability and storage requirements for each DAS will be independent of other processors
The capability to allow presentation of plots comprised of data from current files and from previously stored flights or baseline engineering analysis data
The DAS must provide the capability to create, debug, and validate specialized applications software
Each DAS will consist of:

- A black and white CRT with the capability to:
  - o Display up to 16 raw or calculated scrolling time histories on eight annotated grids
  - o Display 10 raw or calculated parameters plus time in half screen tabulated format
  - o Display ¼ screen cross plots
  - o Reverse or freeze the scrolling time histories
  - o Select start/stop times from the scrolling time history display for further data processing
- A color CRT to display data from complex computational programs run from a data file created in real time. This display will have the capability for two and three dimensional graphics requirements and simplified subsystem schematic line diagrams with numeric displays at points representing key areas of interest
- A strip chart recorder with the following capabilities
  - o Display at least eight raw or calculated parameters plus time on edge pen on a continuous basis unless stopped at the recorder
  - o Computer controlled parameter selection and scaling
  - o Pre-initialized setups selected via keyboard controls
- A hardcopy device capable of output from either the time history or analysis CRT display
- A repeater scope showing the Test Conductor's out of limits/discrete CRT display

Each Test Conductor Station consists of:

- A color CRT with the ability to display
  - o Up to 24 out of limit conditions from a maximum of 100 items being limit check
  - o Up to 150 discrete measurements by title in a grid type pattern
  - o Current flight condition information including time, Mach number, altitude, gross weight, etc
- A black and white CRT capable of:
  - o Producing its own displays
  - o Repeating any DAS time history display
- A strip chart recorder with the same capabilities as the DAS recorder.

ce these requirements were released, a start up team was organized with representatives from Grumman Data Systems and rman's Flight Test Department. This led to the formation of a NDCS design team in September 1982. The design team ed the original requirements, added additional requirements, and issued, in the beginning of December 1982, a System Re- ments Document for the NDCS. This document formed the basis for the design work to follow.

TEM DESIGN

ce the requirements were established, the program moved into the preliminary design phase. At the beginning, the design established the following high level design goals:

Meet flight test requirements through the 1990s
Design for ease of future upgrade/expansions
Limit primary hardware cost to $1.5 million U.S. dollars
Keep manpower costs under $3.5 million U.S. dollars
Have a demonstration prototype by the fourth quarter of 1984
Have an operational prototype by the fourth quarter of 1985
Be fully operational by the end of the second quarter of 1986
Station-wide ATS compatibility.

h these goals and the system requirements in mind, the team produced the baseline configuration shown in Fig. 3 by the Preliminary Design Review date in March of 1983.

e baseline configuration is a distributed processing architecture system centered around a local area network. This design sents a considerable departure from the original centralized system shown in Fig. 1, but was the logical choice to meet the and requirements discussed above. The possible vertical movement in the DAS host computer lends itself toward expand- /. Without changing the system software one can progress upwards through Digital Equipment Corporation's extensive product line. Horizontal growth can be accommodated by simply adding DASs to the network. Additional growth dimen- are possible by adding communications trunks, additional preprocessors, other array processors, additional mass memo- and other special devices to the network. Single-points of failure are minimized and even with the sudden loss of an asset, stem may be rapidly reconfigured with little risk. Each asset will be independently and rapidly re-assigned from one data n to another.

s system allows low-risk simultaneous real time/non-real time activities (post test analysis, hardware and software enance, and application program development). In addition, concurrent secure/non-secure operations are now possible by are and software isolation.

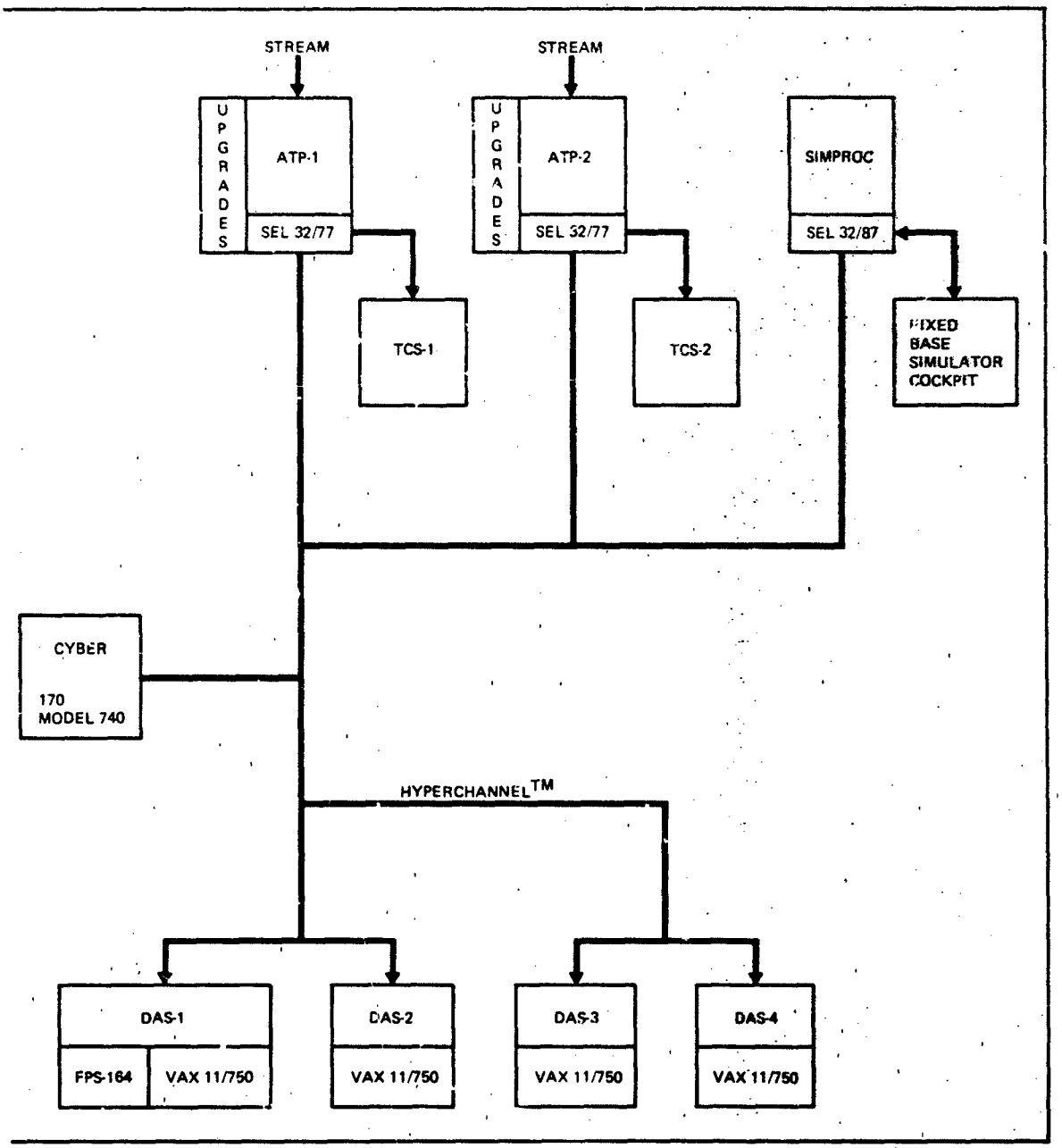

Fig. 3 NDCS Baseline Configuration

he local area network, using Network Systems' HYPERchannel™ communication line, permits the integration of several erent computers (CDC, SEL, VAX) into one system. The network and its interface hardware allow the selection of the right :hine for the right job. By carefully planning the network, the traumas associated with a multi-vendor system are eliminated. shown in Fig. 3, the network allows the integration of two ATS assets not directly associated with NDCS (Flight Test Fixed e Simulator and Floating Point Systems 164 Array Processor) into the system. The SEL 32/87 minicomputer used by the ulator can become a third preprocessor, if needed in the future, and will be used to supply data to the DASs during NDCS elopment. This frees the ATPs to support the current real time system. The array processor provides high speed computa- al power required for such tasks as advanced flutter analysis.

ata flow within the system starts at the ATS front-end with reception of the telemetry signal from the test vehicle. The data ien passed to the ATP for digital and engineering units conversion. Predefined groups of parameters are then selected from total data stream and passed to the respective DASs demanding data at that time over the HYPERchannel™. A master ll data file of the total stream is recorded at the ATP on a disk storage device. Data received at each DAS is processed in time by its own minicomputer (VAX-11/750) for display on a "time history display" and a strip chart recorder. These data also recorded on a local recall data file for further processing by the main analysis programs.

he DAS will consist of two CRT displays (time history and analysis), one strip chart recorder, one repeater scope of the t Conductor's out of limits/discrete display, one hardcopy device, and provisions for individual communications control

nels. In addition to the hardware shown in Fig. 4, each DAS will have a VAX 11/750 minicomputer to perform the computa-nal and overall control functions and two disks for storage of analysis software, data base files, raw data received from the TP, and calculated output data files.

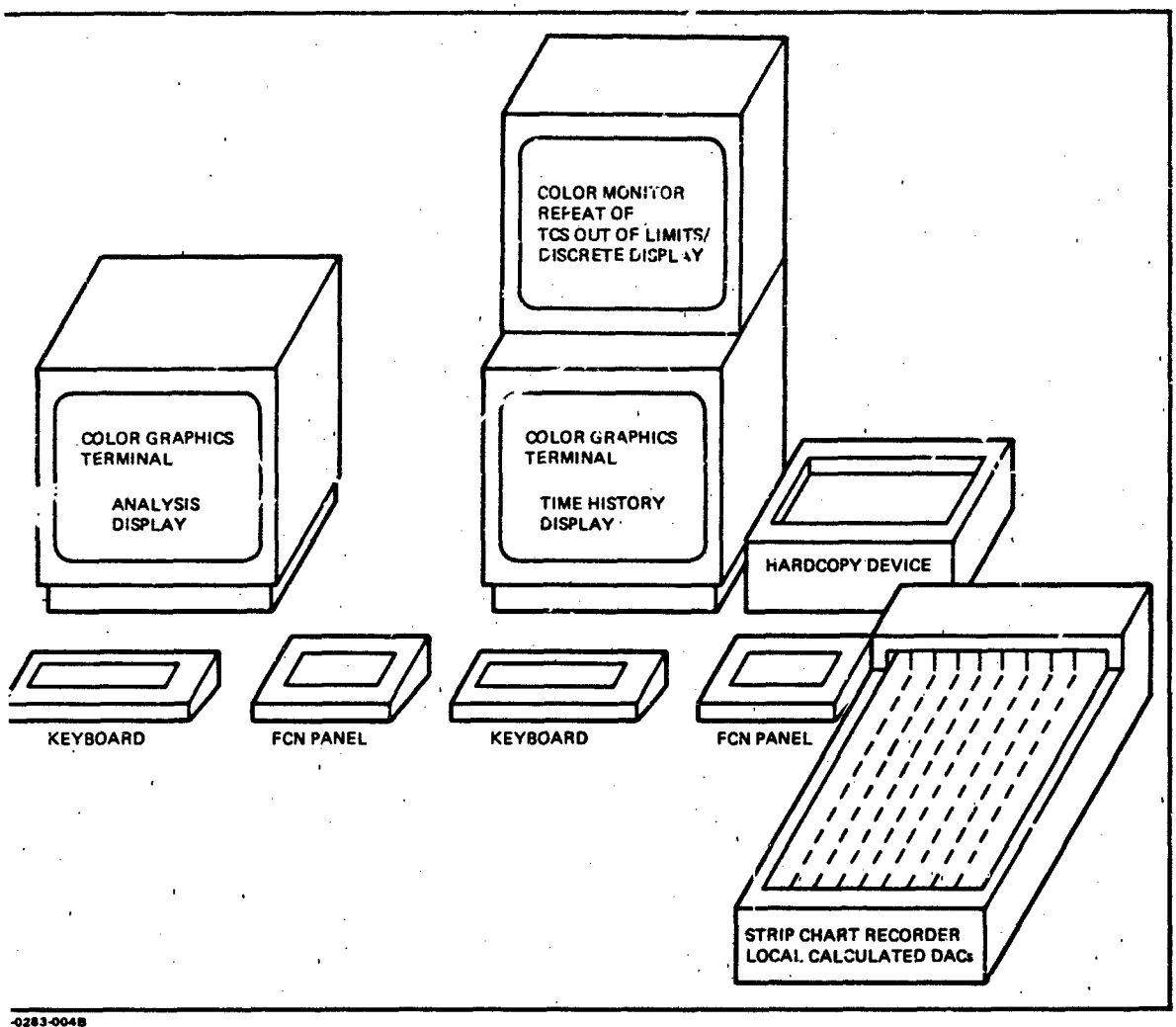

-0283-004B

Fig. 4 DAS Hardware

The "time history display" is intended primarily for real time data analysis. It will be capable of displaying raw or calculated a in the form of scrolling time histories, tabulations, cross plots, or any combinations of these. Besides data and test maneu-validation, the analyst at this display will be able to select start/stop times for further analysis on the "analysis display." e selection process will be made from the scrolling time history displays via a vertical cursor. Selection can be made as the a passes the cursor on the screen or the screen can be frozen and the cursor moved to the appropriate position on the time tory.

The strip chart recorder will provide additional real time monitoring capability for raw or calculated data. A total of eight ameters may be displayed at one time with the capability to switch to any one of several other sets of predefined parameters a touch sensitive function panel. The strip chart will automatically be annotated to identify which group of parameters is be-displayed.

Most answers will be displayed on the analysis screen. Test maneuvers time sliced at the time history display will be proc-ed behind real time from data stored on the local recall disk file. This allows complex, time consuming calculations to be formed without the constraint of keeping up with the real time data stream. Data can be output in a flexible array of formats luding tabulations, cross plots, multi-parameter plots, time histories, and annotated schematic dra vings. In addition, data m previous flights, or estimated data, will be displayed together with the current data. Extensive use of color will be made enhance data readability. Since each DAS is independent of the others, data analysis can continue long after the test maneu-s have been flown by accessing the local recall data file or the master recall file at the ATP if it is not transferring real time a. This will not effect the rest of the flight operation.

The hardcopy device will provide permanent output copy of the data from either the time history or analysis display. The plays will not be noticeably effected when hardcopy is requested. Copies will be available approximately 15 seconds after the uest is made. Although the current plans call for black and white copies, color may be feasible before the prototype system s on-line in 1985.

The repeater scope with the Test Conductor Stations out of limits/discrete display provides continuous real time flight condition information. The out-of-limits data are displayed at the DAS to minimize the chance of a critical out-of-limits condition being missed. With the increasing amount of discrete information that needs to be displayed, the repeater scope eliminates the requirement for other DAS displays to provide these data.

The configuration of the Test Conductor Station was not finalized until late 1983 when it was decided to make two of the DASs into combination DAS/Test Conductor Stations. This decision was based on the strong desire of the Flight Test Department for the Station to have full capability, as specified in the requirements document, and the desire to keep the hardware costs within limits. In the Test Conductor Station configuration (Fig. 5), the analysis display will become the out of limits/discrete display and the time history CRT will be used to monitor the time history display from any DAS active on the same data stream. The test conductor will also be able to generate displays from his own software programs. The other equipment will be used in the same manner as a DAS. The Test Conductor Station will act as the overall controller for the data stream, configuring the ATP via communications over the HYPERchannel™ and assigning DASs as well as controlling the data flow within the stream.

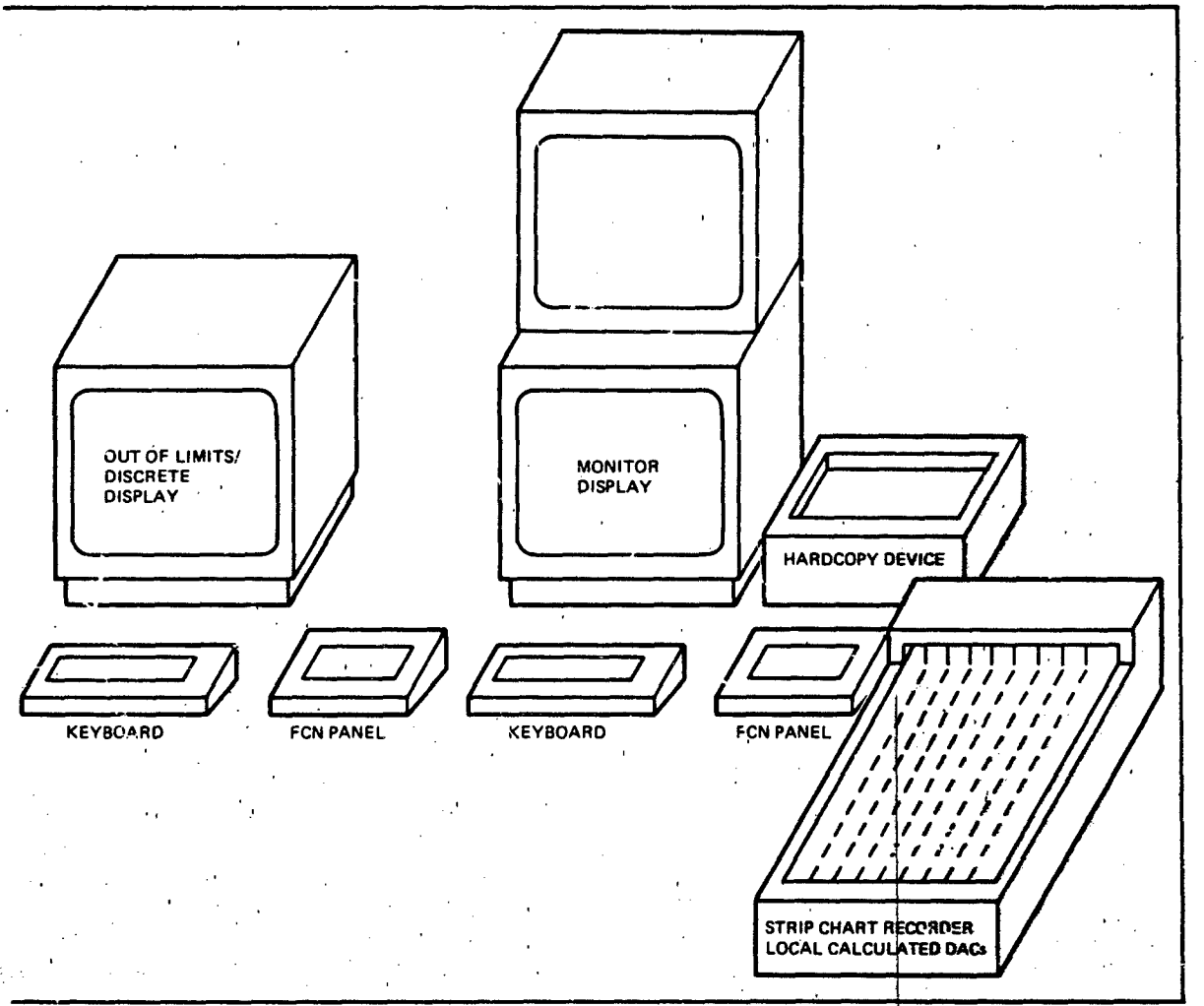

84-0283-005B

Fig. 5 Test Conductor Station Hardware

After the first preliminary design review, the initial hardware was ordered and the system software structure defined. By the second preliminary design review, the implementation plan was established and was based on a series of prototypes (see the latter portion of the development schedule, Fig. 2) to provide early hands-on experience. The design effort continued through 1983 and has resulted in several changes to the baseline configuration (See Fig. 6).

The current NDCS configuration utilizes the combination DAS/Test Conductor Station arrangement discussed previously and new VAX cluster™ System which centralizes the mass storage devices (disk/tape) and provides a high speed computer interconnect between them and the Test Conductor and DAS. These new features have allowed data selection and the master recall file to be moved from the ATP to the DAS side of the local area network. This provides greater accessibility to the master recall file for the DASs and Test Conductor Station and means extremely large files can be accommodated without isolated dedicated mass storage hardware at the ATP. The ATP can be left essentially unchanged, eliminating the need for the hardware and software updates required with the baseline configuration.

Just as the VAX cluster™ System has provided additional advantages to the NDCS, future hardware and software products will be used wherever possible to improve the system. The early hands-on experience which this prototype approach provides, will allow refinements to be made before the NDCS becomes fully operational in 1986. All this will provide the next generation of real time testing with a technological jump in capability to meet the demands of the future.

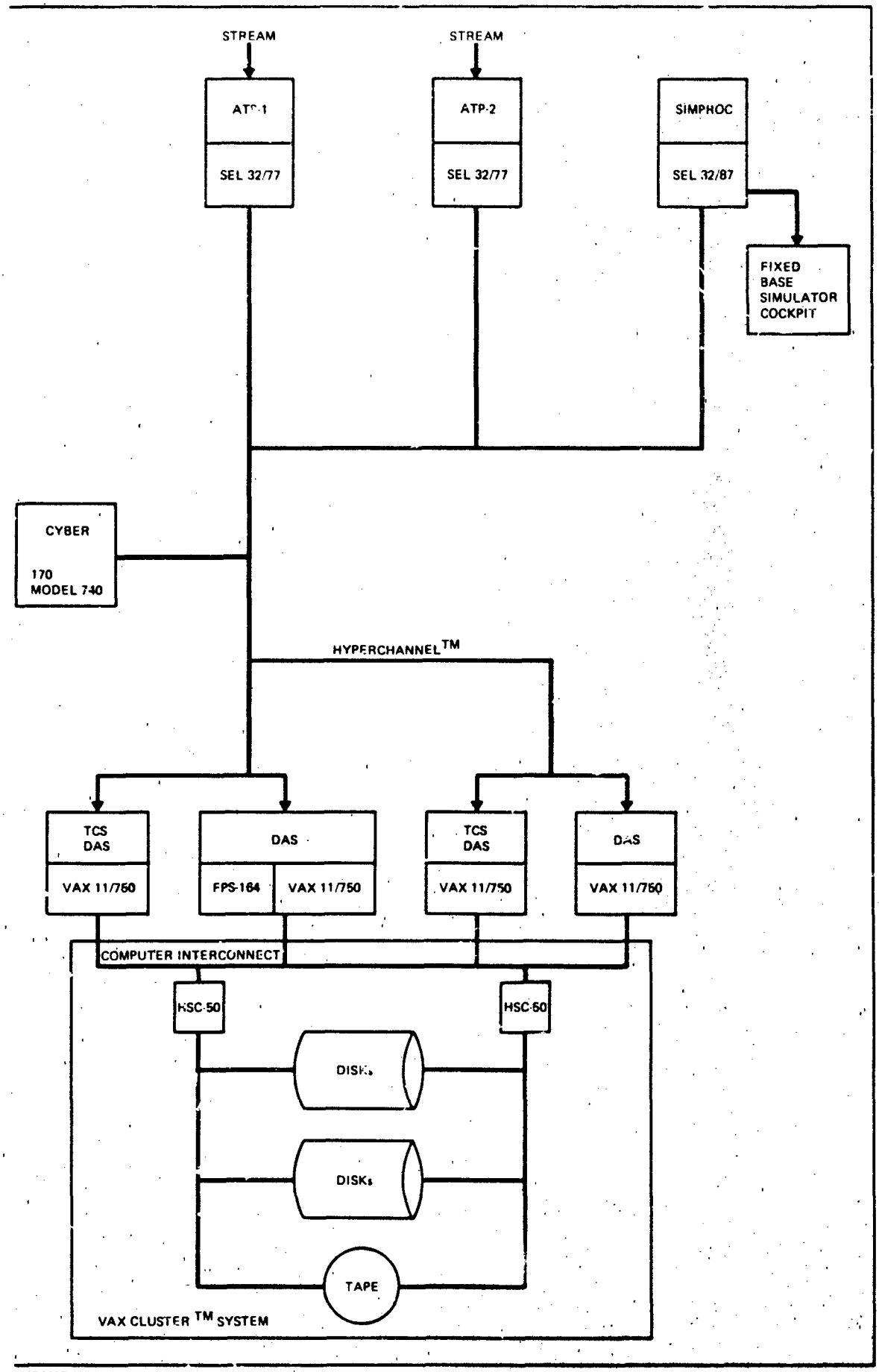

Fig. 8 Current NDCS Configuration

USING AN AIRBORNE CO_2 CW LASER FOR FREE STREAM AIRSPEED AND WINDSHEAR MEASUREMENTS

by

Alan A. Woodfield
Royal Aircraft Establishment, Bedford MK41 6AE, England

and

J. Michael Vaughan
Royal Signals and Radar Establishment, Malvern, Worcs.

RY

Applications of a Laser True Airspeed System (LATAS) in flight are described with les from trials with an exceptionally reliable and rugged system developed by the RAE RSRE and installed on the RAE HS 125 research aircraft. The LATAS system is briefly ibed. Its remote sensing capability makes it particularly useful for measuring ow conditions before they are disturbed by the aircraft. This is demonstrated with ts from flight tests of LATAS as a self-contained pressure error measurement system combined with total pressure and total temperature measurements), and also results windshear measurements in a severe thunderstorm downburst (microburst). The possible sion of the system to measure turbulence by using a conical scanning beam is ibed, and several other possible uses such as an airspeed sensor that can iminate instantaneously between small amplitude gusts and large disturbances for ng an 'intelligent' autothrottle, or a combined 3-axis air data and 3-axis ground ity sensor for helicopters.

INTRODUCTION

One of the perennial problems in flight testing has been measurement of the turbed airflow conditions of static pressure, speed and flow direction, and lence. All the usual sensors, such as pitot-static pressure tubes and wind vanes and more exotic variants (Ref 1) can only measure air flow conditions at their location e aircraft. This local airflow has been disturbed from the free stream conditions by resence of the aircraft and special calibration flights have to be made to find the ionship between the sensor measurements and the undisturbed free stream conditions 2). These calibrations are usually made in steady state conditions and require polation to use in conditions where steady flight cannot be achieved, eg stall, lift aries, zoom climb, flight in ground effect, etc. Also the frequency response of the rbed airflow is unknown and causes uncertainties in the measurement of turbulence.

All these problems could be overcome if it was possible to measure the air tions ahead of the aircraft before they are disturbed by its presence. These tions are found about 10 fuselage diameters (or wing mean chords) ahead of the aft at subsonic speeds. (At supersonic speeds a conventional short nose probe is ate as air disturbances cannot propagate forward of the main shock wave). Thus a e that can measure airflow conditions some 20-100 m ahead of an aircraft would remove eed for the special calibrations, provide true data in unsteady flight conditions, ive uncontaminated data on turbulence. A focussed CW laser doppler system with al scanning will measure the total air velocity vector at these sorts of ranges. In paper results from flight tests with a non-scanning laser doppler system are used to strate the capabilities of these systems to measure undisturbed air velocities.

Since about 1970 the RAE have been collaborating with RSRE in the design and testing CW laser doppler systems (sometimes known as laser radars or LIDARS) for airspeed ements. The main aim initially was to establish the feasibility of using these ns to make remote measurements of the wind so that very large changes (wind shear) be identified. The first system tested was ground based (Fig 1) and housed in a with an accompanying caravan to hold the data processing equipment. The system used opes with a primary reflector of 30 cm diameter and worked out to ranges of about 1 However, in common with many similar systems, it required frequent attention to ain the optical system aligned and the laser tuned to the P20 line without any erence from nearby off-axis modes. Despite these problems the system could be kept d and stable for a day or two without adjustment, and its effectiveness in detecting shear was very good. This led to the development of a compact and reliable system ight tests in the RAE HS125 aircraft. This Laser True Airspeed System (LATAS) (Refs and 5) has now been flying in the RAE HS125 for 3.5 years and this paper will be the system, which has proved to be both rugged and reliable. The goal of a eterodyne system that can be switched on like a light bulb and requires no ments has at last been achieved.

Flight test results have shown that systems of this type could be used for many ent tasks in aviation. This paper describes the use of the LATAS system for ining pressure errors (pe) in air data systems and measuring turbulence, including

2. THE LATAS SYSTEM

2.1 SYSTEM DESCRIPTION

The various components of the LATAS system are shown in Fig 2. All of these items are of UK manufacture and, although they are for an experimental system, they have been put through many of the vibration and temperature tests required for production equipments. Most of the items were very advanced when specified back in 1978 but are now readily available. The three most important items are the Optics Head, Surface Acoustic Wave (SAW) Spectrum Analyser and the Video Integrator.

The Optics Head was designed and built at RSPE. Its general layout is shown in Fig 3. The main beam from the 3 watt Ferranti Wave Guide Laser is transmitted through a Germanium plate set at the Brewster angle and then focussed at a given distance using a remotely adjustable expanding lens. The returning signal is received through the same lenses and after a change of polarisation it is reflected off the Germanium plate. This signal is then mixed with a small proportion of the main beam and focussed onto the Mullard CMT detector. The detector has a frequency response better than 100 MHz and is cooled to -196° K using high pressure pure air or 'white spot' nitrogen.

The coaxial monostatic system, with the same optics for transmitter and receiver, is particularly convenient and also tends to minimise effects of beam distortion when propagating through an inhomogeneous atmosphere. Detailed studies have been made of the optimum choice of system parameters, and also of theoretical and experimental signal to noise ratio with calibrated standard targets (Ref 7). These show that within experimental error the equipment performs at the ideal quantum limited level with no unaccountable losses. The beam waist, from which the strongest return signals are received can be set at distances up to nearly 300 m ahead of the output lens, which is only 15 cm in diameter. The dc current level from the detector is directly related to the power in the local oscillator beam and provides a convenient measure of the main laser power. The dc current is also used in an electronic locking loop to maintain the laser automatically on the P(20) transition by inserting a very narrow band optical filter, which transmits the P(20) line, in the local oscillator path.

The Optics Head (Fig 4), is shown here installed in the nose of the HS125, where the infra-red beam is transmitted through a 20 cm diameter Germanium window (Fig 5) with a special diamond-like surface coating to withstand abrasion and insect and raindrop impact. The Optics Head also includes the HT power supplies for the laser and the complete unit is only 68 x 32 x 29 cm. Cooling is from a simple radiator and fan assembly and is used, together with a 100 W heater mat, to maintain the laser between about 25° and 45° C. This has proved adequate for ambient temperatures from -60° to 35° C.

The output from the detector travels about 12 m back to the MESL (Racal-Decca) SAW Spectrum Analyser in the cabin of the HS 125. A sample of 25 microseconds is taken by the SAW and transformed within a further 35 microseconds into the frequency plane and transmitted to the Video Integrator. The SAW has a total bandwidth of 25 MHz and with four switchable offsets can cover the frequency range up to 62.5 MHz. 1 MHZ is equivalent to just over 10 kt so this gives a true airspeed range of up to 635 kt, with an ample 50% overlap between each of the four bands.

In the Video Integrator, which was made by Cambridge Consultants Ltd (CCL), the transformed signal from the SAW is converted into a frequency spectrum with 834 channels that are each 30 kHz wide. To improve the signal to noise ratio for low signals the Integrator will then accumulate a succession of SAW samples. The number of integrations may be set between 1 and 16000 on the airborne system. With 100 integrations for a single sample the overall sample rate can be about 160 per second.

In the aircraft system, the spectrum from the Integrator is then processed in another CCL unit to measure the main features of the velocity signature. This summary of the total spectrum and many other items describing the configuration of the laser system are then transferred to displays and the recording system. The form of the signal obtained from the system at various stages is shown in Fig 6. The strongest signal comes from the region where the illumination is greatest and thus the velocity of the peak of the frequency spectrum is usually that of the air at the beam waist. The maximum and minimum frequencies of the spectrum correspond to the highest and lowest velocities within the range where signals are detectable. In the LATAS system these are measured by the spectrum width and average ('centroid') velocity at an adjustable level below the peak. All these measurements together with the height of the spectrum are made in real time on the aircraft. These numbers and the complete spectrum are displayed in the cabin and recorded on the Plessey PV 1513 digital recording system for further analysis. Fig 7 shows a typical velocity spectrum recorded in calm air at a height of 13310 ft. The spectrum is clear and unambiguous. This remains true even for small signal levels and makes the identification of the loss of signal very straightforward.

Doppler signals from the LATAS system are unaffected by heavy rain, or dense cloud or fog unless visibility drops to less than about 50 m (Ref 6). If the particles in the air are sub-micron size then the infra-red beam suffers little attenuation when compared with visible radiation. Thus infra-red beams are unaffected by smokes and hazes even though visibility at optical wavelengths may be reduced.

2.2 RELIABILITY

A principle aim of the RAE/RSRE research has been to demonstrate that the LATAS system is both effective and reliable as a means for measuring air velocities. Normally one would anticipate that a 'one off' experimental system such as this would be less reliable and require more frequent adjustment than an eventual production version. It was therefore a very pleasant surprise to find that:

a. the system has only needed adjustment after removing the laser, which has been a rare event.

b. the 20 cm Germanium window in the nose of the aircraft, Fig 8, shows no sign of any damage to its diamond-like coating after 3.5 years of flying, which included flights through soft hail.

After a few months of initial teething troubles the system has only suffered four failures in 3.5 years. Two of these involved the laser and two were failures of power supplies to the signal processing equipment. The present laser has been operating for 22 months with only one removal for adjustment after 18 months.

One subjective measure of the reliability of the system is that it has been demonstrated in flight on 17 occasions to outside parties without a failure. The authors believe that a reliable production version of the LATAS system can be made now using current technology and available UK equipment.

2.3 SAFETY

The infra-red (10.6 micron wavelength) radiation from the LATAS system is not able to enter the eye and thus cannot damage the retina. The radiation levels at the focus of the beam are high, but, because of the small beam diameter, only a small crossing velocity of about 1 m/s is needed to reduce the radiation level below the minimum standard for human exposure. Thus in flight the LATAS system is totally safe and there are no operating restrictions. When both aircraft and target are stationery on the ground then suitable safety precautions must be taken.

3. PRESSURE ERROR MEASUREMENTS

The LATAS system measures airspeed ahead of the aircraft, where it is not affected by the airflow around the fuselage and wings. With the usual air pressure sensors (pitot and static pressure) it is reasonably easy to measure the freestream pitot (stagnation) pressure, but the static pressure measured at the aircraft is usually different from the freestream static pressure. Static pressure (Fig 15) for a given aircraft configuration is a function of freestream speed, pressure, temperature and direction. By very careful choice the static pressure ports can be located where the difference from freestream pressure is small, particularly at normal cruise and landing conditions. However, all height standards for safe separation from the ground and other aircraft depend on static pressure measurements, which are converted into a pressure height. To ensure that all aircraft display the same height scale, they have to be calibrated to measure the pressure error (pe) of each model of an aircraft throughout its full height and speed range.

The present methods of calibration (Ref 1) rely on comparison with a reference pressure measured by a calibrated aircraft which uses photography to establish any height differences (or similar flights past ground based tracking towers), or comparison with measurements from a towed static sensor (Trailing Static), which is on a long enough tow to be outside the influence of the aircraft. This latter method requires a major installation on the test aircraft.

The Tower Fly-By at low altitude is satisfactory and convenient, but can only cover a very limited part of the flight envelope. Flights with a calibrated aircraft are costly and difficult (eg the range of speeds of the two aircraft will rarely be the same).

With the LATAS measuring the undisturbed freestream speed and the ability to measure the true stagnation pressure at the aircraft, only a measure of freestream temperature is required to derive the freestream static pressure. Like stagnation pressure the freestream stagnation temperature is also reasonably easy to measure on an aircraft.

Relationships between the free stream airflow parameter of Mach number M, Calibrated Airspeed, V_c, Static Temperature, T_o, and Static Pressure, p_o can be derived directly from the measurements of free stream True Airspeed, V_t by LATAS and the measurements at the aircraft of free stream stagnation (pitot) pressure p_t, and absolute stagnation (total) temperature, T_t. At subsonic speeds the relationships are:

$$M = [m^2/(1-0.2\ m^2)]^{0.5} \quad (1)$$

$$V_c = a_{ISA}\,5\ [((Pt/P_{...A})(1 - (1-0.2\ m^{...})^{3.5})+1)^{1/...} - 1]^{0.5} \quad (2)$$

$$T_o = T_t(1-0.2\ m^2) \quad (3)$$

$$p_o = p_t(1-0.2\ m\ )^{3.5} \qquad (4)$$

where a_{ISA} = speed of sound as ISA standard sea level

p_{ISA} = ambient pressure at ISA standard sea level

$m = (V_t/\cos\alpha)/(a_{ISA}(T_t/T_{ISA})^{0.5})$ (3)

α = angle between laser line of sight and the flight path

T_{ISA} = absolute static temperature at ISA standard sea level

It can be noted that

$$(1-0.2\ m^2)^{-1} = (1+0.2\ M^2) \qquad (4)$$

and thus eqns (2), (3) and (4) are easily recognisable as standard flow equations.

From these equations the sensitivity of the derived free stream conditions to measurement errors can be calculated. It should be noted that the 'α' terms only apply to a fixed laser. If a conical scanning system is used then 'α' can be eliminated, but errors in scanning angle must be considered.

Sensitivity of derived free stream static pressure to errors in all measured quantities is highest at high speeds at sea level and decreases with increasing height. With standard deviation in measurements of

V_t	0.1 Kt
T_t	0.2 deg K
p_t	0.3 mb
α	0.2 deg at α = 5 deg

then the standard deviation of derived quantities will be:

	Standard Deviation			
	p_o mb(ft)	V_c Kt	M	T_o Deg K
Sea level, M = 0.3	0.3(8)	0.1	0.0002	0.2
Sea level, M = 0.8	0.5(13)	0.2	0.0003	0.2
36000 ft, M = 0.8	0.2(21)	0.2	0.0004	0.2

In determining pe it is usual to calculate a pressure coefficient, C_{ps}, of the aircraft static pressure source, ps, where in subsonic flight

$$C_{ps} = \frac{p_s - p_o}{p_t - p_o} \qquad (7)$$

(NOTE: This compressible form of coefficient is used in preference to the incompressible coefficient, whose divisor is $0.7\ p_o\ M^2$).

In the terms of eqns (1)-(4), eqn (7) may be rearranged as

$$C_{ps} = 1 - (1-p_s/p_t)/((1-0.2\ m^2)^{-3.5} - 1) \qquad (8)$$

To establish the capabilities of a laser doppler system for measuring free stream conditions and direct measurement of pe the LATAS system on the HAE HS 125 is being used for a series of tests. These are:

a. Tower Fly-by. Comparison of free stream static pressure conditions from LATAS measurements with those derived from kinetheodolite height measurements and ground reference pressure.

b. High altitude flights with UK pe standard aircraft. As (a), but at high altitude.

c. Measurements of the pe of the HS 125 over a variety of flight conditions to check flight to flight repeatability.

At the time of writing the first of these has been successfully completed; the last is underway and the middle item is due to start shortly. In addition the HS 125 has flown in close formation with a recent European airliner to check its pe, and also with the RAE BAC 1-11 civil avionics research aircraft to check its true airspeed calibration, which is used for its advanced navigation systems.

Results from the Tower Fly-by, Fig 10, show a random scatter of data with no relation to aircraft flight conditions. The mean difference in pressure height derived from the LATAS and that from the Kinetheodolite measurements is -1.4 ft and the standard deviations of this difference is 9.6 ft. Thus, as predicted the combination of LATAS, total pressure and total temperature provides a good quality source of free stream static pressure.

Time histories of a steady flight condition, Fig 11, show the measured and derived conditions. Points to note are:

a. fluctuations in LATAS airspeed are also present in total pressure after a lag due to the distance of the LATAS measuring point ahead of the aircraft and the pneumatic system lag in the aircraft pitot system.

b. derived free stream static pressure differs from the static pressure source on the aircraft by a constant amount.

If turbulence is present then the lags in the pitot system are more obvious, and, the derived free stream static pressure has increased scatter, Fig 12.

At first sight one would expect to be able to reduce this scatter by correcting the total pressure for lag and the LATAS true airspeed for its lead. However, in practice, in addition to the noise introduced by the differentiation required for the correction, there will be some remaining scatter because the turbulence changes with time between being seen by the LATAS and reaching the aircraft. Also the LATAS is not usually looking along the flight path and will not see exactly the same turbulence on the aircraft. Thus it is desirable to avoid turbulence if possible as with all other methods of measuring pe.

An example of the HS 125 pe at 20000 ft altitude derived directly from the on-board LATAS system is shown in Fig 13. This shows data from several flights in pressure coefficient form (eqns (7) and (8)) as a function of incidence angle, and also as height error against incidence angle. A height change of 15 ft at 20000 ft altitude is equivalent to a pressure difference of 0.3 mb and this is about the largest difference of individual points from a mean line. The consistency is much better than the earlier data of Ref 6 (Fig 16), although the distinctive hump at about 1½ deg incidence is present in all the data. The earlier data of Ref 6 was subsequently found to have been affected by a fault with the stabilized supply to the temperature sensor, which jumped between two fixed levels in an unpredictable manner. The very low level of scatter is remarkably good for pe measurements by any method.

A system such as LATAS could be installed as, say, a temporary replacement for the weather radar and would give complete freedom to establish pe's throughout the full range of configurations and flight envelopes.

The preliminary results with LATAS are very promising. One area where the LATAS system could be particularly useful is in determining true stall speeds and establishing the minimum safe approach speeds for new aircraft. It is essential to maintain a safe speed margin on the approach, but it is very disadvantageous to have approach speeds higher than necessary because of the increased landing distance and tyre wear.

4. WIND SHEAR AND TURBULENCE MEASUREMENTS

4.1 THUNDERSTORM WIND SHEAR

Initial interest in the LATAS system was in its potential to meet the need for a sensor to measure large changes of wind before an aircraft encounters them. Action can then be taken to alleviate the dangers of these wind sheears. At present wind shear is responsible for the loss of about 2 airliners each year. The most recent was in thunderstorm conditions in July 1982 at New Orleans and killed 153 people (all 145 people in the aircraft and 8 on the ground), and seriously injured 9 people on the ground (Ref 8). The aircraft had just taken off and crashed into a residential area 3/4 nm from the airport. At the time of this tragic accident the RAE HS125 was near Denver, Colorado investigating the nature of the severe wind shears which are associated with thunderstorms. The aircraft with its LATAS system was taking part in the Joint Airport Weather Studies (JAWS) Project which was sponsored by the US National Center for Atmospheric Research (NCAR), the University of Chicago and the US Federal Aviation Administration (FAA). The project has amassed a wide range of data on thunderstorm and other severe weather events from a comprehensive set of ground based sensors, including laser and doppler radars, and aircraft from the National Oceanic and Atmospheric Agency (NOAA), NCAR, the National Aeronautics and Space Administration (NASA), University of Wyoming and the RAE.

Among the many events recorded by the RAE HS125 were several severe downbursts such as that shown in Fig 14. This is the type of wind shear that is believed to have caused

Among the many events recorded by the RAE HS125 were several severe downbursts such as that shown in Fig 14. This is the type of wind shear that is believed to have caused the New Orleans, and several earlier accidents. The main features are the very large (nearly 40 kt) and rapid changes of headwind and the strong downdraught of about 1200 ft/min. The downdraught is shown in Fig 14 by the 3 deg increase in the average pitch attitude used to maintain height. If the HS125 had been flying at the much lower speeds used for landing and take-off then this wind shear would have resulted in a large loss of height. Fig 15 shows a model of the flow in a microburst developed from a vortex ring model suggested by Caracena at a Wind Shear Workshop at the University of Tennessee Space Institute, USA in October 1982. This model is able to explain several features that were observed from the HS125 during the JAWS flights, such as dust curtains rising to over 1000 ft around the perimeter of several microbursts. This could not be explained by the more usual vertical jet model which would produce dust blowing radially from the centre of the microburst with very little tendency to rise. The vortex ring model also produces intense downflows near the ground and, by keeping the energy of the flow contained, it requires less total energy to produce large velocities than the jet model. It also explains the smaller peaks in horizontal velocity observed (Fig 14) at the beginning and end of the microburst at 36 and 54 seconds. This suggests that the HS125 penetrated the microburst just below the upper vortex ring. The aircraft was at a safe height of about 1000 ft above the ground. Fig 16 shows the LATAS system measuring the same wind shear just over 2 sec before it reaches the aircraft, which is equivalent to 250 m distance. The width of the spectrum peak is also interesting as it clearly differentiates between small scale turbulence and significant wind shear. This point is seen more clearly in Fig 17 which shows a sequence of signal spectra from the same time history. By following the sequence it is possible to see each changing wind entering and leaving the tube illuminated by the laser. This tube reaches out to about 700-800 m ahead of the aircraft.

The LATAS sensor has two unique advantages over other airborne sensors:

a. it can measure wind at a known distance ahead of the aircraft, and

b. it can measure the change of wind over distances up to nearly three times its measuring distance.

The range to the beam waist of only 250 m may seem quite short. It corresponds to about 4 sec lead at typical jet transport landing speeds. However, the aim is to provide a system which will enable safe penetration of wind shear. If the wind is measured too far ahead of the aircraft, then any wind shear can change with time or may move sideways relative to the aircraft. Thus there will be only a limited band of distances which will give adequate lead without giving a significant amount of false data. To help identify a suitable distance a laser sensor was simulated during studies of wind shear effects on aircraft. The results showed, Fig 18, that there was a significant advantage in controlling the aircraft using the airspeed measured by a laser at 300 m ahead, but that increasing that distance to 600 m produced no further improvements. On the basis of these tests the maximum range to the beam waist was specified as 300 m for the LATAS system.

The ability of the laser to identify the maximum difference in wind speed over a distance of about 800 m gives it a unique ability to separate wind shear from turbulence before the disturbance reaches the aircraft. This is a capability that autothrottle designers have been seeking for some time. The main problem is that the only speed signal available on all aircraft is airspeed and control of this is essential for large wind variations. But it is not possible to differentiate between large changes and small changes until after they have happened at the sensor. This means that autothrottle systems may on the one hand be sensitive to all airspeed changes, resulting in the discomfort and wear and tear associated with the throttles chasing the smallest changes, or alternatively the system only responds to large changes, making it sluggish. Some improvement can be obtained by using accelerometers to maintain a ground speed until airspeed changes exceed certain limits. However, these systems still require the airspeed of the aircraft itself to change significantly before they respond. The LATAS system can identify a large shear well ahead of the aircraft and even before it reaches the beam waist. This means that throttle activity can be restricted to the conditions where it is really needed without introducing additional lag. A laser system thus provides the signals for an intelligent autothrottle, which will be responsive without unnecessary engine activity.

The wind shear research programme at RAE Bedford is now considering various ways in which the signals from the LATAS (and several more conventional sensors) can be presented to the pilot and automatic control systems and allow safe operations in the presence of severe wind shear.

1.2 TURBULENCE

As mentioned in the introduction, it is difficult to correct for the disturbances from an aircraft when measuring airflow. This is particularly true for turbulence as all corrections are derived from steady flight conditions and, although it is known that airflow disturbances are also time dependent, there is no way of applying corrections for this. A LATAS type of system with conical scanning would seem to overcome these problems and provide a direct measurement of true airspeed. If the cone semi-angle is P, then the air velocity along its axis, V_x, and perpendicular to the axis, V_z, are obtained as:

$$V_x = [V_g + V_{(g+\pi)}]/2\cos P$$

$$V_{zg} = [V_g - V_{(g+\pi)}]/2\sin P$$

where 'g' is the cone rotation angle for which V_z is a maximum.

hese values will be averages for the period of the conical traverse. With a matched cone iameter and distance travelled in a single conical traverse then a minimum wavelength is efined. For example at 300 kt (150 m/s) true airspeed a minimum wavelength of 15 m could e obtained with a 15 degree cone semi-angle at a range of 30 m with a 0.1s conical raverse time. There would be little difficulty achieving these rates and angles with a canning version of LATAS and indeed, with only a relatively short range requirement, the iameter of the main lens could be significantly reduced.

It is interesting to note that a LATAS system always shows air velocity components elation to the optics head. Thus, if velocity and attitude reference systems are close o the optics head, there will be negligible effects from angular rates. In contrast, it s rarely possible to get incidence (and sideslip) sensors close to the reference systems ecause they are usually mounted on long nose booms to reduce aircraft interference ffects and good reference systems are usually too bulky to locate on the boom. These ystems need significant corrections for angular rates and any structural flexing of the oom.

The LATAS signals are not affected by heavy precipitation (Ref 6) and, with a range et at 30 m, it would not be affected by dense clouds until visibility fell below about 0-20 m. Some simple anti-icing on the aircraft windows would give the system an xcellent all weather capability.

. FUTURE APPLICATIONS

The remarkable reliability and ruggedness of the experimental LATAS system has emonstrated that commercial 'fit and forget' CW Doppler Laser systems are a practical roposition with the present state of the art. As mentioned earlier, the LATAS has never eeded any adjustment or special treatment during over 3 years of flight trials (except or the rare occasions when the laser was changed).

Four possible applications for such systems have already been discussed, viz:

a. pressure error measurement without any external influence on the airflow and including measurements during manoeuvres such as the approach to the stall,

b. wind shear detection at distances of several hundred meters ahead of an aircraft to give time to counterbalance the response lags of the aircraft and its engines,

c. intelligent autothrottle speed sensor using the ability of the laser to differentiate between turbulence and wind shear at the same time as it measures airspeed,

d. all weather turbulence measurements, at wavelengths of 15 m or greater, without interference from the trials aircraft.

Three other possible applications also spring to mind and there will doubtless be any others.

First the LATAS system can be used in the conical scan mode, as used for turbulence easurement, to identify the the crossflow air velocities in addition to the axial flow or normal air data purposes. The frequency response will be lower than a fixed laser ut still adequate for most applications.

Second the beam scanning could be arranged to scan the ground and the wheels during anding (Fig 19) and the signals could be used to spin the wheels to give zero slip at ouchdown and thus considerably reduce tyre wear. The laser system can give very precise peed information with a good frequency response and thus has the potential for matching yre and groundspeeds to a fraction of a knot.

Third, a system could be used to provide helicopters with a complete air data and hree axis ground velocities (Fig 20). The air data is measured ahead of the rotor ownwash, which is difficult to take into account using air data sensors on the fuselage. he horizontal ground velocities and climb rate can be measured using a vertical axis onical scan. These velocities can be used to establish a steady hover by maintaining ero velocity. The usual problems of identifying zero velocity with a Doppler system can y overcome with a laser.

Further developments of frequency modulated and pulsed Doppler CO_2 lasers will lead o systems which can measure range to solid objects as well as velocity components. Also t is reasonable to expect that the need for high pressure or liquid gas for cooling etectors will become a thing of the past with developments in thermo-electric cooling.

In conclusion, it is relevant to remember that most of the more sophisticated lements are common to the systems needed for all the tasks mentioned in this paper. Only

e scanning system with its demodulator and the final processing of the Doppler Spectra e specific to individual applications.

PERENCES

) W. Wuest: Pressure and flow measurements. AGARDograph No.160, Volume 11, July 1980.

) J.A. Lawford and K.R. Nipress: Calibration of air-data systems and flow direction sensors. AGARDograph No.300, Volume 1, Sept 1983.

) R. Callan, J. Cannell, R. Foord, R. Jones, J.M. Vaughan, D.V. Willetts and A.A. Woodfield: Proc. 5th National Quantum Electronics Conference, Hull 1981, Pub. J. Wiley & Sons Ltd., Chichester, England.

) R. Callan et al: RSRE Research Review No.6, 1982, Paper 39.

) C. Bullock: Turbulence detection by laser. Interavia Magazine 1/1981, pp. 82-83.

) A.A. Woodfield and J.M. Vaughan: Airspeed and wind shear measurements with an airborne CO_2 continuous wave laser. RAE TR 83061, July 1983 (also Chap 7, AGARDograph No.272, June 1983).

) R. Foord, R. Jones, J.M. Vaughan and D.V. Willetts: Precise comparison of experimental and theoretical signal to noise ratios in CO_2 laser heterodyne systems. (To be published).

) Aircraft Accident Report - Pan American World Airways, Clipper 759, N4737, Boeing.

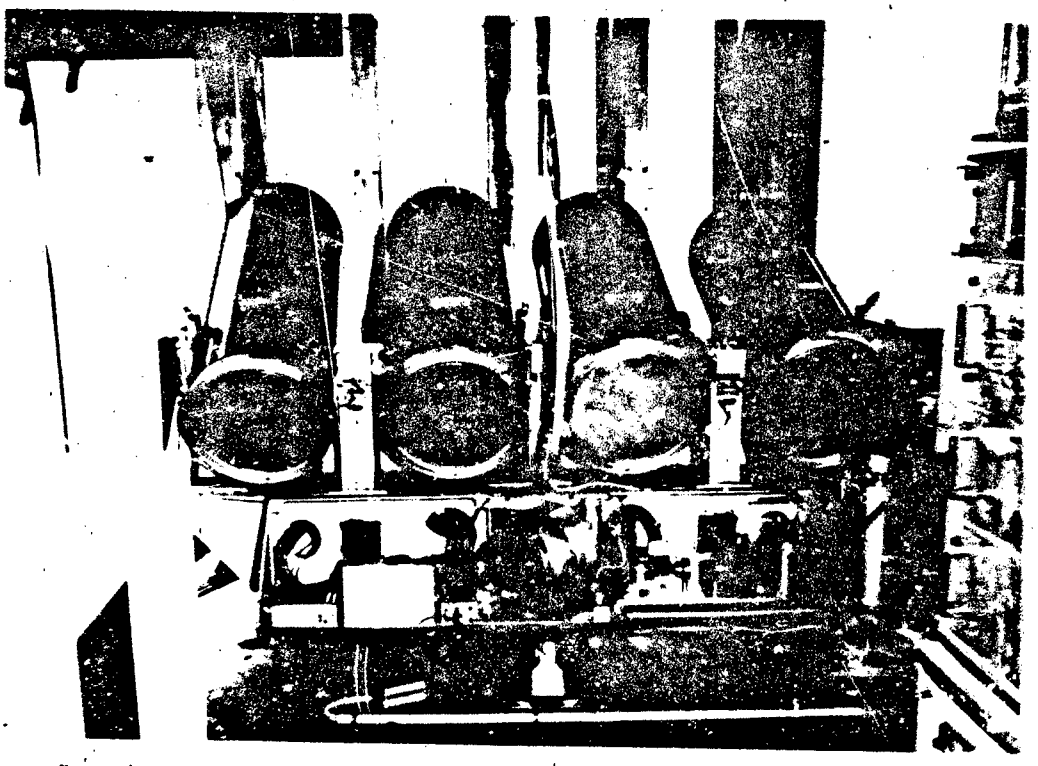

Fig. 1 The Combined Wind And Vortex Experimental Range (CWAVER) equipment. In one mode of operation the outgoing laser beam was switched between the four telescopes in which the range and elevation could be rapidly altered.

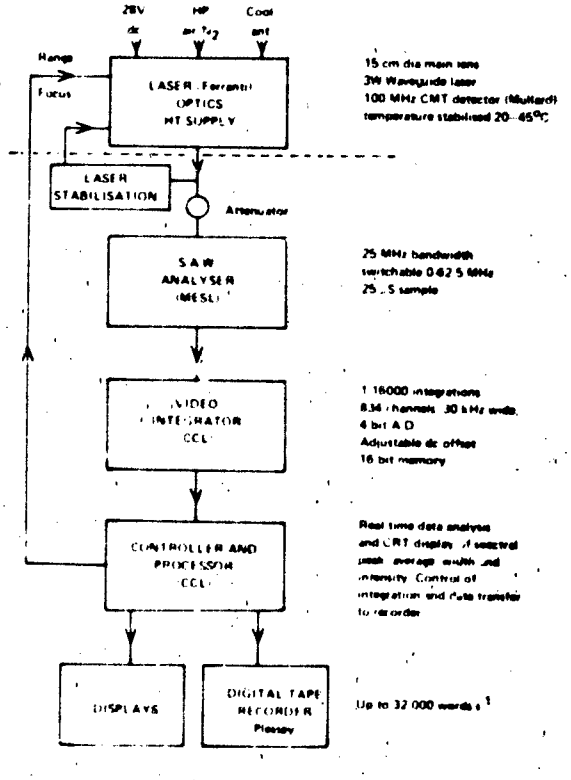

Fig. 2 Block diagram of the Laser True Airspeed System (LATAS). The principal equipment parameters are shown and also (in brackets) the manufacturers.

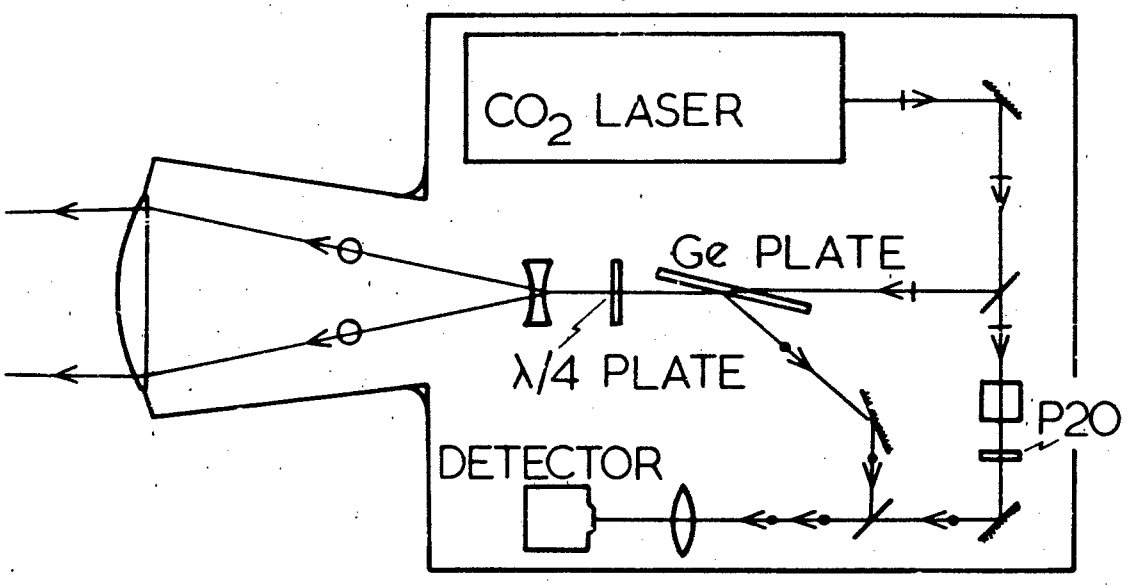

Fig. 3 The layout of the Optics Head in the LATAS equipment. Polarisation techniques and germanium and quarter wave plates promote good efficiency.

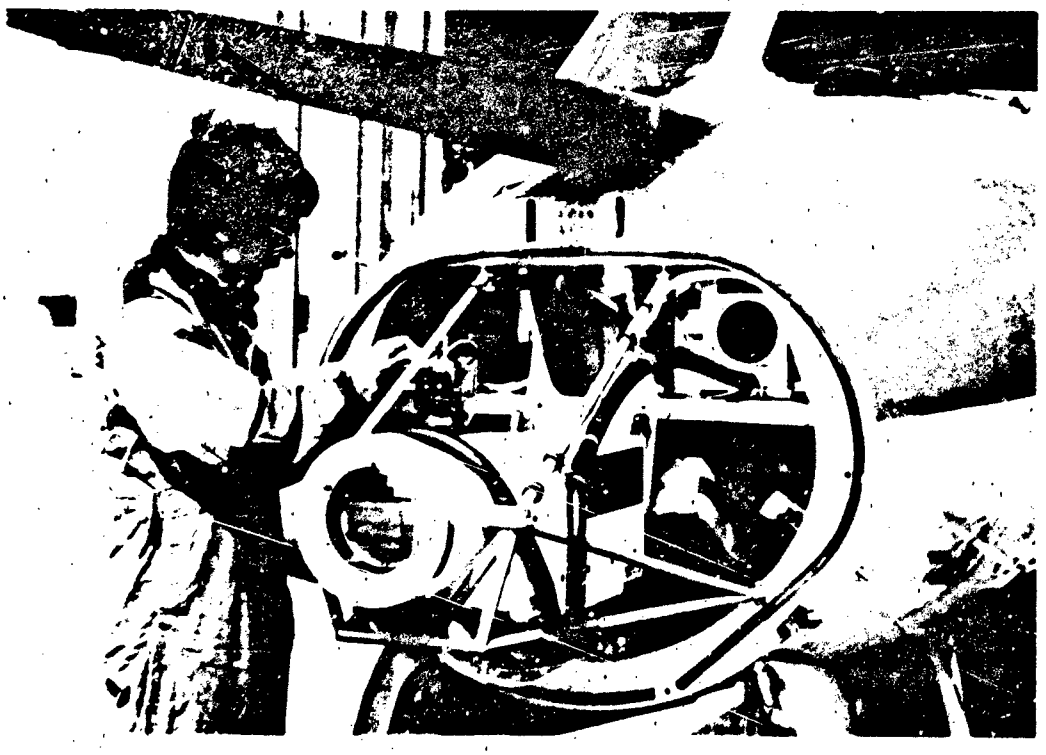

Fig. 4 The Optics Head mounted in the nose of the HS125 trials aircraft of Flight Systems Department, RAE Bedford.

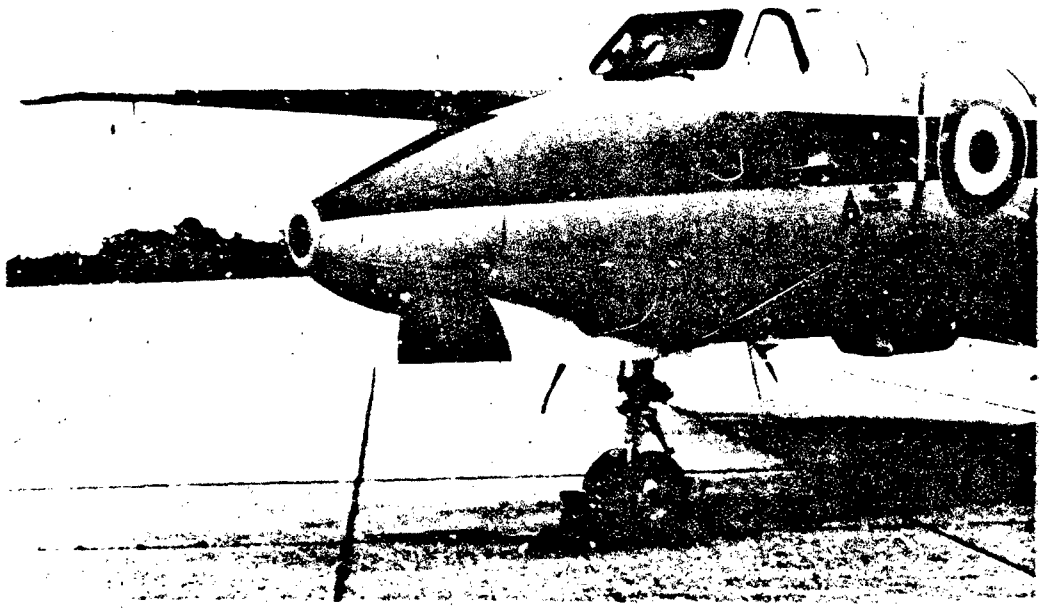

Fig. 5 The HS125 aircraft showing the nose cone and 20 cm diameter germanium window. See also fig. 8.

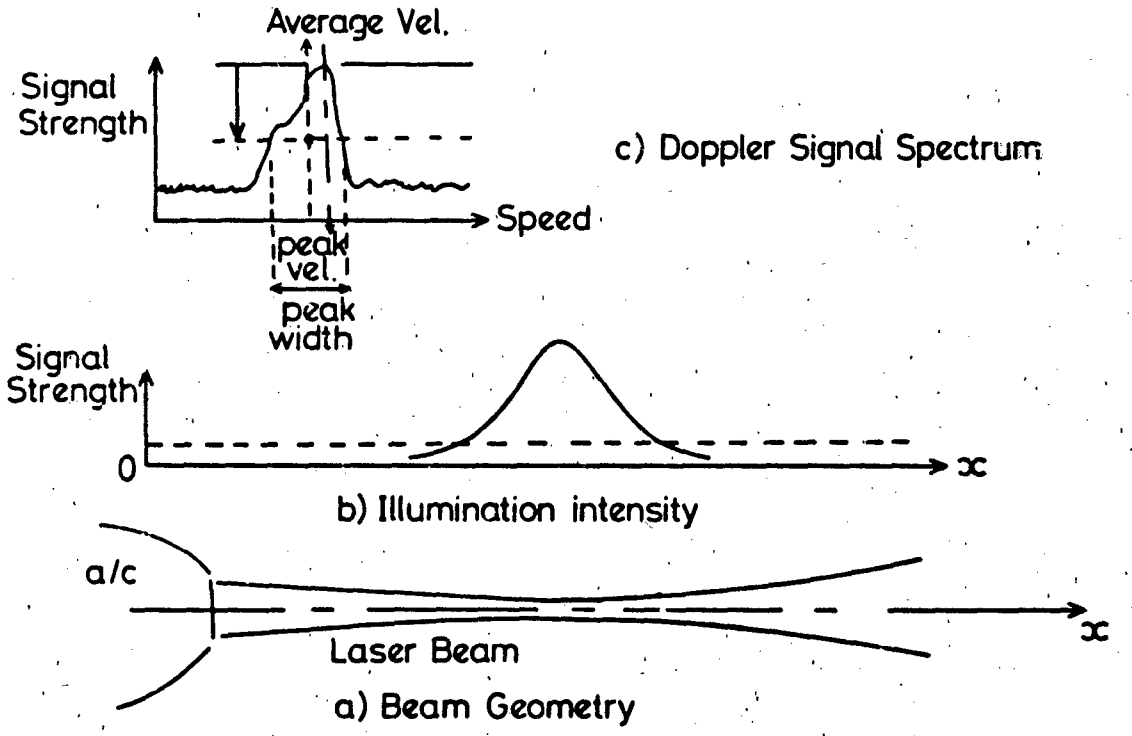

Fig. 6 Parameters of a focussed CW laser anemometer showing schematically the laser beam, the illumination, and Doppler spectrum.

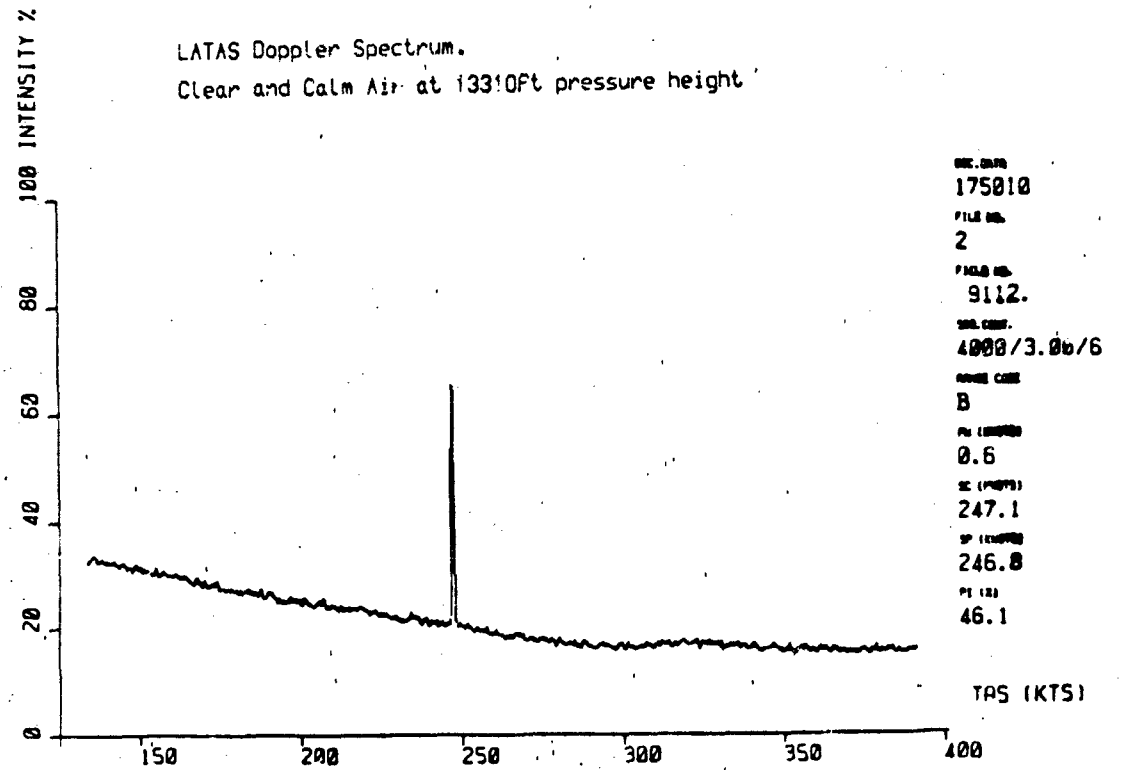

Fig. 7 LATAS Doppler spectrum in clear and calm air at 13310 ft pressure height. Note the narrow Doppler signal with peak corresponding to a true airspeed of 246.8 knots.

Fig. 8 The nose cone of the HS125 aircraft showing the germanium window and diamond-like hard coating (supplied by Barr and Stround), after two years of flying. The nose cone shows considerable surface abrasion after about 30 flights since repainting.

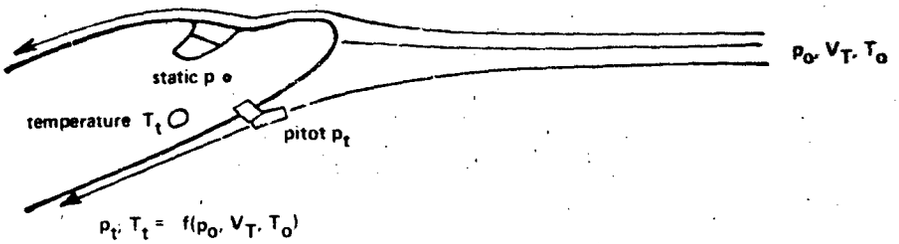

p_t, T_t = $f(p_o, V_T, T_o)$

$p \sim p_o$, $(p-p_o) = f(p_o, V_T, T_o$, flow direction, aircraft shape)

CALIBRATION OF $(p-p_o)$

Present Method: Compare pressures after correcting for Δh

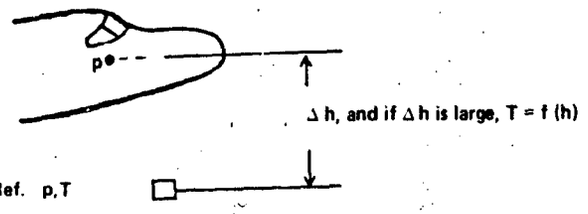

LATAS Method: $p_o = p_t \left\{ 1 - (V_T/87.13)^2/T_t \right\}^{3.5}$

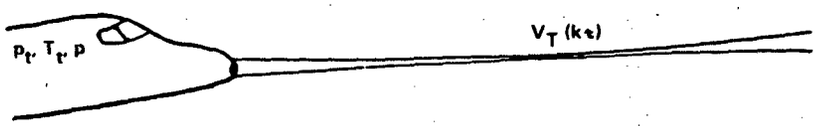

Fig. 9 Calibration of pressure error $(p-p_o)$; comparison of present method and LATAS method.

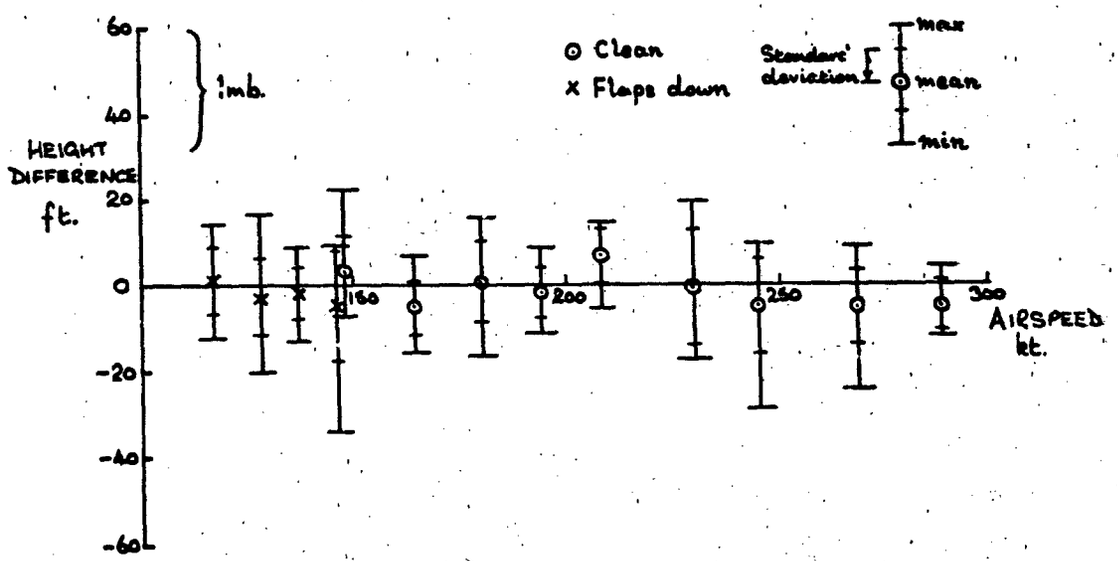

Fig. 10 Comparison of LATAS and kinetheodolite pressure height. "Tower fly-by" tests.

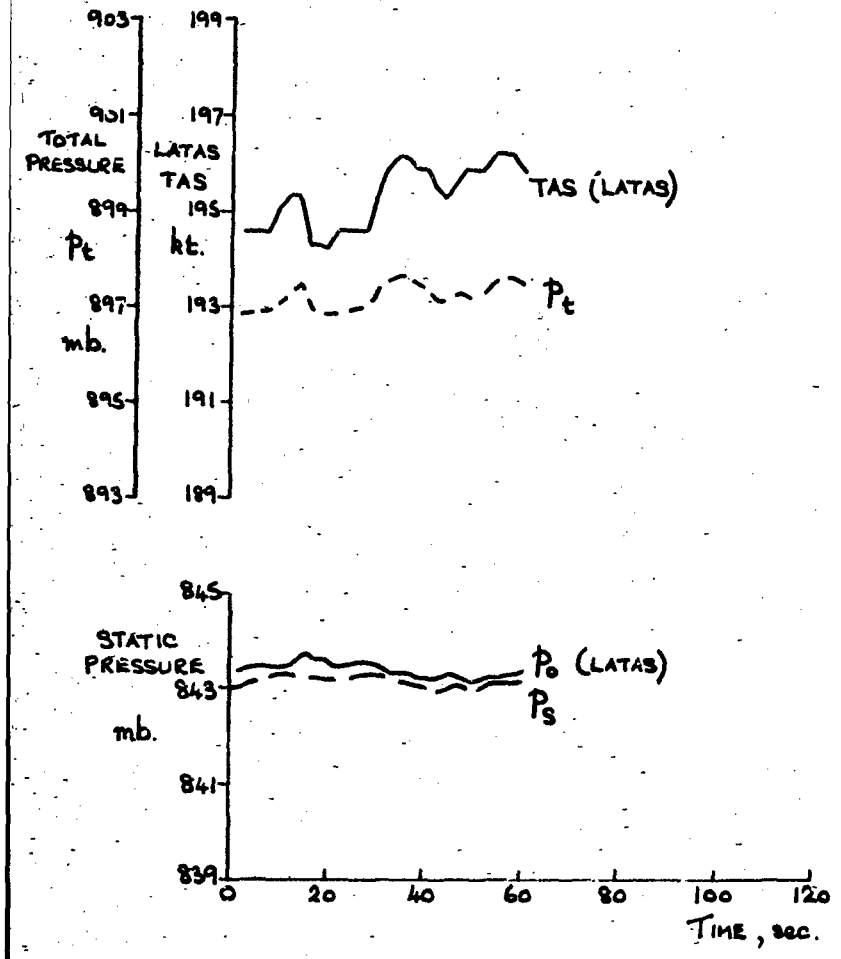

Fig. 11 Time history of recorded data and derived static pressure. 19000 ft altitude and negligible turbulence.

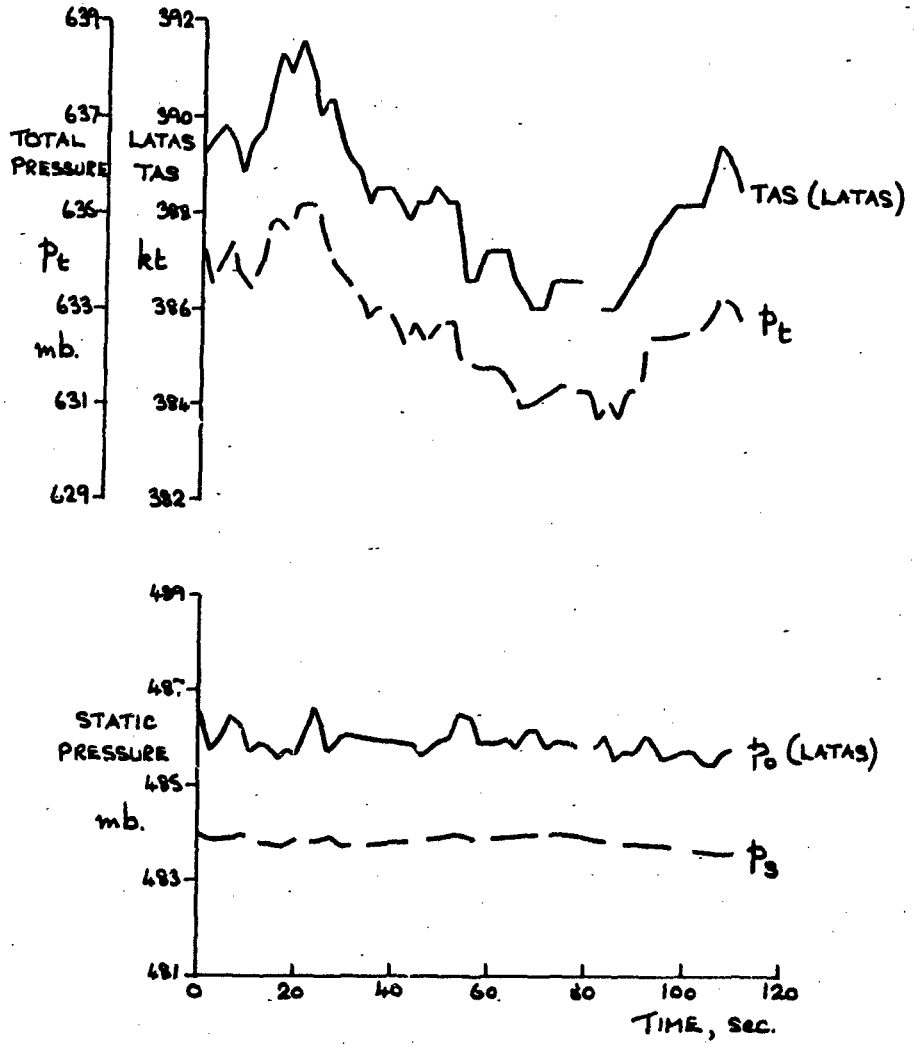

Fig. 12 Time history of recorded data and derived static pressure. 19000 ft altitude and detectable clear air turbulence.

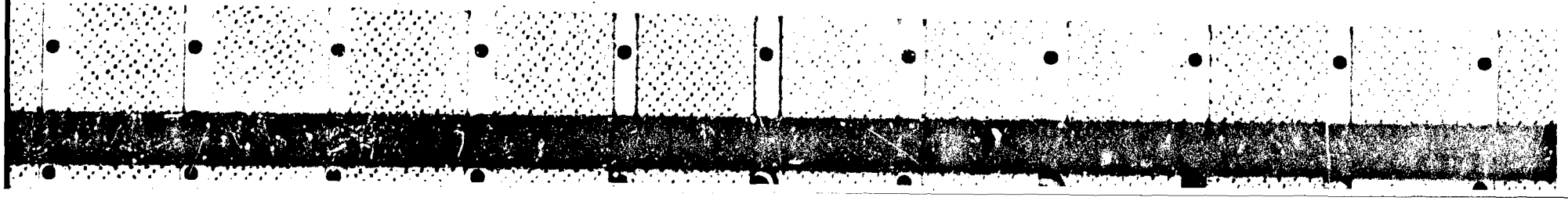

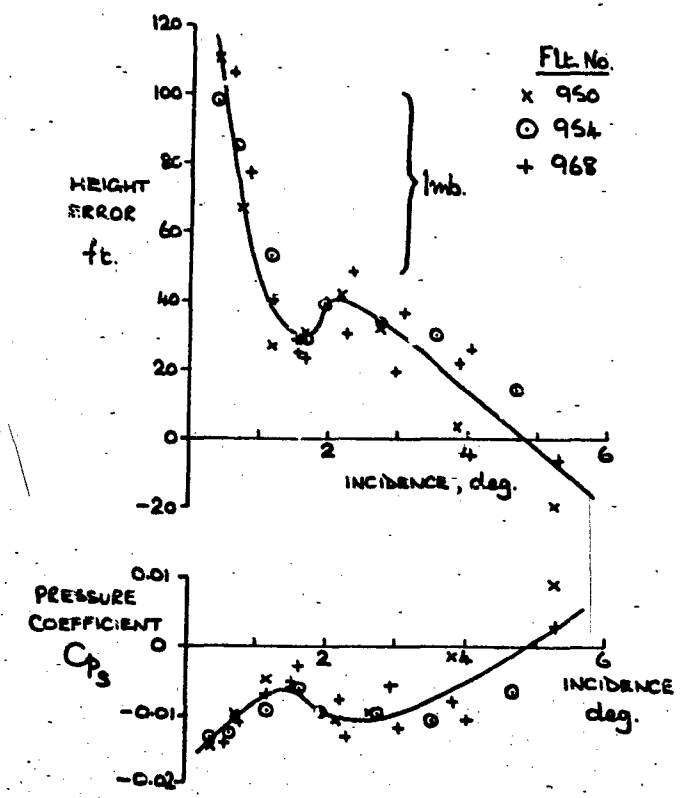

Fig. 13 HS125 pressure errors at 20000 ft measured by on-board LATAS.

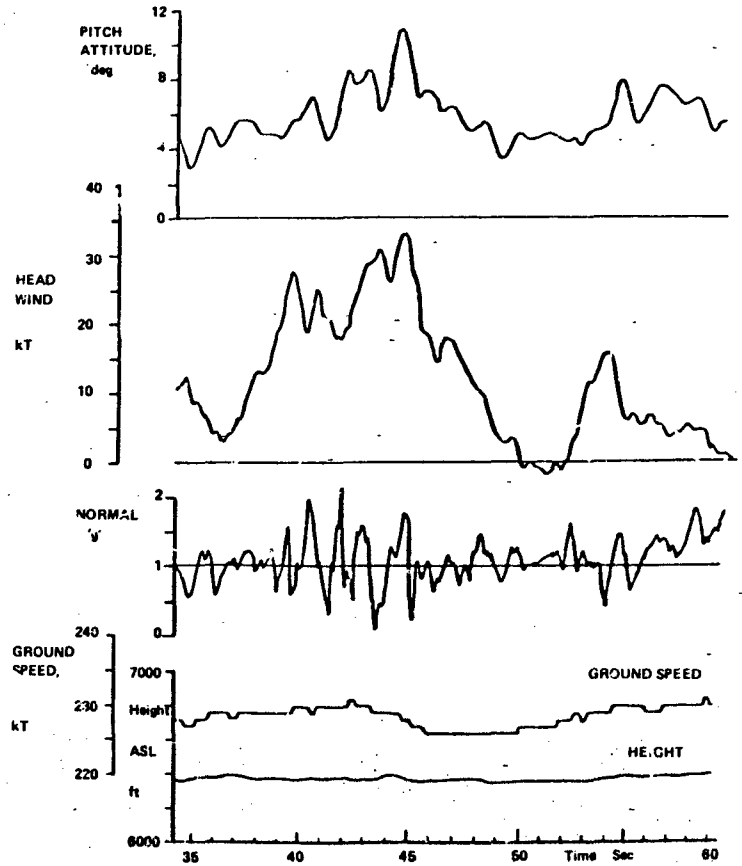

Fig. 14 Passage through a thunderstorm microburst recorded at the JAWS project in Colorado (Flight 792, pm 14 July 1982, run 3).

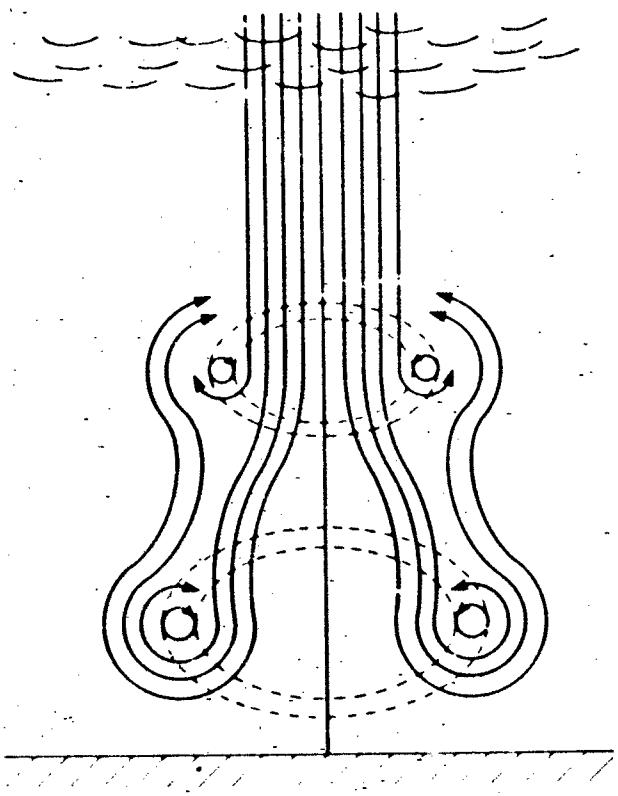

Fig. 15 Vortex model of a microburst showing streamlines.

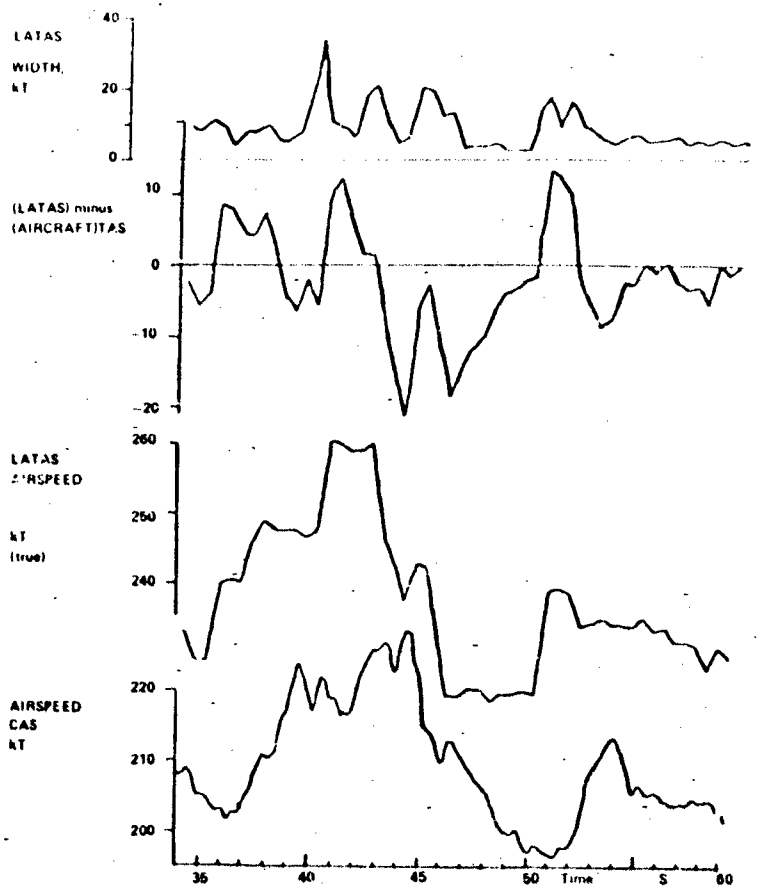

Fig. 16 Passage through a thunderstorm microburst showing the response of the RAE/RSRE LATAS system. (Flt 792, pm 14 July 1982, run 3, JAWS project). Note the 2 sec lead (corresponding to ~ 250m) of the LATAS airspeed.

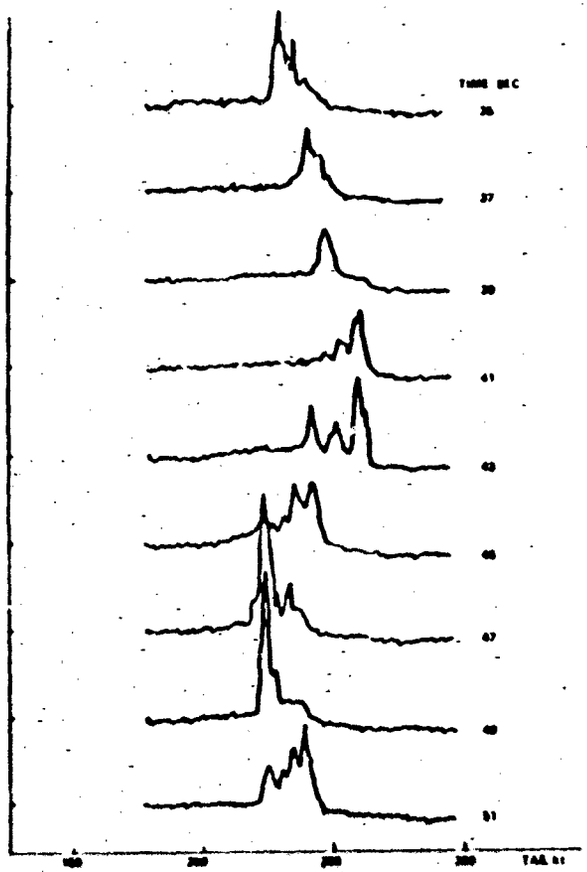

Fig. 17 Successive LATAS Doppler spectra on passage through a thunderstorm microburst. The reference times are the same as for figures 14 and 16 (Flt 792, pm 14 July 1982, run 3).

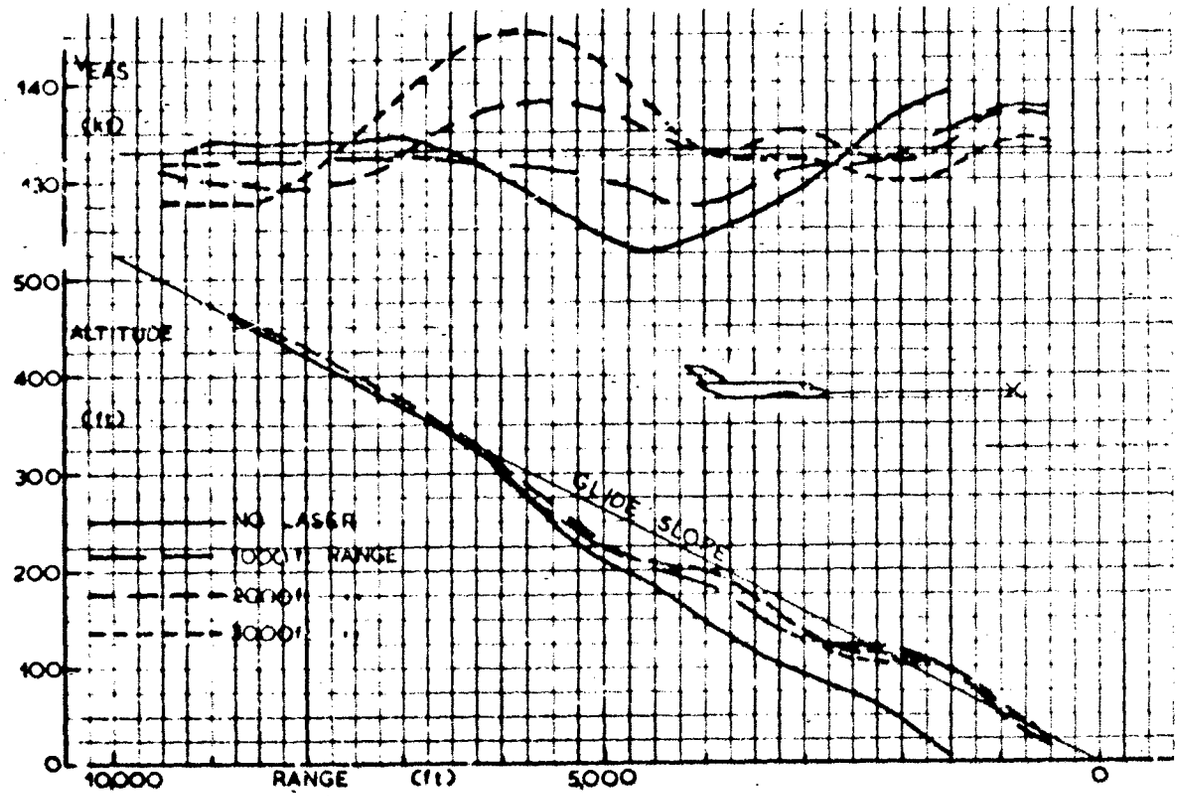

Fig. 18 Flight simulations of a coupled approach through thunderstorm windshear, for a BAC 1-11 medium jet transport, with and without LATAS type advance warning from different ranges. The thunderstorm cell was set at 4,500 ft range, and offset 1500 ft.

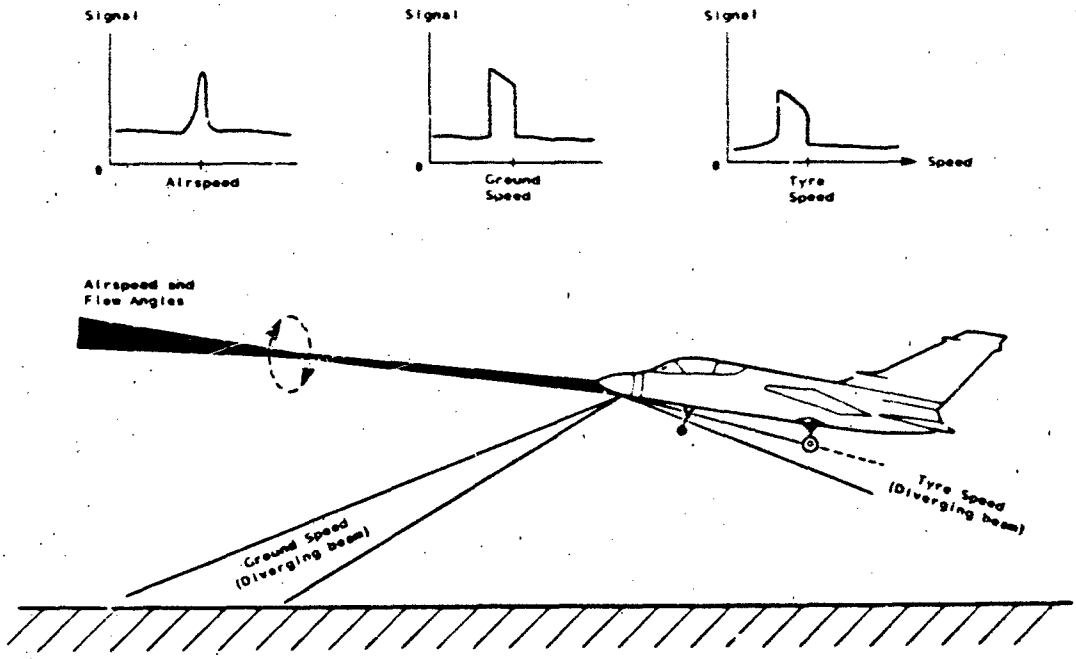

Fig. 19 CW Laser Doppler system for airspeed, ground speed and tyre speed.

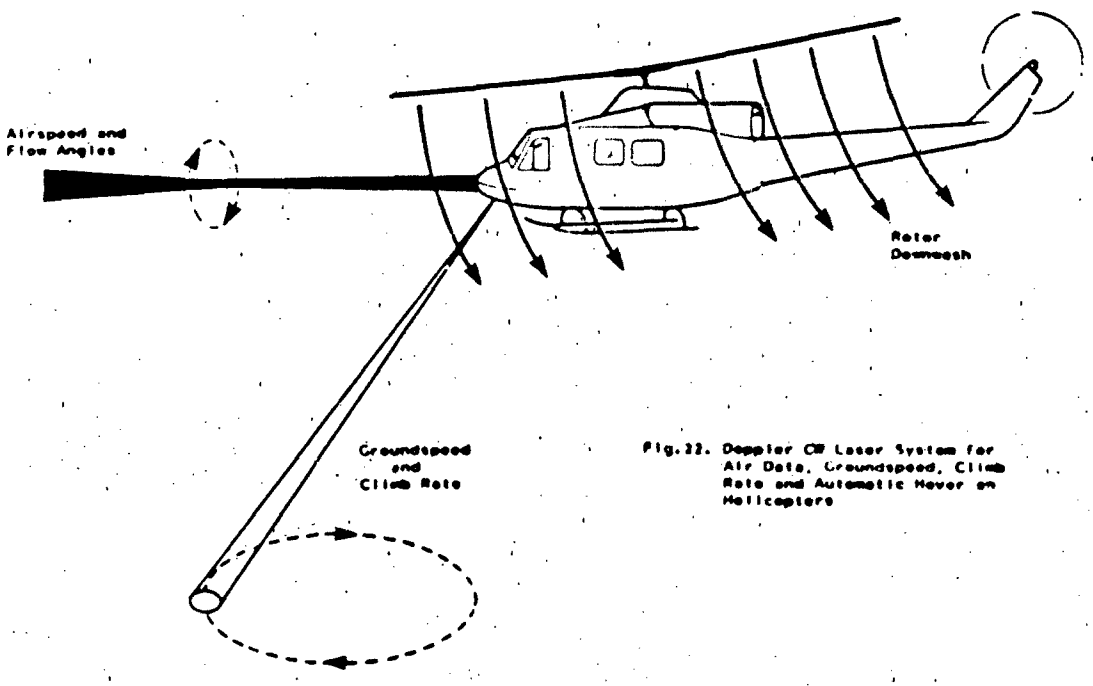

Fig. 20 CW Laser Doppler system for air data, ground speed, climb rate and automatic hover on helicopters.

Fig.22. Doppler CW Laser System for Air Data, Groundspeed, Climb Rate and Automatic Hover on Helicopters

NAVSTAR GPS APPLICATIONS TO TEST AND TRAINING

Kingston A. George and John B. McConnell
Air Force Western Space and Missile Center (XRQ)
Vandenberg Air Force Base, California 93437

ABSTRACT

This paper summarizes a fifteen-month study on the uses of the NAVSTAR Global Positioning System (GPS) at the National Ranges operated by the United States Army, Navy, and Air Force for weapon system development, test, and training. It was conducted by a special triservice committee chartered by the Office of the Undersecretary of Defense for Research and Engineering. The primary objectives were to evaluate GPS application areas, identify and analyze technical issues, and recommend cost- and mission-effective applications.

The study found that GPS technology will have a wide variety of use at the ranges with significant cost advantages and that the technical issues, some of which are quite challenging, do not pose serious obstacles to widespread employment. It will be necessary to design and develop a new family of GPS receiver hardware for range uses since the current generation of receivers does not satisfy the accuracy, data rate and continuity, and size demands of the typical range environment. The study provided the family definitions for GPS range equipment and the basis for a joint-service development program under Air Force direction at Eglin AFB, Florida.

INTRODUCTION

The NAVSTAR Global Positioning System (GPS) is a three-dimensional navigation system that will employ eighteen satellites in circular 20,200 kilometer (12 hour period) orbits (Figure 1). By listening to four or more satellites, users of GPS can derive position, velocity, and time with high precision and uniform accuracy on a global basis(1). NAVSTAR GPS is being developed by a triservice Joint Program Office located at the Air Force's Space Division Headquarters in Los Angeles, California. The six satellites presently in orbit provide a few hours each day for equipment development and testing. The operational satellites will be placed in orbit beginning in 1986 and full 24-hour capability will be achieved by late 1988 or early 1989.

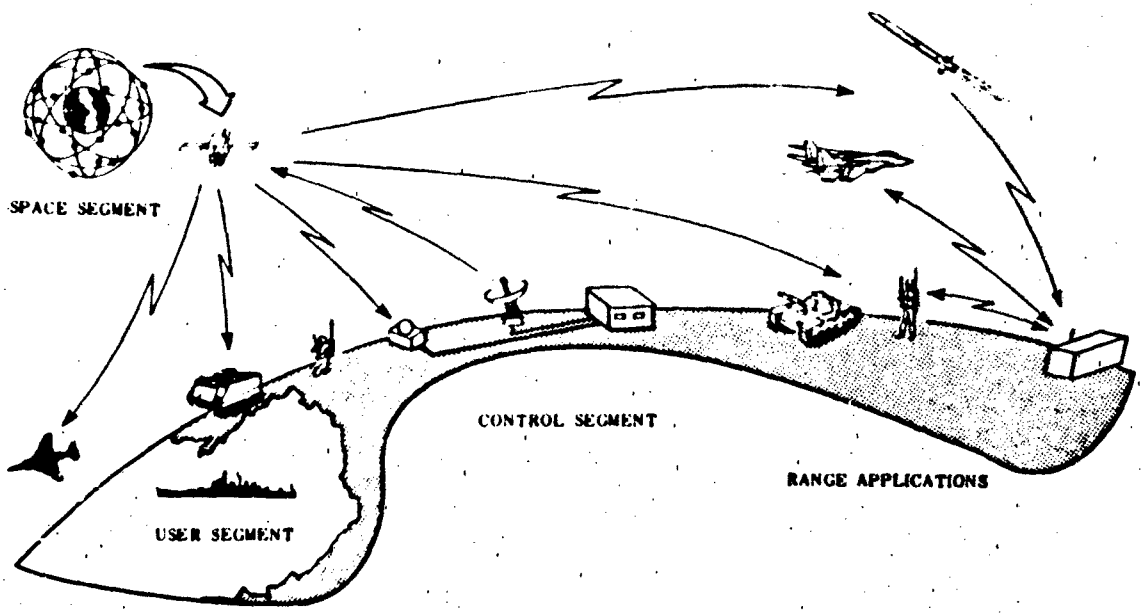

FIGURE 1 NAVSTAR GPS OVERVIEW

The advent of GPS offers a major opportunity for fielding a standardized, cost competitive Time-Space-Position Information (TSPI) system on the national ranges. A GPS-based TSPI system would provide precise and uniform tracking accuracy to unlimited numbers of test articles between the surface and low earth orbit. The individual ranges would have to invest in telemetry data link upgrades and data handling systems, but might be able to avoid the high capital investments of other types of TSPI equipment (phased-array radars, time-multiplexing systems, etc.) in future expansion and improvement programs. On the other hand, there are several significant performance and implementation issues that need to be resolved before the potential benefits of GPS as a test range asset can be realized.

The Department of Defense (OUSDRE/DDT&E) issued a memorandum to the three services in y, 1981 requesting that the Air Force lead a triservice study of GPS applications to st and evaluation ranges and the training ranges. The objectives were:

- Evaluate generic test and evaluation and training requirements for GPS application.
- Identify and analyze the technical problems associated with GPS applications.
- Recommend interim and long-term applications of GPS.

The third objective was expanded during the course of the study to include lentification of a lead organization and development of a management approach to a ng-term equipment acquisition program.

The study committee was organized in September, 1981 with two members each from the my, Navy and Air Force range organizations. A final report was delivered in January, 83(2). The triservice study group has continued to function as an advisory committee the organization selected as the developer of range equipment: the Instrumentation rectorate of the Air Force Armament Division (AD/YI) at Eglin AFB, Florida(3).

NCEPTUAL TSPI EQUIPMENT

TSPI data can be obtained by using onboard GPS receivers or frequency translators. receiver processes the satellite signals and outputs either raw or corrected TSPI data hich can be recorded or transmitted to the ground through a telemetry data link. A anslator receives the GPS signals and retransmits them on a different frequency for tection and processing on the ground. Translators use up telemetry bandwidth rapidly cause at least two megahertz is needed for each simultaneously operating translator. A ceiver system uses less than 100 kilohertz of bandwidth, thus permitting large numbers users to be active at the same time.

Receivers are good candidates for aircraft and test articles with high recovery ates so that the GPS equipment can be reused. Being simpler, smaller, and less pensive than receivers, translators are well-suited for small test articles that are pendable or likely to exhibit a high attrition rate such as missiles and drones. In neral, the type of onboard equipment chosen for a particular application will be ictated by performance requirements, form-fit factors, and costs relative to the test ticle itself.

A range system concept employing a digital translator is shown in Figure 2. The rrier for the retransmitted signal is derived from the translator local oscillator and sed at the receiving site to aid signal tracking and correct translator local oscillator ror(4). Vehicle position and velocity are then estimated using special processing gorithms(5). Both analog and digital translators have been built and tested, thus rifying the concepts(6,7).

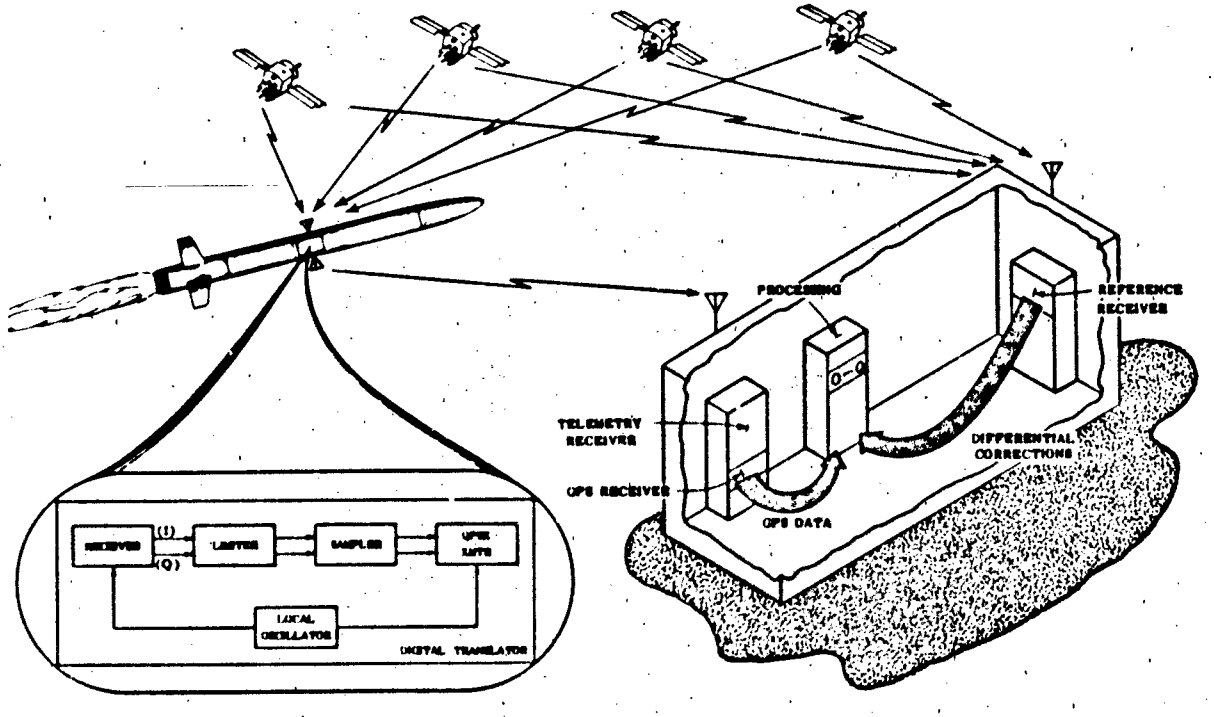

FIGURE 2 TRANSLATOR SYSTEM CONCEPT

In the course of the study, two types of receivers for use on test vehicles were defined(Figure 3): A Low Dynamic Set and a High Dynamic Set. The Low Dynamic unit would be used in applications where output data is required once or twice per second at most and when accelerations are less than 10 meters/sec^2 (infantry, ground vehicles and ships). This Set would operate on the GPS L1 frequency only with two detection channels alternately switched among satellite signals to generate the basic range and range rate data.

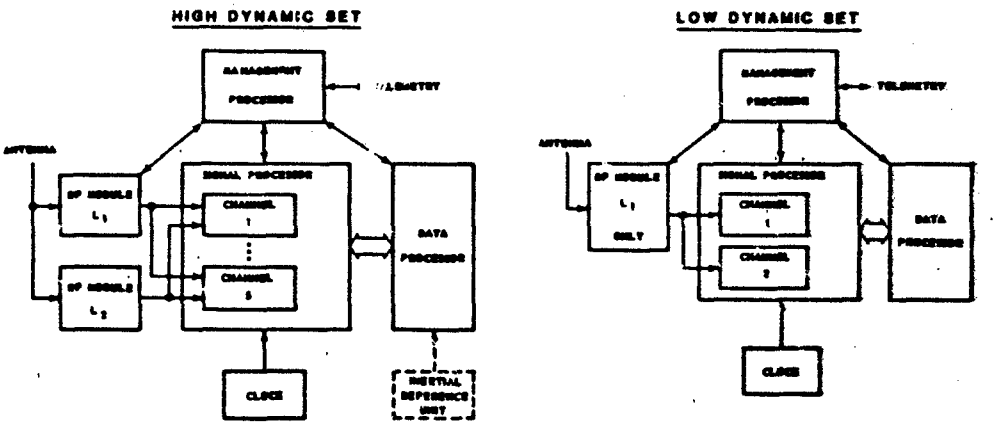

FIGURE 3 INSTRUMENTATION CONCEPTS

The High Dynamic Set would be suitable for vehicles with accelerations up to a maximum of 100 meters/sec^2 (aircraft, helicopters and drones). This unit would operate on both L1 and L2 frequencies, simultaneously track at least four satellite signals and produce new TSPI estimates at rates up to twenty per second corrected for ionospheric delays. In addition to producing absolute TSPI estimates, the High and Low Dynamic Sets could also operate in the differential mode described in the next section.

PERFORMANCE ISSUES

The principal categories of concern with regard to performance are data quality (rate, accuracy, precision and dynamic lag) and data continuity (time-to-first-fix* and data dropouts). Many of the items in these categories are closely allied with the "implementation issues" discussed in the next section.

The TSPI requirements for a wide variety of scenarios and test articles for more than forty service ranges were compiled and analyzed. Based on this compilation, eight idealized (generic) ranges were defined(Table 1) along with typical data requirements (Table 2). Proposed GPS configurations were analyzed to estimate the capabilities of properly designed equipment in the range environment, and a box is drawn around those items in Table 2 that are either stressing for GPS or GPS cannot satisfy. Overall, GPS is effective in meeting most of the requirements and will offer better performance than conventional (non-GPS) systems in many cases.

GENERIC RANGES		ARMY										NAVY					AIR FORCE				
		SMRR	EMP	TPO	EPG	TCATA	CDEC	OTHER TECOM	RTC	BOARDS	PMTC	PMRF	NATC	NOC	APGTF	TRAINING RANGES	EDWC	TPWC	APGTC	NTTR	GULF RANGE TYPE II
TRAINING AND OT&E	AIR	●		●						●	●		●	●				●	●	●	●	
	LAND	●	●	●		●	●		●				●									
	SEA (FIXED)									●	●			●								
	SEA (MOVING)														●							
DT&E AND OT&E	LONG RANGE	●	●			●				●	●		●	●		●	●					
	EXTENDED RANGE	●	●																			
	SHORT RANGE (LAND)	●		●	●	●	●	●	●	●			●					●	●	●	●	●
	SHORT RANGE (WATER)		●							●	●	●		●	●	●	●				●	

TABLE 1 GENERIC RANGE RELATIONSHIPS TO DOD RANGES

*Elapsed time from set initialization to subsequent output of accurate TSPI data.

TEST PERFORMANCE PARAMETERS	TRAINING AND OT&E				DT&E AND OT&E			
	AIR	LAND	SEA (FIXED)	SEA (MOVING)	LONG RANGE	EXTENDED RANGE	SHORT RANGE (LAND)	SHORT RANGE (WATER)
REALTIME ACCURACY - POSITION (M) - VELOCITY (M/SEC)	[3] - 60 0.03 - 5	5 - 9 1 - 3	60 30	300 - - -	6 - 30 0.2 - 2	[2] - 6 2	[2] - 30 0.3 - 7	[2] - 30 0.3 - 7
DATA RATE (#/SEC)	1 - 20	1 - 10	5	1 - 5	20	20	1 - [100]	1 - 20
POST TEST ACCURACY - POSITION (M) - VELOCITY (M/SEC)	[0.3] - 60 0.03 - 5	[2] - 10 1 - 3	[-] 0.03 - 2	TBD - - -	[3] - 6 [0.003] - 0.03	10 [0.003] - 0.006	[0.6] - 5 0.03 - 3	[0.6] - 5 0.03 - 3
SCORING (M)	[0.3 - 3]	[0.3 - 2]	- - -	- - -	15	[0.3]	[0.3 - 2]	[0.3 - 2]
NUMBER OF TEST ARTICLES	1 - 90	2 - 2000	50	60 - 125	3 - 10	1	12 - 20	12 - 20
COVERAGE - ALTITUDE (KM) - DISTANCE (KM)	0.3 - 30 60 X 110	0 - 3 60 X 60	0.03 - 15 140 X 140	0 - 20 650 X 930	90 280 X 9260	0.03 - 9 190 X 1100	0 - 30 90 X 280	0 - 30 230 X 370

[ ] STRESSING FOR GPS [ ] GPS CANNOT SATISFY

TABLE 2 TSPI REQUIREMENTS SUMMARY

The GPS error budget is dominated by systematic errors in satellite location and nal transmission delays through the ionosphere. These systemic errors can be readily ibrated using a GPS reference receiver at a surveyed site to compute differential rections(Figure 4). The corrections can then be used in real-time or recorded for t-flight data improvement. A test program is underway to determine the size of the ion around the reference receiver for which the corrections are valid, with liminary findings that the minimum radius is probably greater than several hundred ometers.

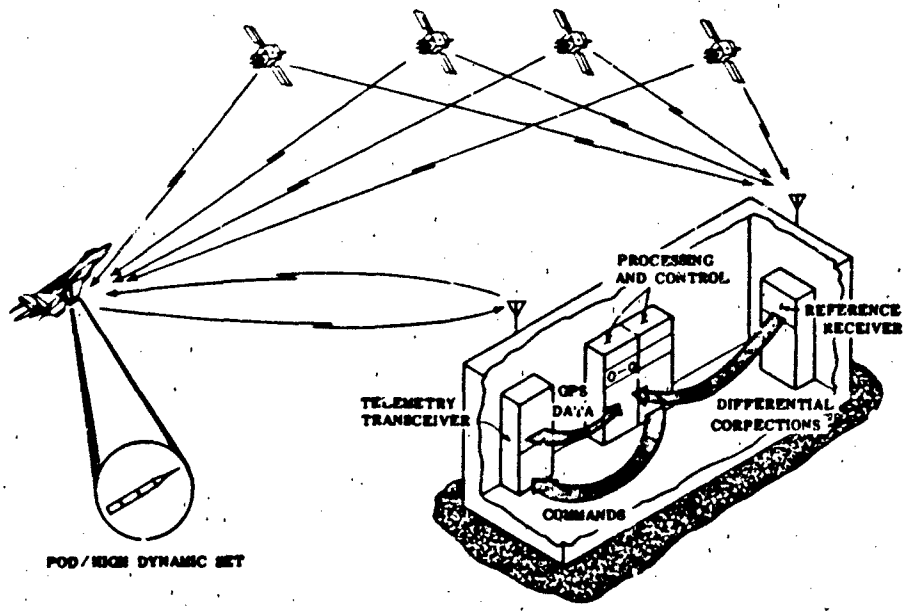

FIGURE 4 POD SYSTEM CONCEPT

Each GPS satellite transmits a navigation signal containing a precise(P) code and a ar/acquisition(C/A) code. Expected TSPI accuracies for authorized users of these es are shown in Table 3. The P-code is significantly better for absolute position and ocity determination but in the differential mode (using a P-code reference receiver) n codes provide essentially equivalent velocity accuracies with the P-code being only ghtly better for position determination(8). Since P-code is less susceptible to tipath errors and since P-code receivers are only slightly more complex and costly, P- e is recommended for receiver applications. The C/A code is selected for translator lications because significantly less bandwidth is required (2 megahertz vs 20 hertz).

		ABSOLUTE		DIFFERENTIAL	
		P-CODE	C/A CODE	P-CODE	C/A CODE
REALTIME	POSITION (M)	14	30*	8	18
	VELOCITY (M/S)	0.2	1*	0.04	0.04
POST MISSION	POSITION (M)	7	30*	6	7
	VELOCITY (M/S)	0.1	1*	0.04	0.04

CONDITIONS: APPROXIMATE THREE DIMENSIONAL RSS ERROR, PDOP = 3
POINTWISE SOLUTIONS (1 Hz POSITION, 10 Hz VELOCITY)
NO MULTIPATH ERRORS OR UNCOMPENSATED DYNAMICS
* NO IONOSPHERIC REFRACTION CORRECTION

TABLE 3 EXPECTED GPS TSPI ACCURACY

The performance of current receivers with respect to data continuity is not isfactory for applications on the ranges. The time-to-first-fix must be reduced from nutes" to a few seconds, and reacquisition after signal loss (for example, when an craft banks and masks the GPS antenna) lowered to a fraction of a second. Three hniques have been proposed to improve data continuity. First, rapid signal uisition methods have been defined and are being tested(9). Secondly, an inertial erence unit integrated with the GPS receiver could provide data through a masking iod and assist the receiver tracking loops to quickly reacquire. Lastly, fixed ground ulated satellites, "pseudolites", at key locations could reduce or eliminate outages. ever, pseudolites may present interference and signal capture problems due to the ge differences in signal strength with the satellites.

LEMENTATION ISSUES

The key implementation issues concern the cost-effectiveness of a GPS approach pared with existing instrumentation systems, and the future integration of GPS ipment at the ranges. The generic ranges were analyzed from a cost-benefit standpoint uming future evolution of both non-GPS and GPS equipment suites(10). The "Mobile Sea" ge was omitted because a fully developed system at sea did not exist and comparative ts could not be obtained. Figure 5 shows the twenty year life-cycle cost results for remaining seven generic ranges, all normalized to a hypothetical present day k-cost baseline. In other words, the cost comparison was done from the present time ward assuming an existing suite of non-GPS instrumentation that must be maintained, rated, modernized, and improved in future years.

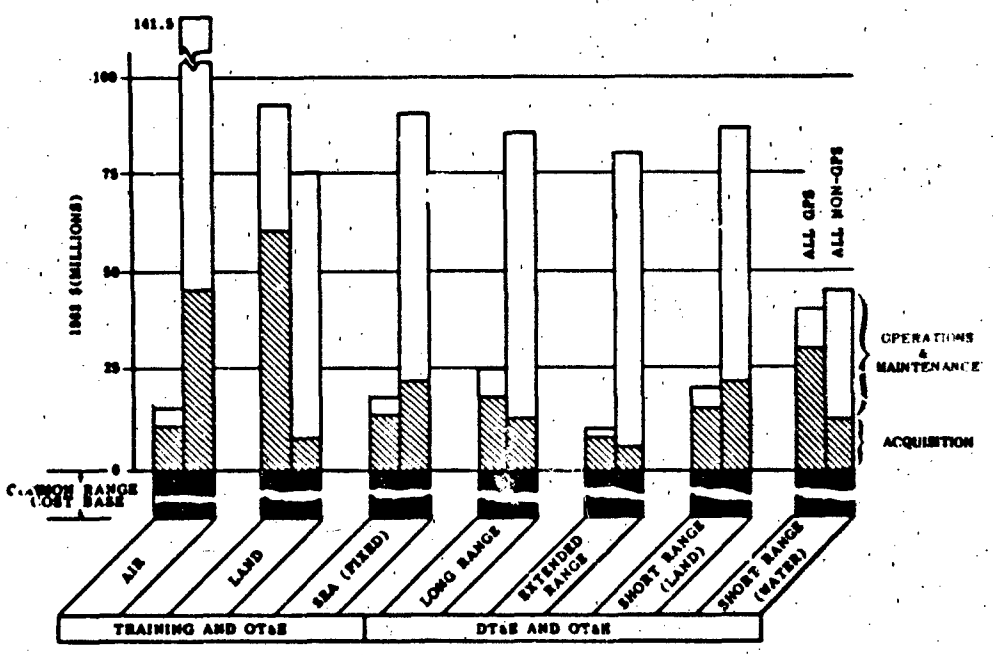

FIGURE 5 DIFFERENTIAL LIFE CYCLE COST SUMMARY

The analysis assumed "very extensive" use of GPS and "practically no" use of GPS, le neither extreme will actually occur. Further, the generic ranges are idealized resentations, while the real-world ranges combine the functions of several generic ges in one geographic location. A far more extensive investigation would be required nap these "generic" savings back into the 40-odd existing ranges to arrive at a total savings. However, an estimate of the bounds of savings was derived by several roximate methods. The results indicate the potential overall cost savings to the DOD, en that the appropriate equipment is developed in a timely fashion, are certainly in ess of $300 million and may approach $1 billion over the twenty year life-cycle cost iod.

As an aside, the "Land Training and OT&E" range is the only generic range which does favor GPS over non-GPS. This partially reflects the conservative nature of the ulations, since the higher values of GPS cost estimates and the lower values of ventional systems were used. Further, the costs of GPS receivers are expected to fall idly over the next few years as new integrated circuit chips are developed, hence this e-cycle cost comparison may be overly conservative.

There are also technical issues associated with implementing GPS on the ranges. For ple, TSPI systems with different telemetry bands, power levels, and modulation are on the various ranges, and appropriate provisions would have to be made to modate these differences. The development of the family of range equipment could be mplished in a modular fashion so that different telemetry transmitters, for ihstance, d be interfaced with the receiver. Similarly, provisions could be made to add an tial reference unit, use different preamplifiers with various antenna arrangements, change the shape factor within certain limits to fit various test articles. The lidates for development are shown in Table 4. The Advanced High Dynamic Set is a ier development risk; however, recent data from manufacturers of GPS equipment suggest GPS receivers of 1600 cc in volume or smaller are feasible in the next few years. rly, a smaller receiver could be used in more applications in the range environment.

	KEY FAMILY MEMBERS	VOLUME (CC)	TEST ARTICLES
NEAR-TERM TECHNOLOGY	LOW DYNAMIC SET	3000-4000	INFANTRY GROUND VEHICLES SHIPS
	HIGH DYNAMIC SET	5000-6000	AIRCRAFT HELICOPTERS DRONES (FULL SCALE)
	TRANSLATOR	500-1500	MISSILES DRONES (SUB SCALE)
GROWTH OBJECTIVE	ADVANCED HIGH DYNAMIC SET	~ 1600	AIRBORNE

TABLE 4 INSTRUMENTATION DEVELOPMENT CANDIDATES

Though not part of the family development, two other types of GPS receivers are rtant to the test range community. Timing receivers, which are commercially lable today, are competitive in price and accuracy with atomic standards and are ady in use. Geodetic receivers capable of providing surveys to a precision of a few imeters are presently being tested(11).

ARY

The potential benefits of GPS as a source of Time-Space-Position Information (TSPI) been established and the Department of Defense has initiated a development program r Air Force auspices at Eglin Air Force Base in Florida. A family of GPS equipment being developed consistent with that proposed by the triservice study group and fly described in this paper. There are several performance and implementation issues to be resolved, but none appear to pose serious obstacles to widespread applications PS on the ranges.

The present GPS user equipment is not suitable as-is for the majority of uses on the es since it was not designed to satisfy range requirements for data quality and inuity, and is not compatible with existing range data systems. However, appropriate instrumentation for range use can be developed with available technology. The all cost avoidance is very difficult to estimate, but is believed to be several reds of millions of dollars for the combined range activities in the Department of nse over the next twenty years.

?ERENCES

GPS NAVSTAR User's Overview; Deputy for Space Navigation Systems, NAVSTAR Global sitioning System Joint Program Office, PO BOX 92960, Worldway Postal Center, Los geles, California 90009, September 1982; Document YEE-82-009.

Kingston A. George, et al; Prepared by the Western Space and Missile Center (XRQ), denberg AFB, California 93437 for the Office of the Undersecretary of Defense search and Engineering Deputy Director of Test and Evaluation; GPS Range Applications dy Final Report, January 1983 (No reference number).

Thomas P. Hancock; Air Force Systems Command Armament Division; Tri-Service nagement Plan for the Development and Acquisition of GPS Range Equipment; Proceedings the IEEE 1983 National Telesystems Conference, November 1983; IEEE Catalog Number 83CH 75-2, pp 182-186.

John B. McConnell, Robert B. Pickett; Western Space and Missile Center and Federal ctric Corporation; GPS Translator Tracking System Implementations at the Test Ranges; ceedings of the IEEE 1983 National Telesystems Conference, November 1983; IEEE Catalog ber 83CH 1975-2, pp 239-245.

Richard A. Brooks; Trajectory Estimation Using Translated GPS Signals; Proceedings of IEEE 1983 National Telesystems Conference, November 1983; IEEE Catalog Number 83CH 75-2, pp 246-253.

T. Thompson; Johns Hopkins University Applied Physics Laboratory; Performance of the RACK/Global Positioning System Trident Missile Tracking System; Proceedings of the E 1980 Position Location and Navagation Symposium; IEEE Catalog Number 80CH 1957-4, 445-449.

Larry L. Warnke, Edwin E. Westerfield; Johns Hopkins University Applied Physics oratory; Use of GPS for Determining Position of Drifting Buoys; Proceedings of the E 1983 National Telesystems Conference, November 1983; IEEE Catalog Number 83CH 75-2, pp 209-213.

Richard A. Brooks, et al; Prepared by Federal Electric Corporation for the Western ce and Missile Center (XRQ), Vandenberg AFB, California 93437; GPS Error Budgets, uracy, and Applications Considerations for Test and Training Ranges, December 1982; C TR82-2.

E. D. Holm, E. E. Westerfield; Johns Hopkins University Applied Physics Laboratory; PS Fast Acqusition Receiver; Proceedings of the IEEE 1983 National Telesystems ference, November 1983; IEEE Catalog Number 83CH 1975-2, pp 214-218.

Harold Jones, et al; Prepared by The Analytical Sciences Corporation for the Air ce Western Space and Missile Center; GPS Range Applications Study Final Report; December 1982, WSMC TR82-3.

M. L. Sims, C. R. Griffin; Naval Surface Weapons Center and Applied Research oratory; GPS Geodetic Receiver System Testing; Proceedings of the IEEE 1983 National esystems Conference, November 1983; IEEE Catalog Number 83CH 1975-2, pp 415-419.

AN EXTENDED REAL-TIME MICROWAVE AIRPLANE POSITION SYSTEM

P. L. Pereboom J. H. Lincoln R. N. Snow
Boeing Commercial Airplane Company
PO Box 3707 Mail Stop 24-71
Seattle, Washington 98124 USA

IARY

eal-time Microwave Airplane Position System (MAPS) is currently being used by The ng Company for noise certification testing. The system measures ranges and range es from several ground transponders to an airplane, and computes the airplane tion using a Kalman Filter algorithm. Airplane position relative to a fixed earth dinate system is available for recording and cockpit display five times per second.

arisons of position data from MAPS with data from Boeing photo-theodolite systems shown that MAPS accuracy is better than two meters when the airplane is within the gn envelope of the ground transponder array. Unfortunately, the minimum practical tude of a design envelope is 50 meters, so MAPS cannot be used for takeoff and ling tests.

bridge the gap from the ground to 50 meters altitude, an alternate source of tude information is required. The problems of obtaining absolute altitude rmation from other sources have been well documented. Radio altimeters are depen- on smooth, hard reflective surfaces, and measure only the local altitude above nd level. Pressure altimeters are dependent on the whims of Mother Nature. tial Reference Unit (IRU) altitude is not accurate enough for performance data over time periods because of biasing from the double integration of accelerometer rs. However, radio altimeters give excellent altitude information when over a ay, pressure altimeters give an excellent indication of a local change in altitude, an IRU is an excellent source of vertical speed data.

report examines the inclusion of these alternate sources of altitude data in the an Filter used by MAPS. Filter initialization was modified to include the ulation of bias errors found in the other sources derived from the original er's estimate of airplane location. The measurement matrix was expanded to include alternate sources in a manner that places emphasis on the most reliable sources of with respect to the airplane's location.

exterded filter was verified through computer simulations, which provided a direct ure of the effects of the filter on the output data. Comparisons of "true" tion, original filter output and enhanced filter output were made to determine e effects. Actual flight data that had been recorded during previous testing was introduced to the filter for comparison with the original filter and with photo-dolite data.

ACE

e position data collected by Boeing Flight Test during airplane development and ification testing has historically depended upon photo-theodolite systems. How-, in 1981 Boeing acquired a microwave system that provides accurate position data an airplane is at least 50 meters above the ground. The Kalman Filter algorithm by the system was extended to allow altitude and altitude rate input from an pendent source. This extension broadened the flight regime of the system to also ude the space from ground level to 50 meters above ground level.

extended system was developed using simulated microwave and altitude input. It was analyzed and verified using both simulation and actual flight data. Data from e flight tests including three approaches, five flybys, and two takeoffs of Boeing and 767 airplanes were used during the verification. Comparisons of airplane tion given in X, Y, Z coordinates were made from data collected from the microwave em, the extended microwave system, and the photo-theodolite systems.

results from the comparisons show that the Extended MAPS provides output position that is not restricted to a particular altitude regime, and is within one meter of actual airplane position at least 90% of the time.

GROUND

of the space position data obtained at Boeing Flight Test involves gathered data ltitudes from 0 to 1000 meters at surveyed test ranges from two to ten kilometers . Prior to acquisition of the Microwave Airplane Positioning System (MAPS), most tion data was obtained using one of two photo-theodolite systems. The Airplane tion and Attitude Camera System (APACS) uses a forward looking camera mounted near

front of an airplane to take time coordinated pictures of airport runway lights to rmine the airplane's position and attitude when the runway lights are in the field iew of the camera. A down-looking camera system takes pictures of surveyed targets testing requirements preclude the use of runway lights. APACS is the most rate positioning system available, but the use of runway lights limits the range of to 100 meters altitude while the lights are in view. The down-looking camera em has a practical altitude range from 20 to 1000 meters and requires extensive e setup prior to testing. Both of these systems require a considerable amount of -test processing before confirming that test requirements were accomplished.

primary use of the down-looking camera system is noise certification testing use of the time and expense associated with noise testing, real time data and pilot ance information became a priority item when test planning began for the 757 and airplanes. The results of a study of real time space position possibilities cated that a microwave ranging system would fulfill the accuracy requirements and w a good measure of flexibility and portability. The MAPS was built for The Boeing any by the Cubic Corporation in 1981.

is used to provide accurate real time and post test position data for noise certi- tion testing. It determines airplane position from ranges and range rates measured 3 to 11 ground transponders placed at surveyed locations on a test range.

ire 1 illustrates the equipment included in MAPS. After an initialization period system enters a 200 millisecond output cycle, which includes eight 25-millisecond it cycles. The operation of the system as the output cycle proceeds is outlined)w.

Based on the latest position estimate, the computer selects eight transponders that will provide the best position solution at the end of the cycle.

Eight input cycles are performed; one for each of the selected transponders. During each input cycle the following operations take place:

* The computer instructs the interrogator to obtain data from a specific transponder.
* The interrogator encodes the transponder identification and sends a signal to the transponders.
* The transponder with the proper code returns a signal to the interrogator.
* The interrogator decodes the return signal and passes range and range rate values to the computer.
* The computer applies calibration and atmospheric corrections to the data and, through use of a Kalman filter, updates the estimated airplane position and extrapolates an estimate for the next input cycle.

The computer sends the extrapolated position to the pilot's display for airplane guidance and the updated position to a tape recorder for post-test analysis.

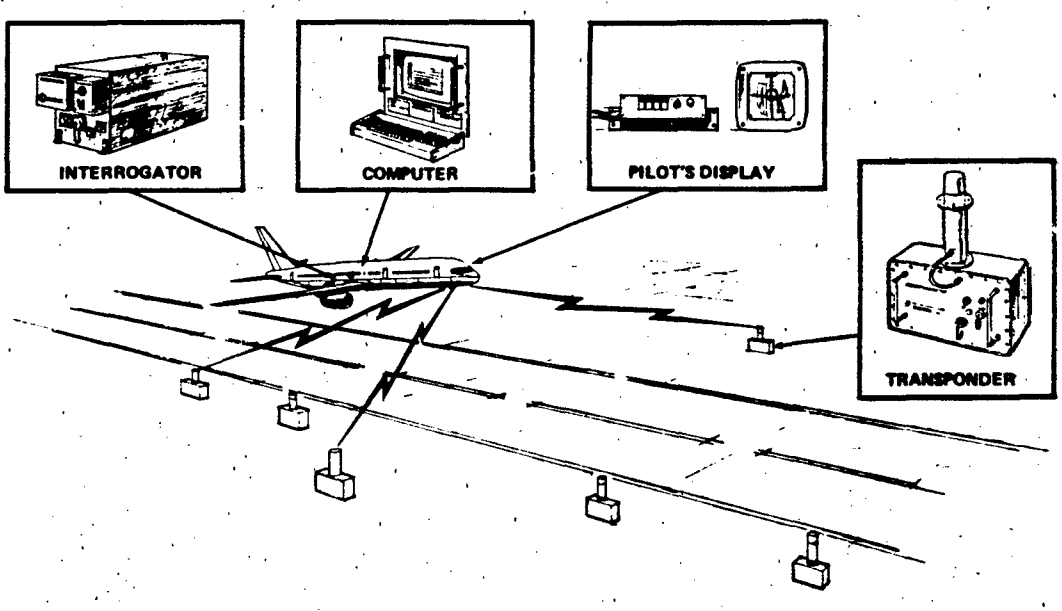

Figure 1. Microwave Airplane Positioning System Components

arison data were generated using both APACS and the down-looking camera system ng the MAPS acceptance test; an automatic approach test using a Boeing 737; and the e certification test of the 767. The results of these tests indicated that MAPS ut is within two meters of the true position at least 95 percent of the time at tudes above 50 meters. The 50 meter minimum altitude results from the combination he geometric dilution of precision (GDOP) inherent in geometrical systems, and the tical limit on the number of ground transponders deployed.

oon as the usefulness and accuracy of the system was recognized, a study began to nd its test regime to the ground using data that is generally available on test raft. If possible, MAPS could then be used for takeoff and landing performance s and multi-segment automatic approach tests.

NSION OF THE MICROWAVE AIRPLANE POSITION SYSTEM

Alternate Sources of Altitude Data

alternate sources of altitude data available on test airplanes are pressure alti-, radio altitude and the inertial reference unit (IRU) altitude. Pressure tude provides accurate, short-term altitude change information. Because of local ations in the atmosphere, there is usually a bias between the pressure altitude e mean sea level and the actual mean sea level altitude, but for short distances, bias may be considered constant. The radio altimeter provides very accurate tude above ground level when measured over a hard surface, but the altitude data mes erratic over grass and trees. Altitude data from the inertial reference unit ot as satisfactory as either pressure altitude or radio altitude, but IRU vertical d is better than those derived from the other systems.

nature of each of the altitude systems determined how they would be included in . After MAPS has established an accurate time history of altitude data, pressure tude is used to predict the altitude changes as the system descends below its ht regime. Radio altitude is used to establish an accurate altitude when the em is below its flight regime and is over a runway. IRU vertical speed is used at times.

MAPS Kalman Filter

heart of MAPS is a linearized Kalman filter that provides position output with ect to a fixed coordinate system. The state of the filter consists of the onents of the position and velocity of the airplane. The current state is related future state via a set of linear equations called the System Model. The rements of range and range rate are related to the state via a set of linearized ions called the Measurement Model. These are expressed as follows:

State of the System:

$$\{X\} = \begin{Bmatrix} xpos \\ xvel \\ ypos \\ yvel \\ zpos \\ zvel \end{Bmatrix}$$

System Model:

$$\{X(k+1)\} = [PHI]\{X(k)\} + \{W\}$$

where:

k and k+1 indicate times k and k+1

$$[PHI] = \begin{bmatrix} 1 & dt & 0 & 0 & 0 & 0 \\ 0 & 1 & 0 & 0 & 0 & 0 \\ 0 & 0 & 1 & dt & 0 & 0 \\ 0 & 0 & 0 & 1 & 0 & 0 \\ 0 & 0 & 0 & 0 & 1 & dt \\ 0 & 0 & 0 & 0 & 0 & 1 \end{bmatrix}$$

dt = Time between computational cycles, and

{W} = System modeling errors associated with the components of the state

Measurement Model:

ion-linear relationship between the range and range rate measurements from a ground ponder and the state of the system is:

$$\{Z(k)\} = \{h(x(k))\} + \{V\}$$

expands to:

$$\begin{Bmatrix} \text{rangei} \\ \text{rratei} \end{Bmatrix} = \begin{Bmatrix} \text{SQRT((xpos-xti)**2 + (ypos-yti)**2 + (zpos-zti)**2)} \\ \text{((xpos-xti)*xvel+(ypos-yti)*yvel+(zpos-zti)*zvel)/rangei} \end{Bmatrix} + \begin{Bmatrix} V1 \\ V2 \end{Bmatrix}$$

where:
xti, yti, zti are the coordinates of the transponder being used, and
{V} are the expected errors in the measurements

expressions were linearized by expanding them in Taylor Series about the latest position output.

$$\{Z(k)\} = \{h(X(k-1))\} + [H(k-1)]\{X(k)-X(k-1)\} + \{V\}$$

where:

$$[H(k-1)] = \frac{\partial h(X(k-1))}{\partial X(k-1)}$$

Kalman extrapolation and update equations that derive from the problem definition is follows:

Extrapolation Equations:

$$\{Xe(k)\} = [PHI]\{Xu(k-1)\}$$

$$[Pe(k)] = [PHI][Pu(k-1)][PHI]^T + [Q]$$

Update Equations:

$$[K(k)] = [Pe(k)][H(k)]^T\left[[H(k)][Pe(k)][H(k)]^T + [R]\right]^{-1}$$

$$\{Xu(k)\} = \{Xe(k)\} + [K(k)]\{Z(k) - h(Xe(k))\}$$

$$[Pu(k)] = \left[[I] - [K(k)][H(k)]\right][Pe(k)]$$

where:
The e and u suffixes indicate the extrapolated and updated values of the attached parameter, respectively.

[K] is the Kalman Gain matrix

[Q] is the system error co-variance matrix

$$Q = \begin{bmatrix} .1 & 0 & 0 & 0 & 0 & 0 \\ 0 & 1. & 0 & 0 & 0 & 0 \\ 0 & 0 & .1 & 0 & 0 & 0 \\ 0 & 0 & 0 & 1. & 0 & 0 \\ 0 & 0 & 0 & 0 & .1 & 0 \\ 0 & 0 & 0 & 0 & 0 & 1. \end{bmatrix}$$

R is the measurement error co-variance matrix

$$R = \begin{bmatrix} 0.0625 & 0.0 \\ 0.0 & 0.005184 \end{bmatrix}$$

Extended MAPS Kalman Filter

ding the definition of the Kalman filter to accept altitude and vertical speed only requires changes to the Measurement Model. The output of the system remains same, so the state of the system does not change, and since the state does not ge, the System Model does not change.

leasurement Model becomes:

$$\begin{Bmatrix} \text{rangei} \\ \text{rratei} \\ h \\ hd \end{Bmatrix} = \begin{Bmatrix} \text{SQRT((xpos-xti)**2 + (ypos-yti)**2 + (zpos-zti)**2)} \\ \text{((xpos-xti)*xvel+(ypos-yti)*yvel+(zpos-zti)*zvel)/rangei} \\ zpos \\ zvel \end{Bmatrix} + \begin{Bmatrix} V1 \\ V2 \\ V3 \\ V4 \end{Bmatrix}$$

where h is altitude, and hd is vertical speed

$$R = \begin{bmatrix} 0.0625 & 0.0 & 0.0 & 0.0 \\ 0.0 & 0.005184 & 0.0 & 0.0 \\ 0.0 & 0.0 & 0.1 & 0.0 \\ 0.0 & 0.0 & 0.0 & 0.1 \end{bmatrix}$$

Initialization of Altitude Data

The measurements h and hd for altitude and vertical speed are not the raw values as measured by one of the various instruments, but they are those raw values with biases removed using an initialization process.

For descending flights, the original MAPS algorithm is used until certain conditions call for the extended algorithm. However, the initialization process begins when the airplane passes through 150 meters. A running one-second average of the differences between pressure altitude and MAPS altitude is maintained until the extended algorithm is called. The average is then subtracted from the input pressure altitude to remove the bias. An identical procedure is used for correction of vertical speed.

For ascending flights below 60 meters, or level flights that do not have adequate altitude for accurate altitude determination, the radio altimeter values are used along with a constant correction value that removes biases due to the differing reference values. A variable correction factor that compensates for the difference between the MAPS coordinate system and runway elevation is used. Vertical speed bias is ignored in these instances. The pressure altitude initialization process described above is started so that pressure data can be introduced when the end of the runway is reached.

Extended MAPS Operation

During the discussion of MAPS it was pointed out that the altitude data was acceptable at altitudes above 50 meters. However, this limit is strongly dependent on the design of the ground transponder array. For this reason, during descending flights the Extended MAPS algorithm was designed to check the geometry of the airplane-ground transponder relationship, beginning at 100 meters. If the elevation angle from the closest ground transponder to the airplane is less than 17 degrees, the extended algorithm is used. In all cases, the extended algorithm is used below 60 meters.

During ascending or low-level flybys, the extended algorithm is used at the beginning of the flight. When the end of the runway is reached, pressure altitude is substituted for radio altitude, and the original algorithm is used when the airplane is above 60 meters and the elevation angle from the closest transponder to the airplane is greater than 20 degrees.

VERIFICATION

Verification of the Extended MAPS was accomplished using a two-stage approach. First, simulations of both MAPS and Extended MAPS were developed to provide a direct comparison of actual airplane position and calculated position. Then actual recorded flight test data was used as input to Extended MAPS for comparison with recorded MAPS and photo-theodolite data.

This approach was required because the down-looking camera system used for comparison during the acceptance testing of MAPS is not as accurate as MAPS itself. Therefore, while it was possible to establish the acceptability of MAPS, it was not possible to assign a definitive accuracy. The results of that testing show that the error in MAPS data has a standard deviation of not more than four meters when the system's altitude is above the design minimum for the transponder array being used.

Flight Simulations

A predetermined flight path was used for development of the input data for both MAPS and Extended MAPS. Among the comparisons made are those illustrated in Figure 2. These flight paths were level flybys with the addition of a five-meter altitude sine wave and a three-meter longitudinal sine wave superimposed. The nominal altitudes for the flight paths were 100, 50 and 25 meters. The addition of the sine wave motions is intended to ensure that a non-linear flight path is used to stress the filter's ability. The transponder array used for this simulation is illustrated in Figure 3. This array was chosen as one that fulfills the requirements for a 50-meter flyby using MAPS.

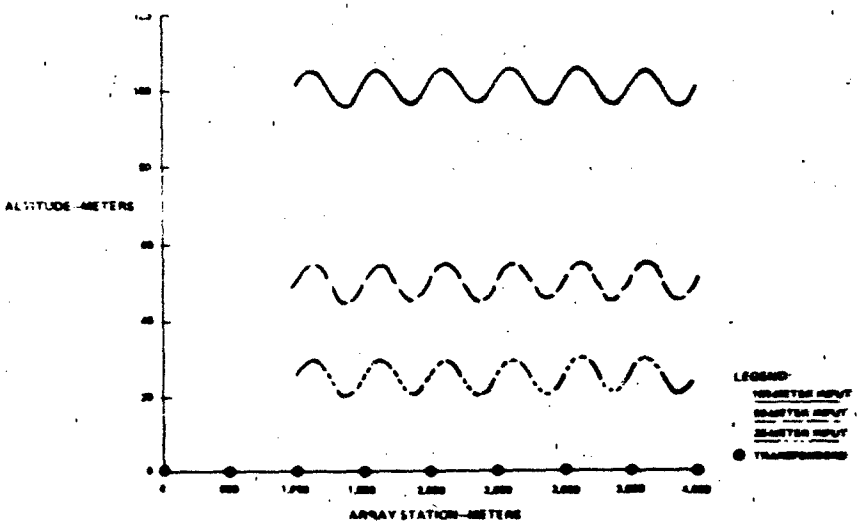

Figure 2. Simulator Input Data

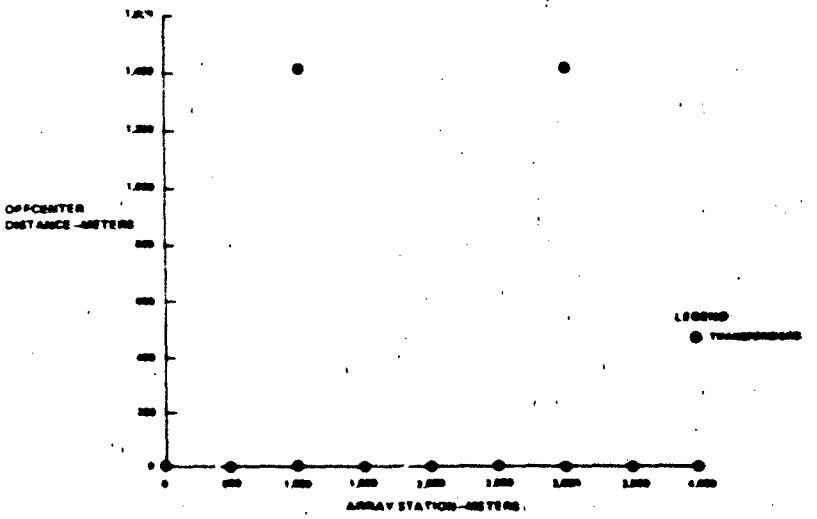

Figure 3 Simulator Transponder Array

e input data for the simulation was developed through the addition of errors that re randomly selected from normal error distributions. The errors assigned to the ansponder locations had a zero mean and a standard deviation of 0.3 meters, and tual locations used in calculating range data were determined by randomly selecting e errors from a normal distribution. A different selection was made for each flight th simulated. Errors for the ranges and range rates used as input were similarly signed zero means and 0.4 meter and 0.02 meter/second standard deviations, spectively. These values were determined from the manufacturer's specifications and mparison of simulation results with actual flight test results. Ranges and range tes were zeroed out for transponders that were more than 1000 meters behind the mulated position to model transponder blanking by the fuselage of an airplane. On a ndom basis, one percent of the ranges were zeroed out also. This allowed for mulated random transponder blanking from unknown sources.

rors for the altitude data for Extended MAPS simulations were generated having zero ans and 0.5 meter and 0.5 meter/second standard deviations respectively for altitude d vertical velocity.

me representative results from the simulators are shown in Figure 4. These results e from the three flight paths described above. For this comparison the Extended MAPS

two systems converge at higher altitudes. Note that the altitude comparisons at 100 meters are quite similar, and the deviation increases at the lower altitudes. The table below summarizes these data.

Standard Deviation of Output Errors (meters)

	MAPS			Extended MAPS		
	X	Y	Z	X	Y	Z
100 Meter Flyby	0.3	0.4	0.7	0.4	0.4	0.3
50 Meter Flyby	0.3	0.4	0.9	0.4	0.4	0.3
25 Meter Flyby	0.3	0.4	1.6	0.3	0.4	0.3

Each of these results is from three separate 30-second simulation flights.

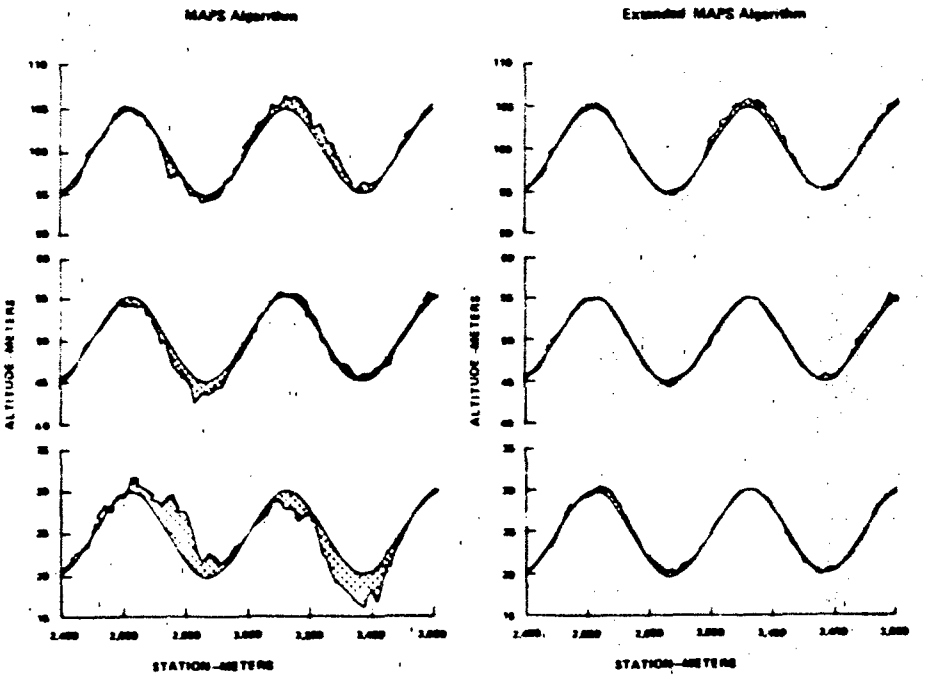

Figure 4. Simulator Data

These particular conditions were executed several times with different error selections, and takeoff and landing flight paths were also investigated. The results from these simulations are summarized in the altitude error versus altitude graph shown in Figure 5. These results show the expected trends. Without a direct altitude input, the system output degrades at altitudes below 100 meters. The addition of this input results in altitude output that is approximately as good as the input.

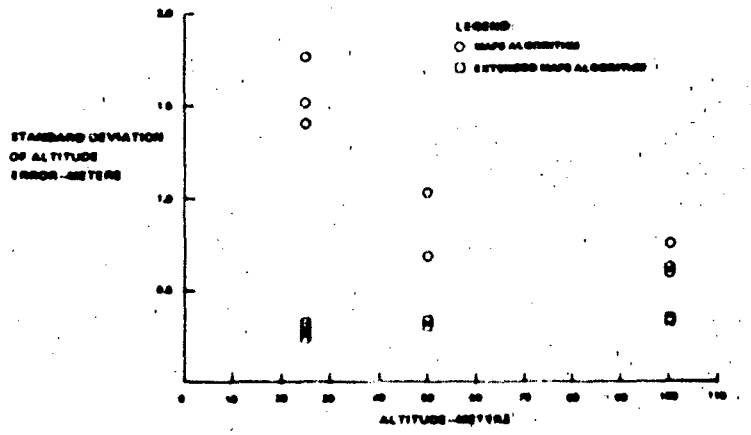

Figure 5. Simulator Data

ta from three flight tests were investigated for comparison with the simulation data. e purposes of this phase of the verification were to show that Extended MAPS would erate using actual data and to gather sufficient comparison data to validate the ulation results. The difficulty in comparing MAPS data with photo-theodolite data two-fold. The most accurate theodolite system, APACS, can only gather data at latively low altitudes, and the down-looking camera system gathers data only at dis-ete points in the test array. Therefore, gathering a statistically significant pling for comparison at all altitudes requires an inordinate amount of flight time. other practical reason for relying on the simulator is that each flight test has ique requirements that determine the transponder array to be used. The array signed for the test may not be conducive to gathering the comparison data required r a complete analysis.

e three tests used for this analysis were an Automatic Approach test of a Boeing del 737, the acceptance test of MAPS, using the same airplane, and the Noise Certi-cation of the Boeing 767. Several flights from each test were analyzed, and presentative flights are discussed below to illustrate the results.

Boeing 737 - Automatic Approach Test

e 737 automatic approach test was the first use of MAPS as a data gathering system. fact, timing was such that the test came before MAPS had been officially accepted by eing. In order to verify the low altitude part of the MAPS output data, portable nway lights were placed prior to the approach end of the runway in order to extend ACS altitude capability to 150 meters. The transponder array used during this test illustrated in Figure 6. The variable spacing used for the centerline transponders s intended to allow accurate altitude output from 1000 meters altitude at 16 lometers to 50 meters at 0.5 kilometer. The purpose of the test was to compare the ight path of the airplane with instrument landing system measurements for the last 16 lometers of the approach. Comparison data from APACS was only available for the last o kilometers.

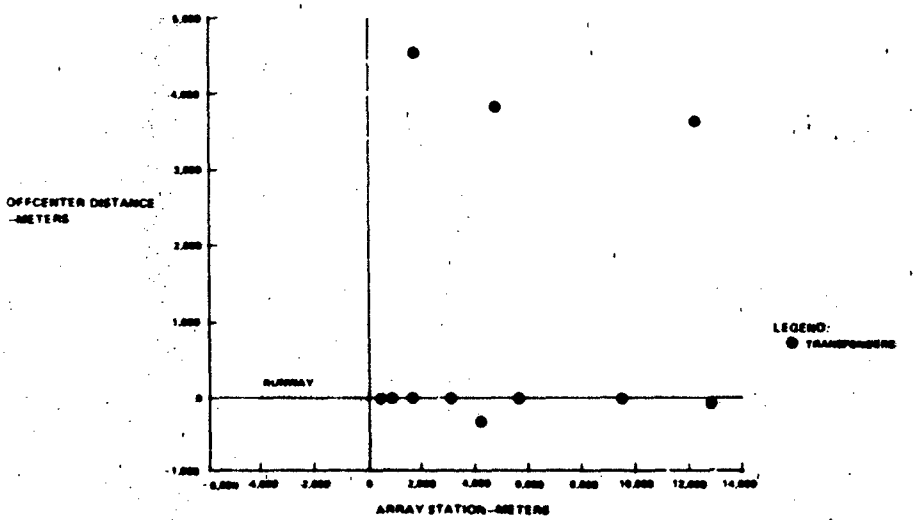

Figure 6. 737 Approach Test Transponder Array

ree approaches from this test were used for comparison of MAPS and Extended MAPS ta. Figure 7 shows the comparison of APACS, MAPS, and Extended MAPS altitude data r the last kilometer of one of these approaches. Extended MAPS used corrected essure altitude, and corrected altitude rate from different static pressure sources input, together with the MAPS ranges and range rates recorded during the test. ile altitude rate from the inertial reference system would have been a more desirable urce for altitude rate data, it was not available. Note that the data was ended at e runway threshold because the transponders were almost entirely blanked out at that int.

ing APACS as the "true" position, the standard deviation of MAPS results can be timated as one-third of the maximum excursion from the APACS data. That means that e standard deviation of the error is less than one meter at 70 meters altitude, proximately one meter at 50 meters, and over two meters at 20 meters. The Extended PS result shows that the standard deviation of the error is less than one meter for e entire approach.

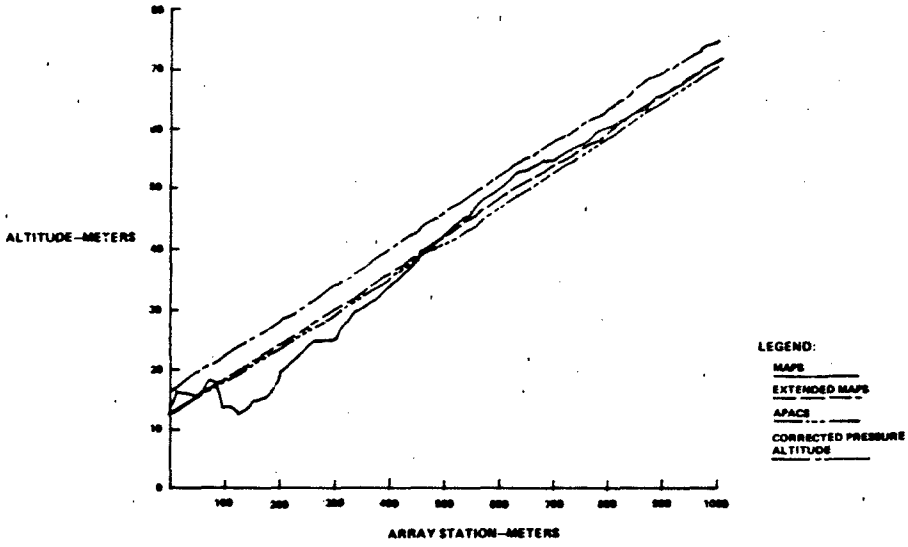

Figure 7. 737 Approach Test

Boeing 737 - MAPS Acceptance Test

The second test using MAPS was its acceptance test in Glasgow, Montana. Fourteen flights were used to evaluate MAPS as an acceptable system for Noise Certification testing. Five of the flights were used for this analysis, and data from one of these is discussed in detail.

The array used during the 14 evaluation flights is illustrated in Figure 8. It was designed for a minimum altitude of 100 meters over the entire range. Figure 9 presents the comparison data for a 90-meter flyby over the runway. It was chosen because it represents a classic example of the geometric dilution of precision (GDOP) that the extended system was designed to correct. Because the flight is lower than the design limits of the array, the ranges from the transponders do not have enough resolution to establish an accurate altitude unless the airplane is very close to a transponder station. Note that the MAPS output is very good as the airplane passes over each transponder, but appears to degenerate until approaching another. During this test, the down-looking target locations coincided with the centerline transponder locations. At these locations all three systems agree within one meter. By comparing the altitude curves, one may conclude that the MAPS output is the one in error between the transponders because it becomes so erratic. This data falls within the specifications required of MAPS, but there is a great deal of room for improvement.

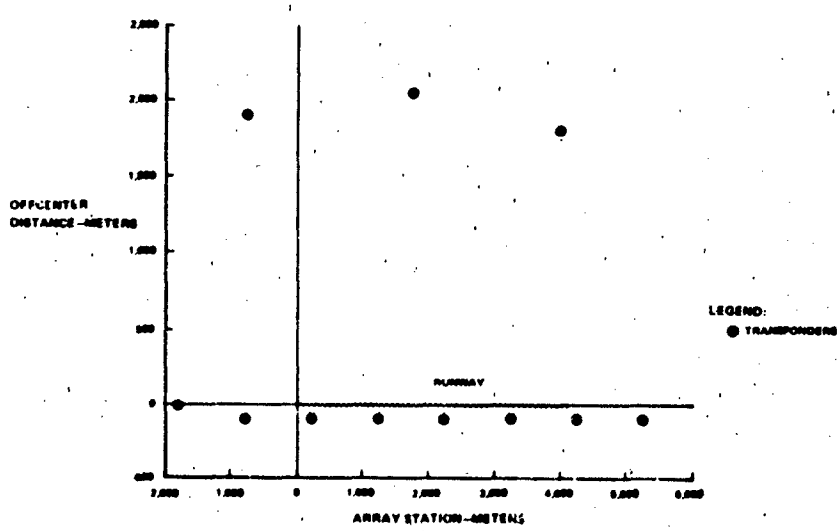

Figure 8. MAPS Acceptance Test Transponder Array

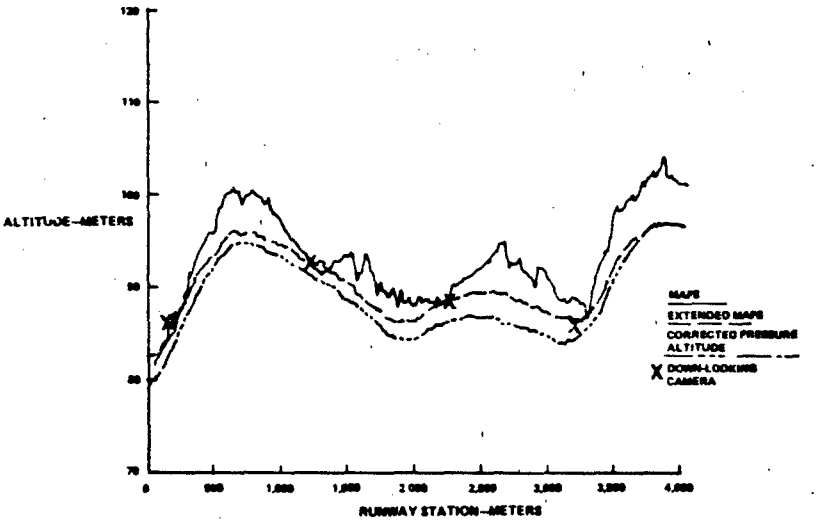

Figure 9. MAPS Acceptance Test

Boeing 767 - Noise Certification Test

767 noise certification test in Palmdale, California, was the first production use APS. The transponder array used was designed to provide accurate data at altitudes 0 meters and higher over the east half of the runway, and 150 meters and higher 3 meters east of the runway. The array is illustrated in Figure 10. All test hts were flown within these constraints, so the addition of altitude data input d not improve those results. The initial takeoffs from two days of testing were yzed to show the potential for the use of Extended MAPS in takeoff performance ing. The first of these is illustrated in Figure 11.

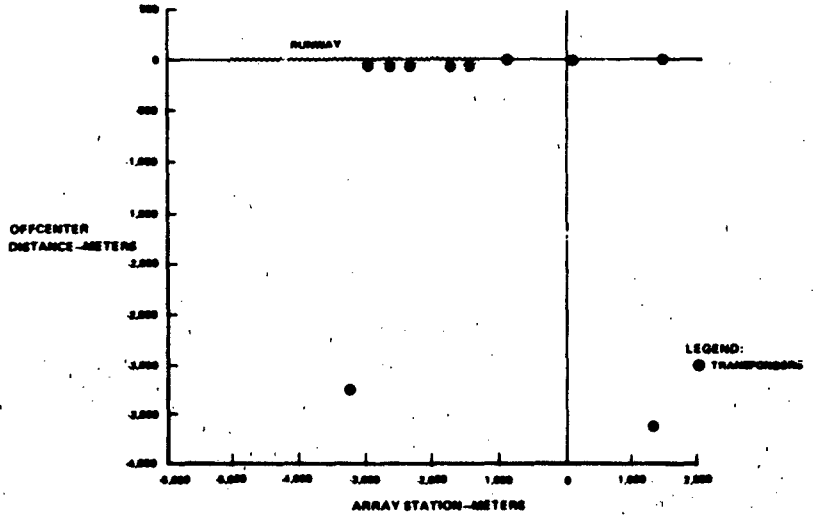

Figure 10. 767 Noise Certification Test Transponder Array

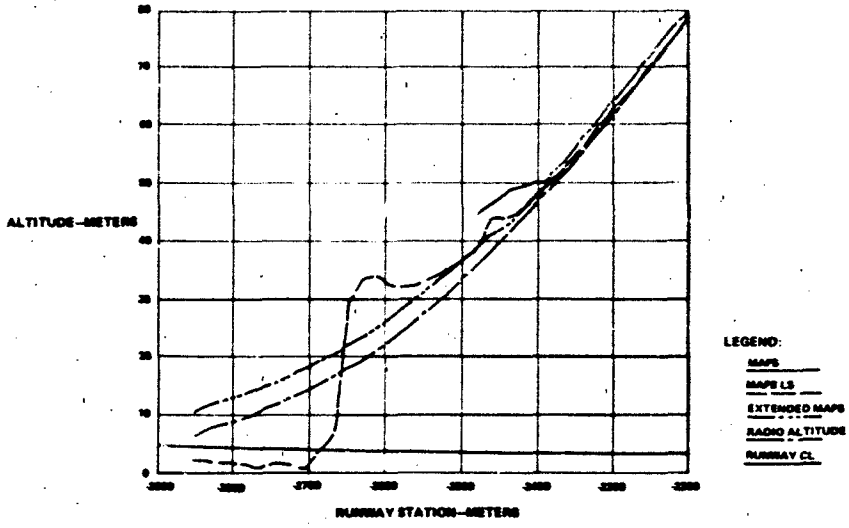

Figure 11. 767 Takeoff

ote that the MAPS onboard data did not start until the airplane reached an altitude of meters. This occurred because the system could not initialize until then. By rcing initialization after the fact, the trace entitled MAPS LS was calculated. This ace provides a view of the behavior of the MAPS Kalman filter if it had initialized. e Extended MAPS solution appears to provide a much more accurate solution, but the mparison is marred because there is no camera data to support this conclusion. To rrect this shortfall, the flight was reversed and rerun as an approach, for which we ve some knowledge from the 737 approach test. Figure 12 contains this comparison and nfirms that the Extended MAPS altitude data is accurate.

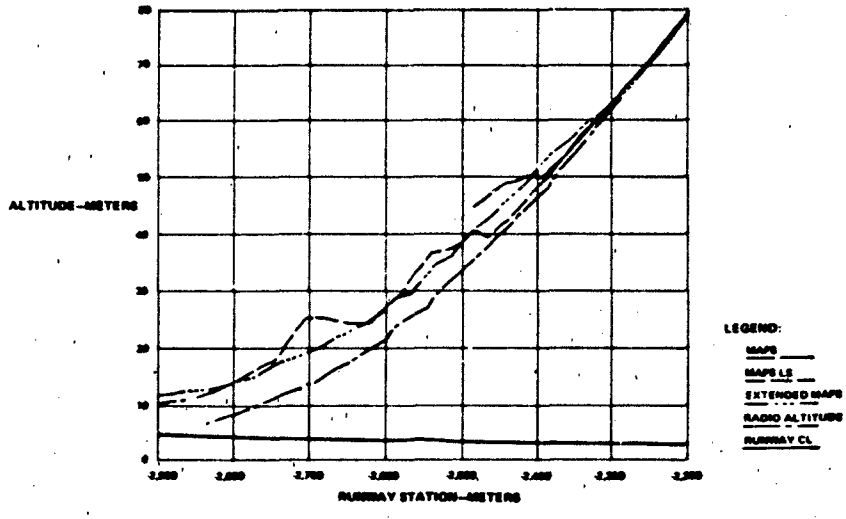

Figure 12. 767 Takeoff With Reversed Input

NCLUSIONS

is evident from the data comparisons during verification that the Extended MAPS tends the usefulness of MAPS from the ground to design altitude of a transponder ray. Figure 13 summarizes all of the data examined during this investigation. Since e MAPS acceptance test was the only one that used a transponder array designed for 0-meter minimum altitude, the errors from that test were applied to one-half the own altitudes in order that the MAPS output not be biased. Note that the design titudes of the various arrays (50 meters) coincides with the point at which the MAPS titude solution begins to diverge. At higher altitudes, the Extended MAPS and MAPS lutions approach each other. Also note that the simulation data agrees with the ight data. Therefore, it may be used when studying either system.

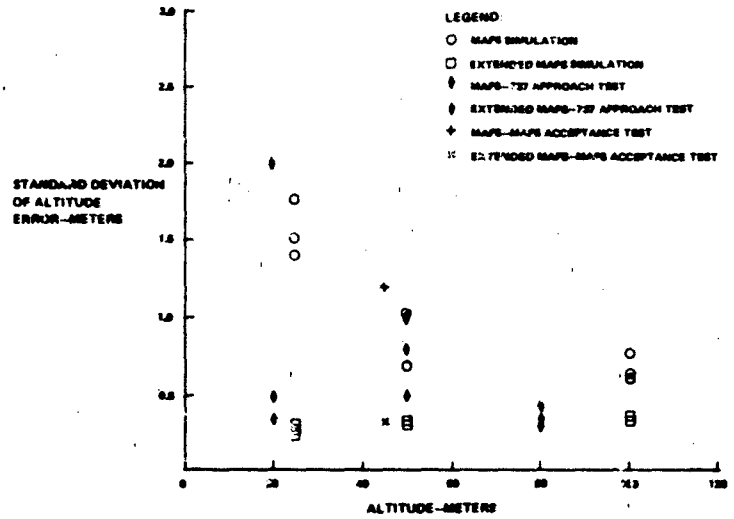

Figure 13. Summary of Results

servative estimate derived from these results is that the Extended MAPS output des output data that is within one meter of the actual position at least 90 nt of the time.

E DEVELOPMENT

elative simplicity of the changes to MAPS that resulted in such a significant gain ·ages us to continue to extend the system. With the inclusion of more data from ial reference systems and altitude sensors, the number of transponders required d be reduced considerably. For tests that do not require a fixed reference, the ponder requirement may be eliminated altogether. Development in this direction ·educe operational requirements of the system and make it much more flexible.

GENERAL INTEGRATED MULTIPURPOSE INFLIGHT CALIBRATION SYSTEM (GIMICS)

by

Rüdiger Gandert
Rüdiger Karmann

Institut für Flugmechanik

Deutsche Forschungs- und Versuchsanstalt
für Luft- und Raumfahrt e.V. (DFVLR)
D 3300 Braunschweig-Flughafen, West-Germany

IARY

n 1985 the new Advanced Technology Testing Aircraft System (ATTAS) will be operable at DFVLR in Braunschweig. Owing to the wide application spectrum of ATTAS and the varied e of users, a flight test instrumentation system having a very high degree of flexi-ty and testability was required. It was therefore decided that a versatile built-in : and calibration system called GIMICS should form an integral part of the ATTAS ht test instrumentation system. GIMICS is an intelligent, computer-controlled system ng dedicated access to the ATTAS subsystems. The system architecture and application ibility of GIMICS will be presented.

NTRODUCTION

he DFVLR has been involved since 1971 in the design, utilization and operation of the 320 In-Flight Simulator.

sing special equipment and instrumentation of this In-Flight Simulator the dynamic acteriscics of different transport aircrafts could be simulated in 5 degrees of free-under realistic conditions. Based on more than ten years of experience with the HFB in various national and international programs the DFVLR started in 1981 the develop-of the **Advanced Technology Testing Aircraft System ATTAS.** MBB-VFW and the DFVLR developing in close cooperation the ATTAS In-Flight Simulator based on a VFW 614 raft, which includes a dual fail passive redundancy concept thus also enabling compu-controlled take-off, landing and high-speed flights in the simulation mode.

FVLR - ADVANCED TECHNOLOGY TESTING AIRCRAFT SYSTEM ATTAS

ig. 1 shows the principal blockdiagram of the ATTAS-VFW 614 instrumentation. It in-es the following:

sic controls and instruments for the safety pilot who operates the original chanical links to the different motivators. The safety pilot can switch off the Fly--Wire (FBW)-Control System in emergency cases.

y-by-Wire-Controls and experimental instruments for the evaluation pilot who controls e aircraft in the FBW simulation modes using various computers and electro-hydraulic tuators.

nsors, signal conditioning and additional avionics to identify the actual aircraft atus.

Central Communication Computer for intercommunication between the Fly-by-Wire stem, the Experiment Control Computer Systems and the operator using the operator nel computer system

lemetry and analog taperecorder for data transmission and recording.

t is obvious that this complex test instrumentation for the In-Flight Simulator ATTAS h will be used by a varied range of users over a wide application spectrum requires atile check-out, test and calibration aids to minimize unpredictable downtimes and to mize the benefit-to-cost ratio.

n the basis of over 10 years of user experience gained with the In-Flight Simulator 320, the DFVLR designed and realized the so-called "General Integrated Multipurpose light Calibration System "GIMICS" which forms an essential part of the ATTAS urement System. GIMICS is a flexible system used for

stem Checkout

e-Flight/In-Flight Test

e-Flight/In-Flight Calibration

stem Monitoring

the following section GIMICS is presented and discussed, showing its range of ap-
ion a:d flexibility.

IC OBJECTIVES OF GIMICS

achieve a high quality level of In-Flight-Simulation, it is necessary to use high
y and high accuracy sensors, signal conditioning and actuators. The whole mesure-
:hain from sensor to actuator including the computer system has to be tested and
ated in given time intervals to guarantee the required static and dynamic accuracy.
uld thereby be stressed that essential aspects of the testing and calibration such
dynamic calibration of control surface transfer functions can only be performed
tically under flight conditions. GIMICS therefore contains as an integral part a
te test and calibration system which allows signal input- and response measurement
computer control at different points in the measurement chain.

ther essential aspects of GIMICS are:

ssibility to raw analog transducer signals,

te controlled testability of signal conditioning,

uter-controlled adaption of signal conditioning parameters to different flight test
s,

grated Pulse Code Modulation (PCM) data-acquisition and monitoring (Quicklook),

isition and monitoring of measurement system housekeeping data,

age of test and calibration results,

ty lockout of test and calibration functions from flight test system during criti-
In-Flight simulation phases,

le to use with menu oriented computer control.

s system is currently under development. A more detailed description is now given
following.

'AS EXPERIMENTAL FLIGHT CONTROL SYSTEM

. 2 shows a further simplified block diagram of the ATTAS experimental flight con-
system. We can discern three system levels of decreasing significance for flight
.

highest level shows the computer systems of the Fly-by-Wire system. It consists of
Fly-by-Wire computer, the Experimental Control Computer, as well as a Terminal
uter at both the tailplane and cockpit regions of the aircraft. At these points
emely safety critical aircraft flight functions are housed. The system is thus only
ssible to the experimenter via the Central Communication Computer.

second level is the **Signal Conditioning and PCM System.** Its primary task is to
lition the raw sensor data for the Fly-by-Wire system. It also contains an integra-
PCM system to transfer all data of the Experimental Flight Control System to magne-
tape and via telemetry to the ground.
ng safety critical flight phases, the **Signal Conditioning and PCM System** can be
ked by the Fly-by-Wire system so as not to disturb the highly critical uppermost
em level.

lower level is the **Test and Calibration System.** It has no influence on the
ty of the aircraft. It consists of a basic set of standard measuring instruments.

SUREMENT SYSTEM AND GIMICS

neral

two lower levels of Fig. 2 are to be understood as the measuring system. This
n is again represented in Fig. 3.

measurement system consists of two subsystems, the **Signal Conditioning and PCM**
in the upper half of the figure and the **Test and Calibration System** in the
half.

Signal Conditioning and PCM System consists in the simplex case of two signal
ioning units (SC Units) of the same type in an 1/1 ARINC ATR housing. The boxes are
where data is concentrated and further processed, i.e. in the cockpit and tail-
regions of the aircraft. Certain signals from the tailplane area initially pass
h the special signal conditioning unit (SSC Unit). In this unit, the signals of
sensors are conditioned which cannot be dealt with by the standardized components

he SC boxes. These are the signals from the base aircraft itself, which have to be anically decoupled and/or whose voltage level lies outside the standard signal level conditioning). Apart from these signal conditioning components there are yet further onents installed in the SC Units. These form, in conjunction with the **Test and** oration **System**, GIMICS.

Signal Conditioning and PCM System

1 Signal Conditioning Unit (SC Unit)

ig. 4 shows the structure of the SC Unit. A unit can condition a maximum of 48 analog or signals. Groups of 4 analog channels together with power supply for attendant ors are housed on one card. The conditioned sensor signals proceed in analog form to I/O units of the Fly-by-Wire system, as well as to the local subunits of the integra- PCM system.

part of the SC unit essential to GIMICS is the built-in central calibration unit n is connected via the calibration bus (CAL BUS) with the **Test and Calibration** em. Within each SC box there is a local version of the CAL BUS which leads to the al conditioning channels of the SC Unit. Each SC box contains its own microprocessor n has access via the local control bus to the signal channels and the calibration ce.

1.1 Standard Signal Conditioning Channel

ig. 5 describes in schematic form the essential components and signal paths of a al conditioning channel. Each of the 48 channels of a SC unit is characterized by the owing features:

ftware-controlled gain over a range from 1 to 1024

ftware-controlled offset compensation from - 10 to + 10 VDC with 12 bit resolution

off frequency selectable via plug-in module

rall error smaller than 0.5 % over the range - 25°C to 65°C

tiple signal paths for test and calibration facilities (GIMICS)

ne sensor signal arrives at a programmable instrumentation amplifier via an adapta- module. From there it proceeds via a three-pole Butterworth-filter and a buffer to output. Each channel has a DAC to compensate any static sensor signal voltages. The cation of the various primary sensor elements to the signal conditioning channel is rmed via the plug-in adaptation module. A part of the signal conditioning channel ntial to GIMICS is formed by the three relays A, B and C. With their help, various and calibration functions are possible:

calibration signal from the local CAL BUS proceeds via relay A to the input of the nditioning channel. The corresponding reaction is passed via relay C to the receive ne of the LOCAL CAL BUS. In this way the transfer function of the conditioning chan- can be determined.

calibration voltage is fed via relay B into the adaptation module. The response ceived via relay C depends on both the function of the amplifier and the filter, as l as on the correct state of the sensor, including its input lines, as the sensor lances the network of the adaptation module.

the adaptation module is a purely passive network, the raw sensor signal can be racted via relay B. The transfer direction on the transmit line of the local CAL BUS then reversed.

1.2 Calibration Centre

n essential component of GIMICS is the calibration centre, one of which is present in SC Unit. It has the following tasks:

vanic decoupling of the calibration signal from and to the test and calibration tem to avoid ground loops.

enuation of high level calibration voltages to test high amplification signal chan- s.

eration of signal voltages in the stand-alone mode of the SC Unit.

sekeeping signal switching.

g. 7 shows the block diagram of the single local calibration centre present in each x. A calibration signal from the **Test and Calibration System** via the CAL BUS is d via a buffer amplifier to the transmit line of the local CAL BUS. A precise, digi- adjustable attenuator is connected in this signal path. It is thus possible to

e the necessarily small input voltages for high amplification signal conditioning
s and whilst also sending high level, relatively noise-immune excitation voltages
CAL BUS running throughout the whole aircraft. The response of the tested signal
oning channel passes via a relay G, a buffer amplifier and a relay H back to the
. The signal paths can furthermore be so connected (relays D, F and G) that the
r function of the components lying in the calibration path are determined before
ual measurement signal paths are calibrated. With the aid of a housekeeping multi-
values of interest from the SC Units, such as temperatures, operating and refe-
voltages and currents can be measured. The local calibration centre possesses in
n its own precise calibration primary sensor element. Using this, an SC Unit can
ed and calibrated completely in the stand-alone mode. The sum of all errors lying
calibration path in the local calibration centre is smaller than 0.15 % FSD with a
ture range from -25°C to 65°C.

Local Processor (CPU)

SC Unit contains its own microcomputer. Its tasks are:

nication with the SC master unit via the signal conditioning control bus for
nd input and status response

etrization of the SC components and the calibration centre

ction of the internal signal paths of the SC Unit

test

-alone operation of the unit

SC Unit has a further interface for a standard terminal, whereby the unit can be
d in the laboratory in stand-alone mode.

ingal Conditioning Master Unit (SCMU) Fig. 3

Signal Conditioning Master Unit (SCMU) has the following tasks:

ol of the signal conditioning and calibration functions in the SC Units

ol of the PCM subsystems in the SC Units and generation of the programmed PCM

ction of the program-selected data from the PCM-frame for "quick-look"

ge of signal conditioning and PCM-system parameters in a non-volatile memory
g power off

nication between the **Signal Conditioning and PCM-System** and the **Test and
ration System**

rder to fulfil these tasks, all SC Units are connected via two digital bus systems
e **Signal Conditioning Master Unit:**

ignal conditioning control bus (SCC BUS) and

CM BUS

SCC BUS is a modified RS-232-C interface, via which the parameters of the condi-
channels are set in the SC boxes and the diverse test and calibration functions
system are controlled.

digitized measurement values pass from the SC units via the PCM BUS to the PCM
in the **Signal Conditioning Master Unit.** The PCM BUS operates in two cycles.
first phase the SCMU outputs a 16 bit address to select a signal channel. In the
phase, the transfer direction is reversed and the selected, digitized measurement
rom an SC Unit is placed on the bus.

t bus systems are optically decoupled in each unit in order to avoid ground loops
r the spatially widely distributed system.

2 Calibration Bus (CALBUS)

h CAL BUS is one of the most important parts of GIMICS. It consists of an analog
t line and an analog receive line which lead to all SC Units of the system and
s these with the **Test and Calibration System.** The calibration bus signals are
tted via true differential signal lines and are doubly shielded so as to prevent
as possible falsification of their transmitted signals by external noise sources.
e aid of this bus, actuation signals pass from the **Test and Calibration System**
to selected components of the **Signal Conditioning and PCM System** and the
e signals are returned to TACS.

g. 8 summarizes the possible calibration paths dealt with in the measurement system.
ire:

lination of raw sensor data

: signal input to the adaptation module

.bration of the calibration centres in the SC units

: and calibration of signal conditioning channels

2 Further Interfaces

:re are two further external interfaces to the **Signal Conditioning and PCM**
is:

lA channel from the Central Communication Computer and a

idard RS 232 connection to the **Test and Calibration System**

:a of interest are passed from the experimental flight control system via the DMA
:l into the PCM system. The second interface forms the main connection between the
. **Conditioning and PCM Systems** and the **Test and Calibration System.**

:st and Calibration System (TACS)

: lower part of Fig. 3 shows the **Test and Calibration System** within the ATTAS
'ement system. Whereas the components of the **Signal Conditioning and PCM System**
istributed throughout the whole aircraft, the **Test and Calibration System** is
itrated at an operating panel for the measurement system operator (Fig. 9). The
and Calibration System consists basically of a precision digital multimeter, a
:ion voltage source and an analog relay scanner. The system is enhanced by a pro-
:ble word selector for the analog representation of selected words from a PCM frame.

graphic display serves to provide a quick-look representation of the variety of test
:libration functions. The equipment at this level is connected via an IEEE 488 bus,
.-proven bus in the measurement field, to the most important GIMICS computer. These

Calibration Control Computer

Calibration Control Computer controls all functions of the **General Integra-**
ltipurpose In-Flight Calibration System GIMICS. These comprise:

ing up of the parameters of the SC channels and the PCM subsystem,

rol of the test and calibration tasks,

em monitoring,

rol of all equipment in the **Test- and Calibration System** and

unication with the ATTAS Fly-by-Wire System via the Central Communication Computer

Fluke 1720A was chosen as the **Calibration Control Computer** for the following
s:

interfaces are standarized,

ly programmable in various languages,

iciently flight-robust and installable in 19" racks and

able without keyboard via a touch-sensitive display.

Basic Software

tware has currently been implemented in the **Calibration Control Computer**, which
as a basis for the yet to be implemented, varied and complex test and calibration
re, but which is already employed during the integration of GIMICS into the air-
This software relies on basic data records which are generated on the ground with
d of interactive programs using a keyboard. On switching-on, GIMICS is completely
lized using these data records. In the aircraft itself, only the touch-sensitive
y of the **Calibration Control Computer** is used.

user is guided via menus. Input is achieved by simply touching the corresponding
oint (softkey). This allows even complicated operation sequences to be performed
t recourse to a manual.

ICATION OF GIMICS

flexibility and application potential of GIMICS can be illustrated by the dynamic
it calibration procedure of the flight control system consisting of:

:er

:ohydraulic actuator

lucer and

. conditioning

:omplete control loop is shown in Fig. 10.

:amming is done in the following steps:

:uction of the tailplane terminal computer to accept additive analog control sig-
for the dedicated electrohydraulic actuator to be superposed with the current
ol signal.

:ction of the analog cal-in signal path in the signal conditioning unit to the
nal computer and the cal-out path from the transducer to the relay scanner of the
and Calibration System.

:ction of the cal-in path to the noise source i.e., the X-output of a spectrum
ser and connection of the Y-input of the analysis instrumentation to the cal-out
using the relay scanner.

inally, transfer of the analyzer output data to the Calibration Control Computer
rom there to graphics generator for display if required.

procedure the transfer functions or dynamic characteristics of the control loop
easured using zero mean value noise source and stochastic analysis methods with-
ificant disturbance to the actual flight.

USIONS

eral Integrated Multipurpose In-Flight Calibration System GIMICS presented
one answer to the ever increasing complexity of flight test instrumentation and
es in the fields of In-Flight Simulation. The modular and integrated concept
) an optimum transparency in the complex hardware and software comprising the
ntrol system. For this reason GIMICS is one of the most important tools for ATTAS

development,

acceptance testing,

check out and

operation

pe that the concept represented by GIMICS will widen the techniques for checkout,
and calibration over a wide range of application of the DFVLR ATTAS In-Flight
r.

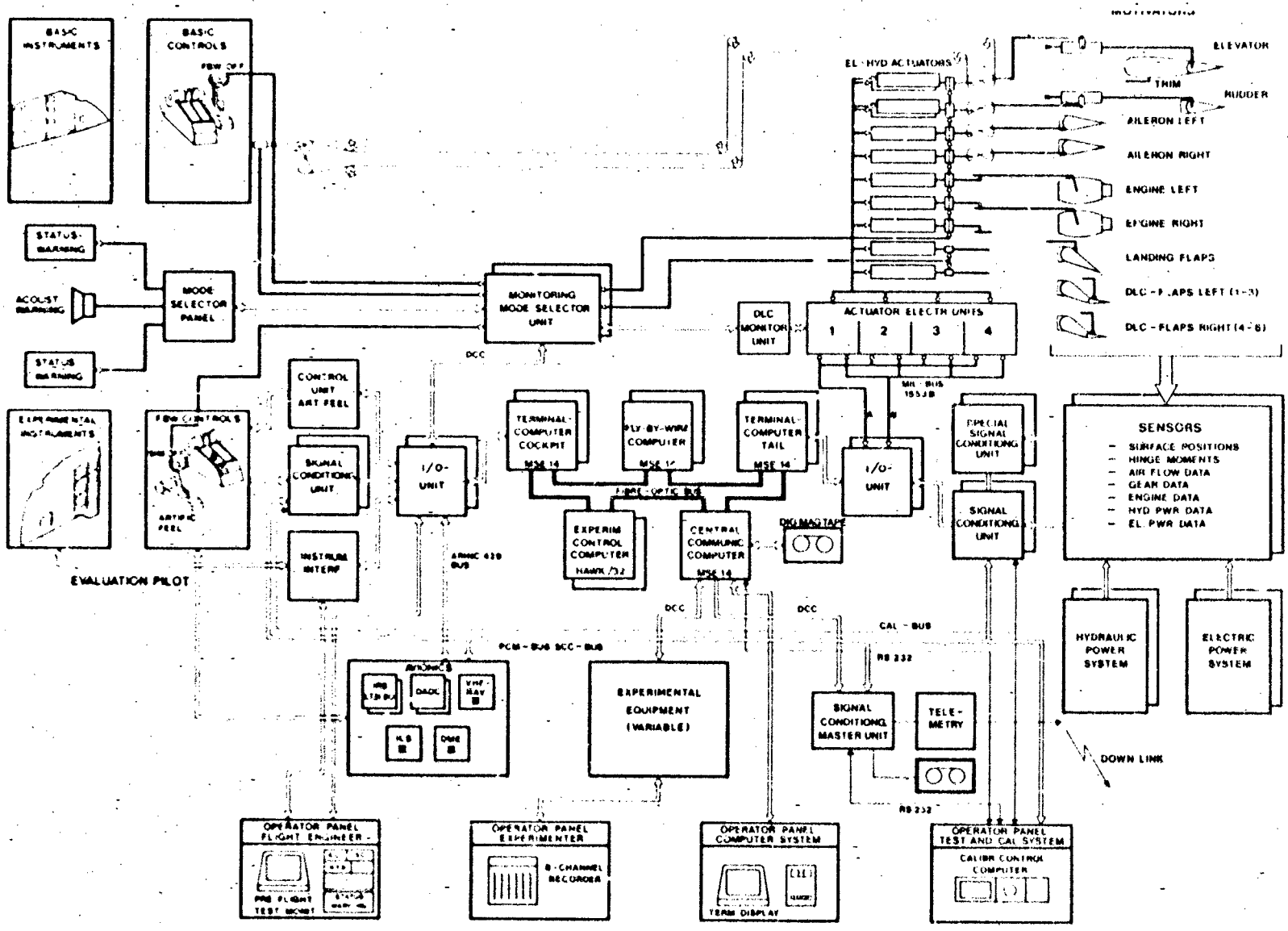

FIG. 1 AFTAS EXPERIMENTAL FLIGHT CONTROL SYSTEM

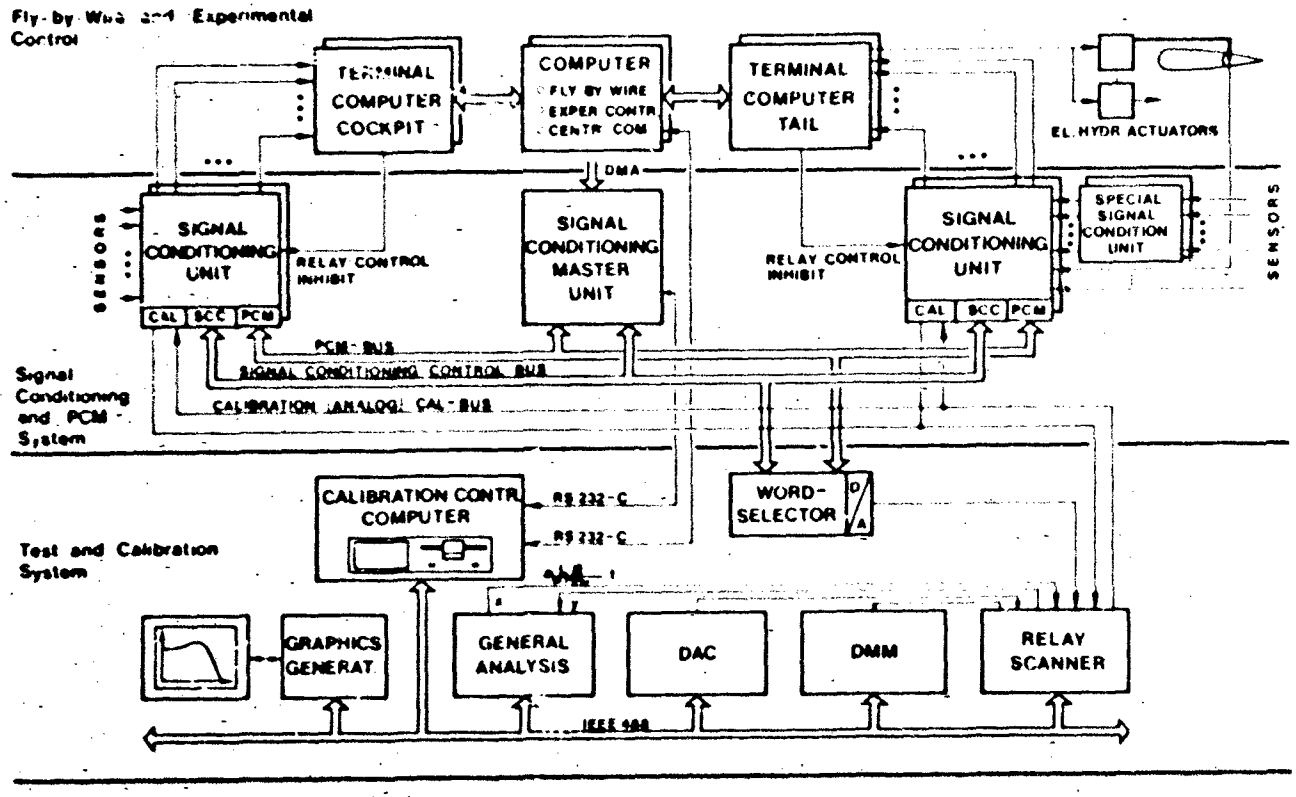

FIG. 2 ATTAS FLY-BY-WIRE AND MEASURING SYSTEM

DFVLR

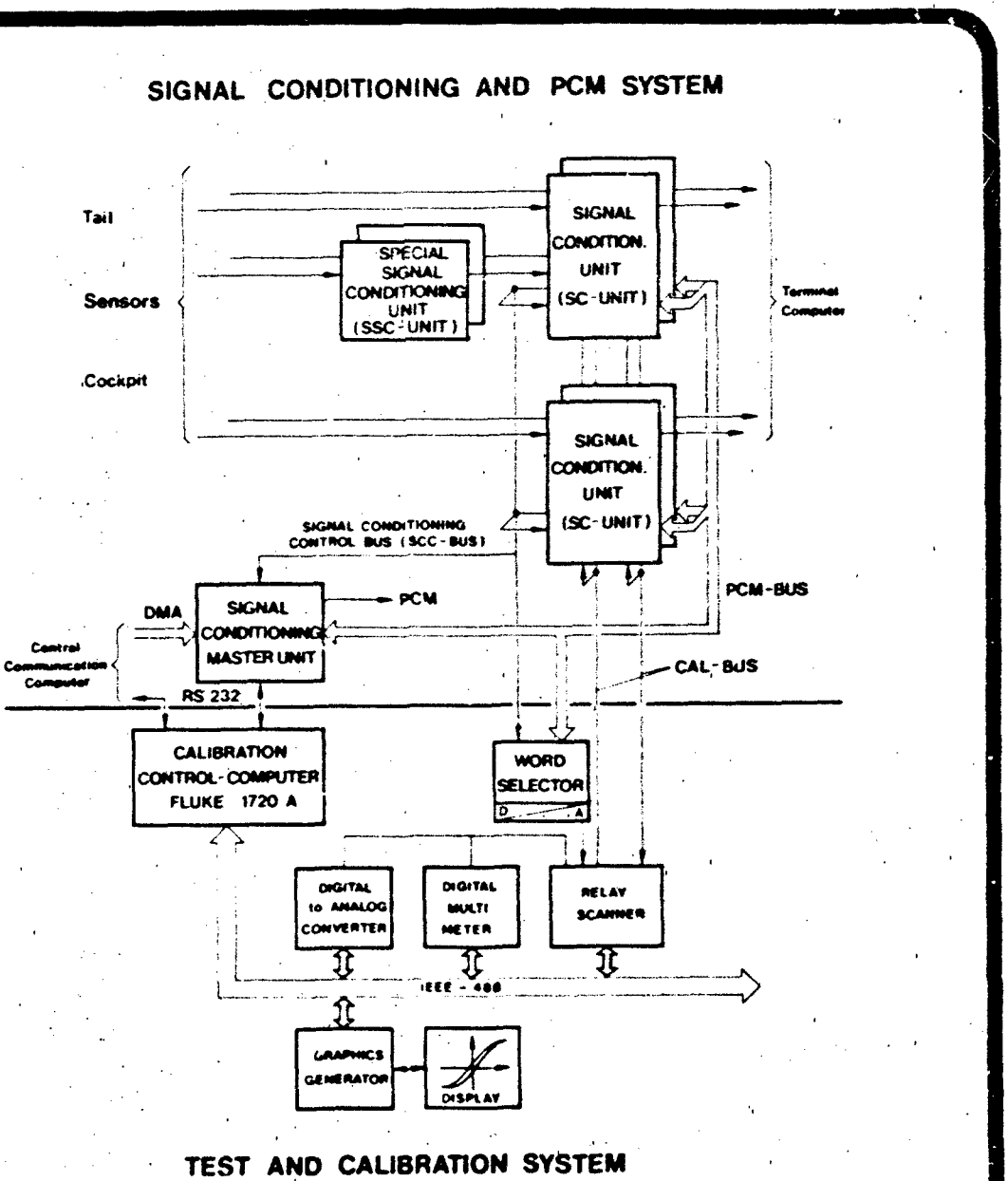

FIG. 3 ATTAS MEASURING SYSTEM

DFVLR

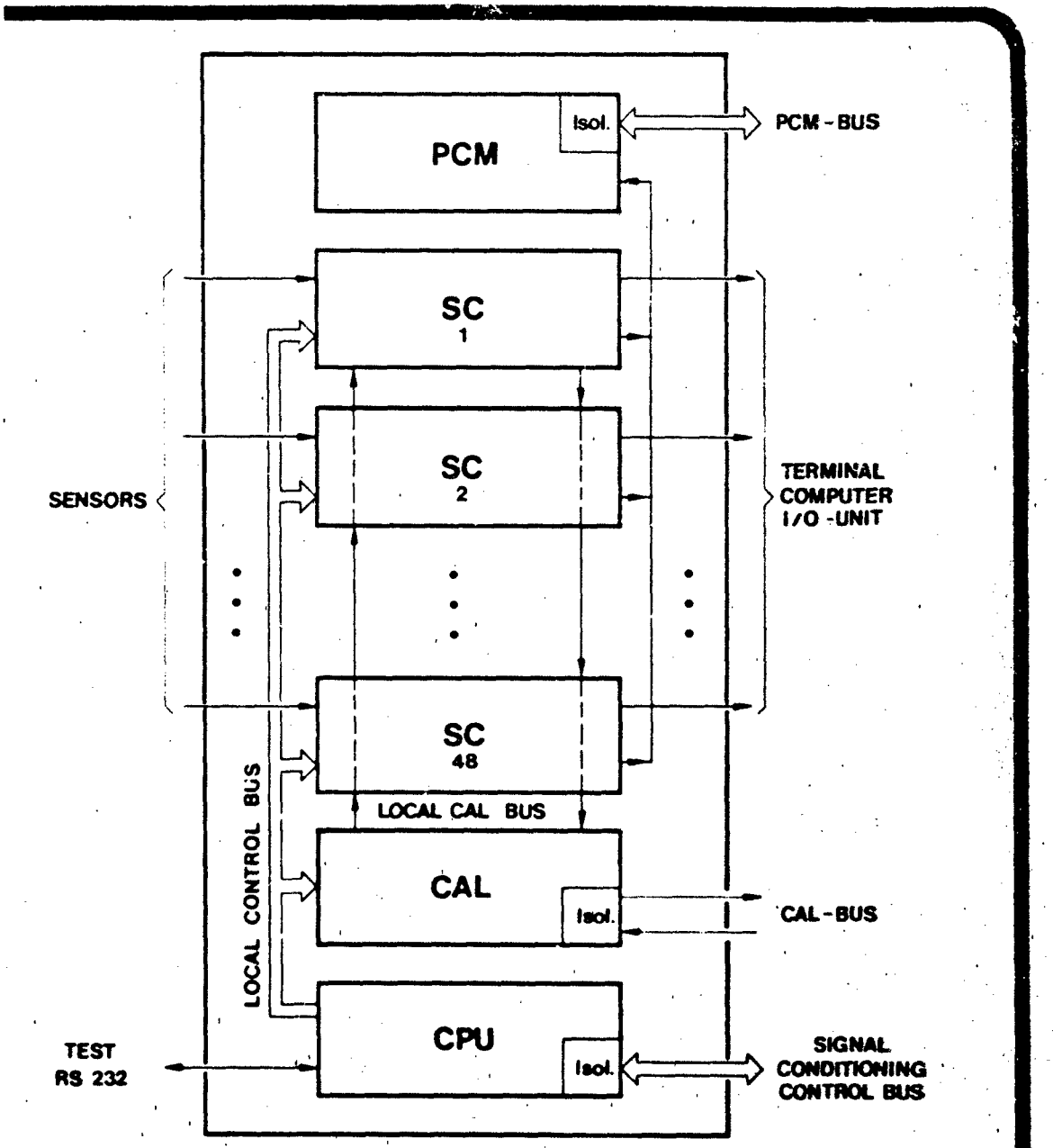

FIG. 4 SIGNAL CONDITIONING UNIT BLOCK DIAGRAM

DFVLR

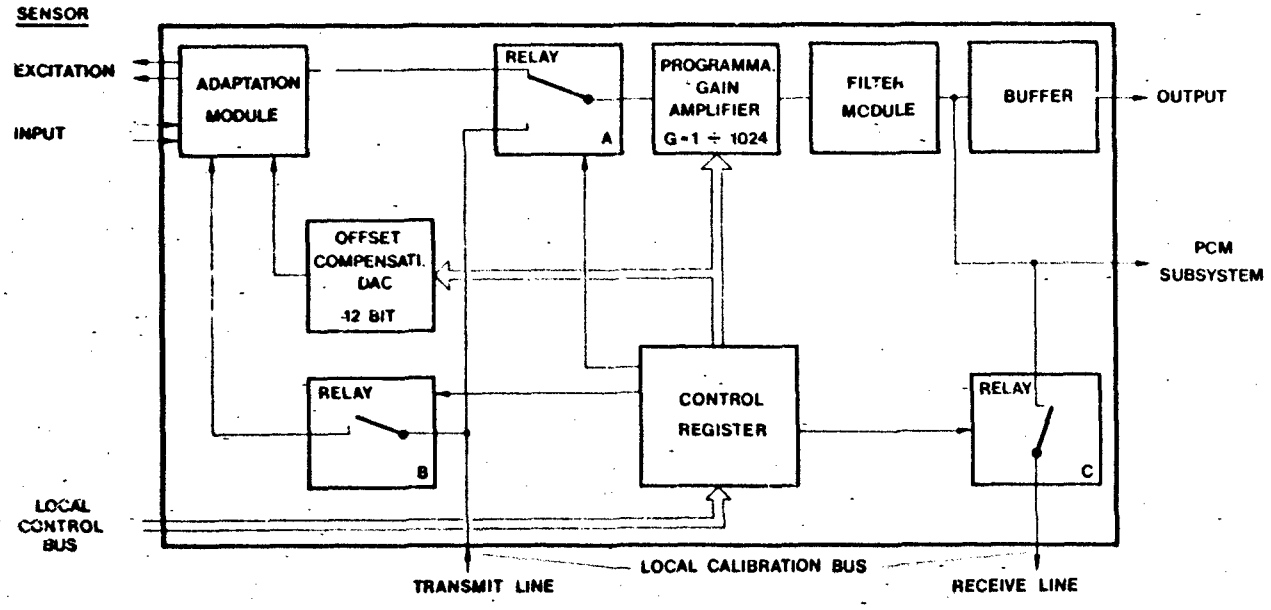

FIG. 5 SIGNAL CONDITIONING CHANNEL BLOCK DIAGRAM

DFVLR

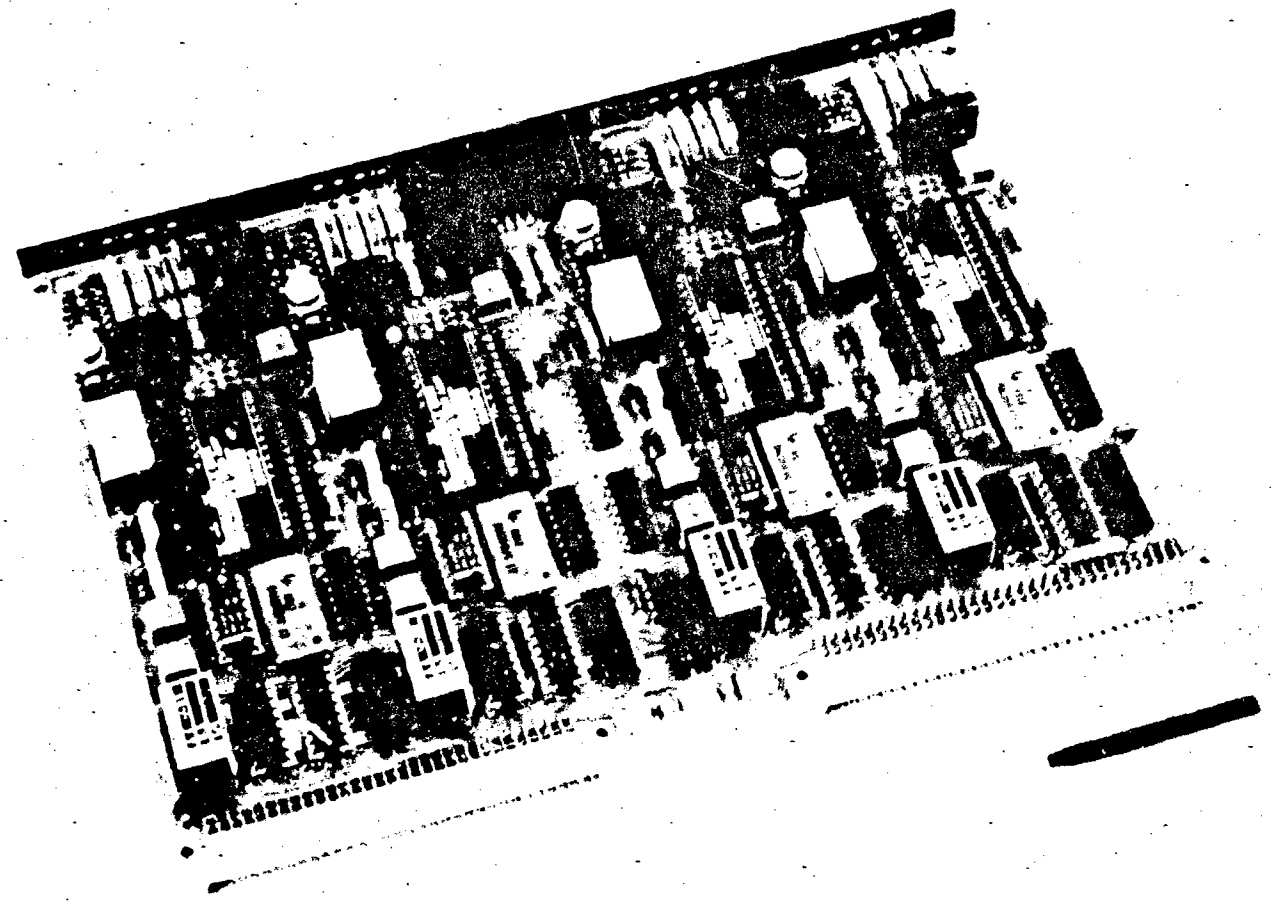

FIG. 6 ANALOG SIGNAL CONDITIONING BOARD (4 CHANNELS)

DFVLR

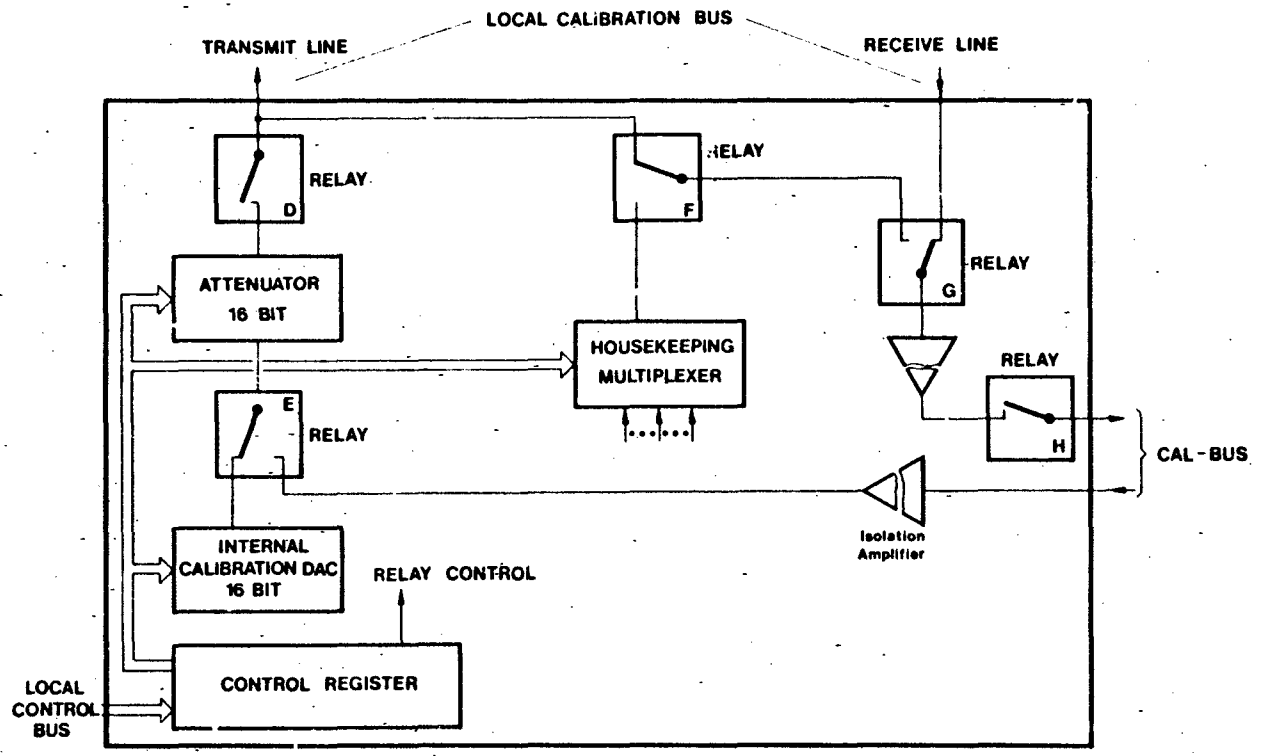

FIG. 7 LOCAL CALIBRATION CENTRE BLOCK DIAGRAM

DFVLR

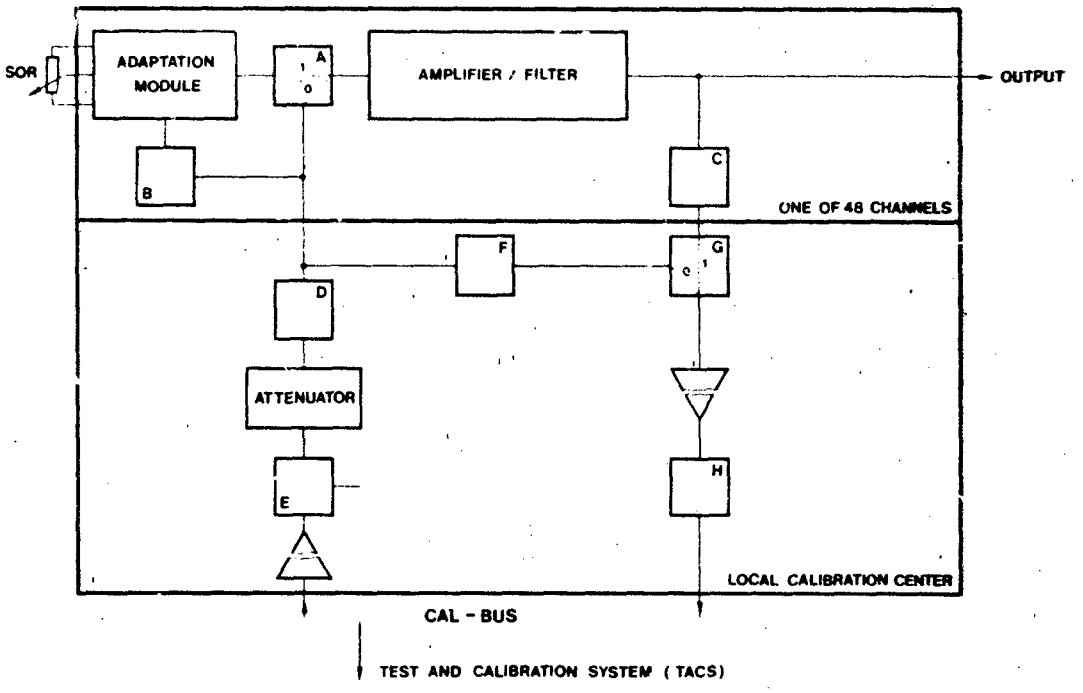

TASK:	SIGNALPATH:
Sensor Raw Data Examination	Sensor, B, F, GO, H, TACS
Test Voltage Superposing	TACS, E, D, B, A1, C, G1, H, TACS
Local Calibration Centre Verification	TACS, E, D, F, GO, H, TACS
Signal Conditioning Channel Test and Calibration	TACS, E, D, AO, C, G1, H, TACS

G. 8 SIGNAL PATHS FOR TEST AND CALIBRATION TASKS

DFVLR

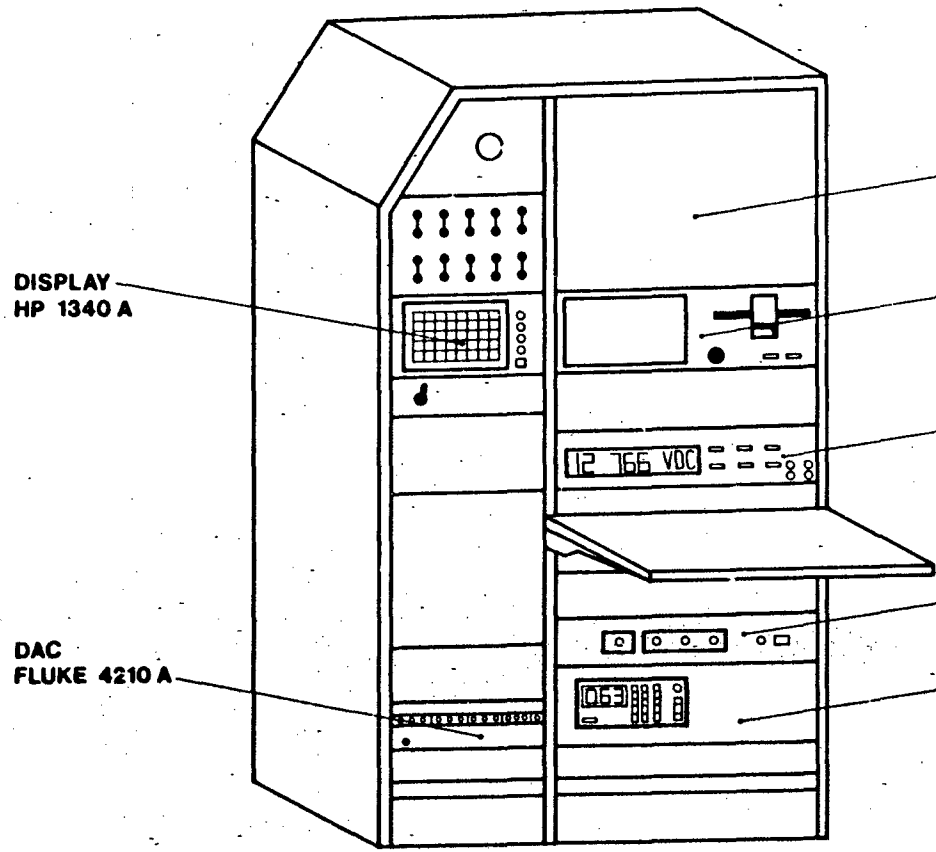

FIG. 9 TEST AND CALIBRATION SYSTEM OPERATOR PANEL

DFVLR

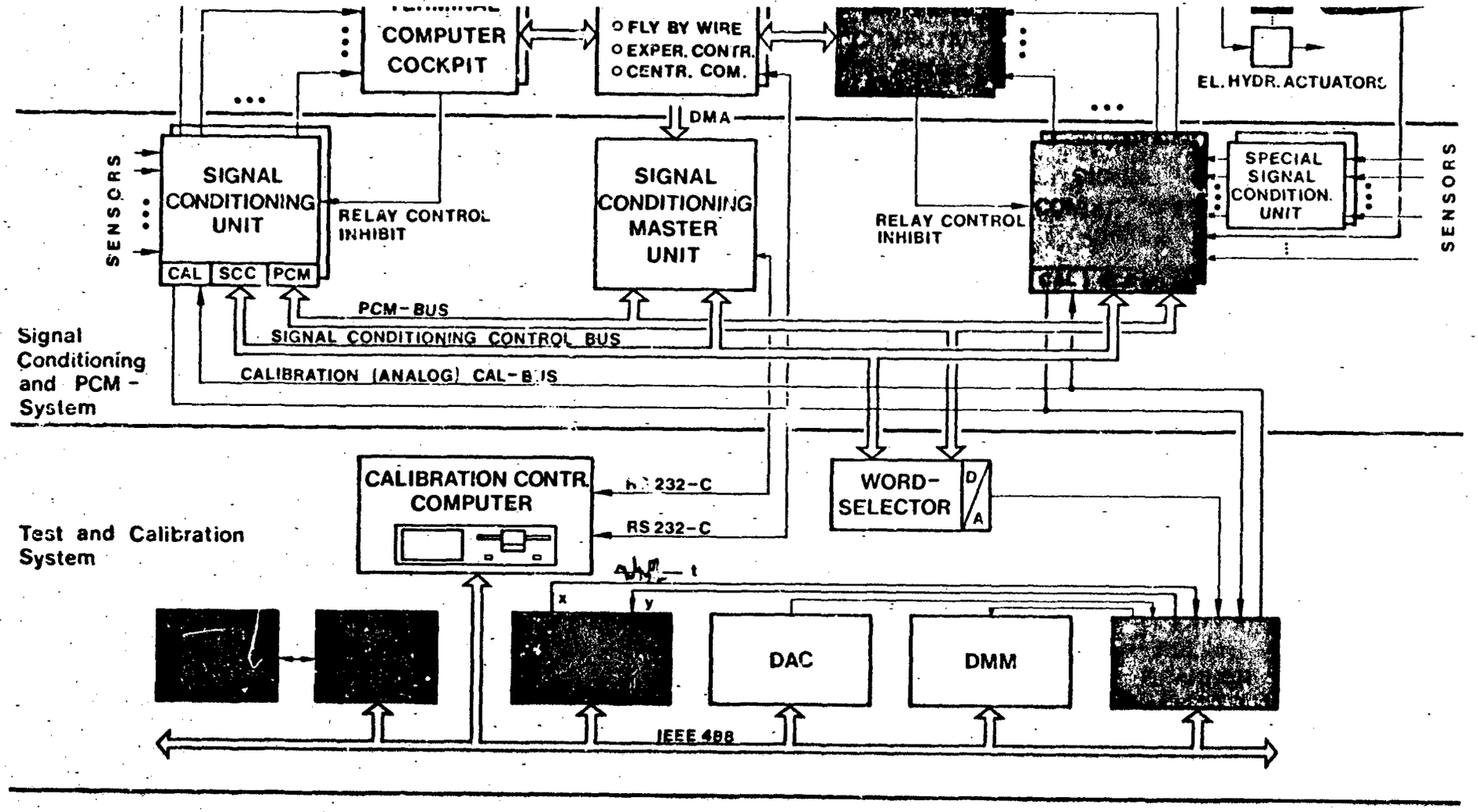

FIG. 10 DYNAMIC IN-FLIGHT CALIBRATION

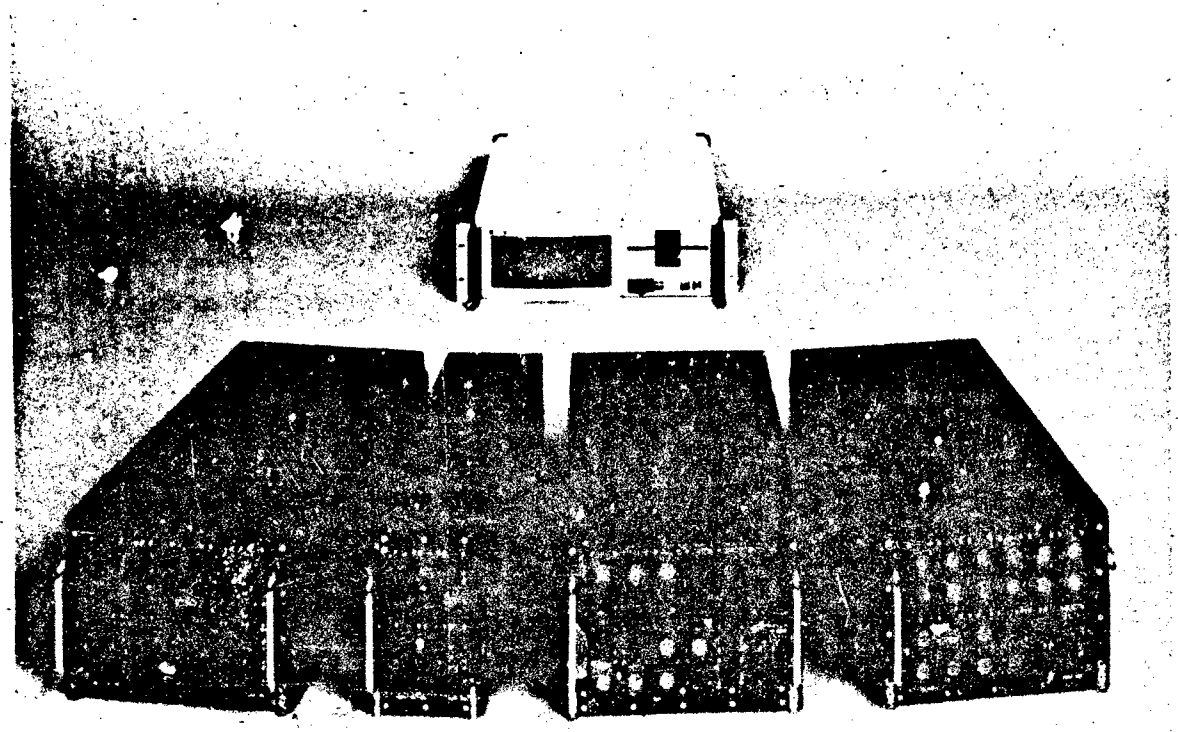

FIG. 11 ATTAS MEASURING SYSTEM; SC-UNITS, SSC-UNIT MASTER UNIT AND CALIBRATION CONTROL COMPUTER

DFVLR

THE DEVELOPMENT OF AN AIRBORNE INSTRUMENTATION COMPUTER SYSTEM FOR FLIGHT TEST

Glenn A. Bever
NASA Ames Research Center
Dryden Flight Research Facility
P.O. Box 273
Edwards, California 93523
U.S.A.

ımentation interfacing frequently requires the linking of intelligent systems together, as well as the link itself to be intelligent. The airborne instrumentation computer system (AICS) was develdress this requirement. Its small size, approximately 254 by 133 by 140 mm (10 by 5¼ by 5½ in), ous, and modular-board configuration give it the ability to solve instrumentation interfacing and on problems without forcing a redesign of the entire unit. This system has been used on the F-15 digital electronic engine control (DEEC) and its follow-on engine model derivative (EMD) project, OV-1C Mohawk aircraft stall-speed warning system. The AICS is presently undergoing configuration a an F-104 pace aircraft and on the advanced fighter technology integration (AFTI) F-111 aircraft.

JRE

advanced fighter technology integration	LSB	least significant byte
airborne instrumentation computer system	LSI	large-scale integration
Aeronautical Radio, Inc. specification number	MIL-STD-1553	military standard number
digital electronic engine control	MSB	most significant byte
direct memory access	PCM	pulse code modulation
electrically erasable programmable read-only memory	PROM	programmable read-only memory
engine model derivative	RAM	random access memory
erasable programmable read-only memory	RMDU	remote multiplexer digitizer unit
input/output	RS-232C	Electronics Industry Association standard number
liquid crystal display	TTL	transistor-transistor logic
	USART	universal synchronous/asynchronous receiver transmitter

UCTION

creasing digital nature of aircraft being tested at NASA Ames Research Center's Dryden Flight acility has increased the need for flexible digital instrumentation systems. Test aircraft typi- digital systems of unique design on board and researchers need to derive data from those systems. raft often have minimal space for flight-test instrumentation. This paper addresses the need for hat is capable of interfacing special digital systems to pulse code modulation (PCM) systems and nboard engineering calculations and display. The development of the system is discussed, and amples are described.

OBLEMS

ft instrumentation systems used at NASA Ames Dryden are built either in-house or by a contractor. ject is designed in-house, NASA has the choice of selecting those systems that correspond well to g experience and data reduction methods. When an instrumentation system is contractor built (off- is frequently of a unique design, or of a design that does not lend itself to merge gracefully mes Dryden data systems.

e space on an aircraft is limited, there is typically very little room to house an instrumenta- m.

t requirements, regardless of where they originate, tend to be evolutionary. Because of unfore- requirements, new ideas, or lack of foresight, instrumentation systems may require modifications. rs to be a minor modification can cause significant changes in the overall system.

im: data reduction is desired on a number of flight projects that are flown at Ames Dryden. The ion for these requirements include: saving flight time by immediately determining if a data run ad the required data; helping the pilot identify a potential problem in his flight systems and

m to take corrective action; dynamically changing the flight plan based on observed data; and
e postflight data reduction tasks.

h flights are becoming longer in duration and are increasing in frequency. This puts real-time
ion facilities at a premium. Postflight data reduction is a time-consuming process and require-
se of this facility add significant delays in providing researchers with flight data. Methods
the time requirements on these facilities are therefore desirable.

, manpower and budget constraints are increasingly becoming a problem.

t, a small, versatile, programmable, and inexpensive digital interface and calculation system is

ION

ns to problems are derived from experience, knowledge, and the use of available equipment. The
esented here is not necessarily in the order of that which was followed, but all of the items
ial in the production of the final result. At all times, simplicity and flexibility of design
n mind, as was serviceability of the equipment. An effort was made to solve many instrumenta-
ms at once by developing multipurpose and standardized units.

ection

buses were considered. Design goals included simplicity of bus architecture, small size, and
y of low-cost commercial boards and prototype building cards. The STD bus (Ref. 1) met those
s. It was designed to work with 8-bit microprocessors and has an 8-bit data path. An 8-bit
sor (as opposed to more complicated, newer 16-bit microprocessors) was deemed adequate for most
applications. The bus supplies circuit boards with +5 V, +12 V, and -12 V. No onboard regula-
equired for transistor-transistor logic (TTL) circuitry, thus saving board space.

re

puter enclosure has to be as small as possible to fit in the limited space of most aircraft,
e enough to accommodate three wire-wrapped prototype cards or six printed circuit cards. This
minimum of 15.875 mm (0.625 in) spacing between card slots. As prototype cards are debugged
ocated and fixed) and made into printed circuits, more space is available for additional proto-
this way, the same enclosure can be used by both prototype and final systems. A number of these
manufactured at Ames Dryden without detailing the mounting of power supplies and connectors.
each project the flexibility to determine what interface connectors to use on the AICS. Signals
tionally grouped in different connectors. Inexpensive off-the-shelf connectors can then be used,
es the problem of special connectors being out of stock.

mputer Board Selection

r of interface cards were commercially available for the STD bus, but the available microproc-
were not functional in a very small system. Since as much room as possible should remain in
re for project-dependent interfaces, the basic general purpose computer and standard input-
uitry should be contained on one card. Because some projects require the processing of signif-
ts of real-time complex engineering equations, an arithmetic or floating-point processor was
e the card needed to withstand rugged flight environments, and one was not available that satis-
the above requirements, a decision was made for an in-house design of the microcomputer board.

E SYSTEM DESCRIPTION

S consists of an enclosure approximately 254 by 133 by 140 mm (10 by 5¼ by 5½ in) and contains
ard microcomputer that plugs into an industry-standard STD backplane. This backplane accom-
her commercially available or specially designed interface boards. The enclosure itself can be
to fit the needs of the individual project with respect to power supplies and external connec-
ical project configurations yield an AICS power consumption of under 50 W. Having the power
rmined by the project allows state-of-the-art power converters to be used as they become avail-
1 is an internal view of the F-15 digital electronic engine control (DEEC) prototype AICS and
s an enclosed AICS as used in the OV-1C aircraft.

rt of the AICS system is a microcomputer board that plugs into a wide-spaced STD bus backplane
ns six card slots. There are enough standard peripheral components on the processor board so
ve remaining STD bus slots can be devoted to special system requirements.

mputer Board Description

gle-board computer uses six-layer printed circuit technology to accommodate a number of large-
gration (LSI) components on a single board measuring 14.3 by 165.1 by 1.6 mm (4.5 by 6.5 by
The board contains:

8C85A microprocessor.

8231A floating-point arithmetic processor.

ilobytes of 2732 erasable programmable read-only memory (EPROM).

kilobytes of either 2716 EPROM or 6116 random access memory (RAM) plus 256 bytes of RAM in an 55 RAM input-output (I/O) port.

o 8251 universal synchronous/asynchronous receiver transmitters (USART) that can be used either th TTL signals or RS-232C level signals provided by the 75188 line driver and the 75189 line ceiver.

ree 16-bit programmable timers in an 8253 programmable timer (two used for USART bit rate ntrol).

bits of parallel I/O using the 8155.

ress decoding using 82S131 programmable read-only memory (PROM).

) bus interface.

ight-qualified, low-profile sockets that every integrated circuit plugs into.

ard configuration controlled by jumpers on the user interface connector.

is a simplified block diagram of the single-board computer and Fig. 4 is a photograph of the board. One reason the 8085A microprocessor (Ref. 2) was chosen was because of its superior circuitry. It allows direct inputs for one unmasked and three masked interrupts with various is of level and edge triggering, as well as allowing one line for up to seven externally vec- rupts. Because instrumentation projects are intensely real-time oriented, interrupts are used . Good priority interrupt circuitry on the microprocessor chip can reduce the microcomputer ponent count.

85A is clocked by a crystal operating at a frequency of 6.144 MHz. It yields a microcycle time A typical instruction completes in 2 to 3 μs. Address, data, and control lines (such as , Clock, I/O-Memory select, Address Latch Enable, and Reset) are bused to all of the peripheral

55 provides two 8-bit and one 6-bit parallel input/output ports, 256 bytes of static RAM, and a rammable timer for the board (Ref. 2). Two 2732 EPROMs (Ref. 2) provide the board with 8 kilo- ogram memory, with the remaining 2 kilobytes of memory being either a 2716 EPROM (Ref. 2) or a ef. 3).

1 integrated circuits (Ref. 2) provide USARTs to the board. Their bit rates are determined by ogrammable timer which allows separate control of the two 8251 bit rates. The USARTs can be to operate in either a synchronous mode at 0 to 64,000 bits per second or in an asynchronous o 19,200 bits per second. The 75189 and 75188 integrated circuits (Ref. 4) provide RS-232C I/O l interfacing.

oard address decoding is provided by three 82S131 PROMs (512 by 4 bits each). Use of PROM lows maximum flexibility in determining onboard addresses (there is no fragmentation of memory esses — all addresses are contiguous and unique) as well as allowing offboard direct memory ces to access the computer board's memory. Use of discrete logic to accomplish these tasks up too much room on the board.

y the most important factor in making this board universally applicable to many real-time instru- ystems is the use of the 8231A arithmetic processor. The 8231A integrated circuit is a powerful hat will perform single- and double-precision fixed-point, as well as floating-point arithmetic fic calculations (Ref. 2). Thus all of the mathematical operations can be offloaded to the processor which contains a 32-bit wide internal data path. Benchmark testing has indicated that wentyfold-savings in execution time can be realized by using the arithmetic processor (Ref. 5). imes of floating-point instructions in the arithmetic processor vary considerably; for example, g-point multiply instruction takes approximately 50 μs and a cosine operation takes 1.34 ms

1A is interfaced to the 8085A through the 8-bit data bus, control lines for Read and Write, select, and the least significant address line. This address line, in conjunction with Read ignals, tells the 8231A what types of operations it will be doing; (for example, data entry or The 8085A passes data and commands to the 8231A, and receives results back from the 8231A. Data nternally on a stack in the 8231A. The data stack is either 16 bits or 32 bits wide, depending ation. The 8085A is typically programmed to wait for the completion of each command it sends to This is the most straightforward way to program it. The 8085A could, however, be programmed the 8231A instruction, continue with 8085A instructions, and check the status of the 8231A only sult is required by the 8085A. This would increase the information processing rate (throughput) es, but generally the arithmetic operations are done contiguously. Therefore, the program would not be enhanced by this alternate scheme. It would, however, require a larger code space the extra status checks required.

ry Interface

ry systems at Ames Dryden use data words that are between 8 and 12 bits long — typically, nboard computer systems that need to interface to the telemetry system frequently have word are 16 bits long. Two asynchronous activities are taking place in the system: data coming S from the onboard computer or data system, and data being passed from the AICS to the

...6 bits does not get half transferred in 16 bits) at a time when the telemetry system is request- whole transfer out. This is accomplished by latching all 16 bits and transferring them all at the time to a 16-bit memory. When the telemetry system requests data, all 16 bits are read out of memory ce and stored in a register where the telemetry system can access them.

o interface the AICS with a remote multiplexer digitizer unit (RMDU) PCM system, two boards were ned. Fig. 5 is a simplified block diagram of the circuitry on these boards. One board contains the y accessible by the PCM system and the other contains the direct memory access (DMA) controller that CM system uses to interrogate the PCM memory. The basic operation can be summarized as follows: The al processor places data in the two 8-bit latches, then simultaneously writes them into the PCM acces- memory as a single 16-bit value. The PCM input port is organized in 10-bit units. When the PCM sys- equests a value through a PCM word request signal, the "glitch" detector (a glitch is a spurious asyn- ous signal that is to be ignored) verifies the validity of the request. A divide by two latch acti- the DMA controller every second PCM word request. The DMA controller presents the requested 16-bit to the PCM input port within 4 μs. The most significant 10 bits are taken by the PCM on that request. ext PCM word equest multiplexes the lower order 6 bits without requiring another memory read. The nd of cycle signal resets the divide by two latch to ensure synchronization of the DMA activity with elemetry system. It also terminates the DMA activity for that cycle. This signal is required only to synchronize the telemetry data map with the interface, but continuous use of this signal ensures transient improper operation will not cause the interface to lose synchronization for very long.

...ice Output

...is board was designed to interface the processor with a speech synthesizer through the STD bus. 5 is a simplified block diagram of this board. It uses a Votrax SC-01 phoneme speech synthesizer 6) that has 64 different phonemes. Circuitry has been added to allow extended pitch control. An integrated circuit (Ref. 2) is used to control various onboard functions, as well as provide 2 kilo- of onboard EPROM for word tables or additional programming space. Use of a phoneme-based speech esizer allows customized vocabularies to be programmed and tested inexpensively. (Phoneme synthe- s sound mechanical, yet are intelligible.)

...ftware Design

...rogramming the AICS for a specific project is a major part of the application effort. To effectively ...lish that, software development tools are required. One of the tools available at Ames Dryden is a ...ful relocating cross assembler on a minicomputer. Instead of filling up the AICS memory with an exist- ...rating system and spending a lot of time working around it (and locating the problems, or "bugs"), ...stem software was completely designed and tailored to the particular needs of flight test instru- ...ion. This optimized the code size, as well as providing in-house knowledge of the inner software ...gs.

...e instrumentation requirements that dictate the software design include: functionally optimized code ...verhead); the ability to stand alone (nonvolatile program memory); optimal utilization of hardware; ...mplicity. In order to achieve functionally optimized code, all code was written in assembly language. ...evel computer language compilers that optimize code were not available for this system. Extensive user-definable operation codes (macros) in the macro assembler raised the level of programming to ... that of a high-level language, but retained optimizing characteristics by assembling only what was ...d. The use of a librarian allowed linkage of only those routines required by the programming. The a microprocessor hardware emulator allowed program development to proceed without requiring the pro- ...development code to be part of the microprocessor software. The use of the real-time hardware emula- ... an indispensable tool in developing microprocessor systems in a time-effective manner.

...easons for programming in a high-level language (such as FORTRAN or PASCAL) include the need for: ...ted input/output; floating-point formula calculations; and ease of programming and debugging (find- ...rors). Using macro coding, formatted input/output and floating-point formula calculations were ...olished. Ease of programming usually implies separation from hardware, which, by the nature of this ..., is undesirable. A reasonable compromise has been achieved by the use of libraries of macros and ...tines.

...PROM DATA STORAGE TECHNIQUE

... data acquisition systems requiring small amounts of data, electrically erasable programmable read- ...emory (EEPROM) is useful in providing nonvolatile storage. It allows flight-dependent documentation ...nd calibration coefficients to be entered without requiring removal of components for programming. ...s not require battery backup, it is inexpensive, and because it is solid state it has no moving The technique of using EEPROM for data storage was used on the OV-1C aircraft stall warning system ...re flight parameters at moments determined by the pilot. After engine shutdown, data could be off- (in both uncalibrated and calibrated forms) directly from the AICS to a printer to provide hardcopy flight data.

...VIRONMENTAL CONSIDERATIONS

...haustive environmental tests have not yet been conducted on the AICS. However, one configuration ...ted in section 8.2 has been vibrated to NASA process specification 21-2, curve A (12g from ...2 to ...). Forced air ventilation of at least 0.850 m^3/min (30 ft^3/min) has been used on all flying systems. ...omponents used on the microprocessor board are available in military-specified (MIL-SPEC, harsh envi- ...t) forms. The temperature regimes of current applications have allowed the use of commercial grade ...ents, thus saving development cost.

F-15 EMD (DEEC)

The AICS is presently being used on the F-15 aircraft DEEC and its follow-on engine model derivative) project. This aircraft is fitted with two DEEC computers. Fig. 9 is a simplified block diagram of F-15 DEEC instrumentation system. The AICS is acting as the interface between the two DEEC computers the PCM system. Each of the DEEC computers sends 16-bit data asynchronously to the AICS in 8-bit tums at 9600 bits/sec. Each data frame consists of 100 16-bit words, including 1 16-bit synchroniza- word. The USARTs on the AICS microprocessor board receive this data and interrupt the microprocessor, i in turn decommutates the data and places it in the memory on the PCM memory card. The telemetry sys- retrieves this data as described in section 4.2. Status words are formed by the AICS to determine the th of the system, including program status, data-stream status, and synchronization status. This sta- information is passed to the telemetry system for real-time evaluation.

The number of words per frame of asynchronous data, as well as the number of DEEC engines (one or two) ed, has varied. Since the AICS is a microprocessor-based design, only software modifications have been ired to reconfigure it for the different configurations.

OV-1C Aircraft Stall Warning

The AICS is also being used to test a stall warning concept aboard a United States Army OV-1C Mohawk raft (Ref. 7) in a joint NASA/Army project. Fig. 8 is an overall block diagram of the OV-1C stall ing system. This system represents the most complex use of the AICS to date, and serves to illustrate otential power of the AICS. It provides nearly all of the functions associated with real-time data ection and display including:

1. data acquisition via two 10-bit digital inputs;

2. data acquisition via nine analog inputs;

3. sensor calibration assistance;

4. real-time engineering unit calculations;

5. real-time control of synchro-driven cockpit indicator needles displaying airspeed and stall speed;

6. a voice synthesized aural warning of approaching stall to the pilot;

7. audible sensor limit warning to the flight test engineer;

8. nonvolatile data storage;

9. real-time data display of uncalibrated instrumentation counts, as well as engineering unit data; and

10. postflight dump of the raw data or engineering unit data for immediate analysis.

of a hand-held liquid crystal display (LCD) keyboard data entry and display unit (Fig. 9) allows the it test engineer to access flight data and enter selected coefficients.

dvanced Fighter Technology Integration (AFTI) F-111 Aircraft

The AFTI program is studying the concept of a variable camber wing on an F-111 airplane. It has a com- control system that is controlled by two airborne computers. This system was designed by a contractor s another example of the requirement of a unique interface to NASA's PCM system. The AICS hardware for this interface task is nearly identical to the set used on the F-15 aircraft. It was only neces- to add one line receiver card. Because of the flexibility inherent in the microprocessor-based design e AICS, the remaining modifications required by the project were completed in the software.

PLANNED APPLICATIONS

-104 Pace Aircraft

evelopment is underway to use the AICS as a real-time calculation and display system for aircraft g work. It would, based on pitot/static pressure sensor input, provide altitude, airspeed, and ion-error corrected Mach number display to the pilot or flight test engineer, as well as optionally t this information into the PCM system for comparison with ground data calculations. Fig. 10 is a ified block diagram of this instrumentation system.

ntegrated Sensor System Front Panel Controller

he microcomputer board developed for AICS is also being used in a ground-based project as a control- or data entry and display via an ARINC-429 data bus (Ref. 8). The ARINC-429 bus is used as the com- ation bus for state-of-the-art strapdown inertial navigation systems being used at Ames Dryden. The software development tools that were used for the airborne AICS are also used for this project.

nned enhancements to the system include the ability to: interface with different types of PCM sys- h addition to the RMDU); interface with the MIL-STD-1553 data bus (Ref. 9); and decommutate data oard PCM systems so that the AICS can take advantage of telemetered data rather than requiring the interface to the sensors directly.

e-integrated parameters, such as current aircraft weight, could be calculated in real time on an t using the AICS. These parameters could be passed on to the flight recorder or ground stations. ild simplify postflight data reduction by allowing time-integrated flight parameters to be observed requiring that a flight tape be replayed for integration.

increase the system information processing rate, multiprocessing could be used in the AICS. the STD bus, by virtue of its simplicity, is not designed for multiprocessing, it could be d by electrically splitting the STD backplane into two or more individual STD buses. The micro- rs on each bus could then be responsible for different processes and communicate with each other their parallel or serial I/O lines on the user interface connector. Thus a division of labor e achieved without altering the bus architecture or requiring substantial rewriting of system e.

ther approach for increasing the system's information processing rate is to use peripheral proc- on boards that are interfaced to the host microcomputer board through the STD bus. The host micro- would act as overall system controller, but the peripheral processors could handle special purpose uirements.

SI manufacturing techniques improve, more powerful microcomputer components are being built in packages that use less power than previously possible. This offers the possibility of using these erful microcomputers in a system the size of the AICS. In order to maintain the current STD bus e for compatibility, an 8-bit data path would need to be maintained off the microcomputer board, 6-bit (or larger) data path could be used on the microcomputer board itself to increase bandwidth.

NCLUSIONS

ible aircraft instrumentation interfaces such as the airborne instrumentation computer system re obtained by using a microprocessor-based system design. Large-scale integration (LSI) tech- llows these computer systems to be small enough to fit in most test aircraft. Because of soft- ls; project modifications can frequently be made without requiring hardware redesigns. A common ardware can be used for several projects, thus decreasing the overall cost of engineering each The use of a floating-point arithmetic processor allows real-time engineering equation calcula- take place onboard the aircraft for display in the cockpit or for telemetering to the ground. rtens the time requirements for a ground-based real-time data reduction facility. Onboard calcu- f time-integrated parameters (such as gross weight) simplifies postflight data reduction by allow- -integrated flight parameters to be observed without having to replay an entire flight tape to e them. This saves in postflight data reduction time. Significant savings in data analysis and ntation modification times are realized using this design.

ES

Bus Technical Manual and Product Catalog, 1982, Pro-Log Corporation, Monterey, Calif., 1-1 to 2-5.

onent Data Catalog, 1982, Intel Corporation, Santa Clara, Calif.

emories, 1980, Hitachi, San Jose, Calif., pp. 71-73.

Linear and Interface Circuits Data Book for Design Engineers, 1973, Texas Instruments rporated, First Ed., pp. 8-95 to 8-102.

1 Speech Synthesizer Data Sheet, 1980, Votrax, Troy, Mich.

er, Douglass O. and Bever, Glenn A., An Automated Stall-Speed Warning System, 1984, TM-84917.

11A/Am9512 Floating-Point Processor Manual, 1981, Advanced Micro Devices, Sunnyvale, Calif., 43 to 49.

33 Digital Information Transfer System (DITS) ARINC Specification 429-6, 1982, Aeronautical o, Inc., Annapolis, Md.

STD-1553 Multiplex Applications Handbook, 1982, SCI Systems, Inc., Huntsville, Ala.

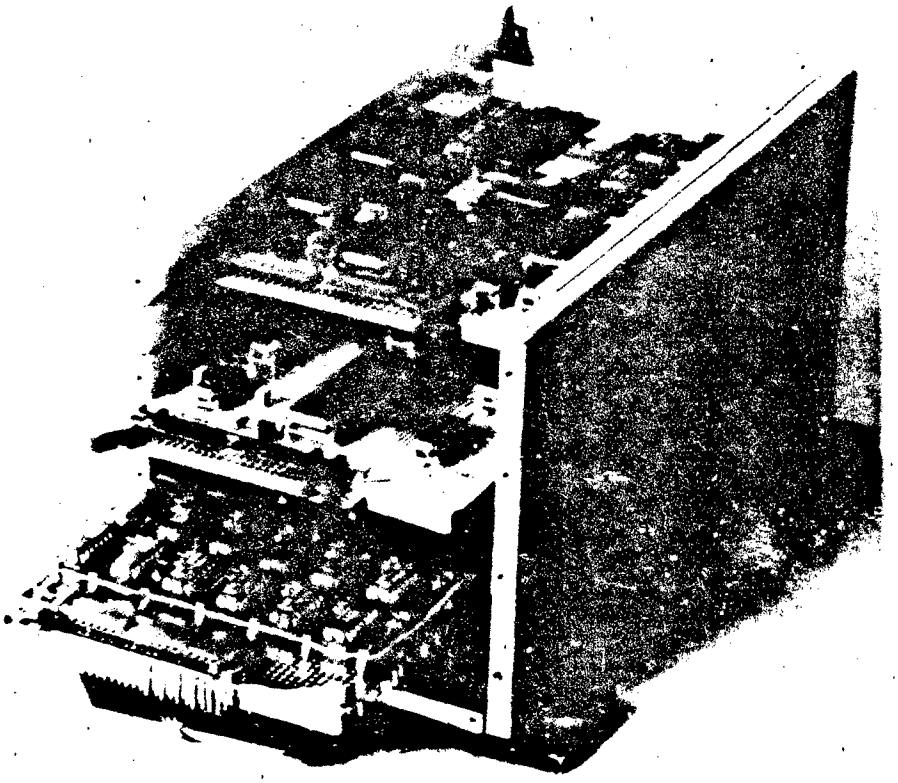

Figure 1. AICS box (DEEC prototype configuration).

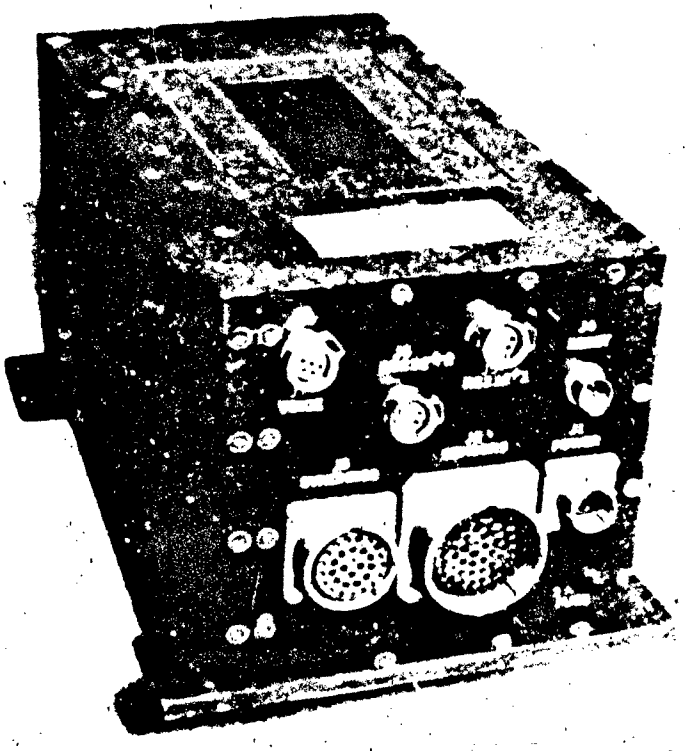

Figure 2. AICS box (OV-1C configuration).

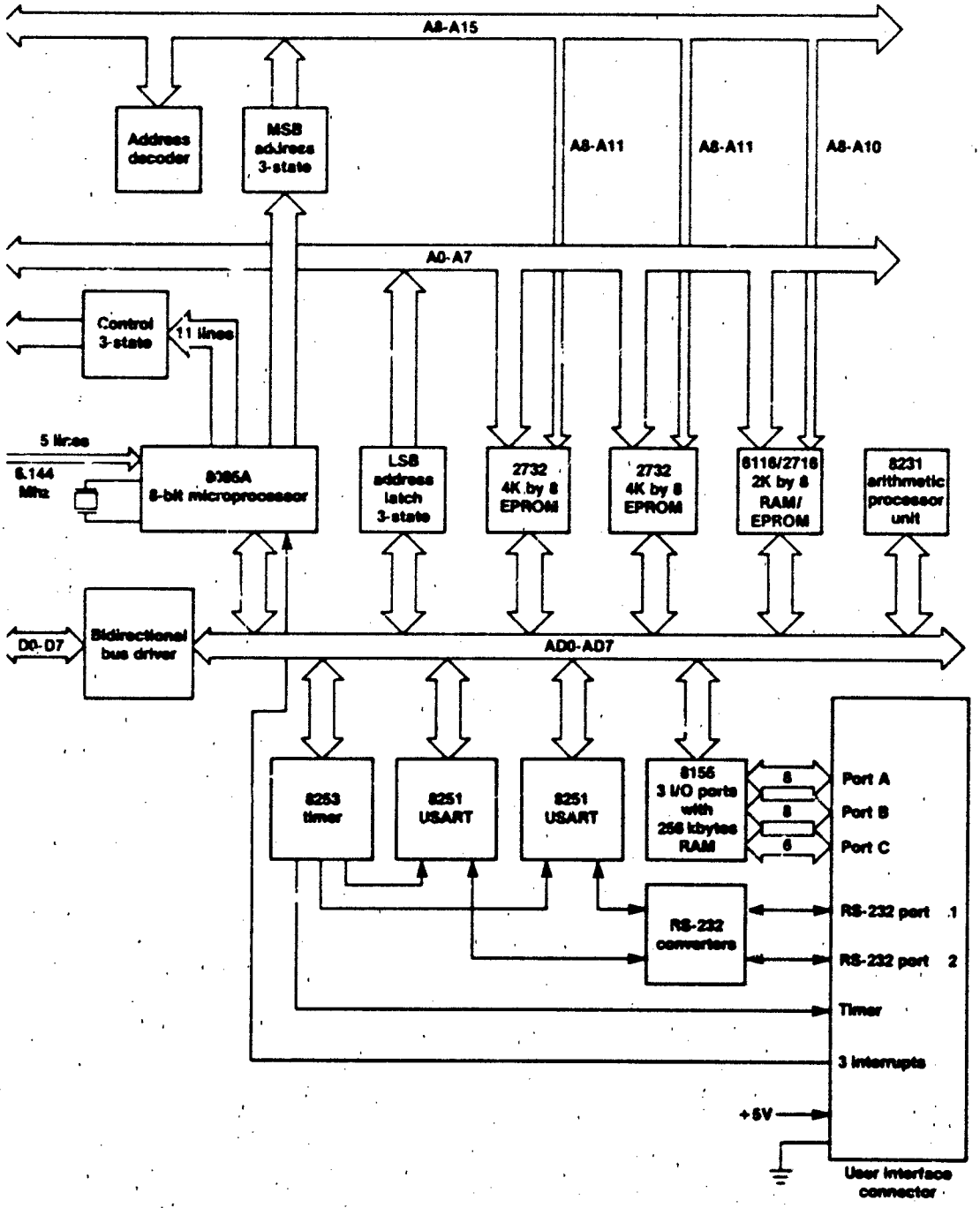

Figure 3. Simplified block diagram of a single-board microcomputer.

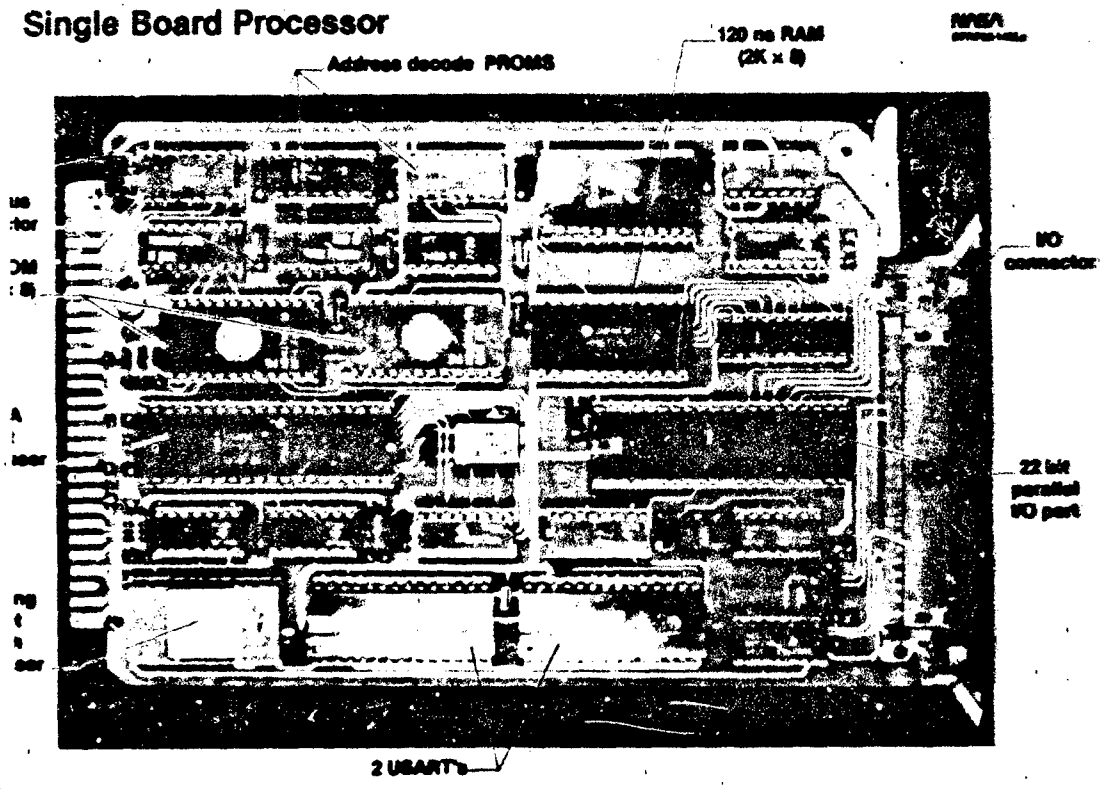

Figure 4. Single-board microcomputer.

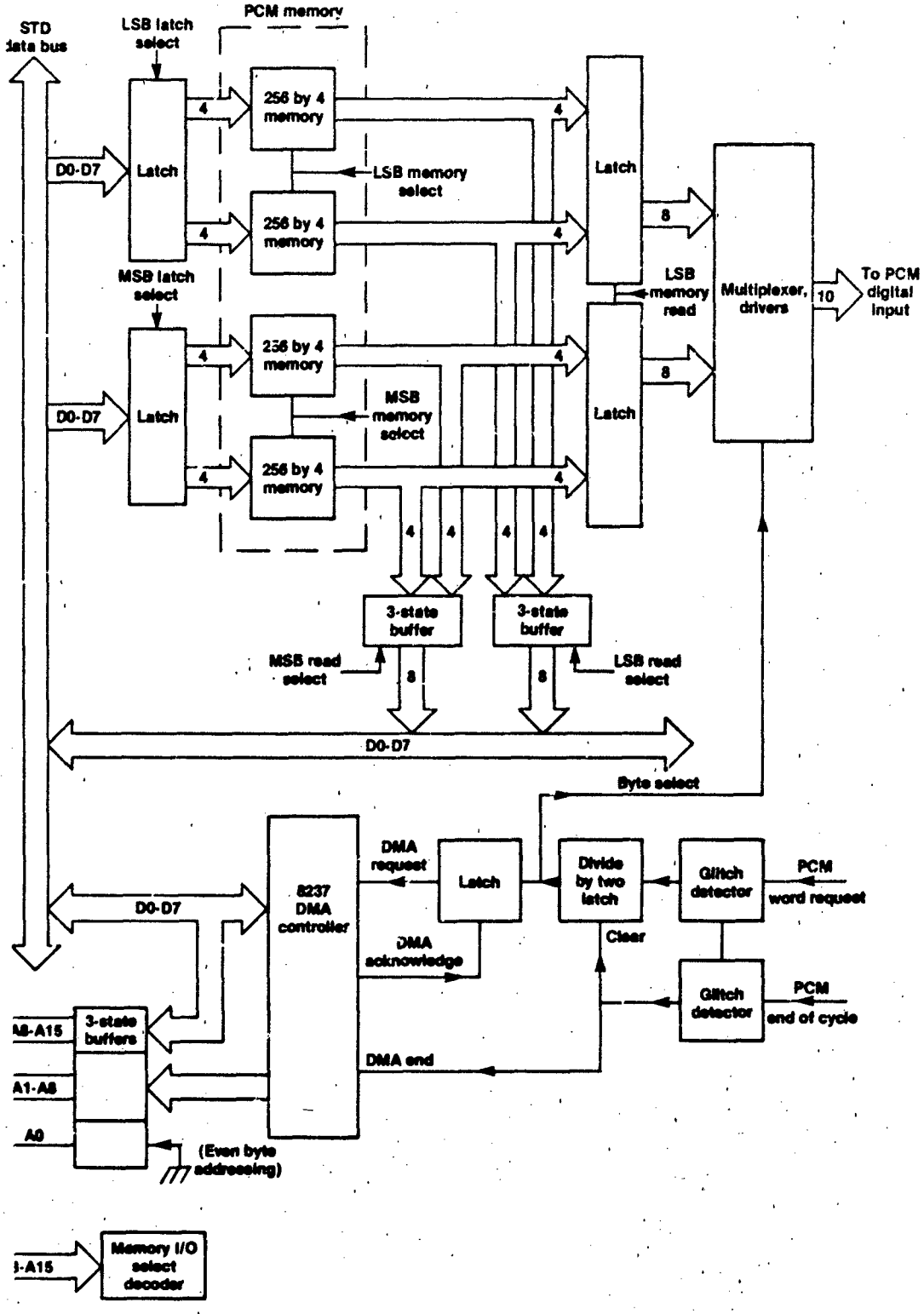

Figure 5. Simplified block diagram of a PCM interface.

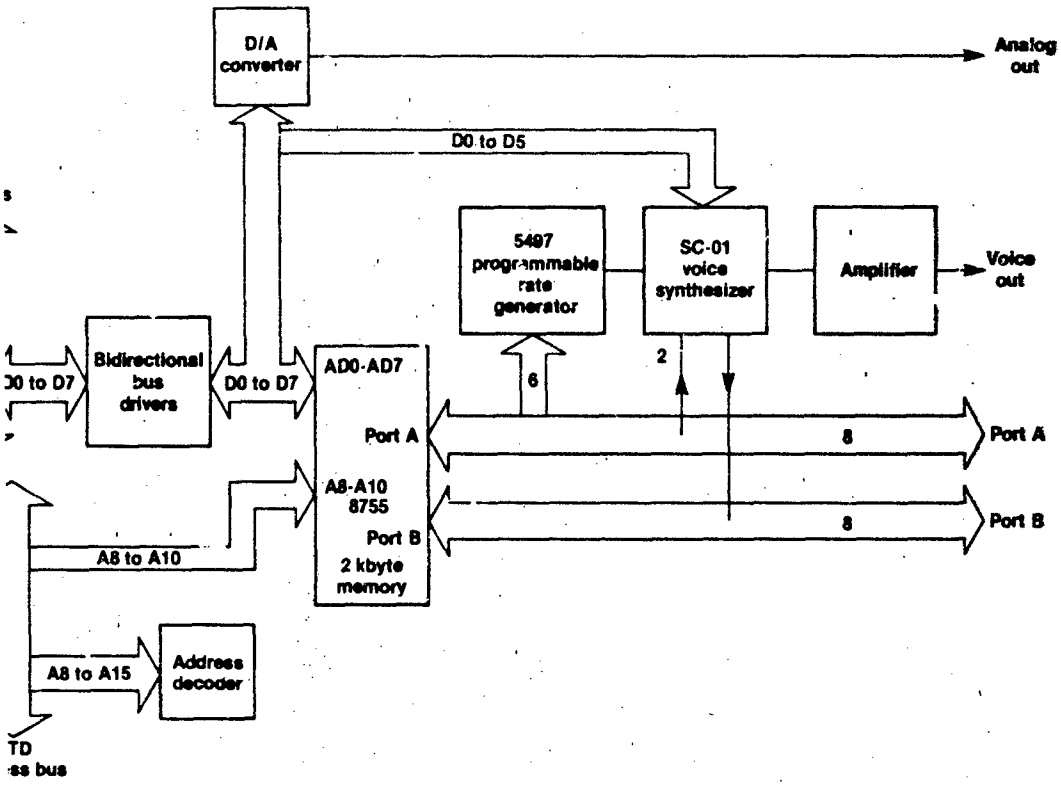

Figure 6. Simplified block diagram of a voice synthesizer.

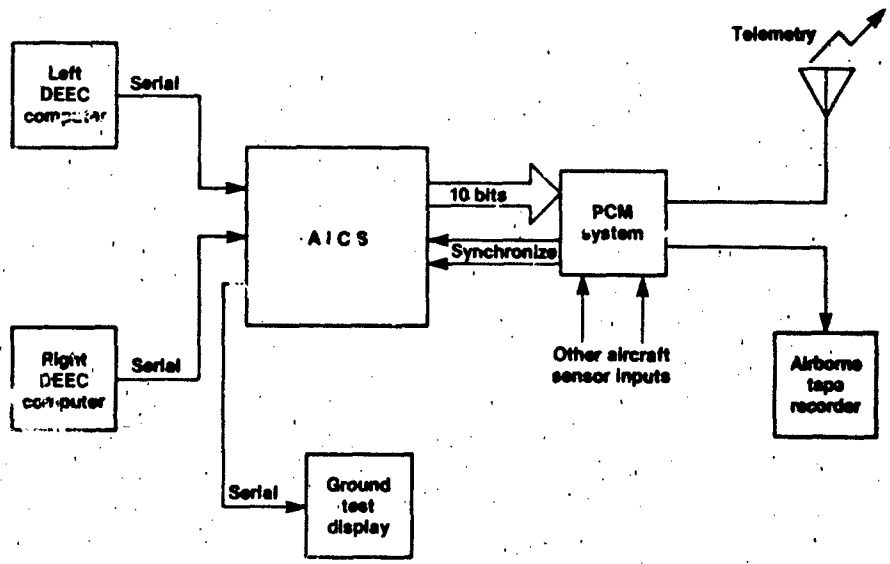

Figure 7. Simplified block diagram of the F-15 DEEC instrumentation system.

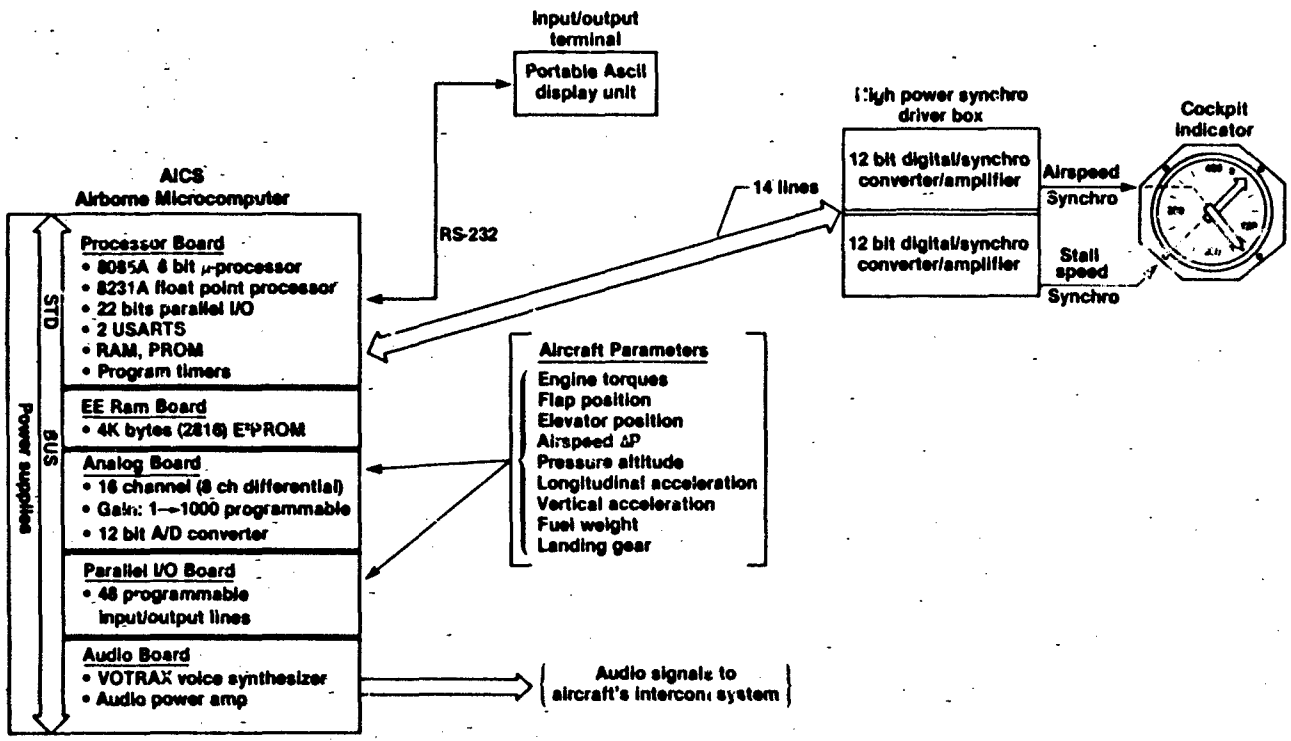

Figure 6. Overall block diagram of the OV-1C stall-warning system.

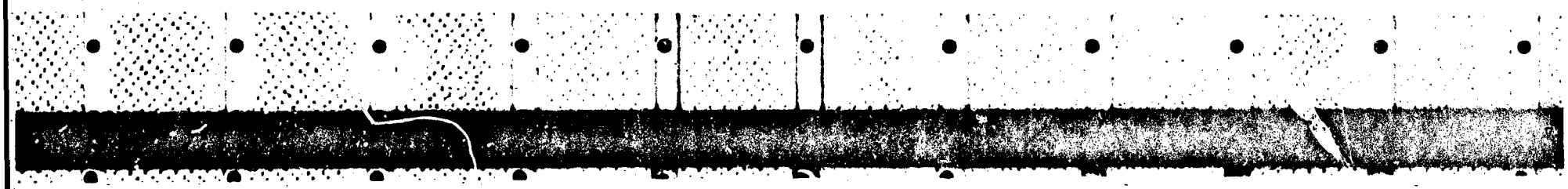

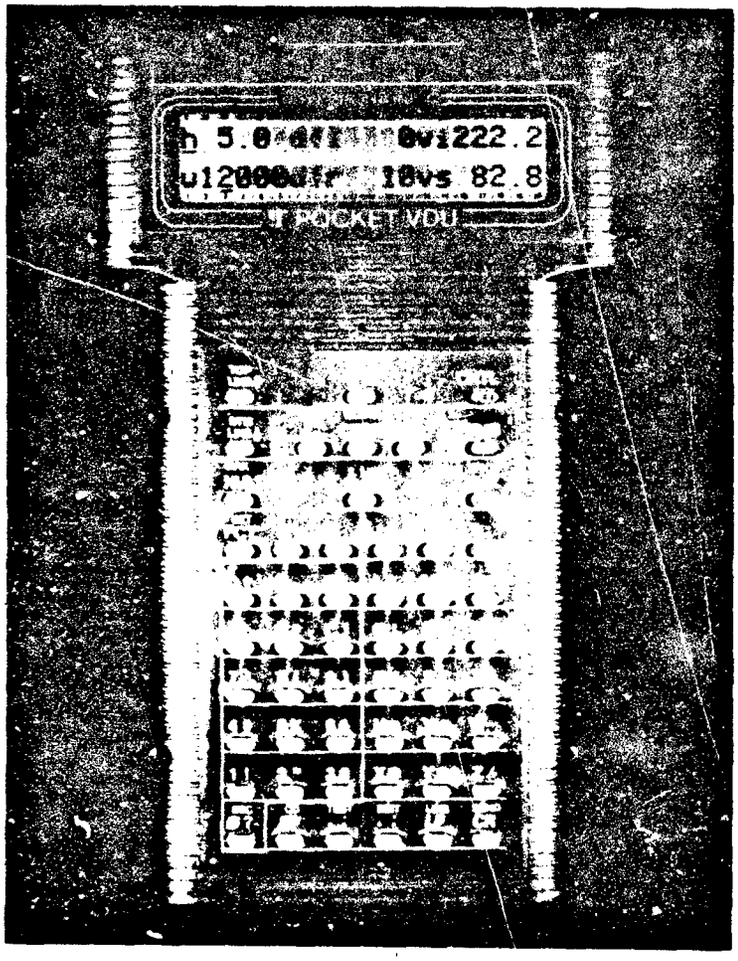

Figure 9. Portable LCD display unit.

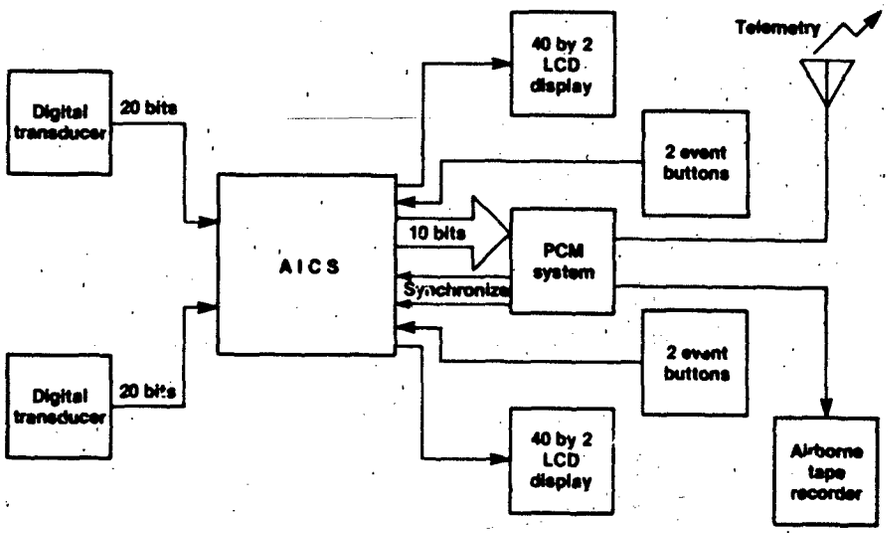

Figure 10. Simplified block diagram of an F-104 Pace instrumentation system.

REPORT DOCUMENTATION PAGE

nt's Reference	2. Originator's Reference	3. Further Reference	4. Security Classification of Document
	AGARD-CP-373	ISBN 92-835-0359-7	UNCLASSIFIED

tor Advisory Group for Aerospace Research and Development
North Atlantic Treaty Organization
7 rue Ancelle, 92200 Neuilly sur Seine, France

FLIGHT TEST TECHNIQUES

ed at the Flight Mechanics Panel Symposium held in Lisbon, Portugal, 2–5 April 1984.

(s)/Editor(s)	9. Date
Various	July 1984
's/Editor's Address	**11. Pages**
Various	380

ıtion Statement This document is distributed in accordance with AGARD policies and regulations, which are outlined on the Outside Back Covers of all AGARD publications.

rds/Descriptors

Flight tests	Avionic test units
Flight characteristics	Checkout
Performance tests	

t

proceedings contain the twenty-five papers presented at the AGARD Flight Mechanics Symposium on Flight Test Techniques, held in Lisbon, Portugal, 2–5 April 1984. main headings of Performance and Flying Qualities, Systems Testing, and Instrumenta- ıd Facilities, papers were given on: Lift-Drag; Parameter Identification; High-Angle g; Flight and Release of External Stores; Pilot Workload; Avionics, Navigation and ns Systems; H.U.D.; Real-Time Analysis and Test Control; Airborne Computation alibration; Laser Measurement of True Airspeed and Windshear; Clearance for Repaired ay Operation.

AGARD Conference Proceedings No.373
Advisory Group for Aerospace Research and Development, NATO
FLIGHT TEST TECHNIQUES
Published July 1984
380 pages

These proceedings contain the twenty-five papers presented at the AGARD Flight Mechanics Panel Symposium on Flight Test Techniques, held in Lisbon, Portugal, 2–5 April 1984. Under main headings of Performance and Flying Qualities, Systems Testing, and Instrumentation and Facilities, papers were given on Lift-Drag; Parameter Identification; High-Angle Testing; Flight and Release of External Stores; Pilot Workload; Avionics, Navigation and Weapons Systems; H.U.D.;

P.T.O.

AGARD-CP-373

Flight tests
Flight characteristics
Performance tests
Avionic test units
Checkout

AGARD Conference Proceedings No.373
Advisory Group for Aerospace Research and Development, NATO
FLIGHT TEST TECHNIQUES
Published July 1984
380 pages

These proceedings contain the twenty-five papers presented at the AGARD Flight Mechanics Panel Symposium on Flight Test Techniques, held in Lisbon, Portugal, 2–5 April 1984. Under main headings of Performance and Flying Qualities, Systems Testing, and Instrumentation and Facilities, papers were given on Lift-Drag; Parameter Identification; High-Angle Testing; Flight and Release of External Stores; Pilot Workload; Avionics, Navigation and Weapons Systems; H.U.D.;

P.T.O.

AGARD-CP-373

Flight tests
Flight characteristics
Performance tests
Avionic test units
Checkout

AGARD Conference Proceedings No.373
Advisory Group for Aerospace Research and Development, NATO
FLIGHT TEST TECHNIQUES
Published July 1984
380 pages

These proceedings contain the twenty-five papers presented at the AGARD Flight Mechanics Panel Symposium on Flight Test Techniques, held in Lisbon, Portugal, 2–5 April 1984. Under main headings of Performance and Flying Qualities, Systems Testing, and Instrumentation and Facilities, papers were given on Lift-Drag; Parameter Identification; High-Angle Testing; Flight and Release of External Stores; Pilot Workload; Avionics, Navigation and Weapons Systems; H.U.D.;

P.T.O.

AGARD-CP-373

Flight tests
Flight characteristics
Performance tests
Avionic test units
Checkout

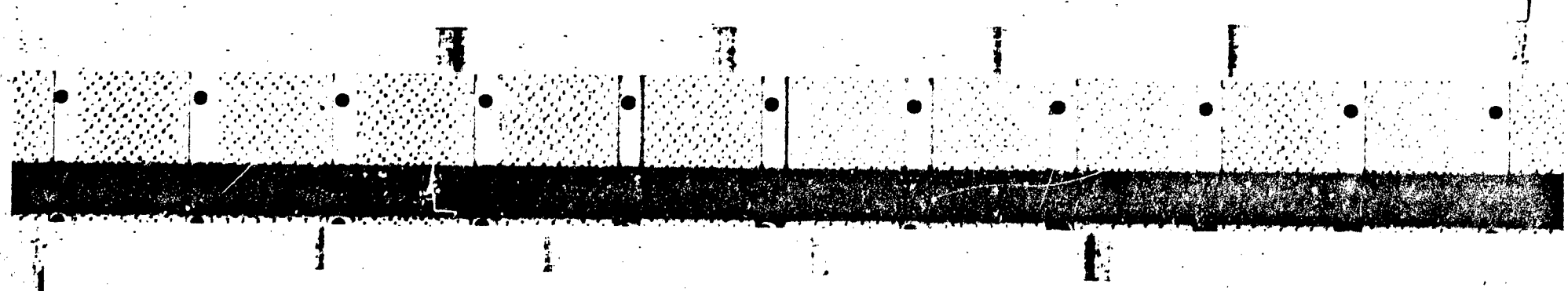

Measurement of True Airspeed and Windshear; Clearance for Repaired Runway Operation. ISBN 92-835-0359-7	Measurement of True Airspeed and Windshear; Clearance for Repaired Runway Operation. ISBN 92-835-0359-7
Real-Time Analysis and Test Control; Airborne Computation and Calibration; Laser Measurement of True Airspeed and Windshear; Clearance for Repaired Runway Operation. ISBN 92-835-0359-7	Real-Time Analysis and Test Control; Airborne Computation and Calibration; Laser Measurement of True Airspeed and Windshear; Clearance for Repaired Runway Operation. ISBN 92-835-0359-7

AGARD
NATO OTAN
ANCELLE · 92200 NEUILLY-SUR-SEINE
FRANCE
Telephone 745.08.10 · Telex 610176

DISTRIBUTION OF UNCLASSIFIED AGARD PUBLICATIONS

es NOT hold stocks of AGARD publications at the above address for general distribution. Initial distribution of AGARD s is made to AGARD Member Nations through the following National Distribution Centres. Further copies are sometimes om these Centres, but if not may be purchased in Microfiche or Photocopy form from the Purchase Agencies listed below.

NATIONAL DISTRIBUTION CENTRES

donnateur AGARD – VSL
Major de la Force Aérienne
tier Reine Elisabeth
d'Evere, 1140 Bruxelles

nce Science Information Services
irtment of National Defence
wa, Ontario K1A OK2

K
ish Defence Research Board
rbrogades Kaserne
enhagen Ø

.E.R.A. (Direction)
Avenue de la Division Leclerc
20 Châtillon sous Bagneux

IY
ninformationszentrum Energie,
sik, Mathematik GmbH
nforschungszentrum
514 Eggenstein-Leopoldshafen 2

lenic Air Force General Staff
earch and Development Directorate
argos, Athens

D
ector of Aviation
Flugrad
ykjavik

ITALY
Aeronautica Militare
Ufficio del Delegato Nazionale all'AGARD
3, Piazzale Adenauer
Roma/EUR

LUXEMBOURG
See Belgium

NETHERLANDS
Netherlands Delegation to AGARD
National Aerospace Laboratory, NLR
P.O. Box 126
2600 A.C. Delft

NORWAY
Norwegian Defence Research Establishment
Main Library
P.O. Box 25
N-2007 Kjeller

PORTUGAL
Direcção do Serviço de Material
da Força Aerea
Rua da Escola Politécnica 42
Lisboa
Attn: AGARD National Delegate

TURKEY
Department of Research and Development (ARGE)
Ministry of National Defence, Ankara

UNITED KINGDOM
Defence Research Information Centre
Station Square House
St. Mary Cray
Orpington, Kent BR5 3RE

UNITED STATES
National Aeronautics and Space Administration (NASA)
Langley Field, Virginia 23365
Attn: Report Distribution and Storage Unit

THE UNITED STATES NATIONAL DISTRIBUTION CENTRE (NASA) DOES NOT HOLD STOCKS OF AGARD PUBLICATIONS, AND APPLICATIONS FOR COPIES SHOULD BE MADE DIRECT TO THE NATIONAL TECHNICAL INFORMATION SERVICE (NTIS) AT THE ADDRESS BELOW.

PURCHASE AGENCIES

he or Photocopy
. Technical
tion Service (NTIS)
rt Royal Road
eld
22161, USA

Microfiche
ESA/Information Retrieval Service
European Space Agency
10, rue Mario Nikis
75015 Paris, France

Microfiche or Photocopy
British Library Lending
Division
Boston Spa, Wetherby
West Yorkshire LS23 7BQ
England

s for microfiche or photocopies of AGARD documents should include the AGARD serial number, title, author or editor, and ion date. Requests to NTIS should include the NASA accession report number. Full bibliographical references and abstracts of AGARD publications are given in the following journals:

ic and Technical Aerospace Reports (STAR)
ed by NASA Scientific and Technical
ation Branch
Headquarters (NIT-40)
gton D.C. 20546, USA

Government Reports Announcements (GRA)
published by the National Technical
Information Services, Springfield
Virginia 22161, USA

Printed by Specialised Printing Services Limited
40 Chigwell Lane, Loughton, Essex IG10 3TZ

ISBN 92-835-0359-7

END

END

FILMED

1-85

DTIC